

Arthritis & Rheumatology

An Official Journal of the American College of Rheumatology
www.arthritisrheum.org and wileyonlinelibrary.com

GENERAL INFORMATION

TO SUBSCRIBE

Institutions and Non-Members

Email: wileyonlinelibrary.com
Phone: (201) 748-6645
Write: Wiley Periodicals LLC
Attn: Journals Admin Dept
UK
111 River Street
Hoboken, NJ 07030

Volumes 73, 2021:
Institutional Print Only:

Institutional Online Only:
Institutional Print and
Online Only:

Arthritis & Rheumatology and Arthritis Care & Research:
\$2,422 in US, Canada, and Mexico
\$3,089 outside North America

\$2,422 in US, Canada, Mexico, and outside North America
\$3,029 in US, Canada, and Mexico; \$3,862 outside
North America

For submission instructions, subscription, and all other information visit: wileyonlinelibrary.com.

Arthritis & Rheumatology accepts articles for Open Access publication. Please visit <https://authorservices.wiley.com/author-resources/Journal-Authors/open-access/onlineopen.html> for further information about OnlineOpen.

Wiley's Corporate Citizenship initiative seeks to address the environmental, social, economic, and ethical challenges faced in our business and which are important to our diverse stakeholder groups. Since launching the initiative, we have focused on sharing our content with those in need, enhancing community philanthropy, reducing our carbon impact, creating global guidelines and best practices for paper use, establishing a vendor code of ethics, and engaging our colleagues and other stakeholders in our efforts.

Follow our progress at www.wiley.com/go/citizenship.

Access to this journal is available free online within institutions in the developing world through the HINARI initiative with the WHO. For information, visit www.healthinternetwork.org.

Disclaimer

The Publisher, the American College of Rheumatology, and Editors cannot be held responsible for errors or any consequences arising from the use of information contained in this journal; the views and opinions expressed do not necessarily reflect those of the Publisher, the American College of Rheumatology and Editors, neither does the publication of advertisements constitute any endorsement by the Publisher, the American College of Rheumatology and Editors of the products advertised.

Members:

American College of Rheumatology/Association of Rheumatology Professionals

For membership rates, journal subscription information, and change of address, please write:

American College of Rheumatology
2200 Lake Boulevard
Atlanta, GA 30319-5312
(404) 633-3777

ADVERTISING SALES AND COMMERCIAL REPRINTS

Sales: Kathleen Malseed, National Account Manager
E-mail: kmalseed@pminy.com
Phone: (215) 852-9824
Pharmaceutical Media, Inc.
30 East 33rd Street, New York, NY 10016

Production: Patti McCormack
E-mail: pmccormack@pminy.com
Phone: (212) 904-0376
Pharmaceutical Media, Inc.
30 East 33rd Street, New York, NY 10016

Publisher: Arthritis & Rheumatology is published by Wiley Periodicals LLC, 101 Station Landing, Suite 300, Medford, MA 02155

Production Editor: Ramona Talantor, artprod@wiley.com

ARTHRITIS & RHEUMATOLOGY (Print ISSN 2326-5191; Online ISSN 2326-5205 at Wiley Online Library, wileyonlinelibrary.com) is published monthly on behalf of the American College of Rheumatology by Wiley Periodicals LLC, a Wiley Company, 111 River Street, Hoboken, NJ 07030-5774. Periodicals postage paid at Hoboken, NJ and additional offices. POSTMASTER: Send all address changes to Arthritis & Rheumatology, Wiley Periodicals LLC, c/o The Sheridan Press, PO Box 465, Hanover, PA 17331. **Send subscription inquiries care of** Wiley Periodicals LLC, Attn: Journals Admin Dept UK, 111 River Street, Hoboken, NJ 07030, (201) 748-6645 (nonmember subscribers only; American College of Rheumatology/Association of Rheumatology Health Professionals members should contact the American College of Rheumatology). **Subscription Price:** (Volumes 73, 2021: Arthritis & Rheumatology and Arthritis Care & Research) Print only: \$2,422.00 in U.S., Canada and Mexico, \$3,089.00 rest of world. For all other prices please consult the journal's website at wileyonlinelibrary.com. All subscriptions containing a print element, shipped outside U.S., will be sent by air. Payment must be made in U.S. dollars drawn on U.S. bank. Prices are exclusive of tax. Asia-Pacific GST, Canadian GST and European VAT will be applied at the appropriate rates. For more information on current tax rates, please go to www.wileyonlinelibrary.com/tax-vat. The price includes online access to the current and all online backfiles to January 1st 2017, where available. For other pricing options including access information and terms and conditions, please visit <https://onlinelibrary.wiley.com/library-info/products/price-lists>. Terms of use can be found here: <https://onlinelibrary.wiley.com/terms-and-conditions>. **Delivery Terms and Legal Title:** Where the subscription price includes print issues and delivery is to the recipient's address, delivery terms are Delivered at Place (DAP); the recipient is responsible for paying any import duty or taxes. Title to all issues transfers Free of Board (FOB) our shipping point, freight prepaid. We will endeavor to fulfill claims for missing or damaged copies within six months of publication, within our reasonable discretion and subject to availability. **Change of Address:** Please forward to the subscriptions address listed above 6 weeks prior to move; enclose present mailing label with change of address. **Claims** for undelivered copies will be accepted only after the following issue has been received. Please enclose a copy of the mailing label or cite your subscriber reference number in order to expedite handling. Missing copies will be supplied when losses have been sustained in transit and where reserve stock permits. Send claims care of Wiley Periodicals LLC, Attn: Journals Admin Dept UK, 111 River Street, Hoboken, NJ 07030. If claims are not resolved satisfactorily, please write to Subscription Distribution c/o Wiley Periodicals LLC, 111 River Street, Hoboken, NJ 07030. **Cancellations:** Subscription cancellations will not be accepted after the first issue has been mailed. **Journal Customer Services:** For ordering information, claims and any enquiry concerning your journal subscription please go to <https://hub.wiley.com/community/support/onlinelibrary> or contact your nearest office. **Americas:** Email: cs-journals@wiley.com; Tel: +1 781 388 8598 or +1 800 835 6770 (toll free in the USA & Canada). **Europe, Middle East and Africa:** Email: cs-journals@wiley.com; Tel: +44 (0) 1865 778315. **Asia Pacific:** Email: cs-journals@wiley.com; Tel: +65 6511 8000. **Japan:** For Japanese speaking support, Email: cs-japan@wiley.com. **Visit our Online Customer Help** available in 7 languages at <https://hub.wiley.com/community/support/onlinelibrary>. **Back Issues:** Single issues from current and prior year volumes are available at the current single issue price from csjournals@wiley.com. Earlier issues may be obtained from Periodicals Service Company, 351 Fairview Avenue-Ste 300, Hudson, NY 12534, USA. Tel: +1 518 822-9300, Fax: +1 518 822-9305, Email: psc@periodicals.com. Printed in the USA by The Sheridan Group.

Arthritis & Rheumatology

An Official Journal of the American College of Rheumatology
www.arthritisrheum.org and wileyonlinelibrary.com

VOLUME 74 • January 2022 • NO. 1

In This Issue	A9
Journal Club	A10
Clinical Connections	A11
Special Articles	
Notes from the Field: Global Rheumatology Research: Frontiers, Challenges, and Opportunities <i>Joshua B. Bilsborrow, Ingris Peláez-Ballestas, Bernardo Pons-Estel, Christiaan Scott, Xiping Tian, Graciela S. Alarcon, Richard Bucala, Laura B. Lewandowski, and Evelyn Hsieh</i>	1
Editorial: Reexamining Remission Definitions in Rheumatoid Arthritis: Considering the Twenty-Eight-Joint Disease Activity Score, C-Reactive Protein Level, and Patient Global Assessment <i>David T. Felson, Diane Lacaille, Michael P. LaValley, and Daniel Aletaha</i>	5
Editorial: Lung Inflammation, NETosis, and the Pulmonary Initiation of Anti-Citrullinated Protein Antibody Response: What Came First, the Chicken or the Egg? <i>Jeremy Sokolove</i>	10
Review: Systemic Sclerosis-Associated Interstitial Lung Disease: How to Incorporate Two Food and Drug Administration-Approved Therapies in Clinical Practice <i>Dinesh Khanna, Alain Lescoat, David Roofeh, Elana J. Bernstein, Ella A. Kazerooni, Michael D. Roth, Fernando Martinez, Kevin R. Flaherty, and Christopher P. Denton</i>	13
COVID-19	
Disease Flare and Reactogenicity in Patients With Rheumatic and Musculoskeletal Diseases Following Two-Dose SARS-CoV-2 Messenger RNA Vaccination <i>Caoilfhionn M. Connolly, Jake A. Ruddy, Brian J. Boyarsky, Iulia Barbur, William A. Werbel, Duvuru Geetha, Jacqueline M. Garonzik-Wang, Dorry L. Segev, Lisa Christopher-Stine, and Julie J. Paik</i>	28
Humoral and Cellular Immune Responses to SARS-CoV-2 Infection and Vaccination in Autoimmune Disease Patients With B Cell Depletion <i>David Simon, Koray Tascilar, Katja Schmidt, Bernhard Manger, Leonie Weckwerth, Maria Sokolova, Laura Bucci, Filippo Fagni, Karin Manger, Florian Schuch, Monika Ronneberger, Axel Hueber, Ulrike Steffen, Dirk Mielenz, Martin Herrmann, Thomas Harrer, Arnd Kleyer, Gerhard Krönke, and Georg Schett</i>	33
Rheumatoid Arthritis	
Association of Sputum Neutrophil Extracellular Trap Subsets With IgA Anti-Citrullinated Protein Antibodies in Subjects at Risk for Rheumatoid Arthritis <i>Yuko Okamoto, Stephanie Devoe, Nickie Seto, Valerie Minarchick, Timothy Wilson, Heather M. Rothfuss, Michael P. Mohning, Jaron Arbet, Miranda Kroehl, Ashley Visser, Justin August, Stacey M. Thomas, Laura Lenis Charry, Chelsie Fleischer, Marie L. Feser, Ashley A. Frazer-Abel, Jill M. Norris, Brian D. Cherrington, William J. Janssen, Mariana J. Kaplan, Kevin D. Deane, V. Michael Holers, and M. Kristen Demoruelle</i>	38
Osteoarthritis	
Role of Ciliary Protein Intraflagellar Transport Protein 88 in the Regulation of Cartilage Thickness and Osteoarthritis Development in Mice <i>Clarissa R. Coveney, Linyi Zhu, Jadwiga Miotla-Zarebska, Bryony Stott, Ida Parisi, Vicky Batchelor, Claudia Duarte, Emer Chang, Eleanor McSorley, Tonia L. Vincent, and Angus K. T. Wann</i>	49
Magnetic Resonance Imaging-Assessed Subchondral Cysts and Incident Knee Pain and Knee Osteoarthritis: Data From the Multicenter Osteoarthritis Study <i>Thomas A. Perry, Terence W. O'Neill, Irina Tolstykh, John Lynch, David T. Felson, Nigel K. Arden, and Michael C. Nevitt</i>	60
Spondyloarthritis	
Safety and Efficacy of Upadacitinib in Patients With Active Ankylosing Spondylitis and an Inadequate Response to Nonsteroidal Antiinflammatory Drug Therapy: One-Year Results of a Double-Blind, Placebo-Controlled Study and Open-Label Extension <i>Atul Deodhar, Désirée van der Heijde, Joachim Sieper, Filip Van den Bosch, Walter P. Maksymowych, Tae-Hwan Kim, Mitsumasa Kishimoto, Andrew Ostor, Bernard Combe, Yunxia Sui, Alvina D. Chu, and In-Ho Song</i>	70
Psoriatic Arthritis	
Identification and Evaluation of Serum Protein Biomarkers That Differentiate Psoriatic Arthritis From Rheumatoid Arthritis <i>Angela Mc Ardle, Anna Kwasnik, Agnes Szentpetery, Belinda Hernandez, Andrew Parnell, Wilco de Jager, Sytze de Roock, Oliver FitzGerald, and Stephen R. Pennington</i>	81

Systemic Lupus Erythematosus

Induction of Interferon- γ and Tissue Inflammation by Overexpression of Eosinophil Cationic Protein in T Cells and Exosomes

Huai-Chia Chuang, Ming-Han Chen, Yi-Ming Chen, Yi-Ru Ciou, Chia-Hsin Hsueh, Ching-Yi Tsai, and Tse-Hua Tan 92

Brief Report: Anti-Double-Stranded DNA Antibodies Recognize DNA Presented on HLA Class II Molecules of Systemic Lupus Erythematosus Risk Alleles

Hideaki Tsuji, Koichiro Ohmura, Hui Jin, Ryota Naito, Noriko Arase, Masako Kohyama, Tadahiro Suenaga, Shuhei Sakakibara, Yuta Kochi, Yukinori Okada, Kazuhiko Yamamoto, Hitoshi Kikutani, Akio Morinobu, Tsuneyo Mimori, and Hisashi Arase 105

Phase III/IV, Randomized, Fifty-Two-Week Study of the Efficacy and Safety of Belimumab in Patients of Black African Ancestry With Systemic Lupus Erythematosus

Ellen Ginzler, Luiz Sergio Guedes Barbosa, David D'Cruz, Richard Furie, Kathleen Maksimowicz-McKinnon, James Oates, Mittermayer Barreto Santiago, Amit Saxena, Saira Sheikh, Damon L. Bass, Susan W. Burriss, Jennifer A. Gilbride, James G. Groark, Michelle Miller, Amy Pierce, David A. Roth, and Beulah Ji 112

Vasculitis

Phase IIa Global Study Evaluating Rituximab for the Treatment of Pediatric Patients With Granulomatosis With Polyangiitis or Microscopic Polyangiitis

Paul Brogan, Rae S. M. Yeung, Gavin Cleary, Satyapal Rangaraj, Ozgur Kasapcopur, Aimee O. Hersh, Suzanne Li, Dusan Paripovic, Kenneth Schikler, Andrew Zeff, Claudia Bracaglia, Despina Eleftheriou, Pooneh Pordeli, Simone Melega, Candice Jamois, Jacques Gaudreault, Margaret Michalska, Paul Brunetta, Jennifer C. Cooper, Patricia B. Lehane, and the PePRS Study Group 124

A Worldwide Pharmacoepidemiologic Update on Drug-Induced Antineutrophil Cytoplasmic Antibody-Associated Vasculitis in the Era of Targeted Therapies

Samuel Deshayes, Charles Dolladille, Anaël Dumont, Nicolas Martin Silva, Basile Chretien, Hubert De Boysson, Joachim Alexandre, and Achille Aouba 134

Myositis

Time-Dependent Analysis of Risk of New-Onset Heart Failure Among Patients With Polymyositis and Dermatomyositis

Chun-Yu Lin, Hung-An Chen, Tsai-Ching Hsu, Chun-Hsin Wu, Yu-Jih Su, and Chung-Yuan Hsu 140

Pediatric Rheumatology

Effect of Clonally Expanded PD-1^{high}CXCR5-CD4⁺ Peripheral T Helper Cells on B Cell Differentiation in the Joints of Patients With Antinuclear Antibody-Positive Juvenile Idiopathic Arthritis

Jonas Fischer, Johannes Dirks, Julia Klausner, Gabriele Haase, Annette Holl-Wieden, Christine Hofmann, Stephan Hackenberg, Hermann Girschick, and Henner Morbach 150

Autoimmune Disease

Variants on the *UBE2L3/YDJC* Autoimmune Disease Risk Haplotype Increase *UBE2L3* Expression by Modulating CCCTC-Binding Factor and YY1 Binding

Jaanam Gopalakrishnan, Kandice L. Tessner, Yao Fu, Satish Pasula, Richard C. Pelikan, Jennifer A. Kelly, Graham B. Wiley, and Patrick M. Gaffney 163

Letters

Hypogammaglobulinemia in Rheumatoid Arthritis Patients Treated With Rituximab: Should We Switch Biologics?

Comment on the Article by Fraenkel et al

Gerasimos Evangelatos, Melina Moschopoulou, Alexios Iliopoulos, and George E. Fragoulis 174

Reply

Liana Fraenkel, Joan M. Bathon, Bryant R. England, E. William St.Clair, and Elie A. Akl, on behalf of the ACR RA Guideline Author Group 175

Importance of Internal and External Validity in Clinical Research: Comment on the Article by Fatima et al

Yusuke Matsuo, Yoshie Yamada, Jun Miyata, Tetsuro Aita, and Takashi Yoshioka 175

Considerations for a Study Using the Health Assessment Questionnaire to Predict All-Cause Mortality in

Early Rheumatoid Arthritis: Comment on the Article by Fatima et al

Po-Yun Ko, Da-Ming Yeh, and James Cheng-Chung Wei 176

Functional Capacity at 1 Year Predicts All-Cause Mortality in Patients With Rheumatoid Arthritis: Comment on the Article by Fatima et al

Richard K. Jacoby and Johannes J. Rasker 177

Reply

Safoora Fatima, O. Schieir, E. C. Keystone, M. F. Valois, S. J. Bartlett, L. Bessette, G. Boire, G. Hazlewood, C. Hitchon, D. Tin, C. Thorne, V. P. Bykerk, and J. E. Pope, on behalf of the CATCH Investigators 178

Cover image: The figure on the cover (from Coveney et al, pages 49–59) is a confocal microscopy image depicting RNA scope signal in chondrocytes within articular cartilage. The image shows increased expression of *Gli1* mRNA (red), indicative of elevated Hedgehog signaling upon cartilage-specific deletion of the primary cilia gene *Ift88* in young adult mice. Blue signal (DAPI) shows cell nuclei.

In this Issue

Highlights from this issue of *A&R* | By Lara C. Pullen, PhD

Belimumab in Patients of Black African Ancestry

Renal involvement is more common and severe in systemic lupus erythematosus (SLE) patients of Black African ancestry. In this issue, Ginzler et al (p. 112) conclude that belimumab remains a suitable treatment option for SLE management in patients of Black African ancestry even though it did not achieve the primary end point in a randomized study. They report the results from the first randomized, placebo-controlled clinical trial in SLE focusing on patients of self-identified Black race. The study was initiated as one of the postapproval commitments for belimumab.

Treatment with belimumab 10 mg/kg intravenous was well tolerated, and the study identified no new safety signals. The most noteworthy finding in the trial was the large difference in SLE Responder Index (SRI)–SLE Disease Activity Index 2000 (SLEDAI-2K) response in the open-label extension phase. The SRI–SLEDAI-2K response during the open-label extension was much greater than the primary analysis at 52 weeks. While the team introduced the SRI–SLEDAI-2K intending to increase sensitivity to treatment response relative to the SRI–SELENA–SLEDAI used in previous clinical trials, they did not achieve the predicted increase in sensitivity.

The study included patients who were generally less immunologically active than the overall population included in the pivotal phase III studies, and the immunoglobulin and SLE biomarker responses from the study were consistent with those in the pivotal belimumab studies. When the investigators performed a regional analysis of the primary end point, they found that patients in the rest-of-world subgroup had a higher response to belimumab compared with placebo than did the US/Canada subgroup. The authors propose that regional baseline differences in complement levels may have contributed to this difference.

Insights into the Role of Sputum NET Subsets in RA

Although rheumatologists still do not know the exact etiology of rheumatoid arthritis (RA), multiple studies indicate that patients who ultimately develop RA first experience autoimmunity and inflammation in the lung. This observation has led some researchers to postulate an important role for neutrophil extracellular trap (NET) formation in the lungs in the development of RA. In this issue, Okamoto et al (p. 38) report results consistent with the hypothesis that inflammation leads to increased citrullinated histone H3 (Cit-H3) protein–expressing NETs, which then promote local mucosal anti-citrullinated protein antibody (ACPA) generation. This is the first study to show that not only are RA patients more prone to spontaneous NET formation in the lung, but those at risk for RA also have sputum NET remnants that are associated with IgA anti-cyclic citrullinated peptide (anti-CCP).

The investigators began by using immunofluorescence imaging to document that spontaneous Cit-H3–expressing NET formation

was higher in sputum neutrophils from at-risk subjects and RA patients compared to controls. Of note, total sputum NET formation and Cit-H3+ NETosis were not significantly increased when based on age, sex, or history of chronic lung disease. When the researchers specifically assessed at-risk subjects, they found that sputum IgA ACPA correlated with the percentage of neutrophils that underwent Cit-H3+ NET formation as well as the levels of Cit-H3+ NET remnants. They also found that sputum macrophages in subjects at risk for RA and RA patients had diminished endocytic function relative to controls.

Using a mediation model, researchers determined that sputum inflammatory proteins were associated with sputum IgA ACPA via a pathway mediated by Cit-H3+

NET remnants. Moreover, sputum from at-risk individuals induced Cit-H3+ NET formation in correlation with sputum levels of interleukin-1 β (IL-1 β), IL-6, and tumor necrosis factor. While the authors believe that these observations suggest a causal relation, they acknowledge that it is also possible that ACPA, which can trigger NET formation, may result in driving forward the process of increased NETosis.

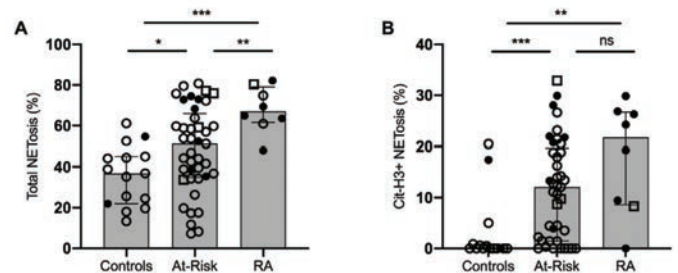


Figure 1. Sputum NET formation (known as NETosis) and association with sputum IgA anti-CCP. **A** and **B**, Percentage of sputum neutrophils that underwent total NETosis (DNA+MPO+) (**A**) and Cit-H3+ NETosis (DNA+MPO+Cit-H3+) (**B**) in ex vivo unstimulated culture in healthy controls (n = 15), subjects at risk for RA (n = 41), and RA patients (n = 8).

Upadacitinib Safe and Effective for Active AS

The primary goal of therapy in ankylosing spondylitis (AS) is to maximize a patient's quality of life by controlling the signs and symptoms of disease and preserving physical function and social participation. **p. 70** **Deodhar et al** (p. 70) report that treatment of patients with active AS with upadacitinib 15 mg once daily resulted in sustained and consistent efficacy over 1 year. Moreover, patients who switched from placebo to upadacitinib at week 14 showed similar efficacy to those who received continuous upadacitinib. The SELECT-AXIS 1 study is the first to report 1-year data on a JAK inhibitor in AS.

Of 187 patients enrolled, 178 completed week 14 on the study drug and entered the open-label extension. The study included only

1 dose of upadacitinib (15 mg once daily) and did not include an active comparator. At week 64, patients in both the continuous upadacitinib and the placebo-to-upadacitinib groups achieved similar rates of improvement as measured by the Assessment of Spondylo-Arthritis International Society criteria for 40% improvement (ASAS40) or Ankylosing Spondylitis Disease Activity Score (ASDAS). More than 70% of patients achieved these end points based on nonresponder imputation (NRI), and $\geq 81\%$ achieved the end points based on as-observed analyses. In addition, $\geq 34\%$ (NRI) and $\geq 39\%$ (as-observed analysis) achieved ASDAS showing inactive disease or ASAS showing partial remission at week 64. When the researchers looked at mean changes in pain, function, and inflammation from baseline (week 0) to week

64, they found consistent improvement or sustained maintenance through the study.

The investigators also documented that upadacitinib was well tolerated over 237.6 patient-years of exposure with no new or unexpected safety signals beyond those already seen in clinical development programs in rheumatoid arthritis and psoriatic arthritis. There were no reports of serious infections, major adverse cardiovascular events, venous thromboembolic events, gastrointestinal perforation, or deaths. None of the patients developed new-onset uveitis, and events were observed only in patients with a history of uveitis. The authors conclude by suggesting that upadacitinib may help address an unmet need for patients with AS who have active disease and an inadequate response to nonsteroidal anti-inflammatory drugs.

Journal Club

A monthly feature designed to facilitate discussion on research methods in rheumatology.

A Worldwide Pharmacoepidemiologic Update on Drug-Induced AAV in the Era of Targeted Therapies

Deshayes et al, *Arthritis Rheumatol* 2022;74:134–139

Little is known about the epidemiology and the spectrum of the drugs involved or suspected in drug-associated antineutrophil cytoplasmic antibody-associated vasculitis (AAV). Since drug-induced AAV seems to exhibit a better prognosis than primary AAV due to possible self-healing after withdrawal of the culprit drug, updating data on new targeted therapies is useful. The data in the literature supporting the role of a drug in the onset of AAV mainly rely on case reports or short series, implicating established treatments. Because of the rarity of AAV, and a possible long delay between the introduction of the drug and the clinical event, this adverse reaction is rarely evoked and is difficult to prove. The authors collected data on adverse drug reactions from the World Health Organization pharmacovigilance database. For each retrieved drug, a case–noncase analysis was performed, and disproportionate reporting was calculated using the information component (IC). The IC is a validated Bayesian indicator that compares the number of cases observed for a specific drug–adverse drug reaction pair with the number of cases expected for that pair given the hypothesis of an independent distribution of the reporting of the adverse drug reaction and the drug in the database.

Among the more than 20 million suspected adverse drug events reported in the database, a total of 483 case reports of

drug-associated AAV were retrieved. These involved 15 drugs that showed significant disproportionate reporting. This data mining approach allows for the automated detection of drug safety signals associated with rare events such as AAV and for the description of the largest series of cases and drugs involved in drug-induced AAV. The significant associations found do not imply causality, but they should be considered hypothesis-generating.

To conclude, this expansive pharmacoepidemiologic method is a first step to retrieve and prioritize all drugs suspected in rare diseases such as drug-induced AAV, after which experimental and observational studies are required as a second step to confirm these findings.

Questions

1. What was previously known in drug-associated AAV?
2. Why did the authors choose a pharmacovigilance-based data mining approach?
3. What are the main limitations and the strengths of this method?
4. How does this method of drug safety epidemiology compare with other methods?

In this Issue

Highlights from this issue of *A&R* | By Lara C. Pullen, PhD

Belimumab in Patients of Black African Ancestry

Renal involvement is more common and severe in systemic lupus erythematosus (SLE) patients of Black African ancestry. In this issue, Ginzler et al (p. 112) conclude that belimumab remains a suitable treatment option for SLE management in patients of Black African ancestry even though it did not achieve the primary end point in a randomized study. They report the results from the first randomized, placebo-controlled clinical trial in SLE focusing on patients of self-identified Black race. The study was initiated as one of the postapproval commitments for belimumab.

p. 112

Treatment with belimumab 10 mg/kg intravenous was well tolerated, and the study identified no new safety signals. The most noteworthy finding in the trial was the large difference in SLE Responder Index (SRI)–SLE Disease Activity Index 2000 (SLEDAI-2K) response in the open-label extension phase. The SRI–SLEDAI-2K response during the open-label extension was much greater than the primary analysis at 52 weeks. While the team introduced the SRI–SLEDAI-2K intending to increase sensitivity to treatment response relative to the SRI–SELENA–SLEDAI used in previous clinical trials, they did not achieve the predicted increase in sensitivity.

The study included patients who were generally less immunologically active than the overall population included in the pivotal phase III studies, and the immunoglobulin and SLE biomarker responses from the study were consistent with those in the pivotal belimumab studies. When the investigators performed a regional analysis of the primary end point, they found that patients in the rest-of-world subgroup had a higher response to belimumab compared with placebo than did the US/Canada subgroup. The authors propose that regional baseline differences in complement levels may have contributed to this difference.

Insights into the Role of Sputum NET Subsets in RA

Although rheumatologists still do not know the exact etiology of rheumatoid arthritis (RA), multiple studies indicate that patients who ultimately develop RA first experience autoimmunity and inflammation in the lung. This observation has led some researchers to postulate an important role for neutrophil extracellular trap (NET) formation in the lungs in the development of RA. In this issue, Okamoto et al (p. 38) report results consistent with the hypothesis that inflammation leads to increased citrullinated histone H3 (Cit-H3) protein–expressing NETs, which then promote local mucosal anti-citrullinated protein antibody (ACPA) generation. This is the first study to show that not only are RA patients more prone to spontaneous NET formation in the lung, but those at risk for RA also have sputum NET remnants that are associated with IgA anti-cyclic citrullinated peptide (anti-CCP).

The investigators began by using immunofluorescence imaging to document that spontaneous Cit-H3–expressing NET formation

was higher in sputum neutrophils from at-risk subjects and RA patients compared to controls. Of note, total sputum NET formation and Cit-H3+ NETosis were not significantly increased when based on age, sex, or history of chronic lung disease. When the researchers specifically assessed at-risk subjects, they found that sputum IgA ACPA correlated with the percentage of neutrophils that underwent Cit-H3+ NET formation as well as the levels of Cit-H3+ NET remnants. They also found that sputum macrophages in subjects at risk for RA and RA patients had diminished endocytic function relative to controls.

Using a mediation model, researchers determined that sputum inflammatory proteins were associated with sputum IgA ACPA via a pathway mediated by Cit-H3+

NET remnants. Moreover, sputum from at-risk individuals induced Cit-H3+ NET formation in correlation with sputum levels of interleukin-1 β (IL-1 β), IL-6, and tumor necrosis factor. While the authors believe that these observations suggest a causal relation, they acknowledge that it is also possible that ACPA, which can trigger NET formation, may result in driving forward the process of increased NETosis.

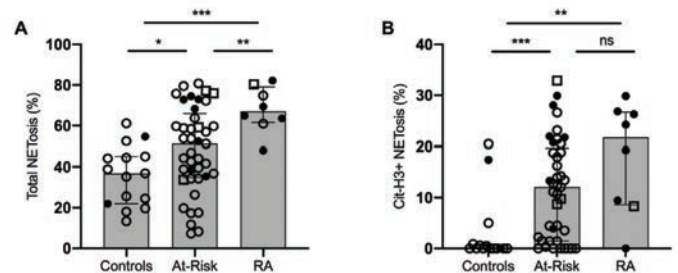


Figure 1. Sputum NET formation (known as NETosis) and association with sputum IgA anti-CCP. **A** and **B**, Percentage of sputum neutrophils that underwent total NETosis (DNA+MPO+) (**A**) and Cit-H3+ NETosis (DNA+MPO+Cit-H3+) (**B**) in ex vivo unstimulated culture in healthy controls (n = 15), subjects at risk for RA (n = 41), and RA patients (n = 8).

Upadacitinib Safe and Effective for Active AS

The primary goal of therapy in ankylosing spondylitis (AS) is to maximize a patient's quality of life by controlling the signs and symptoms of disease and preserving physical function and social participation. **p. 70** **Deodhar et al** (p. 70) report that treatment of patients with active AS with upadacitinib 15 mg once daily resulted in sustained and consistent efficacy over 1 year. Moreover, patients who switched from placebo to upadacitinib at week 14 showed similar efficacy to those who received continuous upadacitinib. The SELECT-AXIS 1 study is the first to report 1-year data on a JAK inhibitor in AS.

Of 187 patients enrolled, 178 completed week 14 on the study drug and entered the open-label extension. The study included only

1 dose of upadacitinib (15 mg once daily) and did not include an active comparator. At week 64, patients in both the continuous upadacitinib and the placebo-to-upadacitinib groups achieved similar rates of improvement as measured by the Assessment of Spondylo-Arthritis International Society criteria for 40% improvement (ASAS40) or Ankylosing Spondylitis Disease Activity Score (ASDAS). More than 70% of patients achieved these end points based on nonresponder imputation (NRI), and $\geq 81\%$ achieved the end points based on as-observed analyses. In addition, $\geq 34\%$ (NRI) and $\geq 39\%$ (as-observed analysis) achieved ASDAS showing inactive disease or ASAS showing partial remission at week 64. When the researchers looked at mean changes in pain, function, and inflammation from baseline (week 0) to week

64, they found consistent improvement or sustained maintenance through the study.

The investigators also documented that upadacitinib was well tolerated over 237.6 patient-years of exposure with no new or unexpected safety signals beyond those already seen in clinical development programs in rheumatoid arthritis and psoriatic arthritis. There were no reports of serious infections, major adverse cardiovascular events, venous thromboembolic events, gastrointestinal perforation, or deaths. None of the patients developed new-onset uveitis, and events were observed only in patients with a history of uveitis. The authors conclude by suggesting that upadacitinib may help address an unmet need for patients with AS who have active disease and an inadequate response to nonsteroidal anti-inflammatory drugs.

Journal Club

A monthly feature designed to facilitate discussion on research methods in rheumatology.

A Worldwide Pharmacoepidemiologic Update on Drug-Induced AAV in the Era of Targeted Therapies

Deshayes et al, *Arthritis Rheumatol* 2022;74:134–139

Little is known about the epidemiology and the spectrum of the drugs involved or suspected in drug-associated antineutrophil cytoplasmic antibody-associated vasculitis (AAV). Since drug-induced AAV seems to exhibit a better prognosis than primary AAV due to possible self-healing after withdrawal of the culprit drug, updating data on new targeted therapies is useful. The data in the literature supporting the role of a drug in the onset of AAV mainly rely on case reports or short series, implicating established treatments. Because of the rarity of AAV, and a possible long delay between the introduction of the drug and the clinical event, this adverse reaction is rarely evoked and is difficult to prove. The authors collected data on adverse drug reactions from the World Health Organization pharmacovigilance database. For each retrieved drug, a case–noncase analysis was performed, and disproportionate reporting was calculated using the information component (IC). The IC is a validated Bayesian indicator that compares the number of cases observed for a specific drug–adverse drug reaction pair with the number of cases expected for that pair given the hypothesis of an independent distribution of the reporting of the adverse drug reaction and the drug in the database.

Among the more than 20 million suspected adverse drug events reported in the database, a total of 483 case reports of

drug-associated AAV were retrieved. These involved 15 drugs that showed significant disproportionate reporting. This data mining approach allows for the automated detection of drug safety signals associated with rare events such as AAV and for the description of the largest series of cases and drugs involved in drug-induced AAV. The significant associations found do not imply causality, but they should be considered hypothesis-generating.

To conclude, this expansive pharmacoepidemiologic method is a first step to retrieve and prioritize all drugs suspected in rare diseases such as drug-induced AAV, after which experimental and observational studies are required as a second step to confirm these findings.

Questions

1. What was previously known in drug-associated AAV?
2. Why did the authors choose a pharmacovigilance-based data mining approach?
3. What are the main limitations and the strengths of this method?
4. How does this method of drug safety epidemiology compare with other methods?

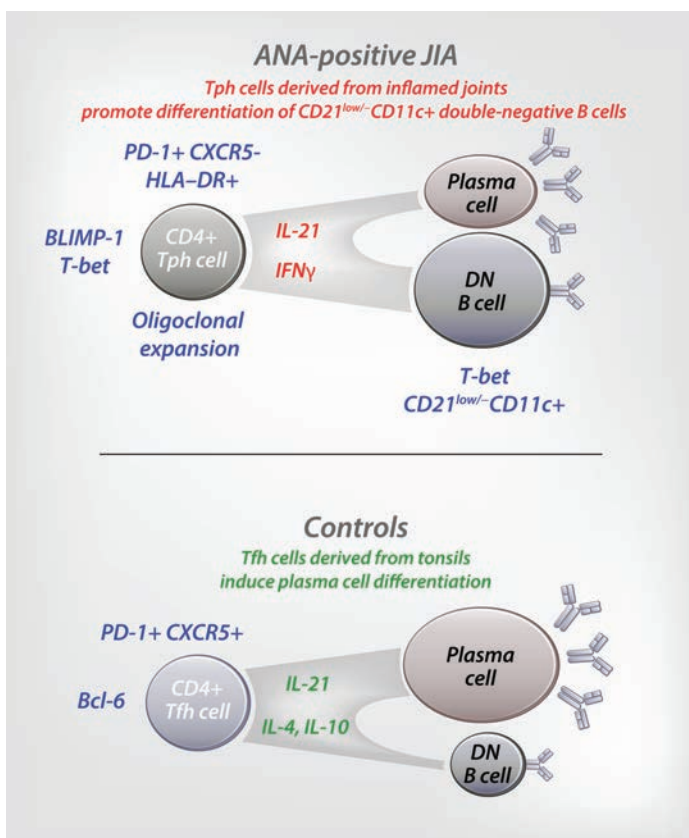
Clinical Connections

Effect of Clonally Expanded PD-1^{high}CXCR5–CD4+ Tph Cells on B cell Differentiation in the Joints of Patients With ANA-Positive JIA

Fischer et al, *Arthritis Rheumatol* 2022;74:150–162

CORRESPONDENCE

Henner Morbach, MD: morbach_h@ukw.de



KEY POINTS

- ANA-positive JIA is characterized by expansion of synovial PD-1^{high}CXCR5–HLA–DR+CD4+ T cells resembling Tph cells.
- These Tph cells displayed signs of oligoclonal expansion and coexpress IL-21 and IFN γ .
- Tph cells induced plasma cell differentiation as potent as classic tonsil Tfh cells, but also skewed B cells toward a T-bet-expressing CD21^{low/-}CD11c⁺ phenotype.

SUMMARY

Antinuclear antibody (ANA)–positive juvenile idiopathic arthritis (JIA) seems to constitute a clinically homogenous group of patients that is also characterized by synovial B cell hyperactivity. T follicular helper (Tfh) cells have been implicated in the pathogenesis of many autoimmune diseases; however, we do not fully understand the role of CD4+ T cells in promoting local B cell dysregulation in JIA. Fischer et al therefore investigated the phenotype and function of synovial CD4+ T cells that promote aberrant B cell activation in the joints of ANA-positive JIA patients. Within the joints of these patients, they demonstrated an expansion of programmed death 1 (PD-1)^{high}CXCR5–HLA–DR+CD4+ T cells, which exhibited signs of clonal expansion. These T cells phenotypically resembled peripheral T helper (Tph) cells with an extrafollicular chemokine receptor pattern and coexpression of interleukin-21 (IL-21) and interferon- γ (IFN γ). In contrast to tonsillar Tfh cells derived from controls that expressed IL-21 with IL-4 and IL-10, and particularly induced plasma cell differentiation in vitro, synovial fluid Tph cells from JIA patients additionally skewed B cell differentiation toward a CD21^{low/-}CD11c⁺ phenotype partially by provision of IL-21 and IFN γ . Additionally, in the synovial fluid of JIA patients, Tph cell frequencies correlated with the appearance of CD21^{low/-}CD11c⁺CD27–IgM– double-negative (DN) B cells. Hence, the characteristic expansion of Tph cells and CD21^{low/-}CD11c⁺ DN B cells in the joints of ANA-positive JIA patients might reflect the autoimmune response present at the site of inflammation.

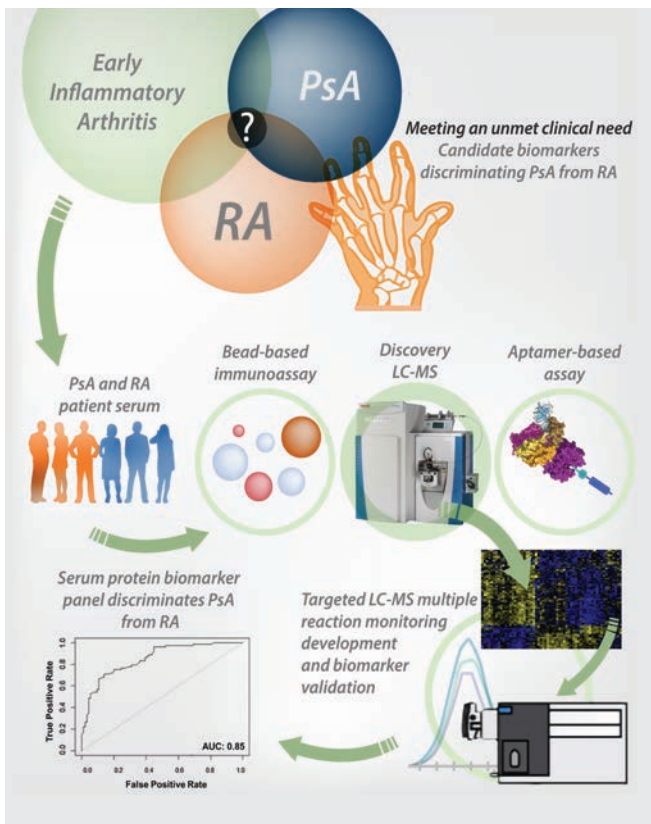
Identification and Evaluation of Serum Protein Biomarkers That Differentiate Psoriatic Arthritis From Rheumatoid Arthritis

Mc Ardle et al, *Arthritis Rheumatol* 2022;74:81–91

CORRESPONDENCE

Stephen Pennington, PhD: stephen.pennington@ucd.ie

Oliver FitzGerald, MD, FRCPI, FRCP(UK): oliver.fitzgerald@ucd.ie



SUMMARY

Early diagnosis and management of psoriatic arthritis (PsA) leads to better long-term outcomes; however, due to its complex presentation, the diagnosis of PsA may be delayed or inaccurate. It can be difficult to separate early PsA from other forms of arthritis, such as rheumatoid arthritis (RA), as the clinical features may be similar and there are no diagnostic features or laboratory tests that will identify an individual as having PsA. Early and accurate diagnosis can have important consequences, as different arthropathies may require different treatment. It is clear that the development of a diagnostic blood test would allow for earlier and more accurate diagnosis and improved clinical decision making in PsA.

Mc Ardle et al demonstrated that by analyzing blood samples from patients with recent-onset symptoms of PsA or RA, using a combination of proteomic technologies, it was possible to identify a blood-based protein signature that can distinguish PsA from RA. During follow-up studies, a targeted liquid chromatography mass spectrometry (LC-MS)–based approach was used to refine the protein signature, and a highly multiplexed and robust assay was developed. This assay was then used to evaluate the signature using blood samples from a second independent cohort of individuals with PsA and RA. This resulted in the refinement of the signature and confirmation of its ability to differentiate those with PsA from those with RA, even in early disease. While large-scale and multicenter validation is now required, the identification of a highly specific protein signature that can discriminate PsA from RA will enhance current clinical practice in PsA by enabling accurate early diagnosis and consequent selection of the most appropriate treatment.

KEY POINTS

- Delayed, missed, or inaccurate diagnosis has significant consequences for individuals with PsA.
- A signature of blood-based protein biomarkers that can differentiate those with PsA from those with RA has been developed.
- LC-MS–based proteomics is an indispensable tool for the identification and verification of putative protein biomarkers.

NOTES FROM THE FIELD

Global Rheumatology Research: Frontiers, Challenges, and Opportunities

Joshua B. Bilsborrow,¹ Ingris Peláez-Ballestas,² Bernardo Pons-Estel,³ Christiaan Scott,⁴ Xinping Tian,⁵ Graciela S. Alarcon,⁶ Richard Bucala,⁷ Laura B. Lewandowski,⁸ and Evelyn Hsieh¹

Introduction

Rheumatologic and musculoskeletal diseases (RMDs) are important causes of morbidity and mortality worldwide (1). The World Health Organization (WHO) considers musculoskeletal conditions to be the leading causes of disability worldwide, and the greatest independent contributors to chronic pain (2). Population-based surveys from low- and middle-income countries (LMICs) have demonstrated similar rates of RMDs compared with high-income countries (3). However, in many low-resource settings rheumatology remains underdeveloped with regard to health care access, clinical practice, education, training, and research (4).

A review of the adult and pediatric rheumatology literature published between May 2019 and May 2020 and indexed in PubMed and Web of Science Core Collection (for details, see Supplementary Information on Literature Search Procedure and Parameters, on the *Arthritis & Rheumatology* website at <http://onlinelibrary.wiley.com/doi/10.1002/art.41980/abstract>) demonstrated that, among the top 20 nations according to author location, the only LMICs represented were Brazil and India; the overwhelming majority of authors were from high-income countries (Figure 1A). This discrepancy highlights the substantial knowledge gap regarding the global burden of RMDs, and the need to expand research capacity in LMICs to better understand how differing geographies, ethnic and genetic backgrounds, environmental variations, endemic infections, and health system disparities influence the epidemiology and outcomes of RMDs around the world.

Dr. Lewandowski's work was supported by the National Institute of Arthritis and Musculoskeletal and Skin Diseases Intramural Research Program. Dr. Hsieh's work was supported by the NIH/Fogarty International Center (grant K01-TW009995) and a Rheumatology Research Foundation K Supplement Award.

¹Joshua B. Bilsborrow, MD, MHS, Evelyn Hsieh, MD, PhD: Yale University School of Medicine, New Haven, Connecticut, and Veterans Affairs Connecticut Healthcare System, West Haven VAMC, West Haven, Connecticut; ²Ingris Peláez-Ballestas, MD, PhD: Hospital General de México Dr. Eduardo Liceaga, Mexico City, Mexico; ³Bernardo Pons-Estel, MD: Centro Regional de Enfermedades Autoinmunes y Reumáticas, Rosario, Argentina; ⁴Christiaan Scott, MBChB: Red Cross War Memorial Children's Hospital and University of Cape Town, Cape Town, South Africa; ⁵Xinping Tian, MD, PhD: Peking Union Medical College Hospital, Beijing, China; ⁶Graciela S. Alarcon, MD: University

A call to action

We convened an innovative session at the 2019 American College of Rheumatology (ACR) Annual Meeting, titled *Frontiers and Opportunities in Global Rheumatology Research*, which brought together researchers from different parts of the globe to address the critical need to improve rheumatology research capacity and training opportunities. This session—cosponsored by the ACR Committee on Research, the National Institute of Arthritis and Musculoskeletal and Skin Diseases (NIAMS), and the Fogarty International Center (FIC)—addressed the unique challenges and rewards of building global collaborative platforms and explored opportunities for research training and funding. The session opened with remarks from NIAMS and FIC leaders, followed by presentations from researchers representing 3 different geographic regions who have developed ongoing and successful international collaborations. Approximately 100 participants attended the session, including health care providers, research scientists, trainees, and administrators representing the Americas, Africa, Europe, Asia, and Oceania.

The presentations provided an informed and thoughtful starting point for the subsequent open forum discussion, which encouraged viewpoints and perspectives from the audience members coming from around the world. During this open forum, audience members asked questions and shared their own experiences in global rheumatology research. Two scribes recorded the themes. Attendees also completed a brief survey to evaluate the session and to share additional perspectives.

of Alabama at Birmingham, and Universidad Peruana Cayetano Heredia, Lima, Perú; ⁷Richard Bucala, MD, PhD: Yale University School of Medicine, New Haven, Connecticut; ⁸Laura B. Lewandowski, MD, MS: National Institute of Arthritis and Musculoskeletal and Skin Diseases, NIH, Bethesda, Maryland.

Author disclosures are available at <https://onlinelibrary.wiley.com/action/downloadSupplement?doi=10.1002%2Fart.41980&file=art41980-sup-0001-Disclosureform.pdf>.

Address correspondence to Evelyn Hsieh, MD, PhD, Section of Rheumatology, Allergy and Immunology, Yale University School of Medicine, 300 Cedar Street, TAC S-525, PO Box 208031, New Haven, CT 06520-8031. Email: evelyn.hsieh@yale.edu.

Submitted for publication March 16, 2021; accepted in revised form September 14, 2021.

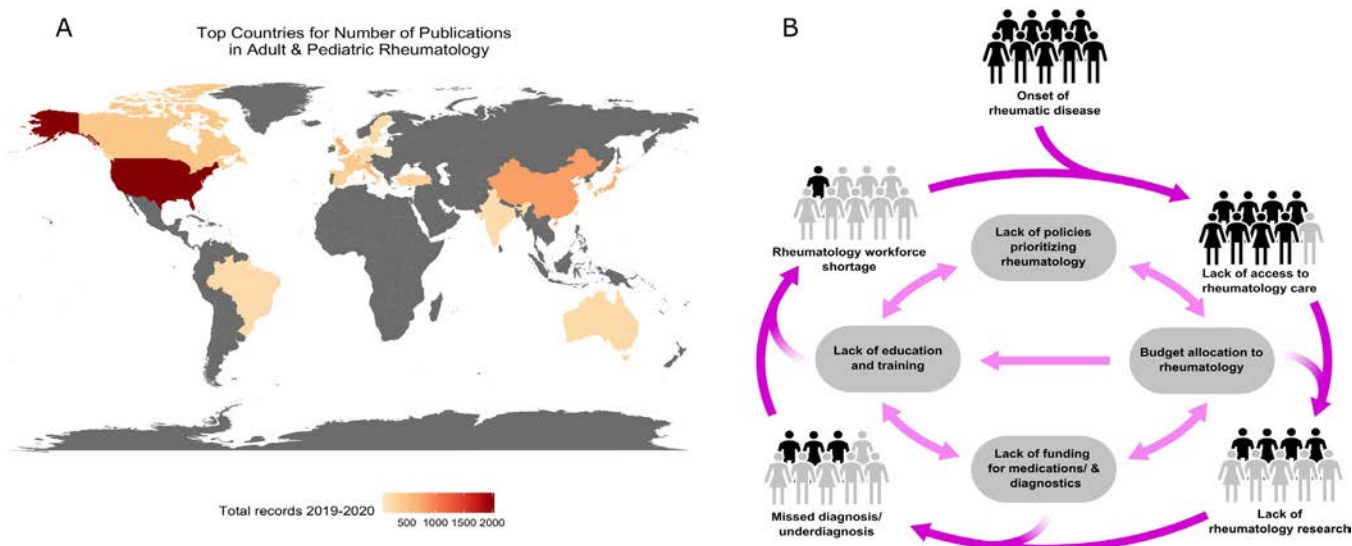


Figure 1. The scope and vicious circle of the global rheumatology research gap. **A**, Map demonstrates the top 20 countries represented by authors of publications in adult and pediatric rheumatology from May 2019 to May 2020. **B**, Without a rheumatology-trained workforce, a vicious circle develops, leading to decreased access to care and decreased research regarding the mechanisms, epidemiology, treatments, and outcomes of rheumatic and musculoskeletal diseases. These factors contribute to missed diagnoses, undertreatment of rheumatic diseases, and poor outcomes. Underreporting of rheumatic diseases drives underrecognition and underfunding at the national and institutional levels for rheumatology care, research, education, and health policy and funding. The human images represent the number of patients with rheumatic disease; black indicates patients diagnosed and gray indicates those missed or underdiagnosed. With each vicious circle, more patients are missed, and the problem is compounded.

Themes

Several key themes emerged from the session and should be prioritized for further exploration by all stakeholders working to advance global rheumatology research platforms, including investigators (mentors and trainees), institutions, policy makers, and funders.

Research funding. Funding for research can be a significant obstacle for academic rheumatologists, especially at the early career stage. Funding is even more challenging for rheumatologists pursuing global health research careers. Whereas certain fields (e.g., infectious disease and oncology) have a comparatively robust landscape of global funding mechanisms, many RMD funding agencies restrict their awards to domestic investigators and institutions or stipulate that funds must be spent in the “home country,” which limits the possibilities for international work.

In the US, the National Institutes of Health (NIH) has historically been an important resource for global health research funding. NIH funding agencies have increased their global research support by 140% between 2011 and 2018 (5). During their opening remarks, the NIAMS and FIC speakers encouraged researchers to consider developing proposals for global projects with translatable applications to the health and welfare of US patients. Similarly, government funding agencies from other

countries face obligations within their programs and initiatives to balance global priorities with advancing the health and welfare of their domestic populations.

Other potential sponsors include nongovernmental organizations and private pharmaceutical enterprises. The Rheumatology Research Foundation, Wellcome Trust, and International League of Associations for Rheumatology were highlighted as just some of the funders that have supported international collaborations to further rheumatology research and education. Moving forward, diversification and growth of potential funding sources for global RMD research is imperative.

Finally, it was acknowledged that noncommunicable disease (NCD)–specific funding agencies may have an interest in expanding globally but may hesitate due to lack of familiarity with the research landscape in LMICs, and limited experience working with foreign institutions from an administrative and regulatory standpoint. One approach to bridge these gaps is to partner with existing global health programs. For example, the FIC Global Health Program for Fellows and Scholars provides 12-month mentored, hands-on global health research experiences to trainees from the US and LMICs through an extensive network of well-established LMIC sites (6). While initially heavily focused on communicable diseases, over the years the program’s portfolio has expanded to include a broad spectrum of NCD-related topics. This expansion was made possible through

cosponsorship by institutes and centers with expertise in NCDs, including the National Heart Lung Blood Institute, the National Cancer Institute, and more recently, NIAMS.

Mentorship and research training opportunities.

Early-career investigators also face significant challenges in finding mentorship in the field of global rheumatology. Many LMICs have a limited number of rheumatology providers (or none), and those individuals may not have sufficient time beyond clinical care to engage in research, much less provide mentorship and training (7). In many cases those individuals may not have received formal research training due to the paucity of local opportunities. Their institutions also may not offer incentives for conducting research or may lack the collaborative networks with universities or public health departments needed to make research practical. This vicious circle severely jeopardizes the pipeline for future rheumatology researchers in regions where data on RMDs are most lacking (Figure 1B). Early-career investigators may encounter difficulties identifying global rheumatology mentors within their institutions. As such, individuals who are interested in global rheumatology research may need to consider mentorship relationships with established international collaborators in other specialties. Fortunately, there are growing networks of international rheumatologists and musculoskeletal disease experts such as the Global Alliance for Musculoskeletal Health (GAMH) (<https://gmusc.com>) and the COVID-19 Global Rheumatology Alliance (GRA) (<https://rheum-covid.org>) to which new investigators can reach out.

Infrastructure. In many LMICs health care budgets can be extremely limited, and NCDs have not historically been prioritized. As such, the capacity to build and maintain infrastructure for basic rheumatology care is often lacking (8). The scarcity of rheumatology-related resources and infrastructure creates pragmatic barriers to research. Rheumatic diseases are complex, and many diagnoses require access to laboratory and imaging studies for confirmation. Clinical, translational, and basic science research have a range of physical infrastructure and technical capacity needs, including consistent and accurate medical record-keeping systems; clinical or laboratory research space, equipment, and technology; ability to collect, store, and analyze biologic specimens; animal laboratory facilities; trained and dedicated institutional review boards; research staff with technical support skills; and investigators trained in research methods, statistics, and manuscript and grant writing. A lack of research infrastructure may be compounded by language barriers and lower institutional incentives to publish (9). While acknowledging the dedication and resourcefulness of teams that have successfully overcome these challenges to generate high-quality research platforms in low-resource settings, during the open forum discussion participants simultaneously voiced the very tangible ways in which limitations in one or more of these areas can significantly

challenge feasibility, efficiency, and scalability of research efforts and infrastructure.

Creating sustainable platforms for rheumatology research requires longitudinal vision, commitment, interdisciplinary partnerships, and flexibility. For example, in many LMICs the comparatively sophisticated infrastructure for HIV care and research—built through more than 20 years of investment by the global community—is increasingly being leveraged to develop NCD models of care and research, and could be applied to rheumatology as well (10). Given the key role of musculoskeletal health as a driver of many NCD outcomes, partnering directly with other major NCD fields, e.g., cardiology, oncology, pulmonology, or endocrinology, may be a viable strategy (11). Additionally, while investment in rheumatology within an individual country may be modest, regional partnerships that address mutual priorities may offer accessible and synergistic opportunities for research infrastructure development (12). Finally, in order to address wide internal disparities (e.g., urban versus rural) in clinical and research infrastructure, some countries have leveraged the expertise of major academic centers to create national training programs (13).

Health policy and advocacy. Use of scientific evidence has a critical role as a tool to guide advocacy and policy change. The absence of systematically collected epidemiologic data on local burden of RMDs leads to underquantification and underrecognition of these conditions and makes it impossible to measure their impact on important downstream outcomes, such as costs to the health system and individuals, disability, unemployment, and mortality. Without these data, patients, families, providers, and advocates have limited grounds upon which to appeal to national policy makers and international agencies for increased investment in RMD infrastructure and workforce development. Furthermore, if RMDs are not studied in diverse geographic settings and populations, the full spectrum of phenotypes cannot be defined, nor can the environmental, genetic, and sociocultural factors that influence presentation and disease progression. The relationships between components of this vicious circle are illustrated in Figure 1B.

Finally, it is of paramount importance that RMDs are actively integrated into broader global discourse related to NCDs, aging, health systems, and health policy (14). For example, the WHO Model List of Essential Medicines comprises 460 medicines considered to be the most efficacious, safe, and cost-effective that meet minimum needs for a basic health care system to address priority conditions, and serves as the guide for national formularies in >150 countries. The 2019 update included, for the first time, a biologic disease-modifying antirheumatic drug (DMARD) (adalimumab and its biosimilars) in addition to the conventional synthetic DMARDs previously listed. The Pediatric Task Force for Musculoskeletal Health has similarly advocated for changes to address gaps in the pediatric rheumatic diseases section of this list (15).

Conclusions and future directions

The future of global rheumatology research is bright, but much collaborative work remains to be done with partners and stakeholders across all regions, to further develop and expand this nascent field. The global rheumatology community is poised to increase its research efforts and to collaborate on previously unexplored innovative topics. However, in order for this to be possible, key barriers such as the paucity of funding and mentorship, limited research infrastructure in LMICs, and health policies that do not prioritize rheumatology will first need to be addressed.

ACKNOWLEDGMENTS

We would like to thank all of those from the global rheumatology community who participated in the 2019 ACR Annual Meeting session *Frontiers and Opportunities in Global Rheumatology Research* and shared their thoughtful perspectives and experiences. Special appreciation to the ACR, the NIH, NIAMS, and the FIC for cosponsoring this session. We are grateful to Ngozi Afulezi for her support in organizing the session and Dr. Kathleen Vazzana for her contribution to recording the session. We thank Brigit Sullivan, MLS for the literature search, Ya-Ling Lu, MLS for the country annotation of publications, and Alicia Livinski, MLS for critical reading of the manuscript.

AUTHOR CONTRIBUTIONS

All authors were involved in drafting the article or revising it critically for important intellectual content, and all authors approved the final version to be published. Dr. Hsieh had full access to all of the data in the study and takes responsibility for the integrity of the data and the accuracy of the data analysis.

Study conception and design. Peláez-Ballestas, Pons-Estel, Scott, Tian, Alarcon, Bucala, Lewandowski, Hsieh.

Acquisition of data. Bilsborrow, Lewandowski, Hsieh.

Analysis and interpretation of data. Bilsborrow, Lewandowski, Hsieh.

REFERENCES

- Institute for Health Metrics and Evaluation. Global burden of disease 2019. URL: <https://vizhub.healthdata.org/gbd-compare>.
- World Health Organization. Musculoskeletal conditions. URL: <https://www.who.int/news-room/fact-sheets/detail/musculoskeletal-conditions>.
- Oyoo O, Moots RJ, Ganda B. Stepping into the state of rheumatology in East Africa [editorial]. *Rheumatology (Oxford)* 2012;51:1345–6.
- Tikly M, McGill P. Epidemiology: the challenge of practicing rheumatology in Africa. *Nat Rev Rheumatol* 2016;12:630–1.
- Kilmarx PH. Frontiers and opportunities in global rheumatology research: welcoming remarks. Presented at the American College of Rheumatology/Association of Rheumatology Health Professionals Annual Meeting; 2019 November 8–13; Atlanta, GA.
- Fogarty International Center, NIH. Global health program for fellows and scholars. URL: <https://www.fic.nih.gov/programs/pages/scholars-fellows-global-health.aspx>.
- Reveille JD, Muñoz R, Soriano E, Albanese M, Espada G, Lozada CJ, et al. Review of current workforce for rheumatology in the countries of the Americas 2012–2015. *J Clin Rheumatol* 2016;22:405–10.
- Muka T, Imo D, Jaspers L, Colpani V, Chaker L, van der Lee SJ. The global impact of non-communicable diseases on healthcare spending and national income: a systematic review. *Eur J Epidemiol* 2015;30:251–77.
- Ugarte-Gil MF, Alarcón GS. Medical scientific publications from Latin America: a commentary [editorial]. *J Clin Rheumatol* 2019;25:157–8.
- Njuguna B, Vorkoper S, Patel P, Reid MJ, Vedanthan R, Pfaff C, et al. Models of integration of HIV and noncommunicable disease care in sub-Saharan Africa: lessons learned and evidence gaps. *AIDS* 2018;32 Suppl 1:S33–42.
- Budreviciute A, Damiati S, Sabir DK, Onder K, Schuller-Goetzburg P, Plakys G, et al. Management and prevention strategies for non-communicable diseases (NCDs) and their risk factors [review]. *Front Public Health* 2020;8:574111.
- Peláez-Ballestas I, Granados Y, Quintana R, Loyola-Sánchez A, Julián-Santiago F, Rosillo C, et al, the Latin American Study Group of Rheumatic Diseases in Indigenous Peoples (GLADERPO). Epidemiology and socioeconomic impact of the rheumatic diseases on indigenous people: an invisible syndemic public health problem. *Ann Rheum Dis* 2018;77:1397–404.
- Li M, Tian X, Zhang W, Leng X, Zeng X. CRDC: a Chinese rheumatology research platform [review]. *Clin Rheumatol* 2015;34:1347–52.
- Briggs AM, Slater H, Jordan JE, Huckel Schneider C, Kopansky-Giles D, et al. Global Alliance for Musculoskeletal Health. Towards a global strategy to improve musculoskeletal health. URL: <https://gmusc.com/>.
- World Health Organization. 21st WHO model list of essential medicines. URL: <https://www.who.int/groups/expert-committee-on-selection-and-use-of-essential-medicines/essential-medicines-lists>.

EDITORIAL

Reexamining Remission Definitions in Rheumatoid Arthritis: Considering the Twenty-Eight-Joint Disease Activity Score, C-Reactive Protein Level, and Patient Global Assessment

David T. Felson,¹  Diane Lacaille,²  Michael P. LaValley,³ and Daniel Aletaha⁴

Editors' Note: *The Editors of the 5 journals of the American College of Rheumatology and European Alliance of Associations for Rheumatology have been reminded by this editorial that ACR and EULAR have jointly agreed on various classification criteria, definitions, recommendations, or points to consider, which do not always find reflection in manuscripts submitted to the journals. Consequently, in the future, the Editors will enforce the use of the products obtained in the course of joint ACR/EULAR or EULAR/ACR activities in all respective papers. For rheumatoid arthritis this would mean use of the ACR/EULAR or EULAR/ACR classification criteria, remission definitions, recommendations on what to report in clinical trials, and others, as pertinent. The same applies to other diseases. There are valid and important reasons that these activities have been undertaken by ACR and EULAR, and therefore, the conclusions of the various task forces, which have been endorsed by ACR and EULAR, should be respected by investigators and study administrators. This does not mean other methods could not be used in a study, but at the least, the reports should address the methods agreed upon by the 2 organizations. Maintaining uniformity across major publications regarding rheumatoid arthritis remission or other definitions not only allows for more appropriate comparison across analyses, but also enhances readers' ability to interpret results. Author instructions across the 5 journals will more strongly reflect this requirement.*

Over the last 30 years, treatment for rheumatoid arthritis (RA) has improved dramatically. By the early 2000s, disease remission had become a realistic goal, although definitions of remission varied widely, making it difficult to compare treatment strategies and gauge how often remission occurred. In 2009, the American College of Rheumatology (ACR) and the European Alliance of Associations for Rheumatology (EULAR) created a joint committee whose charge was to recommend a definition of remission. Members of the committee suggested a large number of candidate definitions and, using a data-driven consensus process, statisticians and programmers tested these candidates in a bank of RA trial data to see which definitions performed best in predicting long-term good function and lack of radiographic progression.

The committee endorsed a stringent definition using measures from the validated core set of outcome measures.

After reviewing analysis results, the committee selected 2 definitions of remission that were approved by the ACR and EULAR (1,2). The first was a Boolean version in which, to be classified as having attained remission, a patient had to have tender and swollen joint counts of ≤ 1 , a C-reactive protein (CRP) level of ≤ 1 mg/dl, and a patient global assessment of arthritis activity of ≤ 1 (on a 0–10 scale). The second recommended definition was a score of ≤ 3 on the Simplified Disease Activity Index (SDAI) (3), a scoring system that is based on the same core set outcome measures. While designed and validated in trials, these definitions could help assess treatment “success” in clinical practice as well as in trials

This article is published simultaneously in the January 2022 issues of *Annals of the Rheumatic Diseases*, *Arthritis Care & Research*, *RMD Open*, and *ACR Open Rheumatology*.

¹David T. Felson, MD, MPH: Boston University School of Medicine, Boston, Massachusetts, and University of Manchester and the NIHR Manchester Biomedical Research Center, Manchester University NHS Trust, Manchester, UK; ²Diane Lacaille, MD, MHS: University of British Columbia and Arthritis Research Canada, Vancouver, British Columbia, Canada; ³Michael P. LaValley, PhD: Boston University School of Public Health, Boston,

Massachusetts; ⁴Daniel Aletaha, MD, MS, MBA: Medical University of Vienna, Vienna, Austria.

Author disclosures are available at <https://onlinelibrary.wiley.com/action/downloadSupplement?doi=10.1002%2Fart.41959&file=art41959-sup-0001-Disclosureform.pdf>.

Address correspondence to David T. Felson, MD, MPH, Boston University School of Medicine, 650 Albany Street, Suite 200, Boston, MA 02118. Email: dfelson@bu.edu.

Submitted for publication June 19, 2021; accepted in revised form August 24, 2021.

and, in practice, could serve as a “treat-to-target” goal for some patients.

Like all developed criteria, the ACR/EULAR 2011 RA remission criteria were labeled as provisionally approved and awaited validation in an independent sample for final approval. A revised validated version of the remission criteria is pending full approval by ACR/EULAR. Many concerns have arisen since the publication of the provisional remission criteria. Among them is the continuing use in trials of 28-joint Disease Activity Score (DAS28) thresholds (4) to define remission, questions about the use of CRP as an element of remission definitions, and questions about the appropriateness of including patient global assessment in defining RA remission. This editorial will address each of these issues.

Using the DAS28: when “remission” is often not remission

The DAS28 is a widely used measure of disease activity. An ACR committee that critically evaluated RA disease activity measures for use in clinical settings found that the DAS28 met predefined criteria, including providing a score that stratified patients into at least 3 disease activity states, being measurable in the clinical setting, and having adequate psychometric properties. The DAS28 was one of 4 recommended RA disease activity measures (5).

The committee on RA remission considered several DAS28 thresholds as candidate definitions of remission, including the popular threshold of a DAS28 using the CRP level (DAS28-CRP) of <2.6 and an even lower threshold of <2.0 . The DAS28 formula weights swollen joint count half as much as tender joint count and also underweights it relative to CRP (or erythrocyte sedimentation rate [ESR]). Therefore, a patient can achieve a low DAS28 score but still have a substantial number of swollen joints. The committee's analyses showed that 10% of patients with a DAS28 of <2.6 had ≥ 4 swollen joints, and 1 patient had >20 swollen joints. When a lower DAS28 threshold of <2.0 was used, swollen joint counts of 2 or 3 were common and scores of up to 6 possible. In fact, if the tender joint count is 0, values for the other components of the DAS28 become irrelevant (Figure 1). Values of up to 60 (of 100) for patient global assessment are consistent with remission according to the DAS28. Even if the tender joint count is 1, the DAS28 score can be in the remission range when other core set measures show active disease. DAS28-CRP thresholds differ substantially from those obtained with the DAS28 using the ESR (DAS28-ESR) (6), and with the DAS28-ESR, RA would be even more likely to be classified as being in remission when disease is in fact active.

One other major criterion was that patients whose disease was in remission at 6 months or 12 months in a 2-year trial should be likely to have both good and stable functional and radiographic outcomes later in the same trial. Patients in whom DAS28

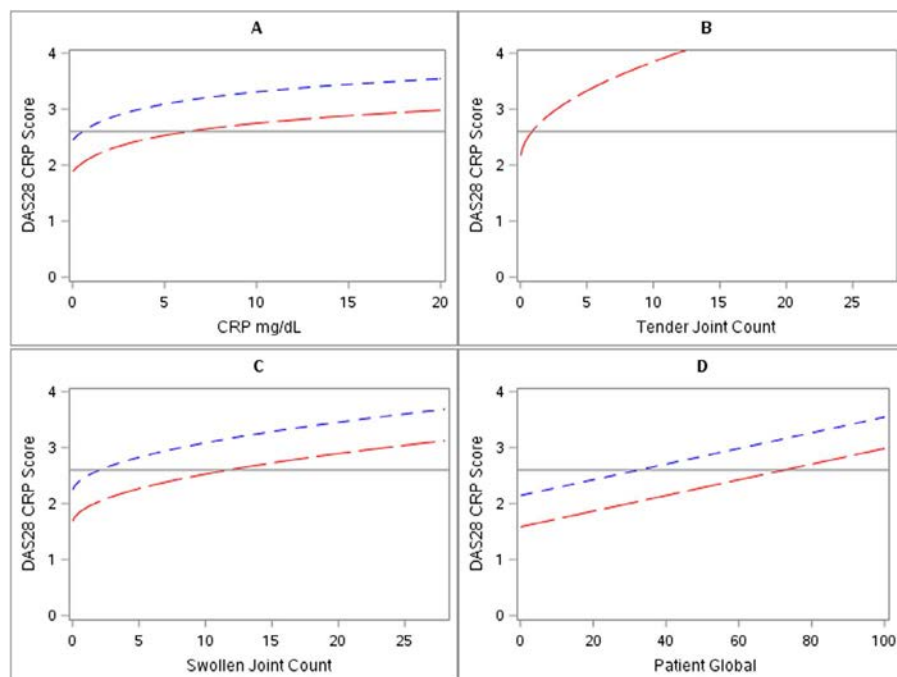


Figure 1. The contribution of each component of the 28-joint Disease Activity Score using the C-reactive protein level (DAS28-CRP) to remission (score <2.6 [solid horizontal line]) when other components are in the range of remission. The DAS28-CRP is composed of 4 components: CRP level (A), tender joint count (TJC) (B), swollen joint count (SJC) (C), and patient global assessment of arthritis activity (D). In each graph, it is assumed that the 3 components other than the one depicted met the threshold for remission (CRP 0.5, TJC 0 [red dashed lines] or 1 [blue dashed lines], SJC 0, patient global assessment 1). Note that when the TJC is 0, most values of CRP and patient global assessment yield a DAS28 of <2.6 (“remission”), and SJC values of <10 yield DAS28 “remission.”

remission was achieved had worse radiographic outcomes than those achieving remission according to other definitions (no change in the Sharp score [7] or the Sharp/van der Heijde score [8]). Ultimately, the committee rejected DAS28 candidates as definitions of remission because swollen joint counts were too high to be consistent with clinical remission and because DAS28 “remission,” even with the use of stricter thresholds, did not predict good combined functional and radiographic outcomes as well as the predictive ability that was observed using the remission definitions selected by the committee.

Other studies carried out since the publication of ACR/EULAR remission criteria provided additional evidence that the DAS28 should not be used to define remission. Saleem and colleagues (9) demonstrated that among patients whose RA was in remission according to the DAS28, power Doppler ultrasound showed considerable disease activity unless disease was also in remission according to the SDAI. Lee et al (10) reported that joint pain was present and persisted in patients whose disease was in remission according to the DAS28 but was absent if remission was classified according to the Boolean definition. Analyses from the AGREE trial of abatacept versus placebo (11) confirmed that patients in whom remission was achieved according to the DAS28 subsequently had worse mean scores on the Health Assessment Questionnaire (HAQ) (12) than those in whom remission was attained according to the SDAI. Schoels and colleagues reported, from an analysis of 3 large multicenter RA trials, that among patients with a DAS28 of <1.9, those whose disease was not in remission according to the ACR/EULAR criteria still had an average of 2–3 swollen joints (13).

Given the problems with use of the DAS28 to define remission, why is it so widely used? First, the DAS28 is a commonly used disease activity measure and it is easy to apply a threshold in data already being acquired, although the requisite elements of the ACR/EULAR definitions of remission are also acquired. Another potential reason relates to industry-sponsored RA trials. A definition based on a DAS28 of <2.6 yields remission rates far higher than definitions endorsed by the ACR/EULAR, and treatments therefore appear more efficacious with use of the DAS28. Further, use of a definition that yields a higher remission rate improves statistical power. The same absolute difference in

remission rates between 2 drugs is more likely to reach statistical significance when remission rates are higher. Finally, DAS28 use is mandated by some regulatory agencies. Many reports do not even include data on other measures of remission.

When remission definitions favor some treatments over others

Reliance on the CRP level to define RA remission is an emerging concern (14). CRP is the second most heavily weighted variable in the DAS28 formula. The armamentarium for treatment of RA includes effective biologic agents that have different effects on CRP; interleukin-6 and JAK inhibitors both directly reduce CRP, whereas abatacept and rituximab do not. If the DAS28-CRP is used in a trial comparing the efficacy of abatacept and JAK inhibitors, even if effects on joint counts and patient-reported outcomes are the same, JAK inhibitors would score better, as seen in one recent trial (15). In another trial comparing biologic agents, the authors acknowledged avoiding use of the DAS28-CRP because of this bias (16). The ACR/EULAR provisional criteria allow for remission definitions that exclude acute-phase reactants, using a 3-variable version of the Boolean definition and the Clinical Disease Activity Index (17) instead of the SDAI. Further, while the full ACR/EULAR remission definitions include acute-phase reactants, they are not weighted as heavily as in the DAS28-CRP (or the DAS28-ESR).

Concerns about inclusion of the patient global assessment

Yet another concern about the provisional definitions of remission has been championed by Ferreira et al (18). They point out that a patient’s global assessment of their arthritis activity often is based on considerations unrelated to current disease activity, such as pain from joint damage, and that this measure should not be included in definitions of remission. The factors that most influence the patient global activity measure are pain and fatigue. Ferreira and colleagues’ analyses suggest that removing the patient global assessment would not compromise the ability to predict later radiographic outcomes in RA, although they acknowledge that patient

Table 1. Proportion of patients with good outcomes (both radiographic and functional) in 3 multicenter rheumatoid arthritis trials*

Patients with good outcomes†	Candidate remission definition	
	TJC, SJC, and CRP level all ≤1	TJC, SJC, CRP level, and patient global assessment all ≤1
In remission, %	46	66
Not in remission, %	17	17
Positive likelihood ratio (95% CI)	3.1 (1.9–5.3)	7.2 (3.5–14.8)

* Excluding patient global assessment compromises the ability to predict good outcomes (from ref. 1). TJC = tender joint count; SJC = swollen joint count; CRP = C-reactive protein; 95% CI = 95% confidence interval.

† Based on remission status at 6 months after baseline. Good radiographic outcome was defined as a change of 0 in the Sharp/van der Heijde score between 12 months and 24 months after baseline. Good functional outcome was defined as a change of 0 in the Health Assessment Questionnaire between 12 months and 24 months after baseline and a score of ≤0.5 at both the 12-month and 24-month time points.

global assessment is a powerful predictor of function (as measured by the HAQ). High patient global assessment scores not only correlate with poor concurrent physical function, but they identify patients whose physical function is worsening (19,20). If patient global assessment is removed, remission criteria no longer predict future patient function well.

In addition to its being the only patient-reported outcome measure included in remission definitions and the importance of including the patient perspective, there are other critical reasons to include patient global assessment as a component of remission. First, the patient global assessment reflects components of disease activity that are otherwise not captured, including fatigue and pain, as well as inflammation in joints not included in a 28-joint count, such as the feet and ankles. This may be why high patient global assessment scores, even when 28-joint counts are low, identify patients at high risk of later functional loss. Second, the patient global assessment is among the most sensitive, if not the most sensitive, outcome measure in RA (20). It improves much more with active RA treatment than with placebo, suggesting that it provides a window into disease activity related to systemic inflammation not detected by tender and swollen joint counts. Therefore, eliminating patient global assessments from RA trial outcomes would compromise the ability to distinguish the comparative efficacy of different treatments. This would occur at a time when, given the large armamentarium of treatments available, there is a particular need to maximize the ability to differentiate their efficacy. In addition, inclusion of patient global assessment markedly increases the likelihood that patients in whom remission is attained will have both good radiographic outcomes and good functional outcomes later (Table 1), and it ensures that the definition of remission captures nonradiographic outcomes that are important to patients.

Conclusions

With remission achievable in RA, making the definition of remission stringent will ensure that patients benefit from comprehensive control of their disease. The DAS28 should not be used to define remission because, even with the use of low thresholds, many patients whose disease is in “remission” will still have a number of swollen joints and active disease. Also, given its dependence on the CRP value, use of the DAS28 makes it difficult to differentiate efficacious treatments with dissimilar effects on acute-phase reactant levels. Defining remission without asking patients to provide any information about their disease activity—not to mention failing to collect data on any patient-reported outcomes—risks losing valuable information on treatment efficacy.

AUTHOR CONTRIBUTIONS

All authors drafted the article, revised it critically for important intellectual content, and approved the final version to be published.

REFERENCES

1. Felson DT, Smolen JS, Wells G, Zhang B, van Tuyl LH, Funovits J, et al. American College of Rheumatology/European League Against Rheumatism provisional definition of remission in rheumatoid arthritis for clinical trials. *Arthritis Rheum* 2011;63:573–86.
2. Felson DT, Smolen JS, Wells G, Zhang B, van Tuyl LH, Funovits J, et al. American College of Rheumatology/European League Against Rheumatism provisional definition of remission in rheumatoid arthritis for clinical trials. *Ann Rheum Dis* 2011;70:404–13.
3. Smolen JS, Breedveld FC, Schiff MH, Kalden JR, Emery P, Eberl G, et al. A simplified disease activity index for rheumatoid arthritis for use in clinical practice. *Rheumatology (Oxford)* 2003;42:244–57.
4. Prevoo ML, van 't Hof MA, Kuper HH, van Leeuwen MA, van de Putte LB, van Riel PL. Modified disease activity scores that include twenty-eight-joint counts: development and validation in a prospective longitudinal study of patients with rheumatoid arthritis. *Arthritis Rheum* 1995;38:44–8.
5. England BR, Tiong BK, Bergman MJ, Curtis JR, Kazi S, Mikuls TR, et al. 2019 update of the American College of Rheumatology recommended rheumatoid arthritis disease activity measures. *Arthritis Care Res (Hoboken)* 2019;71:1540–55.
6. Greenmyer JR, Stacy JM, Sahmoun AE, Beal JR, Diri E. DAS28-CRP cutoffs for high disease activity and remission are lower than DAS28-ESR in rheumatoid arthritis. *ACR Open Rheumatol* 2020;2:507–11.
7. Sharp JT, Young DY, Bluhm GB, Brook A, Brower AC, Corbett M, et al. How many joints in the hands and wrists should be included in a score of radiologic abnormalities used to assess rheumatoid arthritis? *Arthritis Rheum* 1985;28:1326–35.
8. Van der Heijde DM. How to read radiographs according to the Sharp/van der Heijde method [corrected and republished in *J Rheumatol* 2000;27:261–3]. *J Rheumatol* 1999;26:743–5.
9. Saleem B, Brown AK, Keen H, Nizam S, Freeston J, Wakefield R, et al. Should imaging be a component of rheumatoid arthritis remission criteria? A comparison between traditional and modified composite remission scores and imaging assessments. *Ann Rheum Dis* 2011;70:792–8.
10. Lee YC, Cui J, Lu B, Frits ML, Iannaccone CK, Shadick NA, et al. Pain persists in DAS28 rheumatoid arthritis remission but not in ACR/EULAR remission: a longitudinal observational study. *Arthritis Res Ther* 2011;13:R83.
11. Smolen JS, Wollenhaupt J, Gomez-Reino JJ, Grassi W, Gaillez C, Poncet C, et al. Attainment and characteristics of clinical remission according to the new ACR-EULAR criteria in abatacept-treated patients with early rheumatoid arthritis: new analyses from the Abatacept study to Gauge Remission and joint damage progression in methotrexate (MTX)-naïve patients with Early Erosive rheumatoid arthritis (AGREE). *Arthritis Res Ther* 2015;17:157.
12. Fries JF, Spitz PW, Kraines RG, Holman HR. Measurement of patient outcome in arthritis. *Arthritis Rheum* 1980;23:137–45.
13. Schoels M, Alasti F, Smolen JS, Aletaha D. Evaluation of newly proposed remission cut-points for disease activity score in 28 joints (DAS28) in rheumatoid arthritis patients upon IL-6 pathway inhibition. *Arthritis Res Ther* 2017;19:155.
14. Aletaha D, Smolen JS. Remission in rheumatoid arthritis: missing objectives by using inadequate DAS28 targets [review]. *Nat Rev Rheumatol* 2019;15:633–4.
15. Rubbert-Roth A, Enejosa J, Pangan AL, Haraoui B, Rischmueller M, Khan N, et al. Trial of upadacitinib or abatacept in rheumatoid arthritis. *N Engl J Med* 2020;383:1511–21.
16. Hetland ML, Haavardsholm EA, Rudin A, Nordström D, Nurmohamed M, Gudbjornsson B, et al. Active conventional treatment and three

- different biological treatments in early rheumatoid arthritis: phase IV investigator initiated, randomised, observer blinded clinical trial. *BMJ* 2020;371:m4328.
17. Aletaha D, Nell VP, Stamm T, Uffmann M, Pflugbeil S, Machold K, et al. Acute phase reactants add little to composite disease activity indices for rheumatoid arthritis: validation of a clinical activity score. *Arthritis Res Ther* 2005;7:R796–806.
 18. Ferreira RJ, Welsing PM, Jacobs JW, Gossec L, Ndosi M, Machado PM, et al. Revisiting the use of remission criteria for rheumatoid arthritis by excluding patient global assessment: an individual meta-analysis of 5792 patients. *Ann Rheum Dis* 2020. doi: 10.1136/annrheumdis-2020-217171. E-pub ahead of print.
 19. Studenic P, Felson D, de Wit M, Alasti F, Stamm TA, Smolen JS, et al. Testing different thresholds for patient global assessment in defining remission for rheumatoid arthritis: are the current ACR/EULAR Boolean criteria optimal? *Ann Rheum Dis* 2020;79:445–52.
 20. Felson DT, Anderson JJ, Boers M, Bombardier C, Chernoff M, Fried B, et al. The American College of Rheumatology preliminary core set of disease activity measures for rheumatoid arthritis clinical trials. *Arthritis Rheum* 1993;36:729–40.

EDITORIAL

Lung Inflammation, NETosis, and the Pulmonary Initiation of Anti-Citrullinated Protein Antibody Response: What Came First, the Chicken or the Egg?

Jeremy Sokolove 

Multiple findings suggest that, at least in some patients, rheumatoid arthritis (RA)-associated autoimmunity and inflammation may originate in the lung (1,2). However, the exact precipitating events and sequence of subsequent events have not been fully defined.

In this issue of *Arthritis & Rheumatology*, Okamoto et al conclude that individuals at risk of developing RA have increased spontaneous neutrophil extracellular trap (NET) formation (known as NETosis) in sputum, in particular NETs containing citrullinated histone H3 (Cit-H3), and that these levels are associated with the presence of IgA anti-citrullinated protein antibody (ACPA) (3). Such findings have previously been reported, but new data illustrate a revised and enhanced narrative by investigating the pathway of mediation underlying these associations. Specifically, the authors suggest that aberrant NET formation (with the generation of citrullinated proteins) in the lungs of subjects at risk for RA precedes, and potentially mediates, local IgA ACPA generation during the preclinical phase of RA development.

Their study is highly translational and leverages induced sputum obtained from RA patients and subjects considered at risk for RA based on the medical history of their first-degree relatives. The researchers measured NET formation, levels of NET-associated Cit-H3, sputum cytokine concentrations, and levels of macrophages endocytosis.

Previous work from these authors has demonstrated a correlation of levels of serum and pulmonary ACPA with other NET remnants, including DNA-myeloperoxidase (MPO) and DNA-neutrophil elastase (NE), in the sputum of at-risk subjects (2). Therefore, the process of NETosis in the lungs of RA patients and at-risk subjects is known, but the initiators and sequence of events is not obvious.

One presumed sequence is that the generation of ACPA, on the background of genetic predisposition to autoreactivity, results in the generation of ACPA-immune complexes with the ability to

drive cytokine production as well as NETosis (4–6). That this process may be initiated in the lung is logical and supported, at least in some patients, by findings from prior studies by this group and others (2,7). Therefore, the excessive presence of products of NETosis, as well as inflammatory cytokines, in the bronchial lavage fluid of at-risk subjects and patients with clinical RA may be assumed to be driven in large part by the existence of ACPA-immune complexes. Logically, this results in a circular process of citrullinated antigen production, immune complex formation, and propagation of local (and eventually systemic) inflammation, including further production of NET-associated citrullinated antigens as well as cytokines that prime for NETosis (Figure 1).

Notably, this cyclical process must depend on the generation of citrullinated protein antigens over ≥ 2 key time points. The first is the initial generation of citrullinated antigens, which drives initiation of the anticitrulline immune response (including uptake by antigen-presenting cells, presentation to and recognition by autoreactive T cells, with subsequent immune activation and assistance to B cells in initiating the ACPA immune response). Though it is likely that intermittent neutrophilic inflammation results in transient generation of citrullinated proteins in all individuals during periods of airway irritation, such as viral respiratory infections (8), the initiation of anticitrulline autoimmunity is potentially less stochastic and is instead associated with a threshold effect of immune cell priming and antigen load. The study by Okamoto et al suggests that increased generation (and/or reduced clearance) of citrullinated proteins could be a primary driver of the break in tolerance and generation of IgA ACPA which, upon isotype switch, generates the systemic and ultimately articular IgG ACPA response characteristic of RA. Notably, a priming or threshold effect is further suggested by the increased risk of RA among smokers and those with exposure to particulate inhalants (9).

The second critical citrullination event is the generation of antigens recognizable by the ACPA immune response. It is well

Jeremy Sokolove, MD: GlaxoSmithKline, Collegeville, Pennsylvania, and Stanford University, Palo Alto, California.

Author disclosures are available at <https://onlinelibrary.wiley.com/action/downloadSupplement?doi=10.1002%2Fart.41947&file=art41947-sup-0001-Disclosureform.docx>.

Address correspondence to Jeremy Sokolove, MD, GSK Clinical Pharmacology and Experimental Medicine, 1250 South Collegeville Road, Collegeville, PA, 19426. Email: sokolove@stanford.edu.

Submitted for publication June 28, 2021; accepted in revised form August 3, 2021.

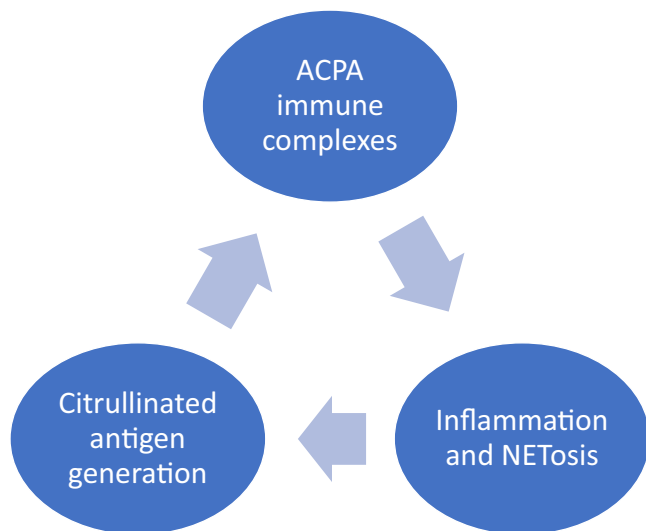


Figure 1. Cycle of inflammation and autoimmunity. Is aberrant activation of pulmonary NETosis and inflammation the precipitating factor in anticitrulline autoimmunity? ACPA = anti-citrullinated protein antibody; NETosis = neutrophil extracellular trap formation.

established that the systemic ACPA immune response precedes the onset of RA, often by decades (10). This observation supports the notion that the generation of citrullinated antigens, in the presence of circulating ACPA which provides the spark, fuels the fire in initiating and propagating RA (11). It remains unclear whether inflammation in the lung follows a similar pattern, whereby circulating ACPA awaits the generation of sufficient citrullinated antigens to allow for immune complex formation and pulmonary inflammation, or whether it is the process of aberrant citrullination that predisposes one to RA by providing sufficient antigens to drive anticitrulline autoimmunity.

In this study, the authors reported significantly higher levels of “spontaneous” NETosis and generation of Cit-H3 in sputum from RA patients and at-risk subjects, compared to controls (median 22%, 12%, and 0%, respectively). Using a mediation model, inflammatory proteins including cytokines and products of complement activation were observed to be associated with sputum IgA ACPA, through a pathway mediated by Cit-H3+ NET remnants. Notably, the only measured citrullinated product of NETosis was Cit-H3, and therefore it cannot be excluded that other citrullinated products of NETosis could similarly (or alternatively) serve as antigens to initiate or propagate the anticitrulline T cell and B cell responses (6).

It remains unclear what might mediate this increased NETosis and Cit-H3 generation in at-risk subjects. Prior studies of the pre-clinical period preceding RA, including the same at-risk population, have demonstrated elevated levels of circulating cytokines and subclinical inflammation (12–14), which would likely be apparent in the lungs via pulmonary circulation. The relative levels of systemic and pulmonary inflammation in the at-risk and clinical RA populations are roughly parallel to those of spontaneous NETosis, suggesting that NETosis could be initiated by systemic

inflammation. However, these studies also found that, in most cases, levels of systemic inflammation preceded the appearance of circulating ACPA (12,13). Additionally, prior studies have suggested that smoking (and presumably exposure to other inhalants) may increase the expression of peptidylarginine deiminase enzymes, thus increasing levels of citrullination in the lung (15), but this study did not specifically define a time frame for this process relative to anticitrulline autoreactivity. In the current study, even after adjustment for smoking, IgA anti-CCP levels remained significantly associated with sputum DNA-Cit-H3 levels ($P = 0.02$), though there was a loss of effect for other NET-associated products, including DNA-MPO and DNA-NE.

So, what is it about this at-risk population that predisposes them to very early lung inflammation? Is it possible that there is a shared environmental effect across first-degree relatives leading to the observed increases in inflammation and NETosis? Perhaps second-hand smoke or concurrent exposure to local environmental inhalants, in the home or in the environment, is to blame. Or perhaps an inherited genetic polymorphism in the pathway leading to increased NETosis (or, alternatively, reduced macrophage efferocytosis/phagocytosis and reduced clearance of NETotic debris) exists. Finally, it is possible that vertical transmission of epigenetic (or shared horizontal inheritance) alterations from those with heavy exposure to smoking or high levels of inflammation underly this predisposition to enhanced NETosis.

Ultimately, the study by Okamoto et al illuminates another potentially key event predisposing subjects to the generation of preclinical RA autoimmunity. Though the predisposing mechanisms have yet to be fully defined, the data supporting a unique predisposition of at-risk subjects to the generation of citrullinated antigens via low-grade pulmonary inflammation and aberrant activation of NETosis provide a newly identified potential “first hit” in the multi-hit process leading to the development of clinical RA.

AUTHOR CONTRIBUTIONS

Dr. Sokolove drafted the article, revised it critically for important intellectual content, and approved the final version to be published.

ADDITIONAL DISCLOSURES

Author Sokolove is an employee of GlaxoSmithKline.

REFERENCES

1. Joshua V, Chatzidionisyou K, Catrina AI. Role of the lung in individuals at risk of rheumatoid arthritis [review]. *Best Pract Res Clin Rheumatol* 2017;31:31–41.
2. Demoruelle MK, Wilson TM, Deane KD. Lung inflammation in the pathogenesis of rheumatoid arthritis [review]. *Immunol Rev* 2020;294:124–32.
3. Okamoto Y, Devoe S, Seto N, Minarchick V, Wilson T, Rothfuss HM, et al. Sputum neutrophil extracellular trap subsets are associated with IgA anti-citrullinated protein antibodies in subjects at risk for rheumatoid arthritis. *Arthritis Rheumatol* 2022;74:38–48.

4. Khandpur R, Carmona-Rivera C, Vivekanandan-Giri A, Gizinski A, Yalavarthi S, Knight JS, et al. NETs are a source of citrullinated autoantigens and stimulate inflammatory responses in rheumatoid arthritis. *Sci Transl Med* 2013;5:178ra40.
5. Chowdhury SC, Giaglis S, Walker UA, Buser A, Hahn S, Hasler P. Enhanced neutrophil extracellular trap generation in rheumatoid arthritis: analysis of underlying signal transduction pathways and potential diagnostic utility. *Arthritis Res Ther* 2014;16:R122.
6. Sohn DH, Rhodes C, Onuma K, Zhao X, Sharpe O, Gazitt T, et al. Local joint inflammation and histone citrullination provides a murine model for the transition from preclinical autoimmunity to inflammatory arthritis. *Arthritis Rheumatol* 2015;67:2877–87.
7. Klareskog L, Catrina AI. Autoimmunity: lungs and citrullination [review]. *Nat Rev Rheumatol* 2015;11:261–2.
8. Camp JV, Jonsson CB. A role for neutrophils in viral respiratory disease [review]. *Front Immunol* 2017;8:550.
9. Prisco LC, Martin LW, Sparks JA. Inhalants other than personal cigarette smoking and risk for developing rheumatoid arthritis [review]. *Curr Opin Rheumatol* 2020;32:279–88.
10. Rantapää-Dahlqvist S, de Jong BA, Berglin E, Hallmans G, Wadell G, Stenlund H, et al. Antibodies against cyclic citrullinated peptide and IgA rheumatoid factor predict the development of rheumatoid arthritis. *Arthritis Rheum* 2003;48:2741–9.
11. Vossenaar ER, van Venrooij WJ. Citrullinated proteins: sparks that may ignite the fire in rheumatoid arthritis [review]. *Arthritis Res Ther* 2004;6:107–11.
12. Nielen MM, van Schaardenburg D, Reesink HW, Twisk JW, van de Stadt RJ, van der Horst-Bruinsma IE, et al. Increased levels of C-reactive protein in serum from blood donors before the onset of rheumatoid arthritis. *Arthritis Rheum* 2004;50:2423–7.
13. Sokolove J, Bromberg R, Deane KD, Lahey LJ, Derber LA, Chandra PE. Autoantibody epitope spreading in the pre-clinical phase predicts progression to rheumatoid arthritis. *PLoS One* 2012;7:e35296.
14. Hughes-Austin JM, Deane KD, Derber LA, Kolfenbach JR, Zerbe GO, Sokolove J, et al. Multiple cytokines and chemokines are associated with rheumatoid arthritis-related autoimmunity in first-degree relatives without rheumatoid arthritis: Studies of the Aetiology of Rheumatoid Arthritis (SERA). *Ann Rheum Dis* 2013;72:901–7.
15. Makrygiannakis D, Hermansson M, Ulfgren AK, Nicholas AP, Zendman AJ, Eklund A. Smoking increases peptidylarginine deiminase 2 enzyme expression in human lungs and increases citrullination in BAL cells. *Ann Rheum Dis* 2008;67:1488–92.

REVIEW

Systemic Sclerosis–Associated Interstitial Lung Disease: How to Incorporate Two Food and Drug Administration–Approved Therapies in Clinical Practice

Dinesh Khanna,¹ Alain Lescoat,² David Roofeh,¹ Elana J. Bernstein,³ Ella A. Kazerooni,¹ Michael D. Roth,⁴ Fernando Martinez,⁵ Kevin R. Flaherty,¹ and Christopher P. Denton⁶

Systemic sclerosis (SSc; scleroderma) has the highest individual mortality of all rheumatic diseases, and interstitial lung disease (ILD) is among the leading causes of SSc-related death. Two drugs are now approved by the US Food and Drug Administration (FDA) and indicated for slowing the rate of decline in pulmonary function in patients with SSc-associated ILD (SSc-ILD): nintedanib (a tyrosine kinase inhibitor) and tocilizumab (the first biologic agent targeting the interleukin-6 pathway in SSc). In addition, 2 generic drugs with cytotoxic and immunoregulatory activity, mycophenolate mofetil and cyclophosphamide, have shown comparable efficacy in a phase II trial but are not FDA-approved for SSc-ILD. In light of the heterogeneity of the disease, the optimal therapeutic strategy for the management of SSc-ILD is still to be determined. The objectives of this review are 2-fold: 1) review the body of research focused on the diagnosis and treatment of SSc-ILD; and 2) propose a practical approach for diagnosis, stratification, management, and therapeutic decision-making in this clinical context. This review presents a practical classification of SSc patients in terms of disease severity (subclinical versus clinical ILD) and associated risk of progression (low versus high risk). The pharmacologic and nonpharmacologic options for first- and second-line therapy, as well as potential combination approaches, are discussed in light of the recent approval of tocilizumab for SSc-ILD.

Introduction

Systemic sclerosis (SSc; scleroderma) is a heterogeneous chronic autoimmune disease characterized by vascular damage, inflammation, and fibrosis of the skin and internal organs (1). SSc is the rheumatic disease with the highest individual mortality and has a detrimental impact on quality of life (1,2). Two main subsets of SSc are described based on the distribution of skin involvement: limited cutaneous SSc (lcSSc), characterized by distal skin thickening, and diffuse cutaneous SSc (dcSSc), with

widespread distal and proximal cutaneous changes (3,4). SSc is also characterized by the detection of specific and often mutually exclusive serum autoantibodies (5). A composite classification of SSc patients based on the combination of degree of skin involvement and antibody subtype is now considered more helpful in predicting the disease course, since scleroderma-specific antibodies are predictive of internal organ involvement (6). Patients who develop progressive SSc-associated interstitial lung disease (SSc-ILD) are more likely to be positive for the anti-topoisomerase I antibody (anti-Scl-70 antibody) and antinuclear antibody with

Dr. Khanna's work was supported by the National Institute of Arthritis and Musculoskeletal and Skin Diseases, NIH (grants K24-AR-063120 and R01-AR-070470). Dr. Lescoat's work was supported by the French network of the University Hospitals, Hôpitaux Universitaire du Grand Ouest (grant AAP JCM2020), and a CORECT Visiting grant from Rennes University Hospital. Dr. Roofeh's work was supported by the National Institute of Arthritis and Musculoskeletal and Skin Diseases, NIH (grant T32-AR-007080). Dr. Bernstein's work was supported by the National Institute of Arthritis and Musculoskeletal and Skin Diseases, NIH (grant K23-AR-075112).

¹Dinesh Khanna, MD, MSc, David Roofeh, MD, Ella A. Kazerooni, MD, MS, Kevin R. Flaherty, MD, MS: University of Michigan, Ann Arbor; ²Alain Lescoat, MD, PhD: University of Michigan, Ann Arbor, and University of Rennes 1, Centre Hospitalier Universitaire Rennes, INSERM, École des Hautes Études en Santé Publique, and Institut de Recherche en Santé, Environnement

et Travail, Rennes, France; ³Elana J. Bernstein, MD, MSc: Columbia University Irving Medical Center, New York, New York; ⁴Michael D. Roth, MD: University of California, Los Angeles; ⁵Fernando Martinez, MD, MS: New York University and Cornell University, New York, New York; ⁶Christopher P. Denton, MD, PhD: University College London, London, UK.

Author disclosures are available at <https://onlinelibrary.wiley.com/action/downloadSupplement?doi=10.1002%2Fart.41933&file=art41933-sup-0001-Disclosureform.pdf>.

Address correspondence to Dinesh Khanna, MD, MSc, University of Michigan Scleroderma Program, Division of Rheumatology, Department of Internal Medicine, Suite 7C27 300 North Ingalls Street, SPC 5422, Ann Arbor, MI 48109. Email: khannad@med.umich.edu.

Submitted for publication April 30, 2021; accepted in revised form July 22, 2021.

nucleolar pattern (notably including anti-PM/Scl-75, anti-PM/Scl-100, anti-Th/To, anti-U3 RNP/fibrillarin, anti-RNA polymerase I, or anti-NOR-90 antibodies), regardless of cutaneous subset (6–9).

ILD is among the leading causes of SSc-related death (10). The prevalence of SSc-ILD varies depending on the assessment method (radiography or high-resolution computed tomography [HRCT]), the screening strategy (systematic HRCT versus selection of patients based on the results of pulmonary function tests [PFTs]), the targeted populations (dcSSc versus lcSSc), and differences in geographic location or expertise of the medical center (11,12). In national observational registries and international cohorts, ~65% of SSc patients have or will develop ILD in the course of their disease (11–14).

The high mortality related to SSc-ILD has led to recent randomized controlled trials (RCTs) forging substantial progress in the management of this manifestation (15). Conventional immunomodulatory agents such as cyclophosphamide (CYC) and mycophenolate mofetil (MMF) are evidence-based treatments typically implemented in clinical practice (16,17). More recently, well-conducted phase III RCTs have led to US Food and Drug Administration (FDA) approval of 2 targeted therapies for SSc-ILD (18–22). Nintedanib is a tyrosine kinase inhibitor; in 2019 it became the first medication approved to slow the rate of decline in pulmonary function in patients with SSc-ILD, based on the results of the Safety and Efficacy of Nintedanib in Systemic Sclerosis (SENSCIS) trial (ClinicalTrials.gov identifier: NCT02597933) (18,19). Tocilizumab is a monoclonal antibody targeting the interleukin-6 (IL-6) receptor; in 2021 it became the first biologic medication approved for the same indication, based on the results of the Safety and Efficacy of Subcutaneous Tocilizumab in Adults With Systemic Sclerosis (faSScinate) trial (ClinicalTrials.gov identifier: NCT01532869) and the Study of the Efficacy and Safety of Tocilizumab in Participants With Systemic Sclerosis (focuSSced) (ClinicalTrials.gov identifier: NCT02453256) (20–22).

Despite these recent FDA approvals, the optimal therapeutic strategy for the management of SSc-ILD is yet to be determined, especially given the heterogeneity of the disease (23). The objectives of this review are 2-fold: 1) to review the body of research focused on diagnosis and treatment of SSc-ILD and 2) to propose a practical approach for diagnosis, stratification, management, and therapeutic decision-making in this clinical context. The management strategy proposed in this review reflects the authors' opinions, experience, and clinical practice.

Pathogenic considerations and rationale for available therapeutic options in SSc-ILD

The pathogenesis of SSc-ILD is not fully understood but includes a triad of pathogenic events: endothelial dysfunction, early inflammatory features, and excessive deposition of extracellular matrix (ECM) components produced by activated myofibroblasts (9,24). ECM deposits induce an increased stiffness

of lung tissue with reduction in pulmonary compliance and volumes. These pathogenic events can lead to a restrictive ventilatory defect captured by spirometry alongside impairment in gas exchange; some patients may remain asymptomatic despite evidence of disease on HRCT, whereas the consequences of severe and advancing disease include dyspnea and death.

The direct inhibition of myofibroblast activation or the targeting of other cellular subsets participating in the production of key mediators responsible for myofibroblast activation provide the rationale for candidate drugs in SSc-ILD. Early inciting factors include epithelial and endothelial damage that may be promoted by aberrant innate and adaptive immunity that can produce profibrotic and proinflammatory mediators, inducing myofibroblast activation. Through the production of IL-13 and IL-4, Th2 lymphocytes have a direct impact on fibroblasts and can induce the activation of profibrotic macrophages (M2 macrophages) that notably produce high levels of transforming growth factor β , platelet-derived growth factor (PDGF), and factors from the fibroblast growth factor (FGF) family favoring myofibroblast activation (25–27). The tyrosine kinase inhibitor, nintedanib, inhibits the receptors of vascular endothelial growth factor (VEGF), PDGF, and the FGF family, with subsequent antifibrotic effects (28).

Acute-phase reactants, and specifically IL-6, play an important role in the pathogenesis of SSc-ILD. IL-6 is produced by B cells, proinflammatory macrophages (M1 macrophages), and myofibroblasts (29,30). In vitro studies suggest that IL-6 can favor the expression of IL-4 and IL-13 receptors, with a subsequent increase in profibrotic M2 macrophage polarization (31). The inhibition of the IL-6 receptor by tocilizumab can directly impact myofibroblast activation and M2 macrophage polarization, with potential antifibrotic effects (29,32). Through their impact on the proliferation of fibroblasts, B cells, and T helper lymphocytes, conventional immunomodulatory agents such as MMF, an inhibitor of de novo synthesis of guanosine nucleotides, or the alkylating agent CYC can also have antifibrotic effects (33,34).

Key parameters for the diagnosis, screening, and assessment of SSc-ILD

HRCT is the reference standard for early diagnosis of SSc-ILD (12,35,36). In the majority of patients (70–80%), SSc-ILD is characterized by a pattern of nonspecific interstitial pneumonia that includes parenchymal changes classically located in bi-basal and posterior regions of the lungs, and defined by the presence of reticular abnormalities with peribronchovascular extension and subpleural sparing with absence of honeycombing and frequent ground-glass attenuations (13,37,38) (Figure 1A). Ground-glass opacity in early SSc may represent either inflammation or fibrosis that is below the resolution of the HRCT technique at the level of intralobular septa and interstitium surrounding alveoli. Early radiologic–pathologic correlation studies using HRCT have demonstrated that bronchiectasis or bronchiolectasis within areas

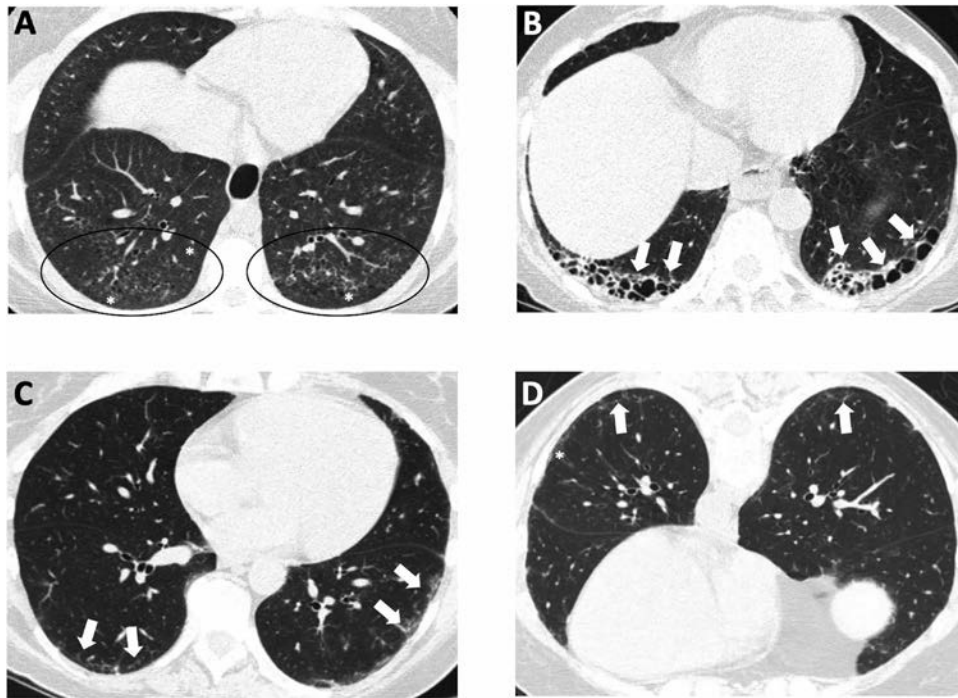


Figure 1. High-resolution computed tomography images of the lungs of 3 different patients with systemic sclerosis (SSc)-related interstitial lung disease (ILD). **A**, Nonspecific interstitial pneumonitis (NSIP) with a lower lobe subpleural predominant distribution of primarily ground-glass opacity (**asterisks** and encircled areas). **B**, Definite usual interstitial pneumonitis with subpleural lower lobe honeycombing (**arrows**). **C** and **D**, Mild ILD on the supine image (**arrows**) (**C**), which could be interpreted as dependent atelectasis; however, it persists on the prone image (**D**), confirming the presence of ILD. The pattern of septal thickening (**arrows**) and ground-glass opacity (**asterisk**) without bronchiectasis is most consistent with NSIP in a patient with SSc.

of ground glass are strong indicators of fibrosis, whereas ground glass without bronchiectasis is strong evidence of inflammation (39). The presence of traction bronchiectasis with minimal ground-glass opacifications is thus more specifically consistent with fibrotic nonspecific interstitial pneumonia. Approximately 10% of patients with SSc-ILD have an HRCT pattern of usual interstitial pneumonia (UIP) defined by subpleural and basal predominant lesions including honeycombing (mandatory criterion) with or without peripheral traction bronchiectasis or bronchiolectasis (Figure 1B).

In patients with connective tissue disease-associated ILD (CTD-ILD), especially rheumatoid arthritis-associated ILD, UIP is predictive of a worse prognosis compared to nonspecific interstitial pneumonia; the specific prognostic value of HRCT patterns in SSc-ILD is more controversial (40). Patient survival in SSc-ILD does not differ between nonspecific interstitial pneumonia and UIP according to the histopathologic patterns on lung biopsy (41). Considering the sensitivity and specificity of HRCT for SSc-ILD and the lack of predictive value of histopathologic patterns in SSc-ILD, lung biopsy is not recommended for the diagnosis and assessment of SSc-ILD. A prone HRCT acquisition is recommended to rule out early ILD, as the predominant bi-basal and posterior localization of HRCT findings in SSc-ILD may produce false-positives due to position-induced changes (i.e., atelectasis) (Figures 1C and D) (42). Quantitative HRCT allows

precise quantification of SSc-ILD lung involvement (the sum of lung involvement with ground-glass opacities, fibrotic reticulations, and honeycombing) and of fibrotic changes (quantification of lung fibrosis, or fibrotic reticulations alone) (43,44). The extent of lung involvement has been demonstrated to have prognostic value; accurately assessing the degree of lung involvement provides a valuable tool for stratifying disease severity and risk of progression (45,46).

Spirometry and gas exchange are the reference standard measurements for the assessment of lung physiology. The impact of SSc-ILD on forced vital capacity (FVC), total lung capacity (TLC), and diffusing capacity for carbon monoxide (DL_{CO}) is a marker of disease severity. In terms of screening and diagnosis, SSc-ILD may initially have only mild or no impact on PFT parameters; normal values of FVC, TLC, and DL_{CO} do not rule out early SSc-ILD (12). In a US multicenter study of patients with early dcSSc, FVC percent predicted (FVC%) <80% had a sensitivity of 63% and a negative predictive value (NPV) of 61% for the detection of SSc-ILD. The combination of FVC% <80% or DL_{CO} % <80% had a sensitivity and NPV of 85% and 70%, respectively, demonstrating that PFTs alone are an inadequate screening tool for the diagnosis of SSc-ILD (12). A European study also demonstrated similar results and highlighted that among patients with normal FVC% but with SSc-ILD on HRCT, 50% had extensive ILD (>20% of parenchymal involvement) (47). In addition, FVC%

in healthy volunteers ranges from 80% to 120%, which can mean that a clinically meaningful decline may be missed in a patient who has declines within the “normal” range of FVC%, e.g., from 110% to 80%. Therefore, it is now accepted that both PFT and HRCT should be performed for initial screening and diagnosis of SSc-ILD (35).

We recommend performing HRCT and PFT for baseline ILD screening in all patients with early SSc (early relates to the onset of their symptoms that are specific for SSc), regardless of cutaneous or autoantibody subtype (36). Every patient with a new diagnosis of SSc-ILD based on HRCT should have initial full PFTs (i.e., spirometry, lung volumes, and DLco) for baseline reference and a 6-minute walk test to assess the impact on gas exchange and exercise capacity. Although the 6-minute walk test can be influenced by different organ involvement in SSc, such as pulmonary vascular disease and cardiac involvement, for example, we use the 6-minute walk test in clinical practice to document baseline distance and oxygen saturation and repeat it annually (or more frequently for new or worsening of symptoms) to assess for decline in both of these parameters (48,49). Clinical scales such as the modified Medical Research Council dyspnea scale or the New York Heart Association functional classification of dyspnea are simple to incorporate in clinical practice and can provide important information to assess for SSc-ILD progression (50,51).

Definitions, risk factors for, and monitoring of the progression of SSc-ILD

There are different definitions for the progression of SSc-ILD. Outcome Measures in Rheumatology (OMERACT) has proposed the definition of “clinically meaningful progression” of CTD-ILD based on the evolution of PFT parameters; this definition can be applied to SSc-ILD. OMERACT defines progression as a $\geq 10\%$ relative decline in FVC% or a 5% to $< 10\%$ relative decline in FVC% and $\geq 15\%$ relative decline in DLco%. The Efficacy and Safety of Nintedanib in Patients With Progressive Fibrosing Interstitial Lung Disease (INBUILD) trial, which focused on fibrotic ILD, has also proposed a composite definition of “progressive fibrosing ILD” as an inclusion criterion, which was notably applied to patients with SSc-ILD (19). In that trial, one of the following criteria was required to fulfill the definition of progression within the prior 24 months: a) $\geq 10\%$ relative decline in FVC%, or b) 5% to $< 10\%$ relative decline in FVC% and worsening of respiratory symptoms or an increased extent of fibrosis on HRCT, or c) worsening of respiratory symptoms and an increased extent of fibrosis on HRCT, regardless of the evolution of FVC%.

The results of the focuSSced trial demonstrate that early treatment should be considered in patients with SSc-ILD at high risk of progression, regardless of the actual progression rate and/or before decline of lung function or progression is identified through close monitoring (21). This approach constitutes a paradigm shift in the field of SSc-ILD and emphasizes the need for

Table 1. Parameters available in clinical practice and associated with progressive SSc-ILD*

Demographic and clinical parameters
Advanced age
Male sex
African American ethnicity
dcSSc
Findings on pulmonary function tests
Low baseline FVC%†
Low baseline DLco%†
HRCT findings
Extent of ILD on HRCT (cutoff value $> 20\%$ of lung parenchyma for total lung involvement)
Serum markers
Anti-Scl-70/topoisomerase I antibody
Nucleolar pattern (especially including anti-Th/To and anti-U3 RNP)
Elevated acute-phase reactant levels, including serum CRP levels greater than the ULN

* SSc-ILD = systemic sclerosis-related interstitial lung disease; dcSSc = diffuse cutaneous SSc; FVC% = forced vital capacity percent predicted; DLco% = diffusing capacity for carbon monoxide percent predicted; HRCT = high-resolution computed tomography; CRP = C-reactive protein; ULN = upper limit of normal.

† Cutoff values vary across studies.

reliable and accessible predictive markers of SSc-ILD progression. The predictive value of such markers in observational studies and RCTs varies according to the targeted populations and the definition of SSc-ILD progression (36,52) (Table 1). Serum markers used in clinical practice, such as anti-topoisomerase I antibodies and elevated C-reactive protein (CRP) values, are associated with SSc-ILD progression (53,54). Other biomarkers, such as KL-6, CCL2, CCL18, CXCL4, or surfactant protein D, may be predictive of the progression of SSc-ILD but are not available in routine practice and are currently used in the context of exploratory clinical research (36,52,55,56). Negative anticentromere antibody and a history of smoking may also constitute risk factors for progressive ILD, although the data are less consistent (6,57).

The heterogeneous rates of disease progression and treatment response underscore the need for close monitoring of patients with SSc-ILD after initial diagnosis or treatment initiation (35,58). The majority of patients who will develop severe SSc-ILD will do so in the first 5 years after the onset of the disease, although late progression may also occur (52). After initial diagnosis of SSc-ILD with baseline HRCT and PFT, follow-up of all SSc-ILD patients should include PFT (FVC and DLco) at least every 6 months for the first 3–5 years from the onset of the first non-Raynaud’s phenomenon manifestation (Table 1) in order to monitor for progression (36,52). Although substantial progress has been made in HRCT techniques, allowing high-quality HRCT with low-dose radiation (typically 1.5–2.5 mSv), the systematic follow-up and monitoring of all SSc-ILD patients with sequential chest HRCT is not currently recommended (35,36). In cases of worsening symptoms or clinically meaningful progression (as defined in the INBUILD trial), a follow-up HRCT can be considered to assess for progressive ILD. Other causes of progressive symptoms such as pulmonary

vascular disease or cardiac involvement should also be considered due to the multifactorial nature of SSc-associated manifestations. In SSc patients without ILD or with stable or controlled ILD after the first 3–5 years, annual PFTs are useful to monitor for both the onset and progression of SSc-ILD and to screen for SSc-associated pulmonary arterial hypertension (PAH) (7,59).

Classification of SSc-ILD and subgroups of patients according to initial severity and risk of progression

SSc-ILD trajectories are divided into 2 large subsets, depending on the initial clinical presentation. Subclinical ILD is defined by the presence of ILD *with* minimal extent on HRCT (usually 5–10% based on visual or computer quantification) *and* no ILD-related clinical symptoms (such as dyspnea and cough) *and* normal initial PFT (including FVC *and* DL_{CO}) or no clinically meaningful decline in PFT, if serial PFTs are available. With the institution of HRCT for screening and diagnosis of SSc-ILD, this subgroup is likely to increase over time. Clinicians also need to use their judgment to assess if symptoms such as cough are related to ILD or to other causes such as silent gastric aspiration or upper airway cough syndrome.

The remaining patients with ILD are classified as having clinical ILD (which comprises the majority of current cases of SSc-ILD due to a lack of universal screening in SSc patients); they are classified by the presence of mild to severe ILD on HRCT *and* one or more of the following features: abnormal initial PFT (including FVC *and/or* DL_{CO}) *and/or* clinically meaningful decline in PFT parameters (including FVC *and/or* DL_{CO}). Clinical ILD is associated with ILD-related symptoms or impact of ILD on daily life.

Within these subsets, patients can be further divided into those with a low risk of progressive ILD (no elevated acute-phase reactants, positive for anticentromere antibody) and high risk of progressive ILD (Table 1). The subgroup of patients with subclinical ILD at high risk of progression (as shown in the focuSSced trial), as well as all patients with clinical ILD, would benefit from early therapeutic intervention for SSc-ILD. Close monitoring (at least every 6 months) is also necessary in patients with subclinical ILD with low risk of progression in order to confirm stability.

Clinical evidence for the management of SSc-ILD based on phase II and III trials

The main therapeutic agents for the treatment of SSc-ILD have immunomodulatory properties, antifibrotic properties, or both (23). The results of the main phase II and III RCTs and their targeted populations are detailed in Table 2.

The Scleroderma Lung Study I (SLS I) evaluated the effects of oral CYC versus placebo in SSc-ILD. SLS I demonstrated that the mean absolute difference in adjusted 12-month FVC% was 2.53% favoring CYC ($P < 0.03$) (16). CYC also improved dyspnea

and quality of life compared to placebo. SLS I is a pivotal study that demonstrated for the first time that SSc-ILD is responsive to immunosuppressive treatment in a clinical trial setting. The Scleroderma Lung Study II (SLS II) demonstrated that treatment of SSc-ILD with MMF for 2 years or CYC for 1 year was associated with statistically significant improvement in FVC% in both arms at 24 months, without a between-arm difference ($P = 0.24$) (17). Significant favorable transitions from ground-glass and/or lung fibrosis HRCT patterns to a normal pattern were observed in both arms of SLS II (44,60). MMF and CYC also improved the modified Rodnan skin thickness score (MRSS) course over 24 months in participants with dcSSc (61). In SLS II, MMF was associated with less toxicity and was better tolerated than CYC. For these reasons, MMF is now considered the standard of care as first-line therapy for SSc-ILD (62).

The SENSICIS trial, a phase III RCT, evaluated the efficacy of nintedanib compared to placebo for patients with SSc-ILD. Patients receiving a stable dose of MMF or methotrexate for at least 6 months prior to randomization were permitted to enroll. The intergroup difference in the annual rate of change in FVC was 41.0 ml per year (95% confidence interval [95% CI] 2.9, 79.0) in favor of nintedanib ($P = 0.04$) (18). The treatment effect of nintedanib on the annual rate of change in FVC was numerically, but not significantly, lower in participants who were taking MMF at baseline than in those not taking MMF (difference between nintedanib and placebo 26.3 ml per year [95% CI –27.9, 80.6] and 55.4 ml per year [95% CI 2.3, 108.5] in the group taking MMF and the group not taking MMF, respectively). In addition, there were marked geographic differences in the background use of MMF. In North America, where the majority of patients were receiving MMF, the difference between treatment arms was even smaller, at 10.3 ml per year (95% CI –27.9, 80.6), but still in favor of nintedanib. As a result, the SENSICIS data suggest a possible additive or synergistic effect from combining MMF and nintedanib, but the details of such a combination require further clarification (63).

The phase II faSScinate and phase III focuSSced trials evaluated the safety and efficacy of tocilizumab in patients with early active dcSSc (20,21). The primary end point was the difference in mean change in MRSS from baseline to week 24 and to week 48 in faSScinate and focuSSced, respectively. Despite a numerical difference in the change in MRSS in favor of tocilizumab, neither trial reached statistical significance at $P < 0.05$ for their primary end points. However, the key secondary end point showed statistically significant and clinically meaningful differences in the change in FVC% from baseline to week 48 in favor of tocilizumab. In faSScinate, patients treated with tocilizumab had a smaller decrease in FVC from baseline to 24 weeks (least squares mean difference 136 ml [95% CI 9, 264]; $P = 0.04$ in favor of tocilizumab) with a numerical effect in favor of tocilizumab also observed at week 48 (least squares mean difference 120 ml [95% CI –23, 262]; $P = 0.099$ in favor of tocilizumab) (20). At both time points,

Table 2. Inclusion criteria, targeted population, and main results of key phase II and III trials including SSC-ILD patients*

Trial name (ref.)	Drug tested	Targeted population (main criteria)	Control group	Background therapy	Total no./no. in active treatment group/no. in control group	% with SSC-ILD in active treatment group/% with SSC-ILD in control group	Pulmonary outcome measure used for efficacy	Main results for the pulmonary outcome measure used
SLS I (16)	CYC	dcSSc or lcSSc; SSC-ILD defined by active alveolitis or GGO on CT; disease duration <7 years; FVC% 45–85%; exertional dyspnea grade ≥2†	Placebo	Potentially disease-modifying medications excluded; prednisone >10 mg/day excluded	158/79/79	100/100	FVC% at 12 months adjusted for baseline FVC	Mean absolute difference in adjusted 12-month FVC 2.53% (95% CI 0.28, 4.79), favoring CYC ($P < 0.03$)
SLS II (17)	MMF	dcSSc or lcSSc; SSC-ILD defined by GGO on CT (with or without reticulation); disease duration <7 years; FVC% 45–80%; exertional dyspnea grade ≥2†	CYC	Potentially disease-modifying medications excluded; prednisone >10 mg/day excluded	142/69/73	100/100	Course of FVC% from 3 to 24 months	Course of FVC% did not differ significantly between the 2 treatment groups ($P = 0.24$); adjusted FVC% improved from baseline to 24 months by 2.19% in the MMF group (95% CI 0.53, 3.84) and 2.88% in the CYC group (95% CI 1.19, 4.58)
SENSCIS (18)	NINT	dcSSc or lcSSc; SSC-ILD with CT showing fibrosis affecting ≥10% of the lungs; FVC% ≥40%	Placebo	Allowed prednisone (up to 10 mg per day) or MMF/MTX at a stable dose for ≥6 months before randomization	580/288/288‡	100/100	Annual rate of decline in FVC (ml/year), assessed over a 52-week period	Adjusted annual rate of change in FVC –52.4 ml per year in the NINT group and –93.3 ml per year in the placebo group (difference 41.0 ml per year [95% CI 2.9, 79.0]; $P = 0.04$)
faSScinate (20)	TCZ	dcSSc with or without ILD; active disease‡; disease duration <5 years	Placebo	No background immunomodulatory therapies allowed	87/43/44	NA	Decline in FVC (ml) at weeks 24 and 48 (secondary outcome); % of patients experiencing worsening of FVC% in each arm	Smaller decrease in FVC for TCZ than for placebo from baseline to 24 weeks (TCZ –34 ml vs. placebo –171 ml; LSM difference 136 ml [95% CI 9, 264]; $P = 0.0368$) but no significant difference from baseline to 48 weeks (TCZ –117 ml vs. placebo –237 ml; LSM difference 120 ml [95% CI –23, 262]; $P = 0.0990$); fewer patients in the TCZ group than in the placebo group had worsening of FVC% at 24 weeks ($P = 0.009$) or at 48 weeks ($P = 0.037$)

(Continued)

Table 2. (Cont'd)

Trial name (ref.)	Drug tested	Targeted population (main criteria)	Control group	Background therapy	Total no./no. in active treatment group/no. in control group	% with SSC-ILD in active treatment group/% with SSC-ILD in control group	Pulmonary outcome measure used for efficacy	Main results for the pulmonary outcome measure used
focuSSced (21)	TCZ	dcSSc with or without ILD; active disease; disease duration <60 months	Placebo group	No background immunomodulatory therapies allowed	212/105/107	67/65	Difference in distribution of change from baseline to week 48 in FVC% (key secondary outcome)	Shift in the distribution of change in FVC% from baseline to week 48 favoring TCZ (van Eleren nominal $P = 0.002$ versus placebo); in patients with SSC-ILD at baseline the LSM of change from baseline in FVC% was -6.4 in the placebo group and 0.1 in the TCZ group (LSM difference between groups 6.5 [95% CI 3.4, 9.5]; $P < 0.0001$)

* SSC-ILD = systemic sclerosis-associated interstitial lung disease; SLS I = Scleroderma Lung Study I; CYC = cyclophosphamide; dcSSc = diffuse cutaneous SSC; lcSSc = limited cutaneous SSC; GGO = ground-glass opacities; CT = computed tomography; FVC% = forced vital capacity percent predicted; 95% CI = 95% confidence interval; MMF = mycophenolate mofetil; SENSICIS = Safety and Efficacy of Nintedanib in Systemic Sclerosis; NINT = nintedanib; MTX = methotrexate; faSScinatate = Safety and Efficacy of Subcutaneous Tocilizumab in Adults With Systemic Sclerosis; TCZ = tocilizumab; NA = not available; LSM = least squares mean; focuSSced = Study of the Efficacy and Safety of Tocilizumab in Participants With Systemic Sclerosis.

† On the Magnitude of Task component of the Mahler Baseline Dyspnea Index.

‡ An additional 3 patients were randomized despite noneligibility, and 1 patient withdrew from the study.
 § Defined as an increase of ≥ 3 on the modified Rodnan skin thickness score (MRSS) at screening compared to the last visit within the previous 1–6 months or new-onset SSC diagnosed within 1 year before screening, involvement of 1 new body area with an increase in MRSS of ≥ 2 or 2 new body areas with increase in MRSS of ≥ 1 , documentation of worsening of skin thickening in the previous 6 months, or ≥ 1 tendon friction rub plus fulfillment of ≥ 1 laboratory criterion (C-reactive protein ≥ 10.0 mg/liter, erythrocyte sedimentation rate ≥ 28 mm/hour, or platelet count $\geq 330,000/\mu\text{l}$).

fewer patients in the tocilizumab group than in the placebo group had worsening of FVC%.

In the focuSSced trial, 68 patients in each arm had SSc-ILD on HRCT (representing 67% and 65% of the patients in the tocilizumab and placebo arms, respectively). In these patients, risk factors for SSc-ILD progression were similar in the tocilizumab and placebo arms, including disease duration (mean \pm SD 23 \pm 17.2 months versus 22.6 \pm 16.6 months), proportion positive for antitopoisoisomerase antibodies (68.7% versus 68.8%), CRP levels (mean \pm SD 11.2 \pm 17.4 versus 8.0 \pm 13.1 mg/liter), baseline FVC% (mean \pm SD 77.7 \pm 13.9 versus 81.5 \pm 14.9), and baseline quantitative ILD (mean \pm SD 20.5 \pm 12.8% versus 16.8 \pm 8.8%) in the tocilizumab and placebo arms, respectively (22). In the focuSSced trial, the least squares mean difference in FVC% in patients with SSc-ILD showed a change from baseline of -6.4% for placebo and $+0.1$ for tocilizumab (least squares mean difference between groups 6.5% [95% CI 3.4, 9.5]; $P < 0.0001$) (21). Post hoc analysis showed that early SSc-ILD was not synonymous with minimal ILD on HRCT, as 41% of the patients had total lung involvement of $>10\%$ to 20%, and 36% had total lung involvement of $>20\%$, determined using a computer-generated algorithm. These data highlighted that the stabilization of lung function in the tocilizumab arm was consistent across all severity groups of SSc-ILD, demonstrating that the effects of tocilizumab were observed in all subgroups (22).

Other targeted biologics such as rituximab (anti-CD20 antibody) and abatacept (CTLA-4lg fusion protein) have shown some beneficial effects on FVC in patients with SSc-ILD (64). In a phase II trial, abatacept showed a nonsignificant reduction in FVC decline at 12 months (least squares mean FVC% 2.79% [95%CI -0.69 , 6.27], favoring abatacept compared to placebo) (64). A similar trend was observed in the open-label extension at month 18 (65). In an open-label trial comparing rituximab to CYC, mean \pm SD FVC% improved from 61.30 \pm 11.28% at baseline to 67.52 \pm 13.59% at 6 months in the rituximab arm, but declined from 59.25 \pm 12.96% to 58.06 \pm 11.23% in the CYC arm, with a mean difference in FVC% at 6 months of 9.46 (95% CI 3.01, 15.90) ($P = 0.003$) (66). A recent Japanese phase II trial evaluating the impact of rituximab on skin involvement also showed promising results with regard to FVC progression, as the change in FVC% from baseline to week 24 was 0.09% in the rituximab group compared to -2.87% in the placebo group (difference 2.96% [95% CI 0.08, 5.84]; $P = 0.04$ favoring rituximab) (67).

The phase II Scleroderma: Cyclophosphamide or Transplantation (SCOT) trial has demonstrated the efficacy of myeloablative chemotherapy with radiation and hematopoietic stem cell transplantation (HSCT) to improve survival in a population of patients with severe SSc. Among the included patients, 100% in the transplantation group and 95% in the CYC control group had SSc-ILD (68). In this RCT, 36% of the patients in the HSCT arm had an improvement in FVC of $\geq 10\%$ compared to 23% of the patients in the CYC arm. The proportion of the patients with a decrease

in FVC of $\geq 10\%$ was lower in the HSCT arm than in the CYC arm (17% versus 41%, respectively). Observational before-and-after HSCT studies also suggest an improvement in the extent of ILD on HRCT, although the small sample size precludes firm conclusions (69).

Lung transplant could be considered for patients with SSc-ILD, especially when other available treatments have failed (70,71). Referral for lung transplant should notably be considered in cases of progressive FVC and DL_{CO} decline despite a combination of immunosuppressive and antifibrotic therapies, worsening symptoms such as dyspnea on exertion (without any other identifiable cause), and/or increasing oxygen requirement (72). In carefully selected patients with mild-to-moderate extrapulmonary manifestations related to SSc, lung transplant for SSc-ILD has shown similar outcomes as in other fibrotic lung diseases or in PAH (73).

Points to consider when interpreting the RCTs of nintedanib and tocilizumab in SSc-ILD

When interpreting the results of SENSICIS and focuSSced, it is important to underscore that the study populations were different in these trials (early active dcSSc in focuSSced, and progressive ILD regardless of the cutaneous subset in SENSICIS), with potential impact on the natural progression rate in the placebo arms. Moreover, background therapies were allowed in SENSICIS, which could have contributed to limiting the decline in FVC in both arms and could have impacted the results regarding extrapulmonary manifestations. The expected decline in FVC after age 25 years in the general population is 25–30 ml/year, which is another point to consider in interpreting the decline in FVC in these phase III trials, notably in the placebo arms (74). In SENSICIS, the decline in FVC in the placebo arm was 93.3 ml (119.3 ml in patients not taking MMF in the placebo group), a 3- to 4-fold greater decline compared to the healthy population (18,63). In focuSSced, the placebo arm showed an absolute decline in FVC of 255 ml, which corresponds to a 10-fold greater decline compared to the healthy population, highlighting that the patients included in the study were at high risk of severe decline (21).

This difference in rate of FVC decline between the 2 trials can be explained by the natural history of SSc-ILD and the underlying pathogenic mechanisms. In focuSSced, the patients included had early dcSSc, with more prominent inflammatory immune features that were captured at a very early phase, without significant SSc-ILD during the screening phase prior to randomization and baseline HRCT (75). These patients were rarely included in previously designed SSc-ILD studies because significant and/or progressive clinical ILD was a required inclusion criterion. Thus, the early treatment of this specific population of patients with inflammatory SSc at high risk of progression may represent a window of opportunity to prevent the decline in pulmonary function in SSc-ILD. The patients included in the SENSICIS trial had clinical ILD, so that we can hypothesize that fibrotic pathways were more established,

with a more predictable decline in FVC that was similar to what was expected based on previous SSc-ILD studies (16,17). Both tocilizumab and nintedanib, nonetheless, showed biologic effects that can be considered disease-modifying in SSc-ILD.

A proposed strategy for the management of SSc-ILD

All patients with SSc-ILD deemed appropriate for pharmacologic treatment should be initiated on immunomodulatory treatment, as the pathogenesis of early ILD includes immune dysfunction and inflammation resulting in fibrosis (Figure 2). Our

treatment decision algorithm for SSc-ILD is provided in Figures 2 and 3. The first step in the treatment decision algorithm is the classification of the patient along the dimension of disease severity (subsets of subclinical ILD or clinical ILD), based on ILD-specific symptoms and clinical impact, extent of ILD on HRCT, and functional impact based on FVC and/or DLco (58,70). All patients with clinical ILD should be considered for immunomodulatory treatment (15,35). If a patient has subclinical ILD, further stratification regarding risk of progressive disease determines if a given patient is a candidate for pharmacologic treatment. Treatment options may be further stratified based on the severity or activity of the extrapulmonary manifestations of SSc.

Conceptual framework for the management of SSc-ILD

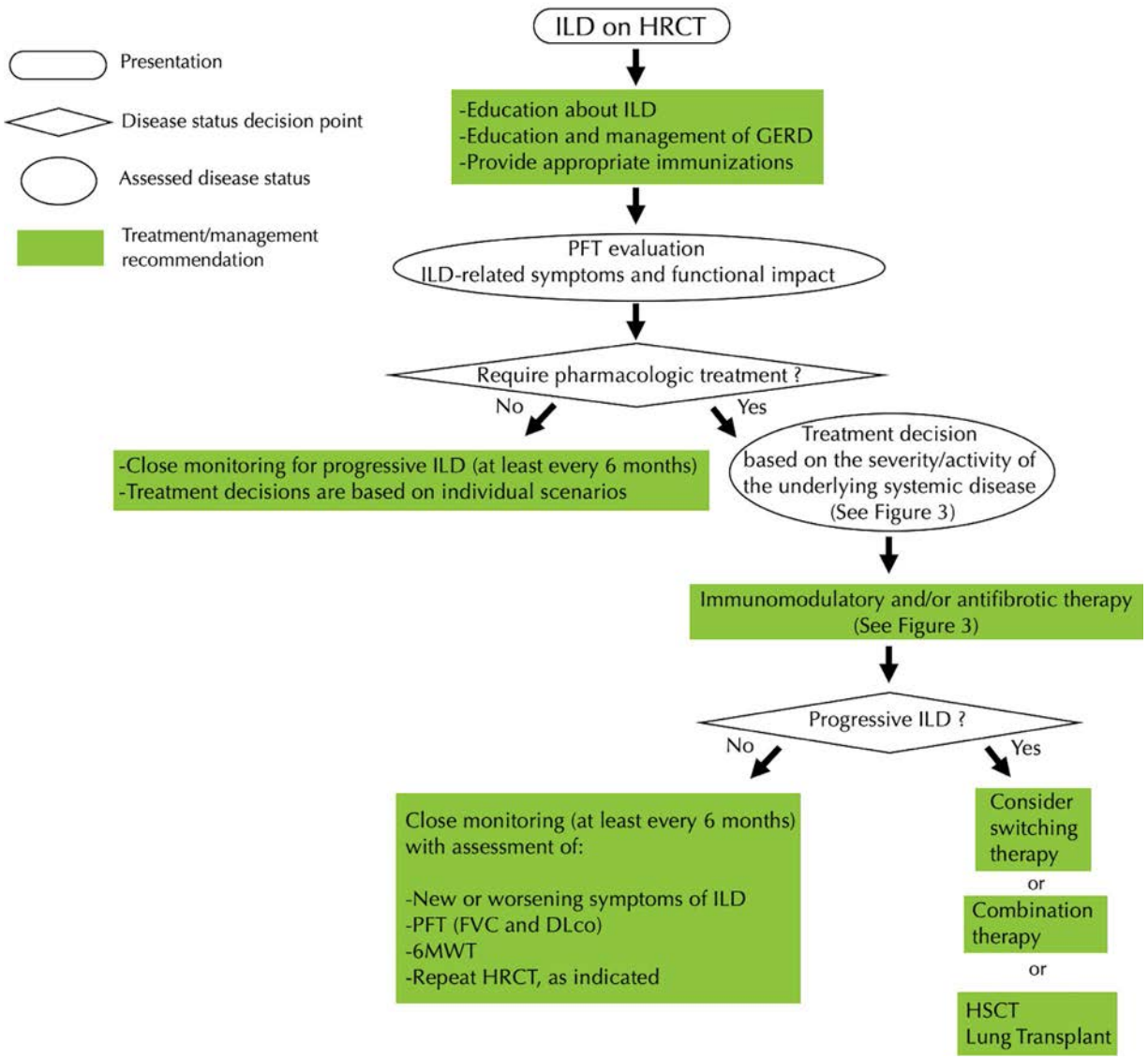
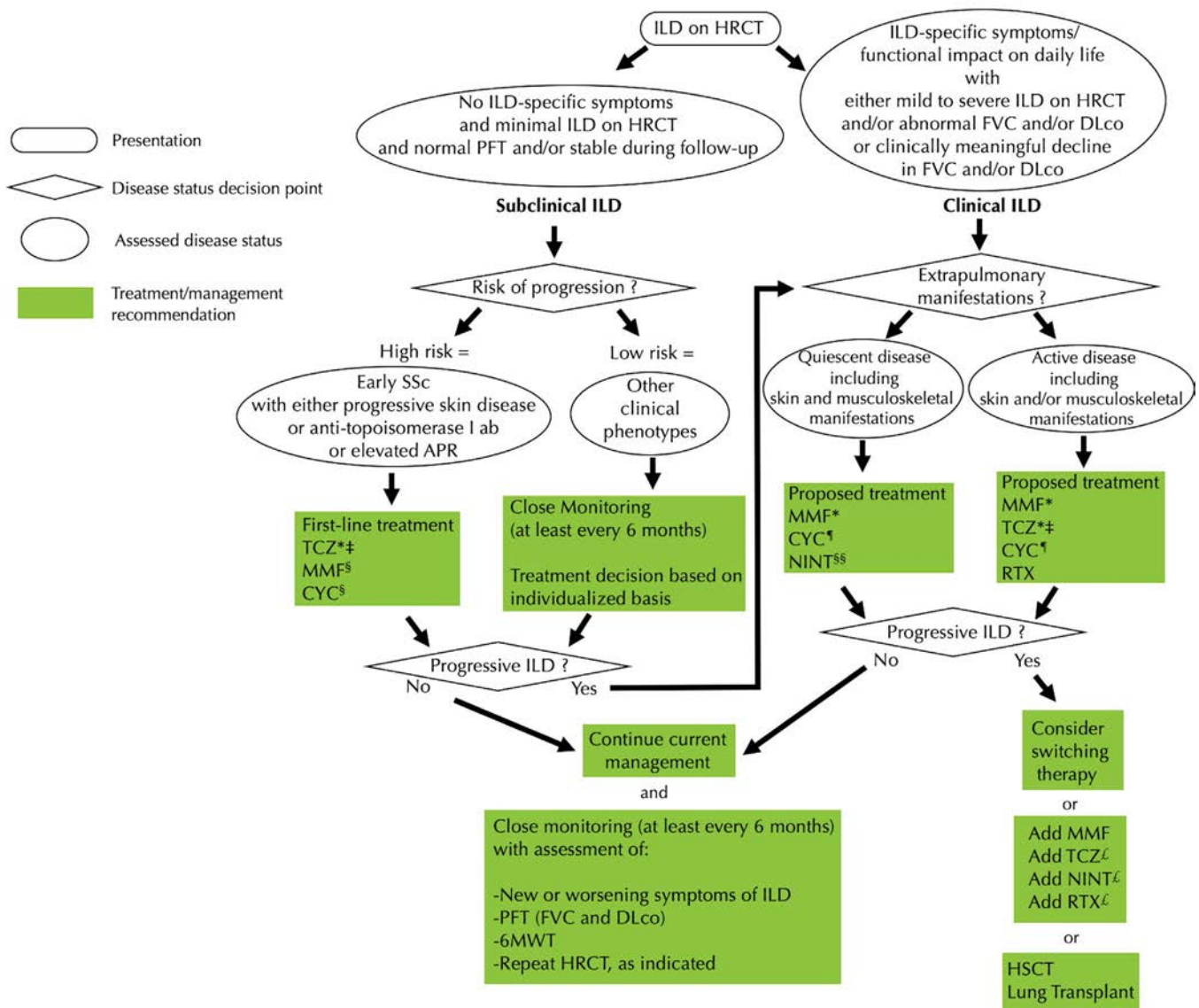


Figure 2. Conceptual framework for the management of systemic sclerosis-associated interstitial lung disease (SSc-ILD). HRCT = high-resolution computed tomography; GERD = gastroesophageal reflux disease; PFT = pulmonary function test; FVC = forced vital capacity; DLco = diffusing capacity for carbon monoxide; 6MWT = 6-minute walk test; HSCT = hematopoietic stem cell transplantation.

Expert opinion on the management of SSc-ILD



*Initial preference.

‡TCZ has only been evaluated in early active dcSSc, no specific data available in early lcSSc.

§ Based on expert opinion and extrapolation of the data from SLS I and SLS II.

§§ Although nintedanib was shown to be superior to placebo in a Phase 3 trial, there were no beneficial effects on skin, musculoskeletal and quality of life.

† Although CYC has two RCTs in SSc-ILD, the toxicity precludes us for advocating it as first line treatment.

£No data supporting combined therapy of two biologic DMARDs or Tyrosine kinase inhibitor with biologic DMARDs.

Figure 3. Expert opinion on the management of systemic sclerosis–associated interstitial lung disease (SSc-ILD). HRCT = high-resolution computed tomography; PFT = pulmonary function test; FVC = forced vital capacity; DLco = diffusing capacity for carbon monoxide; ab = antibody; APR = acute-phase reactants; TCZ = tocilizumab; MMF = mycophenolate mofetil; CYC = cyclophosphamide; NINT = nintedanib; RTX = rituximab; 6MWT = 6-minute walk test; HSCT = hematopoietic stem cell transplantation; dcSSc = diffuse cutaneous SSc; lcSSc = limited cutaneous SSc; SLS I = Scleroderma Lung Study I; RCTs = randomized controlled trials; DMARDs = disease-modifying antirheumatic drugs.

Nonpharmacologic measures. All patients should be educated about ILD, symptom monitoring, and nonpharmacologic management. Nonpharmacologic treatments include receipt of appropriate vaccinations such as influenza, pneumococcal, and COVID vaccines; pulmonary rehabilitation; and

oxygen therapy if indicated. Pulmonary rehabilitation should be offered to those patients with SSc-ILD in whom dyspnea and other aspects of ILD are limiting functional capacity (76). Oxygen therapy should be considered in cases of hypoxemia ($SpO_2 < 88\%$). The 6-minute walk test is useful to evaluate

cardiopulmonary exercise desaturation that would require oxygen therapy.

Patients should be educated about silent aspiration; optimal care of gastroesophageal reflux disease should be undertaken with early initiation of proton-pump inhibitors. Any inhalation of recreational drugs such as tobacco, marijuana, vaping, and other products should be discontinued. Recent studies have highlighted the importance of fostering a good nutritional status to maintain respiratory function in chronic respiratory disorders, especially in patients with gastrointestinal symptoms (77–79). Annual screening for immunosuppressant-induced nonmelanoma skin cancers is also recommended.

Pharmacologic treatment. Data emerging from the recent RCTs of tocilizumab suggest that early treatment with immunomodulatory agents should be considered for patients with subclinical ILD with a high risk of progression (i.e., early SSc with progressive skin disease, or antitopoisomerase antibody, or elevated acute-phase reactants). Tocilizumab may be proposed as initial treatment based on phase II and III trials; patients should be advised to administer the weekly subcutaneous injections in parts of the body spared from or minimally involved with skin thickening, typically the upper, outer/posterior region of the arm (21,80). MMF and CYC remain alternative options, although they lack RCT data in the context of subclinical ILD. In patients with subclinical ILD and a low risk of progression, close monitoring of PFT every 6 months in early SSc is needed, and case-by-case treatment decisions may be considered.

As mentioned above, all patients with clinical ILD should be considered for immunomodulatory treatment (15,35). In the case of quiescent skin and musculoskeletal manifestations, MMF is the preferred initial treatment from the authors' perspective, with CYC and nintedanib as other acceptable first-line options that might be considered. In the case of active disease including skin and/or musculoskeletal manifestations, tocilizumab, CYC, or MMF should be introduced, considering their effects on extrapulmonary manifestations in focuSSced, SLS I, and SLS II, respectively. Rituximab may also be an option, although we usually reserve it for second-line treatment given the absence of randomized double-blind controlled trials for this drug in SSc-ILD (Figure 3). Upfront combination of nintedanib with MMF in patients with active extrapulmonary and rapidly progressive disease is also acceptable first-line therapy (such patients may also be candidates for autologous HSCT). We do not recommend nintedanib alone as first-line therapy in patients with SSc-ILD with active extrapulmonary disease, given the absence of impact on these manifestations in SENSICIS (63).

After treatment initiation, clinical monitoring of FVC and DL_{CO} at least every 6 months is recommended, although in those with progressive ILD, we may consider monitoring FVC and DL_{CO} every 4 months until stabilization is documented (58). In the case of stabilization, first-line treatment should be continued. In the case of worsening respiratory symptoms, other diagnoses, such

as cardiac involvement or pulmonary vascular disease, should be explored. If worsening parenchymal disease is suspected, a repeat HRCT should be performed to confirm progression of ILD. In the event of advancing disease despite first-line therapy, a second-line therapeutic strategy should be employed.

Three main options are proposed as second-line therapeutic strategies (Figure 3): 1) switching to another treatment, 2) considering combination of an immunomodulatory agent with an antifibrotic agent or combining 2 immunomodulatory agents (e.g., MMF and tocilizumab, or MMF and rituximab; although there are no data supporting the efficacy and/or safety of these combination therapies), and 3) considering HSCT. Lung transplant is usually reserved for those with progressive ILD despite trials of different therapies and requires referral to a lung transplant center.

Long-term management. The follow-up of patients from SLS I, SLS II, and the CYC arm of SCOT has suggested that the benefit of immunomodulation was not maintained after discontinuation of the immunomodulatory agent (68,81,82). Although the optimal duration of treatment has not been determined to date, we would recommend at least 5 years of treatment, although many patients need longer-term treatment. This duration should take into account the initial severity of ILD, the evaluation and stabilization of ILD-related symptoms, the extrapulmonary manifestations of SSc, and the risk of ILD progression/relapse once the treatment is stopped. In our practice, ~20–30% of patients experience relapse of skin and/or lung involvement once immunomodulatory therapy is discontinued. To date, there are no clinical data to support dose adjustments, such as decreased MMF dosage, after stabilization of the disease. Lower dosage may limit the risk of long-term side effects, including risk of malignancy, but such adjustments should be based on individual patient preferences and should take into account the initial severity and subsequent impact of progression in case of relapse. As an example, a patient with moderate ILD and FVC% of 70% may have adequate pulmonary reserve to consider dose down-titration but someone with an FVC% of 40% who requires supplemental O₂ therapy would likely not be an appropriate candidate for medication down-titration.

In the case of stabilization on treatment, and/or after treatment discontinuation, PFT should continue to be performed at least every 6 months in all SSc patients for 1–2 years. After this period of close monitoring, all patients should undergo annual PFT, as late progression may occur despite long-term stabilization. Screening for other visceral manifestations, especially PAH, should also be continued according to published screening algorithms (59).

Perspectives on the early introduction of combination therapies and new combinations

Recent RCTs in PAH have demonstrated that substantial progress could be obtained through an early combination of existing drugs (83,84). The combination of biologic disease-modifying

antirheumatic drugs (bDMARDs) with conventional DMARDs (cDMARDs) is widely used and recommended for the treatment of extrapulmonary manifestations in other CTDs, such as rheumatoid arthritis. The complex and overlapping pathobiology involved in SSc-ILD, which involves inflammation, fibrosis, and vascular changes, also supports the potential for combination therapies, as does the finding that a diverse range of drugs has clinical utility. As such, there are many reasons to consider combination therapy as a viable approach for treating SSc-ILD.

The combination of MMF and nintedanib demonstrated a reasonable safety profile in SENSICIS, although the benefit of the combination of the 2 active drugs compared to monotherapy alone could not be fully demonstrated in that trial (63). In the focuSSced trial, patients taking cDMARDs were excluded, precluding any conclusion regarding the safety or efficacy of tocilizumab in combination with MMF or methotrexate (21). Nonetheless, with their differing mechanisms of action, MMF and tocilizumab may have complementary effects (85). However, we need additional data to assess for tradeoffs between the efficacy and safety of this combination. The efficacy and safety of the combination of a biologic such as tocilizumab with a tyrosine kinase inhibitor such as nintedanib is still to be determined. This combination may be especially relevant considering the anti-inflammatory properties of tocilizumab and the potential more specific antifibrotic effects of nintedanib through PDGF and FGF receptor inhibition, as well as its potential impact on vasculopathy through VEGF receptor inhibition (28). The ongoing SLS III (ClinicalTrials.gov identifier: NCT03221257) is investigating the impact of pirfenidone, another antifibrotic agent indicated for the treatment of idiopathic pulmonary fibrosis, as an upfront combination treatment with MMF versus placebo and MMF in patients with SSc-ILD (86).

Conclusions

The current review provides a state-of-the-art practical overview of the management of SSc-ILD. As therapeutic options expand, expert perspective remains an important source of treatment guidance. The recent addition of 2 FDA-approved medications for SSc-ILD has broadened the cache of available treatments; management should be determined by stratifying patients in terms of disease severity, risk of progression, and activity of extrapulmonary disease. Patients with subclinical ILD and a high risk of progression should be provided therapy to prevent lung function loss; tocilizumab has demonstrated benefit in those with a high risk of progression. As shown in the focuSSced trial, early ILD is not necessarily mild ILD. Tocilizumab is effective in attenuating lung function loss along a wide spectrum of lung involvement on HRCT, suggesting it can be utilized in clinical ILD with a spectrum of degree of underlying lung involvement. Nintedanib can be considered as first-line therapy in SSc-ILD but preferentially in those with limited extrapulmonary disease (a rare

scenario in early SSc) or as part of upfront combination therapy for progressive SSc-ILD in patients who are candidates for HSCT.

Immunosuppressive therapy with MMF should also be considered as a primary treatment approach for clinical ILD and particularly in those with other active manifestations. In this setting, MMF has the potential to improve pulmonary function over time in the majority of patients and is similarly active with respect to improvements over time in skin disease, dyspnea, and health-related quality of life (87). Current immunomodulatory and antifibrotic interventions attenuate the impact of SSc-ILD but have yet to demonstrate a long-lasting benefit on how patients feel, function, or survive. Further questions of upfront or sequential combination therapy with immunosuppressives and antifibrotics, or addition of bDMARDs, as done in other rheumatic diseases, remain areas of further research.

AUTHOR CONTRIBUTIONS

All authors drafted the article, revised it critically for important intellectual content, and approved the final version to be published.

REFERENCES

- Denton CP, Khanna D. Systemic sclerosis [review]. *Lancet* 2017; 390:1685–99.
- Frantz C, Avouac J, Distler O, Amrouche F, Godard D, Kennedy AT, et al. Impaired quality of life in systemic sclerosis and patient perception of the disease: a large international survey. *Semin Arthritis Rheum* 2016;46:115–23.
- LeRoy EC, Black C, Fleischmajer R, Jablonska S, Krieg T, Medsger TA, et al. Scleroderma (systemic sclerosis): classification, subsets and pathogenesis. *J Rheumatol* 1988;15:202–5.
- LeRoy EC, Medsger TA. Criteria for the classification of early systemic sclerosis [review]. *J Rheumatol* 2001;28:1573–6.
- Domsic RT, Medsger TA. Autoantibodies and their role in scleroderma clinical care. *Curr Treatm Opt Rheumatol* 2016;2:239–51.
- Nihtyanova SI, Sari A, Harvey JC, Leslie A, Derrett-Smith EC, Fonseca C, et al. Using autoantibodies and cutaneous subset to develop outcome-based disease classification in systemic sclerosis. *Arthritis Rheumatol* 2020;72:465–76.
- Coghlan JG, Denton CP, Grünig E, Bonderman D, Distler O, Khanna D, et al. Evidence-based detection of pulmonary arterial hypertension in systemic sclerosis: the DETECT study. *Ann Rheum Dis* 2014;73:1340–9.
- Chan EK, Damoiseaux J, Carballo OG, Conrad K, de Melo Cruvinel W, Francescantonio PL, et al. Report of the first international consensus on standardized nomenclature of antinuclear antibody HEp-2 cell patterns 2014–2015 [review]. *Front Immunol* 2015;6:412.
- Khanna D, Tashkin DP, Denton CP, Renzoni EA, Desai SR, Varga J. Etiology, risk factors, and biomarkers in systemic sclerosis with interstitial lung disease. *Am J Respir Crit Care Med* 2020;201:650–60.
- Elhai M, Meune C, Boubaya M, Avouac J, Hachulla E, Balbir-Gurman A, et al. Mapping and predicting mortality from systemic sclerosis. *Ann Rheum Dis* 2017;76:1897–905.
- Meyer OC, Fertig N, Lucas M, Somogyi N, Medsger TA. Disease subsets, antinuclear antibody profile, and clinical features in 127 French and 247 US adult patients with systemic sclerosis. *J Rheumatol* 2007;34:104–9.
- Bernstein EJ, Jaafar S, Assassi S, Domsic RT, Frech TM, Gordon JK, et al. Performance characteristics of pulmonary function tests

- for the detection of interstitial lung disease in adults with early diffuse cutaneous systemic sclerosis. *Arthritis Rheumatol* 2020;72:1892–6.
13. Hoffmann-Vold AM, Molberg Ø, Midtvedt Ø, Garen T, Gran JT. Survival and causes of death in an unselected and complete cohort of Norwegian patients with systemic sclerosis. *J Rheumatol* 2013;40:1127–33.
 14. Dougherty DH, Kwakkenbos L, Carrier ME, Salazar G, Assassi S, Baron M, et al. The Scleroderma Patient-Centered Intervention Network Cohort: baseline clinical features and comparison with other large scleroderma cohorts. *Rheumatology (Oxford)* 2018;57:1623–31.
 15. Roofeh D, Distler O, Allanore Y, Denton CP, Khanna D. Treatment of systemic sclerosis-associated interstitial lung disease: lessons from clinical trials. *J Scleroderma Relat Disord* 2020;5:61–71.
 16. Tashkin DP, Elashoff R, Clements PJ, Goldin J, Roth MD, Furst DE, et al. Cyclophosphamide versus placebo in scleroderma lung disease. *N Engl J Med* 2006;354:2655–66.
 17. Tashkin DP, Roth MD, Clements PJ, Furst DE, Khanna D, Kleerup EC, et al. Mycophenolate mofetil versus oral cyclophosphamide in scleroderma-related interstitial lung disease (SLS II): a randomised controlled, double-blind, parallel group trial. *Lancet Respir Med* 2016;4:708–19.
 18. Distler O, Highland KB, Gahlemann M, Azuma A, Fischer A, Mayes MD, et al. Nintedanib for systemic sclerosis-associated interstitial lung disease. *N Engl J Med* 2019;380:2518–28.
 19. Flaherty KR, Wells AU, Cottin V, Devaraj A, Walsh SL, Inoue Y, et al. Nintedanib in progressive fibrosing interstitial lung diseases. *N Engl J Med* 2019;381:1718–27.
 20. Khanna D, Denton CP, Jahreis A, van Laar JM, Frech TM, Anderson ME, et al. Safety and efficacy of subcutaneous tocilizumab in adults with systemic sclerosis (faSScinate): a phase 2, randomised, controlled trial. *Lancet* 2016;387:2630–40.
 21. Khanna D, Lin CJ, Furst DE, Goldin J, Kim G, Kuwana M, et al. Tocilizumab in systemic sclerosis: a randomised, double-blind, placebo-controlled, phase 3 trial. *Lancet Respir Med* 2020;8:963–74.
 22. Roofeh D, Lin CJ, Goldin J, Kim GH, Furst DE, Denton CP, et al. Tocilizumab prevents progression of early systemic sclerosis-associated interstitial lung disease. *Arthritis Rheumatol* 2021;73:1301–10.
 23. Hoffmann-Vold AM, Maher TM, Philpot EE, Ashrafzadeh A, Distler O. Assessment of recent evidence for the management of patients with systemic sclerosis-associated interstitial lung disease: a systematic review. *ERJ Open Res* 2021;7:00235–2020.
 24. Volkmann ER, Varga J. Emerging targets of disease-modifying therapy for systemic sclerosis [review]. *Nat Rev Rheumatol* 2019;15:208–24.
 25. Lescoat A, Ballerie A, Augagneur Y, Morzadec C, Vernhet L, Fardel O, et al. Distinct properties of human M-CSF and GM-CSF monocyte-derived macrophages to simulate pathological lung conditions in vitro: application to systemic and inflammatory disorders with pulmonary involvement. *Int J Mol Sci* 2018;19:894.
 26. Lescoat A, Ballerie A, Jouneau S, Fardel O, Vernhet L, Jeco P, et al. M1/M2 polarisation state of M-CSF blood-derived macrophages in systemic sclerosis [editorial]. *Ann Rheum Dis* 2019;78:e127.
 27. Valenzi E, Bulik M, Tabib T, Morse C, Sembrat J, Bittar HT, et al. Single-cell analysis reveals fibroblast heterogeneity and myofibroblasts in systemic sclerosis-associated interstitial lung disease. *Ann Rheum Dis* 2019;78:1379–87.
 28. Wollin L, Wex E, Pautsch A, Schnapp G, Hostettler KE, Stowasser S, et al. Mode of action of nintedanib in the treatment of idiopathic pulmonary fibrosis [review]. *Eur Respir J* 2015;45:1434–45.
 29. Denton CP, Ong VH, Xu S, Chen-Harris H, Modrusan Z, Lafyatis R, et al. Therapeutic interleukin-6 blockade reverses transforming growth factor- β pathway activation in dermal fibroblasts: insights from the faSScinate clinical trial in systemic sclerosis. *Ann Rheum Dis* 2018;77:1362–71.
 30. Numajiri H, Kuzumi A, Fukasawa T, Ebata S, Yoshizaki-Ogawa A, Asano Y, et al. B cell depletion inhibits fibrosis via suppressing pro-fibrotic macrophage differentiation in a mouse model of systemic sclerosis. *Arthritis Rheumatol* 2021 doi: <https://doi.org/10.1002/art.41798>. E-pub ahead of print.
 31. Mauer J, Chaurasia B, Goldau J, Vogt MC, Ruud J, Nguyen KD, et al. Signaling by IL-6 promotes alternative activation of macrophages to limit endotoxemia and obesity-associated resistance to insulin. *Nat Immunol* 2014;15:423–30.
 32. Gao X, Jia G, Guttman A, DePianto DJ, Morshead KB, Sun KH, et al. Osteopontin links myeloid activation and disease progression in systemic sclerosis. *Cell Rep Med* 2020;1:100140.
 33. Petrova DT, Brandhorst G, Koch C, Schultze FC, Eberle C, Walson PD, et al. Mycophenolic acid reverses TGF β -induced cell motility, collagen matrix contraction and cell morphology in vitro. *Cell Biochem Funct* 2015;33:503–8.
 34. Allison AC, Eugui EM. Mycophenolate mofetil and its mechanisms of action [review]. *Immunopharmacology* 2000;47:85–118.
 35. Hoffmann-Vold AM, Maher TM, Philpot EE, Ashrafzadeh A, Barake R, Barsotti S, et al. The identification and management of interstitial lung disease in systemic sclerosis: evidence-based European consensus statements. *Lancet Rheumatol* 2020;2:e71–83.
 36. Roofeh D, Jaafar S, Vummidi D, Khanna D. Management of systemic sclerosis-associated interstitial lung disease [review]. *Curr Opin Rheumatol* 2019;31:241–9.
 37. Fischer A, Antoniou KM, Brown KK, Cadranel J, Corte TJ, du Bois RM, et al. An official European Respiratory Society/American Thoracic Society research statement: interstitial pneumonia with autoimmune features. *Eur Respir J* 2015;46:976–87.
 38. Raghu G, Collard HR, Egan JJ, Martinez FJ, Behr J, Brown KK, et al. An official ATS/ERS/JRS/ALAT statement: idiopathic pulmonary fibrosis: evidence-based guidelines for diagnosis and management. *Am J Respir Crit Care Med* 2011;183:788–824.
 39. Remy-Jardin M, Giraud F, Remy J, Copin MC, Gosselin B, Duhamel A. Importance of ground-glass attenuation in chronic diffuse infiltrative lung disease: pathologic-CT correlation. *Radiology* 1993;189:693–8.
 40. Takei R, Arita M, Kumagai S, Ito Y, Tokioka F, Koyama T, et al. Radiographic fibrosis score predicts survival in systemic sclerosis-associated interstitial lung disease. *Respirology* 2018;23:385–91.
 41. Bouros D, Wells AU, Nicholson AG, Colby TV, Polychronopoulos V, Pantelidis P, et al. Histopathologic subsets of fibrosing alveolitis in patients with systemic sclerosis and their relationship to outcome. *Am J Respir Crit Care Med* 2002;165:1581–6.
 42. Raghu G, Remy-Jardin M, Myers JL, Richeldi L, Ryerson CJ, Lederer DJ, et al. Diagnosis of idiopathic pulmonary fibrosis: an official ATS/ERS/JRS/ALAT clinical practice guideline. *Am J Respir Crit Care Med* 2018;198:e44–68.
 43. Kim HG, Tashkin DP, Clements PJ, Li G, Brown MS, Elashoff R, et al. A computer-aided diagnosis system for quantitative scoring of extent of lung fibrosis in scleroderma patients. *Clin Exp Rheumatol* 2010;28:S26–35.
 44. Goldin JG, Kim GH, Tseng CH, Volkmann E, Furst D, Clements P, et al. Longitudinal changes in quantitative interstitial lung disease on computed tomography after immunosuppression in the Scleroderma Lung Study II. *Ann Am Thorac Soc* 2018;15:1286–95.
 45. Goh NS, Desai SR, Veeraraghavan S, Hansell DM, Copley SJ, Maher TM, et al. Interstitial lung disease in systemic sclerosis: a simple staging system. *Am J Respir Crit Care Med* 2008;177:1248–54.
 46. Winstone TA, Assayag D, Wilcox PG, Dunne JV, Hague CJ, Leipsic J, et al. Predictors of mortality and progression in

- scleroderma-associated interstitial lung disease: a systematic review. *Chest* 2014;146:422–36.
47. Suliman YA, Dobrota R, Huscher D, Nguyen-Kim TD, Maurer B, Jordan S, et al. Pulmonary function tests: high rate of false-negative results in the early detection and screening of scleroderma-related interstitial lung disease. *Arthritis Rheumatol* 2015;67:3256–61.
 48. Holland AE, Spruit MA, Troosters T, Puhan MA, Pepin V, Saey D, et al. An official European Respiratory Society/American Thoracic Society technical standard: field walking tests in chronic respiratory disease [review]. *Eur Respir J* 2014;44:1428–46.
 49. American Thoracic Society Committee on Proficiency Standards for Clinical Pulmonary Function Laboratories. ATS statement: guidelines for the six-minute walk test. *Am J Respir Crit Care Med* 2002;166:111–17.
 50. The Criteria Committee of the New York Heart Association. Nomenclature and criteria for diagnosis of diseases of the heart and great vessels. 9th ed. Boston: Little Brown & Co; 1994:253–6.
 51. Mahler DA, Wells CK. Evaluation of clinical methods for rating dyspnea. *Chest* 1988;93:580–6.
 52. Distler O, Assassi S, Cottin V, Cutolo M, Danoff SK, Denton CP, et al. Predictors of progression in systemic sclerosis patients with interstitial lung disease [review]. *Eur Respir J* 2020;55:1902026.
 53. Liu X, Mayes MD, Pedroza C, Draeger HT, Gonzalez EB, Harper BE, et al. Does C-reactive protein predict the long-term progression of interstitial lung disease and survival in patients with early systemic sclerosis? *Arthritis Care Res (Hoboken)* 2013;65:1375–80.
 54. Nihtyanova SI, Schreiber BE, Ong VH, Rosenberg D, Moinzadeh P, Coghlan JG, et al. Prediction of pulmonary complications and long-term survival in systemic sclerosis. *Arthritis Rheumatol* 2014;66:1625–35.
 55. Stock CJ, Hoyles RK, Daccord C, Kokosi M, Visca D, De Lauretis A, et al. Serum markers of pulmonary epithelial damage in systemic sclerosis-associated interstitial lung disease and disease progression. *Respirology* 2021;26:461–8.
 56. Salazar GA, Kuwana M, Wu M, Estrada-Y-Martin RM, Ying J, Charles J, et al. KL-6 but not CCL-18 is a predictor of early progression in systemic sclerosis-related interstitial lung disease. *J Rheumatol* 2018;45:1153–8.
 57. Jaeger VK, Valentini G, Hachulla E, Cozzi F, Distler O, Airó P, et al. Smoking in systemic sclerosis: a longitudinal European Scleroderma Trials and Research group study. *Arthritis Rheumatol* 2018;70:1829–34.
 58. Roofeh D, Khanna D. Management of systemic sclerosis: the first five years [review]. *Curr Opin Rheumatol* 2020;32:228–37.
 59. Young A, Moles VM, Jaafar S, Visovatti S, Huang S, Vummidi D, et al. Performance of the DETECT algorithm for pulmonary hypertension screening in a systemic sclerosis cohort. *Arthritis Rheumatol* 2021;73:1731–7.
 60. Kim GH, Tashkin DP, Lo P, Brown MS, Volkman ER, Gjerdtson DW, et al. Using transitional changes on high-resolution computed tomography to monitor the impact of cyclophosphamide or mycophenolate mofetil on systemic sclerosis-related interstitial lung disease. *Arthritis Rheumatol* 2020;72:316–25.
 61. Namas R, Tashkin DP, Furst DE, Wilhalme H, Tseng CH, Roth MD, et al. Efficacy of mycophenolate mofetil and oral cyclophosphamide on skin thickness: post hoc analyses from two randomized placebo-controlled trials. *Arthritis Care Res (Hoboken)* 2018;70:439–44.
 62. Jaafar S, Lescoat A, Huang S, Gordon J, Hinchcliff M, Shah AA, et al. Clinical characteristics, visceral involvement, and mortality in at-risk or early diffuse systemic sclerosis: a longitudinal analysis of an observational prospective multicenter US cohort. *Arthritis Res Ther* 2021;23:170.
 63. Highland KB, Distler O, Kuwana M, Allanore Y, Assassi S, Azuma A, et al. Efficacy and safety of nintedanib in patients with systemic sclerosis-associated interstitial lung disease treated with mycophenolate: a subgroup analysis of the SENSICIS trial. *Lancet Respir Med* 2021;9:96–106.
 64. Khanna D, Spino C, Johnson S, Chung L, Whitfield ML, Denton CP, et al. Abatacept in early diffuse cutaneous systemic sclerosis: results of a phase II investigator-initiated, multicenter, double-blind, randomized, placebo-controlled trial. *Arthritis Rheumatol* 2020;72:125–36.
 65. Chung L, Spino C, McLain R, Johnson SR, Denton CP, Molitor JA, et al. Safety and efficacy of abatacept in early diffuse cutaneous systemic sclerosis (ASSET): open-label extension of a phase 2, double-blind randomised trial. *Lancet Rheumatol* 2020;2:e743–53.
 66. Sircar G, Goswami RP, Sircar D, Ghosh A, Ghosh P. Intravenous cyclophosphamide vs rituximab for the treatment of early diffuse scleroderma lung disease: open label, randomized, controlled trial. *Rheumatology (Oxford)* 2018;57:2106–13.
 67. Ebata S, Yoshizaki A, Oba K, Kashiwabara K, Ueda K, Uemura Y, et al. Safety and efficacy of rituximab in systemic sclerosis (DESIREs): a double-blind, investigator-initiated, randomised, placebo-controlled trial. *Lancet Rheumatol* 2021;3:E489–97.
 68. Sullivan KM, Goldmuntz EA, Keyes-Elstein L, McSweeney PA, Pinckney A, Welch B, et al. Myeloablative autologous stem-cell transplantation for severe scleroderma. *N Engl J Med* 2018;378:35–47.
 69. Launay D, Marjanovic Z, de Bazelaire C, Florea L, Zohar S, Keshtmand H, et al. Autologous hematopoietic stem cell transplant in systemic sclerosis: quantitative high resolution computed tomography of the chest scoring. *J Rheumatol* 2009;36:1460–3.
 70. Roofeh D, Lescoat A, Khanna D. Treatment for systemic sclerosis-associated interstitial lung disease. *Curr Opin Rheumatol* 2021;33:240–8.
 71. Bernstein EJ, Peterson ER, Sell JL, D'Ovidio F, Arcasoy SM, Bathon JM, et al. Survival of adults with systemic sclerosis following lung transplantation: a nationwide cohort study. *Arthritis Rheumatol* 2015;67:1314–22.
 72. Weill D, Benden C, Corris PA, Dark JH, Davis RD, Keshavjee S, et al. A consensus document for the selection of lung transplant candidates: 2014—an update from the Pulmonary Transplantation Council of the International Society for Heart and Lung Transplantation. *J Heart Lung Transplant* 2015;34:1–15.
 73. Jablonski R, Dematte J, Bhorade S. Lung transplantation in scleroderma: recent advances and lessons [review]. *Curr Opin Rheumatol* 2018;30:562–9.
 74. Quanjer PH, Stanojevic S, Cole TJ, Baur X, Hall GL, Culver BH, et al. Multi-ethnic reference values for spirometry for the 3–95-yr age range: the global lung function 2012 equations. *Eur Respir J* 2012;40:1324–43.
 75. Khanna D, Denton CP. Integrating new therapies for systemic sclerosis-associated lung fibrosis in clinical practice. *Lancet Respir Med* 2021;9:560–2.
 76. Dowman LM, McDonald CF, Hill CJ, Lee AL, Barker K, Boote C, et al. The evidence of benefits of exercise training in interstitial lung disease: a randomised controlled trial. *Thorax* 2017;72:610–9.
 77. Nakayama K, Nakajima Y, Tanaka R, Hirata KI, Emoto N. Predictors of long-term outcomes in patients with connective tissue disease associated with pulmonary arterial hypertension. *J Clin Rheumatol* 2020. doi: <https://doi.org/10.1097/RHU.0000000000001447>. E-pub ahead of print.
 78. Kanjrawi AA, Mathers L, Webster S, Corte TJ, Carey S. Nutritional status and quality of life in interstitial lung disease: a prospective cohort study. *BMC Pulm Med* 2021;21:51.
 79. Jouneau S, Crestani B, Thibault R, Lederlin M, Vernhet L, Valenzuela C, et al. Analysis of body mass index, weight loss and progression of idiopathic pulmonary fibrosis. *Respir Res* 2020;21:312.
 80. Suleman Y, Clark KE, Cole AR, Ong VH, Denton CP. Real-world experience of tocilizumab in systemic sclerosis: potential benefit on lung

- function for anti-topoisomerase-positive patients. *Rheumatology (Oxford)* 2021;60:3945–6.
81. Khanna D, Furst DE, Clements PJ, Tashkin DP, Eckman MH. Oral cyclophosphamide for active scleroderma lung disease: a decision analysis. *Med Decis Making* 2008;28:926–37.
82. Volkmann ER, Tashkin DP, Sim M, Li N, Goldmuntz E, Keyes-Elstein L, et al. Short-term progression of interstitial lung disease in systemic sclerosis predicts long-term survival in two independent clinical trial cohorts. *Ann Rheum Dis* 2019;78:122–30.
83. Lajoie AC, Lauzière G, Lega JC, Lacasse Y, Martin S, Simard S, et al. Combination therapy versus monotherapy for pulmonary arterial hypertension: a meta-analysis [review]. *Lancet Respir Med* 2016;4:291–305.
84. Khanna D, Zhao C, Saggarr R, Mathai SC, Chung L, Coghlan JG, et al. Long-term outcomes in patients with connective tissue disease-associated pulmonary arterial hypertension in the modern treatment era: meta-analyses of randomized, controlled trials and observational registries. *Arthritis Rheumatol* 2021;73:837–47.
85. Chandran S, Leung J, Hu C, Laszik ZG, Tang Q, Vincenti FG. Interleukin-6 blockade with tocilizumab increases Tregs and reduces T effector cytokines in renal graft inflammation: a randomized controlled trial. *Am J Transplant* 2020;21:2543–54.
86. Khanna D, Albera C, Fischer A, Khalidi N, Raghu G, Chung L, et al. An open-label, phase II study of the safety and tolerability of pirfenidone in patients with scleroderma-associated interstitial lung disease: the LOTUSS trial. *J Rheumatol* 2016;43:1672–9.
87. Volkmann ER, Tashkin DP, LeClair H, Roth MD, Kim G, Goldin J, et al. Treatment with mycophenolate and cyclophosphamide leads to clinically meaningful improvements in patient-reported outcomes in scleroderma lung disease: results of Scleroderma Lung Study II. *ACR Open Rheumatol* 2020;2:362–70.

BRIEF REPORT

Disease Flare and Reactogenicity in Patients With Rheumatic and Musculoskeletal Diseases Following Two-Dose SARS–CoV-2 Messenger RNA Vaccination

Caoilfhionn M. Connolly,  Jake A. Ruddy,  Brian J. Boyarsky, Iulia Barbur, William A. Werbel, Duvuru Geetha,  Jacqueline M. Garonzik-Wang, Dorry L. Segev, Lisa Christopher-Stine,  and Julie J. Paik 

Objective. To evaluate disease flare and postvaccination reactions (reactogenicity) in patients with rheumatic and musculoskeletal diseases (RMDs) following 2-dose SARS–CoV-2 messenger RNA (mRNA) vaccination.

Methods. RMD patients ($n = 1,377$) who received 2-dose SARS–CoV-2 mRNA vaccination between December 16, 2020 and April 15, 2021 completed questionnaires detailing local and systemic reactions experienced within 7 days of each vaccine dose (dose 1 and dose 2), and 1 month after dose 2, detailing any flares of RMD. Associations between demographic/clinical characteristics and flares requiring treatment were evaluated using modified Poisson regression.

Results. Among the patients, 11% reported flares requiring treatment; there were no reports of severe flares. Flares were associated with prior SARS–CoV-2 infection (incidence rate ratio [IRR] 2.09, $P = 0.02$), flares in the 6 months preceding vaccination (IRR 2.36, $P < 0.001$), and the use of combination immunomodulatory therapy (IRR 1.95, $P < 0.001$). The most frequently reported local and systemic reactions included injection site pain (87% after dose 1, 86% after dose 2) and fatigue (60% after dose 1, 80% after dose 2). Reactogenicity increased after dose 2, particularly for systemic reactions. No allergic reactions or SARS–CoV-2 diagnoses were reported.

Conclusion. Flares of underlying RMD following SARS–CoV-2 vaccination were uncommon. There were no reports of severe flares. Local and systemic reactions typically did not interfere with daily activity. These early safety data can help address vaccine hesitancy in RMD patients.

INTRODUCTION

Since its emergence in December 2019, SARS–CoV-2 has spread worldwide, with an estimated 115 million infections and 5.6 million hospitalizations in the US alone at the time of this report (1). In December 2020, 2 messenger RNA (mRNA)-based COVID-19 vaccines (mRNA-1273 and BNT162b2) were recommended for use by the Advisory Committee on Immunization Practices (2), with >260 million doses administered in the US to date (3). Predicted vaccination uptake of 70–80% is required to

significantly reduce community transmission (4), and addressing vaccine hesitancy is crucial to achieving this goal.

In clinical trials of the SARS–CoV-2 mRNA vaccines, participants reported local and systemic postvaccination reactions (reactogenicity), with greater reactogenicity reported following dose 2 (5,6). Patients with rheumatic and musculoskeletal diseases (RMDs) were not well represented in these trials, and despite the significant morbidity and mortality associated with SARS–CoV-2 infection, studies have shown that many RMD patients remain hesitant about getting vaccinated due to

The analyses described here are the responsibility of the authors alone and do not necessarily reflect the views or policies of the Department of Health and Human Services, nor does mention of trade names, commercial products, or organizations imply endorsement by the US Government.

This work was supported by the Ben-Dov family. Drs. Boyarsky and Garonzik-Wang's work was supported by the National Institute of Diabetes and Digestive and Kidney Diseases, NIH (grants F32-DK-124941 and K23-DK-115908, respectively). Dr. Segev's work was supported by the National Institute of Allergy and Infectious Diseases, NIH (grant K24-AI-144954). Dr. Paik's work was supported by the National Institute of Arthritis and Musculoskeletal and Skin Diseases, NIH (grant K23-AR-073927).

Caoilfhionn M. Connolly, MD, MSc, Jake A. Ruddy, BS, Brian J. Boyarsky, MD, PhD, Iulia Barbur, BSE, William A. Werbel, MD, Duvuru Geetha, MBBS,

Jacqueline M. Garonzik-Wang, MD, PhD, Dorry L. Segev, MD, PhD, Lisa Christopher-Stine, MD, MPH, Julie J. Paik, MD, MHS: Johns Hopkins University, Baltimore, Maryland.

Dr. Connolly and Mr. Ruddy contributed equally to this work.

Author disclosures are available at <https://onlinelibrary.wiley.com/action/downloadSupplement?doi=10.1002%2Fart.41924&file=art41924-sup-0005-Disclosureform.pdf>.

Address correspondence to Julie J. Paik, MD, MHS, Division of Rheumatology, Johns Hopkins University School of Medicine, 5200 Eastern Avenue, Mason F. Lord Building, Center Tower Suite 4100, Baltimore, MD 21224. Email: jpaik@jhmi.edu.

Submitted for publication May 26, 2021; accepted in revised form July 8, 2021.

concerns related to the risk of disease flare (7,8). We previously reported that local and systemic reactions following dose 1 were typically mild (9), but there is a paucity of data on reactions or flares following dose 2. Thus, we sought to evaluate disease flare and reactogenicity in RMD patients following 2-dose SARS-CoV-2 mRNA vaccination.

PATIENTS AND METHODS

Study design and population. We conducted a prospective observational study of RMD patients who received the SARS-CoV-2 mRNA vaccine between December 16, 2020 and April 15, 2021. Patients ages ≥ 18 years with a self-reported diagnosis of RMD who were receiving immunomodulatory therapy were recruited to participate via social media postings by national RMD organizations and advocacy groups. Participants

consented electronically, and the study was approved by the Institutional Review Board at the Johns Hopkins School of Medicine (IRB00248540).

Surveys. Participants first completed an English-language enrollment form containing questions regarding demographic characteristics (age, sex, and race), RMD diagnosis, immunomodulatory regimen, and prior SARS-CoV-2 diagnosis (Supplementary Materials, available on the *Arthritis & Rheumatology* website at <https://onlinelibrary.wiley.com/doi/10.1002/art.41924>). An online questionnaire was distributed 7 days after each vaccine (dose 1 and dose 2), in which participants answered solicited questions about local and systemic adverse events. The questionnaire also allowed participants to enter free-text information about their postvaccination experience and adverse health events. Local symptoms such as pain,

Table 1. Demographic and clinical characteristics of the patients with rheumatic and musculoskeletal diseases, stratified by disease flare requiring treatment or no flare after SARS-CoV-2 mRNA vaccination*

	Overall (n = 1,377)	Disease flare (n = 151)	No disease flare (n = 1,226)	P†
Age, median (IQR) years	47 (37–59)	46 (36–57)	47 (37–60)	0.2
Female sex‡	1,266 (92)	144 (95)	1,122 (92)	0.1
Non-White‡	130 (10)	8 (5)	122 (10)	0.1
Diagnosis				
Inflammatory arthritis§	647 (47)	73 (48)	574 (47)	0.7
SLE	273 (20)	30 (20)	243 (20)	>0.9
Sjögren's syndrome	65 (5)	7 (5)	58 (5)	>0.9
Myositis	66 (5)	6 (4)	60 (5)	0.8
Vasculitis	41 (3)	7 (5)	34 (3)	0.2
Scleroderma	14 (1)	2 (1)	12 (1)	0.7
Overlap CTD¶	271 (20)	26 (17)	245 (20)	0.5
Vaccine type				
BNT162b2	755 (55)	82 (54)	673 (55)	0.9
mRNA-1273	622 (45)	69 (46)	553 (45)	0.9
Therapy type				
Conventional DMARD#	352 (26)	23 (15)	329 (27)	0.002
Biologic**	303 (22)	22 (15)	281 (23)	0.02
Glucocorticoid monotherapy††	35 (3)	6 (4)	29 (2)	0.3
Immunomodulatory monotherapy‡‡	6 (0.4)	1 (1)	5 (0.4)	–
Combination§§	681 (50)	99 (66)	582 (48)	<0.001
Flare in 6 months prior to vaccine	767 (56)	113 (75)	654 (53)	<0.001
Prior COVID-19 diagnosis	50 (3)	11 (7)	39 (3)	0.02

* Flares counted include those that occurred between dose 1 of the SARS-CoV-2 mRNA vaccine up to 1 month after dose 2. Except where indicated otherwise, values are the number (%) of patients. IQR = interquartile range; SLE = systemic lupus erythematosus.

† For comparisons between groups of patients who experienced disease flares and those who did not, categories with an overall count of <10 were not analyzed.

‡ Denominators for these categories differ from the total number, as 1 participant selected “prefer not to answer” for sex, and 23 selected “prefer not to answer” for race.

§ Includes rheumatoid arthritis, ankylosing spondylitis, psoriatic arthritis, reactive arthritis, and inflammatory bowel disease-associated arthritis.

¶ Overlap connective tissue disease (CTD) denotes a combination of ≥ 2 of the above conditions.

Includes azathioprine, hydroxychloroquine, leflunomide, methotrexate, mycophenolate, sulfasalazine, and tacrolimus.

** Includes abatacept, adalimumab, anakinra, baricitinib, belimumab, certolizumab, etanercept, golimumab, infliximab, ixekizumab, rituximab, secukinumab, tocilizumab, tofacitinib, upadacitinib, and ustekinumab.

†† Includes prednisone and prednisone equivalents.

‡‡ P values for intravenous immunoglobulin and subcutaneous immunoglobulin were not calculated due to small sample size.

§§ Denotes conventional disease-modifying antirheumatic drug (DMARD) and biologic drug and/or glucocorticoids, or biologic drug and glucocorticoids.

redness, and swelling, as well as systemic adverse events including fever, fatigue, headaches, chills, vomiting, diarrhea, and myalgia were captured using an ordinal scale; these were graded according to their impact on daily activity including “no interference with daily activity,” “some interference with daily activity,” and “prevention of daily activity.” One month after dose 2, participants completed an online questionnaire pertaining to incidence and prior history of flare, incident flare, as well as symptoms, duration, and treatment. Most questions were in multiple-choice format, and some allowed for an open-ended response if participants felt that no given choice was appropriate. Study data were collected and managed using the REDCap tool, a secure, web-based software platform designed to support data capture for research studies (10).

Statistical analysis. Baseline demographic and clinical characteristics were evaluated using descriptive statistics, stratified by disease flare after vaccination requiring treatment. Binary and categorical variables are expressed as the number and percentage and continuous variables with the median and interquartile range (IQR). Associations between flares requiring treatment and participant characteristics were evaluated with modified Poisson regression with a robust variance estimator, generating incidence rate ratios (IRRs) and 95% confidence intervals (95% CIs). Associations were not calculated for variables with a frequency of <10 patients. Changes in denominators of questions due to participants selecting “prefer not to answer” or not responding are noted in the footnotes of the corresponding tables, as are questions with a multiple-select format for which the sum of responses may exceed the total number. All tests were conducted using a 2-sided α level of 0.05. We performed analyses using Stata software, version 16.1.

RESULTS

Baseline characteristics. A total of 1,377 patients with RMD underwent vaccination with BNT162b2 (55%) or mRNA-1273 (45%) (Table 1). The median (IQR) age was 47 years (37–59 years), with 92% of the patients female and 10% Non-White. The most common RMD diagnoses included inflammatory arthritis (47%), systemic lupus erythematosus (SLE; 20%), and overlap connective tissue disease (20%). The most common therapeutic regimens included combination therapy (50%), conventional disease-modifying antirheumatic drugs (cDMARDs) (26%), and biologic therapy (22%). Combination therapy was defined as treatment with a cDMARD and biologic agent, with or without glucocorticoids, or a biologic agent and glucocorticoid therapy. Three percent of patients reported a prior SARS-CoV-2 infection.

Incidence and characteristics of flares requiring treatment. Of the participants, 767 (56%) reported ≥ 1 flare of their underlying RMD in the 6 months preceding dose

1. One hundred fifty-one patients (11%) reported flares requiring treatment following vaccination, of which the majority (60%) occurred after dose 2 (Supplementary Table 1, <https://onlinelibrary.wiley.com/doi/10.1002/art.41924>). The rate of flares requiring treatment was similar in both vaccine types. Most patients (91%) reported worsening of preexisting symptoms, while 72% reported the onset of a new symptom (Supplementary Figure 1, <https://onlinelibrary.wiley.com/doi/10.1002/art.41924>). Patients with inflammatory arthritis more commonly reported symptoms of worsening joint pain, swelling, and stiffness, while patients with SLE reported worsening joint pain, fatigue, and myalgia (Supplementary Table 2, <https://onlinelibrary.wiley.com/doi/10.1002/art.41924>). Flares that required treatment typically lasted 10 days (IQR 6–22 days) and were most commonly treated with oral glucocorticoids (75%), while 23% of participants reported up-titration of their baseline immunomodulatory therapy. No participant required hospital or intensive care unit admission. Factors found to be

Table 2. Adjusted IRR for experiencing a flare requiring treatment, according to demographic and clinical characteristics*

	Adjusted IRR (95% CI)	<i>P</i>
Age, >55 years	0.79 (0.57–1.11)	0.2
Female sex	1.79 (0.86–3.72)	0.1
White	1.86 (0.93–3.7)	0.1
BNT162b2 vaccine	0.98 (0.72–1.32)	0.9
Flare in 6 months prior to vaccine	2.36 (1.66–3.36)	<0.001
Prior SARS-CoV-2 diagnosis	2.09 (1.21–3.60)	0.008
Diagnosis		
Inflammatory arthritis†	1.06 (0.78–1.43)	0.7
SLE	1.00 (0.69–1.46)	>0.9
Sjögren's syndrome	0.98 (0.48–2.00)	>0.9
Myositis	0.82 (0.38–1.79)	0.6
Vasculitis	1.58 (0.79–3.17)	0.2
Systemic sclerosis	1.31 (0.36–4.76)	0.7
Overlap CTD‡	0.85 (0.57–1.27)	0.4
Therapy type		
Conventional DMARD§	0.52 (0.34–0.80)	0.003
Biologic¶	0.60 (0.39–0.93)	0.02
Glucocorticoid monotherapy#	1.59 (0.75–3.34)	0.2
Immunoregulatory monotherapy**	–	–
Combination††	1.95 (1.41–2.68)	<0.001

* IRR = incidence rate ratio; 95% CI = 95% confidence interval (see Table 1 for other definitions).

† Includes rheumatoid arthritis, ankylosing spondylitis, psoriatic arthritis, reactive arthritis, and inflammatory bowel disease-associated arthritis.

‡ Overlap CTD denotes a combination of ≥ 2 of the above conditions. § Includes azathioprine, hydroxychloroquine, leflunomide, methotrexate, mycophenolate, sulfasalazine, and tacrolimus.

¶ Includes abatacept, adalimumab, anakinra, baricitinib, belimumab, certolizumab, etanercept, golimumab, infliximab, ixekizumab, rituximab, secukinumab, tocilizumab, tofacitinib, upadacitinib, and ustekinumab.

Includes prednisone and prednisone equivalents.

** *P* values for intravenous immunoglobulin and subcutaneous immunoglobulin were not calculated due to small sample size.

†† Denotes conventional DMARD and biologic drug and/or glucocorticoids, or biologic drug and glucocorticoids.

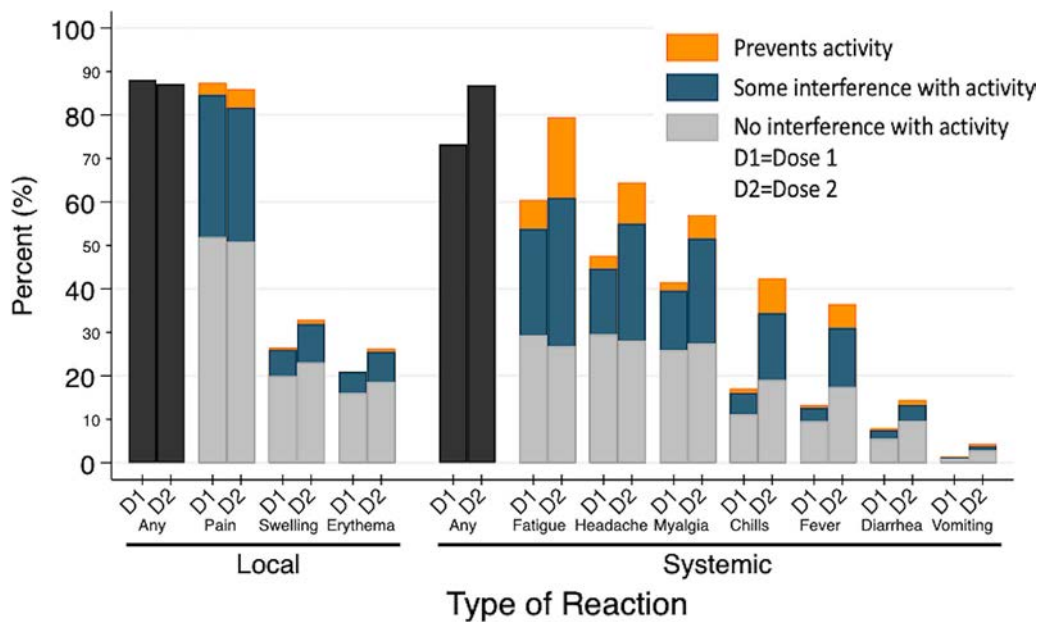


Figure 1. Local site and systemic adverse reactions in 1,377 patients with rheumatic and musculoskeletal diseases within 7 days after doses 1 and 2 of SARS-CoV-2 mRNA vaccination.

associated with flares requiring treatment included a prior SARS-CoV-2 diagnosis (IRR 2.09 [95% CI 1.21–3.60]), a history of flares in the 6 months prior to dose 1 (IRR 2.36 [95% CI 1.66–3.36]), and use of combination therapy (IRR 1.95 [95% CI 1.41–2.68]) (Table 2). Participants receiving cDMARDs (IRR 0.52 [95% CI 0.34–0.80]) or biologic therapy (IRR 0.60 [95% CI 0.39–0.93]) had a lower incidence of flares.

Local and systemic reactogenicity. The most frequently reported local and systemic reactions included injection site pain (87% after dose 1, 86% after dose 2) and fatigue (60% after dose 1, 80% after dose 2) (Figure 1). Reactogenicity increased after dose 2, particularly for systemic reactions, including fatigue (80%), headache (65%), myalgia (58%), and chills (42%). Reports of reactions that prevented daily activities were uncommon, with myalgia (11%) and fatigue (19%) most frequently reported. One patient (0.07%) reported hospital admission for management of diarrhea following dose 2.

DISCUSSION

We studied 1,377 RMD patients who received 2-dose SARS-CoV-2 mRNA vaccinations and did not identify any major safety concerns. There were no reports of severe disease flare. Local and systemic reactions were common, but these were consistent with expected vaccine reactogenicity.

Eleven percent of participants reported flares of their underlying disease that required treatment. No participant required intravenous therapy or hospitalization. Use of combination therapy, as well as reports of flare in the 6 months prior to vaccination were associated

with flares; these factors may be a surrogate for more refractory disease at baseline, and thus the relationship with vaccination is unclear. There was a positive association between prior SARS-CoV-2 infection and flare, which may suggest immunologic priming.

Local and systemic reactions were common, but reassuringly, very few patients reported symptoms that prevented daily activities. Participants reported systemic events (particularly myalgia and fatigue) at higher frequencies than in clinical trials; similar to the trials, reactogenicity increased after dose 2 (5,6). One patient reported hospitalization for management of a systemic event. There were no reported cases of anaphylaxis requiring epinephrine or newly diagnosed SARS-CoV-2 infection.

Limitations of this study include a lack of data on immunomodulatory timing and dosing. We did not assess baseline disease activity, and background rate of flare was not quantified. Most participants were female and white, which may limit generalizability.

The strengths of this study include a national sample with early, novel information about adverse reactions after 2-dose BNT162b2 and mRNA-1273 vaccinations. All data were patient-reported; this is a strength, but given that recruitment was conducted by convenience sampling, the data are also susceptible to responder bias.

Data on vaccine safety in patients with RMD have been lacking, which has contributed to vaccine refusal and hesitancy. It has been shown that RMD patients are more willing to reconsider vaccination if provided with more medical education and recommended by a physician (9). While there are case reports of flares following mRNA vaccination (11,12), this is the first large-scale study evaluating flares and reactogenicity in patients with RMDs. Local and systemic reactions should be anticipated, and setting expectations with patients may alleviate anxiety. This is

particularly relevant given that periodic revaccination may be required in the future (13). These early, reassuring results may ameliorate concern among patients and inform critical discussions regarding vaccine hesitancy or refusal.

In conclusion, in this observational study of 1,377 RMD patients, there were no reports of severe disease flare. Local and systemic reactions were common but typically did not interfere with daily activity. There were no findings that warranted concern about the safety of SARS-CoV-2 mRNA vaccination in patients with RMD. These early data can continue to address vaccine hesitancy in this patient population.

AUTHOR CONTRIBUTIONS

All authors were involved in drafting the article or revising it critically for important intellectual content, and all authors approved the final version to be published. Dr. Connolly had full access to all of the data in the study and takes responsibility for the integrity of the data and the accuracy of the data analysis.

Study conception and design. Boyarsky, Werbel, Garonzik-Wang, Segev.

Acquisition of data. Ruddy, Boyarsky.

Analysis and interpretation of data. Connolly, Ruddy, Barbur, Geetha, Christopher-Stine, Paik.

REFERENCES

- Centers for Disease Control and Prevention. Estimated disease burden of COVID-19. URL: <https://www.cdc.gov/coronavirus/2019-ncov/cases-updates/burden.html>.
- Oliver SE, Gargano JW, Marin M, Wallace M, Curran K, Chamberland M, et al. The Advisory Committee on Immunization Practices' interim recommendation for use of Moderna COVID-19 vaccine: United States, December 2020. *MMWR Morb Mortal Wkly Rep* 2021;69:1653–6.
- Centers for Disease Control and Prevention. Trends in number of COVID-19 vaccinations in the US. URL: <https://covid.cdc.gov/covid-data-tracker/#vaccination-trends>.
- Anderson RM, Vegvari C, Truscott J, Collyer BS. Challenges in creating herd immunity to SARS-CoV-2 infection by mass vaccination. *Lancet* 2020;396:1614–6.
- Polack F, Thomas S, Kitchin N, Absalon J, Gurtman J, Lockhart S, et al. Safety and efficacy of the BNT162b2 mRNA Covid-19 vaccine. *N Engl J Med* 2020;383:2603–15.
- Baden L, El Sahly H, Essink B, Kotloff K, Frey S, Novak R, et al. Efficacy and safety of the mRNA-1273 SARS-CoV-2 Vaccine. *N Engl J Med* 2021;384:403–16.
- Priori R, Pellegrino G, Colafrancesco S, Alessandri C, Ceccarelli F, Di France M, et al. SARS-CoV-2 vaccine hesitancy among patients with rheumatic and musculoskeletal diseases: a message for rheumatologists. *Ann Rheum Dis* 2021;80:956–4.
- Felten R, Dubois M, Ugarte-Gil MF, Chaudier A, Kawka L, Bergier H, et al. Vaccination against COVID-19: expectations and concerns of patients with autoimmune and rheumatic diseases. *Lancet Rheumatol* 2021;3:e243–5.
- Connolly CM, Ruddy JA, Boyarsky BJ, Avery RK, Werbel WA, Segev DL, et al. Safety of the first dose of mRNA SARS-CoV-2 vaccines in patients with rheumatic and musculoskeletal diseases. *Ann Rheum Dis* 2021 doi: <https://doi.org/10.1136/annrheumdis-2021-220231>. E-pub ahead of print.
- Harris PA, Taylor R, Thielke R, Payne J, Gonzalez N, Conde JG. Research electronic data capture (REDCap): a metadata-driven methodology and workflow process for providing translational research informatics support. *J Biomed Inform* 2009;42:377–81.
- Terracina KA, Tan FK. Flare of rheumatoid arthritis after COVID-19 vaccination. *Lancet Rheumatol* 2021;3:e469–70.
- Perrot L, Hemon M, Busnel JM, Muis-Pistor O, Picard C, Zandotti C, et al. First flare of ACPA-positive rheumatoid arthritis after SARS-CoV-2 infection. *Lancet Rheumatol* 2021;3:e6–8.
- Skegg D, Gluckman P, Boulton G, Hackmann H, Karim SS, Piot P, et al. Future scenarios for the COVID-19 pandemic. *Lancet* 2021; 397:777–8.

BRIEF REPORT

Humoral and Cellular Immune Responses to SARS-CoV-2 Infection and Vaccination in Autoimmune Disease Patients With B Cell Depletion

David Simon,¹  Koray Tascilar,¹ Katja Schmidt,¹ Bernhard Manger,¹ Leonie Weckwerth,¹ Maria Sokolova,¹  Laura Bucci,¹ Filippo Fagni,¹  Karin Manger,² Florian Schuch,³ Monika Ronneberger,³ Axel Hueber,¹ Ulrike Steffen,¹ Dirk Mielenz,¹ Martin Herrmann,¹ Thomas Harrer,¹ Arnd Kleyer,¹  Gerhard Krönke,¹ and Georg Schett¹ 

Objective. B cell depletion is an established therapeutic principle in a wide range of autoimmune diseases. However, B cells are also critical for inducing protective immunity after infection and vaccination. We undertook this study to assess humoral and cellular immune responses after infection with or vaccination against SARS-CoV-2 in patients with B cell depletion and controls who are B cell-competent.

Methods. Antibody responses (tested using enzyme-linked immunosorbent assay) and T cell responses (tested using interferon- γ enzyme-linked immunospot assay) against the SARS-CoV-2 spike S1 and nucleocapsid proteins were assessed in a limited number of previously infected ($n = 6$) and vaccinated ($n = 8$) autoimmune disease patients with B cell depletion, as well as previously infected ($n = 30$) and vaccinated ($n = 30$) healthy controls.

Results. As expected, B cell and T cell responses to the nucleocapsid protein were observed only after infection, while respective responses to SARS-CoV-2 spike S1 were found after both infection and vaccination. A SARS-CoV-2 antibody response was observed in all vaccinated controls (30 of 30 [100%]) but in none of the vaccinated patients with B cell depletion (0 of 8). In contrast, after SARS-CoV-2 infection, both the patients with B cell depletion (spike S1, 5 of 6 [83%]; nucleocapsid, 3 of 6 [50%]) and healthy controls (spike S1, 28 of 30 [93%]; nucleocapsid, 28 of 30 [93%]) developed antibodies. T cell responses against the spike S1 and nucleocapsid proteins were found in both infected and vaccinated patients with B cell depletion and in the controls.

Conclusion. These data show that B cell depletion completely blocks humoral but not T cell SARS-CoV-2 vaccination response. Furthermore, limited humoral immune responses are found after SARS-CoV-2 infection in patients with B cell depletion.

INTRODUCTION

Depletion of B cells is an effective therapeutic strategy to treat severe autoimmune disease (1). Diseases with robust activation of B cells and plasma cells, such as rheumatoid arthritis (2), multiple

sclerosis (3), granulomatosis with polyangiitis (4), dermatomyositis (5), IgG4-related disease (6), pemphigus (7), and immune thrombocytopenic purpura (8) are sensitive to B cell targeting. Rituximab, a monoclonal antibody binding the B cell-specific surface molecule CD20, effectively depletes circulating B cells over

Supported by the DFG (grant FOR2886 PANDORA and the CRC1181 Checkpoints for Resolution of Inflammation), the BMBF project MASCARA, the Bavarian State Ministry for Science and Art, the European Research Council Synergy grant 4D Nanoscope, the Innovated Medicines Initiative projects RTCure and Hippocrates, the Emerging Fields Initiative MIRACLE of the Friedrich-Alexander University Erlangen-Nuremberg, and the Else Kröner Memorial Scholarship (grant 2019_EKMS.27 to Dr. Simon).

¹David Simon, MD, Koray Tascilar, MD, Katja Schmidt, PhD, Bernhard Manger, MD, Leonie Weckwerth, Maria Sokolova, MD, Laura Bucci, MD, Filippo Fagni, MD, Axel Hueber, MD, PhD, Ulrike Steffen, PhD, Dirk Mielenz, PhD, Martin Herrmann, PhD, Thomas Harrer, MD, Arnd Kleyer, MD, Gerhard Krönke, MD, Georg Schett, MD: Deutsches Zentrum Immuntherapie, Friedrich-Alexander University Erlangen-Nuremberg, and University Hospital

Erlangen, Erlangen, Germany; ²Karin Manger, MD: Rheumatology Practice Bamberg, Bamberg, Germany; ³Florian Schuch, MD, Monika Ronneberger, MD: Rheumatology Practice Erlangen, Erlangen, Germany.

Author disclosures are available at <https://onlinelibrary.wiley.com/action/downloadSupplement?doi=10.1002%2Fart.41914&file=art41914-sup-0001-Disclosureform.pdf>.

Drs. Simon and Tascilar contributed equally to this work.

Address correspondence to Georg Schett, MD, Department of Internal Medicine 3-Rheumatology and Immunology, Friedrich-Alexander University Erlangen-Nuremberg and Universitätsklinikum Erlangen, Ulmenweg 18, 91054 Erlangen, Germany. Email: georg.schett@uk-erlangen.de.

Submitted for publication April 25, 2021; accepted in revised form June 29, 2021.

a period of several months and shows widespread therapeutic efficacy in patients with autoimmune disease (9). B cell depletion, however, may also seriously impair the development of protective immunity after infection and vaccination. Of note, rituximab treatment has been associated with more severe courses of COVID-19 (10) and impaired immune response to established vaccines (11,12). To date, reliable data on the impact of B cell depletion on the dynamics of protective antibody responses upon infection and vaccination remain sparse (13), while protective antibody responses have been clearly documented in subjects naive to SARS-CoV-2 infection (14) and previously infected immunocompetent subjects (15). The current SARS-CoV-2 pandemic thus provides a unique opportunity to profile the immune response of a naive population to a defined infectious agent. In addition, it allows us to study the magnitude of a newly evolving adaptive immune response to infection and to vaccination in both healthy individuals and in patients with B cell depletion.

PATIENTS AND METHODS

Ethical approval. Ethical approval (no. 157_20 B) to conduct this analysis was granted by the institutional review board of the University Clinic of Erlangen as the responsible ethics committee. Written informed consent was obtained from the study participants.

Patients and controls. Sera from rituximab-treated patients and healthy controls were collected within the COVID-19 study program of the Deutsche Zentrum fuer Immuntherapie (16). This study program was initiated in February 2020 and monitors anti-SARS-CoV-2 antibody responses in healthy controls, COVID-19 patients, and patients with autoimmune diseases (16). Healthy controls did not have an immune-mediated inflammatory disease nor did they receive any treatment with immunomodulatory agents. Vaccinated patients and vaccinated healthy controls did not have any history of COVID-19 or positive COVID-19 polymerase chain reaction results before the analysis.

Rituximab-treated patients and healthy controls were vaccinated with the BNT162b2 messenger RNA (mRNA) SARS-CoV-2 vaccine at official public vaccination centers, based on occupational exposure risk, comorbidities, and age-related risk in accordance with the recommendations of the Robert Koch Institute. Sera were collected ≥ 10 days after the second vaccination and ≥ 30 days after onset of infection in the infected participants. For all participants, we collected demographic data (e.g., age, sex) as well as disease-specific data (e.g., type of autoimmune disease, type of treatment). The elapsed time between antibody testing and either infection (mean \pm SD 3.8 ± 2.9 months [range 1–8 months]) or vaccination (mean \pm SD 3.6 ± 3.0 months [range 1–8 months]) was very similar among the rituximab-treated patients. Patients underwent a mean \pm SD of 5.4 ± 4.3 rituximab infusions, administered at a dose of 1,000 mg every 6 months.

Anti-SARS-CoV-2 antibodies. IgG antibodies against the S1 domain of the spike protein and the nucleocapsid protein of SARS-CoV-2 were tested by 2 Conformité Européenne commercial enzyme-linked immunosorbent assays, according to the protocols of the manufacturers (Euroimmun; Epitope Diagnostics). Optical density (OD) was determined at 450 nm, with a reference wavelength at 630 nm. Cutoffs of <0.8 and <0.2 were considered as negative for IgG antibodies against the spike S1 protein and the nucleocapsid protein, respectively. An in-house neutralization assay for assessment of inhibition of binding to angiotensin-converting enzyme 2 by antibodies was used. Assays were performed in accordance with the guidelines of the German Medical Association with stipulated internal and external quality controls.

Anti-SARS-CoV-2 T cells. The detection of SARS-CoV-2-specific T cells was conducted via an interferon- γ (IFN γ) enzyme-linked immunospot (ELISpot) assay (T-SPOT.COVID; Oxford Immunotec). Isolation of peripheral blood mononuclear cells (PBMCs) was carried out via density-gradient centrifugation. Leucosep tubes (Greiner Bio-One) were filled with 15 ml Lymphoflot (Bio-Rad) and centrifuged briefly to collect the fluid under the membrane. A maximum of 30 ml citrate blood was transferred to the tube and filled up to 50 ml with RPMI 1640 medium (Gibco) that was preheated to 37°C. Cells were centrifuged at 760g for 20 minutes, and the upper layer containing PBMCs was transferred to 50-ml tubes and centrifuged at 610g for 10 minutes. The cell pellet was then washed with 30 ml of RPMI 1640 medium (at 37°C) at 610g for 10 minutes prior to resuspension at a concentration of 2.5×10^6 /ml in AIM-V medium (Gibco) that was preheated to 37°C.

Fifty microliters of either AIM-V medium, Panel A, Panel B, or Positive Control were added to the wells of the precoated multi-titer ELISpot plate (Oxford Immunotec). One hundred microliters of the cell suspension was added to each well and carefully mixed by pipetting. After an incubation period at 37°C with 7% CO₂ for 16–20 hours, the wells were washed 4 times with 200 μ l of phosphate buffered saline (PBS; Gibco). The conjugate reagent was diluted at 1:200 in PBS, and 50 μ l of this dilution was added to each well. Following a 60-minute incubation period at 4°C, the wells were washed 4 times with 200 μ l of PBS. Fifty microliters of substrate solution was added to each well and incubated for 7 minutes. The plate was washed 3 times with H₂O and then air-dried. The spots were counted and analyzed using an ELISpot reader (AID). Results are reported as spot-forming units (SFUs) per 2.5×10^5 cells. According to the manufacturer's guidelines, a response was considered positive when the number of spots in the respective panel was ≥ 8 SFUs above the negative control. Samples with negative controls >10 SFUs were considered invalid.

Statistical analysis. Subject characteristics are presented as the mean \pm SD for continuous data and as the number and percentage for categorical data. We used Wilcoxon's rank sum test for pairwise between-group comparisons of OD from the

anti-spike S1 IgG and anti-nucleocapsid IgG assays. *P* values were adjusted for a family of 6 possible pairwise comparisons per assay using the Bonferroni-Holm method and were considered significant when less than 0.05.

RESULTS

To address the question of whether autoimmune patients in whom peripheral B cells have been depleted are able to develop specific humoral immunity to SARS-CoV-2 vaccination, we screened data from an ongoing longitudinal SARS-CoV-2 antibody study in Germany which measures IgG responses against the SARS-CoV-2 spike S1 and nucleocapsid proteins in patients with autoimmune inflammatory diseases and healthy controls (16). We identified 8 rituximab-treated patients who received the BNT162b2 mRNA SARS-CoV-2 vaccine and 6 rituximab-treated patients who had experienced a clinically symptomatic, mRNA-confirmed infection with SARS-CoV-2. The most frequent COVID-19 related symptoms in the 6 rituximab-treated patients with SARS-CoV-2 infection were cough (*n* = 5), anosmia (*n* = 5), fever (*n* = 4), and dyspnea (*n* = 4). Three patients required hospitalization, and none of them required intensive care. The characteristics of patients and controls are summarized in Table 1.

All 14 rituximab-treated vaccinated or infected patients were tested for anti-SARS-CoV-2 IgG antibodies after having received their second shot of the vaccine or ≥ 4 weeks after the infection, respectively. For control purposes, anti-SARS-CoV-2 IgG antibodies were also tested in 30 healthy controls after SARS-CoV-2 vaccination and in 30 additional healthy controls after SARS-CoV-2 infection. The majority of SARS-CoV-2-infected controls

(93%) developed IgG antibodies against the spike S1 protein (mean \pm SD 5.4 \pm 2.5 at an OD of 450 nm; cutoff for positivity >0.8 at an OD of 450 nm) and all vaccinated controls (100%) developed IgG antibodies against the spike S1 protein (mean \pm SD 8.1 \pm 2.5) (Figure 1A). As expected, IgG antibodies against the nucleocapsid protein were observed only in previously infected controls (mean \pm SD 0.31 \pm 0.09; cutoff for positivity >0.2) but not in vaccinated controls (mean \pm SD 0.10 \pm 0.04).

Although anti-SARS-CoV-2 S1 IgG levels were lower than those in healthy controls, surprisingly, 5 of 6 rituximab-treated SARS-CoV-2-infected patients (83.3%) developed IgG antibodies (mean \pm SD 2.9 \pm 2.2) (Figure 1A). These antibodies in rituximab-treated infected patients also had a similar neutralizing capacity as those in infected controls. In contrast, none of the 8 vaccinated rituximab-treated patients developed anti-SARS-CoV-2 IgG antibodies (mean \pm SD 0.2 \pm 0.3). The mean elapsed time to antibody testing was similar among rituximab-treated patients who had been previously infected (mean \pm SD 3.8 \pm 2.9 months [range 1–8 months]) and those who had been vaccinated (mean \pm SD 3.6 \pm 3.0 months [range 1–8 months]). In addition, the time interval between the last rituximab infusion and infection/vaccination was comparable (infection, mean \pm SD 2.9 \pm 3.8 months; vaccination, mean \pm SD 3.1 \pm 3.7 months).

Peripheral B cells were undetectable or lower than 15 cells/ μ l in all infected and vaccinated patients. Peripheral CD4 and CD8 T cell counts as well as serum levels of IgG, IgA, and IgM did not differ between rituximab-treated patients who previously had a SARS-CoV-2 infection and those who had been vaccinated (Figure 1B). We were also able to assess SARS-CoV-2-specific T cell responses using an IFN γ

Table 1. Characteristics of the autoimmune disease patients with B cell depletion and healthy controls*

	Healthy controls, previously infected (n = 30)	Healthy controls, vaccinated (n = 30)	Patients with B cell depletion, previously infected (n = 6)	Patients with B cell depletion, vaccinated (n = 8)
Age, mean \pm SD years	61.0 \pm 16.6	57.1 \pm 7.5	62.5 \pm 12.8	53.5 \pm 7.7
Female sex	12 (40.0)	23 (76.7)	5 (83.3)	5 (62.5)
Humoral immune response				
Anti-spike S1 IgG, mean \pm SD OD	5.4 \pm 2.5	8.1 \pm 2.5	2.9 \pm 2.2	0.2 \pm 0.3
Anti-spike S1 IgG, OD >0.8	28 (93.3)	30 (100.0)	5 (83.3)	0 (0)
Anti-nucleocapsid IgG, mean \pm SD OD \dagger	0.31 \pm 0.09	0.10 \pm 0.04	0.18 \pm 0.09	0.09 \pm 0.02
Anti-nucleocapsid IgG, OD >0.2 \dagger	28 (93.3)	0 (0)	3 (50.0)	0 (0)
Cellular immune response				
Anti-spike S1 IFN γ >3 SFUs, no. positive/no. tested (%)	4/5 (80)	5/5 (100.0)	6/6 (100.0)	6/8 (75)
Anti-nucleocapsid IFN γ >5 SFUs, no. positive/no. tested (%)	5/5 (100)	0/5 (0)	5/6 (83.3)	0/8 (0)
Disease				
Granulomatosis with polyangiitis	–	–	2 (33.3)	3 (37.5)
Rheumatoid arthritis	–	–	3 (50.0)	3 (37.5)
Multiple sclerosis	–	–	0 (0)	1 (12.5)
Dermatomyositis	–	–	0 (0)	1 (12.5)
IgG4-related disease	–	–	1 (16.7)	0 (0)

* Except where indicated otherwise, values are the number (%) of subjects. IFN γ = interferon- γ ; SFUs = spot-forming units.

\dagger Anti-nucleocapsid IgG was only measured in 6 of the 8 vaccinated patients with B cell depletion.

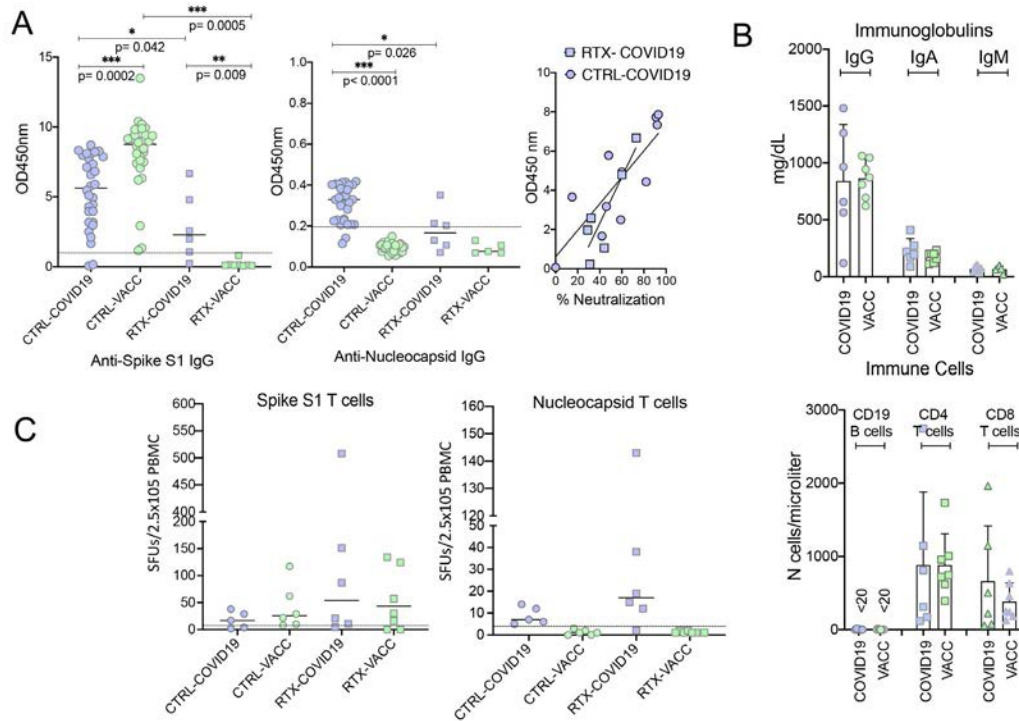


Figure 1. Anti-SARS-CoV-2 immune responses in previously infected patients and vaccinated patients who have undergone B cell depletion. **A**, Antibodies against the spike S1 protein of SARS-CoV-2 (assessed by enzyme-linked immunosorbent assay [ELISA]; Euroimmun) (left) and nucleocapsid protein of SARS-CoV-2 (assessed by ELISA; Epitope) (middle), and correlation between neutralizing antibody activity (percent inhibition of binding of spike S1 protein-expressing cells to angiotensin-converting enzyme 2) and the spike S1 protein antibody response (OD at 450 nm) (right). Tests were performed in 30 healthy controls after SARS-CoV-2 infection (CTRL-COVID-19), 30 healthy controls after SARS-CoV-2 mRNA vaccination (CTRL-VACC), 6 rituximab-treated, B cell-depleted autoimmune disease patients after SARS-CoV-2 infection (RTX-COVID19), and 8 rituximab-treated, B cell-depleted autoimmune disease patients after SARS-CoV-2 mRNA vaccination (RTX-VACC). Symbols represent individual subjects; horizontal lines show the mean. Comparisons were conducted using Wilcoxon's signed rank sum test. **B**, Serum levels of IgG, IgA, and IgM (top) and numbers of CD19 B cells, CD4 T cells, and CD8 T cells (bottom) in rituximab-treated, B cell-depleted autoimmune disease patients after SARS-CoV-2 infection and rituximab-treated, B cell-depleted autoimmune disease patients after SARS-CoV-2 mRNA vaccination. Symbols represent individual subjects; bars show the mean \pm SD. **C**, Enzyme-linked immunospot assay results showing T cell responses to antibodies against the spike S1 protein (left) and the nucleocapsid protein (right) in healthy controls after SARS-CoV-2 infection, healthy controls after SARS-CoV-2 mRNA vaccination, rituximab-treated B cell-depleted autoimmune disease patients after SARS-CoV-2 infection, and rituximab-treated, B cell-depleted autoimmune disease patients after SARS-CoV-2 mRNA vaccination. Symbols represent individual subjects; horizontal lines show the mean. SFUs = spot-forming units; PBMC = peripheral blood mononuclear cell.

ELISpot assay in a limited subset of the patients from each group (Figure 1C). T cell responses against both the spike S1 and nucleocapsid proteins were found after SARS-CoV-2 infection in healthy controls and patients with B cell depletion. Furthermore, the majority of vaccinated patients, including those depleted of B cells, developed a T cell response against the spike S1 protein, but (as expected) no T cell responses against the nucleocapsid protein were found in the vaccinated patients.

DISCUSSION

These data provide interesting and unexpected new insights into the immune response to infection and vaccination in patients with B cell depletion. First, they show that SARS-CoV-2 vaccination fails to trigger significant humoral immune responses in

patients with B cell depletion. This finding may suggest that vaccination should preferentially take place before a B cell-depleting treatment is started in order to mount a significant humoral immune response.

Surprisingly, and in contrast to vaccination, infection with SARS-CoV-2 triggered specific antibody responses, despite the absence of circulating B cells. Although these antibody responses were lower than those in healthy controls, this finding sheds light on the differences between vaccination and infection. While local antigen presentation and T cell and B cell activation may predominate in vaccinated individuals, infection may trigger a much more systemic adaptive immune response. Therefore, residual tissue B cells (e.g., in the bone marrow), which may escape rituximab treatment, could be sufficient to induce a humoral immune response after SARS-CoV-2 infection. Previous biopsy data in rituximab-treated patients, who

were depleted of circulating peripheral B cells, have shown that tissue B cells can escape depletion (17).

Second, our data indicate that SARS-CoV-2 vaccination, like infection, can trigger specific T cell-mediated immune responses even in the absence of peripheral B cells. Such T cell responses may explain why SARS-CoV-2 infection can still be controlled in patients with B cell depletion. In addition, the data suggest that potentially protective T cell-mediated immunity may develop after the vaccination in the absence of B cells.

A limitation of this study is the small number of patients with B cell depletion who were exposed to SARS-CoV-2 infection or vaccination. Although results were highly consistent even in this small sample, further studies will be required. Furthermore, only the BNT162b2 mRNA SARS-CoV-2 vaccine was assessed in this data set, requiring the collection of additional data from other (i.e., vector-based) vaccines. Despite these limitations, the data very consistently showed that T cell responses against SARS-CoV-2 can develop in both vaccinated and previously infected patients with B cell depletion. The data also indicate that SARS-CoV-2 infection, but not vaccination, can in principle trigger limited humoral immune responses against the virus in patients with B cell depletion, indicating that infection can reach and activate residual tissue B cells.

AUTHOR CONTRIBUTIONS

All authors were involved in drafting the article or revising it critically for important intellectual content, and all authors approved the final version to be published. Dr. Schett had full access to all of the data in the study and takes responsibility for the integrity of the data and the accuracy of the data analysis.

Study conception and design. Simon, Tascilar, Krönke, Schett.

Acquisition of data. Simon, Tascilar, Schmidt, Sokolova, Bucci, K. Manger, Schuch, Ronneberger, Hueber, Steffen, Kleyer, Schett.

Analysis and interpretation of data. Simon, Tascilar, B. Manger, Weckwerth, Fagni, Mielenz, Herrmann, Harrer, Krönke, Schett.

REFERENCES

1. Arnagai M. Modulating immunity to treat autoimmune disease. *N Engl J Med* 2016;375:1487–9.
2. Edwards JC, Szczepanski L, Szechinski J, Filipowicz-Sosnowska A, Emery P, Close DR, et al. Efficacy of B-cell-targeted therapy with rituximab in patients with rheumatoid arthritis. *N Engl J Med* 2004;350:2572–81.
3. Hauser SL, Waubant E, Arnold DL, Vollmer T, Antel J, Fox RJ, et al. B-cell depletion with rituximab in relapsing-remitting multiple sclerosis. *N Engl J Med* 2008;358:676–88.
4. Stone J, Merkel PE, Spiera R, Seo P, Langford CA, Hoffman GS, et al. Rituximab versus cyclophosphamide for ANCA-associated vasculitis. *N Engl J Med* 2010;363:221–32.
5. Oddis CV, Reed AM, Aggarwal R, Rider LG, Ascherman DP, Levesque MC, et al. Rituximab in the treatment of refractory adult and juvenile dermatomyositis and adult polymyositis: a randomized, placebo-phase trial. *Arthritis Rheum* 2013;65:314–24.
6. Khosroshahi A, Bloch DB, Deshpande V, Stone JH. Rituximab therapy leads to rapid decline of serum IgG4 levels and prompt clinical improvement in IgG4-related systemic disease. *Arthritis Rheum* 2010;62:1755–62.
7. Joly P, Mouquet H, Roujeau JC, D'Incan M, Gilbert D, Jacquot S, et al. A single cycle of rituximab for the treatment of severe pemphigus. *N Engl J Med* 2007;357:545–52.
8. Braendstrup P, Bjerrum OW, Nielsen OJ, Jensen BA, Clausen NT, Hansen PB, et al. Rituximab chimeric anti-CD20 monoclonal antibody treatment for adult refractory idiopathic thrombocytopenic purpura. *Am J Hematol* 2005;78:275–80.
9. Maloney DG, Liles TM, Czerwinski DK, Waldichuk C, Rosenberg J, Grillo-Lopez A, et al. Phase I clinical trial using escalating single-dose infusion of chimeric anti-CD20 monoclonal antibody (IDEC-C2B8) in patients with recurrent B-cell lymphoma. *Blood* 1994;84:2457–66.
10. Avouac J, Drumez E, Hachulla E, Seror R, Georgin-Lavialle S, El Mahou S, et al. Covid-19 outcomes in patients with inflammatory rheumatic and musculoskeletal diseases treated with rituximab: a cohort study. *Lancet Rheumatol* 2021;3:e419–26.
11. Nived P, Jönsson G, Settergren B, Einarsson J, Olofsson T, Jørgensen CS, et al. Prime-boost vaccination strategy enhances immunogenicity compared to single pneumococcal conjugate vaccination in patients receiving conventional DMARDs, to some extent in abatacept but not in rituximab-treated patients. *Arthritis Res Ther* 2020;22:36.
12. Nazi I, Keltou JG, Larché M, Snider DP, Heddle NM, Crowther MA, et al. The effect of rituximab on vaccine responses in patients with immune thrombocytopenia. *Blood* 2013 12;122:1946–53.
13. D'Silva KM, Serling-Boyd N, Hsu T, Sparks JA, Wallace ZS. SARS-CoV-2 antibody response after COVID-19 in patients with rheumatic disease. *Ann Rheum Dis* 2021 doi: 10.1136/annrheumdis-2020-219808. E-pub ahead of print.
14. Krammer F, Komal S, Alshammary H, Amoako AA, Awawda MH, Beach KF, et al. Antibody responses in seropositive persons after a single dose of SARS-CoV-2 mRNA vaccine. *N Engl J Med* 2021;384:1372–4.
15. Ebinger JE, Fert-Bober J, Printsev I, Wu M, Sun N, Prosko J, et al. Antibody responses to the BNT162b2 mRNA vaccine in individuals previously infected with SARS-CoV-2. *Nat Med* 2021;27:981–4.
16. Simon D, Tascilar K, Krönke G, Kleyer A, Zaiss MM, Heppt F, et al. Patients with immune-mediated inflammatory diseases receiving cytokine inhibitors have low prevalence of SARS-CoV-2 seroconversion. *Nat Commun* 2020;11:3774.
17. Ramwadhoebe TH, Van Baarsen LG, Boumans MJ, Bruijnen ST, Safy M, Berger FH, et al. Effect of rituximab treatment on T and B cell subsets in lymph node biopsies of patients with rheumatoid arthritis. *Rheumatology (Oxford)* 2019;58:1075–85.

Association of Sputum Neutrophil Extracellular Trap Subsets With IgA Anti-Citrullinated Protein Antibodies in Subjects at Risk for Rheumatoid Arthritis

Yuko Okamoto,¹ Stephanie Devoe,² Nickie Seto,³ Valerie Minarchick,² Timothy Wilson,² 
Heather M. Rothfuss,⁴ Michael P. Mohning,⁵ Jaron Arbet,² Miranda Kroehl,² Ashley Visser,²
Justin August,² Stacey M. Thomas,⁵ Laura Lenis Charry,² Chelsie Fleischer,² Marie L. Feser,²
Ashley A. Frazer-Abel,² Jill M. Norris,² Brian D. Cherrington,⁴ William J. Janssen,⁵ Mariana J. Kaplan,³ 
Kevin D. Deane,²  V. Michael Holers,²  and M. Kristen Demoruelle² 

Objective. Mechanisms leading to anti-citrullinated protein antibody (ACPA) generation in rheumatoid arthritis (RA) are hypothesized to originate in the lung. We undertook this study to understand associations between neutrophil extracellular trap (NET) formation in the lung and local ACPA generation in subjects at risk of developing RA.

Methods. Induced sputum was collected from 49 subjects at risk of developing RA, 12 patients with RA, and 18 controls. Sputum neutrophils were tested for ex vivo NET formation, and sputum-induced NET formation of control neutrophils was measured using immunofluorescence imaging. Sputum macrophages were tested for ex vivo endocytosis of apoptotic and opsonized cells. Levels of ACPA, NET remnants, and inflammatory proteins were quantified in sputum supernatant.

Results. Spontaneous citrullinated histone H3 (Cit-H3)-expressing NET formation was higher in sputum neutrophils from at-risk subjects and RA patients compared to controls (median 12%, 22%, and 0%, respectively; $P < 0.01$). In at-risk subjects, sputum IgA ACPA correlated with the percentage of neutrophils that underwent Cit-H3+ NET formation ($r = 0.49$, $P = 0.002$) and levels of Cit-H3+ NET remnants ($r = 0.70$, $P < 0.001$). Reduced endocytic capacity of sputum macrophages was found in at-risk subjects and RA patients compared to controls. Using a mediation model, we found that sputum inflammatory proteins were associated with sputum IgA ACPA through a pathway mediated by Cit-H3+ NET remnants. Sputum-induced Cit-H3+ NET formation also correlated with sputum levels of interleukin-1 β (IL-1 β), IL-6, and tumor necrosis factor in at-risk subjects, suggesting a causal relationship.

Conclusion. These data support a potential mechanism for mucosal ACPA generation in subjects at risk of developing RA, whereby inflammation leads to increased citrullinated protein-expressing NETs that promote local ACPA generation.

The content of this publication is the sole responsibility of the authors and does not represent the official views of the NIH.

Supported by the NIH (grants AR-066712, AR-076450, AI-101990, AI-101981, HL-140039, HD-090541, AR-51749, and GM-103432) and by the Intramural Research Program of the National Institute of Arthritis and Musculoskeletal and Skin Diseases, NIH (project ZIA-AR-041199).

¹Yuko Okamoto, MD: University of Colorado, Aurora, and Tokyo Women's Medical University School of Medicine, Tokyo, Japan; ²Stephanie Devoe, BS, Valerie Minarchick, PhD, Timothy Wilson, MD, Jaron Arbet, PhD, Miranda Kroehl, PhD, Ashley Visser, BS, Justin August, BS, Laura Lenis Charry, BS, Chelsie Fleischer, MA, Marie L. Feser, MPH, Ashley A. Frazer-Abel, PhD, Jill M. Norris, PhD, MPH, Kevin D. Deane, MD, PhD, V. Michael Holers, MD, M. Kristen Demoruelle, MD, PhD: University of Colorado, Aurora; ³Nickie Seto, BS, Mariana J. Kaplan, MD: National Institute of Arthritis and Musculoskeletal and Skin Diseases, NIH, Bethesda, Maryland; ⁴Heather M. Rothfuss, PhD, Brian D. Cherrington, PhD: University of Wyoming, Laramie; ⁵Michael P.

Mohning, MD, Stacey M. Thomas, BS, William J. Janssen, MD: National Jewish Health, Denver, Colorado.

Dr. Norris has received a research grant from Pfizer. Dr. Deane has received consulting fees, speaking fees, and/or honoraria from Bristol Myers Squibb and Janssen (less than \$10,000 each) and research grants from Pfizer and Janssen. Dr. Holers has received consulting fees, speaking fees, and/or honoraria from Bristol Myers Squibb, Janssen, and AdMIRx (less than \$10,000 each) and research grants from Pfizer and Janssen, and owns stock or stock options in AdMIRx. Dr. Demoruelle has received a research grant from Pfizer. No other disclosures relevant to this article were reported.

Address correspondence to M. Kristen Demoruelle, MD, PhD, 1775 Aurora Court, Mail Stop B-115, Aurora, CO 80045. Email: Kristen.Demoruelle@cuanschutz.edu.

Submitted for publication April 8, 2021; accepted in revised form August 3, 2021.

INTRODUCTION

Rheumatoid arthritis (RA) develops in multiple phases, including a “preclinical” phase of systemic autoimmunity that precedes the onset of inflammatory arthritis (IA) (1,2). Anti-citrullinated protein antibodies (ACPAs), often characterized by anti-cyclic citrullinated peptide (anti-CCP) antibodies, are a key autoantibody system in RA. ACPA can be pathogenic in RA-related arthritis models (3,4), yet it is unknown how ACPAs initially form. To study the early steps of ACPA formation, our group has focused on subjects with an elevated risk of developing RA based on familial and/or serologic RA risk factors (5–7). Herein, these subjects are described as “at risk” for RA.

While the exact mechanisms that trigger ACPA generation are unknown, data support the notion that ACPA may originate in the lung (5–11). We have previously identified anti-CCP generation in the lung using induced sputum in RA patients as well as in a portion of subjects at risk for RA (5–7). These studies also found a strong correlation between levels of ACPA and DNA–protein remnants of neutrophil extracellular traps (NETs), including DNA–myeloperoxidase (MPO) and DNA–neutrophil elastase (NE), in the sputum of subjects at risk for RA (6,7). NET formation, commonly termed NETosis, is a mechanism during which neutrophils decondense their nucleus and expel their chromatin in complex with intracellular proteins in response to various stimuli, particularly inflammation or bacteria (12). While NETosis is a common physiologic process, certain NET features have been linked to ACPA and RA (13–17). It is currently unknown whether neutrophils in the lung are inherently more prone to undergo a specific type of NETosis in RA patients or at-risk subjects, and whether citrullinated proteins expressed on NETs are associated with ACPA in the lung.

We hypothesized that ACPAs, specifically IgA ACPA, are formed in the lungs of subjects at risk for RA as the result of increased citrullinated protein-expressing NET formation. In the present study, we specifically investigated citrullinated histone H3 (Cit-H3) expression on NETs, because this molecule and physically associated factors are known to be externalized on a subset of NETs (18), can be a target of ACPA in RA (19), and can be readily identified using currently available antibodies. Importantly, understanding the early steps of ACPA generation, particularly in subjects at risk for RA, can improve the overall understanding of RA development, including the initial loss of tolerance to citrullinated self-antigens and eventual development of clinically apparent IA.

PATIENTS AND METHODS

Study subjects. Subjects were recruited from the Studies of the Etiologies of RA Lung cohort (5–7), which was designed to use induced sputum to study RA-related autoimmunity in the lung during different phases of RA development.

Subjects at risk for RA. We included 49 subjects without IA who were determined to be at risk of developing RA. We defined being at risk for RA as having a first-degree relative with RA and/or having serum ACPA positivity (CCP3.1 IgG/IgA) identified through community health fair, clinic, or research-based blood screenings. In these 49 at-risk subjects, 40 had a first-degree relative with RA (of which 10 of 40 [25%] were also seropositive for ACPA), and 9 were seropositive for ACPA without a known first-degree relative with RA.

RA patients. We included 12 patients who met the RA classification criteria based on medical chart review (20,21). All RA patients were seropositive for ACPA (CCP3.1 IgG/IgA) and were receiving disease-modifying antirheumatic drugs and/or biologics.

Healthy controls. We included 18 healthy controls who were recruited through local advertisement, did not have RA or IA, did not have a first-degree relative with RA, and were seronegative for ACPA.

Sputum collection and processing. All subjects underwent induced sputum collection with nebulized hypertonic saline (10%), as previously described (5–7). Sputum samples were immediately separated into 2 equal portions and processed separately. One portion was processed to obtain the cell-free supernatant, which included dilution with phosphate buffered saline, syringe-based mechanical homogenization, and centrifugation, followed by storage at -80°C with protease inhibitors phenylmethylsulfonyl fluoride and EDTA. Cell-free assays were performed to evaluate levels of ACPA, rheumatoid factor (RF), NET remnants, cytokines, chemokines, complement, and histone protein.

The other portion of the sputum sample was processed to obtain a cell-rich sample, which included extraction of sputum plugs with tweezers, chemical homogenization with dithiothreitol, and filtration. Mechanical homogenization was not performed on this sample. The processed cellular sample was immediately used for cell-based assays, which included *ex vivo* NET formation and macrophage endocytosis assays.

When sputum volume was adequate, all assays were performed. If sample volume was low, only 1 cell-based assay was performed. A flow chart outlining the number of subjects tested for each assay is included in Supplementary Figure 1 (available on the *Arthritis & Rheumatology* website at <http://onlinelibrary.wiley.com/doi/10.1002/art.41948/abstract>). For sputum cell-free testing, all samples with adequate volume were tested for ACPA and RF, and those with remaining volume were also tested for levels of NET remnants, cytokines/chemokines, and complement.

Study visit. Blood and sputum were collected from all subjects. At-risk and control subjects had a 66/68-count joint examination to confirm the absence of IA. Self-administered questionnaires were used to obtain demographic data and history of

smoking and lung disease. For RA subjects, the Multidimensional Health Assessment Questionnaire (MD-HAQ) (22) was completed to measure functional status.

ACPA and RF testing. Serum was tested for ACPA using enzyme-linked immunosorbent assay (ELISA) (Quanta Lite CCP3.1 IgG/IgA; Inova Diagnostics). The cutoff level for positivity was based on the manufacturer's recommendations (≥ 20 units). Sputum supernatant was tested for individual ACPA isotypes, IgG CCP and IgA CCP, using ELISA. IgG anti-CCP was measured using CCP3 (IgG; Inova) with modifications including additional dilutions of the standard curve resulting in a 7-point standard curve. IgA anti-CCP was measured using CCP3.1 (IgG/IgA; Inova) with substitution of the anti-human IgG/IgA conjugate for an anti-human IgA conjugate (horseradish peroxidase-conjugated goat anti-human IgA, no. 2050-05; Southern Biotech) and using an in-house standard curve generated from pooled RA patient serum. Sputum IgG anti-CCP and IgA anti-CCP positivity were established using a separate cohort of 100 healthy controls and setting a cutoff level for positivity at the 95th percentile. Sputum was also tested for IgA RF using ELISA (Quanta Lite RF IgA; Inova Diagnostics).

Shared epitope testing. Blood was tested for RA risk alleles containing the shared epitope using previously described methods (23).

Sputum NET remnant testing. Sputum supernatant was tested for DNA-protein complexes of NET remnants in a blinded manner using previously described methods (6,7,24). Briefly, we used sandwich ELISA to detect DNA-MPO, DNA-NE, and DNA-Cit-H3 protein complexes. Detailed methods for DNA-MPO and DNA-NE testing have been previously described (7). Similar methods were used for DNA-Cit-H3, and the antibody used to coat plates was rabbit anti-human H3 (citrulline R2+R8+R17; Abcam). To control for plate-to-plate variation, 4 control samples were included on every plate and an optical density index was calculated based on the average of these healthy control samples. In addition, a negative and positive control standard were run on each plate to confirm the validity of each plate. All samples were run in duplicate.

Sputum cytokine and chemokine testing. Meso Scale Discovery assays using Custom V-Plex Human Biomarker Panel plates were used to quantify sputum levels of interleukin-1 β (IL-1 β), IL-6, IL-8, IL-10, tumor necrosis factor (TNF), monocyte chemoattractant protein 1 (MCP-1), macrophage inflammatory protein 1 α (MIP-1 α), and MIP-1 β . Spike recovery testing with high and low standards was performed in coordination with the company (Meso Scale Discovery) to confirm that the biologic sample of sputum did not interfere with testing. All sputum samples were tested in duplicate, with mean levels reported in pg/ml.

Sputum complement factor testing. Complement factors Ba, soluble C5b-9, and C3a were measured by ELISA (Quidel). Complement factors C1q, C4, C2, MBL, C4b, C3, factor B, factor D, properdin, C3b, factor H, factor I, and C5a were measured by multiplex Luminex immunoassays (MilliporeSigma). Methods were optimized to measure the low concentration values in sputum, and 3 quality control samples were included in each run. All testing was performed in duplicate, with the resulting mean values reported in ng/ml, except for C5a, which was reported in pg/dl.

Ex vivo sputum NET formation assay. Detailed methods are provided in the Supplementary Materials (<http://onlinelibrary.wiley.com/doi/10.1002/art.41948/abstract>). Briefly, sputum cells were fixed, permeabilized, and stained with anti-MPO and anti-Cit-H3 antibodies. Confocal microscopy was used to quantify NET formation as previously described (25). DNA+MPO+ or DNA+MPO+Cit-H3+ colocalization and morphologic features of DNA extrusion consistent with NET formation were used to identify neutrophils that had undergone total NET formation or Cit-H3+ NET formation, respectively. Percentage of total or percentage of Cit-H3+ NETs was defined as the number of neutrophils with DNA+MPO+ or DNA+MPO+Cit-H3+ NET formation per total neutrophils.

Ex vivo sputum macrophage endocytosis assay. Detailed methods are provided in the Supplementary Materials (<http://onlinelibrary.wiley.com/doi/10.1002/art.41948/abstract>). Briefly, dissociated sputum cells were incubated with apoptotic and opsonized Jurkat cells for 2 hours followed by cell fixation and staining. Microscopy with manual counting was performed to quantify the endocytosis index based on the following formula:

$$\frac{(100 \times \text{number of macrophages with engulfed targets} / \text{total number of macrophages counted}) \times (\text{total number of engulfed targets} / \text{total number of macrophages counted})}{100}$$

Sputum Western blot. Sputum cell-free supernatant from 8 at-risk subjects (3 positive for sputum IgA anti-CCP and 5 negative for sputum IgA anti-CCP) was analyzed by Western blot to determine the levels of Cit-H3 and total H3. Samples were analyzed by equal volume (3 μ l sputum per well) and by total protein level (2 μ g protein per well). A positive control was run with each blot that included 7 ng of in vitro-citrullinated bulk histones. Antibodies were used to detect total H3 (no. ab1791; Abcam) and Cit-H3 (citrulline R2+R8+R17, no. ab5103; Abcam). The volume intensity of bands was calculated by densitometry using Bio-Rad Image Lab software. Each band was normalized to the positive control.

Induction of NETosis by induced sputum.

Detailed methods are provided in the Supplementary Materials (<http://onlinelibrary.wiley.com/doi/10.1002/art.41948/abstract>). Briefly, peripheral blood neutrophils isolated from a control donor were incubated with sputum supernatant for 2 hours followed by fixation and staining with anti-MPO and anti-Cit-H3 antibodies. After accounting for background, levels of NET formation were quantified using the SpectraMax iD5 (Molecular Devices).

Statistical analysis.

Subject demographics, percentage NET formation, levels of sputum protein, macrophage endocytic index, and NET remnants were compared between groups using chi-square and Wilcoxon's rank sum tests, as appropriate. Log-transformed levels of sputum anti-CCP and sputum cytokine, chemokine, and complement factor levels correlated with percentage NET formation, macrophage endocytic index, and NET remnant levels, according to Spearman's correlation. NET remnant levels correlated with MD-HAQ scores, and sputum cytokine, chemokine, and complement levels correlated with sputum-induced NET levels, according to Spearman's correlation. Multivariable linear regression was used to compare sputum percentage NET formation and group status as well as NET remnant levels and log-transformed sputum anti-CCP levels, while adjusting for relevant covariates.

For mediation analyses, we first used established methodologies (26) to create a composite variable to represent the multiple

cytokine/chemokine or complement variables using the first principal component from principal component analysis. The resulting composite score explained 79% and 61% of the total variation among the 8 cytokine/chemokines and 16 complement variables, respectively. The mediation model used the sputum composite score as the effector variable, log-transformed sputum IgA anti-CCP levels as the outcome variable, and sputum NET remnant levels as mediator variables. The model was run with each NET remnant mediator variable separately (DNA-MPO, DNA-NE, and DNA-Cit-H3) to quantify the direct effect and the indirect effect in the model. Significance was determined by a false discovery rate-adjusted bootstrap *P* value of less than 0.05, using the Benjamini and Yekutieli method to account for multiple testing (27). The mediation models were fit using the mediation R package (28,29).

Study approval.

All study procedures were approved by the Colorado Multiple Institutional Review Board and were in compliance with the Declaration of Helsinki. Written informed consent was obtained from all subjects.

RESULTS

Increased spontaneous sputum NET formation in at-risk subjects and RA subjects.

Subject demographic data are described in Supplementary Table 1 (<http://onlinelibrary.wiley.com/doi/10.1002/art.41948/abstract>). Using immunofluorescence

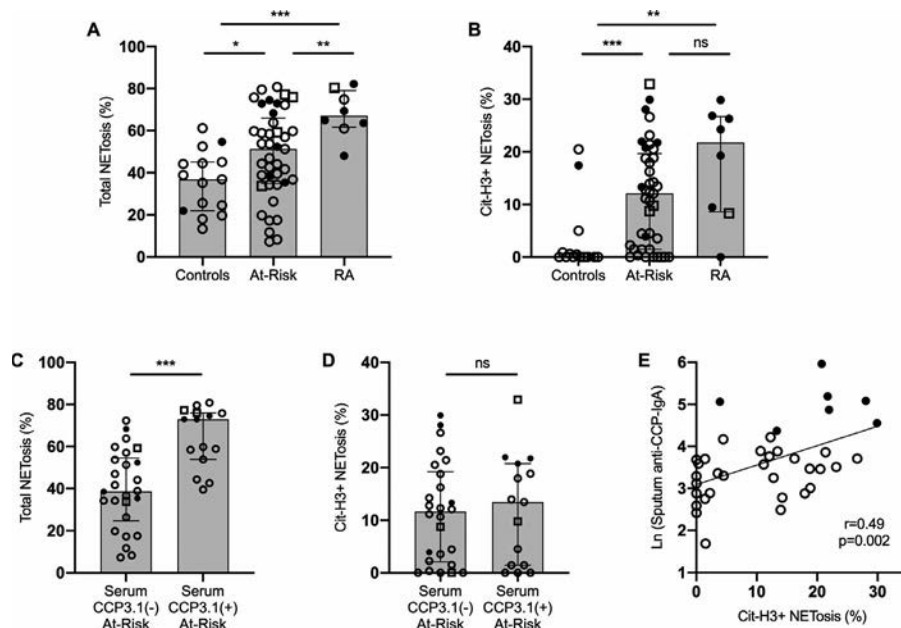


Figure 1. Sputum neutrophil extracellular trap (NET) formation (known as NETosis) and association with sputum IgA anti-cyclic citrullinated peptide (anti-CCP). **A** and **B**, Percentage of sputum neutrophils that underwent total NETosis (DNA+MPO+) (**A**) and citrullinated histone H3-positive (Cit-H3+) NETosis (DNA+MPO+Cit-H3+) (**B**) in ex vivo unstimulated culture in healthy controls ($n = 15$), subjects at risk for rheumatoid arthritis (RA) ($n = 41$), and RA patients ($n = 8$). **C** and **D**, Percentage of sputum neutrophils that underwent total NETosis (**C**) and Cit-H3+ NETosis (**D**) in serum anti-CCP3.1-negative at-risk subjects ($n = 26$) and serum anti-CCP3.1-positive at-risk subjects ($n = 15$). Median levels were compared between groups using Wilcoxon's rank sum test. **E**, Correlation between sputum IgA anti-CCP level and percentage Cit-H3+ NETosis in at-risk subjects ($n = 37$), by Spearman's correlation. Bars show the median and interquartile range. Open circles represent subjects negative for sputum IgA anti-CCP, solid circles represent subjects positive for sputum IgA anti-CCP, and open squares represent subjects in whom sputum IgA anti-CCP was not tested. * = $P < 0.05$; ** = $P < 0.01$; *** = $P < 0.001$. MPO = myeloperoxidase; NS = not significant; Ln = natural logarithm.

imaging of unstimulated sputum cells (representative images in Supplementary Figure 2, <http://onlinelibrary.wiley.com/doi/10.1002/art.41948/abstract>), we found that the percentage of sputum neutrophils that underwent NET formation (DNA+MPO+) and Cit-H3+ NET formation (DNA+MPO+Cit-H3+) was significantly higher in at-risk subjects and RA patients compared to controls (Figure 1A and 1B). For at-risk subjects, RA patients, and controls, the median percentage NET formation values for total NETs were 51%, 67%, and 37% ($P = 0.001$), respectively, and for Cit-H3+ NET formation were 12%, 22%, and 0% ($P < 0.001$), respectively. Among at-risk subjects, sputum total NETosis was significantly higher in those who were seropositive for anti-CCP3.1 (Figure 1C), whereas sputum Cit-H3+ NETosis was similar between at-risk subjects seropositive for anti-CCP3.1 and those seronegative for anti-CCP3.1 (Figure 1D). Increasing levels of Cit-H3+ NETosis significantly correlated with increasing levels of sputum IgA anti-CCP (Figure 1E) but not IgG anti-CCP ($P = 0.88$) in at-risk subjects. There was no significant correlation between total NETosis and IgA anti-CCP or IgG anti-CCP in sputum from at-risk subjects ($P = 0.15$ and $P = 0.12$, respectively). There was also no significant correlation between sputum total or Cit-H3+ NETosis and sputum IgA anti-CCP or IgG anti-CCP among RA patients or control subjects (data not shown).

Of note, sputum total and Cit-H3+ NETosis were not significantly higher based on age, sex, or history of chronic lung disease (data not shown). Because age and history of chronic

lung disease differed between groups, we performed multivariable linear regression and found that sputum total and Cit-H3+ NET formation remained significantly associated with subject group after adjusting for age and history of chronic lung disease ($P < 0.01$). In addition, levels of sputum total and Cit-H3+ NETosis remained significantly higher in at-risk and RA never-smokers compared to controls, and sputum Cit-H3+ NETosis remained significantly correlated with sputum IgA anti-CCP level in at-risk never-smokers (Supplementary Figures 3A–C, <http://onlinelibrary.wiley.com/doi/10.1002/art.41948/abstract>).

Association of sputum Cit-H3 levels with sputum ACPA. Proteins can be released extracellularly during NETosis (30). Using Western blot analysis, we found that median Cit-H3 levels and total H3 protein levels were higher in at-risk subjects with IgA anti-CCP–positive sputum (22% median Cit-H3+ NETosis in these samples based on ex vivo NETosis testing described above) compared to those with sputum negative for IgA anti-CCP (1% median Cit-H3+ NETosis in these samples) (Figures 2A–E). When blots were loaded based on total protein, we also found that the sputum Cit-H3:total H3 ratio was higher in at-risk subjects with sputum positive for IgA anti-CCP (Figure 2F). Total H3 and Cit-H3 levels also correlated with total sputum neutrophil counts ($r = 0.82$, $P = 0.02$, and $r = 0.86$, $P = 0.01$, respectively).

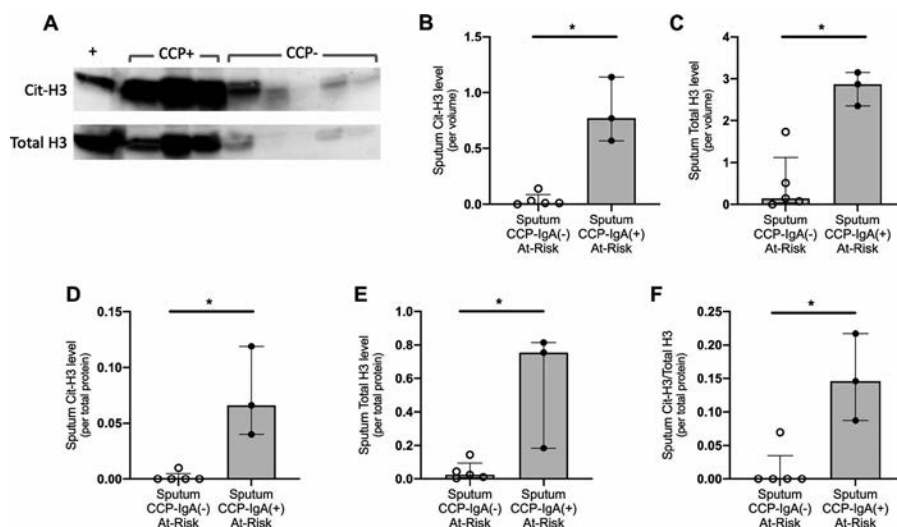


Figure 2. Sputum Cit-H3 levels are associated with sputum IgA anti-CCP levels in subjects at risk for RA. **A**, Western blot imaging of Cit-H3 and total H3 in sputum supernatant from a subset of at-risk subjects (3 subjects with IgA anti-CCP–positive sputum and 5 subjects with IgA anti-CCP–negative sputum). Each well was loaded with 3 μ l of sputum supernatant, and the positive control lane includes in vitro–citrullinated bulk histones. **B** and **C**, Quantified levels of Cit-H3 (**B**) and total H3 (**C**), by sputum volume (3 μ l loaded per well), normalized to the positive control in at-risk subjects positive for sputum IgA anti-CCP and those negative for sputum IgA anti-CCP. **D–F**, Quantified levels of Cit-H3 (**D**), total H3 (**E**), and Cit-H3:total H3 ratio (**F**), by sputum total protein level (2 μ g loaded per well) normalized to the positive control in at-risk subjects positive for sputum IgA anti-CCP and those negative for sputum IgA anti-CCP. Each band volume intensity was calculated using Bio-Rad Image Lab software. Median levels were compared between groups using Wilcoxon’s rank sum test. Bars show the median and interquartile range. Open circles represent subjects negative for sputum IgA anti-CCP, and solid circles represent subjects positive for sputum IgA anti-CCP. * = $P < 0.05$. See Figure 1 for definitions.

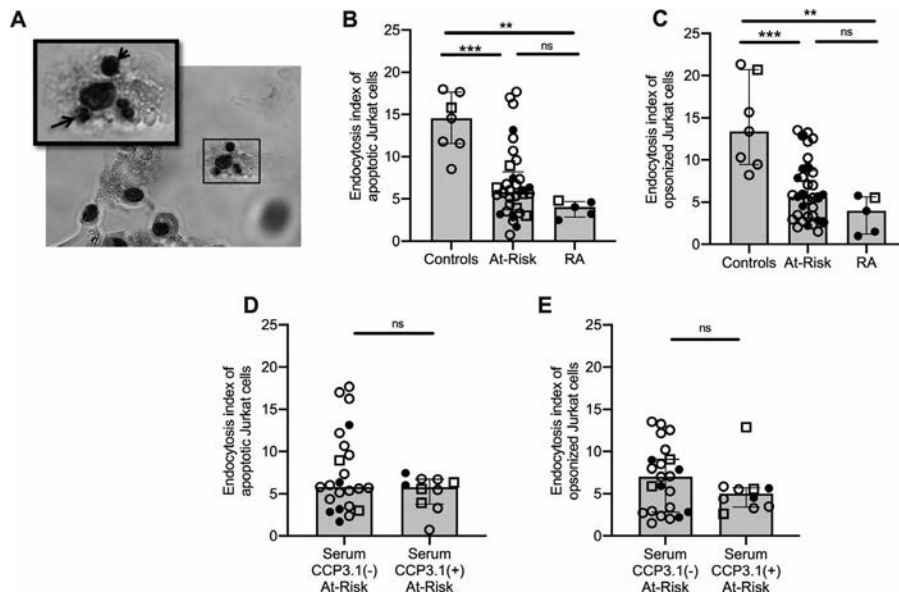


Figure 3. Sputum macrophage endocytosis of apoptotic and opsonized cells. **A**, Representative image of macrophage efferocytosis assay displaying ingestion of apoptotic Jurkat cells (**arrows**) by a sputum macrophage. Original magnification $\times 400$. **B** and **C**, Endocytosis index of apoptotic (**B**) and opsonized (**C**) Jurkat cells in healthy controls ($n = 7$), subjects at risk for RA ($n = 33$), and RA patients ($n = 5$). **D** and **E**, Endocytosis index of apoptotic (**D**) and opsonized (**E**) Jurkat cells in at-risk subjects with serum negative for anti-citrullinated protein antibodies (ACPA) ($n = 23$) and those with serum positive for ACPA ($n = 10$), with ACPA measured using an anti-CCP3.1 (IgG/IgA) enzyme-linked immunosorbent assay. Median levels were compared between groups using Wilcoxon’s rank sum test. Bars show the median and interquartile range. Open circles represent subjects negative for sputum IgA anti-CCP, solid circles represent subjects positive for sputum IgA anti-CCP, and open squares represent subjects in whom sputum IgA anti-CCP was not tested. ** = $P < 0.01$; *** = $P < 0.001$. See Figure 1 for other definitions.

Sputum macrophage endocytosis diminished in at-risk subjects and RA patients. Macrophage endocytosis is needed for effective clearance of NET remnants (31). To globally study macrophage endocytosis, we quantified both efferocytosis of apoptotic cells and phagocytosis of opsonized cells. We found that sputum macrophages from at-risk subjects and RA patients had significant impairments in both efferocytosis (Figure 3B) and phagocytosis (Figure 3C). Among at-risk subjects, there was no difference in endocytosis based on serum anti-CCP3.1 positivity (Figures 3D and E). In addition, sputum macrophage endocytosis did not correlate with sputum IgA anti-CCP level in at-risk subjects ($P = 0.24$ for efferocytosis and $P = 0.10$ for phagocytosis).

Sputum macrophage endocytosis was not significantly associated with age or history of chronic lung disease in any group ($P > 0.05$ for all). Among at-risk subjects, macrophage efferocytosis was higher in women compared to men ($P < 0.01$), and there was a non-significant trend toward lower endocytosis in ever-smokers ($P = 0.08$ for efferocytosis and $P = 0.09$ for phagocytosis). However, when comparing only women or only never-smokers in each group, at-risk subjects and RA patients continued to demonstrate decreased sputum macrophage efferocytosis and phagocytosis compared to controls ($P < 0.05$ for all) (Supplementary Figures 3D and E, <http://onlinelibrary.wiley.com/doi/10.1002/art.41948/abstract>). Endocytosis also remained significantly associated with the subject group when adjusting for sex and ever-smoking in multivariable linear regression ($P < 0.01$).

Correlation of sputum Cit-H3-containing NET remnants with sputum IgA anti-CCP in at-risk subjects. NET remnants represent a composite of NET formation and NET clearance. Consistent with our prior data (7), sputum IgA anti-CCP levels correlated with sputum NET remnant levels of DNA-NE ($r = 0.55$, $P < 0.001$) and DNA-MPO ($r = 0.51$, $P = 0.003$) in at-risk subjects (Figures 4A and B). We also found that sputum DNA-Cit-H3 protein complexes had the strongest correlation with sputum IgA anti-CCP ($r = 0.70$, $P < 0.001$) (Figure 4C). Notably, sputum DNA-Cit-H3 levels were not significantly higher in at-risk subjects as a group compared to healthy controls or RA patients ($P = 0.15$) (Figure 4D), but among at-risk subjects, sputum DNA-Cit-H3 levels were significantly higher in those with sputum IgA anti-CCP positivity ($P = 0.01$) (Figure 4E).

Because IgA RF and smoking have been associated with increased NETosis in humans (6,32,33), we evaluated the influence of these factors. In at-risk subjects, after adjusting for ever-smoking and sputum IgA RF level in linear regression models, sputum IgA anti-CCP remained significantly associated with sputum DNA-Cit-H3 ($P = 0.02$) but not with DNA-MPO ($P = 0.84$) or DNA-NE ($P = 0.06$).

There was no significant correlation between sputum IgA anti-CCP and NET remnant levels in RA subjects (data not shown). However, sputum DNA-Cit-H3 NET remnant levels did demonstrate a significant positive correlation with MD-HAQ score ($r = 0.85$, $P = 0.02$).

Association of sputum cytokines/chemokines with sputum IgA anti-CCP via pathway mediated by DNA-Cit-H3 and DNA-NE NET remnants in at-risk subjects. Multiple inflammatory cytokines can induce NET formation (12,14,34). We found positive correlations between levels of sputum IgA anti-CCP and sputum IL-1 β , IL-6, IL-8, IL-10, TNF, MIP-1 α , and MIP-1 β in at-risk subjects (Supplementary Table 2, <http://onlinelibrary.wiley.com/doi/10.1002/art.41948/abstract>). We then performed a mediation analysis to investigate whether the relationship between a composite cytokine/chemokine score and IgA anti-CCP was mediated by NET remnants. Our outcome of interest was the indirect effect of the model, because it quantified how much of the relationship between cytokine/chemokines and IgA anti-CCP was mediated through NET remnants (Supplementary Figure 4, <http://onlinelibrary.wiley.com/doi/10.1002/art.41948/abstract>). We found that the relationship between the sputum cytokine/chemokine score and sputum IgA anti-CCP was significantly mediated through sputum DNA-Cit-H3 NET remnant levels (indirect effect; $P < 0.001$) (Supplementary Table 3, <http://onlinelibrary.wiley.com/doi/10.1002/art.41948/abstract>) and to a lesser extent DNA-NE (indirect effect; $P = 0.004$).

As outlined in Supplementary Table 3 (<http://onlinelibrary.wiley.com/doi/10.1002/art.41948/abstract>), 86% of the relationship between the sputum cytokine/chemokine score and sputum IgA anti-CCP was mediated by sputum DNA-Cit-H3 levels. This relationship was maintained after adjusting for sputum IgA RF levels ($P = 0.001$ for DNA-Cit-H3; $P = 0.002$ for DNA-NE). The contributions of individual cytokines/chemokines are

outlined in Supplementary Table 4 (<http://onlinelibrary.wiley.com/doi/10.1002/art.41948/abstract>).

Sputum macrophage endocytosis index was not included in the mediation model, because it was not associated with sputum IgA anti-CCP. Of note, when accounting for multiple comparisons, there were no significant correlations between sputum macrophage endocytosis and sputum cytokine/chemokine levels (data not shown), but there was a trend toward sputum macrophage phagocytosis negatively correlating with sputum TNF levels ($r = -0.41$, $P = 0.03$).

Association of sputum complement activation fragments with sputum IgA anti-CCP via pathway mediated by DNA-Cit-H3 NET remnants in at-risk subjects. Complement activation fragments have also been found to induce NETosis (35,36). We identified positive correlations between levels of sputum anti-CCP-IgA and sputum Ba, C2, C4, and factor H in at-risk subjects (Supplementary Table 2, <http://onlinelibrary.wiley.com/doi/10.1002/art.41948/abstract>). Similar to the mediation analysis applied to cytokines/chemokines, we found a significant relationship between the composite sputum complement score and sputum IgA anti-CCP that was mediated through sputum DNA-Cit-H3 NET remnant levels (indirect effect; $P < 0.001$) (Supplementary Table 3, <http://onlinelibrary.wiley.com/doi/10.1002/art.41948/abstract>). We found that 86% of the relationship between the sputum complement score and sputum IgA anti-CCP was mediated by sputum DNA-Cit-H3 levels. We did not find DNA-MPO or DNA-NE to significantly mediate this relationship. Results

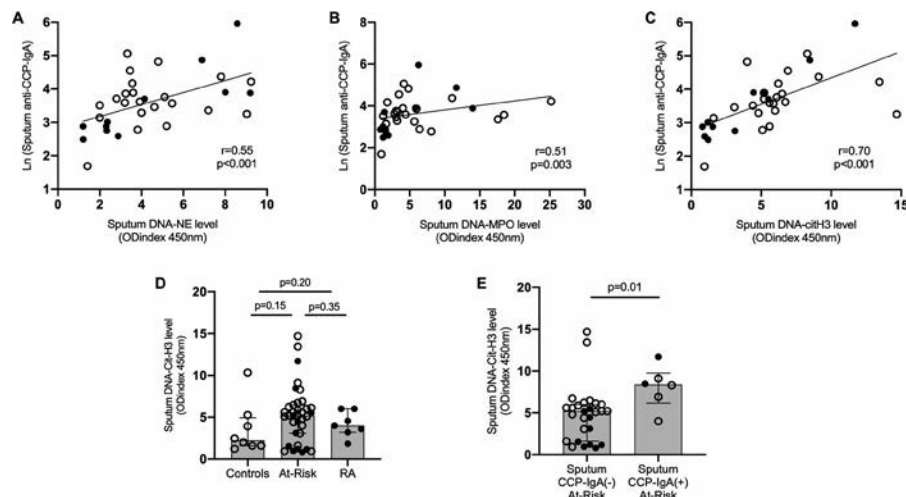


Figure 4. Sputum IgA anti-CCP and NET remnant levels. **A–C**, Correlations between levels of sputum IgA anti-CCP and levels of sputum NET remnants, measured as DNA-neutrophil elastase (DNA-NE) (**A**), DNA-MPO (**B**), and DNA-Cit-H3 (**C**) in at-risk subjects ($n = 33$). Correlations were calculated using Spearman's correlation. **D**, Sputum DNA-Cit-H3 levels in controls ($n = 8$), at-risk subjects ($n = 33$), and RA patients ($n = 7$). **E**, Sputum DNA-Cit-H3 levels in at-risk subjects positive for sputum IgA anti-CCP ($n = 6$) and those negative for sputum IgA anti-CCP ($n = 27$). Median levels were compared between groups using Wilcoxon's rank sum test. Open circles represent subjects negative for serum anti-CCP3.1, and solid circles represent subjects positive for serum anti-CCP3.1. See Figure 1 for definitions.

for individual complement proteins are listed in Supplementary Table 5 (<http://onlinelibrary.wiley.com/doi/10.1002/art.41948/abstract>). Although not included in the mediation model, when accounting for multiple comparisons, there was a non-significant trend toward sputum macrophage phagocytosis negatively correlating with sputum levels of C3a ($r = -0.51$, $P = 0.01$), C2 ($r = -0.47$, $P = 0.02$), C1q ($r = -0.44$, $P = 0.03$), and C3 ($r = -0.44$, $P = 0.03$).

Increase in induction of NETosis due to sputum that contains elevated inflammatory cytokine levels in at-risk subjects. Because our mediation analysis suggested that the relationship between sputum inflammatory proteins and IgA anti-CCP was mediated by DNA–Cit-H3 in at-risk subjects, we evaluated the ability of the sputum from at-risk subjects to induce Cit-H3+ NETs in control neutrophils. We found that among at-risk subjects, induction of Cit-H3+ NETs significantly correlated with sputum levels of IL-1 β , IL-6, and TNF (Figure 5 and Supplementary Table 6, <http://onlinelibrary.wiley.com/doi/10.1002/art.41948/abstract>). There was no significant correlation between sputum complement factor levels and NET induction. There was also no significant correlation between sputum IgA anti-CCP, IgG anti-CCP, or IgA RF level in at-risk subjects and NET induction. In at-risk subjects with IgA anti-CCP–negative sputum, positive correlations remained between the induction of Cit-H3+ NETs and sputum IL-1 β ($P = 0.002$), IL-6 ($P = 0.010$), and TNF ($P = 0.027$), supporting the notion that sputum cytokines in at-risk subjects can induce Cit-H3+ NETs even in the absence of sputum IgA anti-CCP.

DISCUSSION

We demonstrate for the first time that sputum neutrophils from subjects at risk of developing RA and RA patients are more prone to spontaneously undergo NET formation. Of particular interest, in at-risk subjects, IgA anti-CCP levels in the lung were associated with increased Cit-H3–expressing NET formation, and sputum IgA anti-CCP most strongly correlated with Cit-H3–containing NET remnants. Furthermore, we demonstrate that in at-risk subjects, inflammatory cytokines, chemokines, and complement pathway proteins in the lung are associated with sputum IgA anti-CCP through a pathway mediated by Cit-H3–containing NET remnants, and induction of Cit-H3+ NETosis was increased in sputum containing higher levels of IL-1, IL-6, and TNF. Taken together, these data suggest an important role for inflammation-induced citrullinated protein–expressing NETs in the lungs in subjects at risk for RA.

While the exact etiology of RA remains unknown, multiple data indicate that autoimmunity and inflammation begin in the lung in a portion of individuals who ultimately develop RA (7,9,37,38). Data also demonstrate that peripheral blood and synovial fluid neutrophils from RA patients are more prone to NETosis (14). Arthritogenic NET peptides can also be presented to antigen-specific T cells in association with ACPA, suggesting that NETs can be an initial trigger or amplifier of ACPA production (39). Taking these data into account along with our current findings, we propose that neutrophils in the lungs of subjects at risk for RA are more prone to undergoing citrullinated protein–containing NETosis, and IL-1 β –

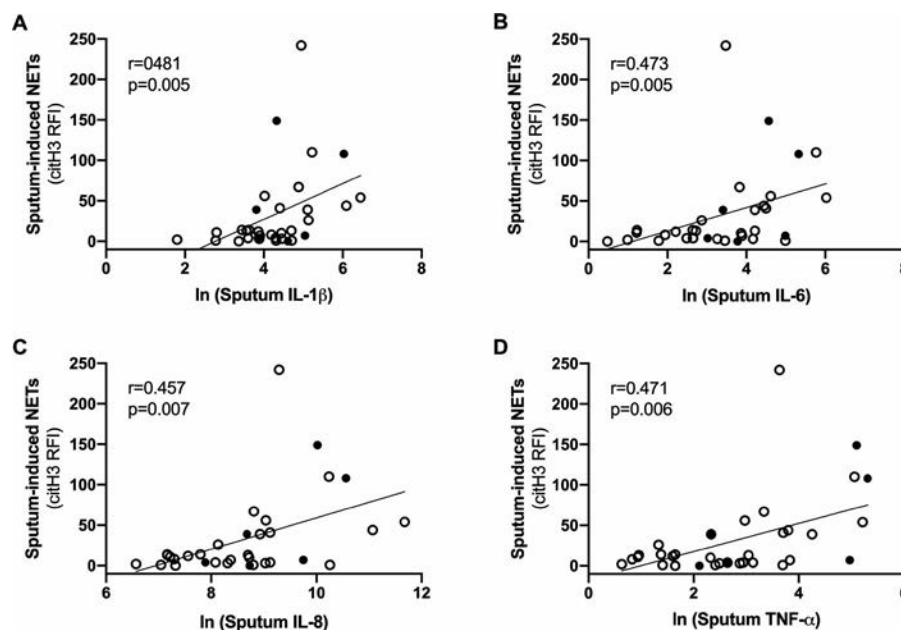


Figure 5. Sputum-induced Cit-H3+ NET formation and sputum cytokine levels. Correlations between levels of sputum-induced Cit-H3+ NET formation in control peripheral blood neutrophils measured by Cit-H3 mean relative fluorescence intensity (RFI) and log-transformed levels of sputum cytokines, including interleukin-1 β (IL-1 β) (A), IL-6 (B), IL-8 (C), and tumor necrosis factor (TNF) (D) in subjects at risk for RA ($n = 33$) were calculated using Spearman's correlation. Open circles represent subjects negative for sputum IgA anti-CCP, and solid circles represent subjects positive for sputum IgA anti-CCP. See Figure 1 for other definitions.

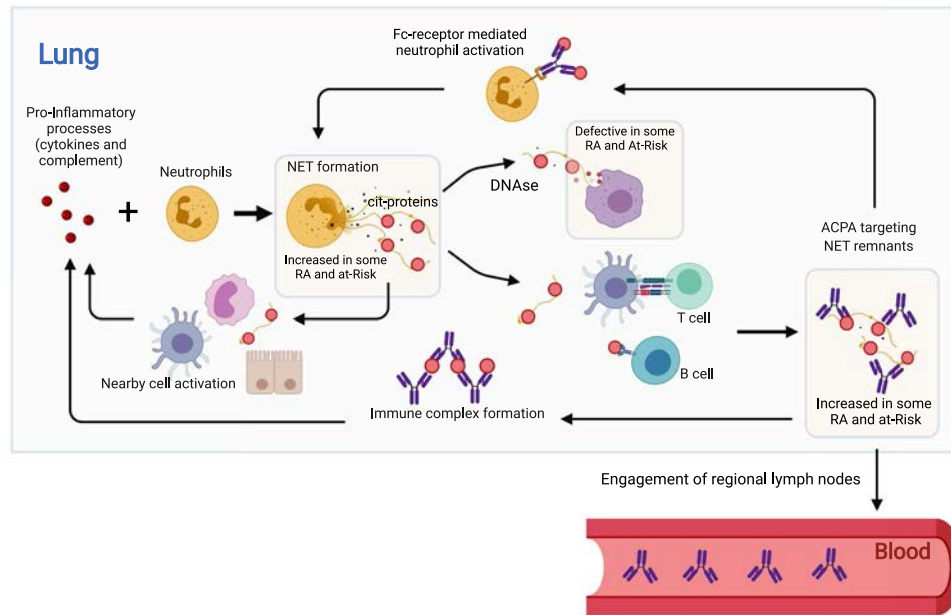


Figure 6. Hypothesis by which NETs in the lung can contribute to anti-citrullinated protein antibody (ACPA) generation. The figure depicts a hypothesis that proinflammatory mediators in the lung, including cytokines and complement proteins, can activate neutrophils to undergo NET formation in the lung. In addition, degradation of NET remnants can be diminished due to defective macrophage endocytosis. The resulting increased NET remnants can lead to ACPA generation in the lung via T cell and B cell activation. Following engagement of regional lymph nodes, this ACPA generation could become systemic and ultimately participate in the initiation and/or propagation of joint inflammation. There are several opportunities for feed-forward enhancement of this process including Fc receptor–mediated NET formation by ACPA and increased inflammatory protein generation via ACPA immune complex formation/deposition or NET activation of nearby cells, including macrophages, dendritic cells, and respiratory epithelial cells that can subsequently produce inflammatory cytokines. Notably, these processes may also occur at sites other than the lung mucosa. Figure created by BioRender.com. See Figure 1 for other definitions.

IL-6-, and TNF-associated inflammation, in particular, lead to an excess accumulation of citrullinated protein–containing NET remnants in the lung that can promote the local formation of ACPA. The factors that drive the inflammation in these subjects are unknown, but candidates are under investigation. We also found that sputum NET remnants in RA subjects correlated with joint disability (i.e., MD-HAQ) and not sputum ACPA levels, suggesting that NETs in the lung may play different roles at different stages of RA development.

In the present study, we found that sputum macrophages in at-risk subjects and RA patients had diminished endocytic function, suggesting that both increased NET formation and decreased NET clearance could contribute to the high levels of NET remnants associated with sputum IgA anti-CCP. While we did not directly evaluate macrophage ingestion of NET remnants in this study, it is assumed that NET ingestion would also be diminished because sputum macrophages in at-risk subjects and RA patients displayed global dysfunction of endocytosis (e.g., decreases in both efferocytosis and phagocytosis), and the receptor for advanced glycation end products can be used for both NET and apoptotic cell ingestion (39,40). Studies have shown that NE, which can be released during NETosis, can reduce lung macrophage efferocytic capacity by cleaving phagocytic receptors on the cell surface (41). Future studies are needed to identify whether similar processes

occur in subjects at risk for RA. In addition to macrophage endocytosis, NETs are cleared through degradation by DNase (31). We were unable to measure sputum DNase enzyme activity in this study, which is a limitation, but going forward, understanding differences in sputum DNase activity in at-risk subjects will be important to determine its contribution to increased levels of sputum NET remnants and RA pathogenesis.

NETs can be divided into several subtypes. The protein cargo externalized and the inflammation triggered by NETs can differ based on the individual and the NET stimulus (14,42–44). While smoking can induce NETosis and could play a role in increased NET formation in at-risk and RA smokers, our findings were independent of smoking, supporting the hypothesis of involvement of other factors. Our study focused on Cit-H3–containing NETs, but other citrullinated proteins have been identified in RA-associated NETs (14). As such, additional studies are needed to explore the full citrullinome of NETs generated in the lung in subjects at risk for RA. In addition, we found increased Cit-H3 and H3 protein levels in sputum associated with IgA anti-CCP in at-risk subjects. The source of Cit-H3 in the sputum could be from NETosis, but other pathways could also contribute, including extracellular release of peptidylarginine deiminase during NETosis (30) and neutrophils externalizing citrullinated proteins through leukotoxic hypercitrullination or complement membrane attack complex insertion

(45). Understanding each distinct pathway that could trigger ACPA through excess citrullinated protein externalization will be of interest.

There are several limitations to our study. It has been demonstrated that ACPA can trigger NET formation (13), which could result in a feed-forward process of increased NETosis. However, we found increased sputum NETosis in at-risk subjects without ACPA in the sputum or serum, suggesting that increased NET formation could be an initial event leading to ACPA formation and not a resultant event caused by ACPA in the lung. NETs can also induce cytokine stimulation from other nearby cells, including airway epithelial cells, and NETs can activate complement (46–48). Therefore, while our data suggest that NET remnants mediate the relationship between inflammatory factors and ACPA, we cannot exclude the possibility that elevation of sputum cytokines and/or complement results in part from the effects of increased NETosis. Figure 6 depicts our hypothesis in the context of the complexities of several possible feed-forward loops that could contribute to further enhancement of lung inflammation and NET formation. Of note, lung inflammation and NET formation triggered by a variety of environmental factors are likely common in most individuals, regardless of their risk for RA. It is likely the generation of a sustained local and subsequently systemic adaptive immune response to citrullinated proteins is the factor that distinguishes individuals with and those at-risk for RA from healthy controls. However, large longitudinal studies of sputum and linked systemic studies of autoimmune status are needed to fully understand the natural history and relationships of lung inflammation and ACPA generation across different sites in groups of individuals who have well-defined outcomes.

In conclusion, we found increased Cit-H3-containing NET formation and NET remnants to be associated with IgA anti-CCP in the sputum of subjects at risk for RA. These data suggest a role for aberrant NET formation in the lung during the preclinical period of RA. They further support the importance of understanding features of sputum neutrophils in at-risk subjects and RA patients, as NET formation and effector mechanisms may be potential future targets that abrogate ACPA generation during the preclinical period of RA.

AUTHOR CONTRIBUTIONS

All authors were involved in drafting the article or revising it critically for important intellectual content, and all authors approved the final version to be published. Dr. Demoruelle had full access to all of the data in the study and takes responsibility for the integrity of the data and the accuracy of the data analysis.

Study conception and design. Okamoto, Devoe, Minarchick, Rothfuss, Mohning, Thomas, Norris, Cherrington, Janssen, Kaplan, Deane, Holers, Demoruelle.

Acquisition of data. Okamoto, Devoe, Seto, Minarchick, Rothfuss, Visser, August, Charry, Fleischer, Feser, Frazer-Abel, Cherrington, Kaplan, Deane, Demoruelle.

Analysis and interpretation of data. Okamoto, Wilson, Rothfuss, Mohning, Arbet, Kroehl, Thomas, Frazer-Abel, Norris, Cherrington, Janssen, Kaplan, Deane, Holers, Demoruelle.

REFERENCES

- Rantapää-Dahlqvist S, de Jong BA, Berglin E, Hallmans G, Wadell G, Stenlund H, et al. Antibodies against cyclic citrullinated peptide and IgA rheumatoid factor predict the development of rheumatoid arthritis. *Arthritis Rheum* 2003;48:2741–9.
- Kokkonen H, Mullahezi M, Berglin E, Hallmans G, Wadell G, Rönneid J, et al. Antibodies of IgG, IgA and IgM isotypes against cyclic citrullinated peptide precede the development of rheumatoid arthritis. *Arthritis Res Ther* 2011;13:R13.
- Harre U, Georgess D, Bang H, Bozec A, Axmann R, Ossipova E, et al. Induction of osteoclastogenesis and bone loss by human autoantibodies against citrullinated vimentin. *J Clin Invest* 2012;122:1791–802.
- Kuhn KA, Kulik L, Tomooka B, Braschler KJ, Arend WP, Robinson WH, et al. Antibodies against citrullinated proteins enhance tissue injury in experimental autoimmune arthritis. *J Clin Invest* 2006;116:961–73.
- Willis VC, Demoruelle MK, Derber LA, Chartier-Logan CJ, Parish MC, Pedraza IF, et al. Sputum autoantibodies in patients with established rheumatoid arthritis and subjects at risk of future clinically apparent disease. *Arthritis Rheum* 2013;65:2545–54.
- Demoruelle MK, Bowers E, Lahey LJ, Sokolove J, Purmalek M, Seto NL, et al. Antibody responses to citrullinated and noncitrullinated antigens in the sputum of subjects with rheumatoid arthritis and subjects at risk for development of rheumatoid arthritis. *Arthritis Rheumatol* 2018;70:516–27.
- Demoruelle MK, Harrall KK, Ho L, Purmalek MM, Seto NL, Rothfuss HM, et al. Anti-citrullinated protein antibodies are associated with neutrophil extracellular traps in the sputum in relatives of rheumatoid arthritis patients. *Arthritis Rheumatol* 2017;69:1165–75.
- Demoruelle MK, Weisman MH, Simonian PL, Lynch DA, Sachs PB, Pedraza IF, et al. Airways abnormalities and rheumatoid arthritis-related autoantibodies in subjects without arthritis: early injury or initiating site of autoimmunity? *Arthritis Rheum* 2012;64:1756–61.
- Klareskog L, Stolt P, Lundberg K, Källberg H, Bengtsson C, Grunewald J, et al. A new model for an etiology of rheumatoid arthritis: smoking may trigger HLA-DR (shared epitope)-restricted immune reactions to autoantigens modified by citrullination. *Arthritis Rheum* 2006;54:38–46.
- Rangel-Moreno J, Hartson L, Navarro C, Gaxiola M, Selman M, Randall TD. Inducible bronchus-associated lymphoid tissue (iBALT) in patients with pulmonary complications of rheumatoid arthritis. *J Clin Invest* 2006;116:3183–94.
- Reynisdottir G, Olsen H, Joshua V, Engstrom M, Forsslund H, Karimi R, et al. Signs of immune activation and local inflammation are present in the bronchial tissue of patients with untreated early rheumatoid arthritis. *Ann Rheum Dis* 2016;75:1722–7.
- Brinkmann V, Reichard U, Goosmann C, Fauler B, Uhlemann Y, Weiss DS, et al. Neutrophil extracellular traps kill bacteria. *Science* 2004;303:1532–5.
- Sur Chowdhury C, Giaglis S, Walker UA, Buser A, Hahn S, Hasler P. Enhanced neutrophil extracellular trap generation in rheumatoid arthritis: analysis of underlying signal transduction pathways and potential diagnostic utility. *Arthritis Res Ther* 2014;16:R122.
- Khandpur R, Carmona-Rivera C, Vivekanandan-Giri A, Gizinski A, Yalavarthi S, Knight JS, et al. NETs are a source of citrullinated autoantigens and stimulate inflammatory responses in rheumatoid arthritis. *Sci Transl Med* 2013;5:178ra40.
- Pratesi F, Dioni I, Tommasi C, Alcaro MC, Paolini I, Barbetti F, et al. Antibodies from patients with rheumatoid arthritis target citrullinated histone 4 contained in neutrophils extracellular traps. *Ann Rheum Dis* 2014;73:1414–22.
- Corsiero E, Bombardieri M, Carlotti E, Pratesi F, Robinson W, Migliorini P, et al. Single cell cloning and recombinant monoclonal antibodies

- generation from RA synovial B cells reveal frequent targeting of citrullinated histones of NETs. *Ann Rheum Dis* 2016;75:1866–75.
17. Lloyd KA, Wigerblad G, Sahlstrom P, Garimella MG, Chemin K, Steen J, et al. Differential ACPA binding to nuclear antigens reveals a PAD-independent pathway and a distinct subset of acetylation cross-reactive autoantibodies in rheumatoid arthritis. *Front Immunol* 2018;9:3033.
 18. Neeli I, Dwivedi N, Khan S, Radic M. Regulation of extracellular chromatin release from neutrophils. *J Innate Immun* 2009;1:194–201.
 19. Janssen KM, de Smit MJ, Withaer C, Brouwer E, van Winkelhoff AJ, Vissink A, et al. Autoantibodies against citrullinated histone H3 in rheumatoid arthritis and periodontitis patients. *J Clin Periodontol* 2017;44:577–84.
 20. Aletaha D, Neogi T, Silman AJ, Funovits J, Felson DT, Bingham CO III, et al. 2010 rheumatoid arthritis classification criteria: an American College of Rheumatology/European League Against Rheumatism collaborative initiative. *Arthritis Rheum* 2010;62:2569–81.
 21. Arnett FC, Edworthy SM, Bloch DA, McShane DJ, Fries JF, Cooper NS, et al. The American Rheumatism Association 1987 revised criteria for the classification of rheumatoid arthritis. *Arthritis Rheum* 1988;31:315–24.
 22. Pincus T, Yazici Y, Bergman M. A practical guide to scoring a Multi-Dimensional Health Assessment Questionnaire (MDHAQ) and Routine Assessment of Patient Index Data (RAPID) scores in 10–20 seconds for use in standard clinical care, without rulers, calculators, websites or computers. *Best Pract Res Clin Rheumatol* 2007;21:755–87.
 23. Kolfenbach JR, Deane KD, Derber LA, O'Donnell C, Weisman MH, Buckner JH, et al. A prospective approach to investigating the natural history of preclinical rheumatoid arthritis (RA) using first-degree relatives of probands with RA. *Arthritis Rheum* 2009;61:1735–42.
 24. Lood C, Blanco LP, Purmalek MM, Carmona-Rivera C, De Ravin SS, Smith CK, et al. Neutrophil extracellular traps enriched in oxidized mitochondrial DNA are interferogenic and contribute to lupus-like disease. *Nat Med* 2016;22:146–53.
 25. Marder W, Knight JS, Kaplan MJ, Somers EC, Zhang X, O'Dell AA, et al. Placental histology and neutrophil extracellular traps in lupus and pre-eclampsia pregnancies. *Lupus Sci Med* 2016;3:e000134.
 26. Song MK, Lin FC, Ward SE, Fine JP. Composite variables: when and how. *Nurs Res* 2013;62:45–9.
 27. Benjamini Y, Yekutieli D. The control of the false discovery rate in multiple testing under dependency. *Ann Statist* 2001;29:1165–88.
 28. Tingley D, Yamamoto T, Hirose K, Keele L, Imai K. mediation: R Package for Causal Mediation Analysis. *J Stat Softw* 2014;59:38.
 29. R Core Team. R: a language and environment for statistical computing. R Foundation for Statistical Computing, Vienna, Austria. 2018. URL: <https://www.R-project.org/>.
 30. Spengler J, Lugonja B, Ytterberg AJ, Zubarev RA, Creese AJ, Pearson MJ, et al. Release of active peptidyl arginine deiminases by neutrophils can explain production of extracellular citrullinated autoantigens in rheumatoid arthritis synovial fluid. *Arthritis Rheumatol* 2015;67:3135–45.
 31. Farrera C, Fadeel B. Macrophage clearance of neutrophil extracellular traps is a silent process. *J Immunol* 2013;191:2647–56.
 32. Aleyd E, Al M, Tuk CW, van der Laken CJ, van Egmond M. IgA complexes in plasma and synovial fluid of patients with rheumatoid arthritis induce neutrophil extracellular traps via FcαRI. *J Immunol* 2016;197:4552–9.
 33. Lee J, Luria A, Rhodes C, Raghu H, Lingampalli N, Sharpe O, et al. Nicotine drives neutrophil extracellular traps formation and accelerates collagen-induced arthritis. *Rheumatology (Oxford)* 2017;56:644–53.
 34. Keshari RS, Jyoti A, Dubey M, Kothari N, Kohli M, Bogra J, et al. Cytokines induced neutrophil extracellular traps formation: implication for the inflammatory disease condition. *PLoS One* 2012;7:e48111.
 35. Palmer LJ, Damgaard C, Holmstrup P, Nielsen CH. Influence of complement on neutrophil extracellular trap release induced by bacteria. *J Periodontol Res* 2016;51:70–6.
 36. Martinelli S, Urosevic M, Daryadel A, Oberholzer PA, Baumann C, Fey MF, et al. Induction of genes mediating interferon-dependent extracellular trap formation during neutrophil differentiation. *J Biol Chem* 2004;279:44123–32.
 37. Holers VM, Demoruelle MK, Kuhn KA, Buckner JH, Robinson WH, Okamoto Y, et al. Rheumatoid arthritis and the mucosal origins hypothesis: protection turns to destruction [review]. *Nat Rev Rheumatol* 2018;14:542–57.
 38. Mankia K, Emery P. Is localized autoimmunity the trigger for rheumatoid arthritis? Unravelling new targets for prevention [review]. *Discov Med* 2015;20:129–35.
 39. Carmona-Rivera C, Carlucci PM, Moore E, Lingampalli N, Uchtenhagen H, James E, et al. Synovial fibroblast-neutrophil interactions promote pathogenic adaptive immunity in rheumatoid arthritis. *Sci Immunol* 2017;2:eaag3358.
 40. Armstrong A, Ravichandran KS. Phosphatidylserine receptors: what is the new RAGE? *EMBO Rep* 2011;12:287–8.
 41. Vandivier RW, Fadok VA, Hoffmann PR, Bratton DL, Penvari C, Brown KK, et al. Elastase-mediated phosphatidylserine receptor cleavage impairs apoptotic cell clearance in cystic fibrosis and bronchiectasis. *J Clin Invest* 2002;109:661–70.
 42. Garcia-Romo GS, Caielli S, Vega B, Connolly J, Allantaz F, Xu Z, et al. Netting neutrophils are major inducers of type I IFN production in pediatric systemic lupus erythematosus. *Sci Transl Med* 2011;3:73ra20.
 43. Skopelja S, Hamilton BJ, Jones JD, Yang ML, Mamula M, Ashare A, et al. The role for neutrophil extracellular traps in cystic fibrosis autoimmunity. *JCI Insight* 2016;1:e88912.
 44. Kenny EF, Herzig A, Kruger R, Muth A, Mondal S, Thompson PR, et al. Diverse stimuli engage different neutrophil extracellular trap pathways. *Elife* 2017;6:e24437.
 45. Konig MF, Abusleme L, Reinholdt J, Palmer RJ, Teles RP, Sampson K, et al. Aggregatibacter actinomycetemcomitans-induced hypercitrullination links periodontal infection to autoimmunity in rheumatoid arthritis. *Sci Transl Med* 2016;8:369ra176.
 46. Leffler J, Martin M, Gullstrand B, Tyden H, Lood C, Truedsson L, et al. Neutrophil extracellular traps that are not degraded in systemic lupus erythematosus activate complement exacerbating the disease. *J Immunol* 2012;188:3522–31.
 47. Wang H, Wang C, Zhao MH, Chen M. Neutrophil extracellular traps can activate alternative complement pathways. *Clin Exp Immunol* 2015;181:518–27.
 48. Sabbione F, Keitelman IA, Iula L, Ferrero M, Giordano MN, Baldi P, et al. Neutrophil extracellular traps stimulate proinflammatory responses in human airway epithelial cells. *J Innate Immun* 2017;9:387–402.

Role of Ciliary Protein Intraflagellar Transport Protein 88 in the Regulation of Cartilage Thickness and Osteoarthritis Development in Mice

Clarissa R. Coveney,  Linyi Zhu,  Jadwiga Miotla-Zarebska, Bryony Stott, Ida Parisi, Vicky Batchelor, Claudia Duarte, Emer Chang,  Eleanor McSorley, Tonia L. Vincent,  and Angus K. T. Wann

Objective. Mechanical and biologic cues drive cellular signaling in cartilage development, health, and disease. Primary cilia proteins, which are implicated in the transduction of biologic and physiochemical signals, control cartilage formation during skeletal development. This study was undertaken to assess the influence of the ciliary protein intraflagellar transport protein 88 (IFT88) on postnatal cartilage from mice with conditional knockout of the *Ift88* gene (*Ift88*-KO).

Methods. *Ift88^{fl/fl}* and *aggrecanCre^{ERT2}* mice were crossed to create a strain of cartilage-specific *Ift88*-KO mice (*aggrecanCre^{ERT2};Ift88^{fl/fl}*). In these *Ift88*-KO mice and *Ift88^{fl/fl}* control mice, tibial articular cartilage thickness was assessed by histomorphometry, and the integrity of the cartilage was assessed using Osteoarthritis Research Society International (OARS) damage scores, from adolescence through adulthood. In situ mechanisms of cartilage damage were investigated in the microdissected cartilage sections using immunohistochemistry, RNAScope analysis, and quantitative polymerase chain reaction. Osteoarthritis (OA) was induced in *aggrecanCre^{ERT2};Ift88^{fl/fl}* mice and *Ift88^{fl/fl}* control mice using surgical destabilization of the medial meniscus (DMM). Following tamoxifen injection and DMM surgery, the mice were given free access to exercise on a wheel.

Results. Deletion of *Ift88* resulted in progressive reduction in the thickness of the medial tibial cartilage in adolescent mice, as well as marked atrophy of the cartilage in mice during adulthood. In *aggrecanCre^{ERT2};Ift88^{fl/fl}* mice at age 34 weeks, the median thickness of the medial tibial cartilage was 89.42 μm (95% confidence interval [95% CI] 84.00–93.49), whereas in *Ift88^{fl/fl}* controls at the same age, the median cartilage thickness was 104.00 μm (95% CI 100.30–110.50; $P < 0.0001$). At all time points, the median thickness of the calcified cartilage was reduced. In some mice, atrophy of the medial tibial cartilage was associated with complete, spontaneous degradation of the cartilage. Following DMM, *aggrecanCre^{ERT2};Ift88^{fl/fl}* mice were found to have increased OARS scores of cartilage damage. In articular cartilage from maturing mice, atrophy was not associated with obvious increases in aggrecanase-mediated destruction or chondrocyte hypertrophy. Of the 44 candidate genes analyzed, only *Tcf7l2* expression levels correlated with *Ift88* expression levels in the microdissected cartilage. However, RNAScope analysis revealed that increased hedgehog (Hh) signaling (as indicated by increased expression of *Gli1*) was associated with the reductions in *Ift88* expression in the tibial cartilage from *Ift88*-deficient mice. Wheel exercise restored both the articular cartilage thickness and levels of Hh signaling in these mice.

Conclusion. Our results in a mouse model of OA demonstrate that IFT88 performs a chondroprotective role in articular cartilage by controlling the calcification of cartilage via maintenance of a threshold of Hh signaling during physiologic loading.

Supported by Versus Arthritis (grants 20205 and 21621). Dr. Coveney's work was supported by the Kennedy Trust for Rheumatology Research (grant KENN181907). Dr. Zhu's work was supported by the European Research Council (grant 743016). Ms. Chang's work was supported by the St. Hughs College, University of Oxford (Student Summer Research award). Ms. McSorley's work was supported by the Magdalen College, University of Oxford (Student Summer Research award). Dr. Wann's work was supported by the Kennedy Trust for Rheumatology Research (KTRR Fellowship).

Clarissa R. Coveney, DPhil (current address: Peabody Museum, Cambridge, Massachusetts), Linyi Zhu, PhD, Jadwiga Miotla-Zarebska, PhD, Bryony

Stott, PhD, Ida Parisi, PhD, Vicky Batchelor, MSc, Claudia Duarte, BSc, Emer Chang, BSc, Eleanor McSorley, BSc, Tonia L. Vincent, MD, PhD, Angus K. T. Wann, PhD: University of Oxford, Oxford, UK.

Dr. Vincent has received consulting fees from Mundipharma and GlaxoSmithKline (less than \$10,000 each). No other disclosures relevant to this article were reported.

Address correspondence to Clarissa R. Coveney, DPhil, Peabody Museum, 5th floor, 11 Divinity Avenue, Cambridge, MA 02138. Email: coveney.coxswain@gmail.com.

Submitted for publication February 2, 2021; accepted in revised form June 3, 2021.

INTRODUCTION

Articular cartilage absorbs and transmits mechanical loads generated by muscle contraction and weight-bearing during physical activity. Cartilage can be broadly divided into a noncalcified zone and a calcified zone adjacent to bone. Total cartilage thickness is allometrically scaled to the size of the organism, ensuring that chondrocytes experience similar force irrespective of the mass of the individual animal (1). Articular cartilage is extremely mechanosensitive, with chondrocytes closely monitoring and remodeling the extracellular matrix in response to physiologic loading (2,3). Physiologic mechanics are critical for cartilage development and homeostasis (4), since their loss has been demonstrated to lead to cartilage thinning (atrophy) (5,6).

Pathologic, supraphysiologic mechanical loading leads to the development of osteoarthritis (OA), in which degradation of the cartilage occurs, resulting in a loss of integrity of the articular surface (6). Cellular responses to mechanical force include the release of fibroblast growth factor receptor type 2 and transforming growth factor β (TGF β) from the matrix upon application of a mechanical load, as well as activation of a hedgehog (Hh) ligand, Indian hedgehog (7–10). A number of other pathways are implicated in cellular mechanotransduction, including connexin and ion channel opening and integrin activation. It is not yet understood how chondrocytes in cartilage integrate these cues as the cartilage matures through adolescence and as adaptation occurs to prepare for lifelong loading.

As in most cells in the body, articular chondrocytes express a single immotile primary cilium (11), a microtubule-based organelle reliant on intraflagellar transport (IFT) proteins, including IFT88. Components of the Hh pathway localize to the cilium, supporting bidirectional modulation of signaling (12). Cilia have been directly linked with other growth factor–signaling pathways such as TGF β signaling, and have also been indirectly linked with a large, growing list of signaling pathways (13), many of which are pertinent to cartilage health. The primary cilium has also been implicated as a “mechanosensory” structure (14). Findings from *in vitro* experiments in chondrocytes have implied that ciliary protein IFT88 is associated with both compression-induced production of extracellular matrix proteins (15) and impaired clearance of aggrecanases, resulting in exacerbated aggrecan degradation (16).

Developmental mutations in ciliary genes, including *Ift88*, result in impaired embryonic patterning as a result of disrupted Hh signaling (17). Cartilage-specific deletion of *Ift88* results in disrupted long bone and articular cartilage formation (18). Cartilage-specific deletion of *Ift80* in mice in the first 2 weeks of postnatal life was found to result in thickening of the articular cartilage (19). However, despite its putative influence over a range of processes that regulate health and disease in cartilage, we have very limited direct knowledge regarding the postdevelopmental influence of

ciliary IFT. We hypothesized that in a mouse model, ciliary protein IFT88 plays a crucial role in mediating cartilage homeostasis in adult animals.

MATERIALS AND METHODS

Animals. *Ift88*^{fl/fl} mice were obtained from The Jackson Laboratory (stock no. 022409) and were maintained as the control line. In parallel, offspring were crossed with *aggrecanCre*^{E^{ERT2}} mice, to generate *aggrecanCre*^{E^{ERT2}};*Ift88*^{fl/fl} mice (i.e., *Ift88*-knockout [*Ift88*-KO]), a mouse line that was originally generated at the Kennedy Institute of Rheumatology (20). The tdTomato reporter mouse line *B6.Cg-Gt(ROSA)26Sor*^{tm14(CAG-tdTomato)Hze}/J was used to confirm tissue-specific Cre recombination (stock no. 007914; The Jackson Laboratory). For all experiments, apart from destabilization of the medial meniscus (DMM) and wheel exercise (in which only male mice were used), both sexes were analyzed. No effect of sex was observed.

Tamoxifen treatment. Tamoxifen (product no. T5648; Sigma-Aldrich) was dissolved using sonication in 90% sunflower oil and 10% ethanol at a concentration of 20 mg/ml. Tamoxifen was administered by intraperitoneal injection at a dose of 50–100 mg/kg (according to the weight of the individual animal) on 3 consecutive days (*aggrecanCre*^{E^{ERT2}};*Ift88*^{fl/fl}, *Ift88*^{fl/fl}, and *aggrecanCre*^{E^{ERT2}};*tdTomato* mice; n = 5–22 per group) stratified by age (4, 6, or 8 weeks of age).

DMM. Mice were given tamoxifen 2 weeks prior to surgery. Male *Ift88*^{fl/fl} control mice and *aggrecanCre*^{E^{ERT2}};*Ift88*^{fl/fl} mice underwent DMM surgery at 10 weeks of age, as previously described (21), or underwent a capsulotomy as sham surgery. Thereafter, the mice were anesthetized using a previously described method (22) and then killed at 8 or 12 weeks after DMM (at 8 weeks, n = 14 *Ift88*^{fl/fl} mice and n = 12 *aggrecanCre*^{E^{ERT2}};*Ift88*^{fl/fl} mice; at 12 weeks, n = 15 *Ift88*^{fl/fl} mice and n = 15 *aggrecanCre*^{E^{ERT2}};*Ift88*^{fl/fl} mice).

Histology. Knee joints from the mice were harvested into 10% neutral buffered formalin (CellPath). The joints were then decalcified (in EDTA), paraffin embedded, and cut coronally through the entire depth of the joint. Sections (4 μ m in thickness) were stained with Safranin O at 80- μ m intervals.

Osteoarthritis Research Society International (OARS) scoring. Safranin O–stained joint sections were assessed using a scoring system for severity of cartilage damage, as described previously (21). OARS scores were assessed by 2 observers (CRC and IP) who were blinded with regard to the mouse group. The summed score method was used (the sum of the 3 highest scores per section, per joint, with a minimum of 9 sections per joint).

Osteophyte quantification. Osteophyte size and maturity, as well as loss of medial tibial cartilage proteoglycan staining, were assessed using a 0–3 scale, as previously described (23).

Cartilage thickness measurements. Thickness measurements were obtained from the mean of 3 measurements from both the medial and lateral tibial plateaus (total of 6 measurements), from 3 consecutive sections in the middle of the joint (total of 18 measurements). The same method was used to measure noncalcified cartilage thickness from the same location from which the total cartilage thickness measurement was obtained. Calcified cartilage thickness was calculated by subtracting the noncalcified cartilage thickness from the total cartilage thickness. All images were independently scored twice; measurements were obtained using ImageJ software (Supplementary Figure 1A, available on the *Arthritis & Rheumatology* website at <http://onlinelibrary.wiley.com/doi/10.1002/art.41894/abstract>).

Subchondral bone measurements. Subchondral bone measurements were obtained using a previously described method (24). Briefly, using ImageJ software, 5 measurements were obtained perpendicular to the articular cartilage plateau, from the chondro–osseous junction to the top of the bone marrow or to the growth plate if there was no bone marrow. Thickness was measured in ≥ 3 sections of each plateau of each knee.

Micro-computed tomography (micro-CT) analysis of bone volume/total volume (BV/TV). Mouse knee joints were scanned using a SkyScan 1172 Micro-CT apparatus in 70% ethanol (10 $\mu\text{m}/\text{pixel}$). A 3-dimensional analysis was used to examine parameters including tissue and bone volume, tissue and bone surface area, trabecular thickness, separation, and volume, and trabecular pattern factor, measured using CTAn (Bruker).

Immunohistochemistry (IHC). Unstained fixed, decalcified coronal sections of the knee joints were deparaffinized, rehydrated, and quenched in 0.3M glycine and treated with proteinase K for 10 minutes. Tissue sections were treated with chondroitinase (0.1 units) for 30 minutes at 37°C, blocked in 5% goat serum and 10% bovine serum albumin in phosphate buffered saline, and permeabilized with 0.2% Triton X-100 for 15 minutes. The cartilage was then incubated overnight at 4°C with one of the following primary antibodies: anti-type X collagen in a 1:50 ratio (product no. ab58632; Abcam), anti-NITEGE in a 1:50 ratio (product no. PA1-1746; Thermo Scientific), IgG control in a 1:50 ratio, or no primary antibody. Sections were washed and incubated with Alexa Fluor 555 secondary antibodies for 30 minutes. Cartilage samples were incubated with the nuclear stain DAPI (in a 1:5,000 ratio), before being mounted in Prolong Gold.

RNA extraction. Articular cartilage was microdissected from the femoral and tibial plateaus using a scalpel (each data point from 2 animals) and was harvested directly into RNeasy lysis buffer (Qiagen) and was transferred to RLT buffer (Qiagen) and were diced before pulverization using a PowerGen 125 Polytron instrument (Fisher Scientific) (3 times for 20 seconds each). RNA in mouse knee cartilage was isolated using an RNeasy micro kit (Qiagen).

Quantitative polymerase chain reaction (qPCR). Using RNA isolated from microdissected knee cartilage, complementary DNA was synthesized (Applied Biosystems) and real-time qPCR was performed using a ViiA 7 real-time PCR instrument on 384 custom-made TaqMan microfluidic cards (product no. 4342253; ThermoFisher). Threshold cycle values were normalized to the mean values for *Gapdh* and *Hprt*. Linear regression analyses were used to assess correlations with *Ift88* expression, and subsequently raw *P* values and corrected *P* (P_{corr}) values (Bonferroni adjusted) were calculated using GraphPad Prism software version 9.

RNAScope analysis. Knee joints were harvested into ice-cold 4% paraformaldehyde and incubated in a refrigerated environment for 24 hours before being transferred into ice-cold 10%, 20%, and 30% sucrose, each for 24 hours. RNAScope probes Mm-Ift88-C1 (product no. 420211-C1) and Mm-Gli1-C2 (product no. 311001-C2) were used in combination with Opal 570 reagent pack signals (product no. FP14880001KT) and 690 reagent pack signals (product no. FP1497001KT) (all from ACD inc.), with the values normalized to those of both positive and negative controls. For further details on slide preparation and more information regarding the imaging protocols applied when using the RNAScope multiplex fluorescent reagent kit version 2 (product no. 323100), see Supplementary Methods (available on the *Arthritis & Rheumatology* website at <http://onlinelibrary.wiley.com/doi/10.1002/art.41894/abstract>).

RESULTS

Thinner medial articular cartilage in adolescent mice following *Ift88* deletion in chondrocytes. To confirm inducible tissue-specific Cre recombination, the *aggrecan*^{Cre^{ERT2}} mouse line was crossed with a tdTomato reporter mouse line, and tamoxifen was administered at 4 and 8 weeks of age. Two weeks following tamoxifen treatment, activation of Cre recombinase was observed in superficial hip articular cartilage chondrocytes (Supplementary Figure 2A, available on the *Arthritis & Rheumatology* website at <http://onlinelibrary.wiley.com/doi/10.1002/art.41894/abstract>), as well as in knee articular cartilage chondrocytes and menisci ($n = 3$) (Figure 1A).

In mice, throughout adolescence and adulthood, articular cartilage was thicker on the medial tibial plateau than on the lateral

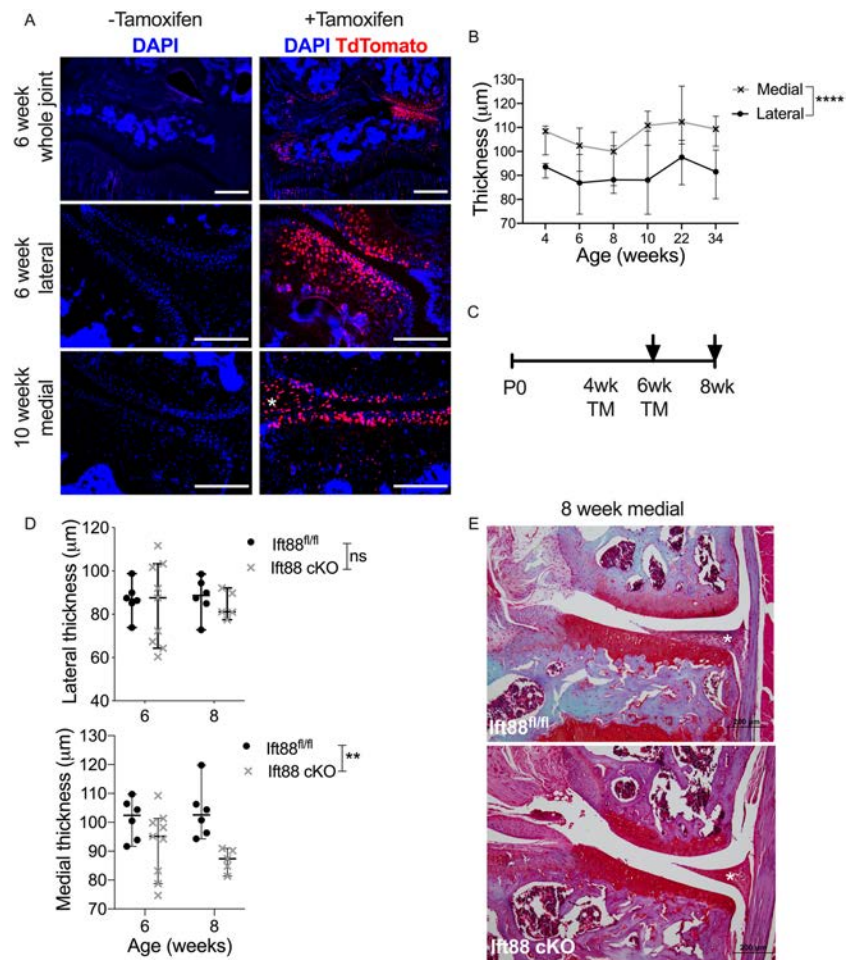


Figure 1. Deletion of *Ift88* in adolescent mice leads to thinner articular cartilage. **A** and **C**, *AggrecanCre^{ERT2}; tdTomato* mice were left untreated or treated with tamoxifen (TM) at ages 4 weeks or 8 weeks (as illustrated by the diagram in **C**; arrows indicate sample collection points), and cryosections of the whole knee joint and the medial and lateral compartments were obtained for immunofluorescence analysis (counterstained with DAPI) (**A**). Bars = 200 μm . **B** and **D**, Thickness of the medial and lateral articular cartilage was assessed in sections from control mice at ages 4, 6, 8, 10, 22, and 34 weeks (**B**), and from *aggrecanCre^{ERT2}; Ift88^{fl/fl}* (*Ift88*-conditional knockout [cKO]) mice and *Ift88^{fl/fl}* control mice at ages 6 weeks or 8 weeks (**D**). Symbols represent individual mice; bars show the median \pm 95% confidence interval. ** = $P < 0.01$; **** = $P < 0.0001$, by two-way analysis of variance. **E**, Images show Safranin O staining of the cartilage from the medial meniscus of a representative *Ift88^{fl/fl}* mouse and *Ift88*-cKO mouse at age 8 weeks, 2 weeks after tamoxifen injection. The white asterisk in **A** and **E** indicates the medial meniscus. NS = not significant.

plateau ($P < 0.0001$) (Figure 1B). *Ift88* was deleted at 4 or 6 weeks of age, and analysis was conducted 2 weeks later (Figure 1C). Deletion of *Ift88* in mice at age 6 weeks resulted in reduced thickness of the medial and lateral knee cartilage, which was significantly different compared to that in the control group (median 82.96 μm [95% confidence interval (95 CI) 81.13–91.56] in *aggrecanCre^{ERT2}; Ift88^{fl/fl}* mice versus 95.58 μm [95% CI] 92.08–99.68] in control mice). A similar effect was not observed when *Ift88* was deleted at 4 weeks of age (Supplementary Figure 2B, available on the *Arthritis & Rheumatology* website at <http://onlinelibrary.wiley.com/doi/10.1002/art.41894/abstract>). Considering each plateau separately, deletion of *Ift88* in mice resulted in a significant reduction in medial cartilage thickness at 6 weeks of age (median thickness 102.42 μm [95% CI 91.7–109.7] in control mice and 94.25 μm [95% CI 78.7–101.3] in

aggrecanCre^{ERT2}; Ift88^{fl/fl} mice) and at 8 weeks of age (median thickness 102.57 μm [95% CI 94.3–119.8] in control mice and 87.36 μm [95% CI 81.35–90.97] in *aggrecanCre^{ERT2}; Ift88^{fl/fl}* mice) (Figures 1D and E). Lateral cartilage thickness was unaffected (Figure 1D).

Thinner calcified articular cartilage resulting from *Ift88* deletion.

In a previous mouse study, reduced thickness of the articular cartilage was associated with acceleration of programmed hypertrophy upon postnatal activation of Hh signaling in mice (25). To assess the effects of *Ift88* deletion on cartilage in maturing mice, we measured the thickness of noncalcified and calcified cartilage (Figure 2A and Supplementary Figure 1A, available on the *Arthritis & Rheumatology* website at <http://onlinelibrary.wiley.com/doi/10.1002/art.41894/abstract>). In control mice, the

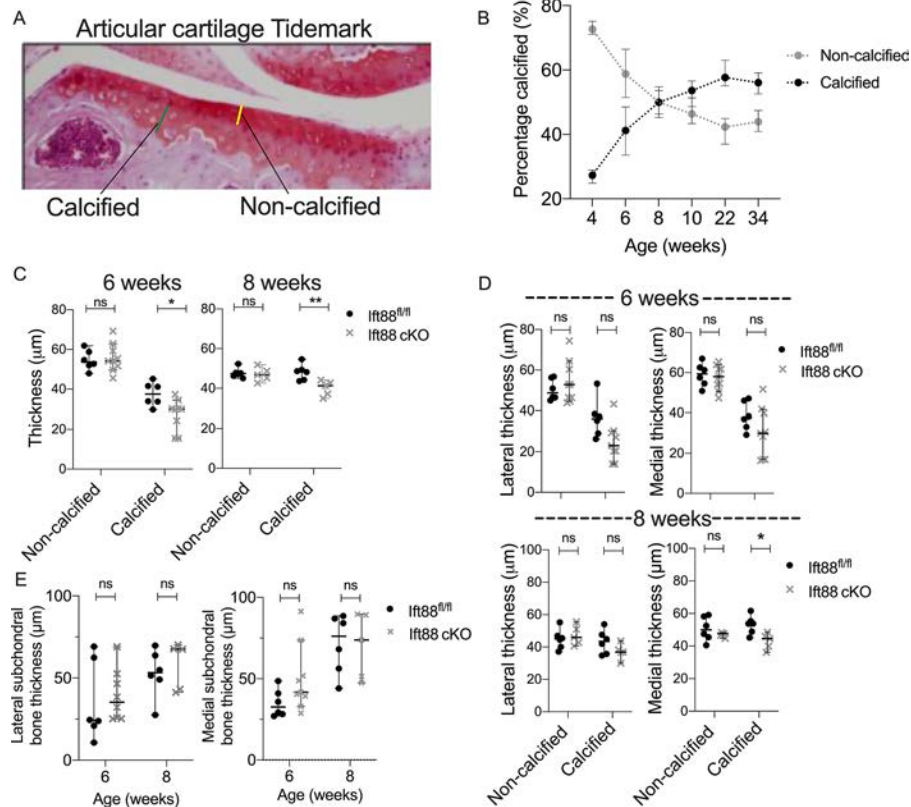


Figure 2. Deletion of *Ift88* in adolescent mice leads to thinner calcified articular cartilage. **A** and **B**, Sections of knee articular cartilage from mice were stained with Safranin O to identify the noncalcified and calcified areas of the cartilage (demarcated by the tidemark) (**A**), and to determine the median percentage of cartilage that was calcified versus noncalcified in sections from mice at different ages ($n = 3$ for 4-week-old mice; $n = 6$ – 19 for all other age groups) (**B**). **C** and **D**, Thickness of the noncalcified and calcified areas of the articular cartilage was compared between *aggrecan-Cre^{ERT2};Ift88^{fl/fl}* (*Ift88*-cKO) mice and *Ift88^{fl/fl}* control mice at ages 6 weeks or 8 weeks, in the whole joint (**C**) or by medial and lateral compartment (**D**). **E**, Median subchondral bone thickness was compared between *aggrecanCre^{ERT2};Ift88^{fl/fl}* (*Ift88*-cKO) mice and *Ift88^{fl/fl}* control mice at ages 6 weeks or 8 weeks. Symbols represent individual mice; bars show the median \pm 95% confidence interval. A minimum of 5 joints was assessed in any group. * = $P < 0.05$; ** = $P < 0.01$, by two-way analysis of variance. See Figure 1 for definitions.

proportion of calcified articular cartilage increased from 25% at 4 weeks of age to 60% by 22 weeks of age (Figure 2B). Deletion of *Ift88* resulted in thinner calcified cartilage at 6 weeks of age (median thickness 37.52 μm [95% CI 29.71–45.17] in control mice and 29.96 μm [95% CI 15.46–34.50] in *aggrecanCre^{ERT2};Ift88^{fl/fl}* mice) and at 8 weeks of age (median thickness 48.43 μm [95% CI 43.62–54.64] in control mice and 41.29 μm [95% CI 34.93–44.17] in *aggrecanCre^{ERT2};Ift88^{fl/fl}* mice), though these reductions were only statistically significant on the medial plateau (Figure 2C). Separating measurements by lateral and medial plateaus revealed reductions in calcified cartilage that were observable across both plateaus and time points, though these reductions were only significant on the medial plateau at 8 weeks of age (Figure 2D).

Histologic measurements of the subchondral bone (Supplementary Figure 1B, available on the *Arthritis & Rheumatology* website at <http://onlinelibrary.wiley.com/doi/10.1002/art.41894/abstract>) revealed that bone thickness approximately doubled between 6 and 8 weeks of age in control mice (Figure 2E). However, deletion of *Ift88* did not result in enhanced bone

thickening. Additionally, there was no tartrate-resistant acid phosphatase staining (Supplementary Figure 1C) in the articular cartilage or the bone beneath, suggesting very little osteoclast activity in the calcified cartilage or subchondral bone at these time points.

Association of reductions in calcified cartilage thickness with articular cartilage atrophy following *Ift88* deletion in mice at 8 weeks of age.

Progressive calcification of articular cartilage continued when mice were between 8 and 22 weeks of age (Figure 2B). Tamoxifen was administered at 8 weeks of age, and joints were collected at 10, 22, and 34 weeks of age (Figure 3A). Deletion of *Ift88* resulted in a 10–20% reduction in the thickness of tibial cartilage at every time point (Figures 3B and C). Based on the mean values across both plateaus, thinning was not cumulative over time and occurred without obvious surface fibrillation, thus representative of atrophy rather than degeneration (3,5,26,27). At 22 and 34 weeks of age, thinning of the medial plateau of *Ift88*-KO mice was significantly greater than

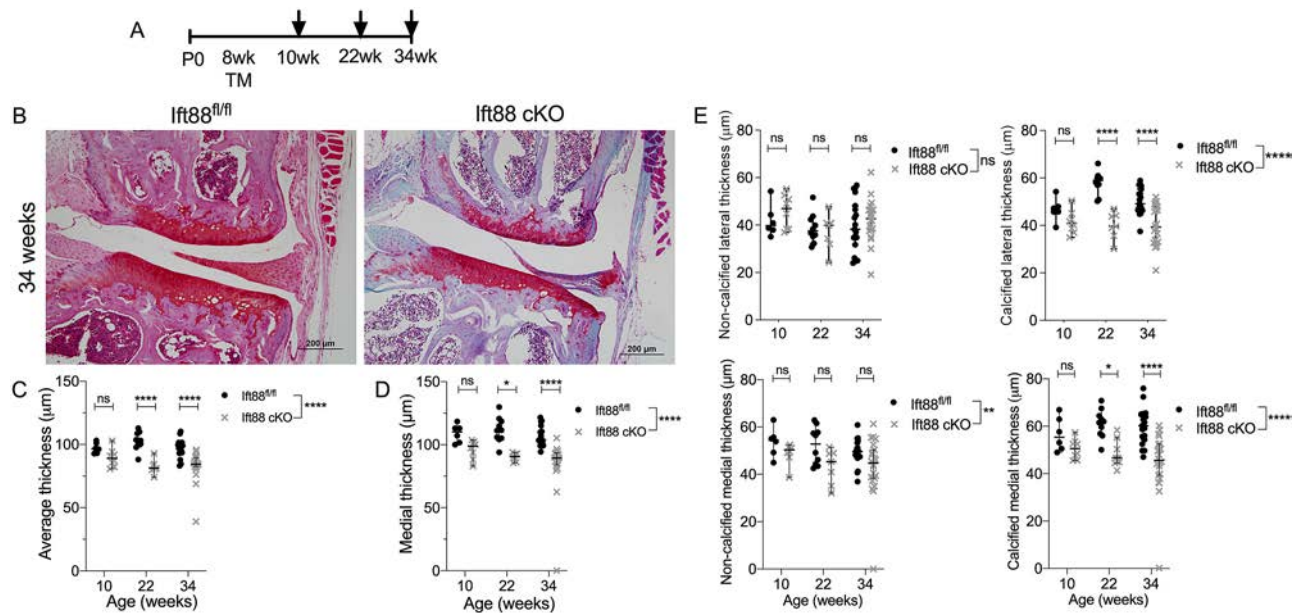


Figure 3. Deletion of *Ift88* in mice at age 8 weeks results in atrophy of the articular cartilage and reduced thickness of the calcified cartilage. **A**, Experimental timeline shows the age of the mice when tamoxifen was injected and the time points when tissue samples were collected (arrows). **B**, Sections of medial articular cartilage from 34-week-old *Ift88* control and *aggrecanCre^{ERT2};Ift88^{fl/fl}* (*Ift88*-cKO) mice were stained with Safranin O for histologic analysis. **C** and **D**, In *Ift88^{fl/fl}* controls and *Ift88*-cKO mice at each age, thickness of the articular cartilage was measured in both the medial and lateral compartments (**C**) and in the medial compartment alone (**D**). **E**, Thickness of the noncalcified and calcified areas of the articular cartilage in both the lateral and medial compartments was compared between groups of mice at each age. Symbols represent individual mice; bars show the median \pm 95% confidence interval. * = $P < 0.05$; ** = $P < 0.01$; **** = $P < 0.0001$, by two-way analysis of variance. See Figure 1 for definitions.

that of control mice. By the time the mice reached 34 weeks of age, the median thickness of the medial plateau was 104.00 μm (95% CI 100.30–110.50) in control mice and 89.42 μm (95% CI 84.00–93.49) in *aggrecanCre^{ERT2};Ift88^{fl/fl}* mice (Figure 3D). Atrophy was milder on the lateral tibial plateaus and was not apparent until mice reached 22 weeks of age (Supplementary Figure 3A, available on the *Arthritis & Rheumatology* website at <http://onlinelibrary.wiley.com/doi/10.1002/art.41894/abstract>).

The effect of *Ift88* deletion on the thickness of the noncalcified cartilage was not statistically significant on either the medial or the lateral plateaus (Figure 3E). In contrast, statistically significant reductions in the thickness of the calcified cartilage were observed on both the medial and the lateral plateaus (medial plateau, median 58.72 μm [95% CI 54.34–65.05] in control mice versus 45.62 μm [95% CI 39.32–52.49] in *aggrecanCre^{ERT2};Ift88^{fl/fl}* mice) (Figure 3E).

Prior evidence has shown that cartilage thinning and accelerated hypertrophy occur in association with reduced numbers of chondrocytes in articular cartilage following reactivation with Hh signaling (25). However, no significant reductions in cell number or density were observed in 10-week-old *aggrecanCre^{ERT2};Ift88^{fl/fl}* mice (Supplementary Figure 3B, available on the *Arthritis & Rheumatology* website at <http://onlinelibrary.wiley.com/doi/10.1002/art.41894/abstract>). TUNEL staining revealed limited apoptosis in both control mice and *aggrecanCre^{ERT2};Ift88^{fl/fl}* mice (Supplementary Figure 3C).

Predisposition of joints to spontaneous OA following atrophy of the medial tibial cartilage.

At 34 weeks of age, *aggrecanCre^{ERT2};Ift88^{fl/fl}* mice developed spontaneous cartilage damage in the medial compartment and this was found to be associated with osteophyte formation, indicating the development of OA (Figure 4A). OARSI scoring revealed a significant increase in cartilage damage scores when mice were 34 weeks of age (Figure 4B), but no significant increase when mice were 22 weeks of age (Supplementary Figure 4A, available on the *Arthritis & Rheumatology* website at <http://onlinelibrary.wiley.com/doi/10.1002/art.41894/abstract>). The highest OARSI scores were found on the medial plateau (Figure 4C). There was no difference in osteophyte scores, except in cartilage displaying severe damage (Figure 4D and Supplementary Figure 4B, <http://onlinelibrary.wiley.com/doi/10.1002/art.41894/abstract>). There were no changes in subchondral bone thickness following *Ift88* deletion in mice at either 10 or 22 weeks of age. By 34 weeks of age, cartilage thinning was associated with a loss of subchondral bone in *aggrecanCre^{ERT2};Ift88^{fl/fl}* mice (Figure 4E and Supplementary Figure 4C, <http://onlinelibrary.wiley.com/doi/10.1002/art.41894/abstract>). Trabecular bone density (BV/TV) in the epiphysis was not affected by deletion of *Ift88* (Supplementary Figure 4D).

Exacerbation of OA severity after surgical joint destabilization and deletion of *Ift88*.

Mice were given tamoxifen at 8 weeks of age, and surgical DMM was performed

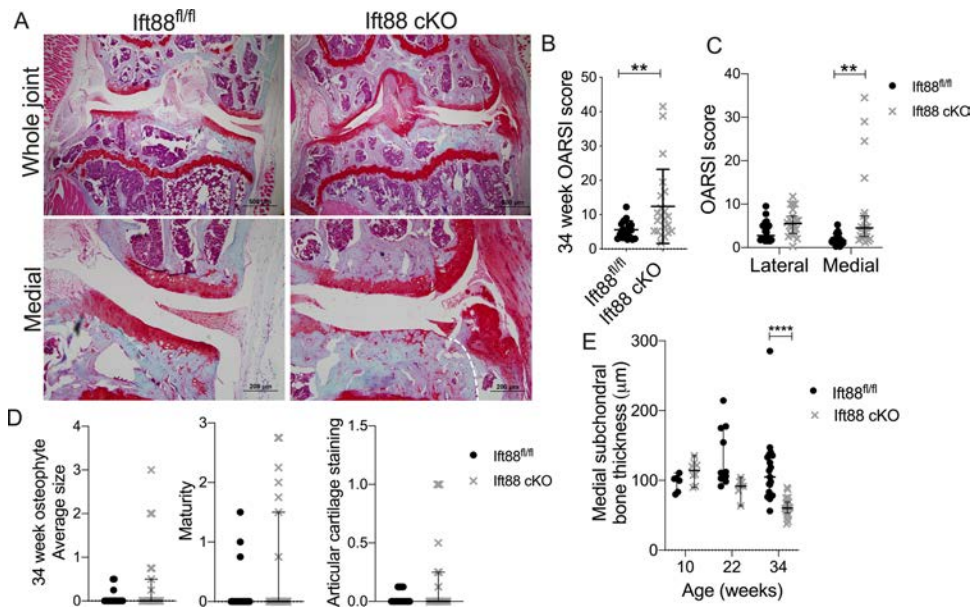


Figure 4. Features of spontaneous osteoarthritis (OA) in *lft88*-conditional knockout [cKO] mice at age 34 weeks. **A**, Whole joint sections and sections from the medial compartment of the articular cartilage from 34-week-old *lft88*^{fl/fl} control and *lft88*-cKO mice were stained with Safranin O for histologic analysis of OA-like features. The **curved white broken line** in the bottom right panel indicates the area of osteophyte formation. **B** and **C**, Summed modified Osteoarthritis Research Society International (OARSJ) scores were used to assess joint damage in articular cartilage sections from 34-week-old *lft88*^{fl/fl} control and *lft88*-cKO mice, in the whole joint (**B**) and by compartment (**C**). ** = $P < 0.01$ by Mann-Whitney test. **D**, Articular cartilage from 34-week-old *lft88*^{fl/fl} control and *lft88*-cKO mice was assessed for median osteophyte size and maturity, as well as for osteophyte staining scores. **E**, Thickness of the subchondral bone was assessed in the medial compartment of articular cartilage from *lft88*^{fl/fl} control and *lft88*-cKO mice at ages 10, 22, or 34 weeks. Symbols represent individual mice (19–22 mice per group); bars show the median \pm 95% confidence interval. **** = $P < 0.0001$ by two-way analysis of variance.

at 10 weeks of age. At either 8 or 12 weeks after surgery, mice were killed and the knee joints were collected, including those from sham-operated mice at the same time points (Figure 5A). Coronal histologic joint sections (Figure 5B) were assessed using summed OARSJ scores of cartilage damage. Deletion of *lft88* resulted in exacerbated disease activity 12 weeks after DMM (mean \pm SD OARSJ score 22.08 ± 9.30 in *lft88*^{fl/fl} mice versus 29.83 ± 7.69 in *aggrecanCre*^{ERT2};*lft88*^{fl/fl} mice [$P < 0.05$]; $n = 15$ mice per group) (Figure 5C). No differences in osteophyte size (Figure 5D and Supplementary Figure 5A, available on the *Arthritis & Rheumatology* website at <http://onlinelibrary.wiley.com/doi/10.1002/art.41894/abstract>), osteophyte maturity, or osteophyte staining scores (Supplementary Figures 5B–E) were observed between control mice and *aggrecanCre*^{ERT2};*lft88*^{fl/fl} mice at either time point after DMM. Further, we observed no difference in the BV/TV of the epiphysis between control mice and *aggrecanCre*^{ERT2};*lft88*^{fl/fl} mice 12 weeks following DMM (Supplementary Figure 5F).

Lack of association between articular cartilage atrophy and markers of matrix catabolism or hypertrophy.

To assess whether *lft88* deletion increased the catabolism of aggrecan, knee joints from control mice and *aggrecanCre*^{ERT2};*lft88*^{fl/fl} mice were probed for protease-generated neopeptides as described previously (22), using an antibody raised against the

synthetic epitope NITEGE, and with an IgG antibody used as an isotype control (Supplementary Figure 6A, available on the *Arthritis & Rheumatology* website at <http://onlinelibrary.wiley.com/doi/10.1002/art.41894/abstract>). The NITEGE signal was weak in sections probed with the IgG positive control antibody (Supplementary Figure 6A), and no differences in NITEGE signaling were observed between the joints from control mice and joints from *aggrecanCre*^{ERT2};*lft88*^{fl/fl} mice (Figure 6A). Moreover, no differences in *ColX* expression, a marker of Hh-driven chondrocyte hypertrophy (28), were observed between *lft88*-KO mice and control mice, as determined by IHC (Figure 6B; results compared against the IgG control are shown in Supplementary Figure 6B).

Results of bulk RNA analyses implicating *Tcf7l2* in cartilage atrophy.

Two weeks after tamoxifen treatment, RNA was isolated from microdissected articular cartilage obtained from the knee joints of 10-week-old *lft88*-KO and control mice (Supplementary Figure 6C, available on the *Arthritis & Rheumatology* website at <http://onlinelibrary.wiley.com/doi/10.1002/art.41894/abstract>). A total of 44 candidate genes, which were all either associated with chondrocyte biology and/or implicated in primary ciliary signaling, were measured using qPCR. Due to the mosaic Cre activity (Figure 1A) and sample pooling, we conducted a correlation analysis to assess correlations between *lft88* expression and expression of the candidate

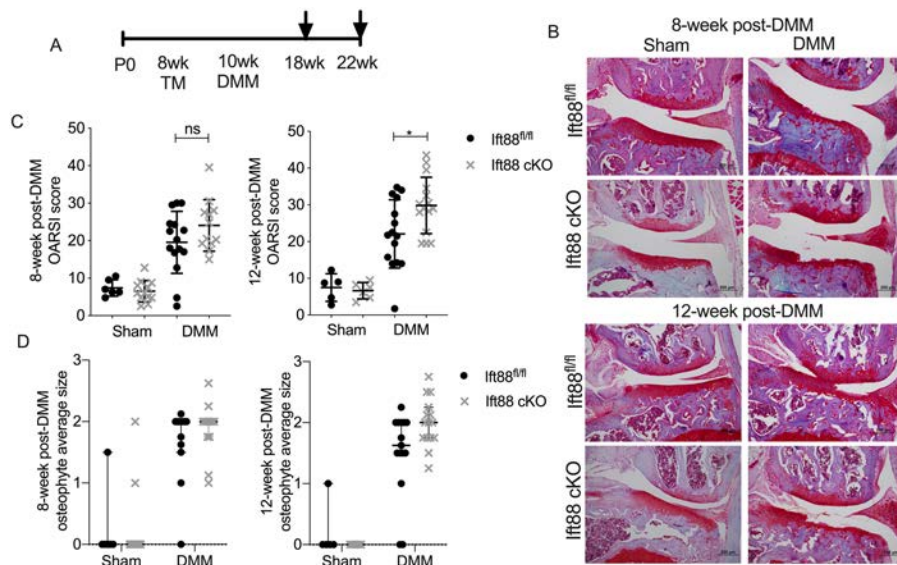


Figure 5. Deletion of *Ift88* in mice exacerbates disease at 12 weeks after surgical destabilization of the medial meniscus (DMM). **A**, Experimental timeline shows the time points for tamoxifen injection and DMM surgery, as well as sample collection (arrows). **B**, Joint sections from the medial compartment of the articular cartilage of sham-operated and DMM-operated *Ift88^{fl/fl}* control and *Ift88*-cKO mice, obtained at 8 weeks and 12 weeks after surgery, were stained with Safranin O for histologic analysis. **C** and **D**, Articular cartilage from sham-operated mice (minimum of 5 mice per group) and DMM-operated mice (12–15 mice per group) were assessed for summed modified Osteoarthritis Research Society International (OARSI) joint damage scores (**C**) and median osteophyte size (**D**) at 8 weeks and 12 weeks after DMM. Symbols represent individual mice; bars show the median \pm 95% confidence interval. * = $P < 0.05$ by two-way analysis of variance. See Figure 1 for other definitions.

genes, with values normalized to the mean values for the 2 most stable housekeeping genes, *Hprt* and *Gapdh* (for all genes see Supplementary Table 1, available on the *Arthritis & Rheumatology* website at <http://onlinelibrary.wiley.com/doi/10.1002/art.41894/abstract>). Expression of the majority of candidate genes did not correlate with *Ift88*, including *Adamts5* and *ColX* (Supplementary Figure 6D), which was consistent with the IHC findings (Figures 6A and B). *Tcf7l2* (29) was the only gene found to be correlated with *Ift88* expression at a level that was statistically significant after Bonferroni correction ($P = 0.0006$, $P_{\text{corr}} = 0.026$, $r^2 = 0.8811$). Levels of *Ctgf*, *Tgfb3*, *Gli2*, and the regulator of cartilage calcification *Enpp1* (30) were positively correlated with *Ift88* expression before Bonferroni correction ($P = 0.002$, $P = 0.0107$, $P = 0.0037$, and $P = 0.009$, respectively) (Figure 6C and Supplementary Figure 6C, available on the *Arthritis & Rheumatology* website at <http://onlinelibrary.wiley.com/doi/10.1002/art.41894/abstract>), but not after Bonferroni correction. Expression of *Gli1* and *Ptch1*, indicators of Hh pathway activation, did not correlate with *Ift88* expression (Supplementary Table 1).

Reduction in *Ift88* expression in *aggrecanCre^{ERT2}; Ift88^{fl/fl}* mouse cartilage revealed using RNAScope analysis. To overcome the limitations of bulk RNA analyses, an RNAScope analysis was performed on cryosections of tibial articular cartilage from 10-week-old control and *aggrecanCre^{ERT2}; Ift88^{fl/fl}* mice ($n = 4$ each) to assess *Ift88* expression, in situ. Results of the RNAScope

analysis revealed that a mean of 39.61% of cells were positive for *Ift88* in control mouse cartilage in comparison to a mean of 27.78% of *Ift88*-positive cells in *aggrecanCre^{ERT2}; Ift88^{fl/fl}* mouse cartilage, indicating a 30% reduction in *Ift88*-positive cells ($P < 0.0001$ by Fisher's exact test) (Figure 6D; for images and contingency data for statistical comparisons, see Supplementary Figure 6E, available on the *Arthritis & Rheumatology* website at <http://onlinelibrary.wiley.com/doi/10.1002/art.41894/abstract>).

Effect of wheel exercise on cartilage atrophy and associated increases in Hh signaling in situ.

RNAScope analysis was performed to investigate the expression of *Gli1*, a marker of Hh pathway activity, in the same cartilage sections in which reduced *Ift88* expression was observed. A mean total of 24.12% of nuclei were positive for *Gli1* in control mouse articular cartilage in comparison to a total of 45.46% of *Gli1*-positive nuclei in *aggrecanCre^{ERT2}; Ift88^{fl/fl}* mouse articular cartilage (Figure 6E). This increase in the percentage of *Gli1*-positive cells, indicative of increased Hh signaling, was statistically significant ($n = 4$ each; $P < 0.0001$) (for raw cell counts, see Supplementary Figure 6E, available on the *Arthritis & Rheumatology* website at <http://onlinelibrary.wiley.com/doi/10.1002/art.41894/abstract>). Analyzing *Gli1* in terms of signal per cell also revealed higher expression of *Gli1* in *aggrecanCre^{ERT2}; Ift88^{fl/fl}* mice (2.88 mean dots per cell per animal) compared to control mice (1.49 mean dots per cell per animal), representing a statistically significant difference ($n = 4$ each; $P < 0.01$) (Figure 6E).

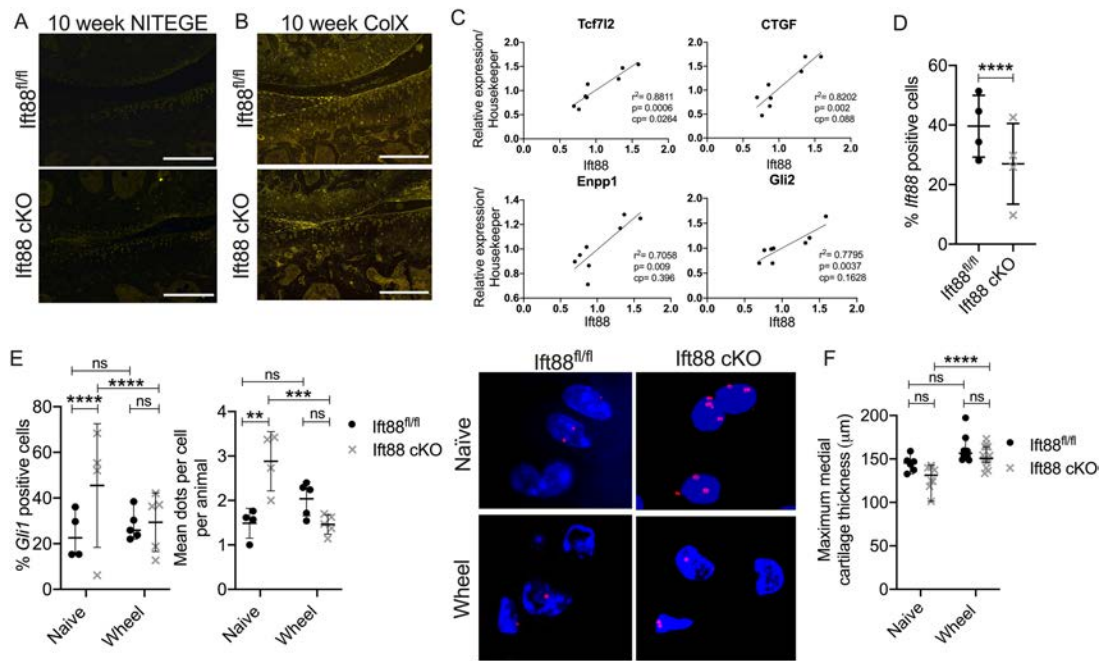


Figure 6. Wheel exercise rescues cartilage atrophy and suppresses increased hedgehog signaling in mouse chondrocytes. **A** and **B**, Immunofluorescence staining of articular cartilage chondrocytes from a representative *lft88^{fl/fl}* control mouse and *lft88*-cKO mouse at age 10 weeks shows expression of the aggrecan neoepitope NITEGE (**A**) and type X collagen (ColX) (**B**). Bars = 200 μ m. **C**, RNA extracted from the microdissected articular cartilage was analyzed using quantitative polymerase chain reaction to identify genes showing a correlation with *lft88* expression. Values were normalized to the mean values for the housekeeping genes *Gapdh* and *Hprt*. Linear regression analyses were performed, and significance was assessed before and after Bonferroni correction (corrected P [cpj]). **D** and **E**, Findings from RNAScope analysis of the articular cartilage chondrocytes show the percentage of chondrocytes that were positive for *lft88* expression in *lft88^{fl/fl}* control and *lft88*-cKO mice (**D**), and the percentage of *Gli1*-positive cells, mean number of *Gli1*-positive dots per cell per mouse, and number of *Gli1*-positive nuclei in *lft88^{fl/fl}* control and *lft88*-cKO exercise-naive mice compared to wheel-exercised mice (**E**). ** = $P < 0.01$; *** = $P < 0.001$; **** = $P < 0.0001$, by two-way analysis of variance. **F**, Maximum medial cartilage thickness was compared between exercise-naive and wheel-exercised *lft88^{fl/fl}* control and *lft88*-cKO mice. **** = $P < 0.0001$ by Fisher's exact test. Symbols represent individual mice; bars show the median \pm 95% confidence interval. See Figure 1 for other definitions.

Mice were given free access to wheel exercise for 2 weeks immediately following the tamoxifen injection administered at 8 weeks of age (over the same time period that atrophy develops). In these experiments, no measurable difference in articular cartilage thickness was observed when comparing control mice to *aggrecanCre^{ERT2};lft88^{fl/fl}* mice (Figure 6F and Supplementary Figure 6F, available on the *Arthritis & Rheumatology* website at <http://onlinelibrary.wiley.com/doi/10.1002/art.41894/abstract>). Wheel exercise did not affect the number of *Gli1*-positive cells or *Gli1* expression per cell in control mice, but, according to findings from both analyses, wheel exercise reduced *Gli1* expression in *aggrecanCre^{ERT2};lft88^{fl/fl}* mice, effectively restoring Hh signaling and cartilage thickness to the levels observed in control mice.

DISCUSSION

In the current study, we explored the influence of ciliary protein IFT88 in postnatal mouse articular cartilage in vivo, by depleting its expression in chondrocytes at different stages of postnatal skeletal maturation. When *lft88* was deleted in the mice at 4, 6,

and 8 weeks of age, we observed rapid cartilage thinning, largely in the calcified cartilage within the medial joint compartment. Thinning was determined to be indicative of atrophy rather than degeneration, since there was no disruption of the articular surface. However, as mice aged, cartilage atrophy was associated with increased severity of spontaneous OA and DMM-induced OA.

We speculate that the *lft88*-dependent effects in the thicker medial compartment of the mouse joint are mechanically driven (6) in a manner analogous to the bone "mechanostat" proposed by Frost in 1987 (31). In essence, this model ensures that chondrocytes mechanoadapt the extracellular matrix so as to experience force within a narrow window (1). Since cartilage thickness can be restored in *lft88*-conditional KO mice with wheel exercise, this suggests that ciliary protein IFT88 may influence, but is not solely responsible for, cartilage mechanoadaptation in vivo. Similar modes of action have been proposed in the context of epithelial response to renal flow (14,32). Our findings contrast with the observation that in mice, deletion of *lft88* during development leads to increased cartilage thickness (17), possibly indicating a changing influence of *lft88* with skeletal maturation.

Since atrophy in *Ift88*-conditional KO mice is largely restricted to calcified cartilage, we speculate that this represents a failure of cartilage hypertrophy during maturation, in a load-dependent manner. Cartilage thinning was not associated with increased matrix catabolism, enhanced subchondral bone thickness, osteoclast activity, or density changes (BV/TV) in the epiphysis, but we cannot exclude the possibility that calcified cartilage is transitioning to the bone in these mice. Calcification of mouse cartilage has recently been linked to *Enpp1*, a pyrophosphatase believed to inhibit calcification through Hh signaling (30). Findings from our molecular analyses indicated that *Enpp1* positively correlates with *Ift88* expression, indicating a reduction in the levels of an inhibitor of calcification in *Ift88*-conditional KO mice. This could result in accelerated ossification analogous to that seen in the growth plates of ciliary protein mutant mice and in articular cartilage upon postnatal activation of Hh (25).

Prior studies investigating congenital mutations (33) or constitutive deletions of *Ift88* (17,18,34) demonstrated that *Ift88* plays a role in mouse limb and joint development. Mouse models targeting other ciliary components, *Kif3a*, Bardet-Biedl syndrome proteins, and *Ift80*, also implicate ciliary machinery in musculoskeletal development (19,28). This influence over skeletal development is also exemplified by the human skeletal ciliopathies (35,36). The most important molecular pathway associated with ciliopathy is Hh, although other pathways have also been described (10,37–41). Hh signaling largely switches off in adulthood (42) but is reactivated in OA (8). We investigated the molecular basis of *Ift88*-dependent cartilage atrophy by identifying the correlation between *Ift88* expression (reflecting efficiency of deletion) and 44 molecules previously demonstrated to be associated with ciliary signaling and cartilage biology. In addition, we explored Hh signaling by directly visualizing *Gli1* expression in murine cartilage using RNAScope. The gene that correlated most strongly with ciliary signaling was transcription factor *Tcf7l2*, previously shown to influence and interact with Hh and β -catenin signaling pathways in cartilage (37). Other genes whose levels correlated with *Ift88* included *Gli2*, *Ctgf*, and *Enpp1*, although these correlations were only statistically significant before Bonferroni correction.

While a gene expression analysis of microdissected mouse cartilage did not show a correlation between *Ift88* and classic Hh pathway molecules (*Gli1*, *Ptch1*), an individual cell analysis using RNAScope revealed increased levels of *Gli1* expression in *aggreCanCre^{ERT2};Ift88^{fl/fl}* mouse chondrocytes, suggesting a reciprocal relationship between Hh signaling and *Ift88*. Therefore, we propose that loss of *Ift88* disrupts ciliary-mediated repression of Hh signaling, resulting in net increases in *Gli1* expression. This is consistent with findings from previous studies in constitutive *Ift88* deletion (18) and endochondromas (43). In this model, our observation that cartilage atrophy was rescued and basal *Gli1* expression levels were normalized in *aggreCanCre^{ERT2};Ift88^{fl/fl}* mice following wheel exercise provides critical evidence of a link with mechanical loading. Our data imply that in postnatal mouse articular cartilage, ciliary protein IFT88 safeguards the progressive

mechanoadaptation of adolescent mouse cartilage, supporting the creation and maturation of fit-for-purpose adult mouse articular cartilage by ensuring appropriate levels of Hh signaling.

As previously described (44), *Ift88* was deleted in mouse chondrocytes using induction of Cre recombinase expression on the aggrecan promoter, which ensured sufficient expression in mice from adolescence through adulthood. Despite the use of this method, we observed only a 40% reduction in *Ift88*-positive chondrocytes in the tibial articular cartilage of *aggreCanCre^{ERT2};Ift88^{fl/fl}* mice. Observations in the tdTomato reporter line of mice indicated that *Ift88* deletion occurred in only a small proportion of chondrocytes, but this was not exclusive to any knee compartment, and therefore it is unlikely that this finding could be attributed to differences between the medial and lateral sides of the knee joint. We also recognize that, due to the challenges associated with imaging cilia in cartilage, we have not yet been able to address the question of whether primary cilia would be negatively impacted as a result of *Ift88* deletion. Thus, we cannot conclude that molecular changes are a direct consequence of the loss of cilia. To date, we have not yet conducted experiments inducing *Ift88* deletion in mice older than age 8 weeks to evaluate whether this gene is as influential later in adulthood, or assessed how behavior of the *aggreCanCre^{ERT2};Ift88^{fl/fl}* mice could be altered.

In summary, these data demonstrate that IFT88 is highly influential in adolescent mouse and adult mouse articular cartilage as a positive regulator of cartilage thickness, guiding cartilage calcification during maturation and safeguarding physiologic Hh signaling in adult mouse cartilage in response to mechanical cues.

AUTHOR CONTRIBUTIONS

All authors were involved in drafting the article or revising it critically for important intellectual content, and all authors approved the final version to be published. Dr. Coveney had full access to all of the data in the study and takes responsibility for the integrity of the data and the accuracy of the data analysis.

Study conception and design. Coveney, Wann.

Acquisition of data. Coveney, Zhu, Miotla-Zarebska, Chang, McSorley.

Analysis and interpretation of data. Coveney, Stott, Parisi, Batchelor, Duarte, Vincent, Wann.

REFERENCES

1. Simon WH. Scale effects in animal joints. I. Articular cartilage thickness and compressive stress. *Arthritis Rheum* 1970;13:244–56.
2. Grodzinsky AJ, Levenston ME, Jin M, Frank EH. Cartilage tissue remodeling in response to mechanical forces [review]. *Annu Rev Biomed Eng* 2000;2:691–713.
3. Palmoski MJ, Brandt KD. Effects of static and cyclic compressive loading on articular cartilage plugs in vitro. *Arthritis Rheum* 1984;27:675–81.
4. Osborne AC, Lamb KJ, Lewthwaite JC, Dowthwaite GP, Pitsillides AA. Short-term rigid and flaccid paralyses diminish growth of embryonic chick limbs and abrogate joint cavity formation but differentially preserve pre-cavitated joints. *J Musculoskelet Neuronal Interact* 2002;2:448–56.

5. Palmoski M, Perricone E, Brandt KD. Development and reversal of a proteoglycan aggregation defect in normal canine knee cartilage after immobilization. *Arthritis Rheum* 1979;22:508–17.
6. Vincent TL, Wann AK. Mechanoadaptation: articular cartilage through thick and thin [review]. *J Physiol* 2019;597:1271–81.
7. Vincent TL, Hermansson MA, Hansen UN, Amis AA, Saklatvala J. Basic fibroblast growth factor mediates transduction of mechanical signals when articular cartilage is loaded. *Arthritis Rheum* 2004;50:526–33.
8. Lin AC, Seeto BL, Bartoszko JM, Khoury MA, Whetstone H, Ho L, et al. Modulating hedgehog signaling can attenuate the severity of osteoarthritis. *Nat Med* 2009;15:1421–5.
9. Tang X, Muhammad H, McLean C, Miotla-Zarebska J, Fleming J, Didangelos A, et al. Connective tissue growth factor contributes to joint homeostasis and osteoarthritis severity by controlling the matrix sequestration and activation of latent TGF β . *Ann Rheum Dis* 2018;77:1372–80.
10. Wu Q, Zhang Y, Chen Q. Indian hedgehog is an essential component of mechanotransduction complex to stimulate chondrocyte proliferation. *J Biol Chem* 2001;276:35290–6.
11. Poole CA, Jensen CG, Snyder JA, Gray CG, Hermanutz VL, Wheatley DN. Confocal analysis of primary cilia structure and colocalization with the Golgi apparatus in chondrocytes and aortic smooth muscle cells. *Cell Biol Int* 1997;21:483–94.
12. Bangs F, Anderson KV. Primary cilia and mammalian hedgehog signaling [review]. *Cold Spring Harb Perspect Biol* 2017;9:a028175.
13. Wheway G, Nazlamova L, Hancock JT. Signaling through the primary cilium. *Frontiers Cell Dev Biol* 2018;6:8.
14. Praetorius HA, Frokiaer J, Nielsen S, Spring KR. Bending the primary cilium opens Ca $^{2+}$ -sensitive intermediate-conductance K $^{+}$ channels in MDCK cells. *J Membr Biol* 2003;191:193–200.
15. Wann AK, Zuo N, Haycraft CJ, Jensen CG, Poole CA, McGlashan SR, et al. Primary cilia mediate mechanotransduction through control of ATP-induced Ca $^{2+}$ signaling in compressed chondrocytes. *FASEB J* 2012;26:1663–71.
16. Coveney CR, Collins I, McFie M, Chanalaris, Yamamoto K, Wann AK. Cilia protein IFT88 regulates extracellular protease activity by optimizing LRP-1-mediated endocytosis. *FASEB J* 2018;32:fj201800334.
17. Haycraft CJ, Zhang Q, Song B, Jackson WS, Detloff PJ, Serra R. Intraflagellar transport is essential for endochondral bone formation. *Development* 2007;134:307–16.
18. Chang CF, Ramaswamy G, Serra R. Depletion of primary cilia in articular chondrocytes results in reduced Gli3 repressor to activator ratio, increased Hedgehog signaling, and symptoms of early osteoarthritis. *Osteoarthritis Cartilage* 2012;20:152–61.
19. Yuan X, Yang S. Deletion of IFT80 impairs epiphyseal and articular cartilage formation due to disruption of chondrocyte differentiation. *PLoS One* 2015;10:e0130618.
20. Lo Cascio L, Liu K, Nakamura H, Chu G, Lim NH, Chanalaris A, et al. Generation of a mouse line harboring a Bi-transgene expressing luciferase and tamoxifen-activatable creER(T2) recombinase in cartilage. *Genesis* 2014;52:110–9.
21. Glasson SS, Askew R, Sheppard B, Carito B, Blanchet T, Ma HL, et al. Deletion of active ADAMTS5 prevents cartilage degradation in a murine model of osteoarthritis. *Nature* 2005;434:644–8.
22. Ismail HM, Miotla-Zarebska J, Troeberg L, Tang X, Stott B, Yamamoto K, et al. JNK2 controls aggrecan degradation in murine articular cartilage and the development of experimental osteoarthritis. *Arthritis Rheumatol* 2015;68:1165–71.
23. Little CB, Barai A, Burkhardt D, Smith SM, Fosang AJ, Werb Z, et al. Matrix metalloproteinase 13-deficient mice are resistant to osteoarthritic cartilage erosion but not chondrocyte hypertrophy or osteophyte development. *Arthritis Rheum* 2009;60:3723–33.
24. Nalesso G, Thomas BL, Sherwood JC, Yu J, Addimanda O, Eldridge SE, et al. WNT16 antagonises excessive canonical WNT activation and protects cartilage in osteoarthritis. *Ann Rheum Dis* 2017;76:218–26.
25. Mak KK, Kronenberg HM, Chuang PT, Mackem S, Yang Y. Indian hedgehog signals independently of PTHrP to promote chondrocyte hypertrophy. *Development* 2008;135:1947–56.
26. Benichou C, Wirotius JM. Articular cartilage atrophy in lower limb amputees. *Arthritis Rheum* 1982;25:80–2.
27. Palmoski MJ, Brandt KD. Running inhibits the reversal of atrophic changes in canine knee cartilage after removal of a leg cast. *Arthritis Rheum* 1981;24:1329–37.
28. Koyama E, Young B, Nagayama M, Shibukawa Y, Enomoto-Iwamoto M, Iwamoto M, et al. Conditional Kif3a ablation causes abnormal hedgehog signaling topography, growth plate dysfunction, and excessive bone and cartilage formation during mouse skeletogenesis. *Development* 2007;134:2159–69.
29. Rockel JS, Yu C, Whetstone H, Craft AM, Reilly K, Ma H, et al. Hedgehog inhibits β -catenin activity in synovial joint development and osteoarthritis. *J Clin Invest* 2016;126:16–63.
30. Jin Y, Cong Q, Gvozdenovic-Jeremic J, Hu J, Zhang Y, Terkeltaub R, et al. Enpp1 inhibits ectopic joint calcification and maintains articular chondrocytes by repressing hedgehog signaling. *Development* 2018;145:dev164830.
31. Frost HM. The mechanostat: a proposed pathogenic mechanism of osteoporoses and the bone mass effects of mechanical and non-mechanical agents [review]. *Bone Miner* 1987;2:73–85.
32. Nauli SM, Alenghat FJ, Luo Y, Williams E, Vassilev P, Li X, et al. Polycystins 1 and 2 mediate mechanosensation in the primary cilium of kidney cells. *Nat Gen* 2003;33:129–37.
33. McGlashan SR, Haycraft CJ, Jensen CG, Yoder BK, Poole CA. Articular cartilage and growth plate defects are associated with chondrocyte cytoskeletal abnormalities in Tg737orpk mice lacking the primary cilia protein polaris. *Matrix Biol* 2007;26:234–46.
34. Chang CF, Serra R. Ift88 regulates hedgehog signaling, Sfrp5 expression, and β -catenin activity in post-natal growth plate. *J Orthop Res* 2013;31:350–6.
35. Huber C, Cormier-Daire V. Ciliary disorder of the skeleton [review]. *Am J Med Genet C Semin Med Genet* 2012;160c:16–74.
36. Wang C, Yuan X, Yang S. IFT80 is essential for chondrocyte differentiation by regulating hedgehog and Wnt signaling pathways. *Exp Cell Res* 2013;319:623–32.
37. Rockel JS, Yu C, Whetstone H, Craft AM, Reilly K, Ma H, et al. Hedgehog inhibits β -catenin activity in synovial joint development and osteoarthritis. *J Clin Invest* 2016;126:1649–63.
38. Clement CA, Larsen LA, Christensen ST. Using nucleofection of siRNA constructs for knockdown of primary cilia in P19.CL6 cancer stem cell differentiation into cardiomyocytes. *Methods Cell Biol* 2009;94:181–97.
39. Wann AK, Chapple JP, Knight MM. The primary cilium influences interleukin-1 β -induced NF κ B signalling by regulating IKK activity. *Cell Signal* 2014;26:1735–42.
40. McFie M, Koneva L, Collins I, Coveney CR, Clube AM, Chanalaris A, et al. Ciliary proteins specify the cell inflammatory response by tuning NF κ B signaling, independently of primary cilia. *J Cell Sci* 2020;133:jcs239871.
41. Anvarian Z, Mykytyn K, Mukhopadhyay S, Pedersen LB, Christensen ST. Cellular signalling by primary cilia in development, organ function and disease [review]. *Nat Rev Nephrol* 2019;15:199–219.
42. Petrova R, Joyner AL. Roles for hedgehog signaling in adult organ homeostasis and repair [review]. *Development* 2014;141:3445–57.
43. Ho L, Ali SA, Al-Jazrawe M, Kandel R, Wunder JS, Alman BA. Primary cilia attenuate hedgehog signalling in neoplastic chondrocytes. *Oncogene* 2013;32:5388–96.
44. Nagao M, Cheong CW, Olsen BR. Col2-Cre and tamoxifen-inducible Col2-CreER target different cell populations in the knee joint. *Osteoarthritis Cartilage* 2016;24:188–91.

Magnetic Resonance Imaging–Assessed Subchondral Cysts and Incident Knee Pain and Knee Osteoarthritis: Data From the Multicenter Osteoarthritis Study

Thomas A. Perry,¹  Terence W. O'Neill,² Irina Tolstykh,³ John Lynch,³ David T. Felson,⁴ Nigel K. Arden,⁵ and Michael C. Nevitt³

Objective. To examine whether knee subchondral cysts, measured on magnetic resonance imaging (MRI), are associated with incident knee osteoarthritis (OA) outcomes.

Methods. We used longitudinal data from the Multicenter Osteoarthritis Study, a community-based cohort of subjects with risk factors for knee OA. Participants without a history of knee surgery and/or inflammatory arthritis (i.e., rheumatoid arthritis and gout) were followed up for 84 months for the following incident outcomes: 1) radiographic knee OA (Kellgren/Lawrence grade ≥ 2), 2) symptomatic radiographic knee OA (radiographic knee OA and frequent knee pain), and 3) frequent knee pain (with or without radiographic knee OA). In a subset of participants, subchondral cysts were scored on baseline MRIs of 1 knee. Multiple logistic regression, with adjustment for participant characteristics and other baseline knee MRI findings, was used to assess whether subchondral cysts were predictive of incident outcomes.

Results. Among the participants with knees eligible for analyses of outcomes over 84 months, incident radiographic knee OA occurred in 22.8% of knees with no baseline radiographic knee OA, symptomatic radiographic knee OA occurred in 17.0% of knees with no baseline symptomatic radiographic knee OA, and frequent knee pain (with or without radiographic knee OA) occurred in 28.8% of knees with no baseline radiographic knee OA and 43.7% of knees with baseline radiographic knee OA. With adjustment for age, sex, and body mass index, the presence of subchondral cysts was not associated with incident radiographic knee OA but was associated with increased odds of incident symptomatic radiographic knee OA (odds ratio 1.92 [95% confidence interval 1.16–3.19]) and increased odds of incident frequent knee pain in those who had radiographic knee OA at baseline (odds ratio 2.11 [95% confidence interval 0.87–5.12]). Stronger and significant associations were observed for outcomes based on consistent reports of frequent knee pain within ~1 month of the study visit.

Conclusion. Subchondral cysts are likely to be a secondary phenomenon, rather than a primary trigger, of radiographic knee OA, and may predict symptoms in knees with existing disease.

INTRODUCTION

Osteoarthritis (OA) is the most common form of arthritis and is a leading cause of global disability, pain, and reduction

in physical function (1). Knee pain is the hallmark feature of knee OA (2) and is the main reason health care is sought among older adults (3). While knee pain may be chronic, many patients experience fluctuations in the presence/

The views expressed herein are those of the authors alone and not necessarily those of the NHS, the NIHR, the Department of Health and Social Care, or Public Health England.

Supported by the Centre for Sport, Exercise, and Osteoarthritis Research Versus Arthritis (grant 21595). The Multicenter Osteoarthritis Study was funded by the NIH (grant UO1 AG18820 to Dr. Felson; grant UO1 AG18832 to Dr. Torner; grant UO1 AG18947 to Dr. Lewis; grant UO1 AG19069 to Dr. Nevitt). The study was also supported by the NIHR Manchester Biomedical Research Centre.

¹Thomas A. Perry, BSc, PhD: University of Oxford and Centre for Sport, Exercise, and Osteoarthritis Research Versus Arthritis, Oxford, UK; ²Terence W. O'Neill, MD: NIHR Manchester Biomedical Research Centre, The University of Manchester and Manchester University NHS Foundation Trust, Manchester, UK, and Salford Royal NHS Foundation Trust, Salford, UK; ³Irina Tolstykh, MS, John Lynch, MD, PhD, Michael C. Nevitt, PhD, MPH: University of California, San Francisco; ⁴David T. Felson, MD, MPH: Centre for Epidemiology Versus Arthritis, Faculty of Biology, Medicine and Health, Manchester Academic Health Science Centre, The University of Manchester, Manchester, UK, NIHR

Manchester Biomedical Research Centre, Manchester University NHS Foundation Trust, Manchester Academic Health Science Centre, Manchester, UK, and Department of Rheumatology, Boston University School of Medicine, Boston, Massachusetts; ⁵Nigel K. Arden, MD, PhD: Nuffield Department of Orthopaedics, Rheumatology and Musculoskeletal Sciences (NDORMS), Botnar Research Centre, University of Oxford, UK, and MRC Lifecourse Epidemiology Unit, Southampton University, Southampton, UK.

Author disclosures are available at <https://onlinelibrary.wiley.com/action/downloadSupplement?doi=10.1002%2Fart.41917&file=art41917-sup-0001-Disclosureform.pdf>.

Address correspondence to Thomas A Perry, PhD, Nuffield Department of Orthopaedics, Rheumatology and Musculoskeletal Sciences (NDORMS), Botnar Research Centre, University of Oxford, Old Road, Oxford OX3 7LD, UK. Email: thomas.perry@ndorms.ox.ac.uk.

Submitted for publication January 14, 2021; accepted in revised form July 1, 2021.

absence of pain and in pain severity (4). Understanding which knee joint structures contribute to the development of structural OA, as radiographic knee OA, and nociceptive activation with radiographic knee pain will help to better clarify the etiology of the disease.

There are considerable magnetic resonance imaging (MRI) data in knee OA research, with a principle focus on the assessment of cartilage, synovitis, and bone marrow lesions (BMLs) (5), though recently there has been a growing interest in the contribution of subchondral cysts to the development of knee OA. Subchondral cysts, also referred to as cystic lesions or bone cysts (6), are defined as regions of markedly increased signal on fluid-sensitive MRI (7) and are typically spherical or ellipsoidal cavities (8). Subchondral cysts are common both in healthy knee joints, occurring in up to 25% of adults age >50 years who have no evidence of radiographic knee OA (9), and in up to 31% of patients with symptomatic knee OA (6). Moreover, using a subsample of subjects in the Multicenter Osteoarthritis Study (MOST), subchondral cysts were shown to occur in the absence of both MRI-assessed BMLs and cartilage loss in men and women with knee OA or at risk for knee OA (10). Despite this evidence, most epidemiologic studies concerning subchondral cysts are in the context of established knee OA. Thus, there is a need for the evaluation of the effect of subchondral cysts on incident knee OA outcomes.

The etiology of subchondral cyst development is unclear (6); however, subchondral cysts in the absence of established radiographic OA may provide a pathway to disease development and pain. Histologic assessment has shown that subchondral cysts contain necrotic bone fragments (11), which may stimulate nociceptive activation, and cystic lesions have shown positive responses to staining for substance P (12), an inflammation marker in pain signaling (13). Data from an *in vivo* study in a rodent model of posttraumatic knee OA induced by meniscectomy showed that subchondral cysts developed within just 12 weeks of injury (14). It is, therefore, possible that subchondral cysts precede the development of more conventional radiographic features including joint space narrowing, osteophytes, and subchondral sclerosis. Subchondral cysts have been shown to contain activated cells that express matrix metalloproteinase 1 (15), which has been linked to joint damage (16). In established knee OA, subchondral cysts typically present adjacent to abnormal joint tissue (11) and have been shown to colocalize with BMLs (12–14). Subchondral cysts have also been found to influence the biomechanical properties of the subchondral bone by affecting bone mineral density (8) and by creating increased intraosseous stress (17). Together, these mechanisms may thereby provide a potential path for the development of knee OA.

In the present study, we aimed to examine the association between MRI-assessed subchondral cysts and incident knee

OA outcomes in participants who were at high risk for developing knee OA over 84 months of follow-up.

PATIENTS AND METHODS

Study design and participants. We used longitudinal data from the MOST study, a prospective, observational study of risk factors for the development and progression of knee OA (<http://most.ucsf.edu/>). Details of the MOST study and study population have been previously published (18). Briefly, 3,026 men and women ages 50–79 years were recruited from 2 US communities and were followed up for up to 84 months. Participants either had evidence of knee OA at baseline or were at high risk for developing the disease. At prespecified time points (baseline, 30 months, 60 months, and 84 months), clinical assessments were performed and knee radiographs and MRIs were obtained.

In the present study, we used data from the “V035WORMS” MRI data set, the largest of 4 MRI subsets which can be used for the analysis of multiple end points. This subsample comprises 1,182 participants who had a readable pair of MRIs of at least 1 knee at 60 months and 84 months. A single index knee MRI obtained from each participant was read for all Whole-Organ Magnetic Resonance Imaging Score (WORMS) features (7), described in more detail below. If a participant had a readable pair of MRIs of both knees at 60 months and 84 months, 1 knee was randomly selected for MRI reading.

All participants underwent weight-bearing posteroanterior fixed-flexion knee radiographs at baseline and follow-up clinic visits. Knee radiographs were graded on a 0–4 scale across the whole knee joint (including the patellofemoral and tibiofemoral regions) using the Kellgren/Lawrence (K/L) scoring criteria (19). Radiographic OA of the whole knee was defined as a K/L grade ≥ 2 in either, or both, the tibiofemoral or patellofemoral joints.

Knee-specific frequent pain was assessed at each clinic visit using a modified version of the National Health and Nutrition Examination Survey (NHANES) questions (20). In accordance with current guidelines, this was considered to be the most suitable measure of current knee pain (21). Participants also completed assessment of frequent knee pain by telephone interview ~30 days prior to each clinical visit. A stricter definition of persistent, frequent knee pain included positive responses to the NHANES questions during both the telephone interview and clinical visits (22–25).

Our goal was to determine the risk of incident radiographic knee OA, incident symptomatic radiographic knee OA, and incident frequent knee pain separately in participants with and without radiographic knee OA in the index knee at baseline. We included only the subset of participants who had a knee with available baseline data on subchondral cysts and other WORMS features (the index knee: 1 knee per participant). Outcomes in index knees were based on radiographic knee OA and knee symptom data from the 60-month and 84-month follow-up visits.

Participants with missing data on baseline radiographic knee OA, baseline frequent knee pain, missing outcomes in the index knee that could not be imputed (see below), and baseline covariate data were excluded. We also excluded participants with evidence of inflammatory arthritis (rheumatoid arthritis and/or gout) and/or a history of knee-related surgery (including knee replacement) at baseline in either knee. In addition, only knees with available baseline data on MRI structural features across all knee subregions were included.

Magnetic resonance imaging. Non-contrast-enhanced MRIs were acquired using a dedicated 1.0T extremity system (OrthOne; ONI Medical Systems) with a 160-mm-diameter circumferential transmit-receive extremity coil. Axial and sagittal proton density-weighted fat-suppressed fast spin-echo sequences were acquired (repetition time 4,800 msec, echo time 35 msec, slice thickness 3.0 mm, interslice gap 0.0 mm, number of slices 32, field of view 140 mm × 140 mm, matrix 288 × 192 pixels, number of excitations 2, echo train length 8 msec) (10).

MRI structural features, including subchondral cysts, BMLs, synovitis/effusions, and cartilage lesions, were semiquantitatively assessed using the WOMBS criteria (7). Subchondral cysts were defined as areas of markedly increased signal intensity in the subarticular bone, with sharply defined, rounded margins and with no evidence of internal marrow tissue or trabecular bone on fluid-sensitive MRI. Subchondral cysts were scored from 0 to 3 across 15 joint subregions (whole knee joint), including the subspinous region of the tibia, with scores related to the extent of regional involvement: 0 = no involvement, 1 = <25% of the region, 2 = 25–50% of the region, and 3 = >50% of the region. BMLs were assessed across the same joint compartments using the same scoring criteria. Synovitis and effusion were scored collectively at the intercondylar and infrapatellar regions only and were not distinguished. Using a previously validated method of semiquantitative assessment for non-contrast-enhanced scans (26), synovitis and effusion were scored from 0 to 3, with 3 representing severe. Cartilage lesions were assessed across 14 subregions (not including the tibia subspinous region), and scored from 0 to 6 (0 = normal signal, 6 = diffuse [$\geq 75\%$ of the region] full-thickness loss).

MRI-assessed subchondral cyst exposure. We used 3 exposure variables to predict incident outcomes. Our first exposure was coded as a binary variable, with 0 representing the absence of subchondral cysts (i.e., no evidence of subchondral cysts across all joint subregions) and 1 representing the presence of subchondral cysts (i.e., evidence of subchondral cysts in at least a single subregion across the knee joint). Our second exposure variable was equal to the maximum subchondral cyst score across the 15 joint subregions (range 0–3), and our final exposure variable was equal to the number of subregions with subchondral cysts present (range 0–15).

Outcome measures. *Incident symptomatic radiographic knee OA.* Incident symptomatic radiographic knee OA was defined as the simultaneous occurrence of a combination of frequent knee symptoms and radiographic knee OA (K/L grade ≥ 2) at one or both of the 60-month or 84-month visits, in an index knee that did not have this combination at baseline.

Incident radiographic knee OA. Incident radiographic knee OA was defined as the occurrence of radiographic knee OA (K/L grade ≥ 2) during follow-up (60 months and 84 months), in an index knee without radiographic knee OA (K/L grade 0–1) at baseline.

Incident frequent pain in knees with or without radiographic knee OA at baseline. Due to a lack of data from other studies concerning the relationship between subchondral cysts and incident knee pain in the absence of radiographic knee OA, and the conflicting data regarding the association between subchondral cysts and knee pain in established knee OA (27–29), we conducted 2 separate incident knee pain analyses: 1) participants without radiographic knee OA (i.e., K/L grade 0–1) in the index knee at baseline and 2) participants with radiographic knee OA in the index knee at baseline. Incident knee pain was defined as the occurrence of frequent knee pain at one or both of the 60-month or 84-month visits, in an index knee that did not have frequent knee pain at baseline.

Covariates. Information on age, sex, and body mass index (BMI) was assessed at baseline. Baseline BML status, synovitis status, and cartilage lesion status were defined as the maximum severity score across the respective knee joint regions assessed. MRI findings were selected for inclusion as covariates in our model based on the available data. There are data to support the notion that subchondral cysts that colocalize with bone marrow lesions (10,30,31) are linked with histologically assessed synovitis (32), and while the exact etiology of subchondral cysts is unclear, it is thought that they may develop in response to cartilage loss with synovial infiltration (6,33).

Statistical analysis. Descriptive statistics were calculated for age, sex, BMI, and MRI findings. To examine the relationship between subchondral cyst exposures and incident outcomes, we performed logistic regression analyses in index knees. Results were presented as odds ratios (ORs) with 95% confidence intervals (95% CIs) for crude and adjusted models. We adjusted for baseline age, sex, and BMI. In additional analyses, we also adjusted for MRI-assessed synovitis (categorical), BML score (categorical), and cartilage lesion score (continuous).

We used imputation (last observation carried forward) to impute missing data on follow-up radiographic knee OA status at the 60-month and 84-month follow-up visits if radiographic knee OA was known to be present at the previous visit (imputed to be present at the visit with missing data) or was known to be absent at the previous visit and the subsequent visit (imputed to be absent at the visit with missing data). We included participants

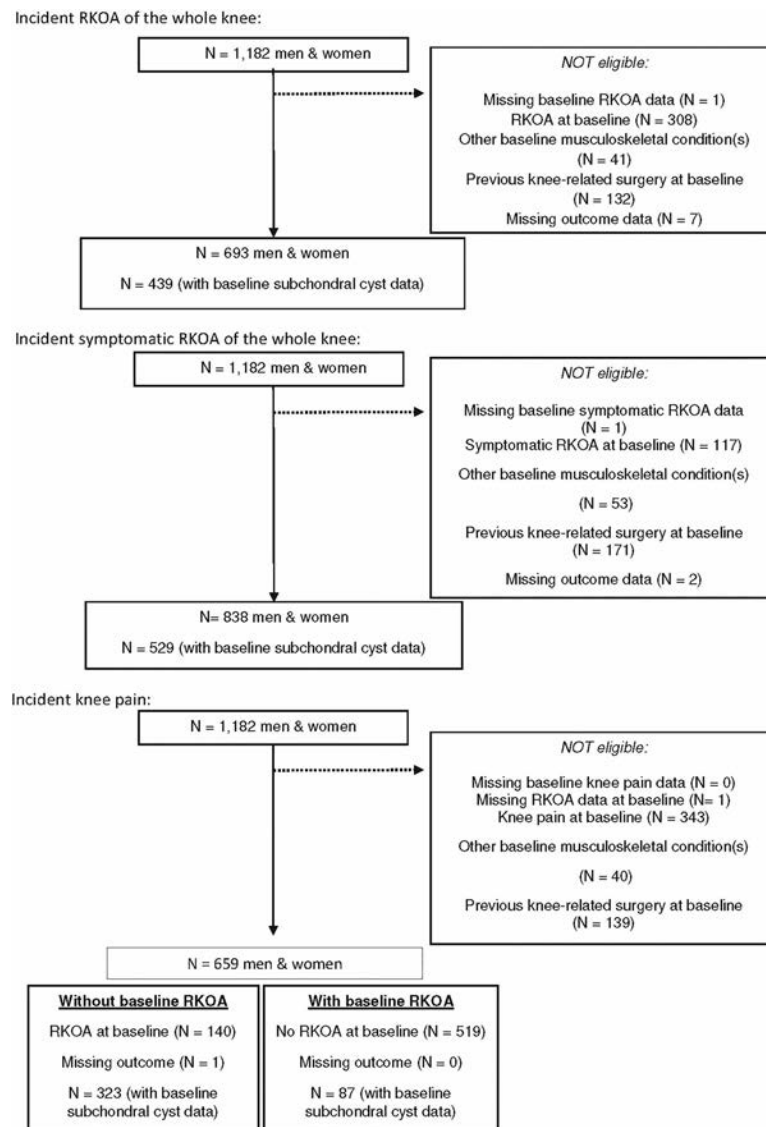


Figure 1. Flow chart of participants eligible for study investigation. RKOA = radiographic knee osteoarthritis.

with missing radiographic knee OA or knee symptom data in cases where it was still possible to determine symptomatic radiographic knee OA status (e.g., negative for radiographic knee OA, missing knee symptom data). For the second exposure variable, maximum subchondral cyst severity score, there were too few knees with a score of 3. Scores of 2 and 3 were combined into a single category of ≥ 2 . Similarly, for the third exposure variable, the number of regions with subchondral cysts, there were too few knees with subchondral cyst involvement across ≥ 2 regions. Therefore, we categorized the data as 0 regions, 1 region, and ≥ 2 regions. We also performed sensitivity analyses using the stricter definition of persistent, frequent knee pain (i.e., positive responses for knee pain during the telephone interview and clinical visit) (22–25) for both incident symptomatic radiographic knee OA and incident knee pain outcomes.

Data availability. All data generated and analyzed in this study are available upon reasonable request. Access to data generated in this study is available upon request from the corresponding author, whereas requests for the MOST data should be submitted to the cohort principal investigators. Information regarding the MOST public use data sets is available at <http://most.ucsf.edu/>.

RESULTS

The distribution of participants with knees eligible for analyses for incident radiographic knee OA, incident symptomatic radiographic knee OA, and incident frequent knee pain (with or without radiographic knee OA at baseline) is presented in Figure 1. Characteristics of the study participants and baseline data on subchondral cysts in the eligible index knees are shown in Table 1. Incident

radiographic knee OA occurred in 22.8% of knees ($n = 100$) eligible for this outcome, and incident symptomatic radiographic knee OA occurred in 17.0% of knees ($n = 90$) eligible for this outcome. Incident frequent knee pain occurred in 28.8% of knees ($n = 93$) without radiographic knee OA at baseline and 43.7% of knees ($n = 37$) with radiographic knee OA at baseline.

Incident symptomatic radiographic knee OA. After adjustment for baseline age, BMI, and sex and using the presence of subchondral cysts (yes/no) as the exposure, knees with evidence of subchondral cysts at baseline had increased odds of incident symptomatic radiographic knee OA compared to knees with no evidence of subchondral cysts (OR 1.92 [95% CI 1.16–3.19]) (Table 2). Using the maximum subchondral cyst

score as the exposure, compared to knees with no subchondral cyst involvement, knees with a maximum subchondral cyst score of 1 (<25% of the region) had a 2-fold increased risk of incident symptomatic radiographic knee OA (OR 1.96 [95% CI 1.15–3.33]); there was no statistically significant association between a maximum subchondral cyst score of ≥ 2 and incident symptomatic radiographic knee OA (OR 1.73 [95% CI 0.53–5.65]). Finally, we observed a statistically significant association between the presence of ≥ 2 regions with subchondral cysts and incident symptomatic radiographic knee OA. After further adjustment for BMLs, synovitis, and cartilage lesions at baseline, there was no longer a statistically significant association between subchondral cyst exposures and incident symptomatic radiographic knee OA.

Table 1. Baseline demographic and clinical characteristics of eligible participants in the MOST study*

	No radiographic knee OA ($n = 439$)	No symptomatic radiographic knee OA ($n = 529$)	No knee pain without radiographic knee OA ($n = 323$)	No knee pain with radiographic knee OA ($n = 87$)
Age, median (IQR) years	60 (11)	60 (12)	60 (11)	64 (13)
Female	268 (61.05)	334 (63.14)	184 (56.97)	64 (73.56)
BMI, median (IQR) kg/m ²	28.65 (6.19)	28.83 (6.11)	28.25 (5.96)	30.14 (5.79)
Right knee as index knee	218 (49.66)	271 (51.23)	159 (49.23)	52 (59.77)
Subchondral cysts				
No	354 (80.64)	409 (77.32)	262 (81.11)	52 (59.77)
Yes	85 (19.36)	120 (22.68)	61 (18.89)	35 (40.23)
Subchondral cyst severity				
0	354 (80.64)	409 (77.32)	262 (81.11)	52 (59.77)
1	76 (17.31)	104 (19.66)	56 (17.34)	28 (32.18)
≥ 2	9 (2.05)	16 (3.02)	5 (1.55)	7 (8.05)
No. of regions with subchondral cysts				
0	354 (80.64)	409 (77.32)	262 (81.11)	52 (59.77)
1	69 (15.72)	89 (16.82)	49 (15.17)	20 (22.99)
≥ 2	16 (3.64)	31 (5.86)	12 (3.72)	15 (17.24)
Bone marrow lesion score				
0	137 (31.21)	143 (27.03)	105 (32.51)	5 (5.75)
1	173 (39.41)	209 (39.51)	133 (41.18)	35 (40.23)
2	92 (20.96)	120 (22.68)	63 (19.50)	27 (31.05)
3	30 (6.83)	49 (9.26)	17 (5.26)	19 (21.84)
Missing†	7 (1.59)	8 (1.51)	5 (1.55)	1 (1.15)
Synovitis score				
0	192 (43.74)	219 (41.40)	137 (42.41)	27 (31.03)
1	196 (44.65)	245 (46.31)	152 (47.06)	46 (52.87)
2	43 (9.79)	54 (10.21)	28 (8.67)	11 (12.64)
3	8 (1.82)	11 (2.08)	6 (1.86)	3 (3.45)
Missing†	0 (0)	0 (0)	0 (0)	0 (0)
Cartilage thickness score‡				
0	57 (12.98)	58 (10.96)	41 (12.69)	1 (1.15)
2	54 (12.30)	58 (10.96)	45 (13.93)	3 (3.45)
2.5	6 (1.37)	7 (1.32)	4 (1.24)	1 (1.15)
3	179 (40.77)	196 (37.05)	134 (41.49)	17 (19.54)
4	6 (1.37)	8 (1.51)	5 (1.55)	2 (2.30)
5	111 (25.28)	144 (27.22)	76 (23.53)	31 (35.63)
6	6 (1.37)	31 (5.86)	3 (0.93)	25 (28.74)
Missing†	20 (4.56)	27 (5.10)	15 (4.64)	7 (8.05)

* Except where indicated otherwise, values are the number (%). Subgroups eligible for assessment of each outcome were not mutually exclusive but were overlapping. MOST = Multicenter Osteoarthritis Study; osteoarthritis = OA; IQR = interquartile range; BMI = body mass index.

† Data were missing for at least 1 region assessed for the given magnetic resonance imaging structure.

‡ Grade 1 on Whole-Organ Magnetic Resonance Imaging Score was not used when scoring cartilage thickness on magnetic resonance imaging.

Table 2. Association between subchondral cysts and incident symptomatic radiographic knee OA*

	Univariate model		Multivariate model 1†		Multivariate model 2‡	
	OR (95% CI) (n = 529)	P	OR (95% CI) (n = 529)	P	OR (95% CI) (n = 500)	P
Presence of subchondral cysts						
No (n = 409/59)	Referent	–	Referent	–	Referent	–
Yes (n = 120/31)	2.07 (1.26–3.38)	0.004	1.92 (1.16–3.19)	0.01	1.53 (0.85–2.75)	0.15
Subchondral cyst severity score						
0 (n = 409/59)	Referent	–	Referent	–	Referent	–
1 (n = 104/27)	2.08 (1.24–3.49)	0.006	1.96 (1.15–3.33)	0.01	1.60 (0.87–2.94)	0.13
≥2 (n = 16/4)	1.98 (0.62–6.34)	0.25	1.73 (0.53–5.65)	0.36	1.14 (0.32–4.10)	0.84
No. of regions with subchondral cysts						
0 (n = 409/59)	Referent	–	Referent	–	Referent	–
1 (n = 89/20)	1.72 (0.97–3.04)	0.06	1.69 (0.95–3.03)	0.08	1.46 (0.76–2.81)	0.25
≥2 (n = 31/11)	3.26 (1.49–7.16)	0.003	2.61 (1.17–5.84)	0.02	1.71 (0.69–4.21)	0.24

* N values represent the number of participants for the given category/number of incident cases of symptomatic radiographic knee osteoarthritis (OA). OR = odds ratio; 95% CI = 95% confidence interval.

† Adjusted for age, sex, and body mass index.

‡ Adjusted for age, sex, body mass index, bone marrow lesion severity, synovitis severity, and cartilage lesions.

In a sensitivity analysis using a stricter definition of persistent, frequent knee pain, in a fully adjusted model (adjusted for age, sex, BMI, and other MRI features), knees in which subchondral cysts were present (OR 2.16 [95% CI 1.18–3.96]), knees with a maximum subchondral cyst score of 1 (OR 2.29 [95% CI 1.23–4.26]), and knees with subchondral cyst involvement at 1 region (OR 2.24 [95% CI 1.16–4.32]) had an increased risk of symptomatic radiographic knee OA (Supplementary Table 1, available on the *Arthritis & Rheumatology* website at <http://onlinelibrary.wiley.com/doi/10.1002/art.41917/abstract>).

Incident radiographic knee OA. After adjustment for age, BMI, and sex, there was no statistically significant association between the presence of subchondral cysts and incident radiographic knee OA compared to knees with no evidence of subchondral cysts (OR 1.20 [95% CI 0.68–2.10]) (Table 3). Similarly, using the maximum subchondral cyst severity score as the

exposure, knees with a maximum grade of 1 (OR 1.25 [95% CI 0.69–2.25]) and a grade of ≥2 (OR 0.81 [95% CI 0.15–4.27]) were not at increased risk for incident radiographic knee OA. Finally, using the number of regions with subchondral cysts as the exposure, there was no statistically significant association between having involvement at 1 region (OR 1.27 [95% CI 0.69–2.34]) or involvement at ≥2 regions (OR 0.93 [95% CI 0.28–3.12]) compared to participants with no evidence of knee subchondral cysts. After further adjustment for synovitis, BMLs, and cartilage lesions, there remained no statistically significant association between subchondral cyst exposures and incident radiographic knee OA.

Incident frequent knee pain. *Index knees without radiographic knee OA at baseline.* Among participants without radiographic knee OA in the index knee at baseline, in a fully adjusted model, there was no statistically significant association between the

Table 3. Association between subchondral cysts and incident radiographic knee OA*

	Univariate model, OR (95% CI) (n = 439)	Multivariate model 1, OR (95% CI) (n = 439)†	Multivariate model 2, OR (95% CI) (n = 417)‡
Presence of subchondral cysts			
No (n = 354/77)	Referent	Referent	Referent
Yes (n = 85/23)	1.34 (0.78–2.29)	1.20 (0.68–2.10)	0.98 (0.52–1.86)
Subchondral cyst severity score			
0 (n = 354/77)	Referent	Referent	Referent
1 (n = 76/21)	1.37 (0.78–2.41)	1.25 (0.69–2.25)	1.01 (0.52–1.95)
≥2 (n = 9/2)	1.03 (0.21–5.05)	0.81 (0.15–4.27)	0.73 (0.13–4.07)
No. of regions with subchondral cysts			
0 (n = 354/77)	Referent	Referent	Referent
1 (n = 69/19)	1.37 (0.76–2.46)	1.27 (0.69–2.34)	1.09 (0.55–2.17)
≥2 (n = 16/4)	1.20 (0.38–3.82)	0.93 (0.28–3.12)	0.64 (0.18–2.27)

* N values represent the number of participants in the given category/number of incident cases of radiographic knee osteoarthritis (OA). None of the odds ratios (ORs) shown were statistically significant. 95% CI = 95% confidence interval.

† Adjusted for age, sex, and body mass index.

‡ Adjusted for age, sex, body mass index, bone marrow lesion severity, synovitis severity, and cartilage lesions.

Table 4. Association between subchondral cysts and incident frequent knee pain without radiographic knee OA at baseline*

	Univariate model, OR (95% CI) (n = 323)	Multivariate model 1, OR (95% CI) (n = 323)†	Multivariate model 2, OR (95% CI) (n = 307)‡
Presence of subchondral cysts			
No (n = 262/76)	Referent	Referent	Referent
Yes (n = 61/17)	0.95 (0.51–1.76)	0.94 (0.50–1.77)	0.93 (0.45–1.91)
Subchondral cyst severity score			
0 (n = 262/76)	Referent	Referent	Referent
1 (n = 56/17)	1.07 (0.57–2.00)	1.08 (0.57–2.07)	1.02 (0.49–2.11)
≥2 (n = 5/0)	–	–	–
No. of regions with subchondral cysts			
0 (n = 262/76)	Referent	Referent	Referent
1 (n = 49/14)	0.98 (0.50–1.92)	1.01 (0.51–2.03)	1.03 (0.48–2.25)
≥2 (n = 12/3)	0.82 (0.22–3.10)	0.69 (0.18–2.67)	0.60 (0.14–2.56)

* N values represent the number of participants for the given category/number of incident cases of knee pain without radiographic knee osteoarthritis (OA). None of the odds ratios (ORs) shown were statistically significant. 95% CI = 95% confidence interval.

† Adjusted for age, sex, and body mass index.

‡ Adjusted for age, sex, body mass index, bone marrow lesion severity, synovitis severity, and cartilage lesions.

presence of subchondral cysts and incident knee pain compared to knees with no evidence of subchondral cysts (OR 0.93 [95% CI 0.45–1.91]) (Table 4). Similarly, using the maximum subchondral cyst severity score as the exposure, knees with a maximum score of 1 were not at increased risk for developing knee pain (OR 1.02 [95% CI 0.49–2.11]). There were no occurrences of incident knee pain in the grade ≥2 group. Finally, using the number of regions with subchondral cysts as the exposure, there was no statistically significant association between subchondral cyst involvement at 1 region (OR 1.03 [95% CI 0.48–2.25]) or at ≥2 regions (OR 0.60 [95% CI 0.14–2.56]) compared to participants with no evidence of subchondral cysts. In a sensitivity analysis using a stricter definition of persistent frequent knee pain, in a fully adjusted model, no statistically significant association was observed between any of the predictors and incident knee pain (Supplementary Table 2, <http://onlinelibrary.wiley.com/doi/10.1002/art.41917/abstract>).

Index knees with radiographic knee OA at baseline. Among participants with radiographic knee OA in the index knee at baseline, there were moderate, but not statistically significant, associations between subchondral cyst exposures and incident knee pain, both in models with adjustment for age, sex, and BMI and in fully adjusted models; e.g., for the association of incident frequent knee pain with presence of subchondral cysts in fully adjusted models, the OR was 2.47 (95% CI 0.87–7.03, $P = 0.091$) (Table 5). However, when we used the stricter definition of persistent, frequent knee pain, presence of subchondral cysts (OR 3.14 [95% CI 1.15–8.59]), subchondral cyst severity score of 1 (OR 3.80 [95% CI 1.33–10.89]), and knees with subchondral cyst involvement at 1 region (OR 4.46 [95% CI 1.39–14.36]) were each statistically significantly associated with increased odds of incident frequent knee pain (Supplementary Table 3, <http://onlinelibrary.wiley.com/doi/10.1002/art.41917/abstract>).

Table 5. Association between subchondral cysts and incident frequent knee pain in knees with radiographic knee OA at baseline*

	Univariate model, OR (95% CI) (n = 87)	Multivariate model 1, OR (95% CI) (n = 87)†	Multivariate model 2, OR (95% CI) (n = 80)‡
Presence of subchondral cysts			
No (n = 262/76)	Referent	Referent	Referent
Yes (n = 61/17)	2.06 (0.86–4.93)	2.11 (0.87–5.12)	2.47 (0.87–7.03)
Subchondral cyst severity score			
0 (n = 262/76)	Referent	Referent	Referent
1 (n = 56/17)	2.32 (0.91–5.91)	2.40 (0.93–6.23)	2.91 (0.96–8.82)
≥2 (n = 5/0)	1.30 (0.26–6.45)	1.26 (0.24–6.57)	1.19 (0.18–7.65)
No. of regions with subchondral cysts			
0 (n = 262/76)	Referent	Referent	Referent
1 (n = 49/14)	2.12 (0.75–6.04)	2.14 (0.75–6.13)	2.85 (0.84–9.63)
≥2 (n = 12/3)	1.99 (0.62–6.34)	2.08 (0.63–6.83)	2.00 (0.50–7.96)

* N values represent the number of participants for the given category/number of incident cases of knee pain with radiographic knee osteoarthritis (OA). None of the odds ratios (ORs) shown were statistically significant. 95% CI = 95% confidence interval.

† Adjusted for age, sex, and body mass index.

‡ Adjusted for age, sex, body mass index, bone marrow lesion severity, synovitis severity, and cartilage lesions.

DISCUSSION

To our knowledge, this study is the first to examine the relationship between subchondral cysts, measured on fluid-sensitive MRI, and incident knee pain (with or without radiographic knee OA of the index knee) and knee OA in a large, long-term study of participants at risk for developing knee OA. In the present study, after adjustment for age, BMI, and sex, we found no association between the presence of subchondral cysts at baseline and incident radiographic knee OA over 84 months of follow-up. Results were similar in analyses that also adjusted for other baseline MRI features (i.e., synovitis, BMLs, and cartilage lesions). In contrast, after adjustment for age, BMI, and sex, the presence of ≥ 1 subchondral cyst(s) and the presence of multiple subchondral cysts at baseline were significantly associated with 1.9–2.6-fold increased odds of incident symptomatic radiographic knee OA. After further adjustment for other baseline MRI features, there was no longer a statistically significant association between any of the exposures and incident symptomatic radiographic knee OA. In addition, we observed no association between subchondral cysts and incident frequent knee pain in knees without radiographic knee OA at baseline. In knees with radiographic knee OA at baseline, we observed a non-statistically significant increase in the odds of incident frequent knee pain over 84 months of follow-up (2.5-fold increase).

In sensitivity analyses, we also examined the incidence of knee pain and symptomatic radiographic knee OA using a stricter definition of persistent, frequent knee pain (22–25) (positive responses reported during both the telephone interview and the clinical visit within ~ 1 month versus the clinical visit only). The rationale for this was that knee OA pain is known to fluctuate in occurrence and severity over time. Using this outcome, after adjustment for age, sex, and BMI, there was a nearly 3-fold significantly increased odds of incident symptomatic OA in knees with subchondral cysts, with the association remaining statistically significant even after further adjustment for other MRI structures (Supplementary Table 1, <http://onlinelibrary.wiley.com/doi/10.1002/art.41917/abstract>). Although using this stricter definition of persistent, frequent knee pain strengthened the association between subchondral cysts and incident knee pain in knees without radiographic knee OA at baseline, the results remained non-statistically significant. In contrast, for incident knee pain in knees with subchondral cysts and radiographic knee OA at baseline, the less strict definition of persistent, frequent knee pain yielded modestly increased, but nonsignificant, odds of incident knee pain, whereas the stricter definition yielded 3–4-fold significantly increased odds of incident knee pain (Supplementary Table 4, <http://onlinelibrary.wiley.com/doi/10.1002/art.41917/abstract>). This finding is consistent with the findings from the symptomatic radiographic knee OA analysis. Since knees with frequent pain that did not have radiographic knee OA at baseline and knees without frequent pain that had

radiographic knee OA at baseline were both eligible for analysis of the incident symptomatic radiographic knee OA outcome, the observed association of subchondral cysts with symptomatic radiographic knee OA may include an increased risk for developing frequent pain in knees with radiographic knee OA at baseline.

These data suggest that knee subchondral cysts may be linked with knee pain, but not with the development of radiographic knee OA. The data further suggest that it may not be useful to focus clinical efforts on identifying individuals with subchondral cysts without radiographic knee OA, as they are not at increased risk for developing knee pain or incident radiographic knee OA. We decided to use pain on most days of the previous month assessed at the clinical visit only as our primary, predefined definition of frequent knee pain, as it was consistent with the recommendations from a recent study that examined the best methods for harmonizing OA and pain among observational cohort studies (21). The stricter definition of persistent, frequent knee pain may represent a more advanced and severe stage of knee pain (22–25), and subchondral cysts may play a role in the development of this type of knee pain.

Our study has several strengths. To our knowledge, it had a longer duration of follow-up compared to earlier investigations of the association of subchondral cysts with incident knee symptoms and knee OA, as well as having a large, well-characterized study cohort. Additionally, the association between subchondral cysts and incident knee OA outcomes was examined using 3 exposures: 1) presence of subchondral cysts (yes/no), 2) maximum subchondral cyst severity score, and 3) number of regions with subchondral cyst involvement. This allowed us to evaluate which attributes of subchondral cysts, presence versus absence and severity, may increase the risk for developing knee OA. We examined the association between subchondral cysts and incident outcomes at a joint level, with 1 index knee assessed per participant. We hypothesized that subchondral cysts would carry an increased risk of incident knee OA only in the index knee, due to the focal damage attributed to the presence of subchondral cysts.

There are also several potential limitations to our study. First, the MOST study cohort is not a random sample of the population, and selection factors that affect both the occurrence of the exposure and the outcomes may be potential sources of bias in our analysis. This could include factors that affect both the availability of baseline MRI data on subchondral cysts and the knee OA and knee pain outcomes. For example, in the sample of knees with baseline MRI data that were available from the MOST study for the present investigation, it is not possible to examine incident total joint replacement as an outcome. This is because patients who underwent knee replacement would not receive MRIs at subsequent visits, and MRIs of knees were only read for changes between baseline and these later visits if they were available at 60 months and 84 months. Whether there is an association between subchondral cysts and subsequent joint replacement is

an important question that should be examined, but one that needs to be addressed using a different sample of knees with MRI readings than the sample from the MOST study used in the present investigation. The knees in this sample may have been more likely to have subchondral cysts at baseline and to develop OA and knee pain. We recognize this as a potential source of bias.

The number of knees with baseline MRI data on subchondral cysts was limited, since we analyzed the subset of knees that had available MRI data from the MOST data set of paired 60-month and 84-month MRI readings. While 4 MRI data sets were available, we used this data set because it was the largest, an important consideration since subchondral cysts and incident knee OA outcomes were both relatively uncommon, and this was the most generalizable sample. The long follow-up in the selected data set ensured an adequate number of radiographic and symptomatic OA outcomes. Thus, by using this MRI data set (baseline, 60 months, and 84 months), we were able to examine the effect of baseline subchondral cyst exposures on all incident outcomes using the same data set and with the same duration of follow-up. However, we recognize that as a result of our choice of data set, we could not investigate short-term outcomes of subchondral cysts.

Defining our pain outcome as incident frequent pain at either, or both, of the 60-month and 84-month time points increased our chances of capturing incident frequent knee pain that comes and goes. Nevertheless, even assessing knee pain every 1–2 years is an insufficient frequency to capture pain that fluctuates, and more frequent follow-up is needed to better understand risk factors for knee pain that fluctuates. The association of subchondral cysts and fluctuating pain, particularly over the short-term, also warrants further investigation.

Compared to the frequency observed in knees with OA (6,34), the low prevalence of subchondral cysts in knees without OA in this study, and the fact that they were not associated with incident radiographic knee OA, suggest that subchondral cysts may not be of clinical use to predict incident knee OA. In addition, we did not examine the effect of subchondral cyst location on the development of compartment-specific incident radiographic knee OA; the number of tibiofemoral-specific and/or patellofemoral-specific subchondral cysts and incident cases would likely be too few for robust statistical testing. Similarly, we were unable to perform further stratification (i.e., incident symptomatic radiographic knee OA stratified according to those with and those without radiographic knee OA at baseline) due to small numbers of participants in these subsets.

Finally, we adjusted for other MRI features, including BMLs, synovitis, and cartilage lesions. The association between subchondral cysts and such findings is still unclear, and it remains unknown where subchondral cysts fall on the causal pathway to disease and pain development. It is possible that adjustment for other baseline MRI features, which may be downstream effects of subchondral cysts, is an overadjustment, thereby limiting the interpretation of the adjusted data, and we acknowledge this as a potential limitation.

In the present study, however, incident symptomatic OA was the only outcome in which adjustment for the other MRI features resulted in substantial changes in the ORs by attenuating the effect, although the association of subchondral cysts with this outcome using the strict definition of knee pain remained significant in the fully adjusted models. Adjusting for other MRI features strengthened the association between subchondral cysts and incident knee pain in those with baseline radiographic knee OA, though it was only of marginal statistical significance, and these findings were corroborated by the results using the more stringent definition.

These data suggest that subchondral cysts are likely to be a secondary phenomenon of knee OA, rather than a primary trigger of radiographic structural change. Subchondral cysts may be associated with the development of knee pain in knees with existing radiographic OA.

ACKNOWLEDGMENT

We would like to express our gratitude to all participants of the MOST study.

AUTHOR CONTRIBUTIONS

All authors were involved in drafting the article or revising it critically for important intellectual content, and all authors approved the final version to be published. Dr. Perry had full access to all of the data in the study and takes responsibility for the integrity of the data and the accuracy of the data analysis.

Study conception and design. Perry, O'Neill, Felson, Nevitt.

Acquisition of data. Perry, Nevitt.

Analysis and interpretation of data. Perry, O'Neill, Tolstykh, Lynch, Felson, Arden, Nevitt.

REFERENCES

1. Felson DT. Osteoarthritis of the knee [review]. *N Engl J Med* 2006; 354:841–8.
2. Neogi T. The epidemiology and impact of pain in osteoarthritis. *Osteoarthritis Cartilage* 2013;21:1145–53.
3. Dominick KL, Ahern FM, Gold CH, Heller DA. Health-related quality of life and health service use among older adults with osteoarthritis. *Arthritis Rheum* 2004;51:326–31.
4. Zhang Y, Nevitt M, Niu J, Lewis C, Torner J, Guermazi A, et al. Fluctuation of knee pain and changes in bone marrow lesions, effusions, and synovitis on magnetic resonance imaging. *Arthritis Rheum* 2011;63:691–9.
5. Kijowski R, Demehri S, Roemer F, Guermazi A. Osteoarthritis year in review 2019: imaging. *Osteoarthritis Cartilage* 2020;28:285–95.
6. Audrey HX, Abd Razak HR, Andrew TH. The truth behind subchondral cysts in osteoarthritis of the knee. *Open Orthop J* 2014;8: 7–10.
7. Peterfy CG, Guermazi A, Zaim S, Tirman PF, Mieux Y, White D, et al. Whole-organ magnetic resonance imaging score (WORMS) of the knee in osteoarthritis. *Osteoarthritis Cartilage* 2004;12:177–90.
8. Burnett WD, Kontulainen SA, McLennan CE, Hazel D, Talmo C, Wilson DR, et al. Knee osteoarthritis patients with more subchondral cysts have altered tibial subchondral bone mineral density. *BMC Musculoskelet Disord* 2019;20:14.
9. Guermazi A, Niu J, Hayashi D, Roemer FW, Englund M, Neogi T, et al. Prevalence of abnormalities in knees detected by MRI in adults

- without knee osteoarthritis: population based observational study (Framingham Osteoarthritis Study). *BMJ* 2012;345:e5339.
10. Crema MD, Roemer FW, Marra MD, Niu J, Lynch JA, Felson DT, et al. Contrast-enhanced MRI of subchondral cysts in patients with or at risk for knee osteoarthritis: the MOST study. *Eur J Radiol* 2010;75:e92–6.
 11. Pouders C, De Maeseneer M, Van Roy P, Gielen J, Goossens A, Shahabpour M. Prevalence and MRI-anatomic correlation of bone cysts in osteoarthritic knees. *AJR Am J Roentgenol* 2008;190:17–21.
 12. Ogino S, Sasho T, Nakagawa K, Suzuki M, Yamaguchi S, Higashi M, et al. Detection of pain-related molecules in the subchondral bone of osteoarthritic knees. *Clin Rheumatol* 2009;28:1395–402.
 13. Fortier LA, Nixon AJ. Distributional changes in substance P nociceptive fiber patterns in naturally osteoarthritic articulations. *J Rheumatol* 1997;24:524–30.
 14. McErlain DD, Ulici V, Darling M, Gati JS, Pitelka V, Beier F, et al. An in vivo investigation of the initiation and progression of subchondral cysts in a rodent model of secondary osteoarthritis. *Arthritis Res Ther* 2012;14:R26.
 15. Kaspiris A, Khaldi L, Grivas TB, Vasiliadis E, Kouvaras I, Dagkas S, et al. Subchondral cyst development and MMP-1 expression during progression of osteoarthritis: an immunohistochemical study. *Orthop Traumatol Surg Res* 2013;99:523–9.
 16. Tetlow LC, Adlam DJ, Woolley DE. Matrix metalloproteinase and pro-inflammatory cytokine production by chondrocytes of human osteoarthritic cartilage: associations with degenerative changes. *Arthritis Rheum* 2001;44:585–94.
 17. McErlain DD, Milner JS, Ivanov TG, Jencikova-Celerin L, Pollmann SI, Holdsworth DW. Subchondral cysts create increased intra-osseous stress in early knee OA: a finite element analysis using simulated lesions. *Bone* 2011;48:639–46.
 18. Segal NA, Nevitt MC, Gross KD, Gross KD, Hietpas J, Glass NA, et al. The Multicenter Osteoarthritis Study: opportunities for rehabilitation research. *PM R* 2013;5:647–54.
 19. Kellgren JH, Lawrence JS. Radiological assessment of osteoarthrosis. *Ann Rheum Dis* 1957;16:494–502.
 20. Felson DT, Naimark A, Anderson J, Kazis L, Castelli W, Meenan RF. The prevalence of knee osteoarthritis in the elderly: the Framingham Osteoarthritis Study. *Arthritis Rheum* 1987;30:914–8.
 21. Leyland KM, Gates LS, Nevitt M, Felson D, Bierma-Zeinstra SM, Conaghan PG, et al. Harmonising measures of knee and hip osteoarthritis in population-based cohort studies: an international study. *Osteoarthritis Cartilage* 2018;26:872–9.
 22. Wise BL, Felson DT, Clancy M, Niu J, Neogi T, Lane NE, et al. Consistency of knee pain and risk of knee replacement: the Multicenter Osteoarthritis Study. *J Rheumatol* 2011;38:1390–5.
 23. Neogi T, Nevitt MC, Yang M, Curtis JR, Torner J, Felson DT. Consistency of knee pain: correlates and association with function. *Osteoarthritis Cartilage* 2010;18:1250–5.
 24. Carlesso LC, Niu J, Segal NA, Frey-Law LA, Lewis CE, Nevitt MC, et al. The effect of widespread pain on knee pain worsening, incident knee osteoarthritis (OA), and incident knee pain: the Multicenter OA (MOST) Study. *J Rheumatol* 2017;44:493–8.
 25. Carlesso LC, Segal NA, Frey-Law L, Zhang Y, Na L, Nevitt M, et al. Pain susceptibility phenotypes in those free of knee pain with or at risk of knee osteoarthritis: the Multicenter Osteoarthritis Study. *Arthritis Rheumatol* 2019;71:542–9.
 26. Roemer FW, Guermazi A, Zhang Y, Yang M, Hunter DJ, Crema MD, et al. Hoffa's fat pad: evaluation on unenhanced MR images as a measure of patellofemoral synovitis in osteoarthritis. *AJR Am J Roentgenol* 2009;192:1696–700.
 27. Perry TA, Parkes MJ, Hodgson RJ, Felson DT, Arden NK, O'Neill TW. Association between bone marrow lesions & synovitis and symptoms in symptomatic knee osteoarthritis. *Osteoarthritis Cartilage* 2020;28:316–23.
 28. Torres L, Dunlop DD, Peterfy C, Guermazi A, Prasad P, Hayes KW, et al. The relationship between specific tissue lesions and pain severity in persons with knee osteoarthritis. *Osteoarthritis Cartilage* 2006;14:1033–40.
 29. Kornaat PR, Bloem JL, Ceulemans RY, Riyazi N, Rosendaal FR, Nelissen RG, et al. Osteoarthritis of the knee: association between clinical features and MR imaging findings. *Radiology* 2006;239:811–7.
 30. Crema MD, Roemer FW, Zhu Y, Marra MD, Niu J, Zhang Y, et al. Subchondral cystlike lesions develop longitudinally in areas of bone marrow edema-like lesions in patients with or at risk for knee osteoarthritis: detection with MR imaging—the MOST study. *Radiology* 2010;256:855–62.
 31. Carrino JA, Blum J, Parellada JA, Schweitzer ME, Morrison WB. MRI of bone marrow edema-like signal in the pathogenesis of subchondral cysts. *Osteoarthritis Cartilage* 2006;14:1081–5.
 32. Yusup A, Kaneko H, Liu L, Ning L, Sadatsuki R, Hada S, et al. Bone marrow lesions, subchondral bone cysts and subchondral bone attrition are associated with histological synovitis in patients with end-stage knee osteoarthritis: a cross-sectional study. *Osteoarthritis Cartilage* 2015;23:1858–64.
 33. Dürr HD, Martin H, Pellengahr C, Schlemmer M, Maier M, Jansson V. The cause of subchondral bone cysts in osteoarthrosis: a finite element analysis. *Acta Orthop Scand* 2004;75:554–8.
 34. Tanamas SK, Wluka AE, Pelletier JP, Martel-Pelletier J, Abram F, Wang Y, et al. The association between subchondral bone cysts and tibial cartilage volume and risk of joint replacement in people with knee osteoarthritis: a longitudinal study. *Arthritis Res Ther* 2010;12:R58.

Safety and Efficacy of Upadacitinib in Patients With Active Ankylosing Spondylitis and an Inadequate Response to Nonsteroidal Antiinflammatory Drug Therapy: One-Year Results of a Double-Blind, Placebo-Controlled Study and Open-Label Extension

Atul Deodhar,¹ Désirée van der Heijde,² Joachim Sieper,³ Filip Van den Bosch,⁴ Walter P. Maksymowych,⁵ Tae-Hwan Kim,⁶ Mitsumasa Kishimoto,⁷ Andrew Ostor,⁸ Bernard Combe,⁹ Yunxia Sui,¹⁰ Alvina D. Chu,¹⁰ and In-Ho Song¹⁰

Objective. To report the efficacy and safety of upadacitinib through 1 year in patients with ankylosing spondylitis (AS).

Methods. In the SELECT-AXIS 1 study, adults with active AS and an inadequate response to nonsteroidal antiinflammatory drugs were randomized to receive upadacitinib 15 mg once daily or placebo. At week 14, patients who had been randomized to receive placebo were switched to upadacitinib, and all patients continued in the open-label extension and received upadacitinib up to week 104; interim data up to week 64 are reported herein.

Results. Of 187 patients, 178 completed week 14 on study drug and entered the open-label extension. Similar proportions of patients in either group (continuous upadacitinib or placebo-to-upadacitinib) achieved Assessment of SpondyloArthritis international Society 40% response (ASAS40) or Ankylosing Spondylitis Disease Activity Score (ASDAS) showing low disease activity at week 64: $\geq 70\%$ of patients achieved these end points based on nonresponder imputation (NRI) and $\geq 81\%$ based on as-observed analyses. Furthermore, $\geq 34\%$ (NRI) and $\geq 39\%$ (as-observed analysis) achieved ASDAS showing inactive disease or ASAS showing partial remission at week 64. Mean changes from baseline (week 0) to week 64 in pain, function, and inflammation showed consistent improvement or sustained maintenance through the study. Among 182 patients receiving upadacitinib (237.6 patient-years), 618 adverse events (260.1 per 100 patient-years) were reported. No serious infections, major adverse cardiovascular events, venous thromboembolic events, gastrointestinal perforation, or deaths were reported.

Conclusion. Upadacitinib 15 mg once daily showed sustained and consistent efficacy over 1 year. Patients who switched from placebo to upadacitinib at week 14 showed similar efficacy versus those who received continuous upadacitinib.

ClinicalTrials.gov identifier: NCT03178487.

Supported by AbbVie.

¹Atul Deodhar, MD: Oregon Health & Science University, Portland;

²Désirée van der Heijde, MD: Leiden University Medical Center, Leiden, The Netherlands; ³Joachim Sieper, MD: Charité Universitätsmedizin Berlin, Berlin, Germany; ⁴Filip Van den Bosch, MD: VIB-UGent Center for Inflammation Research and Ghent University, Ghent, Belgium; ⁵Walter P. Maksymowych, MD: University of Alberta, Edmonton, Alberta, Canada; ⁶Tae-Hwan Kim, MD: Hanyang University Hospital for Rheumatic Diseases, Seoul, Republic of Korea; ⁷Mitsumasa Kishimoto, MD: Kyorin University School of Medicine, Tokyo, Japan; ⁸Andrew Ostor, MD: Cabrini Medical Center and Monash University, Melbourne, Victoria, Australia; ⁹Bernard Combe, MD, PhD: Centre Hospitalier Universitaire de Montpellier and Université de Montpellier, Montpellier, France; ¹⁰Yunxia Sui, PhD, Alvina D. Chu, MD, In-Ho Song, MD: AbbVie Inc., North Chicago, Illinois.

AbbVie is committed to responsible data sharing regarding the clinical trials we sponsor. This includes access to anonymized, individual and trial-level data (analysis data sets), as well as other information (e.g., protocols and Clinical Study Reports), as long as the trials are not part of an ongoing

or planned regulatory submission. This includes requests for clinical trial data for unlicensed products and indications. These clinical trial data can be requested by any qualified researchers who engage in rigorous, independent scientific research, and will be provided following review and approval of a research proposal and Statistical Analysis Plan and execution of a Data Sharing Agreement. Data requests can be submitted at any time and the data will be accessible for 12 months, with possible extensions considered. For more information on the process, or to submit a request, visit the following link: <https://www.abbvie.com/our-science/clinical-trials/clinical-trials-data-and-information-sharing/data-and-information-sharing-with-qualified-researchers.html>.

Author disclosures are available at <https://onlinelibrary.wiley.com/action/downloadSupplement?doi=10.1002%2Fart.41911&file=art41911-sup-0001-Disclosureform.pdf>.

Address correspondence to Atul Deodhar, MD, Oregon Health & Science University, 3181 SW Sam Jackson Park Road, Portland, OR 97239. Email: deodhara@ohsu.edu.

Submitted for publication April 20, 2021; accepted in revised form June 29, 2021.

INTRODUCTION

Ankylosing spondylitis (AS), also known as radiographic axial spondyloarthritis, is a chronic, inflammatory rheumatic disease affecting the axial skeleton, mainly characterized by back pain (including nocturnal back pain) and morning stiffness, and peripheral pain due to arthritis, enthesitis, and extraarticular manifestations (1,2). Irreversible structural damage often occurs, negatively impacting patients' lives (3). To maximize patients' quality of life, therapeutic intervention is necessary to control the signs and symptoms of disease, prevent structural damage, and maintain physical function (4). To achieve these goals, a treatment target for AS should be set at achieving sustained inactive disease or low disease activity (4,5). In recent years, JAK inhibitors have emerged for the treatment of several immune-mediated inflammatory diseases, such as rheumatoid arthritis (RA), psoriatic arthritis (PsA), Crohn's disease, and ulcerative colitis (6–8), and are under investigation as a treatment for AS (9–13).

Upadacitinib, a JAK inhibitor engineered for increased selectivity for JAK1 over JAK2, JAK3, and tyrosine kinase 2 (14), was investigated for the treatment of patients with AS who had an inadequate response to nonsteroidal antiinflammatory drugs (NSAIDs) in the randomized, placebo-controlled phase II/III SELECT-AXIS 1 study (15). The study met its primary end point, with a significantly greater proportion of patients receiving upadacitinib achieving Assessment of SpondyloArthritis international Society 40% response (ASAS40) (16) at week 14 versus placebo (51.6% for upadacitinib 15 mg once daily versus 25.5% for placebo; $P < 0.001$), as well as several multiplicity-controlled secondary end points reflecting significant improvement in disease activity, function, and magnetic resonance imaging outcomes for upadacitinib versus placebo. Upadacitinib was well tolerated, and no serious infections, herpes zoster, malignancy, venous thromboembolic events, or deaths were reported during the first 14 weeks. The objective of this interim analysis of the SELECT-AXIS 1 extension study is to report safety and efficacy, including extraspinal outcomes, in patients with AS receiving upadacitinib 15 mg once daily through 1 year.

PATIENTS AND METHODS

Study design. SELECT-AXIS 1 (ClinicalTrials.gov identifier: NCT03178487) is a randomized, multicenter (62 centers in 20 countries), phase II/III study consisting of a 14-week double-blind, placebo-controlled period 1 and an ongoing 90-week open-label extension period 2 to evaluate the safety and efficacy of upadacitinib 15 mg (Supplementary Figure 1, available on the *Arthritis & Rheumatology* website at <http://onlinelibrary.wiley.com/doi/10.1002/art.41911/abstract>). The methods and results of period 1 have been published previously (15). Briefly, patients were randomized 1:1 to receive upadacitinib 15 mg once daily or placebo for 14 weeks. Patients who completed period 1 were eligible

to enter period 2 and receive open-label upadacitinib 15 mg once daily for 90 weeks, up to week 104. Reported herein are efficacy results at week 64, when all patients continuing in the study had at least 1 year of upadacitinib exposure, including in the placebo-to-upadacitinib switch group. Of note, patients and investigators remained blinded with regard to the patients' period 1 assignment throughout the study.

This study was conducted in accordance with International Council for Harmonisation guidelines and the ethical principles of the Declaration of Helsinki. All patients provided written informed consent, and the study protocol was approved by an institutional review board or independent ethics committee at each study site.

Participants. The study enrolled adult patients (age ≥ 18 years) with AS who met the modified New York criteria (17) based on independent central reading of radiographs of the sacroiliac joints and who had active disease at baseline (i.e., week 0), defined as a Bath Ankylosing Spondylitis Disease Activity Index (BASDAI) (18) score of ≥ 4 and patient's assessment of back pain score of ≥ 4 (on a numerical rating scale [NRS] of 0–10) at screening and baseline visit, and had an inadequate response to ≥ 2 NSAIDs or intolerance to or contraindication for NSAIDs. Patients receiving a stable dose of concomitant conventional synthetic disease-modifying antirheumatic drugs (csDMARDs), oral glucocorticoids, NSAIDs, and analgesics were eligible; patients with prior exposure to JAK inhibitors or biologic DMARDs (such as tumor necrosis factor [TNF] inhibitors and interleukin-17A [IL-17A] inhibitors) were excluded.

Patient and public involvement. This research was done without any formal patient/patient organization involvement in the study design, development of patient-relevant outcomes, interpretation of results, or the writing or editing of the manuscript.

Efficacy end points. Efficacy was assessed based on the percentage of patients achieving ASAS20, ASAS40, ASAS showing partial remission, BASDAI50, and Ankylosing Spondylitis Disease Activity Score (ASDAS) (19) showing inactive disease (ASDAS ID; defined as an ASDAS < 1.3), ASDAS showing low disease activity (ASDAS LDA; < 2.1), ADSAS showing major improvement (ASDAS MI; decrease from baseline ≥ 2.0), and ASDAS showing clinically important improvement (ASDAS CII; decrease from baseline ≥ 1.1) through 64 weeks (20,21). In addition, change from baseline in the ASDAS using the C-reactive protein level (ASDAS-CRP) (22), Bath Ankylosing Spondylitis Functional Index (BASFI) (23), and linear Bath Ankylosing Spondylitis Metrology Index (BASMI) (24) through 64 weeks and Maastricht Ankylosing Spondylitis Enthesitis Score (MASSES) (25), Work Productivity and Activity Impairment (WPAI; on a scale of 0–100) (26), ASAS health index, and AS quality of life (ASQoL) (27) through 52 weeks were assessed. Pain end points included back pain, nocturnal back pain, BASDAI question 2 (back pain), and BASDAI question

3 (peripheral pain/swelling). The proportions of patients achieving BASDAI <4 and normalization of high-sensitivity CRP (hsCRP ≤ 2.87) were evaluated in exploratory analyses.

Safety assessment. One-year safety reports are based on data available on the cutoff date of January 31, 2020, and were assessed as rate of treatment-emergent adverse events (AEs) reported as events per 100 patient-years. Treatment-emergent AEs were defined as AEs that began or worsened in severity after the first dose and through 30 days after the last dose of study medication.

Statistical analysis. One-year efficacy analysis was performed by randomized treatment group sequence in patients receiving upadacitinib 15 mg once daily from baseline throughout periods 1 and 2 (continuous upadacitinib group) and in patients switching from randomized placebo at week 14 (period 1) to open-label upadacitinib 15 mg once daily (period 2). For binary efficacy end points, response rate and 95% confidence interval (95% CI) were reported as-observed and by using nonresponder imputation (NRI) for missing data (patients who prematurely discontinued the study drug were considered as nonresponders for all subsequent visits after discontinuation, and any patient with any missing

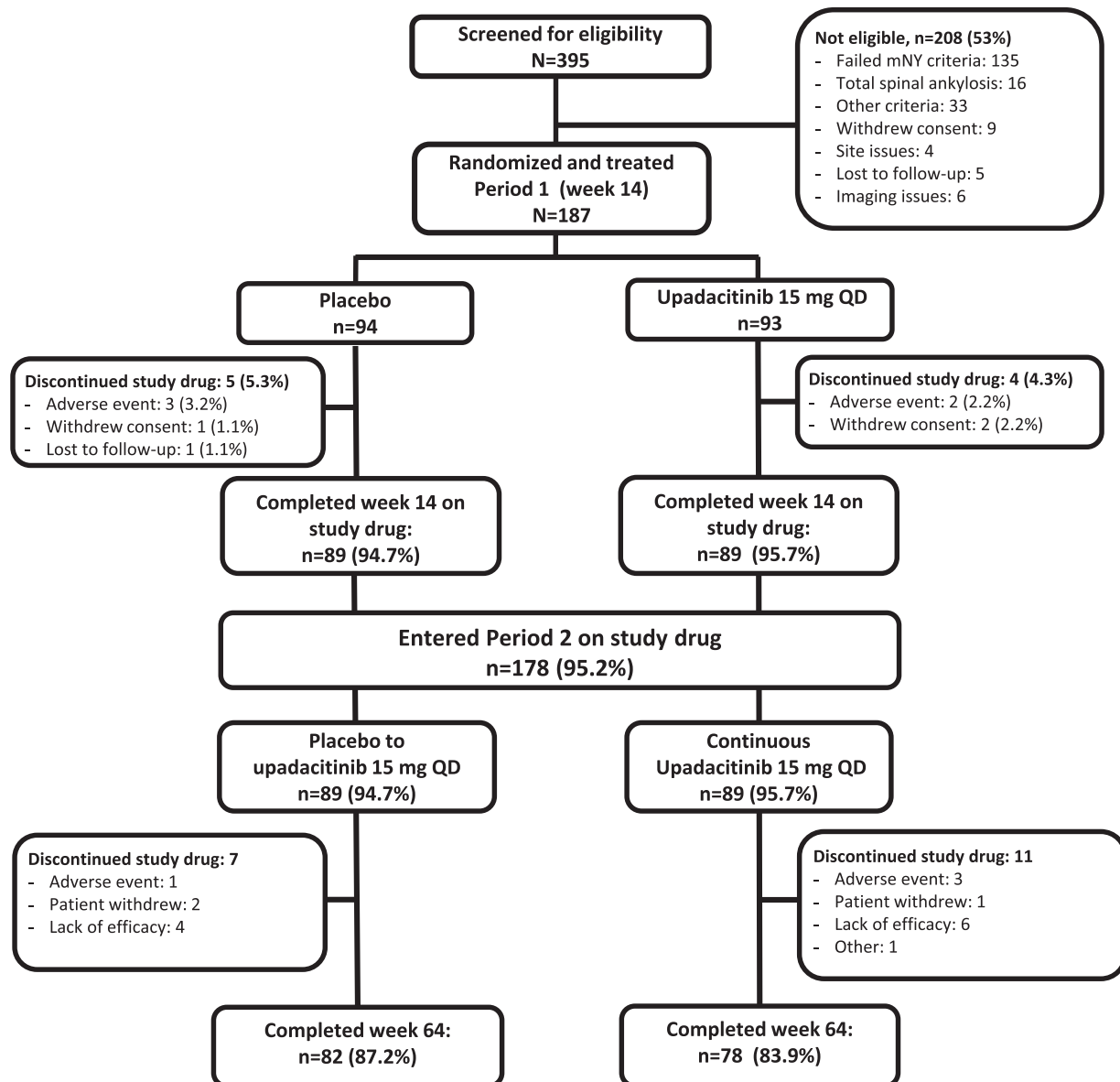


Figure 1. Patient disposition through week 64. Among the reasons for study drug discontinuation in period 2, adverse events included diarrhea, headache, and vertigo in 1 patient; squamous cell carcinoma of the tongue in 1 patient; and headache in 1 patient in the continuous upadacitinib group; and hemiparesthesia (right side) and intervertebral disc protrusion in 1 patient in the placebo-to-upadacitinib group; patient withdrawals included 1 patient who did not wish to administer the medication (lost to follow-up) and 1 patient who did not want to continue the study procedure or the study treatment in the placebo-to-upadacitinib group, and 1 patient who had challenges with transportation to the clinic in the continuous upadacitinib group; the “other” category included 1 patient who moved to a different country. mNY = modified New York; QD = once daily.

value at a specific visit was treated as a nonresponder for that visit). For continuous efficacy end points, descriptive statistics on as-observed data and estimated change from baseline with 95% CI from mixed-effects model repeated measures (MMRM) were reported. MMRM included the categorical fixed effects of treatment, visit, treatment-by-visit interaction, and stratification factor of hsCRP level at screening visit, premature discontinuation flag, and the continuous fixed covariate of baseline value using unstructured variance-covariance matrix. No statistical comparison was performed between the 2 treatment group sequences.

RESULTS

Of the 187 patients randomized to period 1, 178 (89 in the continuous upadacitinib group and 89 in the placebo-to-upadacitinib switch group) completed week 14 on study drug and entered the open-label extension; 160 patients (78 [84%] in the continuous upadacitinib group and 82 [87%] in the placebo-to-upadacitinib switch group) completed week 64 (Figure 1). Lack of efficacy ($n = 10$) and AEs ($n = 4$) were the most common reasons for discontinuation of study drug between weeks 14 and 64.

Up to the data cutoff date, 88% of the patients (160 of 182) who received ≥ 1 dose of upadacitinib 15 mg once daily had at least 52 weeks of exposure to upadacitinib; 34% (62 of 182) had ≥ 18 months of exposure.

Patient demographic and baseline disease characteristics have been reported previously (15). Treatment arms were well balanced; in the upadacitinib and placebo arms, respectively, the majority of patients were male (68% and 73%) and HLA-B27 positive (75% and 78%), the mean age was 47.0 and 43.7 years, and most patients were from Europe (71% and 71%) and White (85% and 81%) (15). The mean duration since AS symptom onset was 14.8 years and 14.0 years, the mean duration since diagnosis was 7.8 years and 6.0 years, the mean ASDAS was 3.5 and 3.7, and the mean hsCRP level was 9.6 mg/liter and 11.7 mg/liter in the upadacitinib and placebo groups, respectively. Concomitant medications in the upadacitinib and placebo arms included NSAIDs (76% and 86%, respectively), csDMARDs (14% and 18%, respectively), and glucocorticoids (6% and 13%, respectively).

Efficacy. The percentage of patients achieving the primary efficacy end point of ASAS40 (52% in the NRI analysis and 54% in the as-observed analysis at week 14) continued to increase throughout the study in the continuous upadacitinib group: 72% and 85% of patients (in the NRI analysis and as-observed analysis, respectively) achieved ASAS40 at week 64 (Figure 2 and Supplementary Table 1, available on the *Arthritis & Rheumatology* website at <http://onlinelibrary.wiley.com/doi/10.1002/art.41911/abstract>). An analogous pattern of improvement was observed in ASDAS LDA (70% in the NRI analysis and 84% in the as-observed analysis), ASDAS ID (34% in the NRI analysis and 42% in the as-observed analysis), and ASAS showing partial remission (40% in the NRI analysis and 46% in the as-observed analysis)

(Figures 2 and 3). Patients who switched from placebo to upadacitinib at week 14 showed a speed of onset and magnitude of response comparable to those in patients who were initially randomized to receive upadacitinib (responses in the switched group at week 64 were 70% in the NRI analysis and 81% in the as-observed analysis for ASAS40; 71% in the NRI analysis and 86% in the as-observed analysis for ASAS LDA; 36% in the NRI analysis and 44% in the as-observed analysis for ASAS ID; and 34% in the NRI analysis and 39% in the as-observed analysis for ASAS showing partial remission) (Figures 2 and 3).

Likewise, the percentage of patients achieving ASAS20 and BASDAI50 (Supplementary Figure 2, available on the *Arthritis & Rheumatology* website at <http://onlinelibrary.wiley.com/doi/10.1002/art.41911/abstract>) and ASDAS CII and ASDAS MI (Supplementary Figure 3, available on the *Arthritis & Rheumatology* website at <http://onlinelibrary.wiley.com/doi/10.1002/art.41911/abstract>) improved throughout the study in the continuous upadacitinib group; patients who switched to upadacitinib from placebo at week 14 showed a rapid onset of response for these end points, with responses at week 64 similar to those observed in patients receiving continuous upadacitinib (Supplementary Figures 2 and 3). At week 64, 88% of patients had a BASDAI < 4 (90% [72 of 80] in the continuous upadacitinib group and 87% [71 of 82] in the placebo-to-upadacitinib switch group).

Mean changes from baseline to 1 year in disease activity, as measured by the ASDAS and pain, including back pain and nocturnal back pain, showed consistent improvement or sustained maintenance throughout the study in the continuous upadacitinib group; a similar magnitude of improvement was seen in the placebo-to-upadacitinib switch group after initiation of upadacitinib at week 14 (Figures 4 and 5 and Supplementary Table 2 and Supplementary Figure 4, available on the *Arthritis & Rheumatology* website at <http://onlinelibrary.wiley.com/doi/10.1002/art.41911/abstract>). Improvements in function (BASFI) and inflammation, based on both clinical (mean of BASDAI questions 5 and 6) and laboratory (hsCRP) end points were also sustained through week 64 (Figure 4 and Supplementary Figure 5 and Supplementary Table 3, available on the *Arthritis & Rheumatology* website at <http://onlinelibrary.wiley.com/doi/10.1002/art.41911/abstract>). Analogous patterns of improvement over time were shown in assessments of quality of life (ASQoL and ASAS health index), spinal mobility (BASMI), enthesitis (MASES), and patient global assessment of disease activity (Supplementary Table 2 and Supplementary Figures 6 and 7, available on the *Arthritis & Rheumatology* website at <http://onlinelibrary.wiley.com/doi/10.1002/art.41911/abstract>).

Among patients who were employed at baseline, the mean WPAI overall work impairment score continued to improve throughout the study in the continuous upadacitinib group (from -20.5 at week 14 [95% CI $-27.1, -14.0$] to -35.6 at week 52 [95% CI $-43.2, -28.0$]; as-observed analysis) and placebo-to-upadacitinib switch group (from -12.3 at week 14 [95% CI $-19.8, -4.8$] to -27.7 at week 52 [95% CI

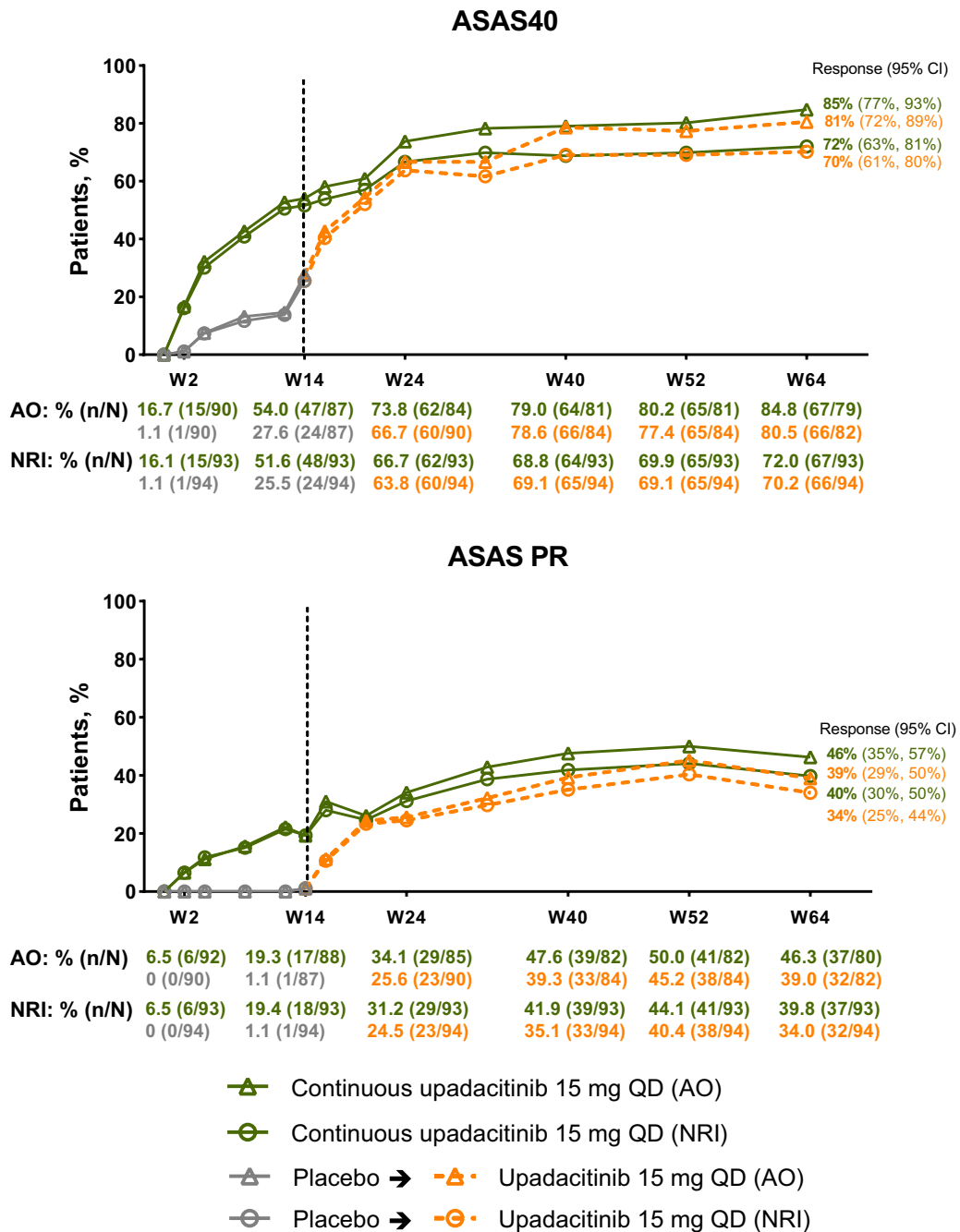


Figure 2. Percentage of patients achieving Assessment of SpondyloArthritis international Society 40% response (ASAS40) and ASAS showing partial remission (ASAS PR) over time. All patients randomized to receive placebo received open-label upadacitinib beginning at week 14. 95% CI = 95% confidence interval; AO = as-observed; NRI = nonresponder imputation; QD = once daily.

–35.4, –20.0]; as-observed analysis). Results were similar in the MMRM analysis (Supplementary Table 4, available on the *Arthritis & Rheumatology* website at <http://onlinelibrary.wiley.com/doi/10.1002/art.41911/abstract>).

Safety. Safety through the January 31, 2020 data cutoff date was assessed in 182 patients (237.6 patient-years) receiving upadacitinib 15 mg once daily during period 1 or 2; a total of 618 AEs (260.1 per 100 patient-years) were reported (Table 1).

The most common AEs were nasopharyngitis (37 events [15.6 per 100 patient-years]), increased blood creatine phosphokinase (28 events [11.8 per 100 patient-years]), and upper respiratory tract infection (26 events [10.9 per 100 patient-years]). The creatine phosphokinase elevation events were all nonserious, none led to study drug discontinuation, and all except 2 were asymptomatic. The 2 symptomatic AEs were based on muscle pain with alternative explanations of increased exercise or physical activity, mild, and resolved with continued study drug treatment. The

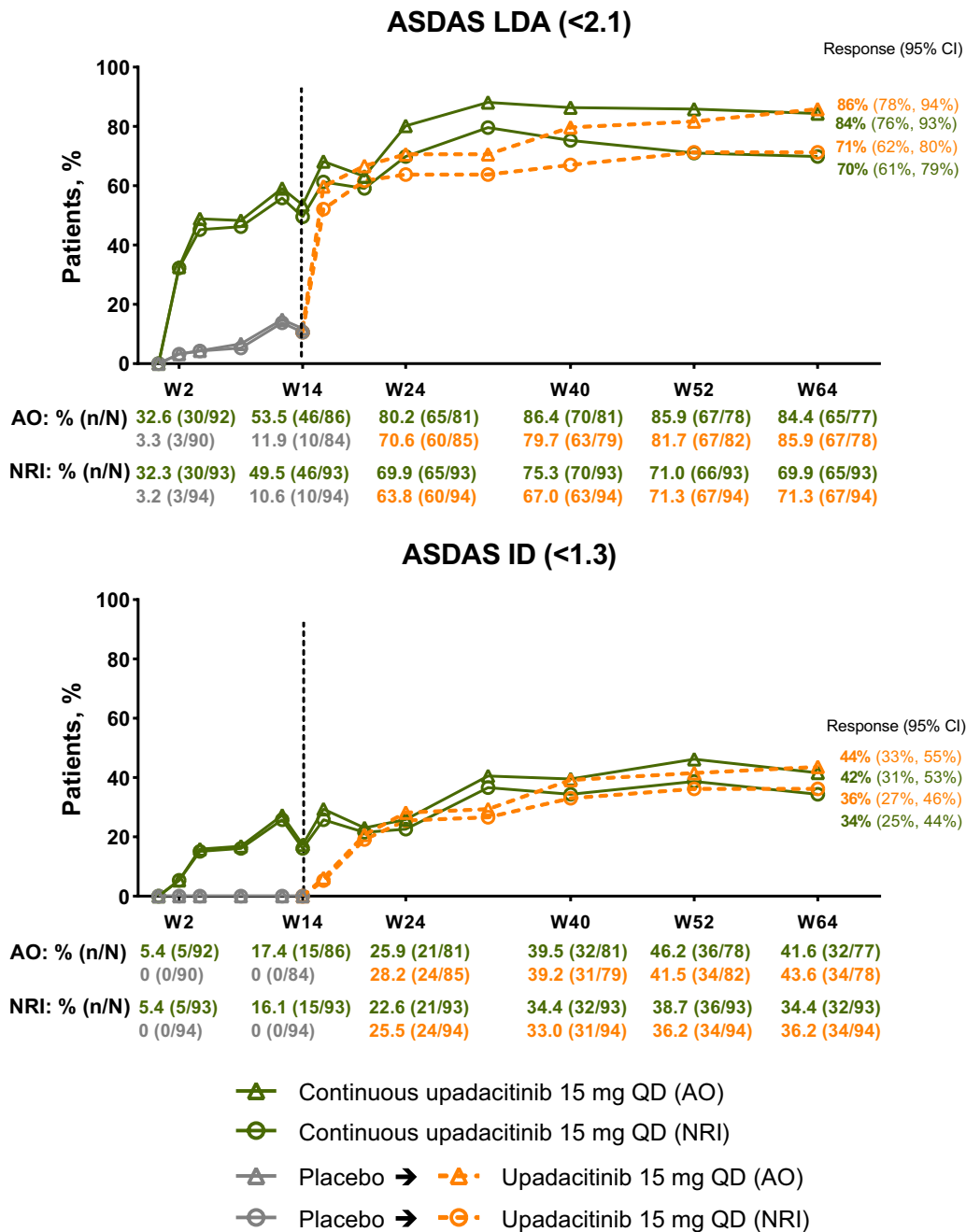


Figure 3. Percentage of patients achieving Ankylosing Spondylitis Disease Activity Score showing low disease activity (ASDAS LDA; <2.1) and ASDAS showing inactive disease (ASDAS ID; <1.3) over time. All patients randomized to receive placebo received open-label upadacitinib beginning at week 14. 95% CI = 95% confidence interval; AO = as-observed; NRI = nonresponder imputation; QD = once daily.

rates of serious AEs (5.9 per 100 patient-years) and AEs leading to discontinuation (6.3 per 100 patient-years) were low (Supplementary Table 5, available on the *Arthritis & Rheumatology* website at <http://onlinelibrary.wiley.com/doi/10.1002/art.41911/abstract>).

No serious infections, active tuberculosis, major adverse cardiovascular events, venous thromboembolic events, gastrointestinal perforation, inflammatory bowel disease (IBD), renal dysfunction, or deaths were reported with upadacitinib treatment; of note, 4 patients (2 in each group) had a history of IBD at baseline. Rates of other events of interest were also

low. The only malignancy reported was a stage IVa squamous cell carcinoma of the tongue in a 61-year-old man (former smoker) after the week 20 visit; per investigator, the event had no reasonable possibility to be related to the study drug but did lead to discontinuation of the study drug as required by the study protocol. Five events of herpes zoster (2.1 per 100 patient-years) in 4 patients were reported; all were nonserious and limited to 1 dermatome, and 1 led to discontinuation of the study drug. Two opportunistic infections (0.8 per 100 patient-years) were reported; both were nonserious events

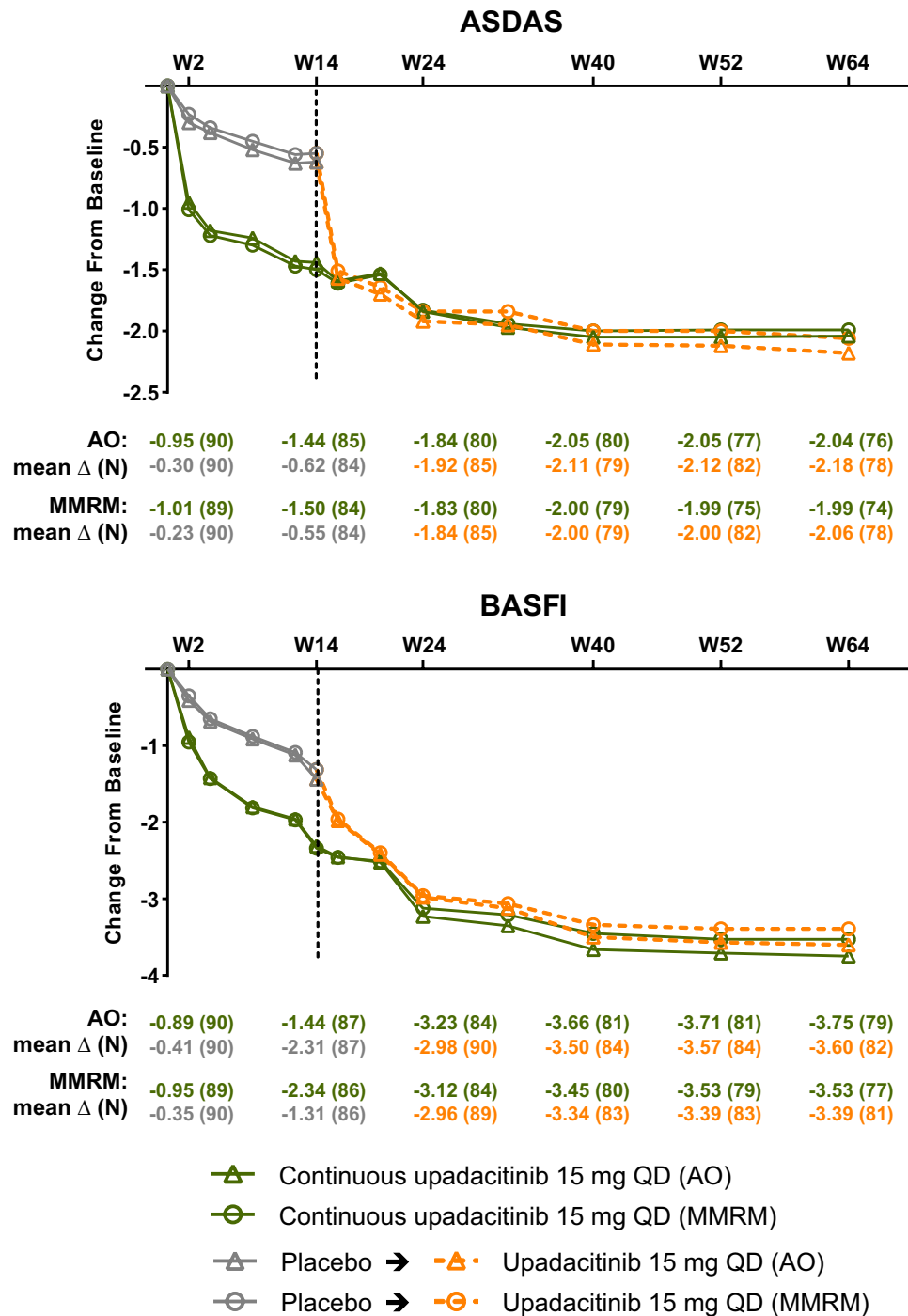


Figure 4. Change from baseline (Δ) in Ankylosing Spondylitis Disease Activity Score using the C-reactive protein level (ASDAS-CRP) and Bath Ankylosing Spondylitis Functional Index (BASFI) over time. All patients randomized to receive placebo received open-label upadacitinib beginning at week 14. AO = as-observed; MMRM = mixed-effects model repeated measures; QD = once daily.

of esophageal candidiasis of moderate severity in the same patient, and neither event led to discontinuation of study drug. Thirteen uveitis events in 8 patients (5.5 per 100 patient-years) were reported; all events occurred in patients with a history of uveitis (Supplementary Table 6, available on the *Arthritis & Rheumatology* website at <http://onlinelibrary.wiley.com/doi/10.1002/art.41911/abstract>). The mean time to onset of

uveitis among these patients was 343 days, and the median was 295 days (range 115–721 days).

All events of neutropenia, anemia, and lymphopenia were non-serious, and none led to study drug discontinuation. The majority of events related to hepatic disorders were based on transient asymptomatic alanine aminotransferase (ALT)/aspartate aminotransferase (AST) elevations, all were nonserious and mild to moderate in

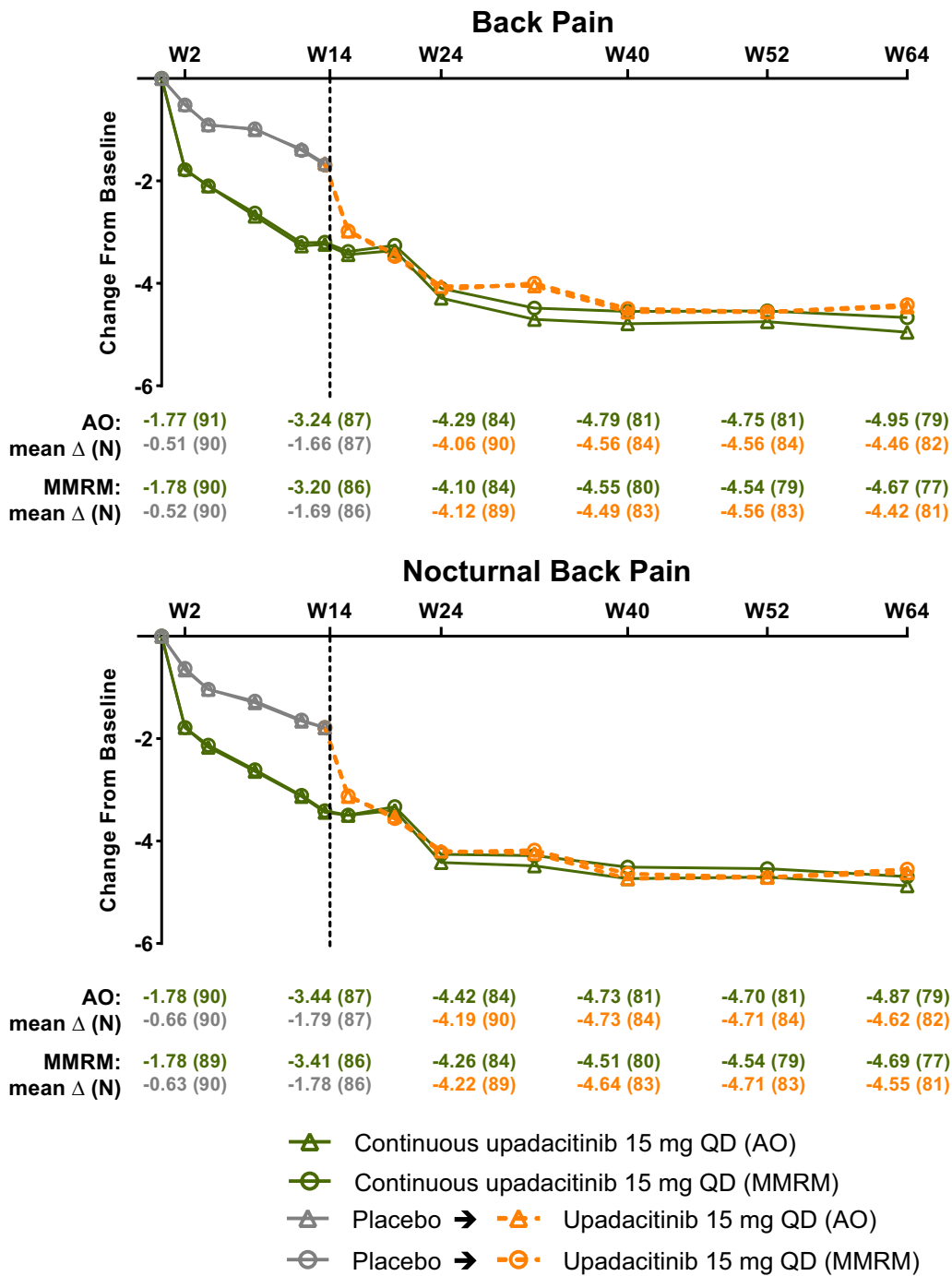


Figure 5. Change from baseline (Δ) in back pain and nocturnal back pain over time. All patients randomized to receive placebo received open-label upadacitinib beginning at week 14. Evaluation of back pain was based on the question, “What is the amount of back pain that you experienced at any time during the last week?” and evaluation of nocturnal back pain was based on the question, “What is the amount of back pain at night that you experienced during the last week?” Both were scored on a numerical rating scale of 0–10. AO = as-observed; MMRM = mixed-effects model repeated measures; QD = once daily.

severity, and none led to study drug discontinuation. One patient experienced a grade 3 (≥ 5 times the upper limit of normal) increase in ALT and 1 patient in AST; no grade 3 or 4 decreases in hemoglobin level or lymphocyte count were observed (Supplementary Table 7, available on the *Arthritis & Rheumatology* website at <http://onlinelibrary.wiley.com/doi/10.1002/art.41911/abstract>).

Five patients experienced grade 3 creatine phosphokinase elevation, and 2 experienced grade 4 elevation; all occurred in young male AS patients, and none led to study drug discontinuation or met the toxicity criteria threshold (Supplementary Table 7). Among these 7 patients, creatine phosphokinase elevations occurred at various time points in relation to the initiation of

Table 1. Treatment-emergent adverse events (AEs) in the all-upadacitinib population*

Any AE	618 (260.1)
Serious AE†	14 (5.9)
AE leading to discontinuation‡	15 (6.3)
Infection	205 (86.3)
Serious infection	0 (0)
Opportunistic infection‡	2 (0.8)
Herpes zoster§	5 (2.1)
Active tuberculosis	0 (0)
Creatine phosphokinase elevation¶	28 (11.8)
Hepatic disorder#	24 (10.1)
Neutropenia**	7 (2.9)
Anemia**	3 (1.3)
Lymphopenia**	2 (0.8)
Renal dysfunction	0 (0)
Gastrointestinal perforation	0 (0)
Malignancy††	1 (0.4)
Adjudicated MACE	0 (0)
Adjudicated VTE	0 (0)
Uveitis‡‡	13 (5.5)
Inflammatory bowel disease	0 (0)
Death	0 (0)

* Values are the number of events (number of events per 100 patient-years) in all patients receiving upadacitinib 15 mg once daily (n = 182; total of 237.6 patient-years). MACE = major adverse cardiovascular event; VTE = venous thromboembolic event.

† See Supplementary Table 5, available on the *Arthritis & Rheumatology* website at <http://onlinelibrary.wiley.com/doi/10.1002/art.41911/abstract>, for more details.

‡ Two nonserious events of esophageal candidiasis occurred in the same 60-year-old patient with a history of gastroesophageal reflux disease. Each event was moderate in severity and assessed by the investigator as having a reasonable possibility of being related to study drug. The study drug was temporarily interrupted for each event but was restarted.

§ Five events in 4 patients; all were nonserious and limited to 1 dermatome.

¶ All events were nonserious, and none led to study drug discontinuation. The majority were asymptomatic and based on creatine phosphokinase increases of <4 times the upper limit of normal.

The majority were based on asymptomatic alanine aminotransferase/aspartate aminotransferase elevations. All were nonserious, and none led to study drug discontinuation.

** All events were nonserious, and none led to study drug discontinuation.

†† Squamous cell carcinoma of the tongue (stage IVa tumor) in a 61-year-old male former smoker (~1 pack per day for 40 years). There was no reasonable possibility the event was related to the study drug, per the investigator.

‡‡ Includes 13 events in 8 patients. All were nonserious and assessed as having no reasonable possibility to be related to the study drug. The majority of events occurred in HLA-B27-positive ankylosing spondylitis patients with a history of uveitis, were mild or moderate in severity, transient, and resolved with local treatment (glucocorticoid eye-drop). One patient discontinued the study. See Supplementary Table 6, available on the *Arthritis & Rheumatology* website at <http://onlinelibrary.wiley.com/doi/10.1002/art.41911/abstract>, for more details.

upadacitinib therapy. Elevations were transient in 5 patients and normalized over time, including the 2 grade 4 increases (Supplementary Figure 8, available on the *Arthritis & Rheumatology* website at <http://onlinelibrary.wiley.com/doi/10.1002/art.41911/abstract>). Mean creatine phosphokinase values showed an increase from baseline over time, but no major differences in mean hemoglobin level, lymphocyte count, or neutrophil count were observed compared with baseline (Supplementary Figure 9,

Arthritis & Rheumatology website at <http://onlinelibrary.wiley.com/doi/10.1002/art.41911/abstract>).

DISCUSSION

SELECT-AXIS 1, the first study to report 1-year data on a JAK inhibitor in AS, showed that upadacitinib 15 mg once daily therapy led to sustained and consistent efficacy over 1 year in both NRI and as-observed analyses in patients with active AS who had an inadequate response to NSAIDs. Improvements were seen in disease activity measures (ASDAS, BASDAI, ASAS, and their components), pain (back pain, nocturnal back pain, and peripheral pain), physical function (BASFI), inflammation (hsCRP), quality of life (ASQoL and the ASAS health index), and other aspects of disease (BASMI and MASES) with continuous upadacitinib therapy. In patients who switched from placebo to upadacitinib at week 14, a similar speed of onset and magnitude of efficacy response was observed through 1 year compared with those who received continuous upadacitinib.

The primary goal of therapy in AS is to maximize a patient's quality of life through control of the signs and symptoms of disease and preservation of physical function and social participation (4), and the SELECT-AXIS 1 study showed wide-ranging benefits of upadacitinib treatment for treating the signs and symptoms of AS. Of note, 39–46% of patients receiving upadacitinib had achieved ASAS showing partial remission or ASDAS ID at the end of 1 year, and >81% reached ASAS40 or ASDAS LDA. Sustained efficacy in AS has also been described for biologic DMARDs, such as TNF or IL-17 inhibitors, and although no head-to-head trials are available, overall, the efficacy of upadacitinib appears to be consistent with that described for TNF and IL-17 inhibitor therapy in AS (28–31). The dropout/retention rate in SELECT-AXIS 1 was also consistent with that for other approved biologic DMARDs (28–30).

Upadacitinib was well tolerated over 237.6 patient-years of exposure, with no new or unexpected safety findings compared with data from the upadacitinib clinical development programs in RA and PsA (32–34). No serious infections, active tuberculosis, venous thromboembolic events, gastrointestinal perforation, major adverse cardiovascular events, renal dysfunction, or deaths were reported. Rates of herpes zoster, opportunistic infections, and malignancy were low and consistent with what has been reported previously in AS patients (35–37). Nonserious and generally asymptomatic events of creatine phosphokinase elevation were observed. Creatine phosphokinase elevations have been observed with JAK inhibitors (9,10,38) and also have been described more frequently with TNF inhibitors in patients with AS than in patients with RA (39,40).

Only limited information is available on the impact of upadacitinib on uveitis and IBD. In this study, no patient developed new-onset uveitis, and events were observed only in patients with a history of uveitis. The rate of uveitis was 5.5 events per 100 patient-years. In addition, no new onset or exacerbation of IBD was observed. Only 4 patients at baseline had a history of IBD in

this study. Whether upadacitinib treatment has an advantage over IL-17 inhibitors, which are not recommended for patients with concomitant active IBD (4), needs further investigation.

Limitations of this study include the open-label nature of period 2, the lack of an active comparator to contextualize efficacy and safety data, and that only 1 dose of upadacitinib was studied. Of note, head-to-head studies in RA and PsA help to put upadacitinib data into context (33,41,42), and upadacitinib exposure–response analyses of the SELECT-AXIS study and of the phase II and III upadacitinib RA studies suggested that upadacitinib pharmacokinetics were similar in patients with AS and patients with RA, and predicted that the 15-mg dose would maximize efficacy in patients with AS (43,44). The upadacitinib 15-mg once daily dose appears to show an optimal benefit–risk profile in RA and PsA (including in PsA patients with axial symptoms) (33,34,42,45,46). In addition, SELECT-AXIS 1 only included a biologic DMARD-naïve population and further evaluation on the effect of upadacitinib in biologic DMARD inadequate responders (as examined in the ongoing SELECT-AXIS 2 study) is needed (47). The strengths of SELECT-AXIS 1 include that it was a well-controlled trial that showed consistent maintenance of response without new safety findings compared with the RA and PsA programs.

In summary, upadacitinib 15 mg once daily showed sustained and consistent efficacy over 1 year in patients with active AS. Patients who switched from placebo to upadacitinib at week 14 showed a similar efficacy response compared with those who received continuous upadacitinib. Safety results were comparable with previous upadacitinib studies. Overall, oral upadacitinib therapy over 1 year was efficacious and well tolerated, suggesting it may help address an unmet need for patients with AS who have active disease and an inadequate response to NSAIDs. The long-term efficacy and safety of upadacitinib, including long-term imaging, will be assessed over 2 years in the SELECT-AXIS 1 extension.

ACKNOWLEDGMENTS

AbbVie and the authors thank the patients, study sites, and investigators who participated in this clinical trial.

AUTHOR CONTRIBUTIONS

All authors were involved in drafting the article or revising it critically for important intellectual content, and all authors approved the final version to be published. Dr. Deodhar had full access to all of the data in the study and takes responsibility for the integrity of the data and the accuracy of the data analysis.

Study conception and design. Deodhar, van der Heijde, Sieper, Van den Bosch, Maksymowych, Kim, Kishimoto, Ostor, Song.

Acquisition of data. Maksymowych, Kishimoto, Ostor, Chu, Song.

Analysis and interpretation of data. Deodhar, Sieper, Van den Bosch, Maksymowych, Kishimoto, Ostor, Combe, Sui, Chu, Song.

ROLE OF THE STUDY SPONSOR

AbbVie funded the study and participated in the study design, research, analysis, data collection, interpretation of data, review, and approval of the manuscript. All authors had access to relevant data and

participated in the drafting, review, and approval of this publication. No honoraria or payments were made for authorship. Medical writing support was provided by M. Hovenden and J. Matsuura of ICON (North Wales, PA) and was funded by AbbVie. Publication of this article was contingent upon approval by AbbVie.

REFERENCES

- Dougados M, Baeten D. Spondyloarthritis [review]. *Lancet* 2011;377:2127–37.
- Sieper J, Poddubnyy D. Axial spondyloarthritis [review]. *Lancet* 2017;390:73–84.
- Strand V, Singh JA. Patient burden of axial spondyloarthritis [review]. *J Clin Rheumatol* 2017;23:383–91.
- Van der Heijde D, Ramiro S, Landewe R, Baraliakos X, Van den Bosch F, Sepriano A, et al. 2016 update of the ASAS-EULAR management recommendations for axial spondyloarthritis [review]. *Ann Rheum Dis* 2017;76:978–91.
- Smolen JS, Schols M, Braun J, Dougados M, FitzGerald O, Gladman DD, et al. Treating axial spondyloarthritis and peripheral spondyloarthritis, especially psoriatic arthritis, to target: 2017 update of recommendations by an international task force. *Ann Rheum Dis* 2018;77:3–17.
- Rinvoq (upadacitinib) prescribing information. North Chicago (IL): AbbVie; 2019.
- Xeljanz (tofacitinib) prescribing information. New York (NY): Pfizer Laboratories; 2019.
- Olumiant (baricitinib) prescribing information. Indianapolis (IN): Lilly, LLC, 2018.
- Van der Heijde D, Deodhar A, Wei JC, Drescher E, Fleishaker D, Hendriks T, et al. Tofacitinib in patients with ankylosing spondylitis: a phase II, 16-week, randomised, placebo-controlled, dose-ranging study. *Ann Rheum Dis* 2017;76:1340–7.
- Van der Heijde D, Baraliakos X, Gensler LS, Maksymowych WP, Tseluyko V, Nadashkevich O, et al. Efficacy and safety of filgotinib, a selective Janus kinase 1 inhibitor, in patients with active ankylosing spondylitis (TORTUGA): results from a randomised, placebo-controlled, phase 2 trial. *Lancet* 2018;392:2378–87.
- Veale DJ, McGonagle D, McInnes IB, Krueger JG, Ritchlin CT, Elewaut D, et al. The rationale for Janus kinase inhibitors for the treatment of spondyloarthritis [review]. *Rheumatology (Oxford)* 2019;58:197–205.
- Onuora S. New positive results for upadacitinib in AS [review]. *Nat Rev Rheumatol* 2020;16:62.
- Deodhar A, Sliwiska-Stanczyk P, Xu H, Baraliakos X, Gensler L, Fleishaker D, et al. Tofacitinib for the treatment of adult patients with ankylosing spondylitis: primary analysis of a phase 3, randomized, double-blind, placebo-controlled study [abstract]. *Arthritis Rheumatol* 2020;72 Suppl 10. URL: <https://acrabstracts.org/abstract/tofacitinib-for-the-treatment-of-adult-patients-with-ankylosing-spondylitis-primary-analysis-of-a-phase-3-randomized-double-blind-placebo-controlled-study/>.
- Parmentier JM, Voss J, Graff C, Schwartz A, Argiriadi M, Friedman M, et al. In vitro and in vivo characterization of the JAK1 selectivity of upadacitinib (ABT-494). *BMC Rheumatol* 2018;2:23.
- Van der Heijde D, Song IH, Pangan AL, Deodhar A, van den Bosch F, Maksymowych WP, et al. Efficacy and safety of upadacitinib in patients with active ankylosing spondylitis (SELECT-AXIS 1): a multicentre, randomised, double-blind, placebo-controlled, phase 2/3 trial. *Lancet* 2019;394:2108–17.
- Rudwaleit M, van der Heijde D, Landewé R, Akkoc N, Brandt J, Chou CT, et al. The Assessment of SpondyloArthritis international Society classification criteria for peripheral spondyloarthritis and for spondyloarthritis in general. *Ann Rheum Dis* 2010;70:25–31.

17. Van der Linden S, Valkenburg HA, Cats A. Evaluation of diagnostic criteria for ankylosing spondylitis: a proposal for modification of the New York criteria. *Arthritis Rheum* 1984;27:361–8.
18. Garrett S, Jenkinson T, Kennedy LG, Whitelock H, Gaisford P, Calin A. A new approach to defining disease status in ankylosing spondylitis: the Bath Ankylosing Spondylitis Disease Activity Index. *J Rheumatol* 1994;21:2286–91.
19. Lukas C, Landewé R, Sieper J, Dougados M, Davis J, Braun J, et al, for the Assessment of SpondyloArthritis international Society. Development of an ASAS-endorsed disease activity score (ASDAS) in patients with ankylosing spondylitis. *Ann Rheum Dis* 2009;68:18–24.
20. Machado PM, Landewe R, Heijde DV, on behalf of the Assessment of SpondyloArthritis International Society (ASAS). Ankylosing Spondylitis Disease Activity Score (ASDAS): 2018 update of the nomenclature for disease activity states. *Ann Rheum Dis* 2018;77:1539–40.
21. Sieper J, Rudwaleit M, Baraliakos X, Brandt J, Braun J, Burgos-Vargas R, et al. The Assessment of SpondyloArthritis international Society (ASAS) handbook: a guide to assess spondyloarthritis. *Ann Rheum Dis* 2009;68 Suppl 2:ii1–44.
22. Machado P, Navarro-Compán V, Landewé R, van Gaalen FA, Roux C, van der Heijde D. Calculating the ankylosing spondylitis disease activity score if the conventional C-reactive protein level is below the limit of detection or if high-sensitivity C-reactive protein is used: an analysis in the DESIR cohort. *Arthritis Rheumatol* 2015;67:408–13.
23. Calin A, Garrett S, Whitelock H, Kennedy LG, O’Hea J, Mallorie P, et al. A new approach to defining functional ability in ankylosing spondylitis: the development of the Bath Ankylosing Spondylitis Functional Index. *J Rheumatol* 1994;21:2281–5.
24. Jenkinson TR, Mallorie PA, Whitelock HC, Kennedy LG, Garrett SL, Calin A. Defining spinal mobility in ankylosing spondylitis (AS): the Bath AS Metrology Index. *J Rheumatol* 1994;21:1694–8.
25. Heuft-Dorenbosch L, Spoorenberg A, van Tubergen A, Landewé R, van der Tempel H, Mielants H, et al. Assessment of enthesitis in ankylosing spondylitis. *Ann Rheum Dis* 2003;62:127–32.
26. Reilly MC, Gooch KL, Wong RL, Kupper H, van der Heijde D. Validity, reliability and responsiveness of the Work Productivity and Activity Impairment Questionnaire in ankylosing spondylitis. *Rheumatology (Oxford)* 2010;49:812–9.
27. Helliwell PS, Doward L, Whalley D, Tennant A, McKenna S, Reynolds S, et al. Psychometric and scaline properties of a new quality of life instrument specific to ankylosing spondylitis [abstract]. *Arthritis Rheum* 1999;42 Suppl:S72.
28. Braun J, Deodhar A, Inman RD, van der Heijde D, Mack M, Xu S, et al. Golimumab administered subcutaneously every 4 weeks in ankylosing spondylitis: 104-week results of the GO-RAISE study. *Ann Rheum Dis* 2012;71:661–7.
29. Sieper J, Landewé R, Rudwaleit M, van der Heijde D, Dougados M, Mease PJ, et al. Effect of certolizumab pegol over ninety-six weeks in patients with axial spondyloarthritis: results from a phase III randomized trial. *Arthritis Rheumatol* 2015;67:668–77.
30. Braun J, Baraliakos X, Deodhar A, Baeten D, Sieper J, Emery P, et al. Effect of secukinumab on clinical and radiographic outcomes in ankylosing spondylitis: 2-year results from the randomised phase III MEASURE 1 study. *Ann Rheum Dis* 2017;76:1070–7.
31. Akkoc N, Khan MA. JAK inhibitors for axial spondyloarthritis: what does the future hold? [review]. *Curr Rheumatol Rep* 2021;23:34.
32. Cohen SB, van Vollenhoven RF, Winthrop KL, Zerbini CA, Tanaka Y, Bessette L, et al. Safety profile of upadacitinib in rheumatoid arthritis: integrated analysis from the SELECT phase III clinical programme. *Ann Rheum Dis* 2020;80:304–11.
33. McInnes I, Anderson J, Magrey M, Merola JF, Liu Y, Kishimoto M, et al. LB0001 efficacy and safety of upadacitinib versus placebo and adalimumab in patients with active psoriatic arthritis and inadequate response to non-biologic disease-modifying anti-rheumatic drugs (SELECT-PsA-1): a double-blind, randomized controlled phase 3 trial [abstract]. *Ann Rheum Dis* 2020;79:16–7.
34. Mease PJ, Lertratanakul A, Anderson JK, Papp K, Van den Bosch F, Tsuji S, et al. Upadacitinib for psoriatic arthritis refractory to biologics: SELECT-PsA 2. *Ann Rheum Dis* 2020;80:312–20.
35. Wang S, Wei JC, Huang JY, Perng WT, Zhang Z. The risk of herpes zoster among patients with ankylosing spondylitis: a population-based cohort study in Taiwan. *Int J Rheum Dis* 2020;23:181–8.
36. Lim DH, Kim YJ, Kim SO, Hong S, Lee CK, Yoo B, et al. The risk of herpes zoster in patients with ankylosing spondylitis: analysis of the Korean National Health Insurance Service-sample cohort database. *Mod Rheumatol* 2018;28:168–73.
37. Yun H, Yang S, Chen L, Xie F, Winthrop K, Baddley JW, et al. Risk of herpes zoster in autoimmune and inflammatory diseases: implications for vaccination. *Arthritis Rheumatol* 2016;68:2328–37.
38. Queeney K, Housley W, Sokolov J, Long AJ. FRI0131 elucidating the mechanism underlying creatine phosphokinase upregulation with upadacitinib. *Ann Rheum Dis* 2019;78:734–5.
39. Cimzia (certolizumab pegol) summary of product characteristics. Bruxelles (Belgium): UCB Pharma, 2020.
40. Park W, Yoo DH, Jaworski J, Brzezicki J, Gnylorybov A, Kadinov V, et al. Comparable long-term efficacy, as assessed by patient-reported outcomes, safety and pharmacokinetics, of CT-P13 and reference infliximab in patients with ankylosing spondylitis: 54-week results from the randomized, parallel-group PLANETAS study. *Arthritis Res Ther* 2016;18:25.
41. Rubbert-Roth A, Enejosa J, Pangan AL, Haraoui B, Rischmueller M, Khan N, et al. Trial of upadacitinib or abatacept in rheumatoid arthritis. *N Engl J Med* 2020;383:1511–21.
42. Fleischmann R, Pangan AL, Song IH, Mysler E, Bessette L, Peterfy C, et al. Upadacitinib versus placebo or adalimumab in patients with rheumatoid arthritis and an inadequate response to methotrexate: results of a phase III, double-blind, randomized controlled trial. *Arthritis Rheumatol* 2019;71:1788–800.
43. Nader A, Mohamed MF, Winzenborg I, Doelger E, Noertersheuser P, Pangan AL, et al. Exposure-response analyses of upadacitinib efficacy and safety in phase II and III studies to support benefit-risk assessment in rheumatoid arthritis. *Clin Pharmacol Ther* 2020;107:994–1003.
44. Ismail M, Nader A, Winzenborg I, Song IH, Othman AA. Exposure-response analyses for upadacitinib efficacy and safety in ankylosing spondylitis—analyses of the SELECT-AXIS I study [abstract]. *Arthritis Rheumatol* 2019;71 Suppl 10. URL: <https://acrabstracts.org/abstract/exposure-response-analyses-for-upadacitinib-efficacy-and-safety-in-ankylosing-spondylitis-analyses-of-the-select-axis-i-study/>.
45. Genovese MC, Fleischmann R, Combe B, Hall S, Rubbert-Roth A, Zhang Y, et al. Safety and efficacy of upadacitinib in patients with active rheumatoid arthritis refractory to biologic disease-modifying anti-rheumatic drugs (SELECT-BEYOND): a double-blind, randomised controlled phase 3 trial. *Lancet* 2018;391:2513–24.
46. Deodhar A, Ranza R, Ganz F, Gao T, Anderson JK, Östör A. Efficacy and safety of upadacitinib in patients with psoriatic arthritis and axial involvement [abstract]. *Arthritis Rheumatol* 2020;72 Suppl 10. URL: <https://acrabstracts.org/abstract/efficacy-and-safety-of-upadacitinib-in-patients-with-psoriatic-arthritis-and-axial-involvement/>.
47. AbbVie, sponsor. A study to evaluate efficacy and safety of upadacitinib in adult participants with axial spondyloarthritis (SELECT-AXIS 2). [ClinicalTrials.gov identifier: NCT04169373](https://clinicaltrials.gov/ct2/show/study/NCT04169373).

Identification and Evaluation of Serum Protein Biomarkers That Differentiate Psoriatic Arthritis From Rheumatoid Arthritis

Angela Mc Ardle,¹  Anna Kwasnik,¹ Agnes Szentpetery,¹ Belinda Hernandez,² Andrew Parnell,¹ Wilco de Jager,³ Sytze de Rook,⁴ Oliver FitzGerald,¹ and Stephen R. Pennington¹

Objective. To identify serum protein biomarkers that might distinguish patients with early inflammatory arthritis (IA) with psoriatic arthritis (PsA) from those with rheumatoid arthritis (RA) and may be used to support appropriate early intervention.

Methods. The serum proteome of patients with PsA and patients with RA was interrogated using nano-liquid chromatography mass spectrometry (nano-LC-MS/MS) (n = 64 patients), an aptamer-based assay (SomaScan) targeting 1,129 proteins (n = 36 patients), and a multiplexed antibody assay (Luminex) for 48 proteins (n = 64 patients). Multiple reaction monitoring (MRM) assays were developed to evaluate the performance of putative markers using the discovery cohort (n = 60 patients) and subsequently an independent cohort of PsA and RA patients (n = 167).

Results. Multivariate machine learning analysis of the protein discovery data from the 3 platforms revealed that it was possible to differentiate PsA patients from RA patients with an area under the curve (AUC) of 0.94 for nano-LC-MS/MS, 0.69 for bead-based immunoassay measurements, and 0.73 for aptamer-based analysis. Subsequently, in the separate verification and evaluation studies, random forest models revealed that a subset of proteins measured by MRM could differentiate PsA and RA patients with AUCs of 0.79 and 0.85, respectively.

Conclusion. We present a serum protein biomarker panel that can separate patients with early-onset IA with PsA from those with RA. With continued evaluation and refinement using additional and larger patient cohorts, including those with other arthropathies, we suggest that the panel identified here could contribute to improved clinical decision making.

INTRODUCTION

Psoriatic arthritis (PsA) is a form of inflammatory arthritis (IA) affecting ~0.25% of the population (1–4). It is a highly heterogeneous disorder associated with joint damage, disability, disfiguring skin disease, and poor patient-related quality of life outcome measures (4). Inherently irreversible and frequently progressive, the process of joint damage begins at or before the clinical onset of disease. Indeed, structural joint damage, which is likely to result in joint deformity and disability, is present in 47% of patients within 2 years of disease onset (3,5). Reductions in

quality of life and physical function are comparable to those in rheumatoid arthritis (RA) and are compounded by the presence of chronic disfiguring skin disease (6–9). Direct and indirect health costs pose a significant economic burden on society and increase with severe physical dysfunction (9).

Early diagnosis and management of PsA leads to better long-term outcomes; however, with no diagnostic laboratory test available, the diagnosis is often delayed or missed, and this has significant consequences for individuals with PsA (10–12). At disease onset, PsA often resembles other forms of arthritis including RA. Despite the clinical similarities between PsA and RA, their distinctive

Supported by the European Commission under the EU FP7 Programme Monitoring Innate Immunity in Arthritis and Mucosal Inflammation (MIAMI) (project grant 305266) and the Health Research Board (grant HRA-HSR-2015-1284). The University College Dublin Conway Institute is supported by the Higher Education Authority of Ireland.

¹Angela Mc Ardle, PhD, Anna Kwasnik, PhD, Agnes Szentpetery, MD, Andrew Parnell, PhD, Oliver FitzGerald, MBBCh, BAO, MRCPI, MRCP, MD, Stephen R. Pennington, PhD: University College Dublin, Dublin, Ireland; ²Belinda Hernandez, PhD: Trinity College Dublin and University College Dublin, Dublin, Ireland; ³Wilco de Jager, PhD: Wilhelmina Children Hospital and University Medical Centre Utrecht, Utrecht, The Netherlands;

⁴Sytze de Rook, PhD: University Medical Centre Utrecht, Utrecht, The Netherlands.

Drs. FitzGerald and Pennington contributed equally to this work.

Dr. Pennington owns stock or stock options in Atturos. No other disclosures relevant to this article were reported.

Address correspondence to Oliver FitzGerald, MBBCh, BAO, MRCPI, MRCP, MD, or Stephen R. Pennington, PhD, University College Dublin, UCD Conway Institute of Biomolecular and Biomedical Research, Dublin, Ireland. Email: oliver.fitzgerald@ucd.ie or Stephen.Pennington@ucd.ie.

Submitted for publication December 8, 2020; accepted in revised form June 8, 2021.

pathologic manifestations often require different treatments. For example, drugs targeting the interleukin-12 (IL-12)/IL-23 and IL-17 pathways, which are highly effective in psoriasis and PsA, are ineffective in RA, while drugs targeting B cells such as rituximab are effective in RA but have not been proven beneficial in PsA (4,13).

PsA is most often diagnosed when a patient presents with musculoskeletal inflammation in the presence of psoriasis and in the absence of rheumatoid factor (RF). However, a clear diagnosis can be difficult, as up to 10% of PsA patients may have RF or anti-citrullinated peptide antibody (ACPA), and joint involvement may precede the development of skin or nail psoriasis in 15% of patients with PsA (14). The Classification of Psoriatic Arthritis (CASPAR) Study Group criteria are accepted as having high sensitivity (98.7%) and specificity (91.4%) in classifying patients with longstanding PsA (15). CASPAR criteria show reduced sensitivity in patients with early disease (87.4%), though specificity is improved (99.1%) (16). CASPAR criteria are valid when including patients in research studies or in clinical trials, but it is recognized that they should not be used for diagnosis and are of little value therefore in a primary care or dermatology setting where specialist rheumatologic expertise is very often not readily available (4,17). An effective clinical laboratory test is needed to improve diagnosis and clinical decision making in PsA.

Ideally, a clinical laboratory test should be based on an easily accessible biologic sample such as blood (10), and we therefore set out to discover serum-based biomarkers that could discriminate between patients with PsA and those with RA. With advances in multiplexed technologies, it has become possible to simultaneously measure multiple analytes. However, in complex biologic fluids such as serum, it is apparent that no single technological platform is capable of measuring the entire protein content of a given sample (3,4,18). For this reason, we undertook a comprehensive and complementary analysis of the serum proteome in a cohort of patients with early IA. We used unbiased nano-liquid chromatography mass spectrometry (nano-LC-MS/MS) for serum samples depleted of abundant proteins to identify differentially expressed proteins. In parallel, aptamer-based and bead-based multiplexed assays were used to target low-abundant proteins not easily detectable by nano-LC-MS/MS. Statistical analysis revealed that proteins identified by nano-LC-MS/MS were the most useful in differentiating individuals with PsA from those with RA. Therefore, in subsequent steps we prioritized these proteins for further investigation.

The translation of biomarkers from discovery to clinical use poses many challenges, not least because of the difficulty of confidently identifying suitable candidates from the discovery phase. Multiple reaction monitoring (MRM), a form of targeted MS, is a highly versatile approach that makes it relatively easy to develop and adapt assays that support the simultaneous measurement of multiple proteins. Assay development times are typically much shorter for MRM assays compared to enzyme-linked immunosorbent assays (ELISAs), and multiplexing of MRM assays

is significantly easier. We therefore exploited the advantages of MRM to undertake a 2-phase approach to progress the candidate protein biomarkers identified in the nano-LC-MS/MS discovery study. First, we undertook a verification phase in which MRM assays for a panel of 150 candidate biomarker proteins identified in the discovery cohort were developed and used to measure protein levels in patients from that cohort; in a second evaluation phase, we adapted the MRM assay to encompass an expanded panel of 173 proteins and used this to measure the proteins in an independent cohort. Figure 1 provides an overview of the study workflow.

PATIENTS AND METHODS

Patients. In the discovery and initial verification phases, a total of 64 patient samples were used, and the extensive clinical characterization of the cohort has previously been described in full by Szentpetery et al (19). Briefly, patients ages 18 to 80 years with recent-onset (symptom duration <12 months), treatment-naive PsA or RA with active joint inflammation were enrolled. PsA patients ($n = 32$) fulfilled the CASPAR criteria (15), and patients with RA ($n = 32$) met the American College of Rheumatology (ACR)/European Alliance of Associations for Rheumatology (EULAR) 2010 classification criteria (20). Baseline serum samples were obtained from each patient using standard methodology, aliquotted, and frozen at -80°C (see Supplementary Document 1 on the *Arthritis & Rheumatology* website at <http://onlinelibrary.wiley.com/doi/10.1002/art.41899/abstract>). The study was approved by St. Vincent's Healthcare Group Ethics and Medical Research Committee, and patients were enrolled only after agreeing to participate in the study and providing informed consent.

Samples from a total of 167 patients were used in the second verification phase. There were 95 patients recruited from a cross-sectional cohort of patients with established PsA who all met CASPAR criteria and 72 patients recruited from the RA Biologics Registry of Ireland who all met ACR/EULAR 2010 classification criteria and had similar levels of active disease as the PsA patients. Again, baseline serum samples were obtained, aliquotted, and frozen at -70°C .

Label-free nano-LC-MS/MS analysis. A detailed description of the unbiased LC-MS/MS workflow has previously been described (10). Briefly, serum samples ($1,700\ \mu\text{g}$) were depleted of the 14 most abundant serum proteins (albumin, transferrin, haptoglobin, IgG, IgA, α_1 -antitrypsin, fibrinogen, β_2 -macroglobulin, α_1 -acid glycoprotein, complement C3, IgM, apolipoprotein A-I, apolipoprotein A-II, and transthyretin) using the Agilent Multiple Affinity Removal System comprising a Hu-14 column (HuMARS14) ($4.6 \times 100\ \text{mm}$; Agilent Technologies, no. 5188-6557) on a Biocad Vision Workstation. Depleted fractions (containing $50\ \mu\text{g}$ protein) were reduced, denatured, and alkylated prior to trypsinization. The digested samples were desalted and purified using C18 resin

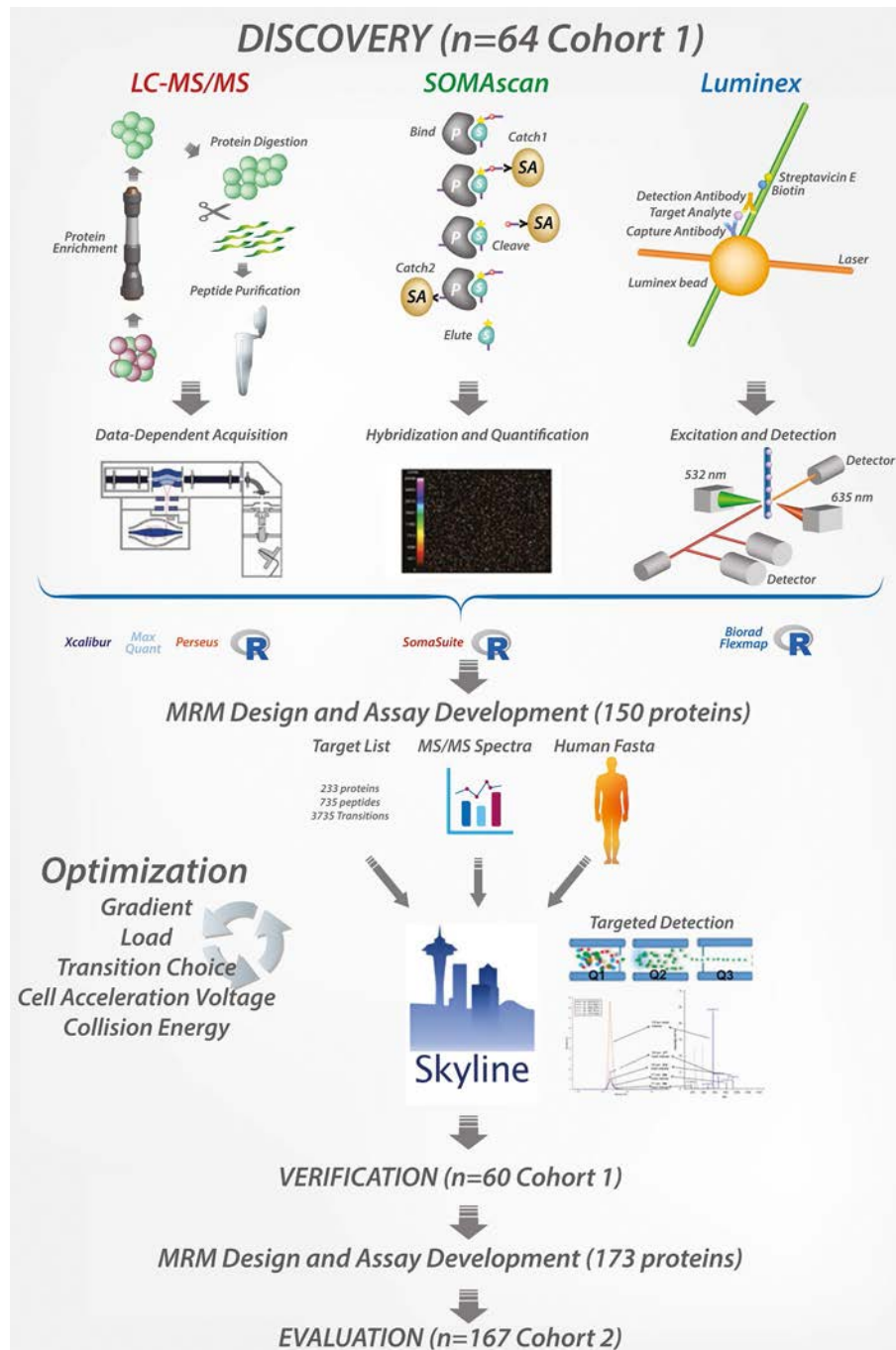


Figure 1. Overview of the experimental workflow. Three platforms were used: nano-liquid chromatography mass spectrometry (nano-LC-MS/MS), aptamer-based immunoassays, and bead-based immunoassays for biomarker discovery. Resulting data were analyzed by univariate and multivariate analysis. Putative biomarkers identified by nano-LC-MS/MS proteins were brought forward for multiple reaction monitoring (MRM) assay development, which was divided into 2 phases. During phase I, it was possible to develop an assay for 150 proteins which were measured in the discovery cohort. During phase II, an assay was developed for 173 proteins which were measured in an independent evaluation cohort. SA = streptavidin.

pipette stage tips. Purified samples were dried under vacuum and resuspended in MS-compatible buffer A (3% acetonitrile, 0.1% formic acid) (21,22). Label-free nano-LC-MS/MS analysis was performed on a Q Exactive mass spectrometer equipped with a Dionex Ultimate 3000 (RSLCnano) chromatography system (ThermoFisher Scientific). Two microliters (equivalent to 2 μ g of digested protein) of each sample were injected onto a fused

silica emitter separated by an increasing acetonitrile gradient over 101.5 minutes (flow rate 250 nl/minute) (10).

Bioinformatic data analysis. As previously reported, nano-LC-MS/MS data were visually inspected using XCalibur software (version 2.2 SP1.48). MaxQuant (version 1.4.12) was then used for quantitative analysis of the LC-MS/MS data, while

Perseus software (version 1.5.0.9) supported statistical analysis (10,23).

Aptamer-based analysis. Individual patient serum samples were subjected to a multiplexed aptamer-based assay developed by Gold et al to measure the levels of 1,129 proteins, as previously reported (10).

Bead-based immunoassay. Individual serum samples were subjected to in-house-developed and validated multiplexed immunoassays measuring 48 analytes. The assays and analyses were undertaken, as previously described, at the Multiplex Core Facility Laboratory of Translational Immunology at the University Medical Centre Utrecht (10).

MRM design and optimization. The development and optimization of MRM assays was performed using Skyline software (version 3.6.0.1062) (MacCoss Lab) (24). Assays for prototypic peptides were developed for all proteins of interest where peptides showed no missed cleavages or “ragged ends” and sequence length was between 7 and 25 amino acids. When possible, peptide sequences with reactive cysteine or methionine residues were avoided but not excluded. An MRM assay was deemed to be analytically validated when it demonstrated the following characteristics: dot product ≥ 0.8 , signal to noise ≥ 10 , data points under the curve ≥ 10 (25), and percentage coefficient of variance showing a retention time $\leq 1\%$ and area $\leq 20\%$ (26). The majority of MRM assays developed significantly exceeded these criteria.

Sample preparation for LC-MRM analysis. *Verification phase.* Crude serum (2 μ l) was added to the wells of 96-well deep well plates (ThermoFisher Scientific) and diluted at 1:50 with NH_4CO_3 (Sigma). RapiGest denaturant (Waters) was resuspended in 50 mM NH_4CO_3 to give a stock solution of 0.1% weight/volume, and 50 μ l of this stock solution was added to each sample so that the final concentration of RapiGest was 0.05%. Plates were covered with adhesive foil (ThermoFisher Scientific), and samples were incubated in the dark at 80°C for 10 minutes. After incubation, plates were centrifuged at 2,000 relative centrifugal force (rcf) at 4°C for 2 minutes to condense droplets. Subsequently, dithiothreitol (DTT) was added to each sample at a final concentration of 20 mM. Samples were then incubated at 60°C for 1 hour followed by centrifugation at 2,000 rcf at 4°C for 2 minutes.

Next, iodoacetamide was added to each sample to give a final concentration of 10 mM, and plates were incubated at 37°C in the dark for 30 minutes. Plates were again centrifuged at 2,000 rcf at 4°C for 2 minutes, and samples were then diluted with LC-MS/MS-grade H_2O to produce a final concentration of 25 mM NH_4CO_3 . Trypsin (Promega) was added to each sample so that the protein:enzyme ratio was 25:1. The reaction was stopped with

the addition of 2 μ l of neat trifluoroacetic acid (Sigma) to each sample and incubated for a further 30 minutes at 37°C. In order to pellet RapiGest, digests were transferred from 96-well plates to 1.5 ml low-bind Eppendorf tubes and centrifuged for 30 minutes at 12,000 rcf. Supernatants were removed and transferred into clean Eppendorf tubes and lyophilized by speed vacuum at 30°C for 2 hours. Lyophilized samples were stored at -80°C until further use.

Evaluation phase. The denaturant used previously (RapiGest) was substituted with 25 μ l denaturant solution comprising 50% trifluoroethanol in 50 mM NH_4HCO_3 with 10 mM DTT, and this mitigated the need for the high-speed spin and transfer of supernatant, which represented an additional processing step less compatible with 96-well plate workflows.

MRM analysis. MRM analysis was performed using an Agilent 6495A triple-quadrupole mass spectrometer with Jet-Stream electrospray source (Agilent) coupled to a 1290 Quaternary Pump HPLC system. Peptides were separated using analytical Zorbax Eclipse Plus C18 (rapid resolution HT 2.1 \times 50 mm, 1.8 μ m, 600-bar columns) (Agilent) before introduction to the triple-quadrupole mass spectrometer. A linear gradient of acetonitrile (99.9% acetonitrile, 0.1% formic acid) 3–75% over 17 minutes was applied at a flow rate of 0.400 μ l/minute with a column oven temperature of 50°C. Source parameters were as follows: gas temperature 150°C, gas flow 15 liters/minute, nebulizer psi 30, sheath gas temp 200°C, and sheath gas flow 11 liters/minute. Peptide retention times and optimized collision energies were supplied to MassHunter (B0.08; Agilent Technologies) to establish a dynamic MRM-scheduled method based on input parameters of 800-msec cycle times and 2-minute retention time windows. The percentage coefficient of variation (%CV) of biologic and technical replicates was used as a measure of variance and was calculated using the following standard calculation: $\%CV = (\text{SD}/\text{mean}) \times 100$.

ELISA analysis. C-reactive protein (CRP) levels were evaluated at St. Vincent's University Hospital using an automated CRPL3 Tina-quant assay (Roche Diagnostics).

Statistical analysis. GraphPad Prism software package (version 7.00) was used to investigate the statistical significance of bead-based immunoassay data, while SomaSuite (version 1.0) was used to analyze aptamer-based assay data. The ability of quantified proteins/peptides to predict the diagnosis (PSa or RA) for individual patients was assessed using the random forest package in R (version 3.3.2). The most important variables in providing the receiver operating characteristic (ROC) area under the curve (AUC) were selected using the variable importance index, and the Gini decrease in impurity was used to assess the importance of each variable. All AUC values were obtained using the ROC R package.

Table 1. Baseline demographic and clinical characteristics of patients in the discovery, verification, and evaluation cohorts*

	Discovery and biomarker verification cohort			Independent cohort for biomarker evaluation		
	Total (n = 64)	PsA (n = 32)	RA (n = 32)	Total (n = 167)	PsA (n = 95)	RA (n = 72)
Age	43.6 ± 13.3	39.6 ± 11.14†	47.7 ± 14.1	53 ± 8.1	52 ± 6.6	55 ± 9.6
Female, no. (%)	37 (58)	15 (47)	22 (69)	89 (53)	51 (54)	38 (53)
Anti-CCP positive, no. (%)	33 (52)	0	26 (81)	49 (29)	1 (1)	48 (67)
RF positive, no. (%)	25 (39)	0	25 (78)	50 (30)	3 (3)	47 (65)
ESR, mm/hour	19.4 ± 16.8	12.0 ± 8.1‡	26.7 ± 20.0	NA	NA	NA
CRP, mg/liter (normal <5)	14.4 ± 19.8	6.6 ± 8.3‡	22.2 ± 24.6	24.9 ± 30.6	28.2 ± 27.8§	20 ± 34.0
DAS28-CRP, median (IQR)	4.2 (1.66–6.88)	3.7 (2.1–5.8)	4.9 (1.7–6.9)	NA¶	NA¶	4.2 (1.1–7.6)
TJC, median (IQR) (range 0–28)	6 (0–23)	4 (0–20)#	8.5 (0–23)	NA¶	10.4 (0–38)¶	8.2 (0–28)
SJC, median (IQR) (range 0–28)	2 (0–12)	1 (0–5)‡	3.5 (0–12)	NA¶	7.2 (0–25)¶	5.2 (0–24)
Dactylitis, no. (%)	NA	10 (31)	NA	NA¶	44 (46.3)	NA
BMI, kg/m ²	28.1 ± 6.3	27.97 ± 6.3	28.24 ± 6.3	28.0 ± 8.6	30.0 ± 10.6‡	27.2 ± 5.1
PASI, median (range)	NA	3.35 (0–27.7)	NA	NA	2.2 (0–14)	NA

* Except where indicated otherwise, values are the mean ± SD. anti-CCP = anti-cyclic citrullinated peptide; RF = rheumatoid factor; ESR = erythrocyte sedimentation rate; NA = not available; IQR = interquartile range; BMI = body mass index; PASI = Psoriasis Area and Severity Index.

† $P < 0.05$ versus rheumatoid arthritis (RA) patients.

‡ $P < 0.01$ versus RA patients.

§ $P < 0.0001$ versus RA patients.

¶ For the validation cohort, 68 and 66 joints were counted for the tender joint count (TJC) and swollen joint count (SJC), respectively, in the psoriatic arthritis (PsA) group, and therefore the Disease Activity Score in 28 joints using the C-reactive protein level (DAS28-CRP) could not be calculated.

$P < 0.001$ versus RA patients.

RESULTS

Patient sample characterization and study design.

For the discovery of novel candidate protein biomarkers, serum samples were collected at baseline from patients with early-onset, treatment-naïve PsA ($n = 32$) and those with early-onset, treatment-naïve RA ($n = 32$). Samples from a second independent cohort (PsA, $n = 95$; RA, $n = 72$) were used to confirm the performance of the putative markers identified during discovery. While these PsA and RA patients may have been receiving treatment at the time of baseline serum sampling, there were similar levels of active disease (as reflected by CRP level, erythrocyte sedimentation rate [ESR], and joint counts) in both patient groups. Key demographic and clinical characteristics for all patients are summarized in Table 1.

Unbiased nano-LC-MS/MS-based protein analysis.

To investigate differential serum protein expression between patients with PsA and those with RA, individual serum samples that had been depleted of high-abundance serum proteins were analyzed by nano-LC-MS/MS using a Q Exactive Hybrid Quadrupole-Orbitrap mass spectrometer. A total of 451 proteins were identified, of which 121 were identified in all 64 individual serum samples. Univariate analysis was applied to the 121 commonly identified proteins, and multivariate analysis was applied to the complete data set. Univariate analysis (Student's t -test using a Benjamini-Hochberg false discovery rate of 0.01) showed that 66 proteins were significantly differentially expressed between PsA and RA (Supplementary Table 1, <http://onlinelibrary.wiley.com/doi/10.1002/art.41899/abstract>). Unsupervised hierarchical cluster and principal components analysis performed using these

66 proteins revealed the overall differences/similarities between serum protein levels in the individual PsA and RA patients; clear within-group clustering and between group separations were observed (Figure 2). Random forest analysis of data from 451 proteins identified in the 64 patient samples demonstrated that patients with PsA and those with RA could be differentiated with an AUC of 0.94 (Table 2) (ROC plot in Supplementary Figure 1A, <http://onlinelibrary.wiley.com/doi/10.1002/art.41899/abstract>).

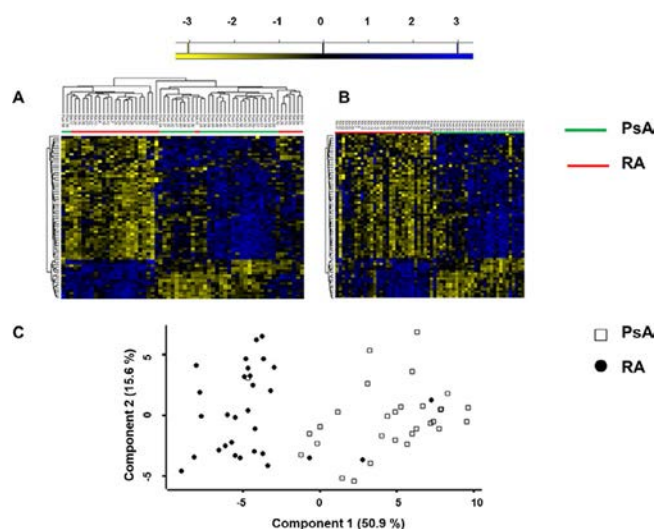


Figure 2. Association of protein signatures with diagnosis of psoriatic arthritis (PsA) or rheumatoid arthritis (RA). **A**, Unsupervised hierarchical cluster analysis. **B**, Supervised hierarchical cluster analysis. **C**, Principal components analysis. Plots were generated for differentially expressed proteins between PsA patients ($n = 30$) and RA patients ($n = 30$). $P < 0.01$ by Benjamin-Hochberg false discovery rate.

Table 2. Determination of protein signatures to predict diagnosis in patients with early PsA and those with RA*

Platform	No.	Correctly predicted/total	AUC
LC-MS/MS	60	55/60	0.94
Aptamer-based immunoassay	36	26/36	0.73
Bead-based immunoassay	64	43/64	0.69

* Area under the curve (AUC) values were generated using predicted probabilities from the random forest model used to discriminate between the groups. PsA = psoriatic arthritis; RA = rheumatoid arthritis; LC-MS/MS = liquid chromatography mass spectrometry.

Taken together, these data strongly suggest that there is a difference in the serum protein profiles between newly diagnosed PsA patients and RA patients. The top 50 proteins providing the AUC are listed in Supplementary Table 2 (<http://onlinelibrary.wiley.com/doi/10.1002/art.41899/abstract>).

Aptamer- and bead-based targeted protein analysis. To extend the breadth and depth of proteome coverage afforded by nano-LC-MS/MS, serum samples were subjected to analysis using 2 complementary protein measurement platforms. Aptamer-based analysis supported the quantification of 1,129 proteins in a subset of the patient samples for PsA ($n = 18$) and RA ($n = 18$). Univariate analysis revealed that 175 proteins were significantly differentially expressed between PsA and RA patients (Supplementary Table 3, <http://onlinelibrary.wiley.com/doi/10.1002/art.41899/abstract>). Multivariate analysis of the data obtained from the aptamer-based analysis revealed that it was possible to discriminate PsA from RA with an AUC of 0.73 (Table 2) (ROC plot in Supplementary Figure 1B, <http://onlinelibrary.wiley.com/doi/10.1002/art.41899/abstract>).

Based largely on their known importance in PsA and RA (3), 48 proteins were selected for analysis using in-house-developed multiplexed bead-based immunoassays (10). Of the 48 proteins targeted, 23 were identified in every sample. *T*-tests revealed that 4 proteins (IL-18 [$P \leq 0.001$], IL-18 binding protein [$P \leq 0.05$], hepatocyte growth factor [$P \leq 0.05$], and tumor necrosis factor receptor superfamily member 6 [$P \leq 0.05$]) were differentially expressed between PsA and RA samples (Supplementary Figure 2, <http://onlinelibrary.wiley.com/doi/10.1002/art.41899/abstract>). Random forest analysis of the bead-based immunoassay data showed that patients could be segregated with an AUC of 0.69 (Table 2 and Supplementary Figure 1C). Compared to the nano-LC-MS/MS analysis, the candidate protein biomarker discovery by both aptamer-based and bead-based assays yielded data sets with reduced predictive power, and therefore the subsequent evaluation process was streamlined to focus only on proteins identified by nano-LC-MS/MS.

LC-MRM verification of nano-LC-MS/MS-identified biomarkers. MRM is a targeted MS technology that is increasingly used to support candidate biomarker evaluation following LC-MS/MS and other protein discovery approaches. Both the cost

of MRM analysis and the time required to develop and optimize MRM assays are considerably less than antibody-based methods (27). For these and other reasons, MRM-based measurement of the nano-LC-MS/MS-identified proteins represents an attractive approach for verification and evaluation of their biomarker performance. The multiplexing capabilities afforded by MRM facilitated the development of an assay that included the top-ranking discriminatory candidate proteins from univariate and multivariate analysis of the nano-LC-MS/MS discovery data described above, but also allowed for the inclusion of additional proteins identified previously during studies of pooled patient samples (data not shown). A total of 233 proteins represented by 735 peptides and 3,735 transitions (5 per peptide) were brought forward for MRM assay development. Of the 233 proteins brought forward, it was possible to develop assays for 150 of them, represented by 299 peptides. The remaining candidates could not be detected reproducibly in crude serum. Of the 50 proteins listed in Supplementary Table 2, 33 were included in the assay.

This MRM assay panel was then used to measure the candidate proteins in 60 patient samples from the discovery cohort. It is noteworthy that to minimize any technical bias, both the pre-analytical processing and MRM analysis were undertaken in a randomized manner. Random forest analysis revealed that using this MRM assay panel it was possible to distinguish PsA from RA with an AUC of 0.79 (Figure 3A). While this initial work was in progress, we independently found an additional 23 candidate biomarker proteins to be capable of identifying other forms of IA (28). MRM assays for these proteins were developed and added to the initial MRM assay panel, yielding a new total number of proteins of 173 (represented by 334 peptides). This expanded panel was used to measure candidate proteins in an independent evaluation cohort of 95 PsA patients and 72 RA patients (Table 1). Seven synthetic isotopically labeled (SIL) peptides were incorporated into the assay to control for potential analytical variation. Summed intensity values from the SIL peptides were used to normalize patient data. Random forest analysis revealed that PsA patients could be separated from those with RA with an AUC of 0.85 (Figure 3B). The proteins ranked as most important in providing the AUC values are reported in Supplementary Table 4 (<http://onlinelibrary.wiley.com/doi/10.1002/art.41899/abstract>).

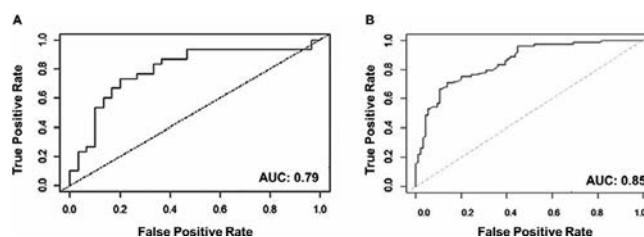


Figure 3. Receiver operating characteristic curve for performance of protein signatures in the discovery cohort ($n = 30$ psoriatic arthritis [PsA] patients and 30 rheumatoid arthritis [RA] patients) (A) and in the independent evaluation cohort ($n = 95$ PsA patients and 72 RA patients) (B). AUC = area under the curve.

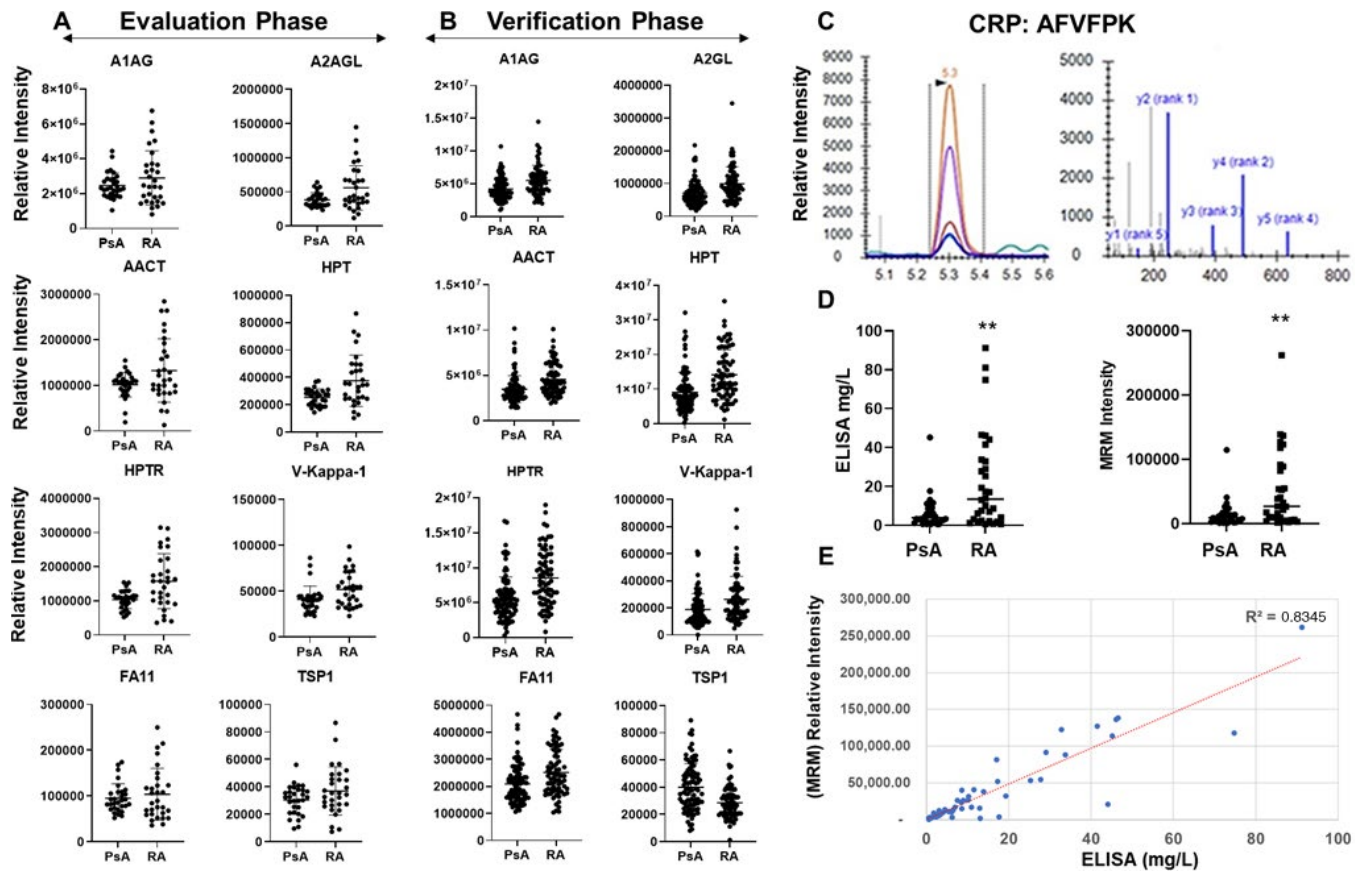


Figure 4. Protein expression changes in PsA and RA, as measured by multiple reaction monitoring (MRM). Eight proteins contributing to the AUC generated during target biomarker verification (AUC 0.79) and evaluation (AUC 0.85) show concordant expression changes in independent cohorts. **A**, During the initial verification phase, α 1-acid glycoprotein 1 (A1AG), coagulation factor XI (FA11), and thrombospondin 1 (TSP-1) were not significantly differently expressed between PsA and RA patients. Proteins α 2-glycoprotein (A2AGL) ($P < 0.006$), α 1-antichymotrypsin (AACT) ($P < 0.020$), haptoglobin (HPT) ($P < 0.001$), and haptoglobin-related protein (HPTR) ($P < 0.015$) were significantly up-regulated in RA. **B**, During a subsequent evaluation phase, α 1-acid glycoprotein 1 ($P < 0.00001$), α 2-glycoprotein ($P < 0.00001$), α 1-antichymotrypsin ($P < 0.00001$), haptoglobin ($P < 0.0001$), haptoglobin-related protein ($P < 0.00001$), $V_{\kappa}1$ ($P < 0.0001$), and coagulation factor XI were significantly up-regulated in RA, while TSP-1 was significantly up-regulated in PsA ($P < 0.00001$). **C**, MRM and mass spectrometry spectrum for C-reactive protein (CRP) levels are shown. **D**, CRP levels analyzed by enzyme-linked immunosorbent assay (ELISA) ($P \leq 0.009$) and MRM ($P \leq 0.006$) are shown. **E**, Pearson's correlation between ELISA and MRM measurements of CRP levels ($R^2 = 0.8345$) is shown. See Figure 3 for other definitions.

The data demonstrate clear overlap between proteins used to distinguish PsA patients from RA patients included in the discovery and verification cohorts. The differential expression levels of these overlapping proteins are illustrated in Figure 4. To this end, α 2-HS glycoprotein, α 1-antichymotrypsin, haptoglobin, haptoglobin-related protein, and RF C6 light chain ($V_{\kappa}1$) were found to be significantly up-regulated in RA patients compared to PsA patients when measured by MRM. Alpha-1-acid glycoprotein and coagulation factor XI were also found to be up-regulated in RA compared to PsA during both biomarker verification and the evaluation phase, but the observation only reached significance during the evaluation phase. This highlights the value in developing MRM assays for large panels of candidate proteins and evaluating them using additional independent patient cohorts. In the case of thrombospondin 1 (TSP-1), the protein was found to be slightly up-regulated in RA patients during verification in the initial discovery

cohort but was significantly up-regulated in PsA patients during the subsequent validation stage. It is evident that the potential PsA versus RA discriminatory role of this protein will require continued evaluation using additional independent cohorts.

Taken together, these observations provide support for the strategy we adopted, i.e., to use discovery experiments to generate an extensive panel of candidates and to use analytically robust MRM assays to verify their performance (using the initial discovery cohort), with a separate cohort of patients for evaluation. It is noteworthy that all samples used here were from patients who underwent detailed and expert clinical evaluation. It is also apparent that the strategy can be used to develop an initial classifier which can be tested and further developed to improve the performance of the predictive algorithm. This ongoing evolution of the MRM assay panel and associated machine learning algorithms represent a new and powerful approach to biomarker development.

Finally, there are at least 2 potential routes to implementing a multiplexed protein biomarker panel in the clinical setting. One is to use MRM assays and the other to develop antibody-based assays for the proteins of interest. To explore the extent to which MRM data may align with ELISA, we compared our MRM data on CRP levels with results obtained by standard clinical laboratory ELISA. MRM measurements were compared to the ELISA measurements in the 60 samples from the discovery set. It was not surprising to find that serum CRP levels were significantly up-regulated in patients with RA compared to those with PsA when measured by both ELISA ($P \leq 0.005$) and MRM ($P \leq 0.001$) (Figure 4D). Interestingly, the CRP values from both platforms were strongly correlated ($R^2 = 0.8345$) (Figure 4E), indicating that protein (peptide) measurements obtained by MRM can provide values similar to those obtained by existing immunoassays.

DISCUSSION

PsA is a complex disease with diverse manifestations; the clinical features observed in individuals with PsA often vary substantially but can overlap with other diseases. Differentiating between PsA and RA can be clinically challenging because of the similarities in their clinical presentation (29). It is increasingly evident that making an accurate diagnosis is important in order to determine which therapeutic strategy to adopt to optimize clinical and radiographic outcomes (30). With no diagnostic laboratory test available, the diagnosis is clinical: it depends on the skills and knowledge of the assessor and is commonly based on the presence of inflammatory musculoskeletal disease in a patient with skin/nail psoriasis and in the absence of RF (31). However, the lack of clear definitions for dermatologists and general practitioners for inflammatory musculoskeletal disease, coupled with inadequate training in musculoskeletal examination techniques, leads to diagnostic uncertainty and delay. As many as 30% of psoriasis patients visiting dermatology practices may have undiagnosed PsA (32). A diagnostic delay of >6 months is not uncommon, and this contributes to poor radiographic and functional outcomes (33,34).

There is a critical need to differentiate PsA from other forms of IA, including RA, and to develop and disseminate new approaches for the objective and sensitive diagnosis of PsA. This is especially important at the early stages of less differentiated disease, when a clear diagnosis and the establishment of disease-appropriate therapy may have the most impact in improving outcomes. Only a few studies have investigated whether there are biomarkers which discriminate between PsA and RA. In one study involving synovial tissue, messenger RNA for vascular endothelial growth factor and angiopoietin 2 were elevated in PsA patients compared to RA patients (35). However, obtaining a synovial biopsy specimen is an invasive procedure, and the discomfort, time, and cost associated with tissue sampling makes it highly undesirable for use in routine clinical practice (35,36). More recently, Siebert et al identified 170

urinary peptides that discriminated between patients with longstanding PsA and those with other arthropathies, including early RA, with an AUC of 0.97 (37). These findings are very promising, but urine collection is especially vulnerable to physiologic variation arising from diet and liquid intake. Additionally, urine tends to be a very diluted matrix high in salt and low in protein concentration. Thus, in the absence of stepwise workflows for sample concentration and clean-up, the quantification of proteins in urine can prove difficult as a result of interfering signals present in the matrix (38).

Serum is well recognized as a suitable sample for biomarker discovery, not least because proteins are shed from relevant affected tissues into the circulation, but also because it is readily obtained under standardized operating procedures (39). Thus, we used serum samples analyzed by 3 proteomic platforms (nano-LC-MS/MS, aptamer-based assays, and bead-based assays). Each platform is capable of measuring a limited but complementary range of proteins present at different abundance levels. This approach was adopted in order to maximize coverage of the serum proteome, and to date it is the most comprehensive analysis of the serum proteome in patients with PsA and those with RA. Although 3 platforms were used to identify putative biomarkers, the data from the unbiased nano-LC-MS/MS analysis proved to be more discriminatory compared to the data from the bead-based and aptamer-based platforms. A potential reason for this is that LC-MS/MS analysis allows for unbiased discovery of biomarkers, whereas the other approaches are limited by having fixed panels of protein markers. Furthermore, the aptamer-based platform uses a single aptamer to capture proteins, thus potentially reducing the specificity of readouts (40). It is also possible that the smaller number of patient samples used in the aptamer-based experiments may have constrained the statistical power of the analysis. With respect to the bead-based immunoassay, the 48 carefully selected proteins we measured may not have included key candidate cytokines and chemokines which could support the differentiation between PsA and RA. The proteins were selected based on their known importance in the pathogenesis of PsA and RA, but the panel was limited by the availability of proteins measurable with the in-house assay.

With no compelling evidence to justify the time and cost required to develop further multiplex antibody-based and/or aptamer-based assays, we instead focused on the nano-LC-MS/MS data and performed follow-up studies using MRM. MRM is an excellent tool for supporting large-scale, multiprotein biomarker studies. It is typically used to narrow an initial list of candidate proteins derived from discovery experiments to the subset that may truly address the clinical question under study (41). MRM analysis is performed using triple-quadrupole mass spectrometers, which inherently have higher sensitivity and greater linear dynamic range than the Orbitrap mass spectrometer used in the discovery experiments here. This boost in sensitivity facilitates the detection of low-abundant proteins in complex samples and therefore reduces

the need for sample pre-enrichment steps. Thus, MRM supports more robust workflows as well as time- and cost-effective assay development compared to traditional antibody-based approaches. MRM is frequently less sensitive than an equivalent immunoassay, and it was for this reason that we did not initially attempt to develop MRM assays for putative markers identified only by the aptamer-based or the bead-based analysis (17,42). The development of MRM immunoassays for these candidate biomarker proteins represents an obvious way in which improving the performance of the existing panel could be explored (43).

In the 2 phases of MRM analysis described here, it was especially interesting to note that a subpanel of 8 proteins (leucine-rich α_2 -glycoprotein, α_1 -antichymotrypsin, haptoglobin, haptoglobin-related protein, RF C6 light chain, α_1 -acid glycoprotein 1, coagulation factor XI, and TSP-1) that were identified as highly discriminatory during the initial verification phase were again confirmed as highly discriminatory during the second evaluation phase. Follow-up *t*-test analysis was performed on this set of proteins, and 7 of 8 proteins were found to be up-regulated in RA compared to PsA during both phases of analysis. TSP-1 was found to be significantly up-regulated in PsA compared RA during the second phase, whereas no significant difference was observed in initial verification. This discordance may relate to differences in the number of patients included in the 2 phases, or it may relate to the differences in the patients included; patients in the initial phase had early-onset, treatment-naïve disease, while those included in the second phase had longer-standing disease and were receiving therapy. This highlights, in part, the advantage of maintaining large panels of proteins for ongoing evaluation in patient cohorts.

Further analysis of this 8-protein subpanel was carried out using a web-based resource "Search Tool for the Retrieval of Interacting Genes/Proteins" (<https://string-db.org/cgi/network.pl>), revealing the biologic functions of these 8 markers of interest (Supplementary Table 5, <http://onlinelibrary.wiley.com/doi/10.1002/art.41899/abstract>). It is interesting to note that this panel is enriched for proteins functionally involved in structural remodeling, angiogenesis, homeostasis, and transportation. This perhaps is not surprising since PsA and RA are characterized by an increase in bone turnover and dysregulated angiogenesis. The radiographic features in PsA and RA can be quite different, with bony erosion observed in both conditions but osteoproliferation only seen in PsA (3). In the context of this investigation, it was not unanticipated that markers of structural remodeling contributed to an algorithm discriminating between individuals with PsA and those with RA. Here, we demonstrated that a major advantage of using MRM is that it allows the investigator to rapidly adapt a panel to include new candidate biomarkers. Our CRP assay that was developed using MRM over a few days also showed values highly correlated with those generated by ELISA.

Our study has several strengths, including the comprehensive and logical approach to biomarker development. Limitations include the modest number of patient samples in both study

phases as well as the absence of healthy and disease controls. Differentiating between PsA and RA is the focus of the current study, but it is not the only challenge faced by clinicians, as it can also be challenging to distinguish PsA from other arthropathies and from patients who have skin psoriasis only (14). This certainly represents a future objective, and assessing this biomarker panel in the appropriate additional cohorts is a critical next step. It is noteworthy that the independent cohort included in the second phase of evaluation included patients that had longstanding disease compared to the discovery cohort, which included those with early-onset disease. Despite this, the 2 cohorts shared similar levels of active disease, as reflected by CRP level, ESR, and joint counts (Table 1). However, it should be noted that the Disease Activity Score using the CRP level (DAS28-CRP) (44) was used as a disease activity measure in the PsA discovery cohort. This is not recommended, since it does not reflect the 68-joint counts recommended for the disease. Notwithstanding this, the DAS28-CRP results show that while lower in PsA, the mean values are not significantly different between the 2 diseases.

It is fair to say that the patients included in this study are representative of those attending IA clinics. We believe that obtaining data and samples from real-world conditions is critically important if our assay is to consistently segregate PsA from RA regardless of disease duration, disease activity, treatment, or comorbidities. The performance of the biomarker panel may reflect a genuine difference in the protein profile between PsA and RA patients, but further work in a larger number of patient samples is needed. It will also be necessary to examine the performance of the panel in distinguishing PsA from other forms of IA and from healthy individuals.

It should be noted that all PsA patients included in both the discovery and verification cohorts met the CASPAR criteria, which was required for inclusion. Therefore, it was not possible in this study to compare the performance of the biomarker panel to that of CASPAR criteria or to test whether a combination of CASPAR criteria and biomarkers is more useful. We intend to address this in a prospective study of psoriasis patients who are being followed up for the development of PsA or in a cohort of patients with early undifferentiated IA. Finally, although non-inflammatory disease controls were not included in our present analysis, it is worth highlighting research by Chandran et al that identified differences in serum proteins in patients with PsA compared to patients with osteoarthritis (45) and patients with psoriasis (46). The protein markers identified in these studies are prime candidates that should be included in future generations of MRM panel assays. At present, there is no diagnostic test for PsA and as a result, the diagnosis is often late or missed, resulting in functional consequences for the patient (12,47). With at least 20% of the patients referred to early arthritis clinics diagnosed as having PsA, there is an urgent need to develop a test to support early detection of this disease (31).

In conclusion, the work described here represents a significant contribution toward the development of such a test. Fundamental

next steps have been outlined, and the MRM approach is ideally suited to support the large-scale studies required to develop and validate a robust panel of distinguishing biomarkers. We believe that with further development it will be possible to establish a diagnostic test for PsA that will reduce diagnostic delay, inform treatment selection, and improve both short-term and long-term outcomes.

ACKNOWLEDGMENT

The authors would like to thank Prof. Anthony G. Wilson (Arthritis Ireland Chair of Rheumatology, UCD Centre for Arthritis Research, School of Medicine, Conway Institute, Belfield, Dublin 4). Prof. Wilson made a fundamental contribution to our study by providing the RA cohort used in our validation analysis.

AUTHOR CONTRIBUTIONS

All authors were involved in drafting the article or revising it critically for important intellectual content, and all authors approved the final version to be published. Dr. Mc Ardle had full access to all of the data in the study and takes responsibility for the integrity of the data and the accuracy of the data analysis.

Study conception and design. Mc Ardle, Szentpetery, Hernandez, Parnell, FitzGerald, Pennington.

Acquisition of data. Mc Ardle, Kwasnik, Szentpetery, de Jager, de Roock, FitzGerald, Pennington.

Analysis and interpretation of data. Mc Ardle, Kwasnik, Szentpetery, Hernandez, Parnell, de Jager, de Roock, FitzGerald, Pennington.

REFERENCES

- Ogdie A, Langan S, Love T, Haynes K, Shin D, Seminara N, et al. Prevalence and treatment patterns of psoriatic arthritis in the UK. *Rheumatology (Oxford)* 2013;52:568–75.
- Ogdie A, Weiss P. The epidemiology of psoriatic arthritis [review]. *Rheum Dis Clin North Am* 2015;41:545–68.
- Mc Ardle A, Flatley B, Pennington SR, FitzGerald O. Early biomarkers of joint damage in rheumatoid and psoriatic arthritis [review]. *Arthritis Res Ther* 2015;17:141.
- McArdle A, Pennington SR, FitzGerald O. Clinical features of psoriatic arthritis: a comprehensive review of unmet clinical needs [review]. *Clin Rev Allergy Immunol* 2018;55:271–94.
- Kane D, Stafford L, Bresnihan B, FitzGerald O. A prospective, clinical and radiological study of early psoriatic arthritis: an early synovitis clinic experience. *Rheumatology (Oxford)* 2003;42:1460–8.
- Husted JA, Gladman DD, Farewell VT, Cook RJ. Health-related quality of life of patients with psoriatic arthritis: a comparison with patients with rheumatoid arthritis. *Arthritis Rheum* 2001;45:151–8.
- Sokoll KB, Helliwell PS. Comparison of disability and quality of life in rheumatoid and psoriatic arthritis. *J Rheumatol* 2001;28:1842–6.
- Lindqvist UR, Alenius GM, Husmark T, Theander E, Holmström G, Larsson PT, on behalf of the Psoriatic Arthritis Group of the Society for Rheumatology. The Swedish Early Psoriatic Arthritis Register—2-year followup: a comparison with early rheumatoid arthritis. *J Rheumatol* 2008;35:668–73.
- Lee S, Mendelsohn A, Sarnes E. The burden of psoriatic arthritis: a literature review from a global health systems perspective. *P T* 2010;35:680–9.
- McArdle A, Butt AQ, Szentpetery A, de Jager W, de Roock S, FitzGerald O, et al. Developing clinically relevant biomarkers in inflammatory arthritis: a multiplatform approach for serum candidate protein discovery. *Proteomics Clin Appl* 2016;10:691–8.
- Ritchlin CT, Kavanaugh A, Gladman DD, Mease PJ, Helliwell P, Boehncke WH, et al. Treatment recommendations for psoriatic arthritis [review]. *Ann Rheum Dis* 2009;68:1387–94.
- Kirkham B, de Vlam K, Li W, Boggs R, Mallbris L, Nab HW, et al. Early treatment of psoriatic arthritis is associated with improved patient-reported outcomes: findings from the etanercept PRESTA trial. *Clin Exp Rheumatol* 2015;33:11–9.
- Yago T, Nanke Y, Kawamoto M, Kobashigawa T, Yamanaka H, Kotake S. IL-23 and Th17 disease in inflammatory arthritis [review]. *J Clin Med* 2017;6:81.
- Butt AQ, McArdle A, Gibson DS, FitzGerald O, Pennington SR. Psoriatic arthritis under a proteomic spotlight: application of novel technologies to advance diagnosis and management [review]. *Curr Rheumatol Rep* 2015;17:35.
- Taylor W, Gladman D, Helliwell P, Marchesoni A, Mease P, Mielants H, on behalf of the CASPAR Study Group. Classification criteria for psoriatic arthritis: development of new criteria from a large international study. *Arthritis Rheum* 2006;54:2665–73.
- Coates LC, Conaghan PG, Emery P, Green MJ, Ibrahim G, MacIver H, et al. Sensitivity and specificity of the classification of psoriatic arthritis criteria in early psoriatic arthritis. *Arthritis Rheum* 2012;64:3150–5.
- Chandran V. Spondyloarthritis: CASPAR criteria in early psoriatic arthritis [review]. *Nat Rev Rheumatol* 2012;8:503–4.
- Gibson DS, Rooney ME, Finnegan S, Qiu J, Thompson DC, Labaer J, et al. Biomarkers in rheumatology, now and in the future [review]. *Rheumatology (Oxford)* 2012;51:423–33.
- Szentpetery A, Herffernan E, Haroon M, Kilbane M, Gallagher P, McKenna MJ, et al. Striking difference of periarticular bone density change in early psoriatic arthritis and rheumatoid arthritis following anti-rheumatic treatment as measured by digital X-ray radiogrammetry. *Rheumatology (Oxford)* 2016;55:891–6.
- Aletaha D, Neogi T, Silman AJ, Funovits J, Felson D, Bingham CO III, et al. 2010 rheumatoid arthritis classification criteria: an American College of Rheumatology/European League Against Rheumatism collaborative initiative. *Arthritis Rheum* 2010;62:2569–81.
- Rappsilber J, Ishihama Y, Mann M. Stop and go extraction tips for matrix-assisted laser desorption/ionization, nanoelectrospray, and LC/MS sample pretreatment in proteomics. *Anal Chem* 2003;75:663–70.
- Turriziani B, Garcia-Munoz A, Pilkington R, Raso C, Kolch W, von Kriegsheim A. On-beads digestion in conjunction with data-dependent mass spectrometry: a shortcut to quantitative and dynamic interaction proteomics. *Biology (Basel)* 2014;3:320–32.
- Cox J, Neuhauser N, Michalski A, Scheltema RA, Olsen JV, Mann M. Andromeda: a peptide search engine integrated into the MaxQuant environment. *J Proteome Res* 2011;10:1794–805.
- MacLean B, Tomazela DM, Shulman N, Chambers M, Finney GL, Frewen B, et al. Skyline: an open source document editor for creating and analyzing targeted proteomics experiments. *Bioinformatics* 2010;26:966–8.
- Molecular and Cellular Proteomics. Targeted Mass Spec Guidelines. URL: <https://www.mcponline.org/guidelines-publication-manuscript-s-describing-development-and-application-targeted-mass>.
- Grant RP, Hoofnagle AN. From lost in translation to paradise found: enabling protein biomarker method transfer by mass spectrometry. *Clin Chem* 2014;60:941–4.
- Picotti P, Bodenmiller B, Aebersold R. Proteomics meets the scientific method. *Nat Methods* 2013;10:24–7.
- Gohar F, McArdle A, Jones M, Callan N, Hernandez B, Kessel C, et al. Molecular signature characterisation of different inflammatory phenotypes of systemic juvenile idiopathic arthritis. *Ann Rheum Dis* 2019;78:1107–13.

29. Haroon M, FitzGerald O. Psoriatic arthritis: complexities, comorbidities and implications for the clinic [review]. *Expert Rev Clin Immunol* 2016;12:405–16.
30. Merola JF, Espinoza LR, Fleischmann R. Distinguishing rheumatoid arthritis from psoriatic arthritis. *RMD Open* 2018;4:e000656.
31. Coates LC, Helliwell PS. Psoriatic arthritis: state of the art review [review]. *Clin Med (Lond)* 2017;17:65–70.
32. Haroon M, Kirby B, FitzGerald O. High prevalence of psoriatic arthritis in patients with severe psoriasis with suboptimal performance of screening questionnaires. *Ann Rheum Dis* 2013;72:736–40.
33. Haroon M, Gallagher P, FitzGerald O. Diagnostic delay of more than 6 months contributes to poor radiographic and functional outcome in psoriatic arthritis. *Ann Rheum Dis* 2015;74:1045–50.
34. Tillett W, Jadon D, Shaddick G, Cavill C, Korendowych E, de Vries CS, et al. Smoking and delay to diagnosis are associated with poorer functional outcome in psoriatic arthritis. *Ann Rheum Dis* 2013;72:1358–61.
35. Fearon U, Griosios K, Fraser A, Reece R, Emery P, Jones PF, et al. Angiotensin, growth factors, and vascular morphology in early arthritis. *J Rheumatol* 2003;30:260–8.
36. Ilie M, Hofman P. Pros: can tissue biopsy be replaced by liquid biopsy? [editorial]. *Transl Lung Cancer Res* 2016;5:420–3.
37. Siebert S, Porter D, Paterson C, Hampson R, Gaya D, Latosinska A, et al. Urinary proteomics can define distinct diagnostic inflammatory arthritis subgroups. *Sci Rep* 2017;7:40473.
38. Chiu M, Lawi W, Snyder SI, Wong PK, Liao JC, Gau G. Matrix effects—a challenge toward automation of molecular analysis. *J Lab Autom* 2010;15:233–42.
39. Wilson R. Sensitivity and specificity: twin goals of proteomics assays. Can they be combined? [review]. *Expert Rev Proteomics* 2013;10:135–49.
40. Joshi A, Mayr M. In aptamers they trust: the caveats of the SOMAscan biomarker discovery platform from SomaLogic. *Circulation* 2018;138:2482–5.
41. Carr SA, Abbatiello SE, Ackermann BL, Borchers C, Domon B, Deutsch EW, et al. Targeted peptide measurements in biology and medicine: best practices for mass spectrometry-based assay development using a fit-for-purpose approach. *Mol Cell Proteomics* 2014;13:907–17.
42. Lange V, Picotti P, Domon B, Aebersold R. Selected reaction monitoring for quantitative proteomics: a tutorial. *Mol Syst Biol* 2008;4:222.
43. Yassine H, Borges CR, Schaab MR, Billheimer D, Stump C, Reaven P, et al. Mass spectrometric immunoassay and MRM as targeted MS-based quantitative approaches in biomarker development: potential applications to cardiovascular disease and diabetes [review]. *Proteomics Clin Appl* 2013;7:528–40.
44. Prevoo ML, van 't Hof MA, Kuper HH, van Leeuwen MA, van de Putte LB, van Riel PL. Modified disease activity scores that include twenty-eight-joint counts: development and validation in a prospective longitudinal study of patients with rheumatoid arthritis. *Arthritis Rheum* 1995;38:44–8.
45. Chandran V, Abji F, Perruccio AV, Gandhi R, Li S, Cook RJ, et al. Serum-based soluble markers differentiate psoriatic arthritis from osteoarthritis. *Ann Rheum Dis* 2019;78:796–801.
46. Chandran V, Cook RJ, Edwin J, Shen H, Pellett FJ, Shanmugarajah S, et al. Soluble biomarkers differentiate patients with psoriatic arthritis from those with psoriasis without arthritis. *Rheumatology (Oxford)* 2010;49:1399–405.
47. Sorensen J, Hetland ML, on behalf of all departments of rheumatology in Denmark. Diagnostic delay in patients with rheumatoid arthritis, psoriatic arthritis and ankylosing spondylitis: results from the Danish nationwide DANBIO registry. *Ann Rheum Dis* 2015;74:e12.

Induction of Interferon- γ and Tissue Inflammation by Overexpression of Eosinophil Cationic Protein in T Cells and Exosomes

Huai-Chia Chuang,¹ Ming-Han Chen,² Yi-Ming Chen,³  Yi-Ru Ciou,¹ Chia-Hsin Hsueh,¹ Ching-Yi Tsai,¹ and Tse-Hua Tan⁴ 

Objective. T cells play a critical role in the pathogenesis of systemic lupus erythematosus (SLE). Serum-derived exosomes are increased in SLE patients and are correlated with disease severity. This study was undertaken to investigate whether T cell–derived exosomal proteins play a role in SLE pathogenesis.

Methods. We characterized proteins in T cell–derived exosomes from SLE patients and healthy controls by MACS-Plex exosome analysis and proteomics. To study the potential pathogenic functions of the exosomal protein identified, we generated and characterized T cell–specific transgenic mice that overexpressed that protein in T cells.

Results. We identified eosinophil cationic protein (ECP, also called human RNase III) as overexpressed in SLE T cell–derived exosomes. T cell–specific ECP–transgenic mice ($n = 5$ per group) displayed early induction of serum interferon- γ (IFN γ) levels ($P = 0.062$) and inflammation of multiple tissue types. Older T cell–specific ECP–transgenic mice ($n = 3$ per group) also displayed an increase in follicular helper T cell and plasma B cell numbers, and in autoantibody levels ($P < 0.01$). Single-cell RNA sequencing showed the induction of IFN γ messenger RNA ($P = 2.2 \times 10^{-13}$) and inflammatory pathways in ECP-transgenic mouse T cells. Notably, adoptively transferred ECP-containing exosomes stimulated serum autoantibody levels ($P < 0.01$) and tissue IFN γ levels in the recipient mice ($n = 3$ per group). The transferred exosomes infiltrated into multiple tissues of the recipient mice, resulting in hepatitis, nephritis, and arthritis.

Conclusion. Our findings indicate that ECP overexpression in T cells or T cell–derived exosomes may be a biomarker and pathogenic factor for nephritis, hepatitis, and arthritis associated with SLE.

INTRODUCTION

Autoimmune diseases are chronic, debilitating, incurable, and life-threatening diseases; patients with autoimmune diseases need to receive treatments throughout their life. Patients with systemic lupus erythematosus (SLE) may have inflammation and tissue damage in the liver, kidney, skin, lung, joint, central nervous system, and other organs (1). Despite recent advances in biologic therapies (such as tocilizumab/anti–interleukin-6 receptor [anti–IL-6R] antibody and adalimumab/anti–tumor necrosis factor [anti-TNF] antibody), 30% of patients with rheumatoid arthritis (RA) and 26–38% of patients with ankylosing spondylitis fail to respond to all therapies (2–4). Furthermore, the majority of patients who show

improvement after treatment do not achieve complete remission, and their response to therapy may diminish over time (5,6). Diagnosis and treatment of SLE are challenging due to complex symptoms and a lack of effective therapeutics (1,6). Identification of novel therapeutic targets will help future development of effective treatments for SLE. Moreover, novel diagnostic/prognostic biomarkers will help to stratify patients who are likely to respond to a specific drug, leading to precision medicine.

T cells promote autoimmune diseases by inducing autoantibody production and inflammatory responses (7–12). Effector memory T cell and Th17 cell numbers are increased in SLE patients (7,13,14). The Th1:Th2 cell ratio is also enhanced in SLE patients (15,16). Th1-secreted interferon- γ (IFN γ) and TNF

Supported by the National Health Research Institutes, Taiwan (grants IM-107-PP-01 and IM-107-SP-01 to Dr. Tan) and the Ministry of Science and Technology, Taiwan (grant MOST-106-2321-B-400-013 to Dr. Tan). Dr. Tan holds a National Bio-Development Foundation Chair in Biotechnology.

¹Huai-Chia Chuang, PhD, Yi-Ru Ciou, MS, Chia-Hsin Hsueh, MS, Ching-Yi Tsai, MS: National Health Research Institutes, Zhunan, Taiwan; ²Ming-Han Chen, MD, PhD: Taipei Veterans General Hospital and National Yang Ming Chiao Tung University School of Medicine, Taipei, Taiwan; ³Yi-Ming Chen, MD, PhD: Taichung Veterans General Hospital, Taichung, Taiwan; ⁴Tse-Hua

Tan, PhD: National Health Research Institutes, Zhunan, Taiwan, and Baylor College of Medicine, Houston, Texas.

Author disclosures are available at <https://onlinelibrary.wiley.com/action/downloadSupplement?doi=10.1002%2Fart.41920&file=art41920-sup-0001-Disclosureform.pdf>.

Address correspondence to Tse-Hua Tan, PhD, 35 Keyan Road, Zhunan 35053, Taiwan. Email: ttan@nhri.edu.tw.

Submitted for publication December 24, 2020; accepted in revised form July 1, 2021.

contribute to macrophage activation and damage of multiple tissue types (15). Th17-secreted IL-17A is a key pathogenic cytokine in inflammation and autoimmune responses (17,18). Th17 cells recruit macrophages and dendritic cells to inflammation sites; Th17 cells also facilitate B cell activation and autoantibody production (17). Conversely, the Treg cell population is decreased in SLE patients (19). Thus, T cell hyperactivation plays a critical role in the pathogenesis of SLE.

Cell-derived exosomes directionally deliver proteins, amino acids, microRNA, or metabolites to targeted cells or tissues to modulate cell or tissue characteristics (20–23). Moreover, T cell-derived exosomal microRNAs modulate immune responses (22,24,25). The number of exosomes in the sera of SLE patients is correlated with disease severity (26). These serum-derived exosomes from SLE patients induce the production of proinflammatory cytokines by impacted peripheral blood mononuclear cells from healthy individuals (26). To date, the surface proteins and intra-exosomal proteins of exosomes in SLE patients, as well as the regulatory mechanisms of exosomal protein-induced inflammation in SLE patients, remain unclear.

Eosinophil cationic protein (ECP; also called human RNase III) is a defense protein; eosinophils release ECP during degranulation against bacterial or parasitic infection (27). ECP disrupts the bacteria membrane through binding to lipopolysaccharide or other bacterial cell wall components (27). In addition to being increased during infection, ECP levels are increased in human patients with allergic asthma or atopic dermatitis (28). Moreover, ECP treatment induces mammalian cell necrosis and inhibits cell growth and proliferation (29–31). ECP treatment also induces cell apoptosis through TNF-caspase signaling (32). To date, the roles of ECP in T cell function and autoimmune disease pathogenesis remain unknown. In this study, we characterized T cell-derived exosomes from SLE patients and identified ECP as a pathogenic exosomal protein.

MATERIALS AND METHODS

Human subjects. This study was conducted in accordance with the Declaration of Helsinki. A total of 50 individuals, including 24 healthy controls, 24 SLE patients, and 2 RA patients, were enrolled. Nine of the SLE patients and the 2 RA patients had been referred to the Division of Immunology and Rheumatology at Taichung Veterans General Hospital in Taiwan. The remaining 15 SLE patients had been referred to the Division of Immunology and Rheumatology at Taipei Veterans General Hospital in Taiwan. Characteristics of the SLE patients are provided in Supplementary Table 1, available on the *Arthritis & Rheumatology* website at <http://onlinelibrary.wiley.com/doi/10.1002/art.41920/abstract>.

The collection of peripheral blood from healthy controls and patients, and the experiments, were approved by the ethics committees of Taichung Veterans General Hospital (#SE17193B) and Taipei Veterans General Hospital (2017-06-003BC). All study participants provided written informed consent prior to enrollment.

Mice. All animal experiments were performed in the AAALAC-accredited animal housing facilities at the National Health Research Institutes (NHRI). All mice were used according to protocols and guidelines approved by the Institutional Animal Care and Use Committee of NHRI. The T cell-specific human ECP-transgenic mouse line was generated at the NHRI Transgenic Mouse Core. The C57BL/6J mouse line (catalog no. 000664), MRL/MpJ mouse line (catalog no. 00486), and the autoimmune lupus model MRL/MpJ-Fas^{lpr} mouse line (catalog no. 000485) were purchased from The Jackson Laboratory. The experiments in this study were performed on sex-matched, 5–38-week-old littermates. For T cell development analyses, 5-week-old, sex-matched mice were used. All mice used in this study were maintained in temperature-controlled and pathogen-free cages.

Generation of T cell-specific ECP-transgenic (Lck-ECP-transgenic) mice. A full-length human ECP coding sequence and a FLAG-tag coding sequence were placed downstream of the proximal Lck promoter, which drives gene expression specifically in T cells (33–35). The transgenic mouse line on a C57BL/6J background was generated using pronuclear microinjection at the NHRI Transgenic Mouse Core.

Reagents and antibodies. Anti-human ECP antibody (catalog no. E-AB-14971) was purchased from Elabscience; anti-CD9 antibody (catalog no. ab92726) was purchased from Abcam. An ExoSparkler Exosome Membrane Labeling Kit (green) was purchased from Dojido Molecular Technologies. Alexa 647-conjugated donkey anti-mouse IgG antibody was purchased from ThermoFisher. PerCP-conjugated anti-mouse CD3 (clone 145-2C11), Pacific Blue-conjugated anti-mouse CD4 (clone RM4-5), phycoerythrin (PE)-conjugated anti-mouse CXCR5 (clone 2G8), PerCP-Cy5.5-conjugated anti-mouse B220 (clone RA3-6B2), and PE-conjugated anti-mouse CD138 (clone 281-2) antibodies were purchased from BD Biosciences. PE-conjugated anti-mouse CD44 (clone IM7), fluorescein isothiocyanate-conjugated anti-mouse CD62L (clone MEL-14), Pacific Blue-conjugated anti-mouse CD21 (clone 7E9), and PE-conjugated anti-mouse CD23 (clone B3B4) antibodies were purchased from BioLegend. Alexa 488-conjugated anti-mouse IL-21 (bs-2621R-A488) antibody was purchased from Bioss. Enzyme-linked immunosorbent assay (ELISA) kits for IL-1 β , IL-6, and TNF were purchased from eBioscience. ELISA kits for antinuclear antibody (ANA), rheumatoid factor (RF), and anti-double-stranded DNA (anti-dsDNA) antibody were purchased from Alpha Diagnostic. The ELISA kit for human ECP was purchased from CUSABIO.

T cell purification. Primary murine T cells were negatively selected from the spleen, lymph nodes, or peripheral blood of mice using magnetically coupled antibodies against CD11b (BD Biosciences), CD11c (BD Biosciences), B220 (BD Biosciences),

CD49b (BioLegend), and Ter-119 (BioLegend) as described previously (35). For human T cell purification, peripheral blood T cells were negatively selected from 10 ml of whole blood from participants using a cocktail of biotin-conjugated antibodies against CD14 (eBioscience), CD11b (BioLegend), CD19 (eBioscience), and CD235a (eBioscience) on a magnetic cell separation column (Miltenyi Biotec) as described previously (14).

Isolation of T cell-derived exosomes. Human or murine T cells (8×10^6) were cultured in 2 ml RPMI 1640 medium for 96 hours without any stimulation. To remove cell debris, supernatants were subjected to centrifugation at 13,000 rpm for 15 minutes. T cell-derived exosomes were precipitated from supernatants by ExoQuick (System Biosciences). For isolation of CD9+ and CD63+ exosomes, precipitated T cell exosomes were

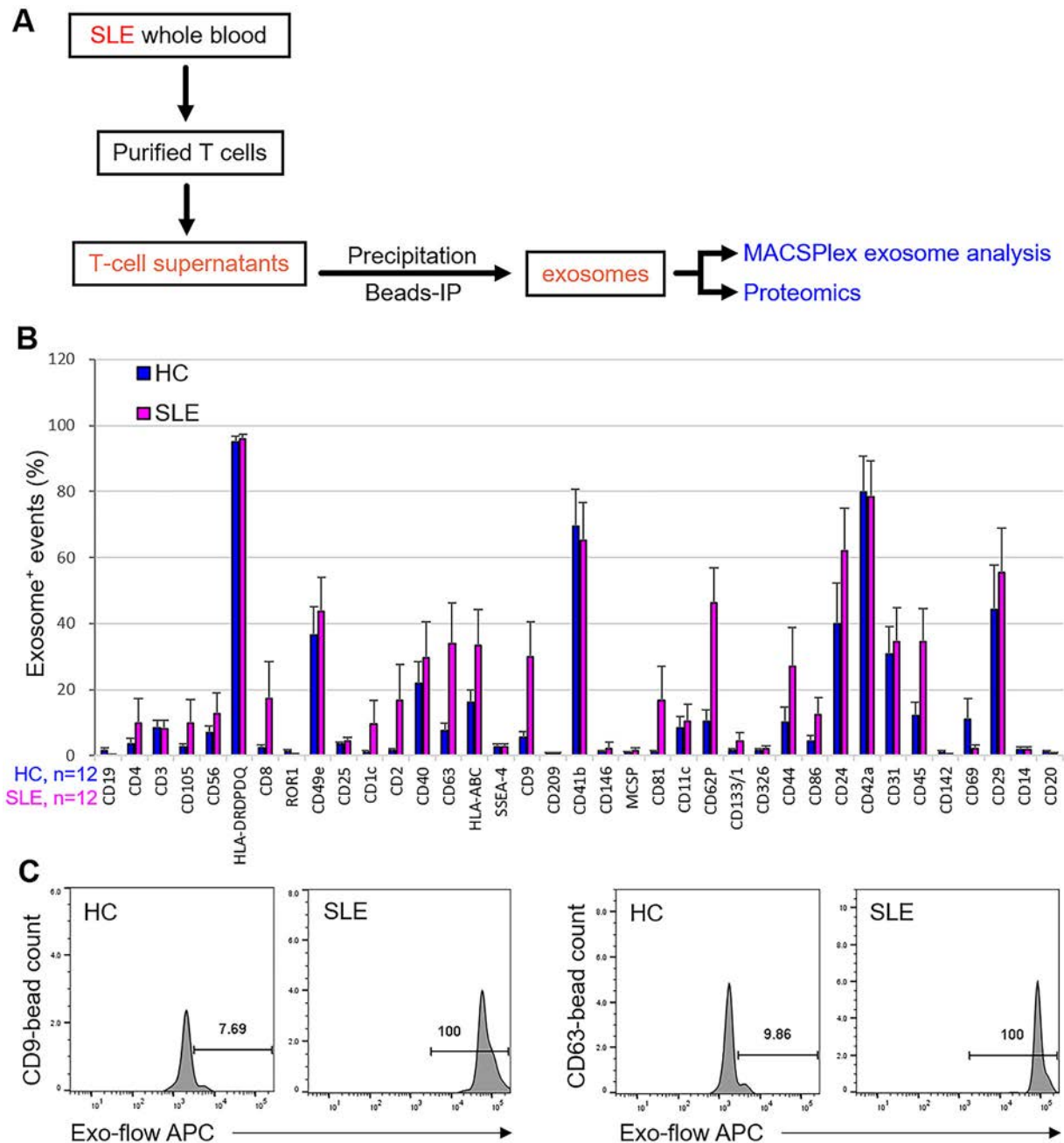


Figure 1. Increased numbers of T cell-derived CD9+ and CD63+ exosomes in patients with systemic lupus erythematosus (SLE). **A**, Experimental design for the characterization of SLE-enriched T cell-derived exosomes. IP = immunoprecipitation. **B**, MACSPlex exosome analysis of T cell-derived exosomes from 12 SLE patients and 12 healthy controls (HCs). Thirty-seven individual surface markers of exosomes were identified using a BD FACSCanto II flow cytometer. Bars show the mean \pm SEM. **C**, Histograms showing the results of MACSPlex analysis of CD9+ and CD63+ exosomes from a representative healthy control and a representative SLE patient. Values are the percent allophycocyanin (APC) positive.

resuspended in phosphate buffered saline (PBS) and then isolated using anti-CD9 or anti-CD63 magnetic beads (System Biosciences). CD9+ and CD63+ exosomes were then eluted with 20 μ l exosome elution buffer (System Biosciences).

Adoptive transfer of T cell-derived exosomes. Murine T cells (8×10^6) from wild-type or Lck-ECP-transgenic mice were cultured in 2 ml RPMI 1640 medium for 96 hours without any stimulation. To remove cell debris, supernatants were subjected to centrifugation at 13,000 rpm for 15 minutes. T cell-derived exosomes were precipitated from supernatants by Exo-Quick (System Biosciences). Exosomes from 12 ml of medium were suspended in 300 μ l of PBS and then intravenously injected into 3 recipient mice (100 μ l/mouse) every 3 days for 9–30 days. For confocal microscopy analysis, exosomes were labeled with green fluorescent dye using an ExoSparkler Exosome Membrane Labeling Kit.

Multiplex exosome flow cytometry assay. To characterize potential surface proteins on T cell-derived exosomes, exosomes were precipitated from T cell supernatants and subjected to bead-based multiplex exosome flow cytometry assay using a MACSPlex Exosome Kit (human; Miltenyi Biotec). The kit contains capture beads conjugated with individual antibodies against 37 known surface markers on different exosomes. The captured exosome signals were analyzed using a BD Canto II flow cytometer.

Single-cell RNA-sequencing data analysis. Murine T cells were purified from the spleens and lymph nodes of wild-type and Lck-ECP-transgenic mice. T cells were analyzed using a BD Rhapsody Single-Cell Analysis System. The single-cell RNA-sequencing data were analyzed using BD SeqGeq software (BD Biosciences) and the R package Seurat. Dimensionality reduction was performed using Uniform Manifold Approximation and Projection; clustering analysis was performed according to individual subsets of variable genes.

Liquid chromatography tandem mass spectrometry (LC-MS/MS) and data analysis. For identification of proteins in T cell-derived exosomes, exosomal proteins were digested with trypsin and subjected to LC-MS/MS analyses on an LTQ Orbitrap Elite hybrid mass spectrometer as described previously (36). The peptide data were analyzed by Mascot MS/MS Ion Search (Matrix Science) with the following conditions: peptide mass tolerance 20 parts per million; fragment MS/MS tolerance 0.6 daltons; allow up to 1 missed cleavage; peptide charge 2+, 3+, and 4+.

Statistical analysis. In vivo experiments were conducted using distinct samples; in vitro experiments were performed at least 3 times. Statistical analysis was performed in Excel, SPSS, or BD SeqGeq. Comparisons between 2 groups were conducted using

Student's unpaired 2-tailed or 1 tailed *t*-test and Wilcoxon's rank sum test. *P* values less than 0.05 were considered significant.

RESULTS

Identification of CD9 and CD63 surface markers in T cell-derived exosomes from SLE patients. Peripheral blood T cells from SLE patients and healthy controls were purified and cultured for 72 hours prior to collection of T cell-derived exosomes. To identify exosomal surface proteins enriched in SLE patients, exosomes in T cell supernatants were subjected to MACSPlex assays (Figure 1A). Exosomes were captured by 37 individual surface marker antibodies conjugated with fluorescent beads, and subjected to flow cytometric analysis (Supplementary Figure 1, available on the *Arthritis & Rheumatology* website at <http://onlinelibrary.wiley.com/doi/10.1002/art.41920/abstract>). The numbers of T cell-derived exosomes were drastically increased in the supernatants of T cells from SLE patients ($n = 12$) compared to those from healthy controls ($n = 12$). Among 37 surface proteins, 16 exosomal surface proteins were increased in SLE patients (Figure 1B). The numbers of T cell-derived CD9+, CD63+, CD62P+, and CD45+ exosomes in SLE patients were high (with signals of >20%) and significantly increased compared to those in healthy controls (Figures 1B and C). CD9 and CD63 are 2 well-known exosomal surface markers; interestingly, T cell-derived CD9+ and CD63+ exosomes had the highest fold induction in SLE patients compared to controls.

Presence of ECP in T cell-derived exosomes from patients with SLE. To characterize the properties of T cell-derived exosomes from SLE patients, T cell-derived CD9+ and CD63+ exosomes isolated from SLE patients and healthy controls were analyzed by mass spectrometry-based proteomics. The proteomics data showed that 130 and 140 proteins were overexpressed in T cell-derived CD9+ exosomes and CD63+ exosomes, respectively, from SLE patients but not in those from healthy controls (Figure 2A). Moreover, many of the exosomal proteins identified were also observed in RA-enriched exosomes; only 15 CD9+ exosomal proteins and 21 CD63+ exosomal proteins were selectively enriched in SLE patients but not RA patients (Figure 2A). The identified SLE-enriched T cell exosomal proteins encompassed protein kinases, protein phosphatases, and metabolic enzymes (Supplementary Table 2, available on the *Arthritis & Rheumatology* website at <http://onlinelibrary.wiley.com/doi/10.1002/art.41920/abstract>).

Notably, one exosomal protein, ECP, which had the highest protein scores, was detected in T cell exosomes from all 5 SLE patient samples included in the mass spectrometry analysis (Figure 2B and Supplementary Table 2). ECP was also determined to be enriched in SLE T cells by proteomics analysis (Supplementary Figure 2A, available on the *Arthritis & Rheumatology* website at <http://onlinelibrary.wiley.com/doi/10.1002/art.41920/abstract>), whereas soluble ECP levels were not increased in the sera of SLE patients (Supplementary Figure 2B). These data

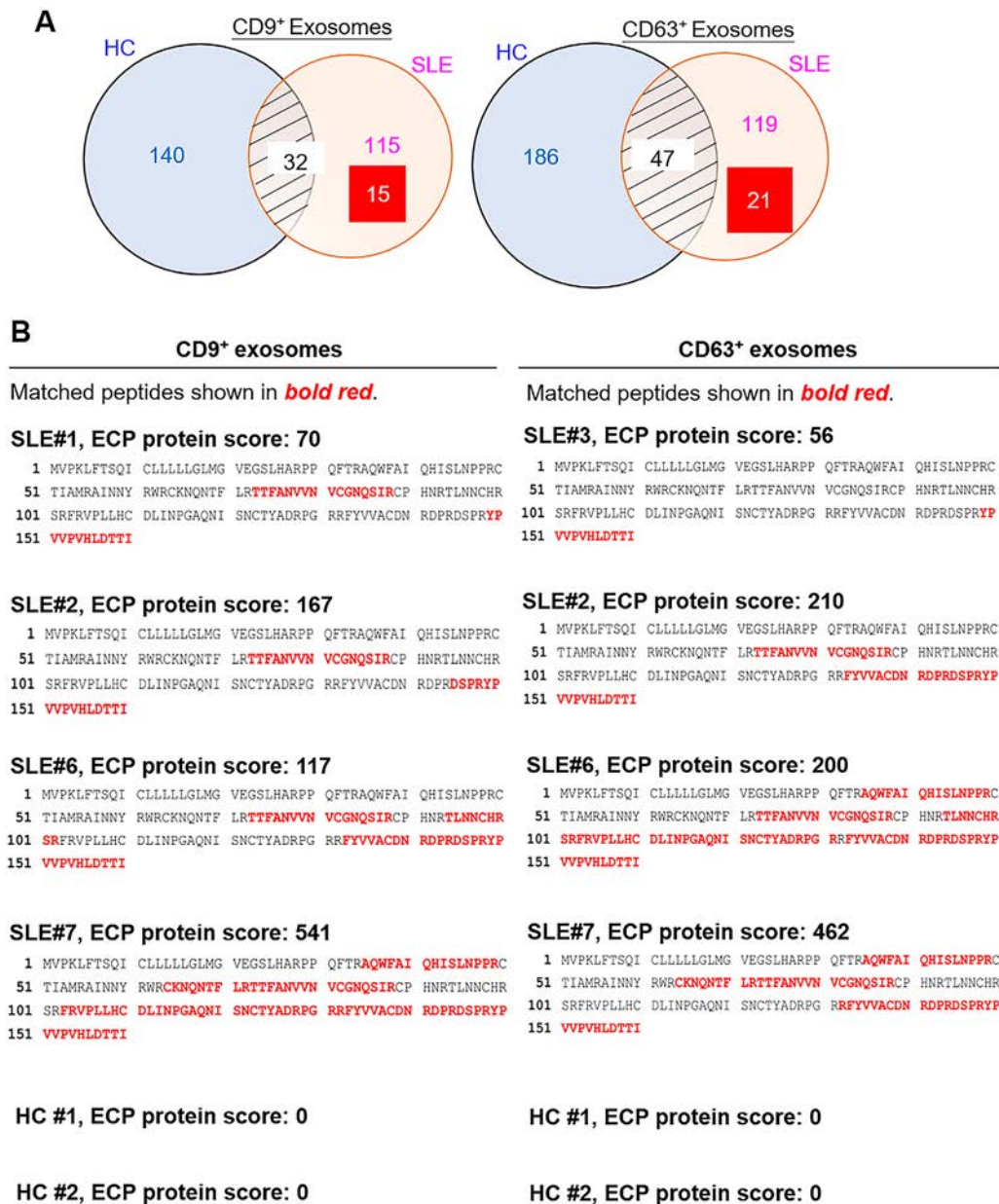


Figure 2. Induction of eosinophil cationic protein (ECP) in T cell–derived CD9⁺ and CD63⁺ exosomes from patients with systemic lupus erythematosus (SLE). **A**, Venn diagrams showing the numbers of proteins that were enriched in T cell–derived CD9⁺ or CD63⁺ exosomes from healthy controls (HCs) only, both healthy controls and SLE patients, and patients with SLE only. Exosomal proteins were identified by mass spectrometry–based protein sequencing. Many of the proteins identified were also enriched in exosomes from patients with rheumatoid arthritis (RA). Values in the rectangles are the number of exosomes that were enriched in SLE patients but not RA patients. **B**, Identification of ECP by mass spectrometry (MS)–based protein sequencing of T cell–derived CD9⁺ and CD63⁺ exosomes from 5 SLE patients (patients 1, 2, 3, 6, and 7). ECP was not detected in T cells from 2 healthy controls (controls 1 and 2). The protein score is the sum of the highest ion scores found by Mascot MS/MS Ion Search for each distinct peptide.

suggest that T cell–derived exosomal ECP may be a biomarker for SLE. Thus, the SLE T cell–enriched exosomal protein ECP was selected for further characterization.

Development of severe inflammation in Lck-ECP–transgenic mice. To study whether SLE-enriched exosomal ECP plays an important role in the pathogenesis of SLE, we generated

and characterized Lck-ECP–transgenic mice (Supplementary Figures 3A and B, available on the *Arthritis & Rheumatology* website at <http://onlinelibrary.wiley.com/doi/10.1002/art.41920/abstract>). ECP was successfully overexpressed in T cells (Supplementary Figure 3C) and T cell–derived exosomes from Lck-ECP–transgenic mice (Figure 3A). T cell–derived exosomes were mostly <200 nm in diameter (Figure 3B and Supplementary Figure 4, available on

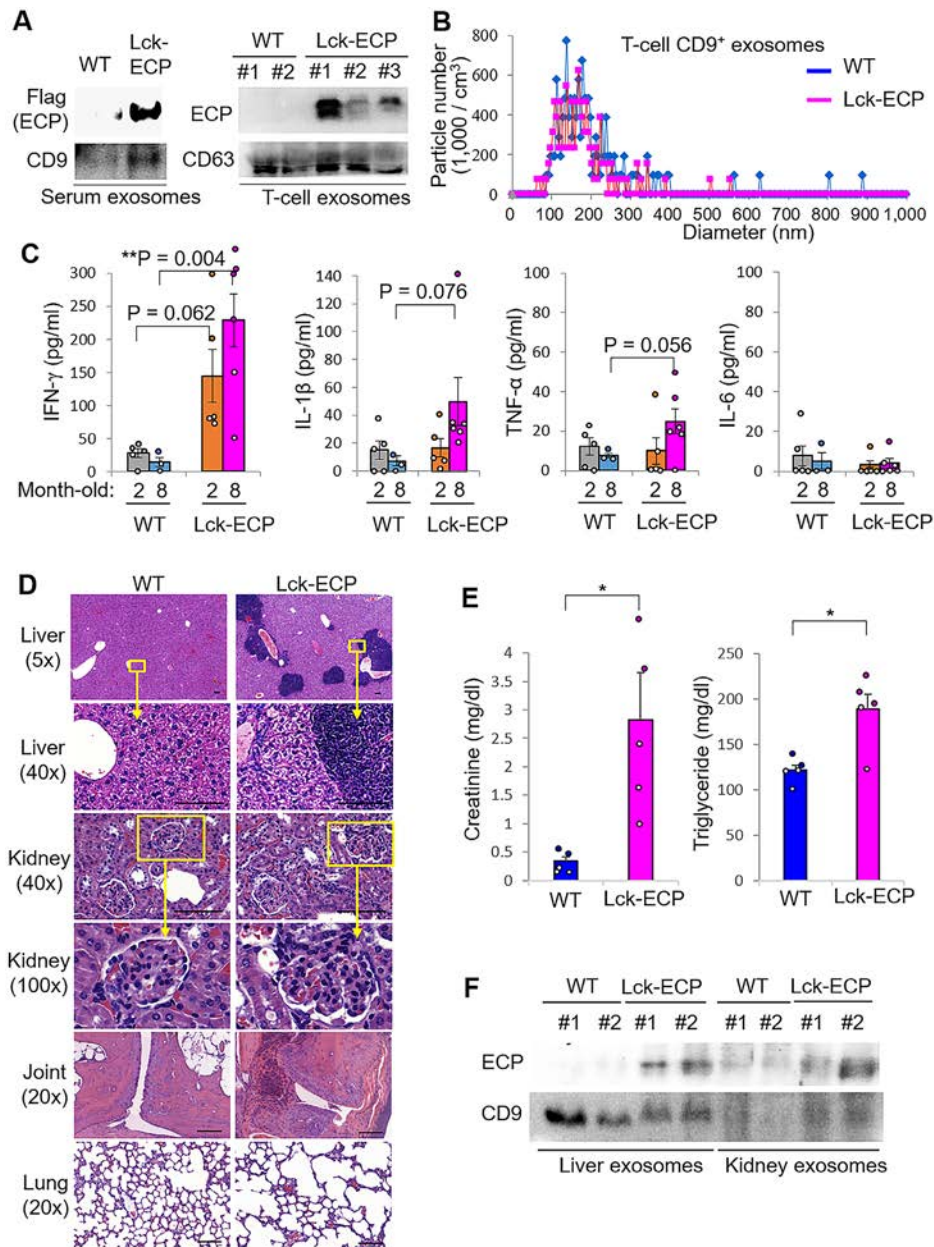


Figure 3. Spontaneous development of severe inflammation in T cell-specific eosinophil cationic protein (ECP)-transgenic (Lck-ECP-transgenic) mice. **A**, Immunoblots showing FLAG-tagged ECP and CD9 protein levels in serum exosomes and T cell-derived exosomes from 3 Lck-ECP-transgenic mice and 2 wild-type (WT) mice. **B**, ZetaView analysis of particle numbers and sizes of CD9+ extracellular vesicles in supernatants from WT and Lck-ECP-transgenic mouse T cells. Extracellular vesicles were isolated by ExoQuick-TC. **C**, Serum levels of interferon- γ (IFN γ), interleukin-1 β (IL-1 β), tumor necrosis factor (TNF), and IL-6 in 2-month-old mice ($n = 5$ per group) and 8-month-old mice ($n = 3$ WT mice and 6 Lck-ECP-transgenic mice), determined by enzyme-linked immunosorbent assay. Each symbol represents an individual mouse; bars show the mean \pm SEM. **D**, Hematoxylin and eosin-stained sections of the liver, kidney, joint, and lung from 8-month-old Lck-ECP-transgenic and WT mice. The bottom panels for liver and kidney show higher-magnification views of the boxed areas in the top panels. Bars = 100 μ m. **E**, Serum levels of creatinine and triglyceride in 38-week-old WT and Lck-ECP-transgenic mice ($n = 5$ per group), measured by serum chemistry assay. Each symbol represents an individual mouse; bars show the mean \pm SEM. **F**, Immunoblot showing FLAG-tagged ECP and CD9 protein levels in exosomes isolated from the liver and kidney tissues of WT and Lck-ECP-transgenic mice. * = $P < 0.05$; ** = $P < 0.01$, by Student's 2-tailed t -test.

the *Arthritis & Rheumatology* website at <http://onlinelibrary.wiley.com/doi/10.1002/art.41920/abstract>). Four-week-old Lck-ECP-transgenic mice displayed normal T cell and B cell development in the thymus and bone marrow, respectively

(Supplementary Figure 5, available on the *Arthritis & Rheumatology* website at <http://onlinelibrary.wiley.com/doi/10.1002/art.41920/abstract>). The peripheral CD4+ cell population was modestly increased, but the CD8+ cell population was

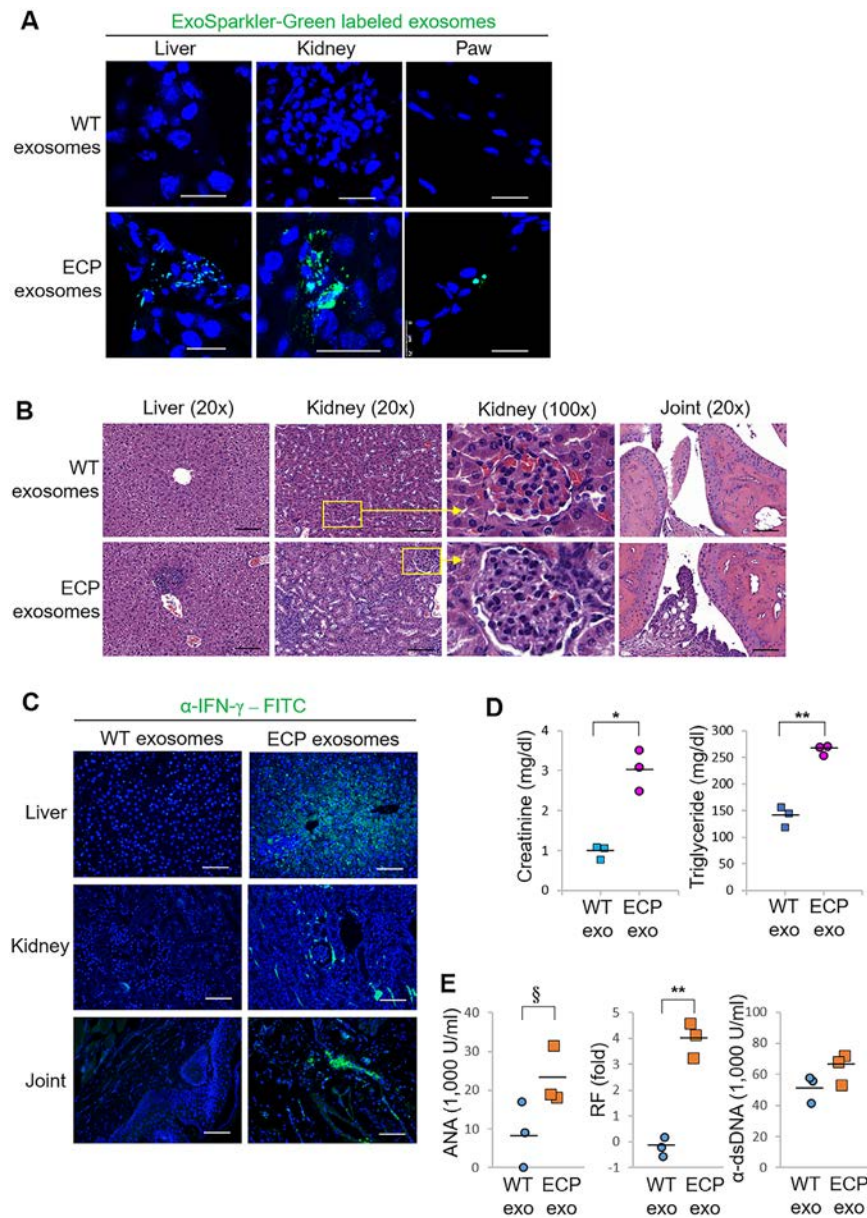


Figure 4. Inflammatory responses in WT mice after adoptive transfer of T cell-derived exosomes (exo) from Lck-ECP-transgenic mice. **A**, Confocal microscopy analysis of fluorescent dye-labeled exosomes (green) in frozen sections of the liver, kidney, and paw from a WT mouse and an ECP exosome recipient mouse. Exosomes were isolated from the supernatants of WT or Lck-ECP-transgenic mouse T cells by ExoQuick-TC. Labeled exosomes were adoptively transferred into recipient mice by intravenous (IV) injection every 3 days for 9 days. Cell nuclei were stained with DAPI. Bars = 25 μ m; original magnification \times 630. **B–E**, Exosomes derived from WT or Lck-ECP-transgenic mouse T cells ($n = 3$ per group) were adoptively transferred into recipient mice by IV injection every 3 days for 30 days. **B**, Hematoxylin and eosin-stained sections of the liver, kidney, and joint from recipient mice. Bars = 100 μ m. Right panels for kidney sections show a higher-magnification view of the boxed areas in the left panels. **C**, Immunohistochemical staining of fluorescein isothiocyanate (FITC)-conjugated anti-interferon- γ (anti-IFN γ) antibody (green) in paraffin-embedded sections of the liver, kidney, and joint from recipient mice. Cell nuclei were stained with DAPI. Bars = 100 μ m. **D**, Serum creatinine and triglyceride levels in recipient mice, determined by serum chemistry assays. **E**, Serum antinuclear antibody (ANA), rheumatoid factor (RF), and anti-double-stranded DNA (anti-dsDNA) antibody levels in recipient mice, determined by enzyme-linked immunosorbent assay. In **D** and **E**, each symbol represents an individual mouse; bars show the mean. * = $P < 0.05$; ** = $P < 0.01$, by Student's 2-tailed t -test; \S = $P < 0.05$ by Student's 1-tailed t -test. See Figure 3 for other definitions.

decreased, in Lck-ECP-transgenic mice (Supplementary Figure 5).

To study whether ECP overexpression in T cells leads to inflammatory responses in mice, we monitored serum cytokine

levels in mice. Two-month-old Lck-ECP-transgenic mice spontaneously developed increased serum levels of the proinflammatory cytokine IFN γ compared to wild-type mice (Figure 3C). Serum levels of TNF, IL-1 β , and IL-6 were not significantly increased in

2-month-old Lck-ECP-transgenic mice, whereas serum levels of IL-1 β and TNF were increased in 8-month-old Lck-ECP-transgenic mice ($P = 0.076$ and $P = 0.056$, respectively), compared to wild-type mice of the same age (Figure 3C). Moreover, 10-month-old Lck-ECP-transgenic mice showed severe inflammation of the liver, kidney, and joint, detected by histologic staining (Figure 3D). Increased serum levels of creatinine and triglyceride also suggest the development of nephritis and hepatitis, respectively, in Lck-ECP-transgenic mice (Figure 3E). To study whether ECP-containing exosomes infiltrate into the inflamed tissues of the liver and kidney, exosomes were isolated from mouse tissue samples and subjected to immunoblotting. The results verified that Lck-ECP-transgenic mouse tissues contained ECP-positive exosomes (Figure 3F). These results suggest that Lck-ECP-transgenic mice spontaneously develop inflammation of multiple tissue types.

Induction of inflammatory responses in recipient mice after adoptive transfer of T cell-derived exosomes from Lck-ECP-transgenic mice. To demonstrate the pathologic functions of ECP-containing exosomes, exosomes from purified Lck-ECP-transgenic mouse T cells were adoptively transferred into wild-type recipient mice through intravenous injection. Confocal microscopy showed that the exosomes derived from T cells from Lck-ECP-transgenic mice (referred to hereafter as ECP exosomes) infiltrated into the tissues of the liver, kidney, and paw of the wild-type recipient mice (Figure 4A). After 4 weeks of adoptive transfer of ECP exosomes, recipient mice displayed induction of infiltrating immune cells in the liver, kidney, and joint synovium (Figure 4B). Hematoxylin and eosin staining suggested the development of hepatitis, nephritis, and arthritis in ECP exosome-recipient mice (Figure 4B).

Consistent with the early induction of serum IFN γ levels in Lck-ECP-transgenic mice, ECP exosomes also stimulated serum IFN γ levels in wild-type recipient mice (Supplementary Figure 6, available on the *Arthritis & Rheumatology* website at <http://onlinelibrary.wiley.com/doi/10.1002/art.41920/abstract>). Liver, kidney, and joint tissues from ECP exosome-recipient mice also showed high IFN γ levels (Figure 4C). Moreover, adoptive transfer of ECP exosomes stimulated serum creatinine and triglyceride levels in wild-type recipient mice (Figure 4D), suggesting the development of nephritis and hepatitis, respectively, in the recipient mice. Furthermore, adoptive transfer of ECP exosomes induced IgG autoantibody in tissues from the wild-type recipient mice, suggesting immune complex deposition (Supplementary Figure 7, available on the *Arthritis & Rheumatology* website at <http://onlinelibrary.wiley.com/doi/10.1002/art.41920/abstract>). Serum levels of ANA and RF, but not anti-dsDNA, were also increased in the recipient mice (Figure 4E), suggesting an induction of autoimmune response by ECP exosomes.

Next, we examined whether MRL/MpJ-Fas^{lpr} mice in the autoimmune lupus model also harbor ECP-containing exosomes.

Consistent with the results described above, we found that ECP levels were indeed induced in serum exosomes and T cell-derived exosomes from MRL/MpJ-Fas^{lpr} mice compared to those of wild-type mice (Supplementary Figure 8, available on the *Arthritis & Rheumatology* website at <http://onlinelibrary.wiley.com/doi/10.1002/art.41920/abstract>). Taken together, these results suggest that T cell-derived exosomal ECP contributes to inflammatory responses.

Induction of growth hormone (GH), TNF superfamily (TNFSF8), and Titin by overexpression of ECP in T cells. To understand the underlying T cell responses that drive spontaneous inflammation in Lck-ECP-transgenic mice, T cells from 8-month-old Lck-ECP-transgenic mice were isolated and subjected to single-cell RNA sequencing. Dimensionality reduction/clustering analyses by Seurat grouped T cells from Lck-ECP and wild-type mice into 11 distinct clusters according to gene expression (Figure 5A). Clusters 1, 2, 5, 10, and 11 were identified as CD4⁺ T cells, while clusters 3, 4, 6, 7, 8, and 9 were identified as CD8⁺ T cells (Figure 5A). According to the expression levels of CD44 and CD62L (Supplementary Figure 9A, available on the *Arthritis & Rheumatology* website at <http://onlinelibrary.wiley.com/doi/10.1002/art.41920/abstract>), cluster 2 was mainly memory T cells, clusters 1 and 3 were identified as naive T cells, and cluster 4 was identified as effector T cells.

ECP overexpression in T cells resulted in decreased numbers of naive CD8⁺ T cells (cluster 3), increased numbers of effector CD8⁺ T cells (cluster 4), and increased numbers of memory CD4⁺ T cells (cluster 2) (Figure 5A). Consistent with these findings, flow cytometry data showed an increase in the numbers of effector memory T cells (CD62L⁻CD44⁺) and central memory T cells (CD62L⁺CD44⁺) in 16-week-old Lck-ECP-transgenic mice (Supplementary Figure 9B). Expression levels of 51 genes, including CD28 and CD69, were significantly up-regulated (>1.166 fold; $P < 0.05$) in Lck-ECP-transgenic mouse T cells (Figure 5B). Clusters 2 and 4 were enhanced in Lck-ECP-transgenic mouse T cells (Figure 5A); both clusters displayed T cell activation and inflammation signatures (Supplementary Figures 9C and D). KEGG pathway analyses revealed that the 51 genes that were up-regulated in Lck-ECP-transgenic mouse T cells belonged to the TNF/NF κ B signaling pathway, IL-2/STAT5 signaling pathway, T cell activation, and inflammatory responses (Supplementary Figure 10, *Arthritis & Rheumatology* website at <http://onlinelibrary.wiley.com/doi/10.1002/art.41920/abstract>). Moreover, GH was the most up-regulated gene in Lck-ECP-transgenic mouse T cells compared to wild-type mouse T cells (Figures 5B and C).

Expression of multiple inflammation-related genes, such as TNFAIP3, TNFSF8, S100a6, and IFN γ , was also significantly increased in Lck-ECP-transgenic mouse T cells (Figures 5B and C). The increased IFN γ expression in Lck-ECP-transgenic mouse

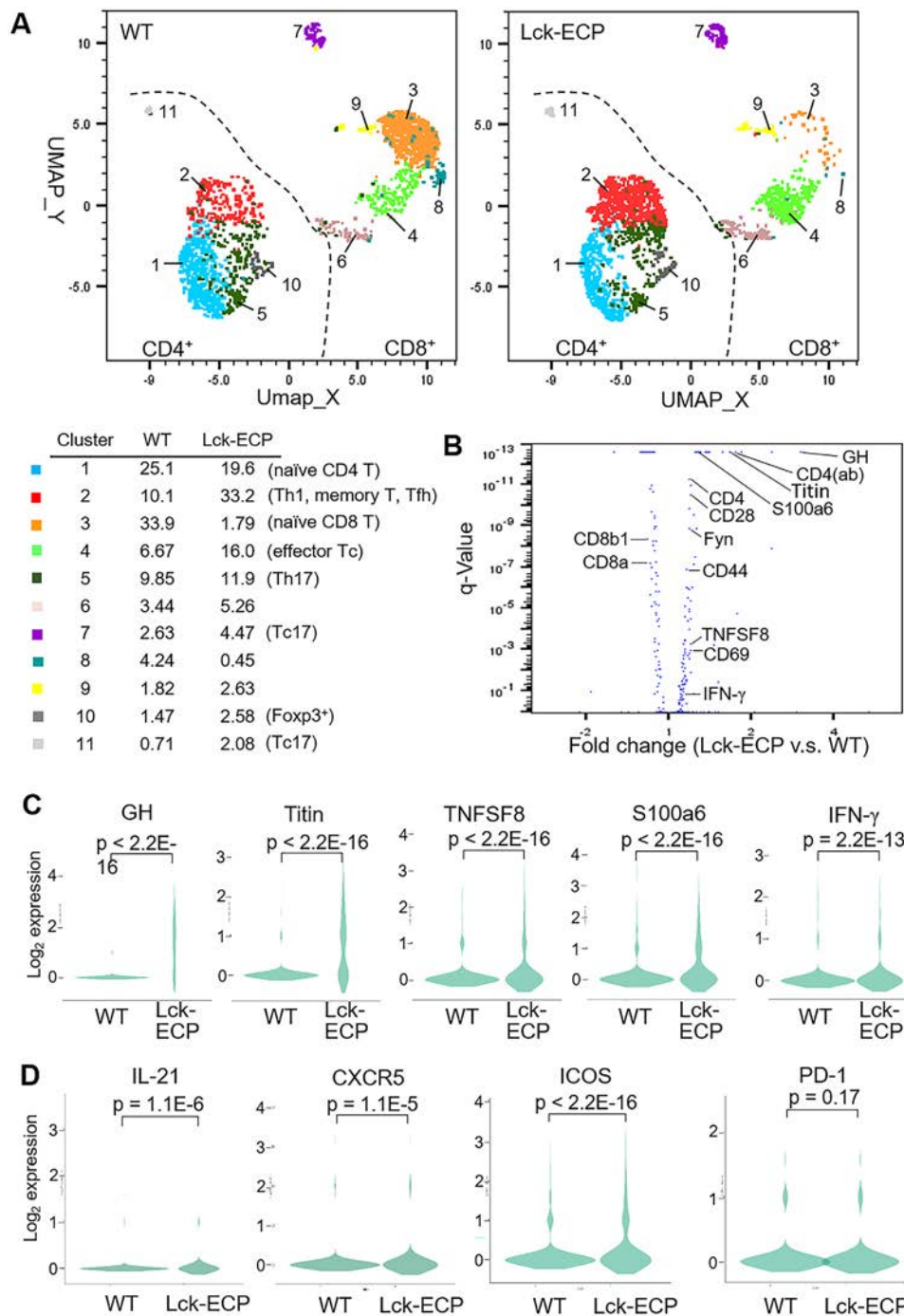


Figure 5. Induction of tumor necrosis factor (TNF) signaling and interferon- γ (IFN γ) production by overexpression of ECP in T cells. **A**, Distribution and classification of T cells from Lck-ECP-transgenic and WT mice. Data were visualized using Uniform Manifold Approximation and Projection (UMAP). Values listed for each cluster are the percentage of the cell subset among all T cells. **B**, Volcano plot showing the selected differentially expressed genes (DEGs) in Lck-ECP-transgenic versus WT mouse T cells. The q values were determined by Fisher's exact test. **C**, Violin plots showing the expression of selected DEGs in WT and Lck-ECP-transgenic mouse T cells. P values were determined by Wilcoxon's rank sum test. **D**, Violin plots showing the expression of follicular helper T (Tfh) cell markers (interleukin-21 [IL-21], CXCR5, inducible costimulator [ICOS], and programmed death 1 [PD-1]) in WT and Lck-ECP-transgenic mouse T cells. P values were determined by Wilcoxon's rank sum test. ab = antibody; GH = growth hormone; TNFSF8 = tumor necrosis factor superfamily 8 (see Figure 3 for other definitions).

T cells (Figure 5C) was consistent with the increased serum IFN γ levels in Lck-ECP-transgenic mice and enhanced Th1 differentiation of Lck-ECP-transgenic mouse T cells (Figure 3C and

Supplementary Figure 11, available on the *Arthritis & Rheumatology* website at <http://onlinelibrary.wiley.com/doi/10.1002/art.41920/abstract>). In vitro Th17 differentiation was also modestly enhanced

in Lck-ECP-transgenic mouse T cells (Supplementary Figure 11). Interestingly, Lck-ECP-transgenic mouse T cells displayed significant induction of Tintin (Figures 5B and C), an intrasarcomeric

filamentous protein, which was also identified in T cell-derived CD9+ exosomes from SLE patients by proteomics (Supplementary Table 2). These results suggest that ECP

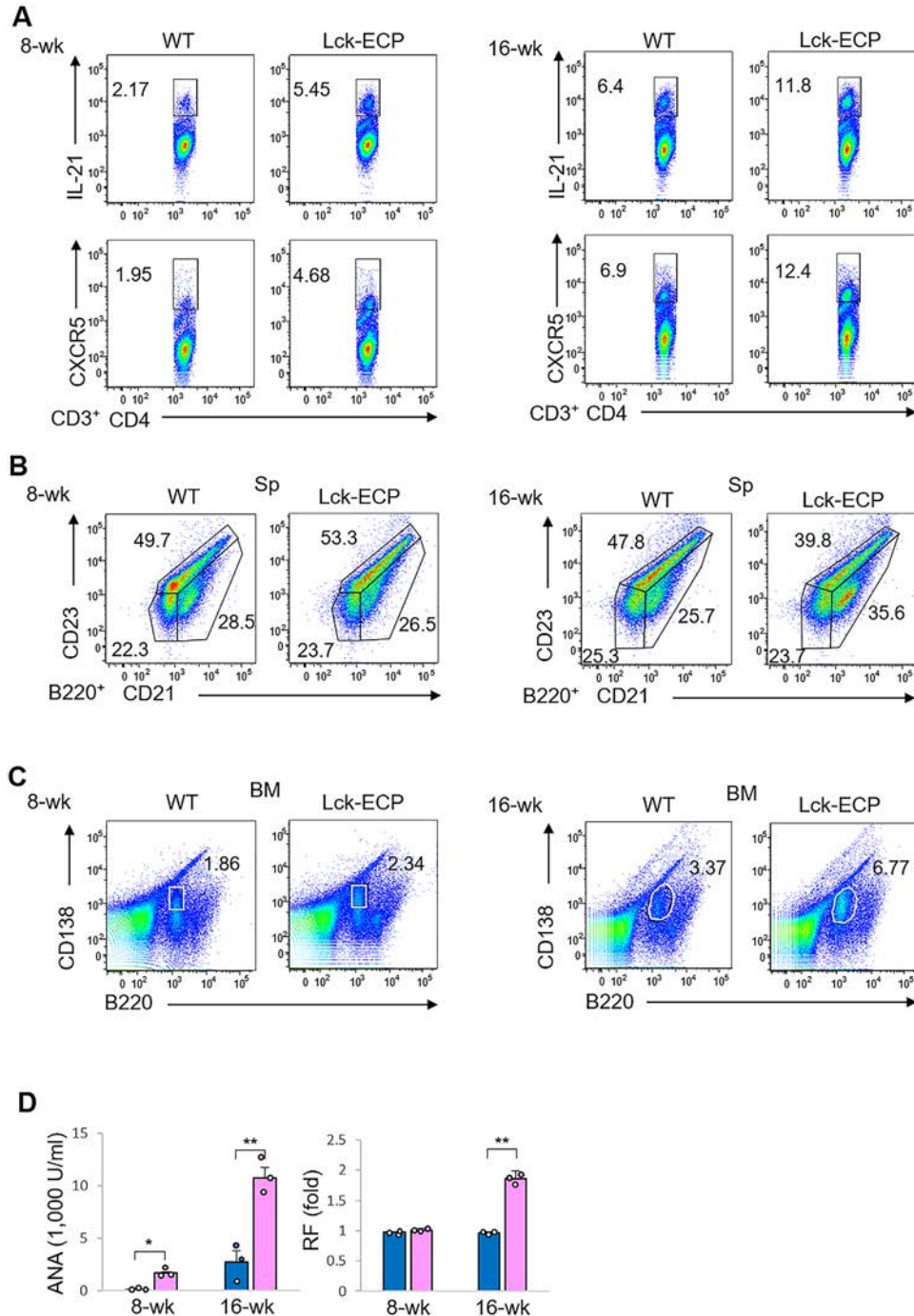


Figure 6. Increase in follicular helper T (Tfh) cell and plasma B cells numbers, and autoantibody levels, in Lck-ECP-transgenic mice. **A**, Flow cytometric analysis of Tfh (CD3+CD4+IL-21+ or CD3+CD4+CXCR5+) cells in the spleens (Sp) of 8-week-old and 16-week-old WT and Lck-ECP-transgenic mice. **B**, Flow cytometric analysis of B220+ B cells (B220+CD21+/mature B or B220+CD23+/naive B cells) in the spleens of 8-week-old and 16-week-old WT and Lck-ECP-transgenic mice. **C**, Flow cytometric analysis of plasma B (B220+CD138+) cells in the bone marrow (BM) of 8-week-old and 16-week-old WT and Lck-ECP-transgenic mice. Values next to the outlined areas in **A–C** are the number of positive cells. **D**, Serum antinuclear antibody (ANA) and rheumatoid factor (RF) levels in 8-week-old and 16-week-old WT mice (blue) and Lck-ECP-transgenic mice (pink), determined by enzyme-linked immunosorbent assay. Each symbol represents an individual mouse; bars show the mean \pm SEM. * = $P < 0.05$; ** = $P < 0.01$, by Student's 2-tailed t -test. See Figure 3 for other definitions.

overexpression in T cells induces T cell activation and inflammatory responses.

Increased numbers of follicular helper T (Tfh) cells and plasma B cells, and increased autoantibody levels, in Lck-ECP-transgenic mice. Lck-ECP-transgenic mouse T cells showed significant induction of mRNA for IL-21, CXCR5, and inducible costimulator (Figure 5D), which are cell markers for Tfh cells. It is notable that programmed death 1 (PD-1) mRNA levels were not significantly increased in Lck-ECP T cells (Figure 5D).

To study whether the Tfh cell population or plasma B cell population was increased in Lck-ECP-transgenic mice, murine spleen cells and bone marrow cells were analyzed by flow cytometry. We found that the percentages of both CD4+IL-21+ T cells and CD4+CXCR5+ T cells were increased in 8-week-old Lck-ECP-transgenic mice compared to wild-type mice (Figure 6A); these 2 T cell subpopulations were further enhanced in 16-week-old mice (Figure 6A). Moreover, the percentage of mature B cells (B220+CD21+) was increased, while the percentage of naive B cells (B220+CD23+) was decreased, in the spleens of 16-week-old but not 8-week-old Lck-ECP-transgenic mice, compared to wild-type mice (Figure 6B). The percentage of plasma B cells (B220^{low}CD138+) was modestly increased in the bone marrow of 8-week-old Lck-ECP-transgenic mice and was further enhanced in 16-week-old Lck-ECP-transgenic mice (Figure 6C).

Histologic analysis also showed an increased number of germinal centers in 16-week-old Lck-ECP-transgenic mice (Supplementary Figure 12, available on the *Arthritis & Rheumatology* website at <http://onlinelibrary.wiley.com/doi/10.1002/art.41920/abstract>). Consistent with these findings, serum levels of ANA were slightly induced in 8-week-old Lck-ECP-transgenic mice and further increased in 16-week-old Lck-ECP-transgenic mice (Figure 6D). Serum levels of RF were also increased in 16-week-old, but not 8-week-old, Lck-ECP-transgenic mice compared to wild-type mice (Figure 6D). These findings suggest that induction of Tfh cells in Lck-ECP-transgenic mice results in an increase in the number of plasma B cells, facilitating subsequent autoantibody production.

DISCUSSION

A key finding of this study was the identification of one novel T cell exosomal protein, ECP, which plays an important role in SLE pathogenesis. ECP overexpression in T cells resulted in enhancement of inflammatory responses and T cell activation. Notably, ECP-containing exosomes from T cells targeted several tissues (such as the liver, kidney, and joint) of the recipient mice, leading to tissue inflammation. These data suggest that ECP-overexpressing T cells or ECP-containing exosomes may act as a causal factor in SLE.

One of the notable findings of this study is that T cell-derived exosomal ECP contributes to autoimmune diseases. This is the first study to show that ECP is an exosomal protein. Extracellular ECP stimulation using ECP recombinant protein induces cell death, including necrosis and apoptosis (29,31,32); however, T cell development in Lck-ECP-transgenic mice was not affected. The data suggest that ECP recombinant protein acts differently from exosomal and intracellular ECP. In support of this notion, soluble ECP levels were not increased in the sera of human SLE patients. These findings also suggest that exosomal ECP and ECP-overexpressing T cells contribute to autoimmune responses through cell death-independent pathways. Furthermore, adoptive transfer of ECP-containing exosomes induced autoantibody production and inflammation expansion; it is likely that the T cell-derived exosomes from Lck-ECP-transgenic mouse T cells contain other inflammatory molecules in addition to ECP proteins.

Besides induction of the proinflammatory cytokine IFN γ , Lck-ECP-transgenic mice manifested the induction of Tfh cells, plasma B cells, and autoantibodies. These results suggest that ECP overexpression in T cells induces the Tfh cell population, facilitating plasma B cell differentiation, leading to overproduction of autoantibodies. Besides induction of plasma B cells through Tfh cells, it is also possible that secreted molecules from ECP-overexpressing T cells or other proteins within ECP+ exosomes may stimulate/activate other potential target cells (e.g., B cells, macrophages, dendritic cells, or osteoclasts), leading to multiple inflammatory phenotypes.

The aforementioned findings are consistent with our single-cell RNA-sequencing data using Lck-ECP-transgenic mouse T cells. First, Lck-ECP-transgenic mouse T cells showed highly increased levels of GH, which induces T cell survival and activation (37,38). Consistent with these findings, T cell activation, T cell proliferation, and adaptive immune response pathways were indeed induced in Lck-ECP-transgenic mouse T cells. Lck-ECP-transgenic mouse T cells also showed induction of IFN γ + Th1 differentiation.

Second, ECP signaling induced several proinflammatory cytokines/chemokines, including TNFSF8 (also called CD30 ligand [CD30L]), S100 proteins, and IFN γ , that may contribute to inflammation of multiple tissue types. CD30L up-regulation is involved in the pathogenesis of human SLE, RA, Hodgkin lymphoma, and anaplastic large cell lymphoma (39). S100 protein enhancement contributes to arthritis and neural degenerative diseases (40,41). Chronic IFN γ overproduction induces hepatotoxicity (42,43); IFN γ also plays a crucial role in the development of nephritis (44,45). Interestingly, our ELISA data also showed early induction of IFN γ in Lck-ECP-transgenic mice. These previous publications and our data suggest that ECP-overexpressing T cells and ECP-containing exosomes cooperate with the aforementioned proinflammatory cytokines/chemokines to induce nephritis, arthritis, and hepatitis in Lck-ECP-transgenic mice and maybe also in human SLE patients.

Third, surface receptors on exosomes may determine their tissue tropisms. It would be interesting to study whether the exosomal olfactory receptor 7D2, identified in this study as being enriched in SLE (Supplementary Table 2), controls the tissue tropism of inflammatory T cell exosomes. Finally, the role of ECP-inducible Titin, an intrasarcomeric filamentous protein, in SLE pathogenesis needs to be explored.

Taken together, these findings indicate that ECP overexpression in T cells contributes to inflammatory responses through both intrinsic and extrinsic events. To distinguish the specific role of ECP in T cells versus exosomes is highly challenging, if not impossible, due to the following two reasons. First, there is no definitive ECP orthologous gene (46) for the generation of ECP-knockout mice. Second, there are no exosome-specific surface markers for the depletion of exosomes *in vivo*.

SLE patients experience damage to multiple organs and complex symptoms (1). Understanding the causal factors of individual symptoms will help in the development of novel therapeutics for SLE. In this study, we found that ECP-containing exosomes induce arthritis, hepatitis, and nephritis in mice. According to our clinical data and proteomics analysis, 5 SLE patients had ECP-containing exosomes derived from T cells, while all of these 5 SLE patients developed arthritis. The data suggest that the novel pathogenic factor, ECP-containing exosome, may also be a biomarker for SLE-associated arthritis. In addition, 2 of these 5 SLE patients have developed nephritis; however, it is difficult to diagnosis SLE-associated nephritis at an early stage. ECP-containing exosomes may help in the early diagnosis of SLE-associated nephritis. Although up to 50% of SLE patients develop hepatitis, the exact diagnosis of hepatitis remains challenging due to complex conditions, including infection, drug treatment, or SLE (47). Notably, Lck-ECP-transgenic mice spontaneously developed hepatitis, suggesting that hepatitis in SLE patients may be a consequence of the induction of ECP-containing exosomes. Thus, exosomal ECP may also be a potential biomarker for SLE-associated hepatitis.

Taken together, our findings suggest that ECP overexpression in T cells or T cell-derived exosomes induces T cell hyperactivation and proinflammatory cytokine production through both intrinsic and extrinsic events, leading to inflammation in multiple organs and autoimmune responses. Thus, ECP-overexpressing T cells and ECP-containing exosomes are potential biomarkers for SLE.

ACKNOWLEDGMENTS

We thank the staff of the Institute of Biological Chemistry of Academia Sinica (Taipei, Taiwan) for mass spectrometry. We thank the staff of the Core Facilities of the National Health Research Institutes (NHRI; Taiwan) for tissue sectioning/H&E staining and confocal microscopy. We thank the staff of the Transgenic Mouse Core of NHRI for generation of Lck-ECP-transgenic mice. We also thank the staff of the (AAALAC-accredited) Laboratory Animal Center of NHRI for mouse housing and serum chemistry assays.

AUTHOR CONTRIBUTIONS

All authors were involved in drafting the article or revising it critically for important intellectual content, and all authors approved the final version to be published. Dr. Tan had full access to all of the data in the study and takes responsibility for the integrity of the data and the accuracy of the data analysis.

Study conception and design. Chuang, Tan.

Acquisition of data. Chuang, M. Chen, Y. Chen, Ciou, Hsueh, Tsai.

Analysis and interpretation of data. Chuang, M. Chen, Y. Chen, Ciou, Hsueh, Tsai, Tan.

REFERENCES

1. Kaul A, Gordon C, Crow MK, Touma Z, Urowitz MB, van Vollenhoven R, et al. Systemic lupus erythematosus [review]. *Nat Rev Dis Primers* 2016;2:16039.
2. Corbett M, Soares M, Jhuti G, Rice S, Spackman E, Sideris E, et al. Tumour necrosis factor- α inhibitors for ankylosing spondylitis and non-radiographic axial spondyloarthritis: a systematic review and economic evaluation. *Health Technol Assess* 2016;20:1-334.
3. Manzi S, Sanchez-Guerrero J, Merrill JT, Furie R, Gladman D, Navarra SV, et al. Effects of belimumab, a B lymphocyte stimulator-specific inhibitor, on disease activity across multiple organ domains in patients with systemic lupus erythematosus: combined results from two phase III trials. *Ann Rheum Dis* 2012;71:1833-8.
4. Smolen JS, Aletaha D, Koeller M, Weisman MH, Emery P. New therapies for treatment of rheumatoid arthritis [review]. *Lancet* 2007;370:1861-74.
5. Breedveld FC, Combe B. Understanding emerging treatment paradigms in rheumatoid arthritis [review]. *Arthritis Res Ther* 2011;13 Suppl 1:S3.
6. Mahieu MA, Strand V, Simon LS, Lipsky PE, Ramsey-Goldman R. A critical review of clinical trials in systemic lupus erythematosus [review]. *Lupus* 2016;25:1122-40.
7. Bluestone JA, Bour-Jordan H, Cheng M, Anderson M. T cells in the control of organ-specific autoimmunity [review]. *J Clin Invest* 2015; 125:2250-60.
8. Suarez-Fueyo A, Bradley SJ, Tsokos GC. T cells in systemic lupus erythematosus [review]. *Curr Opin Immunol* 2016;43:32-8.
9. Chuang HC, Lan JL, Chen DY, Yang CY, Chen YM, Li JP, et al. The kinase GLK controls autoimmunity and NF- κ B signaling by activating the kinase PKC- θ in T cells. *Nat Immunol* 2011;12:1113-8.
10. Li JP, Yang CY, Chuang HC, Lan JL, Chen DY, Chen YM, et al. The phosphatase JKAP/DUSP22 inhibits T-cell receptor signalling and autoimmunity by inactivating Lck. *Nat Commun* 2014;5:3618.
11. Chuang HC, Chen YM, Hung WT, Li JP, Chen DY, Lan JL, et al. Downregulation of the phosphatase JKAP/DUSP22 in T cells as a potential new biomarker of systemic lupus erythematosus nephritis. *Oncotarget* 2016;7:57593-605.
12. Chuang HC, Tan TH. MAP4K family kinases and DUSP family phosphatases in T-cell signaling and systemic lupus erythematosus [review]. *Cells* 2019;8:1433.
13. Suarez-Fueyo A, Barber DF, Martinez-Ara J, Zea-Mendoza AC, Carrera AC. Enhanced phosphoinositide 3-kinase δ activity is a frequent event in systemic lupus erythematosus that confers resistance to activation-induced T cell death. *J Immunol* 2011;187: 2376-85.
14. Chuang HC, Chen YM, Chen MH, Hung WT, Yang HY, Tseng YH, et al. AhR-ROR- γ t complex is a therapeutic target for MAP4K3/GLK^{high}L-17A^{high} subpopulation of systemic lupus erythematosus. *FASEB J* 2019;33:11469-80.
15. Pan L, Lu MP, Wang JH, Xu M, Yang SR. Immunological pathogenesis and treatment of systemic lupus erythematosus [review]. *World J Pediatr* 2020;16:19-30.

16. Dolff S, Bijl M, Huitema MG, Limburg PC, Kallenberg CG, Abdulahad WH. Disturbed Th1, Th2, Th17 and T_{reg} balance in patients with systemic lupus erythematosus. *Clin Immunol* 2011; 141:197–204.
17. Maddur MS, Miossec P, Kaveri SV, Bayry J. Th17 cells: biology, pathogenesis of autoimmune and inflammatory diseases, and therapeutic strategies [review]. *Am J Pathol* 2012;181:8–18.
18. Chuang HC, Tan TH. MAP4K3/GLK in autoimmune disease, cancer and aging [review]. *J Biomed Sci* 2019;26:82.
19. Ohl K, Tenbrock K. Regulatory T cells in systemic lupus erythematosus [review]. *Eur J Immunol* 2015;45:344–55.
20. Alexander M, Hu R, Runtsch MC, Kagele DA, Mosbrugger TL, Tolmachova T, et al. Exosome-delivered microRNAs modulate the inflammatory response to endotoxin. *Nat Commun* 2015;6:7321.
21. Zhao H, Yang L, Baddour J, Achreja A, Bernard V, Moss T, et al. Tumor microenvironment derived exosomes pleiotropically modulate cancer cell metabolism. *Elife* 2016;5:e10250.
22. Song J, Huang J, Chen X, Teng X, Song Z, Xing Y, et al. Donor-derived exosomes induce specific regulatory T cells to suppress immune inflammation in the allograft heart. *Sci Rep* 2016;7:20077.
23. Gunasekaran M, Xu Z, Nayak DK, Sharma M, Hachem R, Walia R, et al. Donor-derived exosomes with lung self-antigens in human lung allograft rejection. *Am J Transplant* 2017;17:474–84.
24. Okoye IS, Coomes SM, Pelly VS, Czieso S, Papayannopoulos V, Tolmachova T, et al. MicroRNA-containing T-regulatory-cell-derived exosomes suppress pathogenic T helper 1 cells. *Immunity* 2014;41:89–103.
25. Mittelbrunn M, Gutierrez-Vazquez C, Villarroya-Beltri C, Gonzalez S, Sanchez-Cabo F, Gonzalez MA, et al. Unidirectional transfer of microRNA-loaded exosomes from T cells to antigen-presenting cells. *Nat Commun* 2011;2:282.
26. Lee JY, Park JK, Lee EY, Lee EB, Song YW. Circulating exosomes from patients with systemic lupus erythematosus induce a proinflammatory immune response. *Arthritis Res Ther* 2016;18:264.
27. Bystrom J, Amin K, Bishop-Bailey D. Analysing the eosinophil cationic protein: a clue to the function of the eosinophil granulocyte [review]. *Respir Res* 2011;12:10.
28. Wardlaw AJ. Eosinophils in the 1990s: new perspectives on their role in health and disease [review]. *Postgrad Med J* 1994;70:536–52.
29. Navarro S, Aleu J, Jimenez M, Boix E, Cuchillo CM, Nogues MV. The cytotoxicity of eosinophil cationic protein/ribonuclease 3 on eukaryotic cell lines takes place through its aggregation on the cell membrane. *Cell Mol Life Sci* 2008;65:324–37.
30. Trautmann A, Schmid-Grendelmeier P, Kruger K, Cramer R, Akdis M, Akkaya A, et al. T cells and eosinophils cooperate in the induction of bronchial epithelial cell apoptosis in asthma. *J Allergy Clin Immunol* 2002;109:329–37.
31. Fredens K, Dahl R, Venge P. The Gordon phenomenon induced by the eosinophil cationic protein and eosinophil protein X. *J Allergy Clin Immunol* 1982;70:361–6.
32. Chang KC, Lo CW, Fan TC, Chang MD, Shu CW, Chang CH, et al. TNF- α mediates eosinophil cationic protein-induced apoptosis in BEAS-2B cells. *BMC Cell Biol* 2010;11:6.
33. Garvin AM, Pawar S, Marth JD, Perlmutter RM. Structure of the murine lck gene and its rearrangement in a murine lymphoma cell line. *Mol Cell Biol* 1988;8:3058–64.
34. Chaffin KE, Beals CR, Wilkie TM, Forbush KA, Simon MI, Perlmutter RM. Dissection of thymocyte signaling pathways by in vivo expression of pertussis toxin ADP-ribosyltransferase. *EMBO J* 1990;9:3821–9.
35. Chuang HC, Tsai CY, Hsueh CH, Tan TH. GLK-IKK β signaling induces dimerization and translocation of the AhR-ROR γ t complex in IL-17A induction and autoimmune disease. *Sci Adv* 2018;4:eat5401.
36. Chuang HC, Chang CC, Teng CF, Hsueh CH, Chiu LL, Hsu PM, et al. MAP4K3/GLK promotes lung cancer metastasis by phosphorylating and activating IQGAP1. *Cancer Res* 2019;79:4978–93.
37. Welniak LA, Sun R, Murphy WJ. The role of growth hormone in T-cell development and reconstitution [review]. *J Leukoc Biol* 2002;71:381–7.
38. Postel-Vinay MC, de Mello Coelho V, Gagnerault MC, Dardenne M. Growth hormone stimulates the proliferation of activated mouse T lymphocytes. *Endocrinology* 1997;138:1816–20.
39. Ofiazoglu E, Grewal IS, Gerber H. Targeting CD30/CD30L in oncology and autoimmune and inflammatory diseases [review]. *Adv Exp Med Biol* 2009;647:174–85.
40. Yammani RR. S100 proteins in cartilage: role in arthritis [review]. *Biochim Biophys Acta* 2012;1822:600–6.
41. Hu J, Ferreira A, Van Eldik LJ. S100 β induces neuronal cell death through nitric oxide release from astrocytes. *J Neurochem* 1997;69:2294–301.
42. Bae HR, Leung PS, Tsuneyama K, Valencia JC, Hodge DL, Kim S, et al. Chronic expression of interferon- γ leads to murine autoimmune cholangitis with a female predominance. *Hepatology* 2016;64:1189–201.
43. Morita M, Watanabe Y, Akaike T. Protective effect of hepatocyte growth factor on interferon- γ -induced cytotoxicity in mouse hepatocytes. *Hepatology* 1995;21:1585–93.
44. Fava A, Buyon J, Mohan C, Zhang T, Belmont HM, Izmirly P, et al. Integrated urine proteomics and renal single-cell genomics identify an IFN- γ response gradient in lupus nephritis. *JCI Insight* 2020;5:e138345.
45. Richards HB, Satoh M, Jennette JC, Croker BP, Yoshida H, Reeves WH. Interferon- γ is required for lupus nephritis in mice treated with the hydrocarbon oil pristane. *Kidney Int* 2001;60:2173–80.
46. Attery A, Batra JK. Mouse eosinophil associated ribonucleases: mechanism of cytotoxic, antibacterial and antiparasitic activities. *Int J Biol Macromol* 2017;94A:445–50.
47. Adiga A, Nugent K. Lupus hepatitis and autoimmune hepatitis (lupoid hepatitis) [review]. *Am J Med Sci* 2017;353:329–35.

BRIEF REPORT

Anti-Double-Stranded DNA Antibodies Recognize DNA Presented on HLA Class II Molecules of Systemic Lupus Erythematosus Risk Alleles

Hideaki Tsuji,¹ Koichiro Ohmura,² Hui Jin,³ Ryota Naito,¹ Noriko Arase,⁴ Masako Kohyama,⁵ Tadahiro Suenaga,⁵ Shuhei Sakakibara,⁶ Yuta Kochi,⁷ Yukinori Okada,⁸ Kazuhiko Yamamoto,⁹ Hitoshi Kikutani,⁶ Akio Morinobu,² Tsuneyo Mimori,² and Hisashi Arase¹⁰

Objective. Specific HLA class II alleles are associated with susceptibility to systemic lupus erythematosus (SLE). The role of HLA class II molecules in SLE pathogenesis remains unclear, although anti-DNA antibodies are specific to SLE and correlate with disease activity. We previously demonstrated that misfolded proteins bound to HLA class II molecules are specific targets for the autoantibodies produced in autoimmune diseases. This study was undertaken to validate our hypothesis that DNA binds to HLA class II molecules in a manner similar to that of misfolded proteins and that DNA bound to HLA class II molecules is involved in SLE pathogenesis.

Methods. We analyzed the binding of DNA to HLA class II molecules, as well as the response of cells expressing anti-DNA B cell receptors (BCRs) to cells expressing the DNA/HLA class II complex.

Results. Efficient binding of DNA to HLA class II molecules was observed in risk alleles of SLE, such as HLA-DRB1*15:01. The efficiency of DNA binding to each HLA-DR allele was positively associated with the risk of SLE conferred by the HLA-DR allele. In addition, reporter cells carrying anti-DNA BCRs were activated by cells expressing DNA/HLA class II complexes.

Conclusion. These results provide evidence that DNA bound to HLA class II molecules is involved in SLE pathogenesis.

Supported by grants from the Japan Agency for Medical Research and Development (grants JP21ek0410088, JP20ek0410053, and JP18K19450 awarded to Dr. H. Arase), by the Ministry of Education, Culture, Sports, Science, and Technology of Japan (Kakenhi Grant-in-Aid JP190H04808 awarded to Dr. H. Arase), and by the Japan Society for the Promotion of Science (Kakenhi Grant-in-Aid JP18H05279 awarded to Dr. H. Arase). Dr. Ohmura's work was supported by a Sanofi research grant.

¹Hideaki Tsuji, MD, PhD, Ryota Naito, MD: Kyoto University, Kyoto, Japan, World Premier International Immunology Frontier Research Center, Osaka University, Suita, Japan, and Research Institute for Microbial Diseases, Osaka University, Suita, Japan; ²Koichiro Ohmura, MD, PhD (current address: Kobe City Medical Center General Hospital, Kobe, Japan), Akio Morinobu, MD, PhD, Tsuneyo Mimori, MD, PhD: Kyoto University, Kyoto, Japan; ³Hui Jin, PhD: Research Institute for Microbial Diseases, Osaka University, Suita, Japan; ⁴Noriko Arase, MD, PhD: Osaka University Graduate School of Medicine, Suita, Japan; ⁵Masako Kohyama, PhD, Tadahiro Suenaga, MD, PhD (current address: Fukushima Medical University, Fukushima, Japan): World Premier International Immunology Frontier Research Center, Osaka University, Suita, Japan, and Research Institute for Microbial Diseases, Osaka University, Suita, Japan; ⁶Shuhei Sakakibara, PhD, Hitoshi Kikutani, MD, PhD: World Premier International Immunology Frontier Research Center, Osaka University, Suita, Japan; ⁷Yuta Kochi, MD, PhD: RIKEN Center for Integrative Medical Sciences, Yokohama, Japan, and Tokyo Medical and Dental University, Tokyo, Japan; ⁸Yukinori Okada, MD, PhD: World Premier International Immunology Frontier Research Center, Osaka University, Suita, Japan, Osaka University Graduate School of Medicine, Suita, Japan, and RIKEN Center for Integrative Medical Sciences, Yokohama, Japan; ⁹Kazuhiko Yamamoto, MD, PhD: RIKEN Center for Integrative Medical Sciences, Yokohama, Japan; ¹⁰Hisashi Arase, MD, PhD:

World Premier International Immunology Frontier Research Center, Osaka University, Suita, Japan, Research Institute for Microbial Diseases, Osaka University, Suita, Japan, and Center for Infectious Disease Education and Research, Osaka University, Suita, Japan.

Dr. Ohmura has received consulting fees, speaking fees, and/or honoraria from AbbVie, Actelion, Asahikasei Pharma, Ayumi, Bristol Myers Squibb, Chugai, Daiichi-Sankyo, Eisai, Eli Lilly, GSK, Janssen, JB Chemicals and Pharmaceuticals, Nippon Kayaku, Nippon Shinyaku, Novartis, Sanofi, and Takeda (less than \$10,000 each) and from Astellas and Mitsubishi Tanabe (more than \$10,000 each) and research grants from those companies. Dr. Yamamoto has received consulting fees, speaking fees, and/or honoraria from AbbVie, Ayumi, Bristol Myers Squibb, Chugai, Eisai Janssen Pharmaceuticals, Mitsubishi Tanabe, Ono Pharmaceutical, and UCB Japan (less than \$10,000 each). Dr. Arase has received consulting fees, speaking fees, and/or honoraria from Hulaimmune, Chugai, Ono Pharmaceutical, Thermofisher, Sanofi, Pfizer, and Taiho Pharmaceutical (less than \$10,000 each). No other disclosures relevant to this article were reported.

Address correspondence to Koichiro Ohmura, MD, PhD, Kyoto University Graduate School of Medicine, Department of Rheumatology and Clinical Immunology, 54 Kawaharacho, Shogoin, Sakyo-ku, Kyoto 606-8507, Japan (email: ohmurako1964@gmail.com); or to Hisashi Arase, MD, PhD, Laboratory of Immunochemistry, World Premier International Immunology Frontier Research Center, Osaka University, Research Institute for Microbial Diseases, Osaka University, Suita, Japan, and Center for Infectious Disease Education and Research, Osaka University, 3-1 Yamadaoka, Suita, Osaka 565-0871, Japan (email: arase@biken.osaka-u.ac.jp).

Submitted for publication April 24, 2020; accepted in revised form June 8, 2021.

INTRODUCTION

Systemic lupus erythematosus (SLE) is an autoimmune disease characterized by B cell hyperactivity and the production of autoantibodies against DNA and various antigens. Although the exact mechanism of anti-DNA antibody production remains unclear, DNA associated with certain molecules appears to be involved in the production of anti-DNA antibodies (1).

Specific HLA class II alleles are associated with susceptibility to SLE (2). However, the role of HLA class II molecules in SLE pathogenesis remains unclear (3). We recently discovered that HLA class II molecules transport misfolded cellular proteins to the cell surface without processing them into peptides. Misfolded proteins were found to be specific targets of autoantibodies in autoimmune diseases (4–6).

When nonimmune cells are exposed to certain cytokines such as interferon- γ (IFN γ) in inflamed tissue, HLA class II expression is induced (7,8). This suggests that misfolded proteins, whose expression on the cell surface is induced by aberrantly expressed HLA class II molecules, might be involved in the pathogenesis of autoimmune diseases (4–6). In addition, elevated blood concentrations of IFN γ (9) and up-regulation of HLA class II expression in the kidneys have been observed in lupus nephritis (8). Furthermore, in patients with active SLE, clearance of apoptotic cells is decreased and circulating DNA levels are elevated (1). Therefore, we hypothesized that DNA might also be associated with HLA class II molecules and that DNA bound to HLA class II molecules might be involved in the activation of B cells expressing anti-DNA B cell receptors (BCRs).

MATERIALS AND METHODS

Cells. HEK 293T cells and B16-F10 cells (RIKEN Cell Bank) were regularly tested for mycoplasma contamination. B16-F10 cells lacking the major histocompatibility complex (MHC) class II transcription activator (CIITA) were generated using pX330 clustered regularly interspaced short palindromic repeat (CRISPR)/CRISPR-associated protein 9 (Cas9) vector.

Patient HLA genotyping data. Odds ratios for the association between HLA-DRB1 alleles and SLE risk were obtained from a high-resolution genotyping of HLA-DRB1 (2). Use of human genomic DNA for HLA genotyping was approved by the ethics committee of RIKEN (no. 2018-26(3)), and all participants provided written informed consent.

Plasmids. Complementary DNAs for different MHC class II alleles from peripheral blood mononuclear cells (3H Biomedical) and Ig α (NM_007655.3) and Ig β (NM_008339.2) were cloned (4,6). HLA-DRB1*01:01 and HLA-DRB1*15:01 containing covalently attached transferrin receptor (RVEYHFLSPYVSPKESP) and SP3 peptides (AILEFRAMAQFSRKTQ) were prepared as previously reported (6,10).

DNA. Genomic DNA was prepared from mouse liver. Biotinylated and phosphorothioate oligonucleotides (5'-biotin-ATGCACTCTGCAGGCTTCTC-3') were synthesized at Fasmac (Atsugi, Japan) and Gene Design (Ibaraki, Japan), respectively.

Analysis of autoantibody binding to the DNA/MHC class II complex. Expression vectors encoding HLA-DR α , HLA-DR β , and green fluorescent protein (GFP) were cotransfected into cells using Polyethylenimine Max (Polysciences) (4,6). After 24 hours, the medium was replaced with medium containing DNA or DNase I (0.1 mg/ml; Roche) and subsequently incubated at 37°C for 24 hours. B16-F10 cells were cocultured with DNA and IFN γ (3.16×10^4 units/ml; PeproTech). HLA-DR was detected with anti-HLA class II monoclonal antibody (mAb) L243 (ATCC), followed by allophycocyanin (APC)-conjugated anti-mouse IgG antibody (Jackson ImmunoResearch). B16-F10 cells were stained with APC-conjugated anti-mouse I-A^b (M5) (BioLegend). DNA was detected with a human anti-DNA mAb (71F12) (11), followed by APC-conjugated anti-human IgG-Fc antibodies (Jackson). Biotinylated DNA was detected with APC-conjugated streptavidin (Jackson ImmunoResearch). Histone H3 was detected with antihistone H3 antibody ab5103 (Abcam), followed by APC-conjugated anti-rabbit IgG antibody (Jackson ImmunoResearch). Stained cells were analyzed using FACSCalibur (Becton Dickinson). The mean fluorescence intensity (MFI) of staining for each molecule on cells was calculated by subtracting the MFI values obtained from cells transfected with GFP alone.

Precipitation and immunoblotting. HLA-DR α and HLA-DR β were cotransfected into HEK 293T cells, and 20-mer biotinylated phosphorothioate oligonucleotides were incubated at 37°C for 24 hours. After precipitation with streptavidin-Sepharose (GE Healthcare), eluates from cell lysates were subjected to sodium dodecyl sulfate-polyacrylamide gel electrophoresis and blotted onto membranes (Millipore). The membranes were incubated with anti-HLA-DR α antibody FL-254 (Santa Cruz Biotechnology) and then with anti-rabbit IgG antibody (ThermoFisher).

Anti-DNA BCR reporter assay. Human IgM (71F12) heavy chain, light chain, Ig α , and Ig β were stably transfected into mouse T cell hybridomas with the NFAT-GFP reporter gene, using the pMXs retroviral expression vector and Plat-E retroviral packaging cells (4,12). Reporter cell reactivity with DNA was confirmed by stimulation with biotinylated DNA (0.2–2 ng/ml) immobilized on a 10 μ g/ml streptavidin-coated plate, and 1×10^4 B16-F10 cells incubated with DNA and IFN γ were cocultured with 1×10^4 reporter cells, DNA, and 3.16×10^4 units/ml IFN γ for 48 hours in 96-well half-area plates (Corning). GFP expression in CD45-positive cells was analyzed using flow cytometry. The production of interleukin-2 (IL-2) in the supernatants was determined using anti-IL-2 mAb (JES6-1A12)

and biotinylated anti-mouse IL-2 mAb (JES6-5H4) (both from eBioscience).

Statistical analysis. Pearson's product-moment correlation coefficient and Student's *t*-test were used to calculate correlations and to generate statistical comparisons. *P* values less than 0.05 were considered significant.

Data availability. All data relevant to this study are available herein as well as in the supplementary data files, and upon request from the corresponding author.

RESULTS

Binding of DNA to HLA class II molecules. We addressed whether DNA could be associated with HLA class II molecules on the cell surface, using SLE patient-derived DNA-specific human mAb 71F12 (11). HEK 293T cells were transfected with HLA-DR15, a susceptibility allele for SLE, and the transfectants were cultured in the presence of genomic DNA for 24 hours. DNA was readily detected on the cell surface of HLA-DR15 transfectants, but was sparsely detected on the mock transfectants (Figure 1A). When cells were

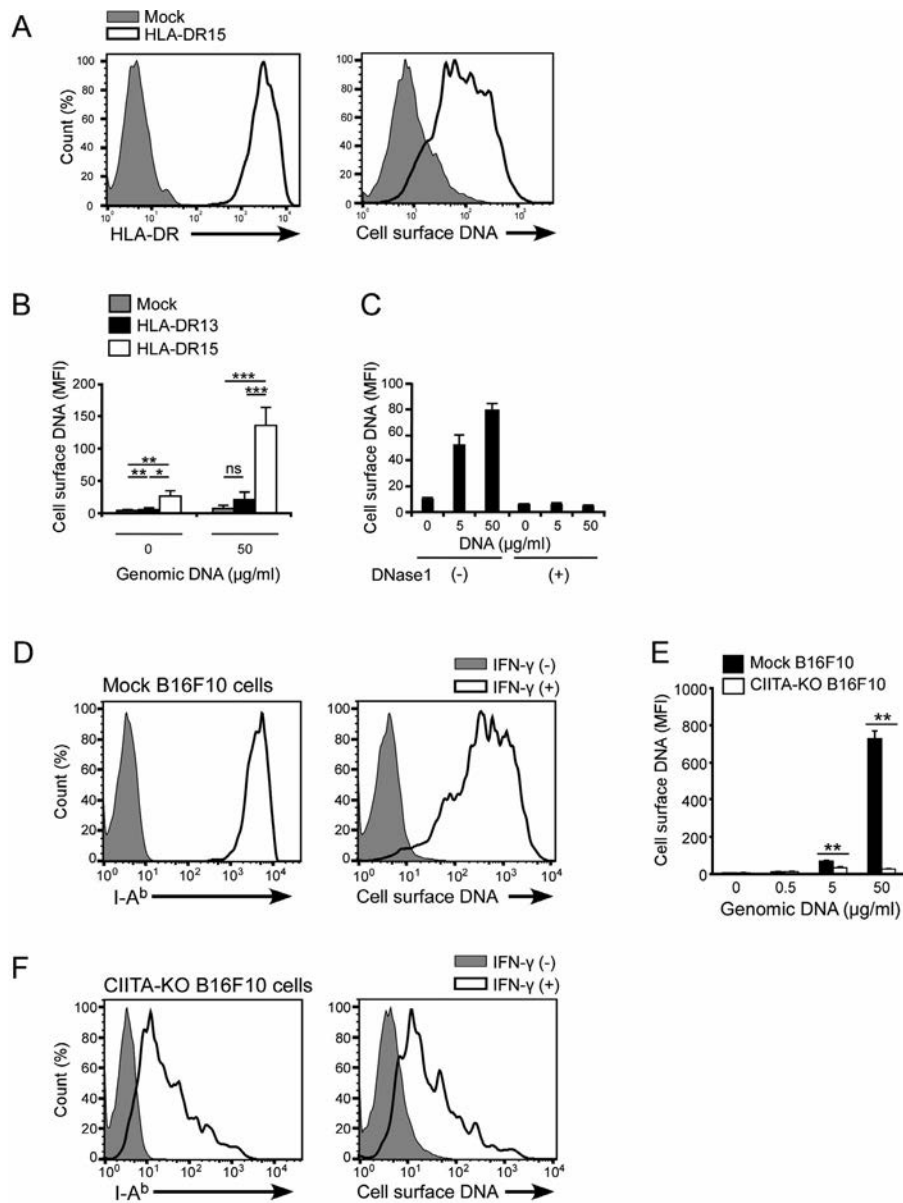


Figure 1. Association of DNA expression on the cell surface with major histocompatibility complex (MHC) class II molecules. **A**, Level of DNA on the cell surface of HEK 293T cells transfected with mock transfectants or HLA-DR15. **B**, Level of DNA on the cell surface of HEK 293T cells transfected with mock transfectants, HLA-DR13, or HLA-DR15. **C**, Level of DNA on the cell surface of HEK 293T cells transfected with HLA-DR15 in the absence or presence of DNase I. **D**, Expression of MHC class II (I-A^b) and cell surface DNA on mock B16-F10 cells in the absence or presence of interferon- γ (IFN- γ) (3.16×10^4 units/ml). **E**, Level of DNA on the cell surface of IFN- γ -stimulated mock B16-F10 cells or MHC class II transcription activator (CIITA)-knockout (KO) B16-F10 cells. **F**, Expression of MHC class II (I-A^b) and cell surface DNA on CIITA-KO B16-F10 cells in the absence or presence of IFN- γ (3.16×10^4 units/ml). Data in **A**, **D**, and **F** are representative of at least 3 independent fluorescence-activated cell sorting experiments. Values in **B**, **C**, and **E** are the mean \pm SD mean fluorescence intensity (MFI). * = $P < 0.05$; ** = $P < 0.01$; *** = $P < 0.001$, by Student's *t*-test with Bonferroni adjustment. NS = not significant.

transfected with HLA-DR13, a protective allele for SLE (2), less DNA was detected on the cell surface than when cells were transfected with HLA-DR15 (Figure 1B). Anti-DNA mAb binding to HLA-DR15 transfectants incubated with DNA was considerably decreased by DNase I treatment (Figure 1C). These results indicated that mAb 71F12 specifically bound to DNA that is associated with HLA class II molecules.

We then analyzed whether DNA is presented on endogenously expressed MHC class II molecules, using B16-F10 cells. B16-F10 is a murine cell line on which MHC class II expression is induced upon IFN γ stimulation (Figure 1D). As in the investigation using MHC class II transfectants, DNA was readily detected on

the surface of IFN γ -stimulated B16-F10 cells after they were incubated with DNA, but not on the surface of unstimulated B16-F10 cells (Figure 1D). CIITA-knockout (KO) B16-F10 cells generated by CRISPR/Cas9 did not express MHC class II upon IFN γ stimulation. Moreover, after stimulation with IFN γ , binding of DNA on the cell surface was significantly increased in cultures with mock B16-F10 cells when compared to CIITA-KO B16-F10 cells (Figure 1E). The binding of DNA to IFN γ -stimulated CIITA-KO B16-F10 cells was at almost the same level as that to unstimulated cells (Figure 1F). These results indicate that DNA can bind to endogenously expressed MHC class II molecules as well as to transfected MHC class II molecules.

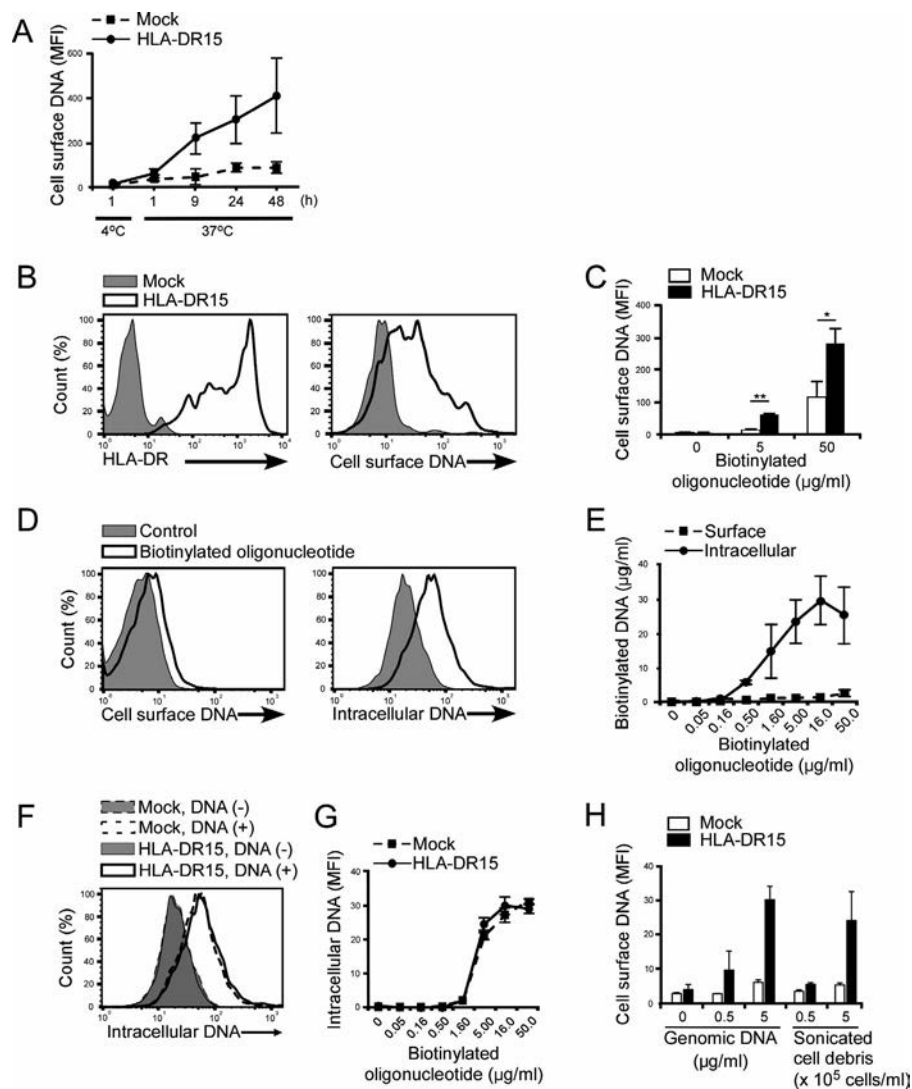


Figure 2. Internalized DNA presented on HLA class II molecules. **A**, Level of DNA on the cell surface of mock-transfected or HLA-DR15-transfected HEK 293T cells cultured with DNA for 1 hour at 4°C or for 1, 9, 24, or 48 hours at 37°C. **B** and **C**, Biotinylated DNA on the cell surface of mock-transfected or HLA-DR15-transfected B16-F10 cells incubated with biotinylated oligonucleotides, expressed as a percent determined by fluorescence-activated cell sorting (FACS) analysis (**B**) and as the mean fluorescence intensity (MFI) (**C**). **D** and **E**, DNA measured on the cell surface or intracellularly in mock-transfected HEK 293T cells in the absence or presence of biotinylated oligonucleotides, expressed as a percent determined by FACS analysis (**D**) and as the MFI (**E**). **F** and **G**, DNA measured intracellularly in mock-transfected or HLA-DR15-transfected HEK 293T cells in the absence or presence of biotinylated oligonucleotides, expressed as a percent determined by FACS analysis (**F**) and as the MFI (**G**). **H**, Level of DNA on the cell surface of mock-transfected or HLA-DR15-transfected HEK 293T cells cultured with genomic DNA or sonicated cell debris. Data in **B**, **D**, and **F** are representative of at least 3 independent experiments. Values in **A**, **C**, **E**, **G**, and **H** are the mean \pm SD. * = $P < 0.05$; ** = $P < 0.01$, by Student's *t*-test.

We next examined whether DNA directly binds to HLA class II molecules on the cell surface or whether endocytosed DNA is presented on HLA class II molecules, similar to peptide antigens. Because endocytosis is affected by temperature, HLA class II transfectants were incubated with DNA at 37°C or 4°C. DNA was detected on HLA–DR15–expressing cells when the cells were incubated with DNA at 37°C, but not at 4°C (Figure 2A). The level of cell surface DNA increased as the incubation time increased on HLA–DR15 transfectants, but remained at low levels on mock transfectants. We further addressed whether HLA class II molecules are involved in endocytosis of DNA using biotinylated oligonucleotides (5′-biotin–ATGCACTCTGCAGGCTTCTC–3′). When biotinylated oligonucleotides were incubated with HLA–DR15 transfectants, the biotinylated DNA was also detected on the cell surface of HLA–DR15–expressing cells with APC-conjugated streptavidin but not on mock transfectants (Figures 2B and C), although DNA was detected intracellularly (Figures 2D and E). There were no differences in the level of intracellular DNA between mock transfectants and HLA–DR15 transfectants

(Figures 2F and G). These results suggest that DNA does not bind directly to HLA class II molecules on the cell surface and that endocytosed DNA is presented on HLA class II molecules. In addition, HLA class II molecules themselves do not affect the endocytosis of DNA.

Because cellular DNA is complexed with certain DNA-binding proteins, such as histone, under physiologic conditions, we analyzed whether nonpurified DNA from sonicated cells was also presented on HLA class II molecules. When HLA–DR15 transfectants were incubated with sonicated HEK 293T cell debris, more DNA was detected on the surface of HLA–DR15 transfectants than on the surface of mock transfectants (Figure 2H). These results indicate that HLA class II molecules can present various types of DNA, including DNA derived from cells.

Involvement of the peptide-binding groove of HLA class II molecules in the binding of DNA. We addressed whether DNA directly binds to HLA class II molecules. Mock transfectants or HLA–DR transfectants were incubated with biotinylated

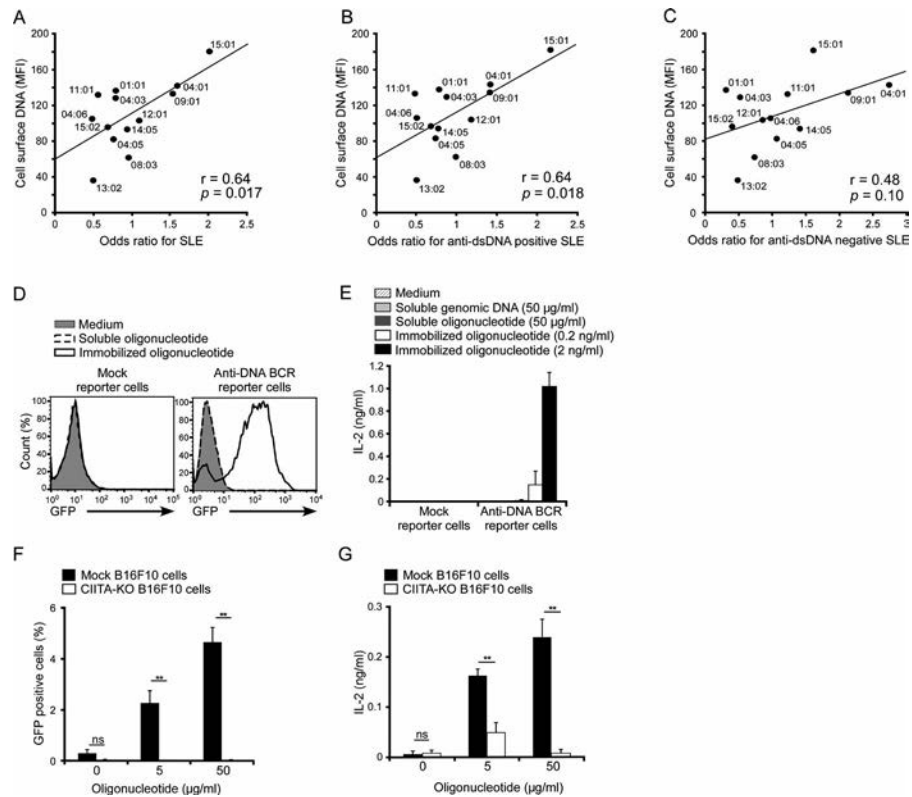


Figure 3. Efficiency of DNA binding to HLA class II molecules and activation of anti-DNA B cell receptors (BCRs) by DNA/major histocompatibility complex (MHC) class II complexes. **A–C**, Mean fluorescence intensity (MFI) of DNA binding to each HLA–DRB1 allele plotted against odds ratios for systemic lupus erythematosus (SLE) susceptibility conferred by each HLA–DRB1 allele in all SLE patients (**A**), anti-double-stranded DNA (anti-dsDNA) antibody–positive SLE patients (**B**), and anti-dsDNA antibody–negative SLE patients (**C**). **D**, Green fluorescent protein (GFP) expression in mock reporter cells or anti-DNA BCR reporter cells cultured with soluble oligonucleotide, immobilized oligonucleotide, or medium alone, determined by fluorescence-activated cell sorting. **E**, Interleukin-2 (IL-2) concentrations in culture supernatants of mock reporter cells or anti-DNA BCR reporter cells cultured with soluble genomic DNA, soluble oligonucleotide, immobilized oligonucleotide, or medium alone. **F** and **G**, Proportions of GFP-expressing reporter cells (**F**) and IL-2 concentrations in culture supernatants (**G**) when anti-DNA BCR reporter cells were cultured with mock B16-F10 cells or MHC class II transcription activator (CIITA)–knockout (KO) B16-F10 cells together with oligonucleotides and interferon- γ . Data in **A–D** are representative of at least 3 independent experiments. Values in **E–G** are the mean \pm SD. ** = $P < 0.01$ by Student's t -test. NS = not significant.

oligonucleotides. The biotinylated oligonucleotides were precipitated from the cell lysates using streptavidin-coupled Sepharose beads, and the precipitates were analyzed by Western blotting. HLA-DR was clearly detected in the precipitates of the oligonucleotides but not in those of the controls (Supplementary Figure 1A, available on the *Arthritis & Rheumatology* website at <http://online.library.wiley.com/doi/10.1002/art.41897/abstract>), suggesting that the DNA was physically associated with the HLA-DR molecules.

Next, we analyzed whether the peptide-binding groove of HLA class II molecules is involved in the binding of DNA. We examined HLA-DR15 molecules with covalently attached SP3 peptides (SP3-pep-HLA-DRB1*15:01), with high affinity for HLA-DR15 (10). Although expression levels of HLA-DR were the same in both wild-type HLA-DR15 and HLA-DR15 with SP3 peptides, the binding of DNA to the HLA-DR15-expressing cells decreased in the presence of the peptides (Supplementary Figures 1B and C). Similar results were observed in HLA-DR1 molecules with covalently attached transferrin receptor peptide (Supplementary Figures 1D and E) (6). These findings demonstrate that the peptide-binding groove of HLA class II molecules is involved in the presentation of DNA.

We further investigated the involvement of histones in the binding of DNA to HLA class II molecules (Supplementary Figures 1F and G). Although DNA was detected on the cell surface of HLA-DR15-expressing cells, histones were not detected on the cell surface, whereas histones were well detected intracellularly, suggesting that DNA binds to HLA class II molecules independently of histones.

Significant correlation of the binding of DNA to HLA-DR with the SLE susceptibility conferred by each HLA-DR allele. We addressed whether the binding of DNA to HLA-DR is associated with the risk of SLE conferred by each HLA class II allele. We analyzed the amount of cell surface DNA bound to HLA-DR with different alleles. HLA-DRB1*15:01, an SLE risk allele, exhibited the strongest binding of DNA. In contrast, DNA barely bound to HLA-DRB1*13:02, an allele that is protective against SLE. A significant positive correlation was observed between the binding of DNA to each HLA-DR allele and the odds ratio for that allele's association with SLE ($r = 0.64$, $P = 0.017$) (Figure 3A). Furthermore, when SLE patients were classified into anti-double-stranded DNA (anti-dsDNA) antibody-positive or anti-dsDNA antibody negative groups, a positive correlation was observed in the anti-dsDNA antibody-positive SLE group ($r = 0.64$, $P = 0.018$), but not in the anti-dsDNA antibody-negative SLE group ($r = 0.48$, $P = 0.10$) (Figures 3B and C). These data suggest that DNA bound to HLA class II molecules is involved in SLE pathogenesis as a target for anti-DNA antibodies.

Activation of reporter cells expressing anti-DNA BCR by cells expressing the DNA/MHC class II complex.

We analyzed whether DNA bound to MHC class II molecules is involved in the activation of B cells expressing anti-DNA BCR.

We generated a membrane form of BCR carrying the variable regions of the mAb 71F12. The 71F12 BCR was transfected into NFAT-GFP reporter cells that express both GFP and IL-2 upon receptor crosslinking (12). Anti-DNA BCR reporter cells expressed GFP and IL-2 when cultured in the presence of immobilized DNA (20-mer phosphorothioate oligonucleotides) (Figures 3D and E), but not when cultured in the presence of soluble DNA, suggesting that soluble DNA alone could not stimulate cells expressing anti-DNA BCR (Figures 3D and E). When the reporter cells were cocultured with IFN γ -stimulated B16-F10 cells in the presence of soluble DNA, they expressed GFP and IL-2 (Figures 3F and G); in contrast, they were not activated by coculture with CIITA-KO B16-F10 cells that do not express MHC class II molecules. These results suggest that anti-DNA BCRs could be activated by DNA bound to MHC class II molecules.

DISCUSSION

We demonstrated that DNA expression on the cell surface occurs through association with MHC class II molecules. The efficiency of the binding of DNA to HLA-DR alleles was significantly correlated with the odds ratios for the risk of SLE conferred by each HLA-DR allele. This indicated that individuals with HLA-DR alleles that are likely to form a complex with DNA are more susceptible to SLE than individuals with HLA-DR alleles that do not form a complex with DNA. HLA-DRB1*13:02 is a risk allele for SLE in African American individuals with anti- β_2 -glycoprotein I antiphospholipid antibody (13), although HLA-DRB1*13:02 is protective against SLE in other populations (2). DNA binding to HLA-DRB1*13:02 was minimal in the current study. These data suggest that DNA bound to HLA class II molecules is not involved in the production of anti- β_2 -glycoprotein I antiphospholipid antibody.

DNA must be incorporated into the cell by endocytosis to be presented by MHC class II molecules. Because DNA is a DAMP, endocytosed DNA might induce cellular stress. Indeed, endoplasmic reticulum (ER) stress is elevated in neutrophils from SLE patients (14). Although the effect of ER stress on antigen presentation is unclear, it might enhance DNA presentation by MHC class II molecules.

GFP reporter cells have been widely used to detect signaling from various cell surface molecules other than T cell receptor (TCR) (12). Because the reporter cells detect all the signals mediated by immunoreceptor tyrosine-based activation motif-containing adaptor molecules, we used them only to detect BCR signaling elicited by antigen recognition. We demonstrated that GFP reporter cells expressing anti-DNA BCR were activated by DNA presented on MHC class II molecules on IFN γ -stimulated B16-F10 cells. Dendritic cells have a more active physiologic role and are more potent antigen-presenting cells than B16-F10 cells. Furthermore, response of memory B cells is much higher than that of naive B cells. Therefore, dendritic cells presenting DNA might efficiently stimulate memory B cells expressing anti-DNA BCR in SLE patients.

Although the pathophysiologic function of anti-DNA antibodies has remained unclear, anti-DNA antibodies bound to DNA/HLA class II complex might induce antibody-dependent cell-mediated cytotoxicity to cause tissue damage.

DNA complexed with HLA class II molecules might exhibit a novel antigenicity for producing anti-DNA antibody. However, we could not induce anti-DNA antibody production by simply immunizing mice with transfectants expressing DNA and MHC class II complexes (data not shown). Therefore, certain unknown factors might be required for anti-DNA production, in addition to DNA/HLA class II complex. DNA-reactive CD4⁺ T cells could be involved in anti-DNA antibody production. However, the TCR recognizing DNA has not been reported (3). Therefore, there is a possibility that bystander T cells recognizing certain antigens other than DNA might be involved in anti-DNA IgG production (15). Alternatively, it is possible that certain peptides containing CD4⁺ T cell epitopes might be associated with DNA, and the DNA/peptide complex presented on HLA class II molecules could be involved in anti-DNA antibody production through activation of CD4⁺ helper T cells. Further studies are required to elucidate how DNA/HLA class II complexes could be involved in anti-DNA antibody production.

ACKNOWLEDGMENT

We thank C. Kita for secretarial assistance.

AUTHOR CONTRIBUTIONS

All authors were involved in drafting the article or revising it critically for important intellectual content, and all authors approved the final version to be published. Dr. H. Arase had full access to all of the data in the study and takes responsibility for the integrity of the data and the accuracy of the data analysis.

Study conception and design. Tsuji, Ohmura, H. Arase.

Acquisition of data. Tsuji, Jin, Naito, Kochi, Okada, H. Arase.

Analysis and interpretation of data. Tsuji, Ohmura, Jin, Naito, N. Arase, Kohyama, Suenaga, Sakakibara, Kochi, Okada, Yamamoto, Kikutani, Morinobu, Mimori, H. Arase.

REFERENCES

1. Rekvig OP. The anti-DNA antibody: origin and impact, dogmas and controversies [review]. *Nat Rev Rheumatol* 2015;11:530–40.
2. Shimane K, Kochi Y, Suzuki A, Okada Y, Ishii T, Horita T, et al. An association analysis of HLA-DRB1 with systemic lupus erythematosus and rheumatoid arthritis in a Japanese population: effects of *09:01 allele on disease phenotypes. *Rheumatology (Oxford)* 2013;52:1172–82.
3. Filaci G, Grasso I, Vignola S, Imro MA, Scudeletti M, Puppo F, et al. DsDNA-specific T-cell lines in systemic lupus erythematosus patients: data suggesting their oligoclonality. *Ann N Y Acad Sci* 1995;756:428–31.
4. Jin H, Arase N, Hirayasu K, Kohyama M, Suenaga T, Saito F, et al. Autoantibodies to IgG/HLA class II complexes are associated with rheumatoid arthritis susceptibility. *Proc Natl Acad Sci U S A* 2014;111:3787–92.
5. Tanimura K, Jin H, Suenaga T, Morikami S, Arase N, Kishida K, et al. β 2-glycoprotein I/HLA class II complexes are novel autoantigens in antiphospholipid syndrome. *Blood* 2015;125:2835–44.
6. Hiwa R, Ohmura K, Arase N, Jin H, Hirayasu K, Kohyama M, et al. Myeloperoxidase/HLA class II complexes recognized by autoantibodies in microscopic polyangiitis. *Arthritis Rheumatol* 2017;69:2069–80.
7. Kambayashi T, Laufer TM. Atypical MHC class II-expressing antigen-presenting cells: can anything replace a dendritic cell? [review]. *Nat Rev Immunol* 2014;14:719–30.
8. Cheah PL, Looi LM, Chua CT, Yap SF, Fleming S. Enhanced major histocompatibility complex (MHC) class II antigen expression in lupus nephritis. *Malays J Pathol* 1997;19:115–20.
9. Wen S, He F, Zhu X, Yuan S, Liu H, Sun L. IFN- γ , CXCL16, uPAR: potential biomarkers for systemic lupus erythematosus. *Clin Exp Rheumatol* 2018;36:36–43.
10. Vogt AB, Kropshofer H, Kalbacher H, Kalbus M, Rammensee HG, Coligan JE, et al. Ligand motifs of HLA-DRB5*0101 and DRB1*1501 molecules delineated from self-peptides. *J Immunol* 1994;153:1665–73.
11. Sakakibara S, Arimori T, Yamashita K, Jinzai H, Motooka D, Nakamura S, et al. Clonal evolution and antigen recognition of anti-nuclear antibodies in acute systemic lupus erythematosus. *Sci Rep* 2017;7:16428.
12. Arase H, Mocarski ES, Campbell AE, Hill AB, Lanier LL. Direct recognition of cytomegalovirus by activating and inhibitory NK cell receptors. *Science* 2002;296:1323–6.
13. Arnett FC, Thiagarajan P, Ahn C, Reveille JD. Associations of anti- β 2-glycoprotein I autoantibodies with HLA class II alleles in three ethnic groups. *Arthritis Rheum* 1999;42:268–74.
14. Sule G, Abuaita BH, Steffes PA, Fernandes AT, Estes SK, Dobry C, et al. Endoplasmic reticulum stress sensor IRE1 α propels neutrophil hyperactivity in lupus. *J Clin Invest* 2021;131:e137866.
15. Horwitz MS, Bradley LM, Harbertson J, Krahl T, Lee J, Sarvetnick N. Diabetes induced by Coxsackie virus: initiation by bystander damage and not molecular mimicry. *Nat Med* 1998;4:781–5.

Phase III/IV, Randomized, Fifty-Two-Week Study of the Efficacy and Safety of Belimumab in Patients of Black African Ancestry With Systemic Lupus Erythematosus

Ellen Ginzler,¹ Luiz Sergio Guedes Barbosa,² David D'Cruz,³ Richard Furie,⁴  Kathleen Maksimowicz-McKinnon,⁵ James Oates,⁶ Mittermayer Barreto Santiago,⁷  Amit Saxena,⁸ Saira Sheikh,⁹  Damon L. Bass,¹⁰ Susan W. Burris,¹⁰ Jennifer A. Gilbride,¹¹ James G. Groark,¹⁰ Michelle Miller,¹⁰ Amy Pierce,¹² David A. Roth,¹⁰ and Beulah Ji¹³

Objective. Enrollment of patients of Black African ancestry with systemic lupus erythematosus (SLE) in phase II and phase III of the belimumab trials was not reflective of the racial distribution observed in the lupus population. This study was undertaken to assess the efficacy and safety of intravenous (IV) belimumab plus standard therapy in patients of self-identified Black race.

Methods. EMBRACE (GSK Study BEL115471; ClinicalTrials.gov identifier: NCT01632241) was a 52-week multi-center, double-blind, placebo-controlled trial in adults of self-identified Black race with active SLE who received monthly belimumab 10 mg/kg IV, or placebo, plus standard therapy. The optional 26-week open-label extension phase included patients who completed the double-blind phase. The primary end point of the study was SLE Responder Index (SRI) response rate at week 52 with modified proteinuria scoring adapted from the SLE Disease Activity Index 2000 (SLEDAI-2K) (SRI-SLEDAI-2K). Key secondary end points included SRI response rate at week 52, time to first severe SLE flare, and reductions in prednisone dose.

Results. The modified intent-to-treat population comprised 448 patients, of whom 96.9% were women and the mean \pm SD age was 38.8 ± 11.42 years. The primary end point (improvement in the SRI-SLEDAI-2K response rate at week 52) was not achieved (belimumab 48.7%, placebo 41.6%; odds ratio 1.40 [95% confidence interval 0.93, 2.11], $P = 0.1068$); however, numerical improvements favoring belimumab were observed, in which the SRI-SLEDAI-2K response rates were higher in those who received belimumab compared with those who received placebo, especially in patients with SLE who had high disease activity or renal manifestations at baseline. The safety profile of belimumab was generally consistent with that observed in previous SLE trials. Adverse events were the primary reasons for double-blind phase withdrawals (belimumab 5.4%, placebo 6.7%).

Conclusion. The primary end point of this study was not achieved, but improvement with belimumab versus placebo was observed, suggesting that belimumab remains a suitable treatment option for SLE management in patients of Black African ancestry.

ClinicalTrials.gov identifier: NCT01632241.

Supported by GlaxoSmithKline (GSK Study BEL115471).

¹Ellen Ginzler, MD, MPH: State University of New York (SUNY) Downstate Health Sciences University, New York; ²Luiz Sergio Guedes Barbosa, MD: Núcleo de Terapia Especializada em Cancerologia (NUTEC), Cuiaba, Brazil; ³David D'Cruz, MD: Guy's Hospital, London, UK; ⁴Richard Furie, MD: Northwell Health, Great Neck, New York; ⁵Kathleen Maksimowicz-McKinnon, DO: Henry Ford Health System, Detroit, Michigan; ⁶James Oates, MD: Medical University of South Carolina and Ralph H. Johnson VA Medical Center, Charleston, South Carolina; ⁷Mittermayer Barreto Santiago, MD: Escola Bahiana de Medicina e Saúde Pública, Salvador Bahia, Brazil; ⁸Amit Saxena, MD: NYU Grossman School of Medicine, New York; ⁹Saira Sheikh, MD: University of North Carolina, Chapel Hill; ¹⁰Damon L. Bass, DO, Susan W. Burris, MSc, James G. Groark, MD, Michelle Miller, MSc, David A. Roth, MD: GlaxoSmithKline, Collegeville, Pennsylvania; ¹¹Jennifer A. Gilbride, MSc: GlaxoSmithKline, Stevenage, UK; ¹²Amy Pierce, BS: Viiv Healthcare, Research Triangle, North Carolina; ¹³Beulah Ji, MD: GlaxoSmithKline, Uxbridge, UK.

Dr. Ginzler has received consulting fees from Janssen (less than \$10,000) and grant support from GlaxoSmithKline, Aurinia, and Genentech. Dr. D'Cruz has received consulting fees and/or honoraria from GlaxoSmithKline. Dr. Furie has received consulting fees from GlaxoSmithKline (less than \$10,000) and grant support from GlaxoSmithKline. Dr. Maksimowicz-McKinnon has received consulting fees and/or honoraria from ChemoCentryx (less than \$10,000). Dr. Saxena has received consulting fees from GlaxoSmithKline, Bristol Myers Squibb, and AstraZeneca (less than \$10,000 each). Dr. Sheikh has received consulting fees from GlaxoSmithKline (less than \$10,000) and has received grant support from Pfizer. Ms. Pierce owns stock or stock options in GlaxoSmithKline. Drs. Bass, Groark, Roth, and Ji and Mses. Burris, Gilbride, and Miller own stock or stock options in GlaxoSmithKline. No other disclosures relevant to this article were reported.

Address correspondence to Damon L. Bass, DO, 1250 South Collegeville Road, Collegeville, PA 19426. Email: damon.l.bass@gsk.com.

Submitted for publication December 3, 2020; accepted in revised form June 10, 2021.

INTRODUCTION

Systemic lupus erythematosus (SLE) is a chronic autoimmune disease that affects multiple organs, including skin, joints, heart, lungs, and kidney (1,2). Black African ancestry is associated with a higher prevalence of SLE, greater disease severity, an increased risk of cardiovascular events, more end-organ damage, and higher mortality rates, compared with a White racial background (3–10).

Belimumab is a human monoclonal antibody that binds to and inhibits the biologic activity of the B lymphocyte stimulator, which plays a key role in B cell selection and differentiation (11,12). The efficacy and safety of intravenous (IV) and subcutaneous belimumab have been demonstrated in phase II and III studies of SLE (13–16). Due to underrepresentation of patients of Black African ancestry in these trials, underpowered subgroup analyses of this population yielded conflicting efficacy data between the phase II and III studies. Post hoc analysis of the phase II study data demonstrated an improved Safety of Estrogens in Lupus Erythematosus National Assessment version of the SLE Disease Activity Index (SELENA–SLEDAI) response in patients of Black African ancestry who received belimumab compared with those who received placebo (17). In contrast, post hoc analysis of pooled data from 2 pivotal phase III studies showed that patients of Black African ancestry had a higher SLE Responder Index (SRI) response rate at week 52 with placebo compared with belimumab (18).

The 52-week EMBRACE study investigated the efficacy and safety of belimumab 10 mg/kg IV plus standard therapy compared with placebo plus standard therapy in adults with SLE of self-identified Black race. This report presents results of the efficacy and safety end point analyses from data collected up to the week 52 visit of the double-blind phase, and

the subsequent 24-week open-label extension phase of EMBRACE. Additionally, results presented include subgroup analyses.

PATIENTS AND METHODS

Study design. EMBRACE (GSK Study BEL115471; ClinicalTrials.gov identifier: NCT01632241) was a phase III/IV, multicenter, randomized, double-blind, placebo-controlled, 52-week study (Figure 1) conducted at 88 centers in Brazil, Colombia, France, South Africa, the UK, and the US. The study consisted of a screening phase of up to 5 weeks and a 52-week double-blind phase (date of initiation [first patient's first visit] February 19, 2013; date of double-blind end point analysis June 18, 2018), followed by an optional 6-month open-label extension phase.

Patients. Full selection criteria are provided in the Supplementary Material (available on the *Arthritis & Rheumatology* website at <http://onlinelibrary.wiley.com/doi/10.1002/art.41900/abstract>). Briefly, for inclusion in the double-blind phase, patients had to be age ≥ 18 years and of self-identified Black race, with a SELENA–SLEDAI score of ≥ 8 at the time of screening and positivity for antinuclear antibodies (titer $\geq 1:80$ and/or anti-double-stranded DNA ≥ 30 IU/ml). Key exclusion criteria included previous treatment with belimumab, severe lupus kidney disease or active nephritis, or central nervous system lupus.

All patients provided written informed consent prior to enrollment. Approval was obtained for all study sites from the ethics committee or institutional review board (IRB) (IRB HGS1006-C1112/tracking QUI1-12-249). The study was conducted in accordance with the ethics principles of the Declaration of Helsinki (19), the International Council for Harmonisation Guidelines for Good Clinical Practice, and any applicable country-specific regulatory

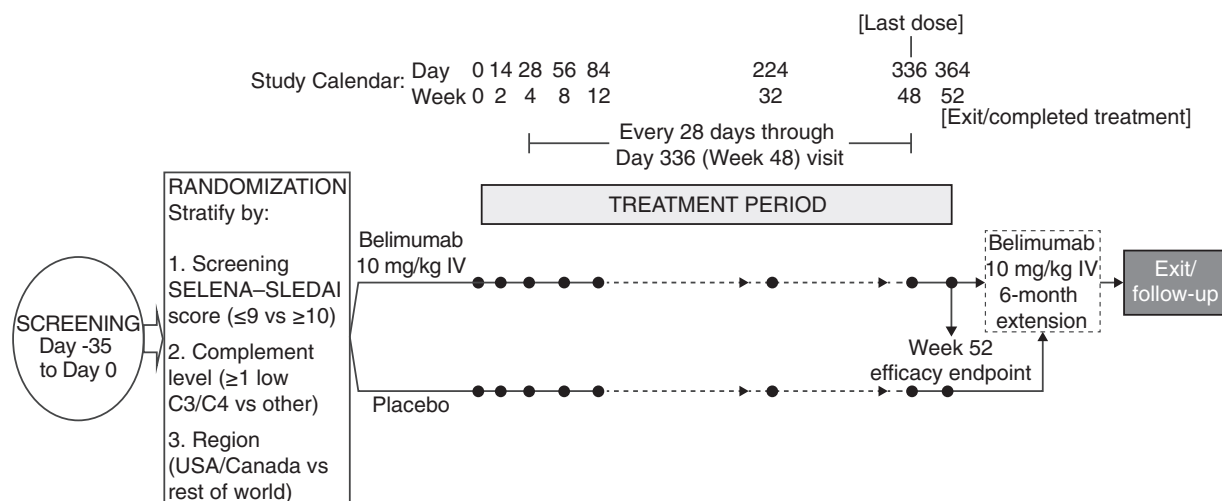


Figure 1. Study design. SELENA–SLEDAI = Safety of Estrogens in Lupus Erythematosus National Assessment–Systemic Lupus Erythematosus Disease Activity Index; IV = intravenous.

requirements. The reporting of this study conforms to the Consolidated Standards of Reporting Trials 2010 guidelines (20).

Randomization and treatment. Using an interactive voice/web response system, patients receiving standard therapy were randomized 2:1 to receive either belimumab 10 mg/kg IV or placebo, which was administered on days 0, 14, and 28 and every 28 days thereafter up to week 48, with a final evaluation at week 52. Randomization was stratified by screening SELENA-SLEDAI score (≤ 9 versus ≥ 10), region (US/Canada versus rest of world), and complement level (≥ 1 test finding showing low C3/C4 [less than the lower limit of normal] versus C3/C4 other [the lower limit of normal or above]). Detailed randomization data are provided in Supplementary Material (<http://onlinelibrary.wiley.com/doi/10.1002/art.41900/abstract>).

Patients who successfully completed the initial 52-week double-blind phase could enter an optional 6-month open-label extension phase, during which they received belimumab 10 mg/kg IV every 28 days plus standard therapy, irrespective of their previous study assignment. The first dose was given at the week 52 (day 364) visit of the double-blind period (day 1 of the open-label extension phase). Patients who completed the 52-week double-blind phase, but did not enter the 6-month open-label extension phase, were required to return for an additional follow-up visit 8 weeks after their last dose. Patients who withdrew early were required to return for an exit visit 4 weeks after their last dose and a follow-up visit 8 weeks after their last dose.

The original protocol plan was to randomize 816 patients, providing $\geq 90\%$ power to detect $\geq 12\%$ absolute improvement in the SRI response rate in the belimumab group compared with the placebo group at a 5% significance level. Due to enrollment challenges, a revised sample size was calculated to include 501 patients (≥ 334 patients in the belimumab group and ≥ 167 patients in the placebo group). This sample size provided $\geq 90\%$ power to detect a minimum 15.55% absolute improvement in SRI-SLEDAI-2K response rate in the belimumab group relative to the placebo group at a 5% significance level (based on the pooled data from efficacy studies BEL112341 and BEL113750) (15,21). These calculations assumed a placebo response rate of 43.95% at week 52.

Study end points and assessments. The primary efficacy end point was the SRI-SLEDAI-2K response rate (defined in the Supplementary Material) at week 52 of the double-blind phase. Unlike in the phase II and phase III studies, the SRI-SLEDAI-2K was selected because of the simplification it offers in proteinuria assessment as compared with the SELENA-SLEDAI proteinuria component; both are clinically meaningful (22). The primary efficacy end point for the open-label extension phase was SRI-SLEDAI-2K response rate at open-label extension week 24. If the open-label extension week 24 data were missing, data from the open-label extension week 28/exit

visit were used. This time point is referred to as “open-label extension week 24” throughout the text. Data related to the primary efficacy end point, e.g., the response rate over time, percentage of patients with a durable SRI-SLEDAI-2K response from week 44 through week 52, time to first SRI-SLEDAI-2K response that was maintained through week 52, and duration of longest SRI-SLEDAI-2K response among patients with ≥ 1 SRI-SLEDAI-2K responses were summarized.

The key secondary end points were SRI-SELENA-SLEDAI at week 52 (open-label extension week 24), time to first severe SLE flare (measured by the SELENA-SLEDAI flare index [SFI]), and proportion of patients whose average prednisone dose had been reduced by $\geq 25\%$ from baseline to ≤ 7.5 mg/day during week 40 through week 52 (open-label extension week 28/exit visit), in patients receiving >7.5 mg/day at baseline. Key renal end points included time to first renal flare over 52 weeks and over 28 weeks in the open-label extension, SELENA-SLEDAI-SLEDAI-2K renal domain improvement at week 52, SELENA-SLEDAI-SLEDAI-2K renal domain worsening at week 52, percentage reduction in proteinuria by visit and at week 52 and open-label extension week 24 and week 28/exit visit among those with baseline proteinuria >0.5 gm/24 hours, and proteinuria shift at week 52 and open-label extension week 24 and week 28/exit visit among those with baseline proteinuria >0.5 gm/24 hours. Renal flare is defined in the Supplementary Material (<http://onlinelibrary.wiley.com/doi/10.1002/art.41900/abstract>).

Biomarkers measured included percentage changes in serum IgG level, anti-dsDNA antibody level (in those who were anti-dsDNA positive [≥ 30 IU/ml] at baseline), and complement (C3 and C4) levels from baseline. Safety was evaluated by monitoring adverse events (AEs), serious AEs (SAEs), AEs of special interest, vital signs, clinical laboratory test results, and immunogenicity up to 8 weeks posttreatment and throughout the open-label extension phase.

Data analyses. For the double-blind phase, safety analyses were performed on the safety population, defined as all patients who were randomized and treated with at least 1 dose of investigational product. Data on the safety population were summarized according to the treatment the patient was randomized to receive rather than by the treatment that was received, but both were the same for this study. Efficacy analyses were performed on the modified intent-to-treat (ITT) population, defined as the safety population minus those patients who had any assessment at any of 3 study sites that were excluded from the efficacy analyses before the database lock because of potential Good Clinical Practice noncompliance.

For analysis of the primary and 3 key secondary efficacy end points, a step-down sequential testing procedure was used as described in the Supplementary Material. The following subgroup analyses were performed for the primary analysis (SRI-SLEDAI-2K response at week 52): region (US/Canada versus rest of

world), baseline SELENA-SLEDAI-SLEDAI-2K score (≤ 9 versus ≥ 10), baseline anti-dsDNA antibody level (≥ 30 IU/ml versus < 30 IU/ml), baseline complement levels (≥ 1 test finding showing low C3/C4 [less than the lower limit of normal] versus C3/C4 other [the lower limit of normal or above]), and baseline complement and anti-dsDNA antibody levels (≥ 1 test finding showing low C3/C4 and anti-dsDNA ≥ 30 IU/ml versus C3/C4 other and anti-dsDNA ≥ 30 IU/ml). The odds of an SRI-SLEDAI-2K response with belimumab treatment versus placebo were estimated using logistic regression analysis.

For the open-label extension phase, all patients received belimumab, no formal statistical hypothesis testing was completed, and all analyses using descriptive statistics were exploratory in nature. Safety analyses were performed on the ITT population, defined as all randomized patients who received ≥ 1 dose of treatment (i.e., at double-blind week 52/open-label extension day 1 or a later open-label extension visit). Efficacy analyses were

performed on the open-label extension modified ITT population, excluding the same patients as described above for the modified ITT population in the double-blind phase.

Data availability. Anonymized individual participant data and study documents can be requested for further research at <http://www.clinicalstudydatarequest.com>.

RESULTS

Patient population. In total, 503 patients were randomized, of whom 496 received at least 1 dose of investigational product (safety population), and 448 comprised the modified ITT population that was included in the efficacy analyses. Three hundred forty-five patients in the modified ITT population completed the 52-week double-blind phase; 334 entered the open-label extension phase, and 313 completed the 6-month open-label

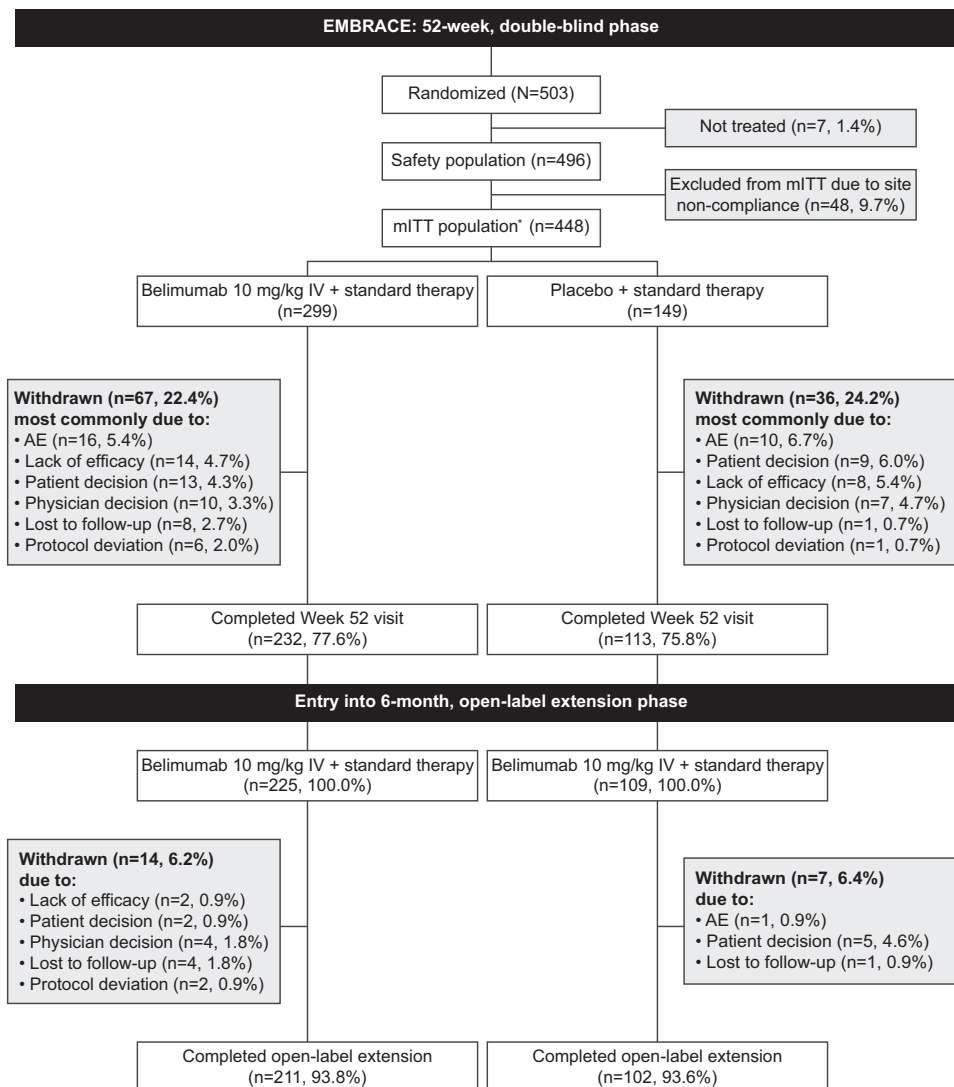


Figure 2. Flow chart of patient disposition. * The modified intent-to-treat (mITT) population consisted of all patients who were randomized and received ≥ 1 dose of the study agent (48 patients were excluded from efficacy analyses due to noncompliance). IV = intravenous; AE = adverse event.

extension phase (Figure 2). The most frequent reasons for withdrawal in the double-blind safety population were AEs (5.8%), patient decision (4.8%), and lack of efficacy (4.8%). In the open-label extension modified ITT population, study closure/termination due to noncompliance at the aforementioned 3 study sites was the main reason for withdrawal (2.8%), followed by patient decision (1.9%), physician decision, and lost to follow-up (both 1.4%).

Patient demographics and baseline characteristics of the modified ITT population were generally similar between treatment

groups and were representative of this type of study design (Table 1 and Supplementary Table 1, available on the *Arthritis & Rheumatology* website at <http://onlinelibrary.wiley.com/doi/10.1002/art.41900/abstract>). In the double-blind phase, patients had a mean \pm SD age of 38.8 ± 11.4 years, 7 patients (1.6%) were age ≥ 65 years, and 96.9% were women.

Baseline disease activity was similar between treatment groups (Table 1), except for a slightly lower percentage of patients in the placebo group with ≥ 1 British Isles Lupus Assessment Group A organ domain involvement (23) (belimumab 17.4%,

Table 1. Patient demographics and baseline characteristics in the modified ITT population*

	Double-blind phase		Open-label extension phase	
	Belimumab, 10 mg/kg IV (n = 299)	Placebo (n = 149)	Continuous belimumab, 10 mg/kg IV (n = 225)	Placebo-to-belimumab, 10 mg/kg IV (n = 109)
Female	290 (97.0)	144 (96.6)	219 (97.3)	107 (98.2)
Age, mean \pm SD years	38.6 \pm 11.1	39.3 \pm 12.2	39.4 \pm 10.6	41.6 \pm 12.1
Race				
Black African ancestry or African American	293 (98.0)	143 (96.0)	220 (97.8)	103 (94.5)
Multiple	6 (2.0)	6 (4.0)	5 (2.2)	6 (5.5)
Region				
US/Canada	131 (43.8)	65 (43.6)	96 (42.7)	44 (40.4)
Rest of world	168 (56.2)	84 (56.4)	129 (57.3)	65 (59.6)
BMI, mean \pm SD kg/m ²	29.46 \pm 7.38†	28.97 \pm 6.96‡	29.48 \pm 7.09§	29.62 \pm 7.02¶
SLE disease duration, mean \pm SD years#	7.3 \pm 7.08**	6.9 \pm 7.38	7.5 \pm 7.29	8.2 \pm 8.03
BILAG organ domain involvement††				
≥ 1 A or 2B	215 (71.9)	107 (71.8)	170 (75.6)	25 (22.9)
≥ 1 A	52 (17.4)	16 (10.7)	42 (18.7)	5 (4.6)
≥ 1 B	273 (91.3)	140 (94.0)	204 (90.7)	51 (46.8)
No A or B	14 (4.7)	4 (2.7)	10 (4.4)	56 (51.4)
SELENA-SLEDAI category				
≤ 9	146 (48.8)	59 (39.6)	109 (48.4)	87 (79.8)
10–11	77 (25.8)	46 (30.9)	56 (24.9)	9 (8.3)
≥ 12	76 (25.4)	44 (29.5)	60 (26.7)	13 (11.9)
SELENA-SLEDAI, mean \pm SD	9.9 \pm 3.52	10.2 \pm 2.90	9.9 \pm 3.31	5.5 \pm 4.20
SELENA-SLEDAI-SLEDAI-2K category				
≤ 9	141 (47.2)	56 (37.6)	106 (47.1)	86 (78.9)
10–11	74 (24.7)	45 (30.2)	53 (23.6)	9 (8.3)
≥ 12	84 (28.1)	48 (32.2)	66 (29.3)	14 (12.8)
SELENA-SLEDAI-SLEDAI-2K score, mean \pm SD	10.2 \pm 3.68	10.5 \pm 3.08	10.2 \pm 3.52	5.7 \pm 4.20
≥ 1 test finding of low C3/C4	108 (36.1)	57 (38.3)	79 (35.1)	34 (31.2)
Anti-dsDNA ≥ 30 IU/ml	181 (60.5)	99 (66.4)	135 (60.0)	63 (57.8)
≥ 1 test finding of low C3/C4 and anti-dsDNA ≥ 30 IU/ml	91 (30.4)	50 (33.6)	66 (29.3)	30 (27.5)
Renal involvement (SLEDAI-2K organ domain)	55 (18.4)	34 (22.8)	39 (17.3)	21 (19.3)
Proteinuria >0.5 gm/24 hours	53 (17.7)	33 (22.1)	37 (16.4)	22 (20.2)
Average prednisone equivalent dose				
0 mg/day	53 (17.7)	22 (14.8)	–	–
0–7.5 mg/day	62 (20.7)	32 (21.5)	–	–
>7.5 mg/day	184 (61.5)	95 (63.8)	–	–

(Continued)

Table 1. (Cont'd)

	Double-blind phase		Open-label extension phase	
	Belimumab, 10 mg/kg IV (n = 299)	Placebo (n = 149)	Continuous belimumab, 10 mg/kg IV (n = 225)	Placebo-to-belimumab, 10 mg/kg IV (n = 109)
Prednisone dose, mean \pm SD mg/day	12.1 \pm 10.71	12.2 \pm 9.95	-	-
Patients receiving treatment				
Steroids	246 (82.3)	127 (85.2)	-	-
Antimalarials	237 (79.3)	124 (83.2)	-	-
Immunosuppressants	167 (55.9)	88 (59.1)	-	-
Aspirin	40 (13.4)	33 (22.1)	-	-
NSAIDs	62 (20.7)	20 (13.4)	-	-
Steroids, immunosuppressants, and antimalarials	113 (37.8)	58 (38.9)	-	-
Steroids and antimalarials only	84 (28.1)	45 (30.2)	-	-
Steroids and immunosuppressants only	28 (9.4)	18 (12.1)	-	-
Steroids only	21 (7.0)	6 (4.0)	-	-
Antimalarials only	25 (8.4)	10 (6.7)	-	-
Immunosuppressants and antimalarials only	15 (5.0)	11 (7.4)	-	-
Immunosuppressants only	11 (3.7)	1 (0.7)	-	-

* Except where indicated otherwise, values are the number (%). Low C3/C4 is defined as less than the lower limit of normal (<90 mg/dl for C3 and <10 mg/dl for C4). ITT = intent-to-treat; IV = intravenous; BMI = body mass index; SLE = systemic lupus erythematosus; BILAG = British Isles Lupus Assessment Group; SELENA-SLEDAI = Safety of Estrogens in Lupus Erythematosus National Assessment-SLE Disease Activity Index; SLEDAI-2K = SLE Disease Activity Index 2000; anti-dsDNA = anti-double-stranded DNA; NSAIDs = nonsteroidal antiinflammatory drugs.

† n = 229.

‡ n = 115.

§ n = 176.

¶ n = 83.

Defined as (treatment start date - SLE diagnosis date + 1)/365.25.

** n = 298.

†† Patients may have been included in >1 category.

placebo 10.7%). There were unexpected imbalances in baseline SELENA-SLEDAI scores and SELENA-SLEDAI-SLEDAI-2K scores, with a larger proportion of patients in the belimumab group having SELENA-SLEDAI scores ≤ 9 (belimumab 48.8%, placebo 39.6%) and SELENA-SLEDAI-SLEDAI-2K scores ≤ 9 (belimumab 47.2%, placebo 37.6%).

Efficacy results. The SRI-SLEDAI-2K response rate at week 52, the primary efficacy end point of the double-blind phase, was numerically but not statistically greater in the belimumab group (48.7%) compared with the placebo group (41.6%) (odds ratio 1.40 [95% confidence interval 0.93, 2.11], $P = 0.1068$). Over time, the SRI-SLEDAI-2K (or SRI-SELENA-SLEDAI) response rates were consistently greater in the belimumab group compared with the placebo group, starting at week 28 (Supplementary Figures 1A and B, <http://onlinelibrary.wiley.com/doi/10.1002/art.41900/abstract>). The SRI-SLEDAI-2K response rate at open-label extension week 24, the primary efficacy end point of the open-label extension phase, was 73.6% and 18.8% in the continuous belimumab group and the placebo-to-belimumab group, respectively, since the start of belimumab treatment (i.e., over 76 weeks in the continuous belimumab group and 24 weeks in the placebo-to-belimumab group). Components of the primary

end point of the double-blind and open-label extension phases are shown in Figure 3.

A durable SRI-SLEDAI-2K response from week 44 through week 52 was achieved by 126 patients (42.3%) in the belimumab group and 48 patients (32.2%) in the placebo group (odds ratio 1.66 [95% confidence interval 1.08, 2.56], $P = 0.0209$). The 25th percentile of the time to SRI-SLEDAI-2K response maintained until week 52 was 116 days (16.6 weeks) in the belimumab group and 204 days (29.1 weeks) in the placebo group (hazard ratio 1.41 [95% confidence interval 1.04, 1.90], $P = 0.0256$) (Supplementary Figure 2, <http://onlinelibrary.wiley.com/doi/10.1002/art.41900/abstract>). The mean \pm SD duration of longest SRI-SLEDAI-2K response among patients with ≥ 1 response was longer in the belimumab group (172.9 \pm 115.65 days [24.7 weeks]) compared with the placebo group (139.1 \pm 110.08 days [19.9 weeks]), resulting in an adjusted treatment difference of 40.10 days (95% confidence interval 14.74, 65.46, $P = 0.0020$).

Since the primary end point did not meet statistical significance, key secondary end points in the prespecified sequence (SRI-SELENA-SLEDAI response, time to first severe SFI flare, and prednisone use) could not be declared as statistically significant. The percentage of SRI-SELENA-SLEDAI responders is presented in the Supplementary Material and in Supplementary

Figure 1B (<http://onlinelibrary.wiley.com/doi/10.1002/art.41900/abstract>). The SELENA–SLEDAI–SLEDAI-2K change from baseline over time is shown in Supplementary Figure 3 (<http://onlinelibrary.wiley.com/doi/10.1002/art.41900/abstract>).

Over the 52-week double-blind phase, patients in the belimumab group had a 23% lower risk of experiencing a severe SFI flare than those in the placebo group (hazard ratio 0.77 [95% confidence interval 0.51, 1.17], $P = 0.2264$). Among patients experiencing a severe SFI flare (58 of 299 [19.4%] in the belimumab group; 37 of 149 [24.8%] in the placebo group), the median time to first severe SFI flare was similar between the belimumab and placebo groups (study day 176 in the belimumab group

versus study day 175 in the placebo group). During the open-label extension phase, 4.0% of patients (9 of 225) and 5.5% of patients (6 of 109) in the continuous belimumab and placebo-to-belimumab groups, respectively, experienced a severe SFI flare.

There was no forced steroid tapering in this study. At baseline, 279 patients (modified ITT population; 184 in the belimumab group and 95 in the placebo group) received prednisone at >7.5 mg/day. Of these patients, 27 (14.7%) in the belimumab group and 12 (12.6%) in the placebo group achieved a reduction in prednisone dose by $\geq 25\%$ from baseline to ≤ 7.5 mg/day during week 40 to week 52 of the double-blind phase (odds ratio 1.30 [95% confidence interval 0.61, 2.80], $P = 0.4996$). In the open-

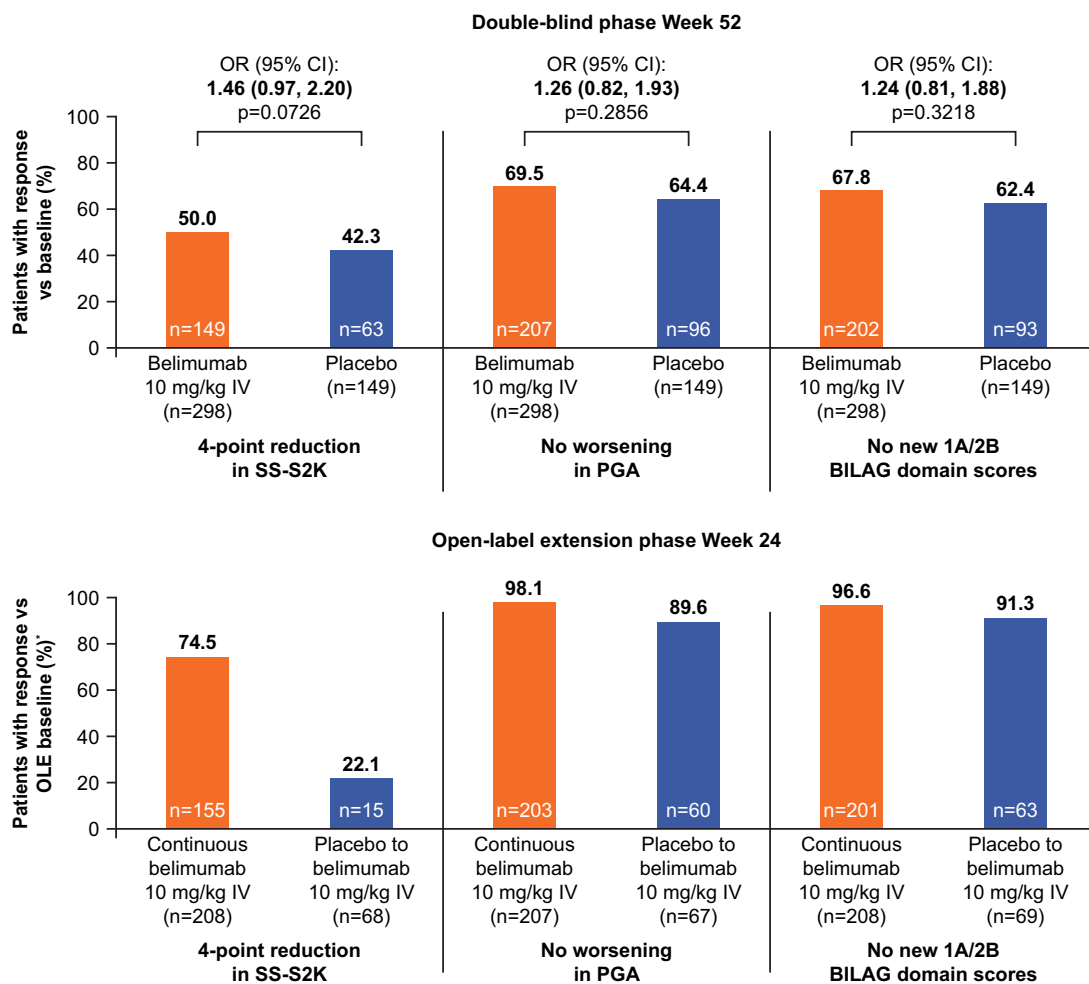


Figure 3. Response rates based on the 3 individual components of the Systemic Lupus Erythematosus (SLE) Responder Index–SLE Disease Activity Index 2000 (SLEDAI-2K) response, with modified SLEDAI scoring for proteinuria, at week 52 of the double-blind phase and at week 24 of the open-label extension (OLE) phase in the modified intent-to-treat population. Odds ratios (ORs) with 95% confidence intervals (95% CIs) and P values were derived using a logistic regression model to compare belimumab with placebo, with covariates of treatment group, baseline Safety of Estrogens in Lupus Erythematosus National Assessment–SLEDAI (SELENA–SLEDAI)–SLEDAI-2K (SS-S2K) score (≤ 9 versus ≥ 10), baseline complement levels (≥ 1 test finding showing low C3/C4 [less than the lower limit of normal] versus C3/C4 other [the lower limit of normal or above]), and region (US/Canada versus rest of world). The open-label extension phase used observed data, and the double-blind phase used nonresponder imputation for withdrawals or treatment failures. The OR was not calculated for the open-label extension phase, as no formal hypothesis testing was performed. * Open-label extension baseline (pre-belimumab) was used for the SELENA–SLEDAI–SLEDAI-2K analysis, with modified SLEDAI scoring for proteinuria, of the open-label extension phase. Patients in the continuous belimumab group received belimumab for 18 months, and those in the placebo-to-belimumab group received belimumab for 6 months. IV = intravenous; PGA = physician global assessment; BILAG = British Isles Lupus Assessment Group.

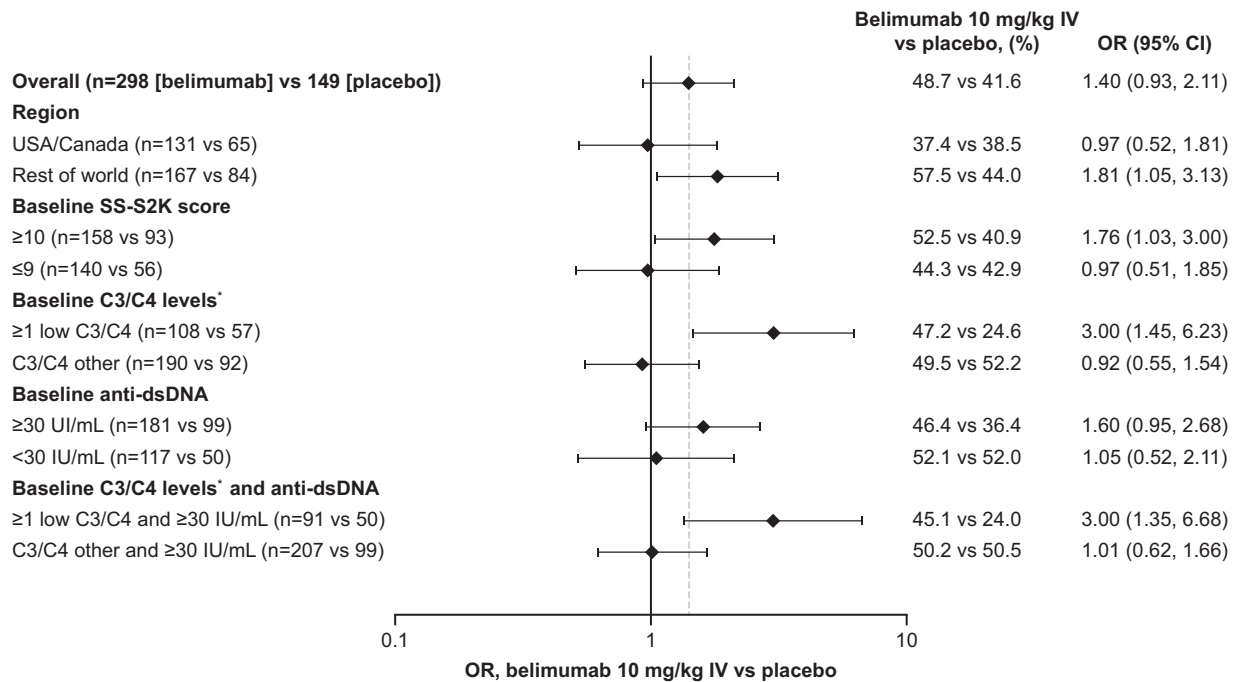


Figure 4. Subgroup analysis of SLE Responder Index–SLEDAI-2K (SS-S2K) response rates at week 52. * Low C3/C4 is defined as C3/C4 levels less than the lower limit of normal (<90 mg/dl for C3 and <10 mg/dl for C4), and C3/C4 other is defined as levels at the lower limit of normal or above. Anti-dsDNA = anti-double-stranded DNA (see Figure 3 for other definitions).

label extension phase, 31.9% of patients (44 of 138) in the continuous belimumab group had achieved a reduction in prednisone dose to ≤7.5 mg/day compared with the start of the double-blind phase, whereas 14.8% of patients (8 of 54) in the placebo-to-belimumab group achieved this compared with the start of the open-label extension phase.

Subgroup analyses revealed that belimumab-treated patients had greater SRI–SLEDAI-2K response rates compared with patients who received placebo if they had the following at baseline: 1) SELENA–SLEDAI–SLEDAI-2K scores ≥10 (52.5% versus 40.9%), 2) positive anti-dsDNA antibody levels (46.4% versus 36.4%), 3) low complement levels (47.2% versus 24.6%), or 4) low complement levels and positive anti-dsDNA (45.1% versus 24.0%) (Figure 4). Patients in the US/Canada had similar SRI–SLEDAI-2K response rates with belimumab as with placebo (37.4% versus 38.5%), whereas those in the rest of the world had a higher response rate with belimumab compared with placebo (57.5% versus 44.0%).

Patients in the double-blind phase who received belimumab had a 46% lower risk of experiencing a renal flare compared with those who received placebo (hazard ratio 0.54 [95% confidence interval 0.21, 1.36], *P* = 0.1880). Among patients who experienced a renal flare (9 of 299 [3.0%] in the belimumab group; 9 of 149 [6.0%] in the placebo group), the median study day of the renal flare was day 196 (range 57–309) in the belimumab group and day 153 (range 30–337) in the placebo group. In the open-label extension phase, 3.1% of patients (7 of 225) in the continuous belimumab group and 4.6% of patients (5 of

109) in the placebo-to-belimumab group experienced renal flares over 28 weeks. Among these patients, the median study day of the renal flare was day 169 (range 162–193) in the continuous belimumab group and day 169 (range 85–197) in the placebo-to-belimumab group.

In the double-blind phase, among patients with baseline SELENA–SLEDAI–SLEDAI-2K renal involvement, more patients in the belimumab group (41.8% [23 of 55]) experienced improvement in this domain compared with those in the placebo group (20.6% [7 of 34]). Among those without baseline SELENA–SLEDAI–SLEDAI-2K renal involvement, the percentage of patients who experienced worsening in this domain was low in both groups (6.1% [15 of 244] in the belimumab group; 7.8% [9 of 115] in the placebo group). Changes in proteinuria by visit in patients in the double-blind phase with baseline proteinuria >0.5 gm/24 hours are shown in Supplementary Figure 4 (<http://onlinelibrary.wiley.com/doi/10.1002/art.41900/abstract>). The median percentage change in proteinuria at week 52 among patients with baseline proteinuria >0.5 gm/24 hours was numerically greater with belimumab treatment compared with placebo (–65.27% [interquartile range –81.1, –38.8], *n* = 38 versus –32.89% [interquartile range –76.6, 36.3], *n* = 23). Among patients with baseline proteinuria >0.5 gm/24 hours in the open-label extension phase, the median percentage change in proteinuria at open-label extension week 24 was –73.99% (interquartile range –91.3, –36.4) in 34 patients receiving continuous belimumab since the start of the double-blind phase and –34.30% (interquartile range –58.8, 29.4) in 17 patients who switched from

Table 2. Summary of treatment-emergent AEs in the safety population*

	Double-blind phase		Open-label extension phase	
	Belimumab, 10 mg/kg IV (n = 331)	Placebo (n = 165)	Continuous belimumab, 10 mg/kg IV (n = 242)	Placebo-to-belimumab, 10 mg/kg IV (n = 117)
Any AE	277 (83.7)	144 (87.3)	152 (62.8)	78 (66.7)
Treatment-related AEs	111 (33.5)	47 (28.5)	36 (14.9)	20 (17.1)
Serious AEs	36 (10.9)	31 (18.8)	13 (5.4)	6 (5.1)
Severe AEs	46 (13.9)	37 (22.4)	9 (3.7)	10 (8.5)
Serious and/or severe AEs	57 (17.2)	46 (27.9)	17 (7.0)	15 (12.8)
AEs resulting in treatment discontinuation	22 (6.6)	12 (7.3)	0	1 (0.9)
Deaths	2 (0.6)	0	0	0

* Values are the number (%). AEs = adverse events; IV = intravenous.

placebo to belimumab at the start of the open-label extension phase. At week 52 of the double-blind phase, 16 patients (42.1%) in the belimumab group and 6 (26.1%) in the placebo group with baseline proteinuria >0.5 gm/24 hours experienced a downward shift in proteinuria to ≤0.5 gm/24 hours. At open-label extension week 24, 20 patients (58.8%) in the continuous belimumab group and 6 (35.3%) in the placebo-to-belimumab group experienced a downward shift in proteinuria to ≤0.5 gm/24 hours since the start of the double-blind phase and the start of the open-label extension phase, respectively.

Biomarker results are shown in Supplementary Table 2 (<http://onlinelibrary.wiley.com/doi/10.1002/art.41900/abstract>). With belimumab versus placebo treatment in the double-blind phase, there was a greater reduction in the percentage change in IgG levels from baseline ($P < 0.0001$) and percentage change in anti-dsDNA levels from baseline ($P = 0.0004$ among patients who were anti-dsDNA positive at baseline). Greater increases in C3 and C4 levels were observed in those who received belimumab versus those who received placebo ($P = 0.0087$ and $P < 0.0001$, respectively).

Safety. In the double-blind phase, the proportion of patients who experienced at least 1 AE was similar between treatment groups (83.7% in the belimumab group; 87.3% in the placebo group). In the open-label extension phase, the proportion of patients who experienced at least 1 AE was 62.8% and 66.7% in the continuous belimumab and placebo-to-belimumab groups, respectively (Table 2 and Supplementary Table 3, <http://onlinelibrary.wiley.com/doi/10.1002/art.41900/abstract>).

The AEs most commonly reported in either treatment group during the double-blind phase were upper respiratory tract infection (14.8% in the belimumab group; 8.5% in the placebo group) and urinary tract infection (13.0% in the belimumab; 12.7% in the placebo group). In the open-label extension phase, in which all patients received belimumab, the AEs most commonly reported (occurring in ≥5% of patients) were upper respiratory tract infection (6.7%), influenza (6.4%), and urinary tract infection (5.6%). AEs in

the double-blind phase occurring more commonly in belimumab-treated patients compared with placebo-treated patients (and occurring in ≥5% of patients) and with a between-group difference in incidence of ≥1% were upper respiratory tract infection, diarrhea, sinusitis, vomiting, cough, and hypertension.

In the double-blind phase, the incidence of SAEs was lower in the belimumab group (10.9%) compared with the placebo group (18.8%), and the SAE with the highest incidence was infections and infestations (3.3% in the belimumab group; 7.9% in the placebo group). There was a similar incidence of infections and infestations between the belimumab group and placebo group (59.2% and 60.0%, respectively) and a similar incidence of serious infections and serious infestations between the belimumab group and placebo group (3.3% and 7.9%, respectively). The rate of opportunistic infection AEs of special interest, including active tuberculosis and herpes zoster, was 0.6% in the belimumab group and 1.2% in the placebo group. Overall, during the open-label extension phase, 5.3% of patients experienced at least 1 SAE.

In total, 6.6% of patients in the belimumab group and 7.3% in the placebo group discontinued treatment due to an AE in the double-blind phase. In the belimumab group, treatment was discontinued most commonly because of lupus nephritis (0.9%). Two patients in the belimumab group (0.6%) died, and none died in the placebo group. Both deaths were considered not to be related to belimumab by the study investigator. The death in 1 patient was attributable to nosocomial meningitis, secondary to an SAE of severe cerebrovascular accident (76 days after administration of the first dose of belimumab, where there was a possibility that the cerebrovascular accident was due to belimumab). The patient had a history of hypertension and infection. The second patient, who received 1 dose of belimumab and developed multidrug-resistant pneumonia 8 days later, died on day 46. There were no deaths in the open-label extension phase, and 1 patient in the placebo-to-belimumab group experienced an AE that resulted in treatment discontinuation (Table 2). No clinically meaningful differences between treatment groups

were found in the incidence of malignancy, postinfusion reactions, or psychiatric disease.

DISCUSSION

To our knowledge, this is the first randomized, placebo-controlled clinical trial in SLE focusing on patients of self-identified Black race. The response to treatment with belimumab 10 mg/kg IV plus standard therapy did not achieve statistical superiority over placebo plus standard therapy when assessed on the basis of the double-blind phase primary end point; however, SRI-SLEDAI-2K response rates were numerically higher in those who received belimumab. Although the magnitude of the treatment group difference favoring belimumab is lower in this study (response rate 49% with belimumab versus 42% with placebo, odds ratio 1.40 [95% confidence interval 0.93, 2.11]) when compared with that observed in the 2 pivotal phase III studies of IV belimumab (response rate in the Study of Belimumab in Subjects with SLE 52-week trial [BLISS-52], 58% with belimumab versus 44% with placebo, odds ratio 1.83 [95% confidence interval 1.30, 2.59]; response rate in the BLISS 76-week trial [BLISS-76], 43% with belimumab versus 34% with placebo, odds ratio 1.52 [95% confidence interval 1.07, 2.15]), the efficacy results are directionally consistent (13,14,24). Our results support the post hoc analysis of the previous phase II study, which showed an improved SELENA-SLEDAI response with belimumab compared with placebo in patients of Black African ancestry (17) and contradicted the post hoc analyses of the pivotal phase III studies (18,25).

The large difference in SRI-SLEDAI-2K response in the open-label extension phase between the 2 treatment groups may be due to the difference in the length of time that patients received belimumab (>76 weeks in the continuous belimumab group versus 24 weeks in the placebo-to-belimumab group). At open-label extension baseline (start of belimumab treatment), the placebo-to-belimumab group also had lower disease activity compared with the continuous belimumab group, which may have made it more difficult to meet the SLEDAI component of the SRI end point.

The durable SRI-SLEDAI-2K response showed a greater difference between treatment groups relative to that in the primary analysis. The time to first SRI-SLEDAI-2K response that was maintained through week 52 occurred earlier in the belimumab group compared with the placebo group, and the belimumab group had a longer duration of SRI-SLEDAI-2K response compared with the placebo group.

The population recruited in this study had a generally lower disease activity than the overall population in the pivotal phase III studies (13,14,16), which may have contributed to the reduced effect size observed. However, subgroup analyses showed higher SRI-SLEDAI-2K responses in the belimumab group compared with the placebo group among patients with high disease activity at baseline (i.e., SELENA-SLEDAI-SLEDAI-2K score ≥ 10 , low complement levels, and low complement levels plus positive

anti-dsDNA). This finding is consistent with subgroup analyses of the pivotal phase III trials, in which patients with high disease activity had a greater SRI-SELENA-SLEDAI effect size with belimumab compared with standard therapy (Supplementary Figure 5, <http://onlinelibrary.wiley.com/doi/10.1002/art.41900/abstract>) (26). These findings add to the growing body of evidence supporting the benefit of belimumab in patients with high disease activity, regardless of race. High disease activity is more common in those of non-White descent, including African descendants (10), and this classification may be useful to practicing clinicians to more easily identify patients who might have an enhanced response to belimumab.

Regional analyses of the primary end point showed that patients in the rest-of-world subgroup compared with the US/Canada subgroup had a higher response to belimumab than to placebo, while those in the US/Canada subgroup had a similar response between treatment groups. A lower proportion of patients in the US/Canada subgroup had low complement levels at baseline than those in the rest-of-world subgroup. Due to this imbalance of baseline disease activity by region, post hoc analyses for response by region and baseline complement level were performed. In patients with low complement levels in both regions, a benefit was observed with belimumab compared with placebo. These regional baseline differences may have contributed to the higher response difference favoring belimumab in the rest-of-world subgroup compared with the US/Canada subgroup.

Renal involvement is more common and severe in patients of Black African ancestry (10,27–29). Although this study was not powered to determine a treatment difference in renal end points, patients treated with belimumab had an improved SELENA-SLEDAI-SLEDAI-2K renal domain score, decrease in proteinuria, and a downward shift in proteinuria among those with high proteinuria at baseline. In this study, the observation that patients with renal manifestations may benefit from treatment with belimumab is supported by the post hoc analysis performed by Dooley et al and was confirmed in the BLISS in Lupus Nephritis study (ClinicalTrials.gov identifier: NCT01639339), which also included patients of Black African ancestry (30,31).

Immunoglobulin and SLE biomarker responses from this study were consistent with those in the pivotal belimumab studies (13,14). The incidences of AEs, and the AE and SAE profile in this study, were consistent with those in the overall SLE population of the BLISS-52, BLISS-76, and BLISS-SC trials (13,14,16). Although patients in the open-label extension continuous belimumab group received more exposure to belimumab than those in the placebo-to-belimumab group, no clinically meaningful safety differences were observed.

This study has several limitations. The introduction of the SRI-SLEDAI-2K as a treatment response end point was expected to increase the sensitivity of the study to identify a between-group treatment difference as compared with that assessed using the SRI-SELENA-SLEDAI, and consequently, the sample size was

reduced from the original protocol (816 to 501 patients). Unfortunately, the predicted increase in sensitivity was not realized and this, combined with the loss of 48 participants from the modified ITT population due to site noncompliance, resulted in reduced power. Despite stratification at screening, a higher proportion of patients in the belimumab group had a SELENA–SLEDAI–SLEDAI-2K score of ≤ 9 at baseline, and the mean baseline SELENA–SLEDAI–SLEDAI-2K score was slightly lower compared with the placebo group. It is possible that a 4-point reduction in the score may therefore have been harder to achieve in the belimumab group compared with the placebo group due to disease changes after screening. Furthermore, subgroup analyses across studies have consistently demonstrated that patients with baseline SELENA–SLEDAI scores of ≥ 10 benefit more from treatment with belimumab compared with those with baseline scores of ≤ 9 (Supplementary Figure 5, <http://onlinelibrary.wiley.com/doi/10.1002/art.41900/abstract>). Therefore, this imbalance may have contributed to the reduction in the overall effect size on the primary end point.

This study was initiated as one of the postapproval commitments for belimumab. The decision not to include forced steroid tapering, which was made to ensure the study design was comparable to that of the pivotal BLISS studies, may have contributed to the inability to differentiate between the 2 groups. Although a reduction in steroid use without mandated tapering has been demonstrated following belimumab treatment (32), steroid tapering is an important consideration for the design of future studies in order to ensure that the full treatment effect of a new medicine may be demonstrated. Other than self-identification, no definitions were applied to the inclusion criteria of Black race. This resulted in the inclusion of a proportion of patients who did not identify as being primarily of Black race but considered themselves of mixed race. Although there is variability in the population of patients who self-identified as being of Black race, this study is unique in the SLE field in that it limits the inclusion criteria by race.

Overall, belimumab 10 mg/kg IV plus standard therapy was generally well tolerated; no new safety signals were observed, and findings were consistent with the known safety profile of belimumab. Efficacy and safety appear to be maintained over time. Although statistical significance was not achieved overall, a greater percentage of patients attained the primary end point in the belimumab group compared with the placebo group. Importantly, patients with baseline high disease activity or renal disease benefited from treatment with belimumab, a finding that adds to the growing body of evidence supporting the benefit of belimumab in these groups (13,14,16,30). This study provides clinically meaningful evidence to inform clinicians regarding the management of SLE in patients of Black African ancestry, especially those with high disease activity, a patient population with high unmet needs.

ACKNOWLEDGMENTS

The authors would like to thank Grace Kang (GlaxoSmithKline) for her contribution to this study. They would also like to thank the

patients and their families, as well as the investigators and support staff.

AUTHOR CONTRIBUTIONS

All authors were involved in drafting the article or revising it critically for important intellectual content, and all authors approved the final version to be published. Dr. Ginzler had full access to all of the data in the study and takes responsibility for the integrity of the data and the accuracy of the data analysis.

Study conception and design. Ginzler, Guedes Barbosa, Santiago, Bass, Burriss, Pierce, Roth, Ji.

Acquisition of data. Ginzler, Guedes Barbosa, D’Cruz, Furie, Maksimowicz-McKinnon, Oates, Santiago, Saxena, Sheikh.

Analysis and interpretation of data. Ginzler, Guedes Barbosa, D’Cruz, Furie, Maksimowicz-McKinnon, Oates, Santiago, Saxena, Sheikh, Bass, Burriss, Gilbride, Groark, Miller, Pierce, Roth, Ji.

ROLE OF THE STUDY SPONSOR

GlaxoSmithKline designed, conducted, and funded this study, contributed to collection, analysis, and interpretation of the data, and supported the authors in development of the manuscript. Medical writing support was provided by Casmira Brazaitis, PhD, of Fishawack Indicia Ltd (Knutsford, UK) and funded by GlaxoSmithKline. All authors, including those employed by GlaxoSmithKline, approved the content of the submitted manuscript. GlaxoSmithKline was involved in the decision to submit the manuscript for publication.

REFERENCES

- Herrada AA, Escobedo N, Iruetagoiena M, Valenzuela RA, Burgos PI, Cuitino L, et al. Innate immune cells' contribution to systemic lupus erythematosus [review]. *Front Immunol* 2019;10:772.
- Menez SP, El Essawy B, Atta MG. Lupus nephritis: current treatment paradigm and unmet needs [review]. *Rev Recent Clin Trials* 2018;13:105–13.
- Stojan G, Petri M. Epidemiology of systemic lupus erythematosus: an update [review]. *Curr Opin Rheumatol* 2018;30:144–50.
- Barbhaiya M, Feldman CH, Guan H, Gómez-Puerta JA, Fischer MA, Solomon DH, et al. Race/ethnicity and cardiovascular events among patients with systemic lupus erythematosus. *Arthritis Rheumatol* 2017;69:1823–31.
- Lewis MJ, Jawad AS. The effect of ethnicity and genetic ancestry on the epidemiology, clinical features and outcome of systemic lupus erythematosus [review]. *Rheumatology (Oxford)* 2017;56:i67–77.
- Munroe ME, Vista ES, Merrill JT, Guthridge JM, Roberts VC, James JA. Pathways of impending disease flare in African-American systemic lupus erythematosus patients. *J Autoimmun* 2017;78:70–8.
- Rees F, Doherty M, Grainge MJ, Lanyon P, Zhang W. The worldwide incidence and prevalence of systemic lupus erythematosus: a systematic review of epidemiological studies [review]. *Rheumatology (Oxford)* 2017;56:1945–61.
- Pons-Estel GJ, Alarcon GS, Scofield L, Reinlib L, Cooper GS. Understanding the epidemiology and progression of systemic lupus erythematosus [review]. *Semin Arthritis Rheum* 2010;39:257–68.
- Uribe AG, Alarcon GS. Ethnic disparities in patients with systemic lupus erythematosus [review]. *Curr Rheumatol Rep* 2003;5:364–9.
- Gonzalez LA, Toloza SM, McGwin G Jr, Alarcon GS. Ethnicity in systemic lupus erythematosus (SLE): its influence on susceptibility and outcomes. *Lupus* 2013;22:1214–24.
- Baker KP, Edwards BM, Main SH, Choi GH, Wager RE, Halpern WG, et al. Generation and characterization of LymphoStat-B, a human

- monoclonal antibody that antagonizes the bioactivities of B lymphocyte stimulator. *Arthritis Rheum* 2003;48:3253–65.
12. Hase H, Kanno Y, Kojima M, Hasegawa K, Sakurai D, Kojima H, et al. BAFF/BlyS can potentiate B-cell selection with the B-cell coreceptor complex. *Blood* 2004;103:2257–65.
 13. Furie R, Petri M, Zamani O, Cervera R, Wallace DJ, Tegzová D, et al. A phase III, randomized, placebo-controlled study of belimumab, a monoclonal antibody that inhibits B lymphocyte stimulator, in patients with systemic lupus erythematosus. *Arthritis Rheum* 2011;63:3918–30.
 14. Navarra SV, Guzmán RM, Gallacher AE, Hall S, Levy RA, Jimenez RE, et al. Efficacy and safety of belimumab in patients with active systemic lupus erythematosus: a randomised, placebo-controlled, phase 3 trial. *Lancet* 2011;377:721–31.
 15. Zhang F, Bae SC, Bass D, Chu M, Egginton S, Gordon D, et al. A pivotal phase III, randomised, placebo-controlled study of belimumab in patients with systemic lupus erythematosus located in China, Japan and South Korea. *Ann Rheum Dis* 2018;77:355–63.
 16. Stohl W, Schwarting A, Okada M, Scheinberg M, Doria A, Hammer AE, et al. Efficacy and safety of subcutaneous belimumab in systemic lupus erythematosus: a fifty-two-week randomized, double-blind, placebo-controlled study. *Arthritis Rheumatol* 2017;69:1016–27.
 17. Stohl W, Hilbert DM. The discovery and development of belimumab: the anti-BLyS-lupus connection. *Nat Biotechnol* 2012;30:69–77.
 18. Benlysta prescribing information. Philadelphia (PA): GlaxoSmithKline; 2021. URL: https://www.gsksource.com/pharma/content/dam/GlaxoSmithKline/US/en/Prescribing_Information/Benlysta/pdf/BENLYSTA-PI-MG-IFU-COMBINED.PDF.
 19. World Medical Association. WMA Declaration of Helsinki: ethical principles for medical research involving human subjects. URL: <https://www.wma.net/policies-post/wma-declaration-of-helsinki-ethical-principles-for-medical-research-involving-human-subjects/>.
 20. Schulz KF, Altman DG, Moher D, Group C. CONSORT 2010 statement: updated guidelines for reporting parallel group randomised trials. *BMJ* 2010;340:c332.
 21. Doria A, Stohl W, Schwarting A, Okada M, Scheinberg M, van Vollenhoven R, et al. Efficacy and safety of subcutaneous belimumab in anti-double-stranded DNA-positive, hypocomplementemic patients with systemic lupus erythematosus. *Arthritis Rheumatol* 2018;70:1256–64.
 22. Gladman DD, Ibanez D, Urowitz MB. Systemic lupus erythematosus disease activity index 2000. *J Rheumatol* 2002;29:288–91.
 23. Yee CS, Farewell V, Isenberg DA, Prabu A, Sokoll K, Teh LS, et al. Revised British Isles Lupus Assessment Group 2004 index: a reliable tool for assessment of systemic lupus erythematosus activity. *Arthritis Rheum* 2006;54:3300–5.
 24. Benlysta summary of product characteristics. Philadelphia (PA): GlaxoSmithKline; 2021. URL: https://gskpro.com/content/dam/global/hcpportal/en_US/Prescribing_Information/Benlysta/pdf/BENLYSTA-PI-MG-IFU.PDF.
 25. US Food and Drug Administration. Belimumab statistical review and evaluation. 2011. URL: https://www.accessdata.fda.gov/drugsatfda_docs/nda/2011/125370Orig1s000StatR.pdf.
 26. Van Vollenhoven RF, Petri MA, Cervera R, Roth DA, Ji BN, Kleoudis CS, et al. Belimumab in the treatment of systemic lupus erythematosus: high disease activity predictors of response. *Ann Rheum Dis* 2012;71:1343–9.
 27. Johnson SR, Urowitz MB, Ibanez D, Gladman DD. Ethnic variation in disease patterns and health outcomes in systemic lupus erythematosus. *J Rheumatol* 2006;33:1990–5.
 28. Feldman CH, Hiraki LT, Liu J, Fischer MA, Solomon DH, Alarcón GS, et al. Epidemiology and sociodemographics of systemic lupus erythematosus and lupus nephritis among US adults with Medicaid coverage, 2000–2004. *Arthritis Rheum* 2013;65:753–63.
 29. Alarcón GS, McGwin G Jr, Petri M, Reveille JD, Ramsey-Goldman R, Kimberly RP, et al. Baseline characteristics of a multiethnic lupus cohort: PROFILE. *Lupus* 2002;11:95–101.
 30. Furie R, Rovin BH, Houssiau F, Malvar A, Teng YK, Contreras G, et al. Two-year, randomized, controlled trial of belimumab in lupus nephritis. *N Engl J Med* 2020;383:1117–28.
 31. Dooley MA, Houssiau F, Aranow C, D’Cruz DP, Askanase A, Roth DA, et al. Effect of belimumab treatment on renal outcomes: results from the phase 3 belimumab clinical trials in patients with SLE. *Lupus* 2013;22:63–72.
 32. Van Vollenhoven RF, Petri M, Wallace DJ, Roth DA, Molta CT, Hammer AE, et al. Cumulative corticosteroid dose over fifty-two weeks in patients with systemic lupus erythematosus: pooled analyses from the phase III belimumab trials. *Arthritis Rheumatol* 2016;68:2184–92.

Phase IIa Global Study Evaluating Rituximab for the Treatment of Pediatric Patients With Granulomatosis With Polyangiitis or Microscopic Polyangiitis

Paul Brogan,¹  Rae S. M. Yeung,² Gavin Cleary,³ Satyapal Rangaraj,⁴ Ozgur Kasapcopur,⁵ Aimee O. Hersh,⁶ 
Suzanne Li,⁷  Dusan Paripovic,⁸ Kenneth Schikler,⁹ Andrew Zeft,¹⁰ Claudia Bracaglia,¹¹  Despina Eleftheriou,¹
Pooneh Pordeli,¹² Simone Melega,¹³ Candice Jamois,¹³ Jacques Gaudreault,¹⁴ Margaret Michalska,¹⁵
Paul Brunetta,¹⁵ Jennifer C. Cooper,¹⁶ Patricia B. Lehane,¹⁷ and the PePRS Study Group

Objective. To assess the safety, tolerability, pharmacokinetics, and efficacy of rituximab (RTX) in pediatric patients with granulomatosis with polyangiitis (GPA) or microscopic polyangiitis (MPA).

Methods. The Pediatric Polyangiitis Rituximab Study was a phase IIa, international, open-label, single-arm study. During the initial 6-month remission-induction phase, patients received intravenous infusions of RTX (375 mg/m² body surface area) and glucocorticoids once per week for 4 weeks. During the follow-up period, patients could receive further treatment, including RTX, for GPA or MPA. The safety, pharmacokinetics, pharmacodynamics, and exploratory efficacy outcomes with RTX were evaluated.

Results. Twenty-five pediatric patients with new-onset or relapsing disease were enrolled at 11 centers (19 with GPA [76%] and 6 with MPA [24%]). The median age was 14 years (range 6–17 years). All patients completed the remission-induction phase. During the overall study period (≤4.5 years), patients received between 4 and 28 infusions of RTX. All patients experienced ≥1 adverse event (AE), mostly grade 1 or grade 2 primarily infusion-related reactions. Seven patients experienced 10 serious AEs, and 17 patients experienced 31 infection-related AEs. No deaths were reported. RTX clearance correlated with body surface area. The body surface area–adjusted RTX dosing regimen resulted in similar exposure in both pediatric and adult patients with GPA or MPA. Remission, according to the Pediatric Vasculitis Activity Score, was achieved in 56%, 92%, and 100% of patients by months 6, 12, and 18, respectively.

Conclusion. In pediatric patients with GPA or MPA, RTX is well tolerated and effective, with an overall safety profile comparable to that observed in adult patients with GPA or MPA who receive treatment with RTX. RTX is associated with a positive risk/benefit profile in pediatric patients with active GPA or MPA.

ClinicalTrials.gov identifier: NCT01750697 and EudraCT database no. 2012-002062-13.

Supported by F. Hoffmann-La Roche. Dr. Yeung's work was supported by the Hak-Ming and Deborah Chiu Chair in Paediatric Translational Research at The Hospital for Sick Children. Drs. Brogan and Eleftheriou's work was supported in part by the NIHR Great Ormond Street Hospital Biomedical Research Centre.

¹Paul Brogan, MBChB, PhD, FRCPC, Despina Eleftheriou, MBChB, PhD, MRCPC: University College London Great Ormond Street Institute of Child Health and Great Ormond Street Hospital NHS Foundation Trust, London, UK; ²Rae S. M. Yeung, MD, PhD, FRCPC: Hospital for Sick Children and University of Toronto, Toronto, Ontario, Canada; ³Gavin Cleary, MBChB, BSc (Hons), MSc, FRCPC: Alder Hey Children's Hospital, Liverpool, UK; ⁴Satyapal Rangaraj, MRCP, MRCPC, DCH: Nottingham University Hospitals NHS Trust, Nottingham, UK; ⁵Ozgun Kasapcopur, MD: Istanbul University–Cerrahpasa, Istanbul, Turkey; ⁶Aimee O. Hersh, MD: Intermountain Primary Children's Hospital, Salt Lake City, Utah; ⁷Suzanne Li, MD, PhD: Hackensack Meridian School of Medicine and Hackensack University Medical Center, Hackensack, New Jersey; ⁸Dusan Paripovic, MD: University Children's Hospital, Belgrade, Serbia; ⁹Kenneth Schikler, MD: Norton Children's Hospital, Louisville, Kentucky; ¹⁰Andrew Zeft, MD, MPH: Cleveland Clinic, Cleveland, Ohio; ¹¹Claudia Bracaglia, MD: IRCCS, Ospedale Pediatrico Bambino Gesù, Rome, Italy; ¹²Pooneh Pordeli, PhD: Hoffmann-La Roche, Mississauga, Ontario, Canada; ¹³Simone Melega, PhD, Candice Jamois, PharmD: Hoffmann-La

Roche, Basel, Switzerland; ¹⁴Jacques Gaudreault, PhD: JIG Pharma Consulting, Basel, Switzerland; ¹⁵Margaret Michalska, MD, Paul Brunetta, MD: Genentech, South San Francisco, California; ¹⁶Jennifer C. Cooper, PharmD, MD: Children's Hospital Colorado and University of Colorado Anschutz Medical Campus, Aurora; ¹⁷Patricia B. Lehane, PhD: Roche Products, Welwyn Garden City, UK.

Qualified researchers may request access to individual patient-level data through the clinical study data request platform (<https://vivli.org/>). Further details on Roche's criteria for eligible studies are available at <https://vivli.org/members/ourmembers/>. For further details on Roche's Global Policy on the Sharing of Clinical Information and how to request access to related clinical study documents, see https://www.roche.com/research_and_development/who_we_are_how_we_work/clinical_trials/our_commitment_to_data_sharing.htm.

Author disclosures are available at <https://onlinelibrary.wiley.com/action/downloadSupplement?doi=10.1002%2Fart.41901&file=art41901-sup-0004-Disclosureform.pdf>.

Address correspondence to Paul Brogan, MBChB, PhD, FRCPC, University College London Institute for Child Health and Great Ormond Street Hospital NHS Foundation Trust, 30 Guilford Street, London WC1N 1EH, UK. Email: p.brogan@ucl.ac.uk.

Submitted for publication September 3, 2020; accepted in revised form June 10, 2021.

INTRODUCTION

The antineutrophil cytoplasmic antibody (ANCA)-associated vasculitides (AAVs) granulomatosis with polyangiitis (GPA) and microscopic polyangiitis (MPA) are rare, potentially organ- and life-threatening, systemic autoimmune small vessel vasculitides. GPA and MPA are associated with the presence of ANCAs against proteinase 3 (PR3) or myeloperoxidase (MPO) (1). Pediatric patients with GPA or MPA share many signs and symptoms of these diseases with adult patients (2). Childhood-onset disease carries considerable disease-related morbidity and mortality, mainly as a result of progressive renal failure or aggressive respiratory involvement (2).

The conventional treatment for severe GPA or MPA in patients is remission induction with cyclophosphamide (CYC) (3) or mycophenolate mofetil (MMF) (4) in combination with glucocorticoids (GCs), usually followed by maintenance with azathioprine (AZA) or methotrexate (5). CYC in combination with GCs does not prevent frequent relapses in the majority of children with GPA or MPA, and this treatment is associated with a significant toxicity risk (2). Relapses may occur more frequently in pediatric patients treated with MMF than in those treated with CYC (4). Pediatric patients with GPA or MPA therefore have major unmet needs, including the lack of improvement in remission rates as well as inability to prevent flares and reduce the toxic effects of GCs and immunosuppressive therapies. Because children and adolescents require treatment during critical periods of growth and development and require treatment for a longer duration than adult patients, it is important to have alternatives to GCs and toxic immunosuppressants.

There is strong evidence to indicate that B cells play a crucial role in the pathogenesis of GPA and MPA (6,7). B cells may contribute to GPA and MPA pathogenesis by acting as antigen-presenting cells, through the production of various cytokines or through ANCA autoantibody production by their progenitor cells (7). Rituximab (RTX) is an anti-CD20 monoclonal antibody that targets and depletes CD20+ B cells. Thus, RTX may disrupt the critical functions of B cells in the pathogenesis and progression of AAVs. The efficacy and safety of RTX as remission-induction treatment in adult patients with severe GPA or MPA were demonstrated in the Rituximab in ANCA-Associated Vasculitis (RAVE) trial (8). RTX, in combination with GCs, was approved worldwide for the treatment of GPA and MPA in adult patients. Recently, the Rituximab versus Azathioprine in ANCA-Associated Vasculitis trial (9) demonstrated the efficacy of RTX for remission maintenance in adult patients with GPA or MPA, leading to regulatory approvals in the US and European Union.

Due to the rare nature of AAVs, controlled clinical trials in pediatric patients with GPA or MPA are difficult to conduct (2). RTX is increasingly being used as a first-line remission-induction treatment in children with AAVs, instead of CYC (10); however, limited data are available regarding pediatric RTX use. Since the

pathogenesis of GPA and MPA is similar in adult and pediatric patients, efficacy can be extrapolated from the outcomes data obtained in adult patients in the RAVE trial (8).

The objective of this first company-sponsored global clinical study was to evaluate the safety, pharmacodynamics (PD), and pharmacokinetics (PK) of RTX in pediatric patients with GPA or MPA. Exploratory efficacy outcomes were also evaluated. Our study led to the US Food and Drug Administration and European Medicines Agency approving RTX for the treatment of GPA and MPA in pediatric patients ≥ 2 years of age in September 2019 and March 2020, respectively (11,12).

PATIENTS AND METHODS

Patient population. Eligibility criteria included being between age 2 years and age 18 years at the time of screening, having received a diagnosis of either GPA (13) or MPA (14), and having newly diagnosed or relapsing disease, defined as the recurrence or new onset of potentially organ- or life-threatening disease (≥ 1 major Birmingham Vasculitis Activity Score [BVAS] for GPA [15]) or disease activity severe enough to require treatment with CYC or immunosuppressive therapy. Exclusion criteria included having received a diagnosis of eosinophilic GPA, having severe disease requiring mechanical ventilation due to alveolar hemorrhage, requiring plasmapheresis or dialysis at the time of screening, or receiving prior treatment with RTX or other B cell-targeted therapy within 6 months prior to the baseline visit.

Written informed consent was obtained from all pediatric patients or from patients' parents or legal guardians, with assent provided by the patient as appropriate, depending on the patient's age and level of understanding. The trial was conducted in accordance with the Declaration of Helsinki. Ethics approval for this study was obtained from the respective institutional review boards or ethics committees (see the Supplementary Methods, available on the *Arthritis & Rheumatology* website at <http://onlinelibrary.wiley.com/doi/10.1002/art.41901/abstract>).

Study design. The Pediatric Polyangiitis and Rituximab Study (PePRS) (clinical study no. WA25615; ClinicalTrials.gov identifier: NCT01750697; European Clinical Trials database no. 2012-002062-13) (see Appendix A for a list of members of the PePRS Study Group) is a phase IIa, international, multicenter, open-label, single-arm uncontrolled study consisting of a screening period of ≤ 28 days and an initial 6-month remission-induction phase followed by a minimum additional 12-month follow-up phase (Supplementary Figure 1, available on the *Arthritis & Rheumatology* website at <http://onlinelibrary.wiley.com/doi/10.1002/art.41901/abstract>).

During the remission-induction phase, RTX was administered as an intravenous (IV) infusion of 375 mg/m² (≤ 1 gm/dose) once a week for 4 consecutive weeks, at baseline (day 1) and on

days 8, 15, and 22. The RTX dose was calculated according to the body surface area of each patient assessed at the screening visit and remained the same for all 4 infusions. Pediatric patients received acetaminophen and an antihistamine prior to each RTX infusion. Before the first RTX infusion, patients received 3 separate IV infusions of methylprednisolone (MP) (each at a dosage of 30 mg/kg/day; maximum dosage of 1 gm/day) at any time after the screening visit, up to and including day 1. If clinically indicated and at the investigator's discretion, up to 3 additional IV infusions of MP could be administered prior to the first RTX infusion. All patients received concomitant oral prednisolone or prednisone (1 mg/kg/day, up to a maximum dosage of 60 mg/day) tapering to ≤ 0.2 mg/kg/day by month 6 (maximum dosage 10 mg/day) and mandatory prophylactic treatment for *Pneumocystis jirovecii* infection. During the remission-induction phase, concomitant use of immunosuppressive agents for GPA or MPA was not permitted. However, patients who experienced a disease flare that could not be controlled using glucocorticoids prior to month 6 could receive standard of care treatment and remain in the study.

During the follow-up phase, further RTX infusions were administered at the discretion of the investigator according to local practice to maintain remission or to treat disease activity. After month 6, other immunosuppressive treatments for GPA or MPA were permitted in accordance with the clinical judgment of the investigator (Supplementary Table 1, available on the *Arthritis & Rheumatology* website at <http://onlinelibrary.wiley.com/doi/10.1002/art.41901/abstract>). After month 18, pediatric patients continued to be followed up at study visits every 3 months until the common closeout date, May 10, 2018, 18 months after the last patient was enrolled.

Outcomes and assessments. The safety and tolerability of RTX were evaluated based on an assessment of all adverse events (AEs) and serious AEs (SAEs), vital signs, and routine laboratory test results. The severity of AEs was graded according to the National Cancer Institute Common Terminology Criteria for Adverse Events (CTCAE) version 4.0. Infusion-related reactions were defined as AEs that occurred during or within 24 hours of an RTX infusion and were classified within the Roche standard AE definition of infusion-related reactions with hypersensitivity (Medical Dictionary for Regulatory Activities [MedDRA] version 20.1; available online at <http://www.meddrasso.com/>). Total serum Ig, IgG, and IgM levels were regularly measured every 8–12 weeks throughout the treatment period and follow-up period. Abnormal laboratory test results indicating prolonged low levels of IgG or IgM were defined as IgG or IgM levels less than the lower limit of normal (LLN) for a ≥ 4 -month period. Antidrug antibody positivity and titers were monitored throughout the study.

During the remission-induction phase, serum samples were collected for a population PK analysis prior to the first, second,

third, and fourth infusions; after the completion of the first and fourth infusions; and subsequently at months 1, 2, 4, and 6. The PK parameters that we assessed included RTX clearance, volume of distribution, and exposure (measured as area under the curve [AUC]). The influence of several covariates, such as demographic characteristics (e.g., body surface area, sex, and the presence of antidrug antibodies), on PK parameters was tested. The relationship between RTX exposure and efficacy, B cell counts, and safety parameters was also assessed. In an exploratory analysis, the PD effects of RTX were evaluated using a longitudinal assessment of circulating CD19+ B cell counts.

All efficacy end points were exploratory in nature. Achievement of remission by months 6, 12, and 18 was assessed, with remission defined based on the Pediatric Vasculitis Activity Score (PVAS) (16), according to either of 2 different definitions: 1) a PVAS score of 0 and achievement of an oral prednisone dose (or prednisolone equivalent dose) of ≤ 0.2 mg/kg/day (maximum dosage of 10 mg/day); or 2) a PVAS score of 0 on 2 consecutive visits ≥ 4 weeks apart, irrespective of the dose of GC being received. Other exploratory efficacy end points included BVAS, physician global assessment of disease activity (evaluated using a 0–100-mm visual analog scale, with 0 defined as no disease activity and 100 defined as maximum disease activity), Pediatric Vasculitis Damage Index (PVDI) (17,18), and cumulative GC dose.

Statistical analysis. We did not conduct formal statistical hypothesis testing for any of the study end points. Nonlinear mixed-effects modeling (NONMEM 7.4.1; ICON Development Solutions) (19) was used to analyze PK data from pediatric and adult patients with GPA and MPA enrolled in this study and the RAVE study (8), respectively, and nonlinear mixed-effects modeling was also used to characterize the sources contributing to variability in the frequency of exposure to RTX.

Exploratory analyses. For the exposure-efficacy analysis, cumulative exposure over the remission-induction phase for each pediatric patient (AUC of cumulative exposure to RTX over 180 days [baseline to month 6] [AUC_{0–180}]) was computed using the individual pediatric patient's dosing history and the individual PK parameters from the final population PK model. Logistic regression models were used to assess the association between the probability of disease being in PVAS-based remission by 6 months and RTX exposure (AUC_{0–180}). A logistic regression model was fitted to these remission data, and a confidence interval (CI) was defined around the regression line. For each exposure value, a 90% CI was defined as the 5th and 95th percentiles of the predictions among 1,000 bootstrap data sets. Logistic regression models were used to assess any correlation between probability of the occurrence of selected AEs and RTX exposure in pediatric patients. The selected AEs included SAEs,

grade ≥ 3 AEs, infusion-related reactions, serious infections, and hypogammaglobulinemia.

For the exploratory efficacy analyses, all data were summarized using descriptive statistics. For binary end points, the number and percentage of patients are presented by visit. At key time points (months 6, 12, and 18), 2-sided 95% CIs were calculated for the percentage of pediatric patients who achieved PVAS-based remission. For continuous end points, the median and interquartile range (IQR) are presented.

RESULTS

Characteristics of the patients at baseline. Between May 23, 2013 and Nov 16, 2016, the study enrolled 25 patients from 11 investigational sites across 6 countries, of whom 17 (68%) were from Europe and 8 (32%) were from North America. Most patients were female (80%), White (68%), and between 12 and 17 years of age (76.0%) (Table 1). A total of 19 patients (76%) had GPA and 6 patients (24%) had MPA. A total of 18 patients (72.0%) had newly diagnosed disease at baseline and 7 patients (28%) had relapsing disease. Two patients (8%) with relapsing disease had received prior CYC therapy, but not within the 4 months prior to the baseline visit. A total of 22 patients (88%) were positive for ANCA at baseline. Of the 3 patients who were negative for ANCA at baseline, 2 patients with relapsing disease were perinuclear ANCA (pANCA)-positive and/or MPO-positive at initial diagnosis, and 1 was a patient with newly diagnosed disease who was positive for pANCA 51 days before the baseline visit. At baseline, the most common disease manifestations were arthralgia/arthritis, nasal crusts/ulcers, hematuria/proteinuria, and purpura (Table 1). A total of 15 patients (60%) experienced renal involvement, 4 patients (16%) experienced major renal disease, and 11 patients (44%) experienced vasculitis-related pulmonary involvement (Table 1).

Treatment regimens. All 25 patients completed the per-protocol RTX regimen (infusions of 375 mg/m² once per week for 4 weeks) and also completed the 6-month remission-induction phase (Supplementary Figure 2, available on the *Arthritis & Rheumatology* website at <http://onlinelibrary.wiley.com/doi/10.1002/art.41901/abstract>). A total of 24 patients completed ≥ 18 months of follow-up; 1 patient withdrew from the study around month 16 due to either an administrative reason or another reason, and was transferred back to a local hospital for care. Eight patients discontinued participation between month 18 and the common closeout date, primarily due to either an administrative reason or some other reason, such as a physician or family decision or transfer to adult care services for their GPA or MPA. There were no withdrawals due to AEs. During the overall study period, patients received 4–28 infusions of RTX. The mean number of infusions per patient was 8. The majority of patients

Table 1. Demographic and baseline clinical characteristics of the patients treated with rituximab (N = 25)*

Sex, female	20 (80.0)
Age, median (range) years	14.0 (6.0–17.0)
Age group	
<12 years	6 (24.0)
≥ 12 years	19 (76.0)
Race	
Asian	4 (16.0)
Black or African American	1 (4.0)
White	17 (68.0)
Other or multiple	3 (12.0)
Height, median (range) cm	154.9 (120.0–175.2)
Weight, median (range) kg	50.9 (23.0–80.8)
Diagnosis	
Newly diagnosed GPA	13 (52.0)
Newly diagnosed MPA	5 (20.0)
Relapsing GPA	6 (24.0)
Relapsing MPA	1 (4.0)
Disease duration, median (range) months	0.5 (0.2–72.1)
ANCA positivity†	22 (88.0)
MPO-ANCA positivity	8 (32.0)
PR3-ANCA positivity	14 (56.0)
Estimated GFR, median (IQR) ml/minute/1.73 m ²	138.0 (120.0–157.0)
PVAS, median (IQR) score (scale 0–63)	8.0 (5.0–15.0)
PhGA, median (IQR) score	46.0 (29.0–71.0)
PVDI, median (IQR) score (scale 0–72)	0.0 (0.0–3.0)
IgG, median (IQR) gm/liter	9.24 (8.5–12.6)
IgM, median (IQR) gm/liter	1.36 (0.8–1.7)
Previous CYC therapy	2 (8.0)
Disease manifestations at baseline	
Arthralgia/arthritis	16 (64.0)
Nasal crusts/ulcers	14 (56.0)
Hematuria	13 (52.0)
Proteinuria	7 (28.0)
Purpura	10 (40.0)
Renal involvement‡	15 (60.0)
Major renal disease§	4 (16.0)
Pulmonary involvement	11 (44.0)

* Except where indicated otherwise, values are the number (%) of patients. MPA = microscopic polyangiitis; MPO = myeloperoxidase; PR3 = proteinase 3; GFR = glomerular filtration rate; IQR = interquartile range; PhGA = physician global assessment of disease activity; PVDI = Pediatric Vasculitis Damage Index; CYC = cyclophosphamide.

† Three patients with relapsing disease were negative for antineutrophil cytoplasmic antibodies (ANCA) at screening but positive for ANCA at the time of the original diagnosis.

‡ According to the Pediatric Vasculitis Activity Score (PVAS) criteria.

§ Based on the definitions in the Birmingham Vasculitis Activity Score for granulomatosis with polyangiitis (GPA), with presence of either red blood cell casts or a significant decline in renal function (rise in creatinine levels $\geq 30\%$ above baseline values or $>25\%$ reduction in creatinine clearance).

(68%) were followed up for 18 months to 3 years, and 6 patients (24%) were followed up for 3–4.5 years. Overall, the total duration of observation was 61.1 patient-years of follow-up.

In total, 17 patients (68%) received additional RTX treatment at or after month 6 until the common closeout date, the dosing of which was variable and determined at the discretion of the treating physician. Among these 17 patients, 5 received infusions of RTX (375 mg/m²) approximately every 6 months administered

once weekly for 4 weeks, and 5 received 1 infusion of RTX (375 mg/m²) every 6 months; a further 7 patients received other, varied doses of RTX within individualized regimens. A total of 9 patients (36%) received ≥ 1 additional immunosuppressive therapy for GPA or MPA between months 6 and 18 (Supplementary Table 1, available on the *Arthritis & Rheumatology* website at <http://onlinelibrary.wiley.com/doi/10.1002/art.41901/abstract>).

Safety based on AEs and SAEs. During the 6-month remission-induction phase, all 25 patients (100%) experienced ≥ 1 AE; 158 AEs were reported, 10 of which were SAEs that occurred in 7 patients (28%) (Table 2). Most AEs (147 [93%], which occurred in 18 patients [72%]), were CTCAE grade 1 or 2 (mild to moderate). A total of 11 grade 3 AEs were reported in 7 patients (28%). No grade 4 or 5 AEs were reported. The most common AEs by MedDRA System Organ Class (SOC) were infections and infestations (31 AEs that occurred in 17 patients [68%]). The most common AEs by MedDRA Preferred Term (PT) were infusion-related reactions, reported in 15 patients (60%), followed by headache, upper respiratory tract infection, and nausea, reported in 4 patients (16%) each (Table 2). The most frequently reported SAEs classified by MedDRA SOC were infections and infestations (3 that occurred in 3 patients [12%]) and vascular disorders (4 that occurred in 3 patients [12%]). The SAEs classified by MedDRA PT that occurred most frequently were related to

worsening GPA (disease flare); these flares were reported to occur in 3 patients (12%) with either GPA ($n = 3$ events) or vasculitis ($n = 1$ event) (Table 2).

During the overall study period (6-month remission-induction and follow-up phases), the safety profile of RTX was consistent with what was reported during the remission-induction phase (Supplementary Table 2, available on the *Arthritis & Rheumatology* website at <http://onlinelibrary.wiley.com/doi/10.1002/art.41901/abstract>). Due to the longer data collection period (up to 4.5 years compared to 6 months), the total number of AEs that were reported was greater (404 AEs were reported to have occurred in 25 patients [100%], 27 of which were SAEs that occurred in 12 patients [48%]). The majority of AEs (370 [92%]) were either grade 1 or 2 in intensity, 32 AEs were grade 3, and 2 AEs were grade 4. No AEs led to discontinuation of study treatment. No deaths, malignancies, progressive multifocal leukoencephalopathy (PML), or other opportunistic infections were reported. During the overall study period, the majority of AEs that resulted in dose modification or treatment interruption were infusion-related reactions (21 AEs that occurred in 10 patients [40%]). The most frequently reported SAEs were consistent with those reported during the remission-induction phase.

Among the SAEs classified by MedDRA SOC, most of them were infections and infestations (9 SAEs that occurred in 7 patients [28%]) and vascular disorders (7 SAEs that occurred in 5 patients [20%]). The SAEs that occurred most frequently by PT were related to worsening GPA and were reported to occur in a total of 6 patients (24%) in conjunction with GPA ($n = 6$ events), ANCA-positive vasculitis ($n = 1$ event), or vasculitis ($n = 1$ event) (Supplementary Table 2, available on the *Arthritis & Rheumatology* website at <http://onlinelibrary.wiley.com/doi/10.1002/art.41901/abstract>).

Infusion-related reactions. Infusion-related reactions predominantly occurred after the first infusion (8 of 25 patients [32%]). The most frequently reported symptoms of infusion-related reactions during the remission-induction phase were rash ($n = 3$ events), headache ($n = 2$ events), rhinorrhea ($n = 2$ events), and pyrexia ($n = 2$ events), occurring in 2 patients each. The incidence of infusion-related reactions decreased with repeated RTX infusions over time (Supplementary Figure 3, available on the *Arthritis & Rheumatology* website at <http://onlinelibrary.wiley.com/doi/10.1002/art.41901/abstract>). One serious infusion-related reaction (generalized edema) was reported and was suspected to be attributable to the concomitant use of GCs. The majority of infusion-related reactions that were reported during the study were grade 1 or 2; 2 nonserious grade 3 infusion-related reactions were reported to occur in 1 patient. No grade 4 or 5 infusion-related reactions were reported.

Infections. During the remission-induction phase, a total of 31 infection-related AEs (serious and nonserious) were reported

Table 2. AEs and SAEs reported during the remission-induction phase in patients treated with rituximab ($N = 25$)

	No. (%) of patients	No. of events
AEs*		
Infusion-related reaction	15 (60.0)	29
Headache	4 (16.0)	4
Upper respiratory tract infection	4 (16.0)	4
Nausea	4 (16.0)	5
Upper abdominal pain	3 (12.0)	3
Constipation	3 (12.0)	3
Arthralgia	3 (12.0)	3
Back pain	3 (12.0)	3
Cough	3 (12.0)	3
Epistaxis	3 (12.0)	3
SAEs		
GPA worsening†	3 (12.0)	4
Influenza	1 (4.0)	1
Lower respiratory tract infection	1 (4.0)	1
Viral gastroenteritis	1 (4.0)	1
Infusion-related reaction‡	1 (4.0)	1
Myopathy	1 (4.0)	1
Bronchial stenosis	1 (4.0)	1

* Only adverse events (AEs) reported in $\geq 10\%$ of patients are shown.

† Includes 4 serious AEs (SAEs) of worsening vasculitis in 3 patients, reported with the Medical Dictionary for Regulatory Activities Preferred Terms granulomatosis with polyangiitis (GPA) (3 events) and vasculitis (1 event).

‡ The event was generalized edema that occurred after the fourth rituximab infusion.

to occur in 17 patients (68%), the most frequent being upper respiratory tract infections (occurring in 4 patients [16%]) (Table 2). The majority of infections (90%) were either grade 1 or 2 and were nonserious, resolving without sequelae. In the overall study period, 105 infection-related AEs, of which the majority (91%) were considered to be nonserious, were reported, occurring in 23 patients (92%). Similar to that observed during the remission-induction phase, the most frequent infections that occurred during the overall study period were upper respiratory tract infections.

A total of 3 serious infections in 3 patients (12%) were reported during the remission-induction phase (Table 2): influenza, lower respiratory tract infection, and gastroenteritis. During the overall study period, 9 serious infections were reported to have occurred in 7 patients (28%), including influenza (occurring in 2 patients [8%]) and lower respiratory tract infection (occurring in 2 patients [8%]) as the most frequently occurring events (Supplementary Table 2, available on the *Arthritis & Rheumatology* website at <http://onlinelibrary.wiley.com/doi/10.1002/art.41901/abstract>). Overall, the majority of serious infections resolved without sequelae.

During the overall study period, 6 of the 18 patients in whom prolonged low serum levels of IgG were observed subsequently experienced a total of 7 serious infections, and 6 of the 19 patients in whom prolonged low serum levels of IgM were observed subsequently experienced a total of 8 serious infections. Most of the infections were reported as being unrelated to study treatment.

Laboratory test results. IgG, IgM, and total Ig serum concentrations decreased from baseline values over the course of the study. Median IgG levels decreased below the LLN within the first month and returned to within-normal limits between months 9 and 12, with a subsequent slight decrease below the LLN observed through month 18 (Figure 1). Median IgM levels fell below the LLN by month 2 and remained below the LLN through month 18 (Figure 1). The proportions of patients with low levels of IgG and IgM at key study points are shown in Supplementary Table 3 (available on the *Arthritis & Rheumatology* website at <http://onlinelibrary.wiley.com/doi/10.1002/art.41901/abstract>). A total of 3 patients experienced hypogammaglobulinemia AEs, for which they received treatment with intravenous immunoglobulin. All of these patients had previous and concomitant use of steroids and immunosuppressive medications. During the study, no clinically significant changes or abnormalities were observed in other laboratory analyses (e.g., chemistry, hematology, urinalysis) and other safety tests (e.g., vital signs, chest radiographs, electrocardiogram).

Immunogenicity. Of 21 evaluable patients, 4 (19%) developed treatment-induced antidrug antibodies during the overall study period. One patient tested antidrug antibody-positive at month 4 and subsequently at each study visit until month 18. This patient achieved PVAS-based remission by month 6, which was maintained through month 18. The 3 other patients tested positive for antidrug antibodies at month 18, and all were in PVAS-

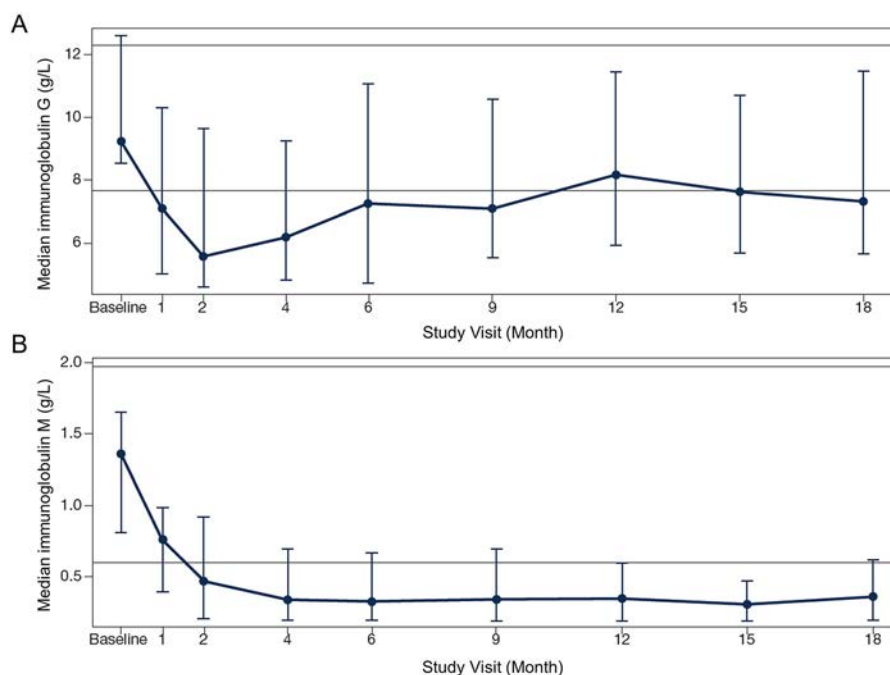


Figure 1. Levels of IgG (A) and IgM (B) at each study visit in the serum of 25 pediatric patients with granulomatosis with polyangiitis or microscopic polyangiitis. Bars show the median with interquartile range. Top and bottom horizontal lines show the lowest upper limit of normal and the highest lower limit of normal (in A, 12.29 gm/liter and 7.68 gm/liter, respectively; in B, 1.97 gm/liter and 0.6 gm/liter, respectively). Color figure can be viewed in the online issue, which is available at <http://onlinelibrary.wiley.com/doi/10.1002/art.41901/abstract>.

based remission at month 18. No serious infusion-related reactions or increases in the occurrence of nonserious infusion-related reactions were observed after the development of antidrug antibodies, and no trends or differences were observed in the type of AEs reported in antidrug antibody-positive patients compared to antibody-negative patients. Two of the patients received repeat RTX treatment after the development of antidrug antibodies, and, as expected, depletion of CD19 B cells occurred following repeated exposure to RTX.

PK analysis. A population PK analysis of the RTX treatment populations was conducted, using 204 serum samples from the 25 pediatric patients in the present study and 487 serum samples from the 97 adult patients with AAVs in the RAVE trial (8). Model parameters for a typical patient (body surface area 1.9 m² and absence of antidrug antibodies), such as RTX clearance (258 ml/day), RTX intercompartmental clearance (317 ml/day), central volume (3,070 ml), peripheral volume (4,160 ml), and terminal half-life (25.6 days), were in the typical range for monoclonal antibodies and were consistent with the known PK of RTX in other autoimmune diseases. The 2 covariates impacting RTX PK were body surface area and the presence of antidrug antibodies. As is typical for monoclonal antibodies, RTX clearance and the volume of distribution parameters increased with body surface area. Because of the effect of body surface area on RTX PK parameters, RTX clearance was lower in pediatric patients compared to adult patients, but RTX exposure (AUC₀₋₁₈₀) was similar between adult patients and pediatric patients because dosages were based on body surface area (Figure 2). As a result, the body surface area-adjusted RTX dosing regimen ensured similar exposure across the whole range of body surface area in pediatric patients with GPA or MPA. Patients with detected antidrug antibodies had 38.2% higher clearance, resulting in a 27.6% lower AUC.

The efficacy-exposure analysis did not show any relationship between RTX exposure variability (in terms of dosing regimens) and achievement of PVAS-based remission (Supplementary Figure 4, available on the *Arthritis & Rheumatology* website at <http://onlinelibrary.wiley.com/doi/10.1002/art.41901/abstract>). Moreover, the exposure-safety analysis did not reveal a relationship between RTX exposure and the occurrence of SAEs grade ≥ 3 , infusion-related reactions, serious infections, or laboratory abnormalities, indicating prolonged low serum levels of IgG, during the remission-induction phase (each $P > 0.05$).

PD analysis. Consistent with its mode of action, RTX treatment resulted in sustained CD19+ peripheral B cell depletion that persisted until at least month 6 (Supplementary Figure 5, available on the *Arthritis & Rheumatology* website at <http://onlinelibrary.wiley.com/doi/10.1002/art.41901/abstract>). By month 18, B cell levels had increased slightly but still remained low (median 58 cells/ μ l), which is consistent with levels in patients receiving repeat RTX treatment. Among the pediatric patients from the current PePRS study

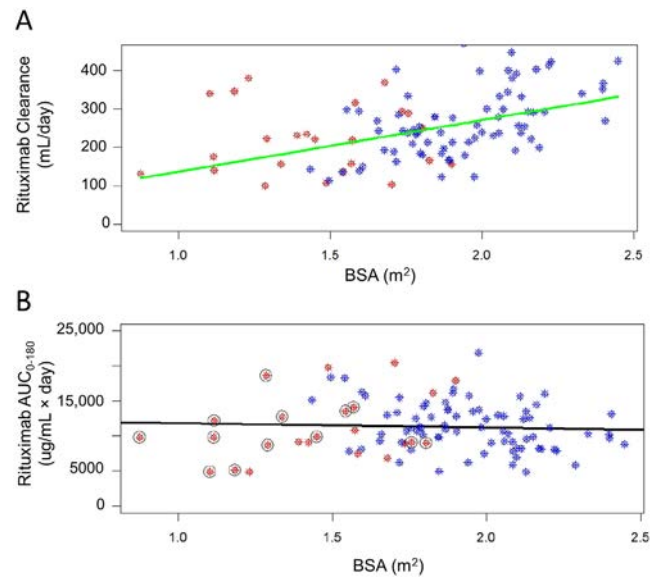


Figure 2. Relationship between the rate of rituximab clearance and body surface area (BSA) (A) and between the cumulative exposure to rituximab over the remission-induction phase (measured as the area under the curve over the first 180 days [AUC₀₋₁₈₀]) and body surface area (B) in antidrug antibody-negative adult and pediatric patients with granulomatosis with polyangiitis or microscopic polyangiitis. Relationships were assessed by linear regression analyses. Red symbols represent predicted individual rituximab clearance (A) and AUC₀₋₁₈₀ values (B) in pediatric patients in the Pediatric Polyangiitis and Rituximab Study. Blue symbols represent the respective predicted individual values in adult patients in the Rituximab in ANCA-Associated Vasculitis trial (8). Circled red symbols in B denote pediatric patients in remission by month 6.

and the adult patients from the RAVE trial, B cell depletion lasted longer in patients with higher levels of exposure (Supplementary Figure 6, available on the *Arthritis & Rheumatology* website at <http://onlinelibrary.wiley.com/doi/10.1002/art.41901/abstract>).

Exploratory efficacy. Disease activity was primarily assessed using PVAS as an exploratory efficacy outcome measure. PVAS was adapted from BVAS for use in childhood vasculitis. PVAS-based remission was achieved in 14 patients (56.0%), 23 patients (92.0%), and 25 patients (100.0%) by months 6, 12, and 18, respectively (Table 3). Of the 25 patients who achieved PVAS-based remission by month 18, remission was achieved in 24 patients according to the criteria of either the first definition of remission or both the first and second definitions of remission, and in 1 patient, only the criteria of the second definition of remission were met. The mean \pm SD duration of remission during the study was 71.7 ± 50.9 weeks. The shortest duration of remission was 6.9 weeks, and the longest was 193.4 weeks (~ 3.5 years). The rate of remission achievement at key study visits is shown in Supplementary Table 4 (available on the *Arthritis & Rheumatology* website at <http://onlinelibrary.wiley.com/doi/10.1002/art.41901/abstract>).

Table 3. Efficacy outcomes in patients treated with rituximab (N = 25) by each follow-up time point*

Achievement of PVAS-based remission, no. (% [95% CI])	
Month 6	14 (56.0 [34.9–75.6])
Month 12	23 (92.0 [74.0–99.0])
Month 18	25 (100.0 [86.3–100.0])
Change in PhGA score from baseline, median (IQR)	
Month 6	–39.0 (64.5–16.0)
Month 12	–39.0 (64.0–16.0)
Month 18	–46.0 (72.0–17.0)

* Seventeen pediatric patients received additional rituximab treatment at or after month 6 until the common closeout date. PVAS = Pediatric Vasculitis Activity Score; 95% CI = 95% confidence interval; PhGA = physician global assessment of disease activity; IQR = interquartile range.

Median PVAS scores decreased through month 18 (Supplementary Figure 7, available on the *Arthritis & Rheumatology* website at <http://onlinelibrary.wiley.com/doi/10.1002/art.41901/abstract>). There was no obvious impact of PR3-ANCA or MPO-ANCA status on remission achievement. A decrease in median physician global assessment of disease activity scores from baseline was reported at months 6, 12, and 18 (Table 3), indicating a reduction in disease activity over the course of the study. The median PVDI was 0 at baseline and 2.0 at months 6, 12, and 18. Thus, after an initial increase in the median PVDI from baseline to month 6 (PVDI score of 0 at baseline to 2.0 at 6 months), no further damage was accrued between months 6 and 18.

During the administration of protocol-defined oral steroids in tapering doses, a clinically meaningful decline in the overall dose of oral GCs was observed from week 1 to month 6 (median prednisolone equivalent dose 45 mg [IQR 35–60] at week 1 to 7.5 mg [IQR 4–10] at month 6). This dose tapering of oral GCs was subsequently maintained at month 12 (median prednisolone equivalent dose 5 mg [IQR 2–10]) and month 18 (median prednisolone equivalent dose 5 mg [IQR 1–5]) (Figure 3).

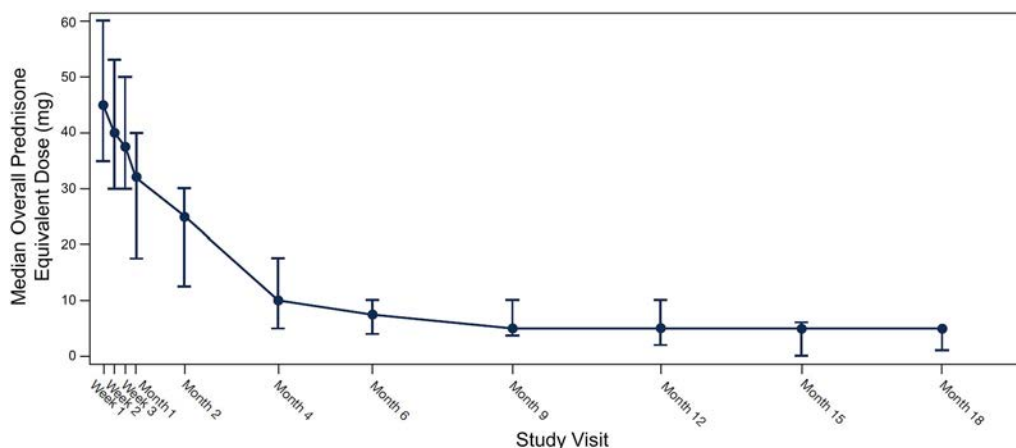


Figure 3. Oral glucocorticoid use over time in 25 pediatric patients with granulomatosis with polyangiitis or microscopic polyangiitis. Bars show the median with interquartile range. Color figure can be viewed in the online issue, which is available at <http://onlinelibrary.wiley.com/doi/10.1002/art.41901/abstract>.

A post hoc sensitivity analysis of the exploratory efficacy outcome (i.e., achievement of PVAS-based remission) was conducted in which 2 patients were excluded who had been continuously receiving additional immunosuppressive therapies (both receiving MMF) between the baseline visit and month 6 and who were considered to be RTX nonresponders. The results of the sensitivity analysis did not change the overall results with regard to the exploratory efficacy outcome at month 6 (data available upon request from the corresponding author). Of the 9 patients who received additional immunosuppressive therapy between months 6 and 18, 5 patients were nonresponders at each of the efficacy time points. Two of these patients received AZA for a short duration (<1 month), which was determined to not have affected whether a patient achieved PVAS-based remission through month 18. Among the 2 patients who received CYC as well as maintenance doses of RTX, efficacy outcomes were variable: PVAS-based remission was achieved at month 12 and month 18 in 1 of the 2 patients, while the other patient was a nonresponder at both time points (Supplementary Table 1, available on the *Arthritis & Rheumatology* website at <http://onlinelibrary.wiley.com/doi/10.1002/art.41901/abstract>).

DISCUSSION

In the PePRS single-arm, open-label clinical study, RTX was evaluated as an alternative treatment option for pediatric patients with GPA or MPA. In the study, safety data regarding RTX use in pediatric patients was consistent with data from adult patients with GPA or MPA, in whom the efficacy and safety profile of RTX is well established. This is the first company-sponsored global clinical trial investigating the use of RTX in pediatric patients with active GPA or MPA. In our study, RTX, administered as 4 weekly IV infusions of 375 mg/m² for remission induction followed by repeat treatment as determined by the treating physician, was

generally safe and well tolerated (for up to 4.5 years). Furthermore, findings from the exploratory efficacy analyses demonstrated a clinical benefit with RTX for achieving PVAS-based remission.

There were no new or unexpected safety findings. The safety profile of RTX in pediatric patients was consistent with the safety profile previously observed in adult patients with GPA or MPA (8) and was consistent with the well-characterized safety profile of RTX for approved autoimmune indications (11,12). Over the course of the study, no patients died or experienced AEs leading to withdrawal, and no malignancies, PML, or other opportunistic infections were reported.

Safety events were associated with confounding/contributory risk factors (e.g., past or concomitant medication use, such as oral GC use), were associated with underlying conditions (GPA or MPA), or were events that were expected with RTX treatment (adverse drug reactions including infusion-related reactions and infections). The most common AEs were infusion-related reactions, which decreased in frequency throughout the study and with repeated treatment. Pretreatment with MP can reduce the incidence and severity of infusion-related reactions (20); however, because patients received high doses of MP prior to the baseline visit, up to day 1, IV MP premedication was optional. The overall incidence and type of infections were characteristic of the general population and pediatric population of AAV patients receiving oral GCs and immunosuppressive therapy.

Low serum levels of IgG or IgM have also been observed in adult patients with autoimmune diseases treated with RTX, which may have no clinical consequence and often do not require specific medical management (21,22). In this study, no consistent pattern in IgG or IgM levels over time was observed, and the majority of patients with prolonged low levels of IgG or IgM did not experience any serious infections. The incidence of antidrug antibodies in pediatric patients (19%) was similar to the incidence observed in adult patients (23% in the RAVE study). In both populations, the presence of antidrug antibodies had no apparent effect on the efficacy, safety, or PD of RTX.

Since RTX dose was based on body surface area, the dosing regimen used in this trial (375 mg/m²) resulted in similar levels of RTX exposure in pediatric patients compared to those observed in adult patients in the RAVE study, in whom a positive benefit/risk profile of RTX was demonstrated (8). Furthermore, the PD effects on CD19 peripheral B cells were similar between pediatric and adult patients, further supporting the idea that efficacy observed in the adult patients could be extrapolated to the pediatric population. There was no relationship between exposure variability and achievement of efficacy outcomes. In addition, findings from the exposure-safety analysis suggested a lack of a relationship between the occurrence of AEs in the safety analysis and RTX exposure.

Clinical disease remission findings from the exploratory efficacy analyses indicated that RTX had an important

clinical benefit, with PVAS-based remission of GPA or MPA achieved in 56%, 92%, and 100% of patients by months 6, 12, and 18, respectively. In a post hoc sensitivity analysis, excluding 2 patients who had received additional immunosuppressive therapies during the remission-induction period did not change the overall exploratory efficacy outcome conclusions at month 6. Despite the important role of GCs in the treatment and control of GPA and MPA, RTX treatment allowed for a clinically meaningful rapid reduction in the tapering dose of oral GCs from the baseline visit to month 6, which was subsequently maintained at months 12 and 18.

This study was not without limitations. Our small sample size limits the generalizability of the findings to all pediatric patients with GPA or MPA. The inclusion of predominantly female patients is consistent with published reports indicating that AAV is more common in female pediatric patients than in male pediatric patients (23). The PePRS study was designed as an open-label, single-arm, uncontrolled study. The lack of a comparator arm prevents direct comparison of the treatment outcomes with conventional standard of care treatments, such as GCs or CYC. However, given the rarity of the disease and alternative treatment options for pediatric patients newly diagnosed as having GPA or MPA or those who were diagnosed as having relapsing GPA or MPA, an open-label design was considered to be the most appropriate and acceptable study design by global ethics and regulatory agencies. Since other induction regimens (i.e., combining RTX with low-dose CYC) were not studied, the question of whether other approaches could induce remission faster and/or improve overall remission rates with acceptable levels of safety could not be answered in this study.

In summary, treatment with 4 weekly infusions of RTX in combination with a tapering dose of oral GCs was demonstrated to have a clinically important effect on remission induction in pediatric patients who were newly diagnosed as having GPA or MPA or in those with relapsing active GPA or MPA. RTX was well tolerated, with an overall safety profile comparable to that observed in adult patients with GPA or MPA who were treated with RTX, and was an effective long-term approach for disease maintenance or for treating relapsing disease through ≥18 months of follow-up.

ACKNOWLEDGMENTS

We would like to thank all the patients and their families, investigators, study coordinators, and staff from the hospitals and research institutions supporting this study. We would also like to thank Dr. John Stone at Massachusetts General Hospital (Boston, MA), Dr. Pavla Dolezalova at Charles University (Prague, Czech Republic), Dr. Fabrizio De Benedetti at IRCCS Ospedale Pediatrico Bambino Gesù (Lazio, Italy), and Leonid Gibiansky of QuantPharm, LLC (North Potomac, MD). Additionally, we thank Claire Stedden, PhD, and Ellen Mercado, PhD, for providing writing support.

AUTHOR CONTRIBUTIONS

All authors were involved in drafting the article or revising it critically for important intellectual content, and all authors approved the final version to be published. Dr. Brogan had full access to all of the data in the study and takes responsibility for the integrity of the data and the accuracy of the data analysis.

Study conception and design. Brogan, Brunetta, Lehane.

Acquisition of data. Brogan, Yeung, Cleary, Rangaraj, Kasapcopur, Hersh, Li, Paripovic, Schikler, Zeft, Bracaglia, Eleftheriou, Brunetta, Cooper, Lehane.

Analysis and interpretation of data. Brogan, Yeung, Cleary, Rangaraj, Kasapcopur, Hersh, Li, Paripovic, Schikler, Zeft, Bracaglia, Eleftheriou, Pordeli, Melega, Jamois, Gaudreault, Michalska, Brunetta, Cooper, Lehane.

ROLE OF THE STUDY SPONSOR

Hoffmann-La Roche had a role in the study design and in the collection, analysis, and interpretation of the data, and the writing of the manuscript. Authors Pordeli, Melega, Jamois, and Lehane are employees of Hoffmann-La Roche.

ADDITIONAL DISCLOSURES

Author Gaudreault is an employee of JJG Pharma Consulting. Authors Michalska and Brunetta are employees of Genentech.

REFERENCES

- Finkelstein JD, Lee AS, Hummel AM, Viss MA, Jacob GL, Homburger HA, et al. ANCA are detectable in nearly all patients with active severe Wegener's granulomatosis. *Am J Med* 2007;120:643.
- Jariwala MP, Laxer RM. Primary vasculitis in childhood: GPA and MPA in childhood [review]. *Front Pediatr* 2018;6:226.
- De Graeff N, Groot N, Brogan P, Ozen S, Avcin T, Bader-Meunier B, et al. European consensus-based recommendations for the diagnosis and treatment of rare paediatric vasculitides- the SHARE initiative. *Rheumatology (Oxford)* 2019;58:656–71.
- Jones RB, Hiemstra TF, Ballarin J, Blockmans DE, Brogan P, Bruchfeld A, et al. Mycophenolate mofetil versus cyclophosphamide for remission induction in ANCA-associated vasculitis: a randomised, non-inferiority trial. *Ann Rheum Dis* 2019;78:399–405.
- Vanoni F, Bettinelli A, Keller F, Bianchetti MG, Simonetti GD. Vasculitides associated with IgG antineutrophil cytoplasmic autoantibodies in childhood. *Pediatr Nephrol* 2010;25:205–12.
- Martin F, Chan AC. Pathogenic roles of B cells in human autoimmunity; insights from the clinic [review]. *Immunity* 2004;20:517–27.
- Popa ER, Stegeman CA, Bos NA, Kallenberg CG, Tervaert JW. Differential B- and T-cell activation in Wegener's granulomatosis. *J Allergy Clin Immunol* 1999;103:885–94.
- Stone JH, Merkel PA, Spiera R, Seo P, Langford CA, Hoffman GS, et al. Rituximab versus cyclophosphamide for ANCA-associated vasculitis. *N Engl J Med* 2010;363:221–32.
- Guillemin L, Pagnoux C, Karras A, Khouatra C, Aumaitre O, Cohen P, et al. Rituximab versus azathioprine for maintenance in ANCA-associated vasculitis. *N Engl J Med* 2014;371:1771–80.
- James KE, Xiao R, Merkel PA, Weiss PF. Variation in the treatment of children hospitalized with antineutrophil cytoplasmic antibody-associated vasculitis in the US. *Arthritis Care Res (Hoboken)* 2017;69:1377–83.
- Rituxan (rituximab) prescribing information. South San Francisco (CA): Genentech; 2019.
- MabThera (rituximab) summary of product characteristics. Grenzach-Wyhlen, Germany: Roche Registration; 2020.
- Ozen S, Pistorio A, Iusan SM, Bakkaloglu A, Herlin T, Brik R, et al. EULAR/PRINTO/PRES criteria for Henoch-Schönlein purpura, childhood polyarteritis nodosa, childhood Wegener granulomatosis and childhood Takayasu arteritis: Ankara 2008. Part II: Final classification criteria. *Ann Rheum Dis* 2010;69:798–806.
- Jennette JC, Falk RJ, Andrassy K, Bacon PA, Churg J, Gross WL, et al. Nomenclature of systemic vasculitides. Proposal of an international consensus conference [review]. *Arthritis Rheum* 1994;37:187–92.
- Stone JH, Hoffman GS, Merkel PA, Min YI, Uhlfelder ML, Hellmann DB, et al, for the International Network for the Study of the Systemic Vasculitides (INSSYS). A disease-specific activity index for Wegener's granulomatosis: modification of the Birmingham Vasculitis Activity Score. *Arthritis Rheum* 2001;44:912–20.
- Dolezalova P, Price-Kuehne FE, Özen S, Benseler SM, Cabral DA, Anton J, et al. Disease activity assessment in childhood vasculitis: development and preliminary validation of the Paediatric Vasculitis Activity Score (PVAS). *Ann Rheum Dis* 2013;72:1628–33.
- Eleftheriou D, Varnier G, Dolezalova P, McMahon AM, Al-Obaidi M, Brogan PA. Takayasu arteritis in childhood: retrospective experience from a tertiary referral centre in the United Kingdom. *Arthritis Res Ther* 2015;17:36.
- Doležalová P, Wilkinson N, Brogan P, Antón J, Benseler S, Brunner J, et al. Paediatric Vasculitis Damage Index: a new tool for standardised disease assessment [abstract]. *Ann Rheum Dis* 2014;73 Suppl 2:696–7.
- Beal S, Sheiner LB, Boeckmann A, Bauer RJ. NONMEM user's guides (1989-2015). Ellicott City (MD): Icon Development Solutions; 2015.
- Emery P, Fleischmann R, Filipowicz-Sosnowska A, Schechtman J, Szczepanski L, Kavanaugh A, et al. The efficacy and safety of rituximab in patients with active rheumatoid arthritis despite methotrexate treatment: results of a phase IIB randomized, double-blind, placebo-controlled, dose-ranging trial. *Arthritis Rheum* 2006;54:1390–400.
- Kado R, Sanders G, McCune WJ. Diagnostic and therapeutic considerations in patients with hypogammaglobulinemia after rituximab therapy [review]. *Curr Opin Rheumatol* 2017;29:228–33.
- Sacco KA, Abraham RS. Consequences of B-cell-depleting therapy: hypogammaglobulinemia and impaired B-cell reconstitution [review]. *Immunotherapy* 2018;10:713–28.
- Calatroni M, Oliva E, Gianfreda D, Gregorini G, Allinovi M, Ramirez GA, et al. ANCA-associated vasculitis in childhood: recent advances [review]. *Ital J Pediatr* 2017;43:46.

APPENDIX A: MEMBERS OF THE PePRS STUDY GROUP

Members of the PePRS Study Group include Kishore Warrior, Samundeeswari Deepak, the NIHR Team at Nottingham University Hospital, Jennifer Weiss, Liza McCann, Clare Pain, Rebecca Nicolai, Susanna Livadiotti, Nur Canpolat, Kenan Barut, Damien Noone, and Diane Hebert.

A Worldwide Pharmacoepidemiologic Update on Drug-Induced Antineutrophil Cytoplasmic Antibody–Associated Vasculitis in the Era of Targeted Therapies

Samuel Deshayes,¹  Charles Dolladille,¹ Anaël Dumont,²  Nicolas Martin Silva,² Basile Chretien,³ Hubert De Boysson,¹ Joachim Alexandre,¹ and Achille Aouba¹

Objective. The literature supporting the role of a specific drug in the onset of drug-induced antineutrophil cytoplasmic antibody–associated vasculitis (AAV) mainly relies on case reports or short series and implicates old treatments. The advent of new treatments may have modified the epidemiology of these adverse drug reactions. This study was undertaken to update the list of drugs associated with AAV by using a pharmacovigilance-based data mining approach.

Methods. We collected data on adverse drug reactions reported using the Medical Dictionary for Regulatory Activities preferred term “anti-neutrophil cytoplasmic antibody positive vasculitis” up to November 2020 from the World Health Organization pharmacovigilance database (VigiBase). For each retrieved drug, a case–noncase analysis was performed, and disproportionate reporting was calculated by using the information component (IC). A positive IC_{025} value, which is the lower end of the 95% credibility interval, was considered significant.

Results. A total of 483 deduplicated individual case safety reports of drug-induced AAV involving 15 drugs with an $IC_{025} > 0$ were retrieved. Of the individuals with drug-induced AAV for whom data on sex were available ($n = 371$), 264 (71.2%) were women. The median age at onset of drug-induced AAV was 62 years (quartile 1 [Q1]–Q3 45–72 years), and the median time from the introduction of the suspected drug to the onset of drug-induced AAV was 9 months (Q1–Q3 1–36 months). Drug-induced AAV was considered serious in 472 (98.1%), and was fatal in 43 (8.9%), of 481 cases. The drugs associated with the highest disproportionate reporting were hydralazine, propylthiouracil, thiamazole, sofosbuvir, minocycline, carbimazole, mirabegron, and nintedanib.

Conclusion. Our findings strengthen the evidence of an association of AAV with previously suspected drugs, but also identify 3 new drugs that may cause drug-induced AAV. Particular attention should be given to these drugs by prescribers and in experimental studies.

INTRODUCTION

Antineutrophil cytoplasmic antibody (ANCA)–associated vasculitis (AAV) includes primary AAV, such as granulomatosis with polyangiitis (GPA), eosinophilic granulomatosis with polyangiitis (EGPA), and microscopic polyangiitis (MPA), as well as drug-induced AAV (1). The identification of drugs involved in this adverse drug reaction has important epidemiologic and clinical implications, because patients diagnosed as having drug-induced AAV seem to have a better prognosis with less severe vasculitis,

resulting in better overall and renal survival and less frequent relapses than seen in those diagnosed as having primary AAV (2–5). In addition, the withdrawal of the culprit drug is sometimes sufficient to achieve resolution of vasculitis in mild cases, without the need for immunosuppressants, and may obviate the need for maintenance treatment (5,6). However, it is difficult to attribute AAV to a suspected drug, and the data in the literature supporting the role of a drug in the onset of AAV mainly rely on case reports or short series and mostly implicate old treatments, such as propylthiouracil, hydralazine, allopurinol, D-penicillamine, minocycline,

¹Samuel Deshayes, MD, Charles Dolladille, MD, Hubert De Boysson, MD, PhD, Joachim Alexandre, MD, PhD, Achille Aouba, MD, PhD: Normandie Université, Université Caen-Normandie, EA4650 SEILIRM, Centre Hospitalier Universitaire de Caen Normandie, Caen, France; ²Anaël Dumont, MD, Nicolas Martin Silva, MD: Normandie Université, Université Caen-Normandie, Centre Hospitalier Universitaire de Caen Normandie, Caen, France; ³Basile Chretien, PharmD: Centre Hospitalier Universitaire de Caen Normandie, Caen, France.

No potential conflicts of interest relevant to this article were reported. Address correspondence to Achille Aouba, MD, PhD, CHU Côte de Nacre–Université Caen Basse Normandie, Service de Médecine Interne et d’Immunologie Clinique, Avenue de la Côte de Nacre, 14000 Caen, France. Email: aouba-a@chu-caen.fr.

Submitted for publication January 28, 2021; accepted in revised form June 10, 2021.

leukotriene antagonists, and, more recently, anti-tumor necrosis factor (7,8). The advent of new treatments may have modified the epidemiology of these adverse drug reactions. We therefore aimed to update the list of drugs associated with drug-induced AAV by using a pharmacovigilance-based data mining approach.

METHODS

Study design. For this retrospective disproportionality analysis, we used the World Health Organization (WHO) pharmacovigilance database (VigiBase), managed by the Uppsala Monitoring Centre (Uppsala, Sweden). As of 2020, this database contained >23,000,000 individual case safety reports (ICSRs) from >130 countries.

We collected data on all adverse drug reactions reported with the Medical Dictionary for Regulatory Activities (MedDRA) version 23.1 preferred term “anti-neutrophil cytoplasmic antibody positive vasculitis” from the introduction of this preferred term in 2006 to November 2020. The drugs considered were those denoted as suspected or interacting. We did not study the following drugs due to potential indication bias, since these drugs are indicated in the management of AAV (9): azathioprine, cyclophosphamide, leflunomide, methotrexate, methylprednisolone, mycophenolic acid, prednisolone, prednisone, rituximab, glucocorticoids, and trimethoprim/sulfamethoxazole.

Each report included administrative information (reporter and reporting region, year and date), patient characteristics (sex and age at onset), drug(s) (suspected, interacting, and concomitant, with start and end dates and dosage), and reaction(s) (including seriousness and death) (10). A serious adverse drug reaction was defined as an adverse drug reaction that caused death; was life-threatening; required or prolonged hospitalization; or led to a

persistent or significant disability, congenital anomaly, birth defect, or to any other medically important condition. The study was approved by the local ethics committee of Caen University Hospital (Comité Local d’Ethique de la Recherche en Santé, no. 2008).

Statistical analysis. For each suspected drug, a case–noncase analysis of AAV reporting was performed. We calculated disproportionality using the information component (IC), as well as the reporting odds ratio (ROR) and its 95% confidence interval. The IC is a validated Bayesian indicator that compares the number of cases observed for a specific drug–adverse drug reaction pair with the number of cases expected for that pair given the hypothesis of an independent distribution of the reporting of the adverse drug reaction and the drug in VigiBase. The IC is computed using the following formula:

$$IC = \log_2([N_{\text{observed}} + 0.5]/[N_{\text{expected}} + 0.5])$$

where $N_{\text{expected}} = (N_{\text{drug}} * N_{\text{adverse reaction}}) / N_{\text{total}}$, and N_{observed} is the actual number of case reports for the drug–adverse drug reaction combination; N_{expected} is the number of case reports expected for the drug–adverse drug reaction combination; $N_{\text{adverse reaction}}$ is the number of case reports for the adverse reaction, regardless of the drug; N_{drug} is the number of case reports for the drug, regardless of the adverse drug reaction; and N_{total} is the total number of case reports in the database. Since the preferred term “anti-neutrophil cytoplasmic antibody positive vasculitis” was introduced in 2006, the IC and ROR were calculated with the number of cases (N_{expected} , N_{drug} , and N_{total}) reported since 2006. The $IC_{0.025}$, which is the lower end of the 95% credibility interval for the IC, was used to test significance (associations were considered significant if $IC_{0.025}$ was greater than 0) (10). Descriptive

Table 1. Drugs with significantly disproportional reporting of an association with AAV in VigiBase, sorted by decreasing $IC_{0.025}$ value*

Drug	No. of ICSRs	No. (%) of fatal reactions	$IC_{0.025}/IC$	ROR (95% CI)	Time from introduction of the drug to onset of AAV, median (Q1–Q3) days/no. with data available
Hydralazine	208	19 (9)	8.2/8.4	2,683.5 (2,269.3–3,173.3)	1,277/1
Propylthiouracil	108	4 (4)	7.2/7.5	1,201.5 (974.8–1,480.9)	1,003 (425–1,959)/19
Thiamazole	40	5 (13)	5.2/5.6	138.7 (100.7–191.1)	411 (58–966)/6
Sofosbuvir	46	0 (0)	4.9/5.3	74.6 (55.3–100.8)	NA
Minocycline	17	0 (0)	3.8/4.6	72.4 (44.7–117.3)	NA
Carbimazole	6	0 (0)	2.0/3.4	44.9 (20.1–100.4)	92/1
Mirabegron	7	2 (29)	1.5/2.7	11.1 (5.3–23.3)	291 (289–415)/3
Nintedanib	6	2 (33)	1.4/2.8	14.2 (6.3–31.7)	56 (36–132)/4
Penicillamine	4	1 (25)	1.4/3.1	170.3 (63.5–456.3)	NA
Influenza vaccine	29	2 (7)	1.3/1.9	4.1 (2.8–6.0)	24 (20–26)/7
Allopurinol	7	2 (29)	1.2/2.4	8.0 (3.8–16.8)	NA
Rifampicin	7	2 (29)	0.6/1.9	4.7 (2.2–9.8)	NA
PEGylated interferon alfa-2b	4	0 (0)	0.3/2.1	7.0 (2.6–18.6)	98/1
Montelukast	4	4 (100)	0.2/1.9	5.8 (2.2–15.5)	NA
Rosuvastatin	6	0 (0)	0.1/1.5	3.4 (1.5–7.5)	NA

* AAV = antineutrophil cytoplasmic antibody-associated vasculitis; $IC_{0.025}$ = lower end of the 95% credibility interval for the information component; ICSRs = individual case safety reports; ROR = reporting odds ratio; 95% CI = 95% confidence interval; Q1 = quartile 1; NA = not available.

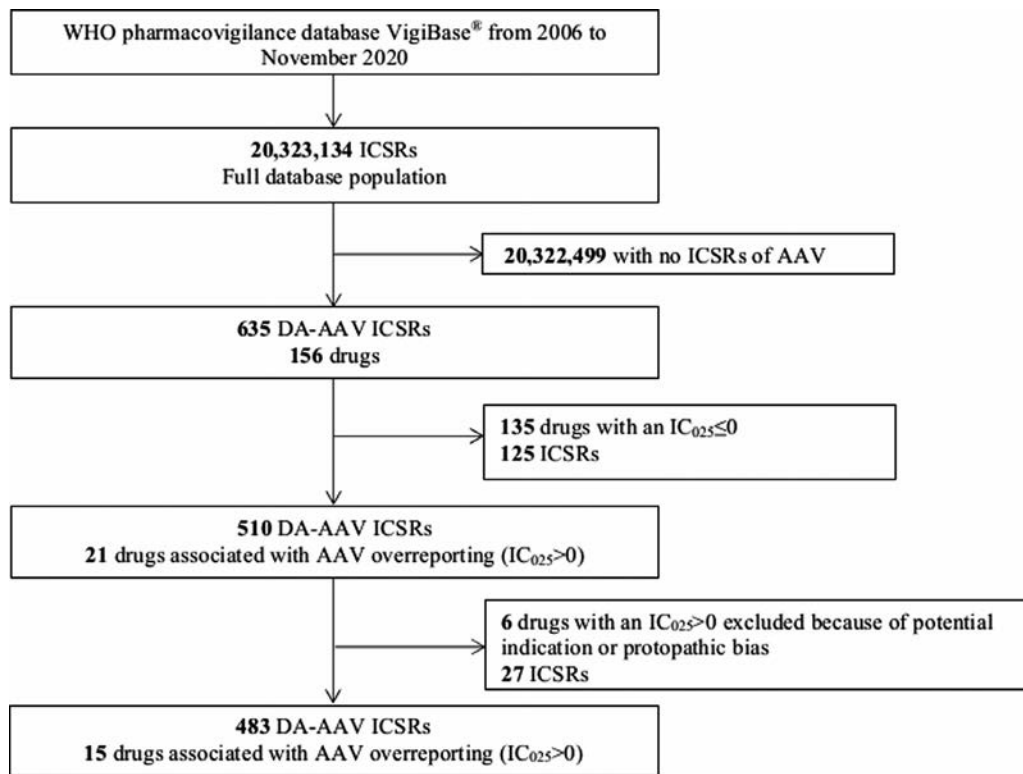


Figure 1. Flow chart of the selection of deduplicated individual case safety reports (ICSRs) of drug-associated antineutrophil cytoplasmic antibody-associated vasculitis (DA-AAV) in the World Health Organization (WHO) pharmacovigilance database VigiBase. IC = information component.

data are presented as the median (quartile 1 [Q1]–Q3) or number (percentage).

RESULTS

A total of 635 deduplicated ICSRs of drug-induced AAV between 2006 and November 2020 were identified in VigiBase. Overall, 15 drugs with an $IC_{025} > 0$ (Table 1), accounting for 483 ICSRs, were included after the exclusion of drugs with potential indication or protopathic biases (Figure 1).

The drugs associated with the highest disproportionate reporting and the highest number of reported cases (Table 1) were hydralazine (IC_{025} 8.2) (43.1%; $n = 208$), propylthiouracil (IC_{025} 7.2) (22.4%; $n = 108$), thiamazole (IC_{025} 5.2) (8.3%; $n = 40$), and sofosbuvir (IC_{025} 4.9) (9.5%; $n = 46$). After hydralazine, the second most frequently reported pharmaceutical class was antithyroid drugs, accounting for 154 ICSRs (31.9%).

These 483 ICSRs originated from 18 different countries, mostly from the US and Japan (52.4% and 27.1%, respectively). Data on reporters were available for 458 ICSRs (94.8%). Of these, the majority were reported by physicians (169 [36.9%]) or other health professionals (255 [55.7%]).

Of the individuals with drug-induced AAV for whom data on sex were available (371 [76.8%] of the ICSRs), 264 (71.2%) were women. After ICSRs associated with antithyroid drugs were excluded, 135 (61.6%) of the ICSRs were for women. The median

age at onset of drug-induced AAV was 62 years (Q1–Q3 45–72 years) (age data were available for 373 ICSRs [77.2%]). The median time between the introduction of the suspected drug and the onset of AAV was 9 months (Q1–Q3 1–36 months) (data available only for 44 ICSRs [9.1%]). This adverse drug reaction was considered serious in 472 (98.1%) cases (data available for 481 ICSRs [99.6%]), and 43 (8.9%) cases were associated with death at the time of reporting.

Regarding the co-reported MedDRA preferred terms, the most frequent were acute kidney injury ($n = 51$), glomerulonephritis rapidly progressive ($n = 42$), pulmonary alveolar hemorrhage ($n = 35$), glomerulonephritis ($n = 29$), and pulmonary renal syndrome ($n = 27$). GPA was co-reported in 11 cases, MPA in 7 cases, and EGPA in 1 case. For exploratory purposes, we listed the drugs with an $IC_{025} > 0$ associated with the preferred terms “granulomatosis with polyangiitis,” “microscopic polyangiitis,” and “eosinophilic granulomatosis with polyangiitis” in Supplementary Tables 1–3, available on the *Arthritis & Rheumatology* website at <http://onlinelibrary.wiley.com/doi/10.1002/art.41902/abstract>.

DISCUSSION

To our knowledge, this is the first systematic pharmacovigilance study focusing on drug-induced AAV, and it includes the largest number of cases and drugs examined to date. In addition

to confirming significant pharmacovigilance signals associated with drugs previously identified as being associated with AAV, such as hydralazine and antithyroid drugs, this study also found a significant overreporting of recently developed drugs in relation to drug-induced AAV, including mirabegron and 2 targeted therapies, sofosbuvir and nintedanib. Ultimately, these data indicate that prescribers should pay specific attention to these drugs, and support the need for experimental studies on AAV pathophysiology and these recently developed drugs.

Multiple hypotheses have been formulated regarding the pathophysiology of drug-induced AAV, and several have been experimentally proven, mainly for propylthiouracil and hydralazine. The main hypotheses include an imbalance in leukotriene receptor stimulation responsible for an increase in the levels of leukotriene B₄, a chemoattractant for eosinophils and neutrophils, in the case of leukotriene antagonist use (11); a modification in the structure of myeloperoxidase within neutrophils, resulting in the induction of ANCA (12); an induction of neutrophil apoptosis by drugs (12); an inhibition of the oxidation activity of myeloperoxidase (13,14); an immunogenicity of drug metabolites (13); an induction of an abnormal conformation and an impaired degradation of neutrophil extracellular traps (15,16); and a reversal of epigenic silencing of neutrophil antigens (17). In addition, causality criteria, at least for some drugs, have previously been reported, such as a temporal association in prospective studies (18), favorable outcome at dechallenge without specific treatment in mild cases (6,19), and relapse after rechallenge (20,21).

The epidemiology of drug-induced AAV could be different from that of primary AAV, with a clear predominance of female patients among those with drug-induced AAV: 71.2% in our study versus ~50% in an international observational study of 967 patients with primary AAV (22). However, the median age at diagnosis in our study (62 years) was similar to that in the previous study (58.3 years) (22). A possible explanation for the higher proportion of female patients with drug-induced AAV is that numerous reports of drug-induced AAV in our cohort were related to antithyroid drugs, and thyroid diseases occur far more frequently in women than in men (23).

Hydralazine is a well-known cause of systemic lupus erythematosus, which occurs in up to 5–15% of patients (24,25). Moreover, several case reports and case series have also described vasculitis involvement with antimyeloperoxidase antibodies associated with the introduction of hydralazine (15,26,27), consistent with the results of our study.

The association between antithyroid drugs and AAV has been extensively studied and has been reported in >250 patients. The majority, i.e., 75%, of these cases of antithyroid drug-induced AAV were associated with thiouracil derivatives (propylthiouracil and benzylthiouracil), and the remaining 25% were associated with methyl mercaptoimidazole derivatives (methimazole/thiamazole and carbimazole) (28). AAV affects ~3% of patients treated with antithyroid drugs (28,29), with an annual incidence estimated at between 5.3 and 7.9 patients per 100,000 (30). These rates are

higher than those in the general population, where the prevalence and annual incidence of primary AAV are estimated to be <0.5% and 3.5 per 100,000, respectively (31–33). Of note, in our study, we found that among antithyroid drugs, the strongest pharmacovigilance signal implicated propylthiouracil, followed by thiamazole, whereas this association was less well described in the literature. Among antithyroid drugs, only benzylthiouracil did not show significant overreporting, but a lack of power cannot be excluded.

Regarding minocyclin, which was identified as being associated with drug-induced AAV in this study, the possibility of information bias (misclassification of the disease) cannot be excluded. Indeed, despite the presence of perinuclear ANCA positivity, the previously described clinical picture in the literature corresponded to polyarteritis nodosa with the involvement of medium-sized vessels (34).

Montelukast, which was also identified as being associated with drug-induced AAV in this study, along with almost every drug associated with EGPA, will be more of a subject of controversy (Supplementary Table 3). Indeed, the hypotheses regarding whether montelukast or other drugs for asthma actually provoke EGPA, or are rather prescribed because of the severity of the asthma that precedes the full spectrum of EGPA (protopathic bias), have not yet been settled because of conflicting results of previous studies (20,35–37).

Regarding other drugs associated with a significant disproportionality in our study, only a few case reports or small case series have been published implicating penicillamine (38,39), influenza vaccine (40), allopurinol (39,41), rifampicin (42), or interferon- α (43). Of note, several previous studies did not find an increased risk of AAV relapse after influenza vaccination (44–46), and the overreporting we found needs to be studied further to exclude bias, including recall and notoriety bias, with regard to this single-injection drug administered once a year. For sofosbuvir, which is a more recently engineered treatment for chronic hepatitis C infection, only 2 articles have been published to our knowledge in the setting of drug-induced AAV (47,48). However, since hepatitis C infection may itself induce ANCAs (49) and cryoglobulinemia production in the context of systemic small vessel vasculitis that may mimic clinical manifestations of AAV, information bias cannot be excluded. However, the high disproportional reporting associated with sofosbuvir in our study is evidence of a need for particular attention to this drug and further observational and experimental studies.

To our knowledge, no case of AAV associated with rosuvastatin, mirabegron, or nintedanib has previously been reported, although we cannot eliminate a protopathic bias with regard to nintedanib (prescription of the drug in response to some early symptoms of the disease). Indeed, nintedanib was mainly engineered to treat idiopathic pulmonary fibrosis, the diagnosis of which requires the exclusion of other causes of lung involvement. Some patterns of fibrotic interstitial lung disease may be observed in the spectrum of AAV, notably as the first manifestation of MPA

(50). Therefore, we cannot exclude the possibility that nintedanib overreporting in our study was secondary to a misdiagnosis of idiopathic pulmonary fibrosis with unrecognized AAV at its onset, and therefore this apparent association should be interpreted with caution. In addition, since nintedanib has shown efficacy for the treatment of interstitial lung involvement secondary to connective tissue diseases such as systemic sclerosis, mixed connective tissue disease, and rheumatoid arthritis (51), the possibility that this new drug will also be offered for the treatment of interstitial lung involvement secondary to AAV cannot be excluded. Therefore, future studies are needed to clarify the potential association with AAV.

Of note, levamisole was not associated with a significant disproportionality in our study, although it is a well-known inducer of AAV. This is probably because levamisole is no longer used as an immunomodulator in humans (withdrawn from the US market in 2000) but as an adulterant for cocaine.

This study has several limitations that are common to studies based on pharmacovigilance databases (10), including notoriety bias (increased number of reports after safety alerts in the media), missing data (including on the delay between the introduction of the drug and the onset of AAV, which was available for <10% of the patients), and bias related to its retrospective and declarative design. Moreover, the significant associations found, defined by a positive IC_{025} , do not imply causality. However, this data mining approach allows for the automated detection of drug safety signals associated with rare events such as AAV and for the description of the largest series of drug-induced AAV.

To conclude, this first worldwide systematic pharmacovigilance study described the largest series of drug-induced AAV cases, implicating several drugs, some of which were already suspected to be a cause of drug-induced AAV. In addition to strengthening the suspected associations between drug-induced AAV and previously reported drugs, such as hydralazine and antithyroid drugs, this study also showed that several recently developed drugs, including sofosbuvir, mirabegron, and nintedanib, are significantly associated with AAV overreporting. Specific prescriber attention to these drugs is needed, as well as experimental and observational studies to confirm these epidemiologic data.

AUTHOR CONTRIBUTIONS

All authors were involved in drafting the article or revising it critically for important intellectual content, and all authors approved the final version to be published. Dr. Deshayes had full access to all of the data in the study and takes responsibility for the integrity of the data and the accuracy of the data analysis.

Study conception and design. Deshayes, Dolladille, Aouba.

Acquisition of data. Deshayes, Dolladille, Chretien, Alexandre, Aouba.

Analysis and interpretation of data. Deshayes, Dolladille, Dumont, Martin Silva, Chretien, De Boysson, Alexandre, Aouba.

REFERENCES

- Jennette JC, Falk RJ, Bacon PA, Basu N, Cid MC, Ferrario F, et al. 2012 revised International Chapel Hill Consensus Conference nomenclature of vasculitides. *Arthritis Rheum* 2013;65:1–11.
- Fujieda M, Hattori M, Kurayama H, Koitabashi Y, on behalf of the Members and Coworkers of the Japanese Society for Pediatric Nephrology. Clinical features and outcomes in children with anti-neutrophil cytoplasmic autoantibody-positive glomerulonephritis associated with propylthiouracil treatment. *J Am Soc Nephrol* 2002;13:437–45.
- Chen YX, Zhang W, Chen XN, Yu HJ, Ni LY, Xu J, et al. Propylthiouracil-induced antineutrophil cytoplasmic antibody (ANCA)-associated renal vasculitis versus primary ANCA-associated renal vasculitis: a comparative study. *J Rheumatol* 2012;39:558–63.
- Yu F, Chen M, Gao Y, Wang SX, Zou WZ, Zhao MH, et al. Clinical and pathological features of renal involvement in propylthiouracil-associated ANCA-positive vasculitis. *Am J Kidney Dis* 2007;49:607–14.
- Gao Y, Chen M, Ye H, Yu F, Guo XH, Zhao MH. Long-term outcomes of patients with propylthiouracil-induced anti-neutrophil cytoplasmic auto-antibody-associated vasculitis. *Rheumatology (Oxford)* 2008;47:1515–20.
- Gao Y, Zhao MH. Review article: drug-induced anti-neutrophil cytoplasmic antibody-associated vasculitis. *Nephrology (Carlton)* 2009;14:33–41.
- Kitching AR, Anders HJ, Basu N, Brouwer E, Gordon J, Jayne DR, et al. ANCA-associated vasculitis [review]. *Nat Rev Dis Primers* 2020;6:71.
- Haute Autorité de Santé. Purpura thrombopénique immunologique de l'enfant et de l'adulte. June 2017. URL: https://www.has-sante.fr/jcms/c_2772874/fr/purpura-thrombopenique-immunologique-de-l-enfant-et-de-l-adulte.
- Yates M, Watts RA, Bajema IM, Cid MC, Crestani B, Hauser T, et al. EULAR/ERA-EDTA recommendations for the management of ANCA-associated vasculitis. *Ann Rheum Dis* 2016;75:1583–94.
- Bihan K, Lebrun-Vignes B, Funck-Brentano C, Salem JE. Uses of pharmacovigilance databases: an overview. *Therapie* 2020;75:591–8.
- McDanel DL, Muller BA. The linkage between Churg-Strauss syndrome and leukotriene receptor antagonists: fact or fiction? *Ther Clin Risk Manag* 2005;1:125–40.
- Bonaci-Nikolic B, Nikolic MM, Andrejevic S, Zoric S, Bukilica M. Antineutrophil cytoplasmic antibody (ANCA)-associated autoimmune diseases induced by antithyroid drugs: comparison with idiopathic ANCA vasculitides. *Arthritis Res Ther* 2005;7:R1072–81.
- Chen M, Gao Y, Guo XH, Zhao MH. Propylthiouracil-induced anti-neutrophil cytoplasmic antibody-associated vasculitis [review]. *Nat Rev Nephrol* 2012;8:476–83.
- Zhang AH, Chen M, Gao Y, Zhao MH, Wang HY. Inhibition of oxidation activity of myeloperoxidase (MPO) by propylthiouracil (PTU) and anti-MPO antibodies from patients with PTU-induced vasculitis. *Clin Immunol* 2007;122:187–93.
- Magro CM, Momtahn S, Harp J. The distinctive histopathology of hydralazine-associated ANCA positive vasculitis: in vivo demonstration of NETosis. *Eur J Dermatol* 2017;27:91–2.
- Nakazawa D, Tomaru U, Suzuki A, Masuda S, Hasegawa R, Kobayashi T, et al. Abnormal conformation and impaired degradation of propylthiouracil-induced neutrophil extracellular traps: implications of disordered neutrophil extracellular traps in a rat model of myeloperoxidase antineutrophil cytoplasmic antibody-associated vasculitis. *Arthritis Rheum* 2012;64:3779–87.
- Aeddula NR, Pathireddy S, Ansari A, Juran PJ. Hydralazine-associated antineutrophil cytoplasmic antibody vasculitis with pulmonary-renal syndrome. *BMJ Case Rep* 2018;2018:bcr2018227161.
- Cin MO, Gursoy A, Morris Y, Aydintug OT, Kamel N, Gullu S. Prevalence and clinical significance of antineutrophil cytoplasmic antibody in Graves' patients treated with propylthiouracil. *Int J Clin Pract* 2009;63:299–302.

19. Grau RG. Drug-induced vasculitis: new insights and a changing lineup of suspects [review]. *Curr Rheumatol Rep* 2015;17:71.
20. Nathani N, Little MA, Kunst H, Wilson D, Thickett DR. Churg-Strauss syndrome and leukotriene antagonist use: a respiratory perspective [review]. *Thorax* 2008;63:883–8.
21. Chen Y, Bao H, Liu Z, Zhang H, Zeng C, Liu Z, et al. Clinico-pathological features and outcomes of patients with propylthiouracil-associated ANCA vasculitis with renal involvement. *J Nephrol* 2014;27:159–64.
22. Pearce FA, Craven A, Merkel PA, Luqmani RA, Watts RA. Global ethnic and geographic differences in the clinical presentations of antineutrophil cytoplasm antibody-associated vasculitis. *Rheumatology (Oxford)* 2017;56:1962–9.
23. Hollowell JG, Staehling NW, Flanders WD, Hannon WH, Gunter EW, Spencer CA, et al. Serum TSH, T₄, and thyroid antibodies in the United States population (1988 to 1994): National Health and Nutrition Examination Survey (NHANES III). *J Clin Endocrinol Metab* 2002;87:489–99.
24. Arnaud L, Mertz P, Gavand PE, Martin T, Chasset F, Tebacher-Alt M, et al. Drug-induced systemic lupus: revisiting the ever-changing spectrum of the disease using the WHO pharmacovigilance database. *Ann Rheum Dis* 2019;78:504–8.
25. Yokogawa N, Vivino FB. Hydralazine-induced autoimmune disease: comparison to idiopathic lupus and ANCA-positive vasculitis [review]. *Mod Rheumatol* 2009;19:338–47.
26. Kumar B, Strouse J, Swee M, Lenert P, Suneja M. Hydralazine-associated vasculitis: overlapping features of drug-induced lupus and vasculitis. *Semin Arthritis Rheum* 2018;48:283–7.
27. Nässberger L, Johansson AC, Björck S, Sjöholm AG. Antibodies to neutrophil granulocyte myeloperoxidase and elastase: autoimmune responses in glomerulonephritis due to hydralazine treatment. *J Intern Med* 1991;229:261–5.
28. Balavoine AS, Glinoe D, Dubucquoi S, Wémeau JL. Antineutrophil cytoplasmic antibody-positive small-vessel vasculitis associated with antithyroid drug therapy: how significant is the clinical problem? [review]. *Thyroid* 2015;25:1273–81.
29. Gao Y, Zhao M, Guo X, Xin G, Gao Y, Wang H. The prevalence and target antigens of antithyroid drugs induced antineutrophil cytoplasmic antibodies (ANCA) in Chinese patients with hyperthyroidism. *Endocr Res* 2004;30:205–13.
30. Noh JY, Yasuda S, Sato S, Matsumoto M, Kunii Y, Noguchi Y, et al. Clinical characteristics of myeloperoxidase antineutrophil cytoplasmic antibody-associated vasculitis caused by antithyroid drugs. *J Clin Endocrinol Metab* 2009;94:2806–11.
31. Berti A, Cornec D, Crowson CS, Specks U, Matteson EL. The epidemiology of antineutrophil cytoplasmic autoantibody-associated vasculitis in Olmsted County, Minnesota: a twenty-year US population-based study. *Arthritis Rheumatol* 2017;69:2338–50.
32. Mohammad AJ, Jacobsson LT, Westman KW, Sturfelt G, Segelmark M. Incidence and survival rates in Wegener's granulomatosis, microscopic polyangiitis, Churg-Strauss syndrome and polyarteritis nodosa. *Rheumatology (Oxford)* 2009;48:1560–5.
33. Mohammad AJ, Jacobsson LT, Mahr AD, Sturfelt G, Segelmark M. Prevalence of Wegener's granulomatosis, microscopic polyangiitis, polyarteritis nodosa and Churg-Strauss syndrome within a defined population in southern Sweden. *Rheumatology (Oxford)* 2007;46:1329–37.
34. Kermani TA, Ham EK, Camilleri MJ, Warrington KJ. Polyarteritis nodosa-like vasculitis in association with minocycline use: a single-center case series. *Semin Arthritis Rheum* 2012;42:213–21.
35. Bibby S, Healy B, Steele R, Kumareswaran K, Nelson H, Beasley R. Association between leukotriene receptor antagonist therapy and Churg-Strauss syndrome: an analysis of the FDA AERS database. *Thorax* 2010;65:132–8.
36. Hauser T, Mahr A, Metzler C, Coste J, Sommerstein R, Gross WL, et al. The leukotriene receptor antagonist montelukast and the risk of Churg-Strauss syndrome: a case-crossover study. *Thorax* 2008;63:677–82.
37. Wechsler ME, Wong DA, Miller MK, Lawrence-Miyasaki L. Churg-Strauss syndrome in patients treated with omalizumab. *Chest* 2009;136:507–18.
38. Rozina T, Fastovets S, Lee O, Kuchieva A, Bulanov N, Moiseev S. D-penicillamine-induced autoimmune disorders. *Dig Liver Dis* 2019;51:1741–2.
39. Choi HK, Merkel PA, Walker AM, Niles JL. Drug-associated antineutrophil cytoplasmic antibody-positive vasculitis: prevalence among patients with high titers of antimyeloperoxidase antibodies. *Arthritis Rheum* 2000;43:405–13.
40. Jeffs LS, Nitschke J, Tervaert JW, Peh CA, Hurtado PR. Viral RNA in the influenza vaccine may have contributed to the development of ANCA-associated vasculitis in a patient following immunisation. *Clin Rheumatol* 2016;35:943–51.
41. Choi HK, Merkel PA, Niles JL. ANCA-positive vasculitis associated with allopurinol therapy. *Clin Exp Rheumatol* 1998;16:743–4.
42. Ji G, Zeng X, Sandford AJ, He JQ. Rifampicin-induced antineutrophil cytoplasmic antibody-positive vasculitis: a case report and review of the literature. *Int J Clin Pharmacol Ther* 2016;54:804–7.
43. Wilson LE, Widman D, Dikman SH, Gorevic PD. Autoimmune disease complicating antiviral therapy for hepatitis C virus infection [review]. *Semin Arthritis Rheum* 2002;32:163–73.
44. Stassen PM, Sanders JS, Kallenberg CG, Stegeman CA. Influenza vaccination does not result in an increase in relapses in patients with ANCA-associated vasculitis. *Nephrol Dial Transplant* 2008;23:654–8.
45. Holvast A, Stegeman CA, Benne CA, Huckriede A, Wilschut JC, Palache AM, et al. Wegener's granulomatosis patients show an adequate antibody response to influenza vaccination. *Ann Rheum Dis* 2009;68:873–8.
46. Jeffs LS, Peh CA, Jose MD, Lange K, Hurtado PR. Randomized trial investigating the safety and efficacy of influenza vaccination in patients with antineutrophil cytoplasmic antibody-associated vasculitis. *Nephrology (Carlton)* 2015;20:343–51.
47. Ahmad YK, Tawfeek S, Sharaf-Eldin M, Elbatea HE, Kobtan A, El-Kalla F, et al. Anti-nuclear cytoplasmic antibody-associated vasculitis: a probable adverse effect of sofosbuvir treatment in chronic hepatitis C patients. *Hospital Pharmacy* 2017;52:294–301.
48. Gadde S, Lee B, Kidd L, Zhang R. Antineutrophil cytoplasmic antibodies crescentic allograft glomerulonephritis after sofosbuvir therapy. *World J Nephrol* 2016;5:547.
49. Palazzi C, Buskila D, D'Angelo S, D'Amico E, Olivieri I. Autoantibodies in patients with chronic hepatitis C virus infection: pitfalls for the diagnosis of rheumatic diseases [review]. *Autoimmun Rev* 2012;11:659–63.
50. Alba MA, Flores-Suárez LF, Henderson AG, Xiao H, Hu P, Nachman PH, et al. Interstitial lung disease in ANCA vasculitis [review]. *Autoimmun Rev* 2017;16:722–9.
51. Flaherty KR, Wells AU, Cottin V, Devaraj A, Walsh SL, Inoue Y, et al. Nintedanib in progressive fibrosing interstitial lung diseases. *N Engl J Med* 2019;381:1718–27.

Time-Dependent Analysis of Risk of New-Onset Heart Failure Among Patients With Polymyositis and Dermatomyositis

Chun-Yu Lin,¹  Hung-An Chen,² Tsai-Ching Hsu,³ Chun-Hsin Wu,¹  Yu-Jih Su,⁴  and Chung-Yuan Hsu⁵ 

Objective. To determine the risk and time trends of heart failure (HF) leading to hospitalization in individuals newly diagnosed as having polymyositis/dermatomyositis (PM/DM) relative to non-PM/DM controls at the general population level.

Methods. A retrospective cohort study was conducted using data from a nationwide insurance database in Taiwan. Patients with incident PM/DM and without a history of HF were selected between 2000 and 2013. Unmatched and propensity score–matched cohorts were established separately. A multivariable Cox proportional hazards regression model was used to estimate the adjusted hazard ratio (HR) for the risk of HF in the unmatched cohort. In the propensity score–matched cohort, general population controls were selected and matched at a 1:1 ratio to the patients with PM/DM based on propensity scores, which accounted for the confounding factors of age, sex, index date (year) of first diagnosis, comorbidities, and medication usage. The cumulative incidence of HF was estimated using the Kaplan-Meier method. A stratified Cox proportional hazards model was used to calculate the HR for the risk of HF events at different follow-up time points among patients with PM/DM compared with non-PM/DM controls in the propensity score–matched cohort.

Results. In the unmatched cohort, the study assessed 2,025 patients with PM/DM and 196,109 general population controls. Results of multivariable Cox regression analysis, adjusted for age, sex, comorbidities, and medication usage, revealed a greater risk of HF leading to hospitalization in the PM/DM group than in the control group (adjusted HR 3.29, 95% confidence interval [95% CI] 2.60–4.18). After matching based on propensity score, a total of 1,997 pairs of PM/DM patients and general population controls were identified. In this propensity score–matched cohort, the cumulative incidence of HF in patients with PM/DM at 3 years, 5 years, and 10 years was 3.3%, 4.4%, and 7.4%, respectively. The absolute difference in HF risk in the PM/DM group compared with the control group was 1.8% at 3 years, 2.1% at 5 years, and 3.0% at 10 years. Compared with general population controls, patients with PM/DM exhibited an augmented risk of HF (HR 2.06, 95% CI 1.36–3.12). Analyses stratified according to follow-up time point revealed that the increased risk of HF persisted for up to 10 years after the PM/DM diagnosis.

Conclusion. These results indicate that the risk of HF leading to hospitalization was increased in patients with PM/DM throughout the study period, supporting the need for greater vigilance in the monitoring of patients with PM/DM for the development of this potentially lethal complication.

INTRODUCTION

Polymyositis (PM) and dermatomyositis (DM) are immune-mediated diseases that are characterized by infiltration of inflammatory cells in the skeletal muscle and progressive muscle

weakness (1,2). Extramuscular manifestations, such as interstitial lung disease, gastrointestinal involvement, and cardiac involvement, can occur in PM/DM (3). Before the 1970s, cardiac involvement was thought to be a rare event in the idiopathic inflammatory myopathies (4). Following the introduction of more sensitive and

Supported by the National Cheng Kung University Hospital (grants NCKUH-11003017 and NCKUH-10803032).

¹Chun-Yu Lin, MD, Chun-Hsin Wu, MD: Division of Rheumatology, Allergy, and Immunology, Department of Internal Medicine, National Cheng Kung University Hospital, College of Medicine, National Cheng Kung University, Tainan, Taiwan; ²Hung-An Chen, MD: Department of Internal Medicine, Chi Mei Medical Center, Tainan, Taiwan; ³Tsai-Ching Hsu, PhD: Chung Shan Medical University, Taichung, Taiwan; ⁴Yu-Jih Su, MD: Gung Memorial Hospital, Kaohsiung, Taiwan; ⁵Chung-Yuan Hsu, MD: Division of Rheumatology, Allergy, and Immunology, Department of Internal Medicine, Kaohsiung Chang Gung Memorial Hospital, and

School of Medicine, College of Medicine, Chang Gung University, Taoyuan, Taiwan.

Author disclosures are available at <https://onlinelibrary.wiley.com/action/downloadSupplement?doi=10.1002%2Fart.41907&file=art41907-sup-0001-Disclosureform.pdf>.

Address correspondence to Chun-Yu Lin, MD, Number 138, Sheng Li Road, Tainan 704, Taiwan (email: linchunyumed@gmail.com); or Chung-Yuan Hsu, MD, Number 123, Ta Pei Road, Niao Sung District, Kaohsiung 83301, Taiwan (email: chungyuango@gmail.com).

Submitted for publication November 14, 2020; accepted in revised form June 23, 2021.

noninvasive techniques into daily practice, there have been more reports of cases of subclinical and clinically relevant cardiac manifestations occurring in patients with PM/DM (5–12). Recent findings in a few epidemiologic studies have indicated that the risk of atherosclerosis and myocardial infarction are higher among patients with PM/DM compared with general population controls (13,14). However, the actual frequency of cardiac manifestations, apart from coronary heart disease, in patients with PM/DM remains uncertain, as there is a paucity of large-scale epidemiologic studies investigating cardiac risks in patients with PM/DM.

The most frequently reported, clinically evident cardiac manifestation in PM/DM is heart failure (HF), but there is a wide variation in its reported frequency, ranging from 32% to 77% (4,5,15). Based on a systematic review, HF is the leading cause of cardiac death in patients with PM/DM, followed by acute myocardial infarction and complete heart block (8). However, previous studies regarding the risk of HF in patients with PM/DM have been limited by several factors, including the following: small numbers of patients studied, cross-sectional study designs, being limited to a single-center study, lack of long-term follow-up data, use of a target population with overlap syndrome, and lack of a matched control population. Consequently, it has been difficult to infer the relative risk of HF in PM/DM. In the present study, we therefore aimed to investigate the risk and magnitude of new-onset HF among patients with PM/DM compared with general population controls, using a nationwide, population-based administrative health database in Taiwan.

PATIENTS AND METHODS

Study design, data source, and ethics approval. An observational, retrospective cohort study design was used. All data were retrieved from the Taiwan National Health Insurance Research Database (NHIRD). The NHIRD was constructed to collate data from a national single-payment health care insurance program that was launched in 1995 in Taiwan. Currently, ~99% of the residents of Taiwan are enrolled in this program. The cost of a wide range of health care services, including ambulatory care, inpatient care, dental treatment, prescription medication use, invasive procedures, and surgeries, are covered by this health insurance program. Therefore, the NHIRD is a rich source of health care information and is one of the most comprehensive administrative health databases in the world. To date, several NHIRD-based epidemiologic and comparative effectiveness studies have been published (16,17). In the NHIRD, the personal information and identification number of each NHIRD enrollee are scrambled to ensure privacy, and thus informed consent for this study was not required. The National Cheng Kung University Hospital Institutional Review Board approved the study protocol (approval no. A-EX-109-017).

Study population. Individuals with a documented diagnosis of new-onset PM/DM were identified between January 1, 2000 and December 31, 2013, using International Classification

of Diseases, Ninth Revision, Clinical Modification (ICD-9-CM) codes (for DM, ICD-9-CM code 710.3; for PM, ICD-9-CM code 710.4). To ensure that only patients with valid diagnoses were included in the PM/DM groups, patients were also required to have catastrophic illness certificates (CICs). In Taiwan, patients with certain types of severe illnesses can apply for CICs in order to be exempted from copayment when seeking medical services for these illnesses. Malignancy, stroke, neurodegenerative diseases, and the majority of systemic autoimmune diseases are categorized as catastrophic illnesses in Taiwan's health care system. In issuing CICs for corresponding diseases, the patient's medical records, laboratory data, and imaging findings are reviewed to ascertain diagnostic accuracy; for example, CICs can be issued to PM/DM patients only when their clinical symptoms and examination results are compatible with the Bohan and Peter criteria for PM/DM (18).

Patients without a CIC for PM/DM-related illnesses were not included in our study. At least 2 independent certified rheumatologists are required to review relevant medical records before the approval of CICs for PM/DM. Therefore, the accuracy of our study in identifying patients with inflammatory myositis was high. The index date was defined as the date of the first diagnosis of PM/DM. Patients who were <18 years of age at the start of the study and those who developed HF before the index date were excluded. Only incident cases were included, and we searched the records before the index date to confirm that no prior diagnosis of PM/DM was made. We also excluded patients who were diagnosed as having other autoimmune diseases, such as systemic lupus erythematosus, systemic sclerosis, or primary Sjögren's syndrome, within a 1-year period prior to the index date, thereby ensuring that there were no overlap syndromes in our enrolled participants.

Selection of non-PM/DM controls. Individuals who were never diagnosed as having PM/DM during the study period were randomly selected from the NHIRD and identified as controls. The index date for each subject in the control group was randomly assigned and corresponded to the distribution of index dates in the PM/DM group. We also excluded from the control group any patients who were <18 years of age at the start of the study and those who were diagnosed as having HF before the matched index date.

Potential confounders. We recorded each patient's age and sex at the time of the index date. In addition, we identified the presence of the following comorbidities using the relevant ICD-9-CM diagnostic codes: diabetes mellitus (ICD-9-CM code 250), hypertension (ICD-9-CM codes 401–405), dyslipidemia (ICD-9-CM code 272), ischemic heart disease (ICD-9-CM codes 410–414), atrial fibrillation (ICD-9-CM code 427.31), peripheral artery disease (ICD-9-CM code 443), chronic obstructive pulmonary disease (COPD) (ICD-9-CM codes 491, 492, and 496), and

chronic kidney disease (ICD-9-CM codes 580–588). We determined whether these comorbidities occurred within a 1-year period before the index date. Patients were categorized as having a certain comorbidity only if the corresponding diagnostic codes were reported in the inpatient claims records at least once or in outpatient claims records more than 3 times.

With regard to medication usage, several medications were identified as pharmacotherapies that had been prescribed to the patients with PM/DM based on a review of the dispensed prescriptions during a 3-month period. The following medications prescribed to patients at least 28 days prior to the index date were recorded: nonsteroidal antiinflammatory drugs (NSAIDs), aspirin, systemic glucocorticoids, statins, warfarin, and digoxin.

Ascertainment of HF diagnoses. The main outcome of this study was new-onset HF, defined as the first hospitalization attributable to acute HF. All HF-related hospital admissions were identified by noting the presence of ICD-9-CM code 428.xx and the primary diagnosis contained within each patient's discharge record. The diagnostic code for HF was validated in the NHIRD database, yielding a positive predictive value for identification of HF of 97.6% (19). The patients with PM/DM and controls were followed up until the first HF-related hospitalization, death, or the end of the study (December 31, 2013), whichever occurred first.

Process of propensity score matching. We studied a propensity score–matched cohort to eliminate the influence of confounding factors and to determine the “marginal effect” of PM/DM on the occurrence of HF (20). To estimate the propensity score, first, a logistic regression model was constructed, with the dependent variable being diagnosis of PM/DM and the independent variables being age, sex, index date (year of first diagnosis), presence of diabetes, hypertension, COPD, hyperlipidemia, chronic kidney disease, atrial fibrillation, and peripheral artery disease, and medication usage, including usage of NSAIDs, aspirin, systemic glucocorticoids, statins, warfarin, and digoxin. Subsequently, the PM/DM cohort was matched with the control cohort at a 1:1 ratio, using nearest-neighbor matching without replacement and a caliper width of 0.1 of the pooled standard deviation of the logit of the propensity score. The adequacy of the balance across these covariates between groups was expressed as the mean standardized difference. If the absolute mean standardized difference between 2 groups was <0.1, the balance of the confounding variable was considered acceptable (21).

Statistical analysis. Continuous variables are presented as the mean \pm SD, and categorical variables as a percentage. HF incidence rates during the follow-up period were calculated by dividing the number of events by the corresponding person-time at risk; results are presented as the number of events per 1,000 person-years. Incidence rate ratios were estimated using Poisson regression. The cumulative incidence of HF in the

PM/DM patients and matched controls was estimated and graphically presented using the Kaplan-Meier method. We used a stratified log-rank test that accounted for the matching property (22) to determine whether significant differences in the HF risk existed between the PM/DM patients and matched controls.

Two different analyses were performed to assess the relative risk of HF associated with PM/DM. First, a multivariable Cox proportional hazards regression model, adjusted for age, sex, comorbidities, and medication usage, was used to derive the “conditional effect” of PM/DM on HF in the cohorts before propensity score matching (20). In other analyses, a stratified Cox model was used to estimate the magnitude of the “marginal effect” of PM/DM on HF at the population level, with stratification based on matched pairs in the cohorts after propensity score matching. The stratified Cox model was suggested in this scenario to account for the propensity score–matched nature of the cohort (22). Tests of the proportional hazards assumption with inspection of log-based survival curves and a scaled Schoenfeld residuals test did not reveal significant violations of the hazards assumption.

We also calculated stratum-specific crude and adjusted hazard ratios (HRs) for the risk of HF at different follow-up time periods (<1 year, <3 years, <5 years, and < 10 years) following the diagnosis of PM/DM. All participants were included for analysis in each period, and patient data were treated as censored observations if a patient did not develop HF at the end of each time period. Subgroup analyses were carried out to examine the moderating effects of various subgroup variables on the association between PM/DM and HF. A significant interaction was determined using the likelihood ratio test. Apart from the stratified Fine and Gray model used in the sensitivity analysis, which was constructed using R, version 3.6.1, all other statistical analyses were performed using the STATA statistical package (version 13.0; StataCorp). All statistical tests were 2-sided, and *P* values less than 0.05 were considered significant.

Sensitivity analyses. We performed a sensitivity analysis in the propensity score–matched cohort using a stratified Fine and Gray competing risk regression model (23), with the event of death used as a competing event. To assess the robustness of our results, a second sensitivity analysis was conducted in which we used the ICD-9-CM diagnostic codes 425.4, 425.9, 402.01, 402.11, 402.91, 404.01, 404.03, 404.11, 404.13, 404.91, 404.93, and 428.xx for the diagnosis of HF, which have been previously validated as having a high sensitivity for identification of HF (96.3%) (24).

We conducted a third sensitivity analysis in which we constructed another logistic regression model to estimate the propensity score. We used the same variables as used in the main propensity score analysis except for the variable of glucocorticoid usage, which was excluded from the propensity score model. Subsequently, the same matching algorithm used in the main

Table 1. Demographic and baseline clinical characteristics of the patients with PM/DM and controls in the unmatched and propensity score-matched cohorts, and standardized mean difference in the propensity score-matched cohort*

Characteristic	Unmatched cohort		Propensity score-matched cohort		Standardized mean difference
	PM/DM (n = 2,025)	Controls (n = 196,109)	PM/DM (n = 1,997)	Controls (n = 1,997)	
Age, mean \pm SD years	50.2 \pm 14.6	43.7 \pm 16.6	50.2 \pm 14.6	50.8 \pm 17.3	-0.038
Sex					0.000
Male	666 (32.9)	98,173 (50.1)	661 (33.1)	661 (33.1)	
Female	1,359 (67.1)	97,936 (49.9)	1,336 (66.9)	1,336 (66.9)	
Comorbidities					
Hypertension	367 (18.1)	19,479 (9.9)	362 (18.1)	406 (20.3)	-0.056
Diabetes mellitus	190 (9.4)	10,516 (5.4)	186 (9.3)	204 (10.2)	-0.030
Ischemic heart disease	136 (6.7)	5,430 (2.8)	131 (6.6)	137 (6.8)	-0.012
Dyslipidemia	212 (10.5)	9,658 (4.9)	206 (10.3)	213 (10.6)	-0.011
Atrial fibrillation	9 (0.44)	482 (0.25)	9 (0.45)	13 (0.65)	-0.027
Chronic kidney disease	54 (2.7)	1,890 (1.0)	53 (2.7)	60 (3.0)	-0.021
COPD	114 (5.6)	2,703 (1.4)	113 (5.6)	99 (5.0)	0.031
Peripheral artery disease	95 (4.7)	726 (0.4)	68 (3.4)	67 (3.3)	0.003
Medication					
Aspirin	95 (4.7)	4,753 (2.4)	86 (4.3)	105 (5.2)	-0.045
NSAID	455 (22.5)	5,739 (2.9)	446 (22.3)	444 (22.2)	0.002
Statin	22 (1.1)	3,237 (1.65)	22 (1.1)	29 (1.4)	-0.031
Glucocorticoid	1,585 (78.3)	5,585 (2.9)	1,557 (77.9)	1,560 (78.1)	-0.004
Warfarin	12 (0.59)	271 (0.14)	9 (0.5)	8 (0.4)	0.008
Digoxin	6 (0.30)	295 (0.15)	6 (0.3)	7 (0.4)	-0.009

* Except where indicated otherwise, values are the number (%). PM/DM = polymyositis/dermatomyositis; COPD = chronic obstructive pulmonary disease; NSAID = nonsteroidal antiinflammatory drug.

analysis was applied in this new calculation of the propensity score.

Availability of data and materials. The data sets used and/or analyzed in the present study are available from the corresponding author upon request.

RESULTS

Clinical characteristics of the patients. Before propensity score matching, a total of 2,025 patients with incident PM/DM and 196,109 non-PM/DM controls were identified between 2000 and 2013. Baseline characteristics of the patients

Table 2. Incidence and risk of HF in patients with PM/DM compared with controls in the unmatched and propensity score-matched cohorts*

	PM/DM	Controls	P
Unmatched cohort			
Total no. of patients	2,025	196,109	-
HF events, no. (%)	90 (4.4)	2,726 (1.4)	-
Total follow-up time, person-years	10,792	1,266,921	-
Follow-up duration, mean \pm SD years	5.3 \pm 4.2	6.5 \pm 4.0	-
Incidence rate per 1,000 person-years	8.3	2.2	-
Incidence rate ratio (95% CI)	3.88 (3.11-4.78)	1.0 (referent)	<0.001
Crude HR for HF (95% CI)	3.87 (3.14-4.78)	1.0 (referent)	<0.001
Adjusted HR for HF (95% CI)†	3.59 (2.90-4.44)	1.0 (referent)	<0.001
Fully adjusted HR for HF (95% CI)‡	3.29 (2.60-4.18)	1.0 (referent)	<0.001
Propensity score-matched cohort			
Total no. of patients	1,997	1,997	-
HF events, no. (%)	89 (4.5)	61 (3.1)	-
Total follow-up time, person-years	10,598	12,884	-
Follow-up duration, mean \pm SD years	5.3 \pm 4.2	6.5 \pm 4.0	-
Incidence rate per 1,000 person-years	8.4	4.7	-
Incidence rate ratio (95% CI)	1.77 (1.27-2.50)	1.0 (referent)	<0.001
HR for HF (95% CI), stratified Cox model	2.06 (1.36-3.12)	1.0 (referent)	<0.001

* HF = heart failure; PM/DM = polymyositis/dermatomyositis; HR = hazard ratio; 95% CI = 95% confidence interval.

† Adjusted for age, sex, comorbidities, and medication usage at baseline (as listed in Table 1, but with exclusion of glucocorticoid usage).

‡ Adjusted for age, sex, comorbidities, and medication usage at baseline (as listed in Table 1).

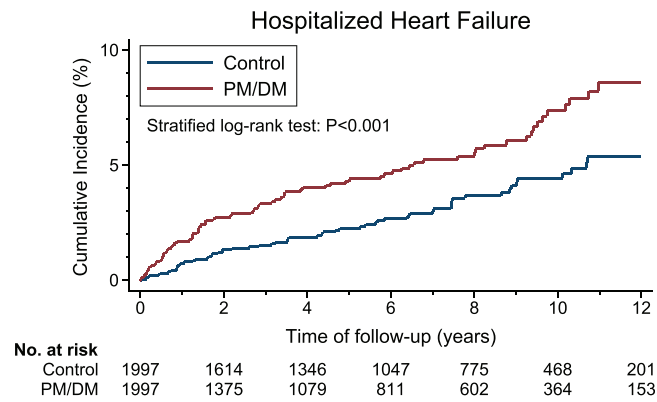


Figure 1. Cumulative incidence of hospitalization for heart failure among patients with polymyositis/dermatomyositis (PM/DM) compared with non-PM/DM control subjects in the propensity score–matched cohort.

with PM/DM and controls are summarized in Table 1. The mean \pm SD age of the PM/DM patients was 50.2 ± 14.6 years, and women accounted for two-thirds of the PM/DM cohort. The most common comorbidities in the PM/DM cohort were hypertension, diabetes mellitus, and dyslipidemia. The prevalence of comorbidities was higher in the PM/DM patients compared with the control group. A high percentage of PM/DM patients were receiving treatment with glucocorticoids and NSAIDs at baseline.

In total, 1,997 pairs of PM/DM patients and controls were included in the propensity score–matched cohort after 1:1 propensity score matching. The absolute standardized differences across all clinical variables, including age, sex, comorbidities,

and medication usage, were < 0.1 , indicating an acceptable balance of confounders between the PM/DM and control cohorts. The mean follow-up duration was estimated to be 5.3 years for the PM/DM patients and 6.5 years for the controls (Table 2).

Occurrence and relative risk of HF. *Conditional effect of PM/DM.* In the unmatched cohort, 90 (4.4%) of the 2,025 patients with PM/DM experienced an HF event. In contrast, of 196,109 controls, 2,726 (1.4%) experienced an HF event (Table 2).

The incidence rate of HF was 8.3 per 1,000 person-years in patients with PM/DM and 2.2 per 1,000 person-years in non-PM/DM controls (Table 2). The HF incidence rate ratio in patients with PM/DM compared with the controls was 3.88 (95% confidence interval [95% CI] 3.11–4.78) in the total unmatched population. The crude HR for HF, calculated using the unadjusted Cox model, was 3.87 (95% CI 3.14–4.78) in patients with PM/DM relative to controls.

The conditional effect of PM/DM, estimated with a multivariable Cox regression model adjusted for age, sex, comorbidities, and medication usage, revealed a similar strength of association of PM/DM with subsequent HF events (adjusted HR 3.29, 95% CI 2.60–4.18). This adjusted effect of PM/DM increased when glucocorticoid usage was not included in the multivariable model (adjusted HR 3.59, 95% CI 2.90–4.44).

Marginal effect of PM/DM. In the propensity score–matched cohort, 89 patients with PM/DM (4.5% of 1,997) and 61 controls (3.1% of 1,997) experienced an HF event (Table 2). The HF incidence rate was 8.4 per 1,000 person-years among patients with PM/DM and 4.7 per 1,000 person-years among non-PM/DM

Table 3. Incidence and risk of HF in patients with PM/DM according to follow-up time interval after the PM/DM diagnosis*

Follow-up time	Unmatched cohort		Propensity score–matched cohort	
	PM/DM	Controls	PM/DM	Controls
<1 year				
Participants, no.	2,025	196,109	1,997	1,997
HF events, no. (%)	30 (1.48)	400 (0.2)	30 (1.5)	14 (0.7)
HR (95% CI)†	5.75 (3.66–9.01)‡	1.0	2.34 (1.24–4.40)§	1.0
<3 years				
Participants, no.	2,025	196,109	1,997	1,997
HF events, no. (%)	54 (2.67)	1,108 (0.56)	54 (2.7)	27 (1.35)
HR (95% CI)†	4.59 (3.34–6.30)‡	1.0	2.32 (1.45–3.71)¶	1.0
<5 years				
Participants, no.	2,025	196,109	1,997	1,997
HF events, no. (%)	67 (3.31)	1,626 (0.83)	66 (3.3)	37 (1.85)
HR (95% CI)†	4.01 (3.03–5.31)‡	1.0	2.25 (1.42–3.57)¶	1.0
<10 years				
Participants, no.	2,025	196,109	1,997	1,997
HF events, no. (%)	85 (4.2)	2,522 (1.29)	84 (4.21)	56 (2.8)
HR (95% CI)†	3.35 (2.62–4.29)‡	1.0	2.09 (1.37–3.19)‡	1.0

* HF = heart failure; PM/DM = polymyositis/dermatomyositis; 95% CI = 95% confidence interval.

† In the unmatched cohort, analyses of the hazard ratio (HR) were adjusted for age, sex, comorbidities, and medication usage at baseline (as listed in Table 1).

‡ $P < 0.001$ versus controls.

§ $P = 0.009$ versus controls.

¶ $P = 0.001$ versus controls.

controls (Table 2). The HF incidence rate ratio in the patients with PM/DM was 1.77 (95% CI 1.27–2.50) relative to controls.

The cumulative incidence of HF was significantly higher in the PM/DM cohort compared with the matched control cohort ($P < 0.001$ by stratified log-rank test) (Figure 1). The cumulative HF incidence at 1, 3, 5, and 10 years among patients with PM/DM was 1.7% (95% CI 1.2–2.4%), 3.3% (95% CI 2.6–4.4%), 4.4% (95% CI 3.5–5.7%), and 7.4% (95% CI 6.0–9.8%), respectively. In contrast, the cumulative HF incidence at 1, 3, 5, and 10 years in the matched controls was 0.75% (95% CI 0.44–1.3%), 1.5% (95% CI 1.1–2.2%), 2.3% (95% CI 1.6–3.2%), and 4.4% (95% CI 3.4–6.0%), respectively. The absolute between-group risk differences at 3, 5, and 10 years were 1.8% (95% CI 0.7–2.9%), 2.1% (95% CI 0.8–3.3%), and 3.0% (95% CI 0.9–5.1%), respectively. The stratified Cox model revealed that the risk of HF associated with PM/DM remained statistically significant (HR 2.06, 95% CI 1.36–3.12).

Risk of HF according to time since diagnosis of PM/DM.

Table 3 presents the risk of HF detected at 4 different follow-up time points (<1 year, <3 years, <5 years, and <10 years) following the PM/DM diagnosis in the unmatched and propensity score-matched cohorts. In the unmatched cohort, the risk of HF in patients with PM/DM was significantly increased at all time points, with the greatest risk observed within the first year after the initial PM/DM diagnosis (adjusted HR 5.75, 95% CI 3.66–9.01). In the propensity score-matched cohort, the relative risk of HF in PM/DM patients compared with controls seemed to be similar across each time point.

Subgroup analysis. The adjusted risks of HF stratified by age, sex, and comorbidities in patients with PM/DM compared with controls are presented in Figure 2. No significant interaction across subgroups was detected, except for the subgroups of atrial fibrillation and chronic kidney disease. Only 9 patients with

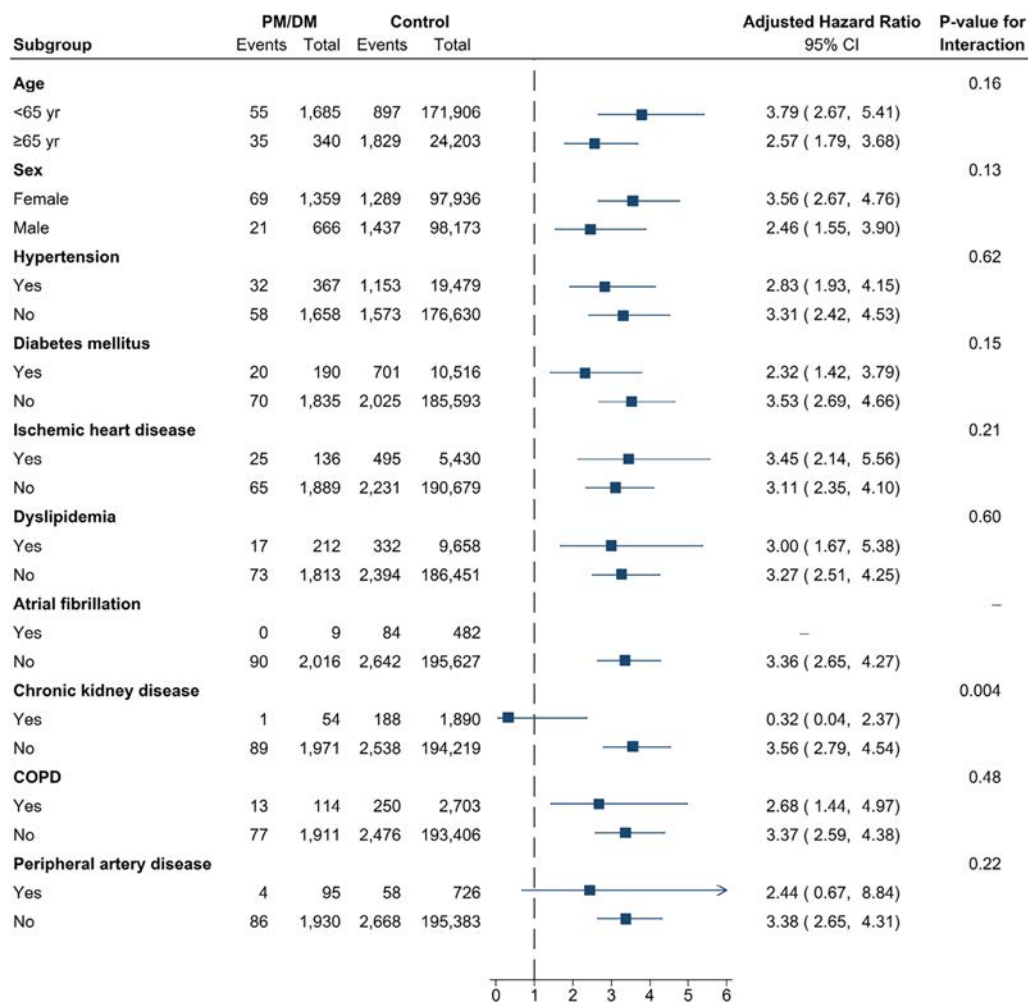


Figure 2. Risk of heart failure (HF) leading to hospitalization among patients with polymyositis/dermatomyositis (PM/DM), according to various subgroups based on demographic and clinical characteristics. Forest plots show the adjusted hazard ratios (with 95% confidence intervals [95% CIs]) for the risk of HF, estimated using a Cox proportional hazards model with adjustment for age, sex, comorbidities, and medication usage. The likelihood ratio test was used to determine the P for interaction. COPD = chronic obstructive pulmonary disease. Color figure can be viewed in the online issue, which is available at <http://onlinelibrary.wiley.com/doi/10.1002/art.41907/abstract>.

Table 4. Sensitivity analyses in the propensity score–matched cohort*

Model	No. of HF events in patients with PM/DM	HR (95% CI)
Primary Cox proportional hazards analysis using diagnostic codes with high positive predictive values	89	2.06 (1.36–3.12)
Cox proportional hazards analysis using diagnostic codes with high sensitivity for HF	95	1.48 (1.02–2.15)
Competing risk regression analysis using a stratified Fine and Gray model	89	1.68 (1.16–2.43)
Matched cohort using a second propensity score–matching model†	89	2.51 (1.78–3.54)

* HF = heart failure; PM/DM = polymyositis/dermatomyositis; HR = hazard ratio; 95% CI = 95% confidence interval.

† The second propensity score was estimated using logistic regression analysis, with age, sex, index date (year) of first diagnosis, presence of diabetes, hypertension, chronic obstructive pulmonary disease, hyperlipidemia, chronic kidney disease, atrial fibrillation, and peripheral artery disease, and usage of nonsteroidal antiinflammatory drugs, aspirin, statins, warfarin, and digoxin as independent variables. Usage of glucocorticoids was not included in this second propensity score model.

PM/DM were identified as having atrial fibrillation, none of whom developed HF. Similarly, the subgroup of PM/DM patients with chronic kidney disease was small, comprising only 54 patients, of whom only 1 developed HF.

Findings from sensitivity analyses. In a sensitivity analysis using the diagnostic codes that were validated as having high sensitivity for identification of HF, we observed that the risk of HF remained higher in the PM/DM group compared with the matched controls (HR 1.48, 95% CI 1.02–2.15) (Table 4). A competing risk regression model analysis yielded similar results as those of the primary analysis with regard to risk of HF in patients with PM/DM (HR 1.68, 95% CI 1.16–2.43). A sensitivity analysis using a second propensity score model (glucocorticoid usage was not included as a matching variable) showed a higher estimated risk of HF in patients with PM/DM compared with controls (HR 2.51, 95% CI 1.78–3.54) than that seen in the primary propensity score–matched analysis.

DISCUSSION

To the best of our knowledge, this is the first nation-scale study in which an unselected, validated cohort of patients with PM/DM was used to investigate the risk of new-onset HF in PM/DM patients compared with controls from the general population. We observed that PM/DM was associated with a

significantly increased risk of HF-related hospitalization throughout the study period. The enhanced risk of HF seemed to be the highest during the first year following the diagnosis of PM/DM.

PM/DM-related inflammation is primarily found in skeletal muscle; however, increasing evidence has shown that the simultaneous occurrence of myocardial inflammation in these patients may have been underestimated (10). An earlier autopsy study of PM/DM patients revealed several histopathologic findings indicative of the presence of interstitial inflammatory cell infiltration, contraction-band necrosis, myocyte degeneration, focal fibrosis, vasculitis, and medial sclerosis of the vessels in the myocardium (25). These pathologic changes resemble the inflammation observed in skeletal muscle, indicating that the heart is also an autoimmune target in PM/DM (26,27). Recently, owing to its noninvasiveness and high resolution, gadolinium-enhanced cardiac magnetic resonance imaging (MRI) has been used to facilitate the detection and diagnosis of myocardial inflammation. In a study conducted in Greece, 20 patients with active PM/DM were evaluated using cardiac MRI, with the results showing that 75% of the study participants exhibited evidence of myocarditis (28). In another study, a total of 16 PM/DM patients without clinically significant cardiac symptoms underwent cardiac MRI, with the findings showing late gadolinium enhancement in 56% of the patients, which indicates a high percentage of inflammatory injury and fibrosis in the myocardium (29). In a more recent study from Germany involving 53 PM/DM patients, myocardial inflammation and fibrosis were detected in 62.3% of the patients who had lesions present mainly in the lateral and inferior segments of the heart (30). Therefore, direct myocardial injury caused by inflammatory cell infiltration or myocarditis is one of the possible mechanisms contributing to the higher risk of HF observed in patients with PM/DM in our study.

It has already been established that systemic inflammation is closely linked to various cardiovascular diseases, including myocardial infarction and ischemic stroke (31). Several autoimmune diseases, such as rheumatoid arthritis, systemic lupus erythematosus, and PM/DM, have been demonstrated to be associated with elevated risks of ischemic heart disease and stroke in various large-scale epidemiologic studies (14,32), in which chronic systemic inflammation was considered as the main contributor independent of traditional risk factors. HF is a clinical syndrome with mixed etiology. For decades, the predominant focus of research on the mechanisms of HF has been analyses of activation of the sympathetic and neurohormonal systems (33,34). In recent years, accumulating evidence has demonstrated that inflammatory mechanisms play a pivotal role in the development and progression of both HF subtypes, HF with preserved ejection fraction and HF with reduced ejection fraction (34–36). Furthermore, inflammation has been observed to be a prevalent phenomenon in HF, which was supported by the findings from a randomized clinical trial in which up to 57% of patients with HF had elevated C-reactive protein levels (37). In addition, elevated serum levels of proinflammatory cytokines, such as tumor necrosis factor

(TNF), interleukin-1 (IL-1), and IL-6, have been observed in patients with HF (34,35). Interestingly, several studies have demonstrated an overexpression of TNF, IL-1, IL-6, IL-17, and type I interferons in the blood or muscle tissue of patients with PM/DM (38,39). Therefore, the causal inflammatory mechanism may be partially shared between PM/DM and HF. It is conceivable that the persisting state of inflammation in patients with PM/DM could lead to subsequent myocardial injury and the development of new-onset HF.

In addition to the effects of PM/DM itself, we must consider that glucocorticoids may increase the risk of HF. Glucocorticoids can bind to the mineralocorticoid receptors, in addition to the glucocorticoid receptors (40,41). Activation of the mineralocorticoid receptor signaling pathway not only increases sodium and fluid retention but also aggravates HF by promoting remodeling through the fibrosis of the atria and ventricles (42). In a large-scale population-based study, treatment with oral glucocorticoids was shown to be associated with an elevated risk of HF (43). Therefore, although glucocorticoids can effectively control disease activity in PM/DM, the subsequent adverse effects on the heart should be noted. Thus, the greater risk of hospitalization for HF observed in patients with PM/DM in the present study may also be attributable to long-term treatment with glucocorticoids, in addition to cardiac involvement.

The risk of cardiac involvement varies among patients with PM/DM, with certain subgroups having a higher risk. The proportion of PM/DM patients who are positive for antimitochondrial antibodies differs between cohorts, and a previous study showed that antimitochondrial antibody positivity may account for ~11% of patients with idiopathic inflammatory myopathies (44). Recently, it has been suggested that antimitochondrial antibody-associated myositis should be considered a distinct inflammatory myopathy phenotype that is frequently associated with myocardial involvement (45). However, we did not analyze the risk of HF in this subgroup, as myositis-related antibody test results were not available in our database.

When we assessed the potential impact of sex and various comorbidities on the association between PM/DM and HF events, we observed differential effects of PM/DM across the subcategories of atrial fibrillation and chronic kidney disease. This variability associated with these 2 comorbidities may be attributed to the fact that the number of patients with PM/DM in these 2 subgroups was relatively small compared with the other subgroups, which made the estimates less reliable. Further research is required to investigate the true moderating effect of these comorbidities.

Previous studies have evaluated the disease course in adult or juvenile patients with DM in the context of treatment with glucocorticoids, and it was observed that DM disease activity was highest during the first 6–12 months following the diagnosis, with improvement in disease activity apparently occurring subsequent to the initiation of glucocorticoid treatment (46–48). In addition, the requirement for use of glucocorticoids to control disease activity was lower after 12 months of treatment (47). Given that

both inflammation resulting from PM/DM and treatment with glucocorticoids may contribute to the development of HF, our findings showing that the risk of HF appeared to be greatest within the first few years of PM/DM diagnosis (according to the findings from the multivariable regression model) could be partly attributable to the subsequent attenuation of disease activity with treatment, as well as to the reduction in glucocorticoid dosage following appropriate treatment in some patients.

There was a certain degree of discrepancy in the estimated impact of PM/DM on the risk of hospitalized HF between the estimates obtained with the multivariable Cox regression model and the estimates obtained with propensity score matching (point estimate of effect 3.29 versus 2.06). This phenomenon could be explained by the difference in the meaning of the term conditional effect and the meaning of the term marginal effect (49). The effect of PM/DM on the occurrence of HF derived from traditional Cox regression analyses adjusted for covariates in our study was referred to as a “conditional estimate or effect”; the resulting HR was conditional on the other covariates in the model (49). In brief, the conditional effect is the average effect of moving an individual from nonexposed to exposed at the individual level. In contrast, the effect of PM/DM estimated from propensity score matching was referred to as the marginal HR (49). The marginal effect denoted the average effect of moving an entire population from nonexposed to exposed at the population level. A previous simulation study revealed that the marginal effect, as measured by the HR or odds ratio, is, in general, closer to the null effect than the conditional effect (50). The divergence between the conditional effect and marginal effect is larger if the model includes more prognostic factors, has stronger covariates, or has a larger exposure/treatment effect (50). Although the strength of the estimated conditional and marginal effects of PM/DM differed in our analysis, their direction was concordant and far away from the effect of null.

The major strength of our study was the use of a nationwide database that includes all levels of health care and almost the entire population of Taiwan; this ensured that selection bias and referral bias were minimized. A broad range of diseases and related medical services are covered by Taiwan’s national insurance program, which enabled us to obtain complete data sets with minimal loss to follow-up. We used CICs, which have been determined to be highly valid for identifying patients with PM/DM; this ensured the high accuracy of the PM/DM diagnosis in our investigation. Furthermore, we conducted sensitivity analyses using different statistical methods and different outcome definitions, and our results remained significant, indicating the robustness of our study findings.

There are, however, some important study limitations that must be mentioned. First, the misclassification of outcomes is an inherent limitation in research based on administrative health databases. However, to minimize the risk of miscoding, we used a diagnostic code for HF that has previously been validated with a high positive predictive value (19). Additionally, even when we

changed the definition of HF using different sets of diagnostic codes with high sensitivity, the association between PM/DM and HF remained significant. Second, we did not have access to data regarding the levels of serum creatinine kinase and acute-phase reactants. Therefore, we could not assess the severity of disease activity in patients with PM/DM, which precluded further analysis of the associated influence on the outcomes. Third, echocardiography results were not available in our study. Therefore, it is not clear whether the higher HF rate observed in PM/DM patients was a result of systolic or diastolic dysfunction.

In summary, the results of the present study from Taiwan indicate a time-dependent increased risk of hospitalization for HF in patients with PM/DM. The risk remains elevated for up to 10 years following the PM/DM diagnosis. These results suggest that there should be increased physician vigilance and awareness regarding this potentially lethal complication. We recommend that rheumatologists regularly assess patients with PM/DM for associated symptoms and signs of HF during clinical management.

AUTHOR CONTRIBUTIONS

All authors were involved in drafting the article or revising it critically for important intellectual content, and all authors approved the final version to be published. Drs. Lin and C. Hsu had full access to all of the data in the study and take responsibility for the integrity of the data and the accuracy of the data analysis.

Study conception and design. Lin.

Acquisition of data. Chen, T. Hsu, Su, C. Hsu.

Analysis and interpretation of data. Wu.

REFERENCES

- Barsotti S, Dastmalchi M, Notarnicola A, Leclaire V, Dani L, Gheorghie K, et al. Performance of the new EULAR/ACR classification criteria for idiopathic inflammatory myopathies (IIM) in a large monocentric IIM cohort. *Semin Arthritis Rheum* 2020;50:492–7.
- Tieu J, Lundberg IE, Limaye V. Idiopathic inflammatory myositis [review]. *Best Pract Res Clin Rheumatol* 2016;30:149–68.
- Jones J, Wortmann R. Idiopathic inflammatory myopathies: a review [review]. *Clin Rheumatol* 2015;34:839–44.
- Lundberg IE. The heart in dermatomyositis and polymyositis [review]. *Rheumatology (Oxford)* 2006;45 Suppl 4:iv18–21.
- Zhang L, Wang GC, Ma L, Zu N. Cardiac involvement in adult polymyositis or dermatomyositis: a systematic review [review]. *Clin Cardiol* 2012;35:686–91.
- Danieli MG, Gelardi C, Guerra F, Cardinaletti P, Pedini V, Gabrielli A. Cardiac involvement in polymyositis and dermatomyositis [review]. *Autoimmun Rev* 2016;15:462–5.
- Schwartz T, Diederichsen LP, Lundberg IE, Sjaastad I, Sanner H. Cardiac involvement in adult and juvenile idiopathic inflammatory myopathies [review]. *RMD Open* 2016;2:e000291.
- Gupta R, Wayangankar SA, Targoff IN, Henneby TA. Clinical cardiac involvement in idiopathic inflammatory myopathies: a systematic review [review]. *Int J Cardiol* 2011;148:261–70.
- Greulich S, Kitterer D, Kurmann R, Henes J, Latus J, Gloekler S, et al. Cardiac involvement in patients with rheumatic disorders: data of the RHEU-M(A)R study. *Int J Cardiol* 2016;224:37–49.
- Liu Y, Fang L, Chen W, Zhu Y, Lin X, Wang Y, et al. Identification of characteristics of overt myocarditis in adult patients with idiopathic inflammatory myopathies. *Cardiovasc Diagn Ther* 2020;10:405–20.
- Lilleker JB, Roberts M, Diederichsen L. Cardiac involvement in inflammatory myopathies and inherited muscle diseases [review]. *Curr Opin Rheumatol* 2020;32:528–33.
- Opinc AH, Makowski MA, Łukasik ZM, Makowska JS. Cardiovascular complications in patients with idiopathic inflammatory myopathies: does heart matter in idiopathic inflammatory myopathies? [review]. *Heart Fail Rev* 2021;26:111–25.
- Ungprasert P, Suksaranjit P, Spanuchart I, Leeaphorn N, Permpalung N. Risk of coronary artery disease in patients with idiopathic inflammatory myopathies: a systematic review and meta-analysis of observational studies [review]. *Semin Arthritis Rheum* 2014;44:63–7.
- Rai SK, Choi HK, Sayre EC, Aviña-Zubieta JA. Risk of myocardial infarction and ischaemic stroke in adults with polymyositis and dermatomyositis: a general population-based study. *Rheumatology (Oxford)* 2016;55:461–9.
- Taylor AJ, Wortham DC, Burge JR, Rogan KM. The heart in polymyositis: a prospective evaluation of 26 patients. *Clin Cardiol* 1993;16:802–8.
- Lin CY, Wu CH, Chen HA, Hsu CY, Wang LH, Su YJ. Long-term renal prognosis among patients with primary Sjogren's syndrome and renal involvement: a nationwide matched cohort study. *J Autoimmun* 2020;113:102483.
- Chang SL, Huang YL, Lee MC, Hu S, Hsiao YC, Chang SW, et al. Association of varicose veins with incident venous thromboembolism and peripheral artery disease. *JAMA* 2018;319:807–17.
- Bohan A, Peter JB, Bowman RL, Pearson CM. A computer-assisted analysis of 153 patients with polymyositis and dermatomyositis. *Medicine (Baltimore)* 1977;56:255–86.
- Lin YS, Chen TH, Chi CC, Lin MS, Tung TH, Liu CH, et al. Different implications of heart failure, ischemic stroke, and mortality between nonvalvular atrial fibrillation and atrial flutter: a view from a national cohort study. *J Am Heart Assoc* 2017;6:e006406.
- Austin PC. The performance of different propensity score methods for estimating marginal hazard ratios. *Stat Med* 2013;32:2837–49.
- Austin PC. Balance diagnostics for comparing the distribution of baseline covariates between treatment groups in propensity-score matched samples. *Stat Med* 2009;28:3083–107.
- Austin PC. Comparing paired vs non-paired statistical methods of analyses when making inferences about absolute risk reductions in propensity-score matched samples. *Stat Med* 2011;30:1292–301.
- Fine JP, Gray RJ. A proportional hazards model for the subdistribution of a competing risk. *J Am Stat Assoc* 1999;94:496–509.
- Su VY, Yang YH, Perng DW, Tsai YH, Chou KT, Su KC, et al. Real-world effectiveness of medications on survival in patients with COPD-heart failure overlap. *Aging (Albany NY)* 2019;11:3650–67.
- Haupt HM, Hutchins GM. The heart and cardiac conduction system in polymyositis-dermatomyositis: a clinicopathologic study of 16 autopsied patients. *Am J Cardiol* 1982;50:998–1006.
- Cavazzana I, Fredi M, Selmi C, Tincani A, Franceschini F. The clinical and histological spectrum of idiopathic inflammatory myopathies [review]. *Clin Rev Allergy Immunol* 2017;52:88–98.
- Day JA, Limaye V. Immune-mediated necrotising myopathy: a critical review of current concepts [review]. *Semin Arthritis Rheum* 2019;49:420–9.
- Mavrogeni S, Bratis K, Karabela G, Stavropoulos E, Sfendouraki E, Kolovou G. Myocarditis during acute inflammatory myopathies: evaluation using clinical criteria and cardiac magnetic resonance imaging. *Int J Cardiol* 2013;164:e3–4.

29. Mavrogeni S, Douskou M, Manoussakis MN. Contrast-enhanced CMR imaging reveals myocardial involvement in idiopathic inflammatory myopathy without cardiac manifestations. *JACC Cardiovasc Imaging* 2011;4:1324–5.
30. Rosenbohm A, Buckert D, Gerischer N, Walcher T, Kassubek J, Rottbauer W, et al. Early diagnosis of cardiac involvement in idiopathic inflammatory myopathy by cardiac magnetic resonance tomography. *J Neurol* 2015;262:949–56.
31. Karim MA, Kartsonaki C, Bennett DA, Millwood IY, Hill MR, Avery D, et al. Systemic inflammation is associated with incident stroke and heart disease in East Asians. *Sci Rep* 2020;10:5605.
32. Durante A, Bronzato S. The increased cardiovascular risk in patients affected by autoimmune diseases: review of the various manifestations. *J Clin Med Res* 2015;7:379–84.
33. Kishi T. Heart failure as an autonomic nervous system dysfunction [review]. *J Cardiol* 2012;59:117–22.
34. Dutka M, Bobiński R, Ulman-Włodarz I, Hajduga M, Bujok J, Pająk C, et al. Various aspects of inflammation in heart failure [review]. *Heart Fail Rev* 2020;25:537–48.
35. Adamo L, Rocha-Resende C, Prabhu SD, Mann DL. Reappraising the role of inflammation in heart failure [review]. *Nat Rev Cardiol* 2020;17:269–85.
36. Gombert-Maitland M, Shah SJ, Guazzi M. Inflammation in heart failure with preserved ejection fraction: time to put out the fire [editorial]. *JACC Heart Fail* 2016;4:325–8.
37. Redfield MM, Chen HH, Borlaug BA, Semigran MJ, Lee KL, Lewis G, et al. Effect of phosphodiesterase-5 inhibition on exercise capacity and clinical status in heart failure with preserved ejection fraction: a randomized clinical trial. *JAMA* 2013;309:1268–77.
38. Kao L, Chung L, Fiorentino DF. Pathogenesis of dermatomyositis: role of cytokines and interferon [review]. *Curr Rheumatol Rep* 2011;13:225–32.
39. Arshanapalli A, Shah M, Veerula V, Somani AK. The role of type I interferons and other cytokines in dermatomyositis [review]. *Cytokine* 2015;73:319–25.
40. Shen JZ, Young MJ. Corticosteroids, heart failure, and hypertension: a role for immune cells? [review]. *Endocrinology* 2012;153:5692–700.
41. Ng MK, Celermajer DS. Glucocorticoid treatment and cardiovascular disease [editorial]. *Heart* 2004;90:829–30.
42. Weber KT. Aldosterone in congestive heart failure [review]. *N Engl J Med* 2001;345:1689–97.
43. Souverein PC, Berard A, Van Staa TP, Cooper C, Egberts AC, Leuffkens HG, et al. Use of oral glucocorticoids and risk of cardiovascular and cerebrovascular disease in a population based case-control study. *Heart* 2004;90:859–65.
44. Shimizu J. Clinical and histopathological features of myositis associated with anti-mitochondrial antibodies [review]. *Rinsho Shinkeigaku* 2013;53:1114–6. In Japanese.
45. Albayda J, Khan A, Casciola-Rosen L, Corse AM, Paik JJ, Christopher-Stine L. Inflammatory myopathy associated with anti-mitochondrial antibodies: a distinct phenotype with cardiac involvement. *Semin Arthritis Rheum* 2018;47:552–6.
46. Johnson NE, Arnold WD, Hebert D, Gwathmey K, Dimachkie MM, Barohn RJ, et al. Disease course and therapeutic approach in dermatomyositis: a four-center retrospective study of 100 patients. *Neuromuscul Disord* 2015;25:625–31.
47. Ramanan AV, Campbell-Webster N, Ota S, Parker S, Tran D, Tyrrell PN, et al. The effectiveness of treating juvenile dermatomyositis with methotrexate and aggressively tapered corticosteroids. *Arthritis Rheum* 2005;52:3570–8.
48. Lim LS, Pullenayegum E, Moineddin R, Gladman DD, Silverman ED, Feldman BM. Methods for analyzing observational longitudinal prognosis studies for rheumatic diseases: a review & worked example using a clinic-based cohort of juvenile dermatomyositis patients [review]. *Pediatr Rheumatol Online J* 2017;15:18.
49. Austin PC. An introduction to propensity score methods for reducing the effects of confounding in observational studies. *Multivariate Behav Res* 2011;46:399–424.
50. Martens EP, Pestman WR, de Boer A, Belitser SV, Klungel OH. Systematic differences in treatment effect estimates between propensity score methods and logistic regression. *Int J Epidemiol* 2008;37:1142–7.

Effect of Clonally Expanded PD-1^{high}CXCR5–CD4⁺ Peripheral T Helper Cells on B Cell Differentiation in the Joints of Patients With Antinuclear Antibody–Positive Juvenile Idiopathic Arthritis

Jonas Fischer,¹ Johannes Dirks,¹ Julia Klaussner,¹ Gabriele Haase,¹ Annette Holl-Wieden,¹ Christine Hofmann,¹ Stephan Hackenberg,¹ Hermann Girschick,² and Henner Morbach¹ 

Objective. Antinuclear antibody (ANA)–positive juvenile idiopathic arthritis (JIA) is characterized by synovial B cell hyperactivity, but the precise role of CD4⁺ T cells in promoting local B cell activation is unknown. This study was undertaken to determine the phenotype and function of synovial CD4⁺ T cells that promote aberrant B cell activation in JIA.

Methods. Flow cytometry was performed to compare the phenotype and cytokine patterns of PD-1^{high}CD4⁺ T cells in the synovial fluid (SF) of patients with JIA and T follicular helper cells in the tonsils of control individuals. *TCRVB* next-generation sequencing was used to analyze T cell subsets for signs of clonal expansion. The functional impact of these T cell subsets on B cells was examined in cocultures in vitro.

Results. Multidimensional flow cytometry revealed the expansion of interleukin-21 (IL-21) and interferon- γ (IFN γ)–coexpressing PD-1^{high}CXCR5–HLA–DR+CD4⁺ T cells that accumulate in the joints of ANA-positive JIA patients. These T cells exhibited signs of clonal expansion with restricted T cell receptor clonotypes. The phenotype resembled peripheral T helper (Tph) cells with an extrafollicular chemokine receptor pattern and high T-bet and B lymphocyte–induced maturation protein 1 expression, but low B cell lymphoma 6 expression. SF Tph cells, by provision of IL-21 and IFN γ , skewed B cell differentiation toward a CD21^{low/–}CD11c⁺ phenotype in vitro. Additionally, SF Tph cell frequencies correlated with the appearance of SF CD21^{low/–}CD11c⁺CD27–IgM– double-negative (DN) B cells in situ.

Conclusion. Clonally expanded CD4⁺ Tph cells accumulate in the joints of ANA-positive JIA patients and, in particular, promote CD21^{low/–}CD11c⁺ DN B cell differentiation. The expansion of Tph cells and DN B cells might reflect the autoimmune response in the joints of ANA-positive JIA patients.

INTRODUCTION

Juvenile idiopathic arthritis (JIA) is the most common childhood rheumatic disease and is characterized by synovial lymphocyte infiltration and progressive joint destruction (1). Findings from functional and genetic analyses indicate that CD4⁺ T helper cells may play a central role in JIA pathogenesis (2). Additionally, autoantibodies (e.g., antinuclear antibodies [ANAs]) can be detected in ~50% of patients with JIA, and the presence of ANAs is correlated with synovial lymphoid neogenesis and B cell

hyperactivity (3). However, the mechanisms that promote the aberrant activation of autoreactive B cells in JIA are still poorly understood.

In JIA patients, the synovial B cell compartment mainly consists of activated memory B cells and, among these, CD21^{low/–}CD11c⁺CD27–IgM– double-negative (DN) B cells seem to be preferentially expanded in the joints of ANA-positive patients (3–7). CD21^{low/–}CD11c⁺ B cells constitute a discrete B cell population that expresses transcription factor T-bet, accumulates in inflamed tissue, and is expanded in many

Supported by the German Research Foundation (grant MO 2160/4-1). Dr. Dirks' work was supported by the Interdisciplinary Center for Clinical Research Würzburg.

¹Jonas Fischer, Johannes Dirks, MD, Julia Klaussner, Gabriele Haase, Annette Holl-Wieden, MD, Christine Hofmann, MD, Stephan Hackenberg, MD, Henner Morbach, MD: University Hospital Würzburg, Würzburg, Germany; ²Hermann Girschick, MD: Vivantes Klinikum im Friedrichshain, Berlin, Germany.

Mr. Fischer and Dr. Dirks contributed equally to this work.

Author disclosures are available at <https://onlinelibrary.wiley.com/action/downloadSupplement?doi=10.1002%2Fart.41913&file=art41913-sup-0001-Disclosureform.pdf>.

Address correspondence to Henner Morbach, MD, Pediatric Immunology, Department of Pediatrics, University Hospital Würzburg, Josef-Schneider-Strasse 2, 97080 Würzburg, Germany. Email: morbach_h@ukw.de.

Submitted for publication December 18, 2020; accepted in revised form June 29, 2021.

autoimmune diseases (8,9). The subset of CD21^{low/-}CD11c+ B cells in humans resembles age-associated B cells in mice, which have been shown to play a central role in the pathogenesis of murine lupus (10). The human CD21^{low/-}CD11c+ B cell population often overlaps with CD27-IgD- DN B cells or atypical memory B cells that are expanded in settings of chronic autoantigen/antigen exposure (11,12). CD21^{low/-}CD11c+ DN B cell differentiation seems to depend on the interaction of these cells with CD4+ T helper cells and their secreted cytokines (7,10,12,13). However, which T helper cell subsets may promote pathogenic B cell responses at the site of inflammation in JIA patients is not yet known.

T follicular helper (Tfh) cells have been implicated in the pathogenesis of many autoimmune diseases (14,15). They are characterized by the lineage-defining transcription factor Bcl-6, high expression of programmed death 1 (PD-1), and the chemokine receptor CXCR5 that recruits them into the follicles of secondary lymphoid organs (16). These cells exert their specific "B helper" function through the secretion of cytokines (e.g., interleukin-21 [IL-21]) and by production of costimulatory molecules (e.g., inducible T cell costimulator, OX40, CD154) (17). In contrast to classic Tfh cells, which act in the germinal centers of secondary lymphoid organs, extrafollicular or peripheral T helper (Tph) cell subsets have been detected in the inflamed joint tissue of patients with autoimmune diseases, and also have been observed in various murine models of autoimmune disease (18,19). In particular, Tph cells that accumulated in the joints of patients with seropositive rheumatoid arthritis (RA) also secreted IL-21 but did not express Bcl-6 and CXCR5, and therefore Tph cells in RA seem to differ from classic Tfh cells (20). Interestingly, IL-21-expressing CD4+ T helper cells could also be detected in the inflamed joints of ANA-positive JIA patients; however, neither the phenotype nor the function of this T helper cell subset has been investigated in detail to date (21). Therefore, in this study, we investigated the occurrence and phenotype of CD4+ T cells that exhibit a "B helper" function at the site of inflammation in JIA patients and examined the functional impact of these cells on B cell differentiation.

PATIENTS AND METHODS

Patients. This study included 53 patients with active JIA, in whom joint puncture had been performed for intraarticular steroid injection (Supplementary Table 1, available on the *Arthritis & Rheumatology* website at <http://onlinelibrary.wiley.com/doi/10.1002/art.41913/abstract>). All patients were followed up at the Children's Hospital at the University Hospital of Würzburg. Human palatine tonsil samples were obtained from patients undergoing tonsillectomy due to recurrent tonsillitis and/or tonsillotomy due to tonsillar hypertrophy. Written informed consent was obtained from the patients' legal guardians. The study protocol was reviewed by the Research Ethics Committee of the University of

Würzburg (approval no. 299/17) and was conducted in accordance with the Declaration of Helsinki.

Sample preparation. Synovial fluid (SF) and peripheral blood (PB) samples were collected in EDTA tubes. Mononuclear cells were isolated using Ficoll density-gradient centrifugation. Tonsil mononuclear cells were obtained using mechanical disaggregation followed by Ficoll density-gradient centrifugation. Cells were stored in liquid nitrogen until used.

Flow cytometry and cell sorting. Details on the flow cytometry and cell sorting procedures and antibodies used are included in Supplementary Materials and Methods (available on the *Arthritis & Rheumatology* website at <http://onlinelibrary.wiley.com/doi/10.1002/art.41913/abstract>).

TCRVB repertoire sequencing. SF CD4+CD45RO+ CXCR5-PD-1^{high}HLA-DR+ and CD4+CD45RO+CXCR5-PD-1^{low/-}HLA-DR- T cells obtained from 4 ANA-positive JIA patients were sorted using flow cytometry. Gene sequencing was performed on each sorted cell subset to identify the *TCRVB* repertoire. Additional details are included in Supplementary Materials and Methods (available on the *Arthritis & Rheumatology* website at <http://onlinelibrary.wiley.com/doi/10.1002/art.41913/abstract>). This targeted locus study project has been deposited at DataBank of Japan/ European Nucleotide Archive/GenBank under the accession no. KEXF00000000. The version described in this report is the first version, accession no. KEXF01000000.

T cell/B cell coculture. A total of 30,000 sorted SF or tonsil CD4+PD-1+ T cells were cocultured with sorted healthy control PB CD19+CD27+IgM- B cells at a 1:1 ratio and were stimulated with staphylococcal enterotoxin B (0.1 µg/ml) in a 96-well plate in 200 µl of RPMI 1640 medium supplemented with 10% fetal calf serum (FCS) and penicillin/streptomycin. For blocking experiments, 10 µg/ml of IL-21 receptor-Fc (R&D Systems), 10 µg/ml of anti-interferon-γ (anti-IFNγ) (cloneB27; BioLegend), and/or 0.1 µg/ml of ruxolitinib (In vivoGen) was added to the cultures. After 7 days, B cell differentiation was analyzed using flow cytometry, and total IgG concentrations in culture supernatants were measured using an in-house enzyme-linked immunosorbent assay (22). To analyze T-bet induction in B cells, T cells were sorted as described above and were cocultured for 48 hours with allogenic B cells that had been immunomagnetically purified from the PB of healthy controls using CD20 microbeads (Miltenyi Biotec). B cells were additionally stimulated with F(ab')₂-anti-IgM (5 µg/ml; The Jackson Laboratory), and in CD19+CD27- gated naive B cells, intracellular T-bet expression was analyzed using flow cytometry.

B cell activation assays. B cells were purified from the PB of healthy controls using CD20 microbeads (Miltenyi Biotec). A total of 30,000 purified B cells were cultured in a 96-well plate

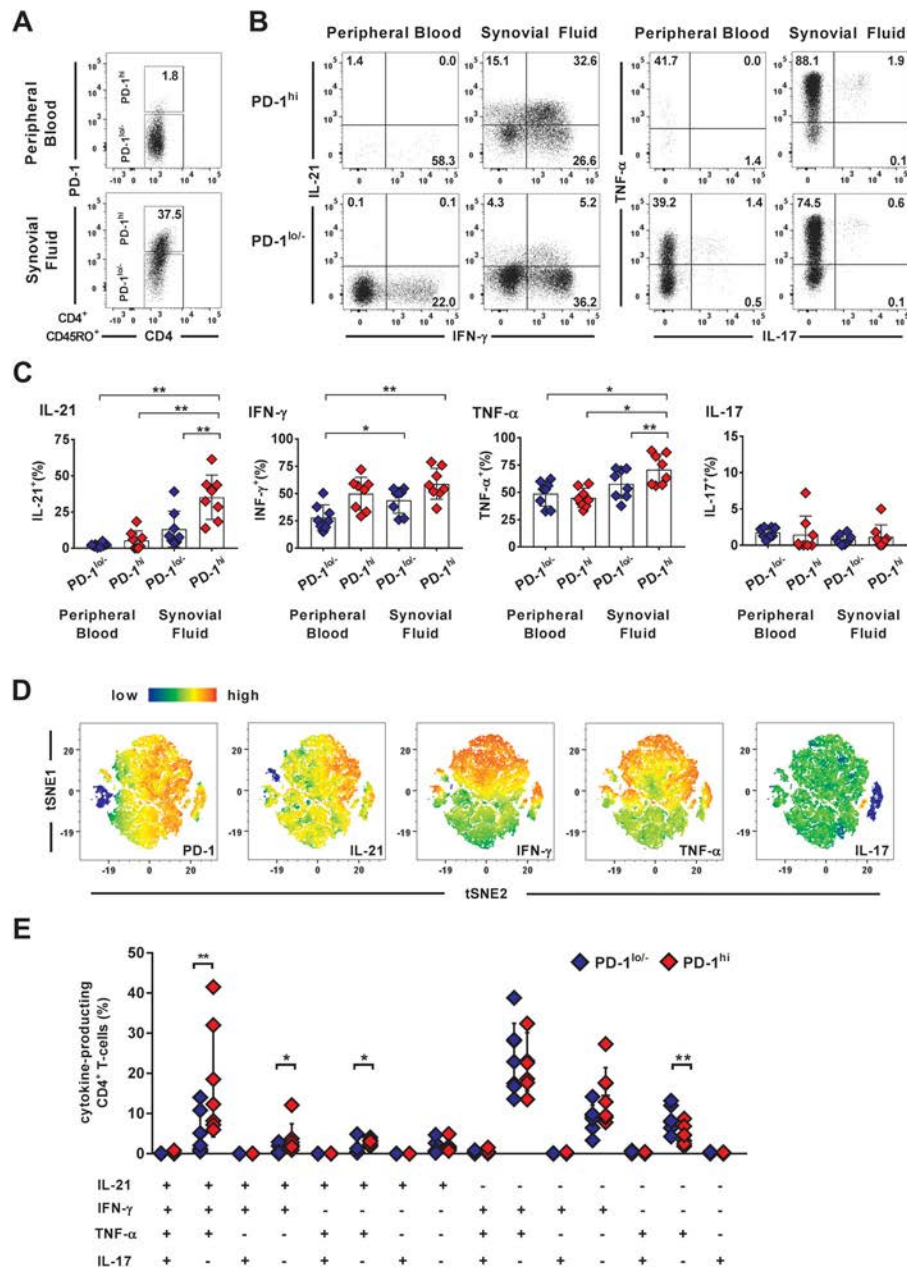


Figure 1. CD4⁺ T cells with high expression of programmed death 1 (PD-1^{high}) are characterized by coexpression of interleukin-21 (IL-21) and interferon- γ (IFN γ) in the synovial fluid (SF) of patients with juvenile idiopathic arthritis (JIA). **A**, Representative dot plots showing PD-1 expression on matched peripheral blood (PB) and SF CD45RO⁺CD4⁺ T cells from 1 patient with JIA. **B** and **C**, Representative dot plots (**B**) and the mean frequencies of cytokine-expressing cells (**C**) within CD45RO⁺PD-1^{low/-} or CD45RO⁺PD-1^{high} CD4⁺ T cells from the PB or SF of JIA patients. **D**, Heatmaps of merged data derived from t-distributed stochastic neighbor embedding (t-SNE) analysis showing expression of PD-1, IL-21, IFN γ , tumor necrosis factor (TNF), and IL-17 on CD4⁺ T cells from the SF of 5 JIA patients. Colors indicate the expression level of each marker. **E**, Polyfunctional cytokine expression data in SF PD-1^{high} or PD-1^{low/-} CD4⁺ T cells. Percentages of CD4⁺ T cells displaying each cytokine coexpression pattern in the SF of 7 JIA patients were determined using flow cytometry, with a Boolean gating strategy. In **C** and **E**, symbols represent individual samples; bars in **C** show the mean \pm SD. * = $P < 0.05$; ** = $P < 0.01$, by one-way analysis of variance with Tukey's multiple comparisons test for comparisons between >2 groups (**C**) and paired t -test for comparisons between 2 groups (**E**). Color figure can be viewed in the online issue, which is available at <http://onlinelibrary.wiley.com/doi/10.1002/art.41913/abstract>.

in 200 μ l of RPMI 1640 medium supplemented with 10% FCS and penicillin/streptomycin in the presence of CD40L (5 μ g/ml) (BioLegend), with the addition of either IFN γ or IL-21 or both (each at a concentration of 100 ng/ml). After 2 days, intracellular expression of T-bet in CD19⁺CD27⁻ gated naive B cells was analyzed using flow cytometry.

Statistical analysis. Statistical analyses were performed using GraphPad Prism software version 8.0. Hierarchical cluster analysis and principal components analysis were performed using ClustVis. Data are expressed as scattered individual values and the mean \pm SD. Either Student's 2-tailed t -test or one-way analysis of variance with Tukey's multiple comparisons test was used

to compare data sets with either 2 or >2 continuous variables, respectively. Pearson's correlation coefficient was used to analyze the correlation between variables. A chi-square test with Yates' correction was used for contingency tables. *P* values less than 0.05 were considered significant.

RESULTS

Correlation of high expression of PD-1 on SF CD4+ T cells with a distinct cytokine pattern characterized by coexpression of IL-21 and IFN γ . We used PD-1 as a surrogate surface marker to explore the SF CD4+ T cell compartment in the joints of patients with JIA for the presence of activated T helper cells with a potential B helper function (e.g., IL-21 expression). The SF CD45RO+CD4+ memory T cell compartment was significantly enriched in PD-1^{high} cells as compared to the CD45RO+CD4+ memory T cell compartment in matched PB samples from each individual patient (mean \pm SD $3.0 \pm 1.7\%$ in the PB versus $34.4 \pm 19.0\%$ in the SF; *P* < 0.001) (Figure 1A). We then investigated whether these PD-1^{high}CD4+ T cells express a distinct cytokine pattern characteristic of B helper cells or whether the high expression of PD-1 in these cells could be indicative of a state of exhaustion (23).

We therefore assessed the capacity of SF PD-1^{high}CD4+ T cells to express IL-21, IFN γ , tumor necrosis factor (TNF), and IL-17 upon restimulation (Supplementary Figure 1, available on the *Arthritis & Rheumatology* website at <http://onlinelibrary.wiley.com/doi/10.1002/art.41913/abstract>). In the SF from patients with JIA, the PD-1^{high} T cell subset was particularly enriched in IL-21-expressing cells, whereas there was only a slight difference in the cytokine patterns seen between SF and PB PD-1^{low/-} T cells and PB PD-1^{high} T cells. Moreover, compared to these other cell subsets, the SF PD-1^{high} T cell population contained high levels of IFN γ -expressing and significantly higher levels of TNF-expressing cells, but similar levels of IL-17-expressing cells (Figures 1B and C). Indeed, up to 40% of SF PD-1^{high} cells showed high expression of IL-21, and >50% of this cell subset showed increased expression of IFN γ and TNF, suggesting that within this cell population, there may be a potential overlap between the "B helper" cytokine signature (i.e., increased levels of IL-21) and the Th1 cytokine signature (i.e., increased levels of IFN γ and TNF) (Figures 1B and C).

To strengthen this hypothesis, we performed an unsupervised analysis of multiparameter flow cytometry-based cytokine expression data derived from the SF CD4+ T cells obtained from 5 JIA patients. A t-distributed stochastic neighbor embedding analysis of SF CD4+ T cells revealed an island of IL-21-expressing T cells that was characterized by high expression of PD-1 together with high expression of IFN γ and TNF, but not IL-17 (Figure 1D). Using a Boolean gating strategy, we further analyzed polyfunctional cytokine combinations at the single-cell level within PD-1^{high} and PD-1^{low/-} SF CD4+ T cells obtained from

7 additional JIA patients. CD4+ T cells that expressed IL-21 together with IFN γ and/or TNF, but not IL-17, were more enriched in PD-1^{high} cells compared to PD-1^{low/-} cells (Figure 1E). Of note, the cytokine pattern of SF PD-1^{high}CD4+ T cells was divergent from classic Tfh cells, since expression of IFN γ and/or TNF could not be observed within IL-21-expressing PD-1^{high}CD4+ T cells derived from tonsil tissue, which, in contrast, contained higher levels of IL-4-expressing T cells and IL-10-expressing T cells compared to that observed in the SF (Supplementary Figures 2A and B, available on the *Arthritis & Rheumatology* website at <http://onlinelibrary.wiley.com/doi/10.1002/art.41913/abstract>).

Therefore, we conclude that IL-21 is a signature cytokine of SF PD-1^{high}CD4+ T cells in JIA patients, but unlike classic Tfh cells, coexpression of IFN γ and TNF also indicates skewing toward a Th1 phenotype. Furthermore, the robust capacity of SF PD-1^{high}CD4+ T cells to express cytokines upon stimulation is evidence against the presence of an exhaustive state that might be indicated by high expression of PD-1.

Signs of activation and an extrafollicular/peripheral migration pattern in PD-1^{high}CD4+ T cells accumulating at the site of inflammation.

Based on the cytokine pattern, we postulated that SF PD-1^{high}CD4+ T cells differ from classic Tfh cells and PD-1^{low/-} memory T helper cells and may rather constitute a distinct T effector subset. Therefore, we further aimed to delineate this T cell subset in more detail by comparing its extended phenotype to that of PD-1^{low/-} memory CD4+ T cells in SF and that of classic Tfh cells in the tonsils from control individuals (Supplementary Figure 3, available on the *Arthritis & Rheumatology* website at <http://onlinelibrary.wiley.com/doi/10.1002/art.41913/abstract>). Indeed, principal components analysis and hierarchical clustering of a flow cytometry data set comprising 17 different markers clearly distinguished SF PD-1^{high} and PD-1^{low/-}CD4+ T cells, as well as tonsil PD-1^{high}CD4+ T cells, the latter representing classic Tfh cells (Figures 2A and B). In contrast to classic Tfh cells derived from tonsils, SF PD-1^{high}CD4+ T cells lacked the chemokine receptor CXCR5 that classically characterizes Tfh cells (Figures 2B–D).

Aside from a lack of CXCR5 expression, both SF CD4+ T cell populations (PD-1^{high} as well as PD-1^{low/-}) significantly differed from classic Tfh cells, as evidenced by a peripheral/inflammatory and extrafollicular migration pattern with increased expression of CCR2, CCR5, and P-selectin glycoprotein ligand 1 (Figures 2B–D and Supplementary Figures 4A and B, available on the *Arthritis & Rheumatology* website at <http://onlinelibrary.wiley.com/doi/10.1002/art.41913/abstract>). Additionally, SF PD-1^{high}CD4+ cells differed from SF PD-1^{low/-}CD4+ cells and also from tonsil Tfh cells by increased expression of activation markers (e.g., HLA-DR, OX40), as well as by high expression of the Th1 transcription factor T-bet, higher expression of B lymphocyte-induced maturation protein 1 (BLIMP-1), and lower expression of Tfh lineage-defining

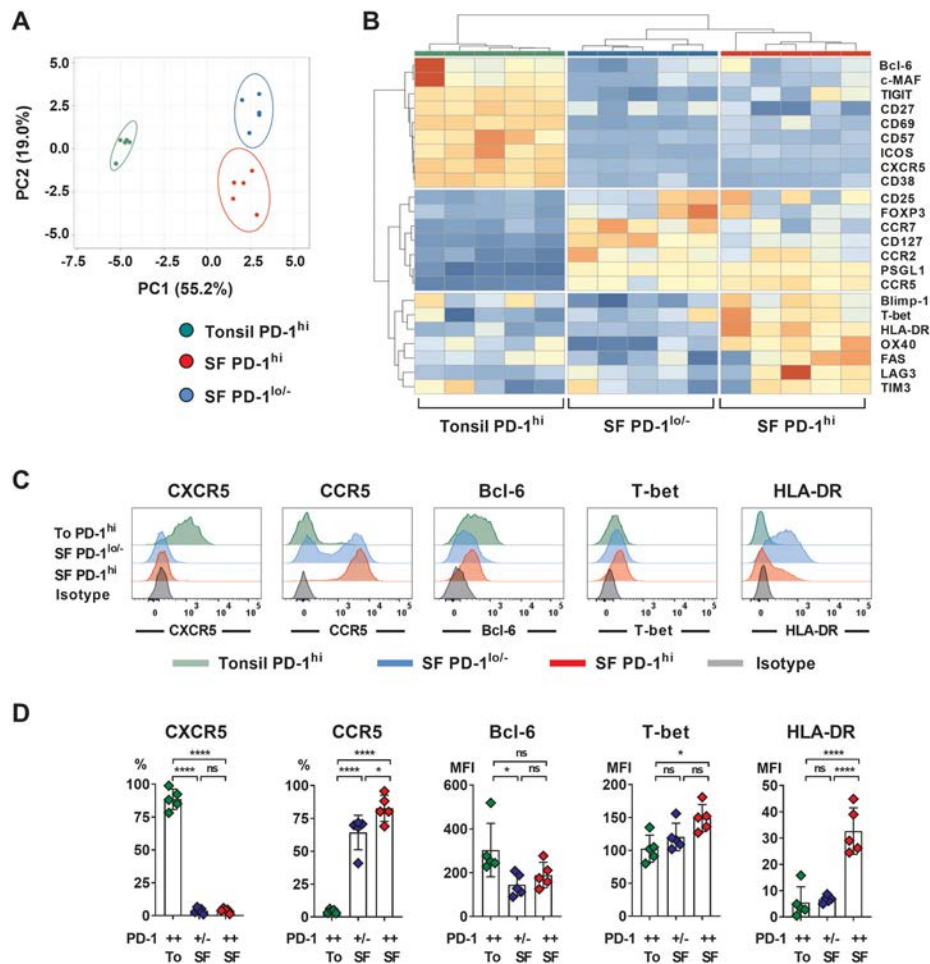


Figure 2. SF PD-1^{high} CD4⁺ T cells show signs of activation and express an extrafollicular/inflammatory migration pattern. **A**, Principal components (PC) analyses of flow cytometry data assessing the phenotypes of SF PD-1^{high} and PD-1^{low/-} CD4⁺ T cells from 5 JIA patients and tonsil PD-1^{high} CD4⁺ T cells from 5 controls. **B**, Unsupervised hierarchical clustering analysis of the 17 different markers from the flow cytometry data set. Patterns of expression are shown as heatmaps, in which colors in each row represent the normalized marker expression, and data are split into 3 clusters. **C**, Representative histograms showing CXCR5, CCR5, Bcl-6, T-bet, and HLA-DR expression on tonsil (To) PD-1^{high} CD4⁺ T cells, SF PD-1^{low/-} CD4⁺ T cells, and PD-1^{high} CD4⁺ T cells. **D**, Flow cytometry analysis of PD-1^{high} and PD-1^{low/-} CD4⁺ T cells from the SF of 5 JIA patients and PD-1^{high} CD4⁺ T cells from the tonsils of 5 controls showing mean frequencies of marker-expressing cells or mean fluorescence intensity (MFI) of marker expression. Symbols represent individual samples; bars show the mean \pm SD. * = $P < 0.05$; **** = $P < 0.0001$, by one-way analysis of variance with Tukey's multiple comparisons test. TIGIT = T cell immunoreceptor with Ig and ITIM domains; ICOS = inducible costimulator; PSGL-1 = P-selectin glycoprotein ligand 1; BLIMP-1 = B lymphocyte-induced maturation protein 1; TIM-3 = T cell immunoglobulin and mucin domain-containing protein 3; NS = not significant (see Figure 1 for other definitions).

transcription factors Bcl-6 and c-MAF (Figures 2B–D and Supplementary Figures 4A and B, available on the *Arthritis & Rheumatology* website at <http://onlinelibrary.wiley.com/doi/10.1002/art.41913/abstract>).

Taken together, these markers established a signature that clearly distinguishes SF PD-1^{high}CD4⁺ T cells from classic Tfh cells as well as PD-1^{low/-} memory T cells. Hence, the extended phenotype of SF PD-1^{high}CD4⁺ T cells is characterized by signs of sustained activation (i.e., enrichment of HLA-DR⁺ cells), an inflammatory/peripheral chemokine receptor pattern

(i.e., enrichment of CXCR5⁺ cells), and a mixed pattern of transcription factors that partially resembles that seen in Tfh cells or Th1 cells.

Since a significant proportion of pathogenic Th1 cells in the joints of JIA patients is derived from a shift of Th17 cells to nonclassic Th1 cells, which can be defined by persistent CD161 expression, we also assessed CD161 expression in SF PD-1^{high}CD4⁺ T cells (24–26). In contrast to tonsil PD-1^{high}CD4⁺ T cells that were shown to have minimal CD161 expression, a considerable percentage of SF PD-1^{high}CD4⁺ T cells expressed

CD161 (Figures 3A and B). We further examined IL-17-expressing and/or IL-21-expressing CD4+ T cell subsets to investigate coexpression of CD161 (Supplementary Figure 5, available on the *Arthritis & Rheumatology* website at <http://onlinelibrary.wiley.com/doi/10.1002/art.41913/abstract>).

As expected, most of the IL-17-expressing cells were CD161+ cells, which was independent of IL-21 coexpression. However, >50% of the IL-21-expressing cells that did not coexpress IL-17 (IL-17-IL-21+) also expressed CD161 (Figures 3C and D). The majority of these IL-21+ cells (including the very rare population of IL-17+IL-21+ cells) were from the PD-1^{high} compartment, whereas the IL-17+ cells that did not coexpress IL-21 were from the PD-1^{low/-} compartment (Figures 3C and D).

Additionally, expression levels of the Th17-defining transcription factor retinoic acid receptor-related orphan nuclear receptor γ t (ROR γ t) within the 3 cell subsets was similar to those of CD161, with lower but residual expression of ROR γ t in IL-17-IL-21+ cells (Figures 3C and D). Expression levels of ROR γ t, as well as CD161, within the cytokine-expressing T cell subsets were independent of IFN γ coexpression (Supplementary Figure 6, available on the *Arthritis & Rheumatology* website at <http://onlinelibrary.wiley.com/doi/10.1002/art.41913/abstract>). Hence, a considerable percentage of PD-1^{high}IL-21+IL-17-CD4+ T cells in the joints of JIA patients coexpress CD161, suggesting that these cells may have originated from the Th17 subset of T helper cells.

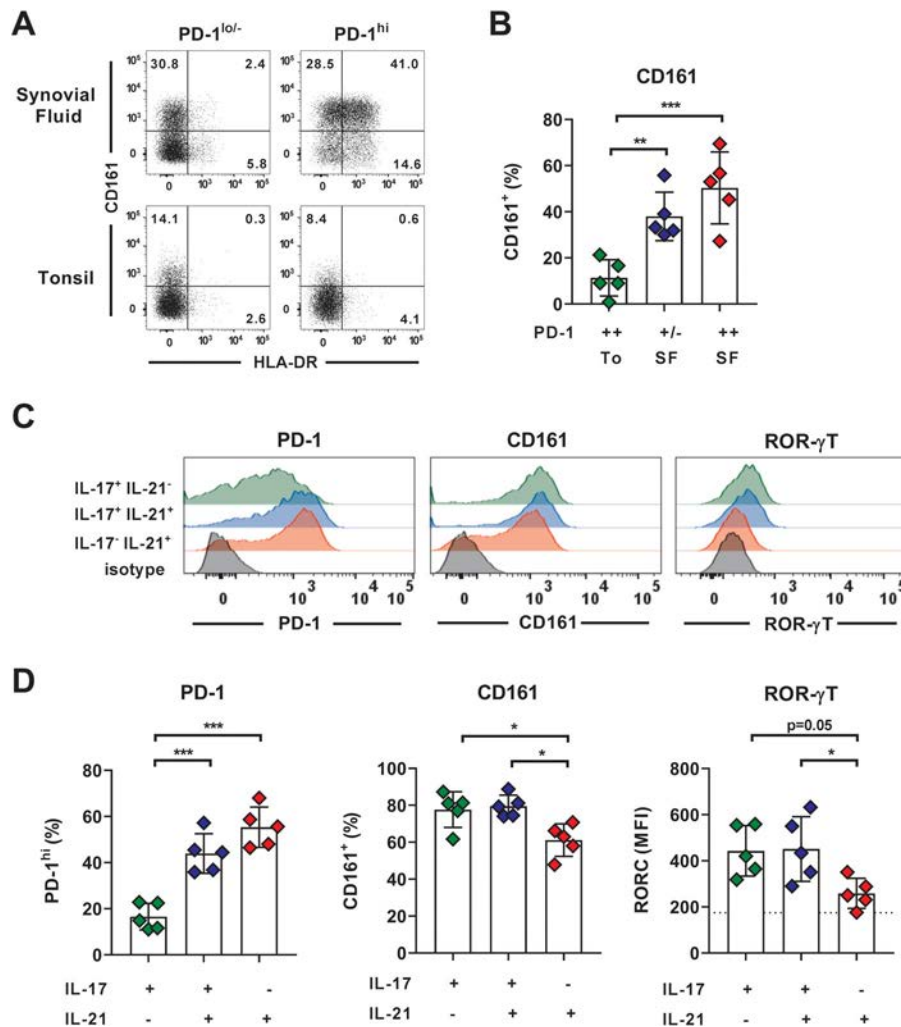


Figure 3. Coexpression of CD161 in PD-1^{high}HLA-DR+ and IL-21+CD4+ T cells from the SF of JIA patients. **A**, Representative dot plots showing CD161 and HLA-DR expression on SF and tonsil PD-1^{low/-} and PD-1^{high} CD4+ T cells. **B**, Mean frequencies of CD161+ cells among PD-1^{high} and PD-1^{low/-} CD4+ T cells from the SF of 5 JIA patients and PD-1^{high} CD4+ T cells from the tonsils (To) of 5 controls. **C**, Representative histograms showing PD-1, CD161, and receptor-related orphan nuclear receptor γ t (ROR γ t) expression in SF IL-17+IL-21-, IL-17+IL21+, and IL-17-IL-21+ CD4+ T cells. **D**, Flow cytometry analysis of IL-17- and/or IL-21-expressing CD4+ T cells from the SF of 5 JIA patients, showing mean frequencies of PD-1+ or CD161+ cells or mean fluorescence intensity (MFI) of ROR γ t expression. In **B** and **D**, symbols represent individual samples; bars show the mean \pm SD. The broken line shows the MFI of the isotype control. * = $P < 0.05$; ** = $P < 0.01$; *** = $P < 0.001$, by one-way analysis of variance with Tukey's multiple comparisons test. See Figure 1 for other definitions. Color figure can be viewed in the online issue, which is available at <http://onlinelibrary.wiley.com/doi/10.1002/art.41913/abstract>.

PD-1^{high}CXCR5-HLA-DR+CD4+ T cells identified as a clonally expanded population in the SF of patients with JIA.

The preferential occurrence of a subset of highly activated effector CD4+ T cells in the joints of JIA patients raises the question of whether this accumulation might be elicited by antigen-driven clonal expansion or rather a random influx into the inflamed joints. The SF PD-1^{high}CXCR5-HLA-DR+CD4+ T cell population (PD-1^{high}) was more enriched in cells expressing Ki-67 compared to the matched PD-1^{low/-}HLA-DR-CD45RO+ memory cell population (PD-1^{low/-}) (Figure 4A), suggestive of recent proliferation *in vivo* and a potential antigen encounter.

Next, we performed *TCRVB* next-generation sequencing on matched SF PD-1^{high} and PD-1^{low/-} T cells from 4 JIA patients (Supplementary Figure 7, available on the *Arthritis & Rheumatology* website at <http://onlinelibrary.wiley.com/doi/10.1002/art.41913/abstract>). Additionally, we analyzed the *TCRVB* repertoire of both T cell populations derived from 2 separate joints from 1 of these patients. Despite the fact that the number of cells in each T cell subset was equal in the matched pairs of SF samples from individual patients, the number of unique clones was lower in the PD-1^{high} T cell subset than in the PD-1^{low/-} T cell subset (Supplementary Table 2, available on the *Arthritis & Rheumatology*

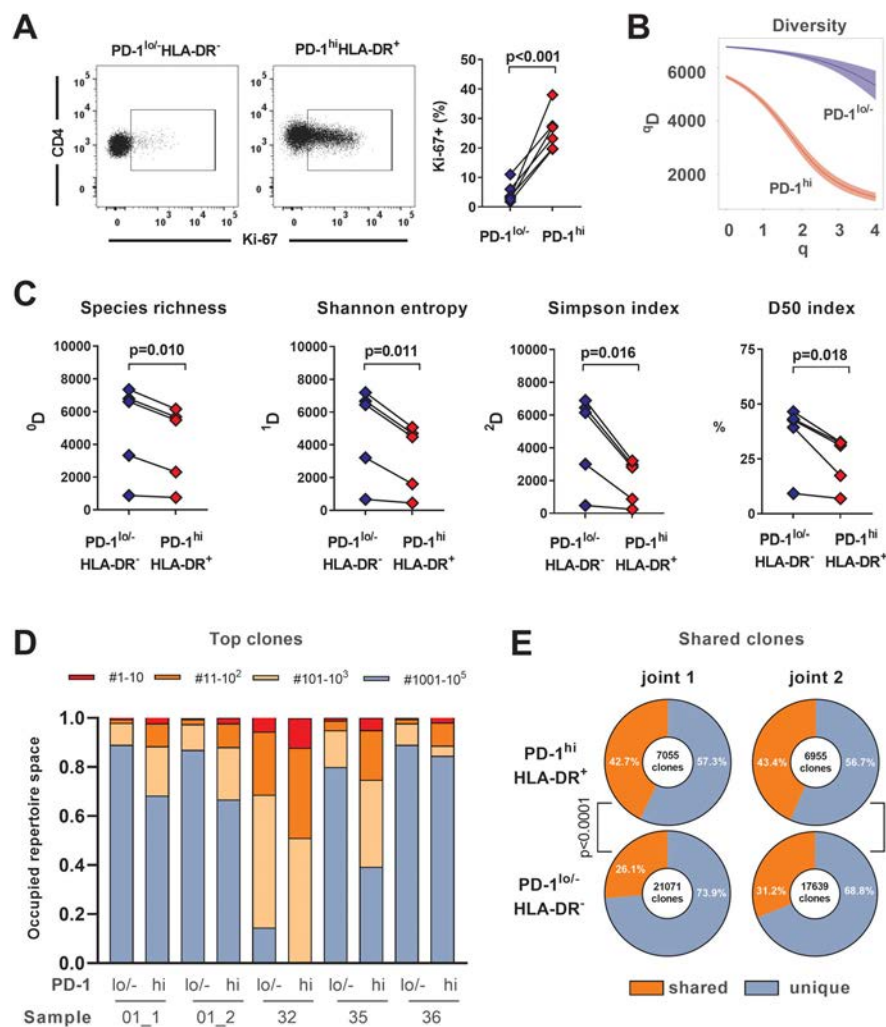


Figure 4. Signs of clonal expansion in SF PD-1^{high}CXCR5-HLA-DR+ CD4+ T cells from patients with JIA. **A**, Representative dot plots showing Ki-67 expression and the Ki-67+ cell frequency within PD-1^{high}CXCR5-HLA-DR+ and PD-1^{low/-}CXCR5-HLA-DR- CD4+ T cells from the SF of 5 JIA patients. **B**, Clonal diversity analysis of the *TCRVB* repertoire in both T cell populations in 5 different joints from 4 JIA patients, using the Hill generalized diversity index. The diversity index (^qD) was calculated over a range of diversity orders (q) and was plotted as a smooth curve. Representative curves from 1 patient are shown. **C**, Representations of species richness (q = 0), Shannon diversity index (q = 1), Simpson diversity index (q = 2), and diversity 50 (D50) index in both T cell subsets. Symbols represent individual values of each T cell population from a single joint sample from the same patient. Significance was determined by paired t-test. **D**, Stacked bar graphs showing the clonal proportion of the top n clonotypes within each T cell subset from the joint samples from 4 JIA patients. **E**, Pie charts showing the proportions of shared clonotypes within both T cell subsets between 2 different joints from the same JIA patient. The proportion of shared clones in the PD-1^{high}CXCR5-HLA-DR+ cells was compared to that of the matched PD-1^{low/-}CXCR5-HLA-DR- T cell subsets from the same joint. P values were determined by chi-square test with Yates' correction. See Figure 1 for other definitions. Color figure can be viewed in the online issue, which is available at <http://onlinelibrary.wiley.com/doi/10.1002/art.41913/abstract>.

website at <http://onlinelibrary.wiley.com/doi/10.1002/art.41913/abstract>).

We therefore analyzed the clonal diversity of each T cell subset using the Hill diversity index as a surrogate marker of clonal expansion, in which q values of 0, 1, or 2 are used, equivalent to measures of diversity such as the species richness, Shannon entropy index, and the inverse Simpson index. Clonal diversity was significantly lower in the PD-1^{high} T cell subset compared to the matched PD-1^{low/-} T cell subset (Figures 4B and C). The D50 index, indicating the frequency of most abundant clones (top clones) of all clones accounting for 50% of all unique sequences, was significantly lower in the PD-1^{high} subset, and the top clones occupied more repertoire space in the PD-1^{high} subset compared to the matched PD-1^{low/-} subset from the same joint sample (Figures 4C and D). These findings indicate

significantly reduced clonal diversity in the PD-1^{high} cell subset, suggestive of a clonally expanded population.

When we assessed the extent of shared clonotypes of cell subsets from 2 different joints in the same patient, we observed that the PD-1^{high} cell subset showed significantly higher clonal overlap than the PD-1^{low/-} subset (Figure 4E). Furthermore, the clonal overlap within samples obtained from different JIA patients was higher in the PD-1^{high} subset than in the PD-1^{low/-} subset (Supplementary Figure 8A, available on the *Arthritis & Rheumatology* website at <http://onlinelibrary.wiley.com/doi/10.1002/art.41913/abstract>). Moreover, a particular set of *TCRVB* and *TCRJB* gene segments was overrepresented in the PD-1^{high} subset in each of the analyzed joint samples obtained from the JIA patients (Supplementary Figures 8B and C). Hence, the PD-1^{high} subset appears to represent a distinct population within SF CD4+

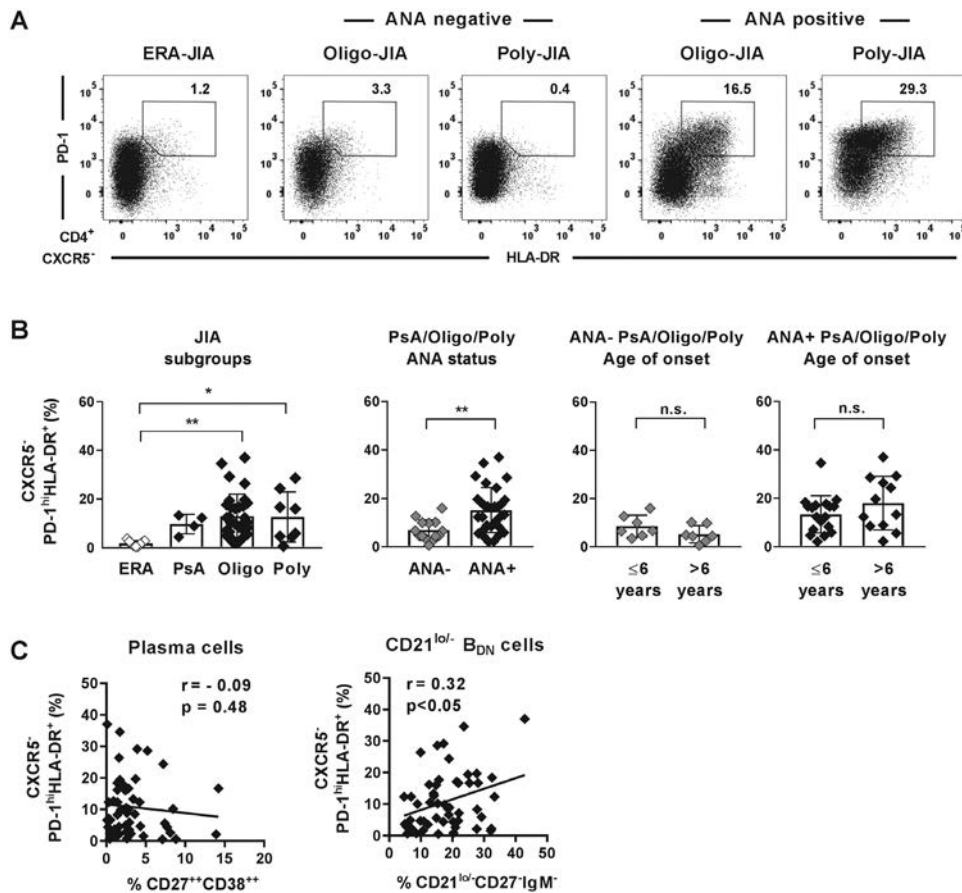


Figure 5. Accumulation of PD-1^{high}CXCR5-HLA-DR+ CD4+ T cells in the joints of antinuclear antibody (ANA)-positive JIA patients is correlated with the proportion of CD21^{low/-} double-negative (DN) B cells. **A** and **B**, Representative dot plots showing PD-1 and HLA-DR expression on SF CXCR5-CD4+ T cells from JIA patients (**A**) and the distribution of SF PD-1^{high}CXCR5-HLA-DR+ CD4+ T cell frequencies stratified according to the subgroup of JIA patients (9 patients with enthesitis-related arthritis [ERA], 32 with oligoarticular JIA [oligo-JIA], 8 with polyarticular JIA [poly-JIA], and 4 with psoriatic arthritis [PsA]-JIA), and within these subgroups (including all JIA patients except for those with ERA), stratified according to ANA status (30 ANA+ patients versus 14 ANA- patients) and age at disease onset (**B**). Symbols represent individual patients; bars show the mean ± SD. * = *P* < 0.05; ** = *P* < 0.01, by unpaired *t*-test for comparison between 2 groups and one-way analysis of variance with Tukey's multiple comparisons test for comparisons between >2 groups. **C**, Correlation between the frequency of SF PD-1^{high}CXCR5-HLA-DR+ CD4+ T cells and frequency of SF CD27++CD38++ plasmablasts/plasma cells and CD21^{low/-} CD27-IgM- DN B cells in 43 JIA patients. Correlations were determined using Pearson's correlation coefficient. See Figure 1 for other definitions.

T helper cells that is clonally expanded and potentially driven by antigens that are present at the site of inflammation.

Correlation of PD-1^{high}CXCR5-HLA-DR+CD4+ T cells in the joints of ANA-positive JIA patients with expansion of CD21^{low/-}CD11c+ DN B cells. The oligoclonal expansion of PD-1^{high}CXCR5-HLA-DR+CD4+ T cells secreting the B helper

cytokine IL-21 at the site of inflammation raises the question of whether this T cell subset might preferentially expand in a distinct subgroup of JIA patients who display a clinical phenotype characterized by signs of B cell dysregulation, such as the presence of ANAs. Therefore, we analyzed the distribution of PD-1^{high} T cells within the SF CD4+ T cell compartment in a larger cohort of JIA patients (Supplementary Figure 9 and Supplementary Table 1,

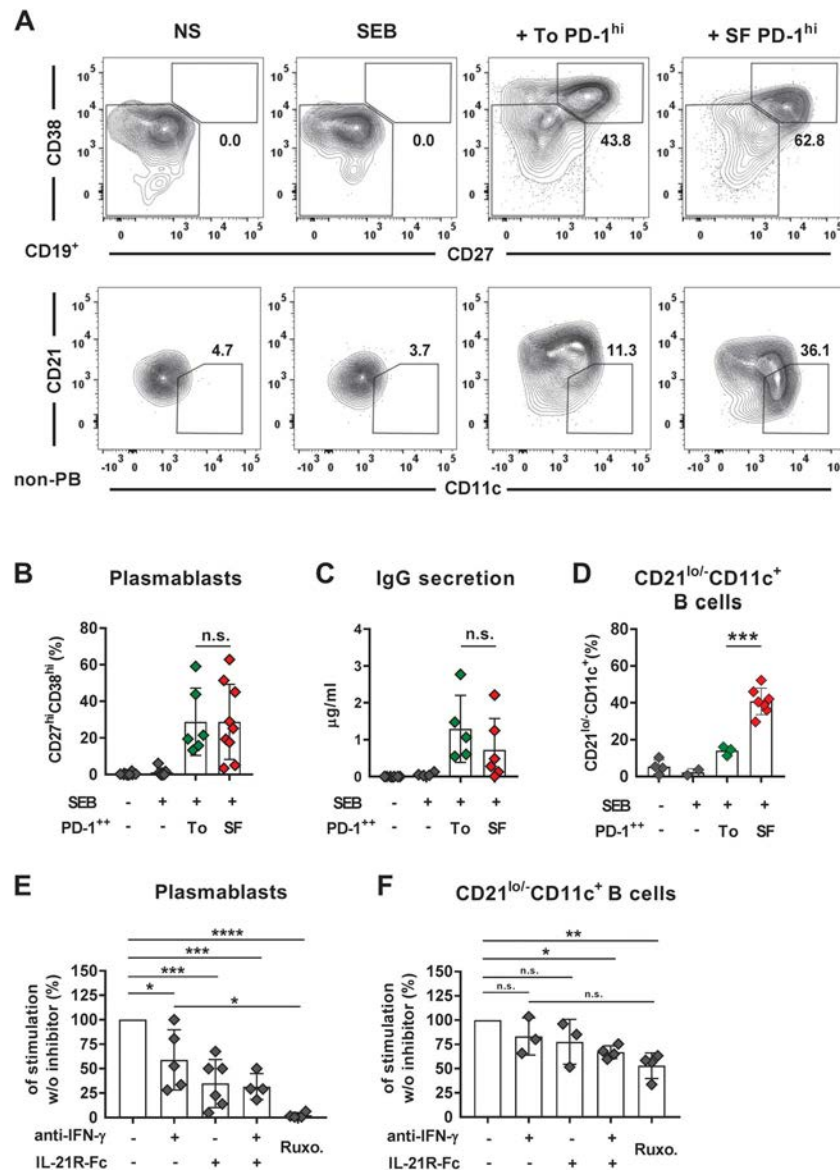


Figure 6. SF PD-1^{high} CD4+ T cells skew B cell differentiation toward a CD21^{low/-}CD11c+ T-bet+ phenotype in vitro. **A**, Representative dot plots showing the frequencies of CD38⁺⁺CD27⁺⁺ plasmablasts (top) and CD21^{low/-}CD11c+ B cells (bottom) in T cell/B cell cocultures in vitro. Cocultures with T cells included CD19+CD27+IgM- switched memory B cells from healthy controls under conditions of no stimulation (NS), using stimulation with staphylococcal enterotoxin B (SEB) alone, or using stimulation with SEB and culturing with sorted PD-1^{high} CD4+ T cells from control tonsils (To) or SF from JIA patients. **B–D**, Frequencies of CD27⁺⁺CD38⁺⁺ plasmablasts and CD21^{low/-}CD11c+ B cells as well as IgG concentration in T cell/B cell cocultures. **E** and **F**, Frequencies of stimulated plasmablasts (**E**) and CD21^{low/-}CD11c+ B cells (**F**) in cocultures of SF PD-1^{high}CD4+ T cells from JIA patients with switched memory B cells from healthy controls in the absence or presence of IL-21 receptor-Fc, anti-IFN γ , and/or the inhibitor ruxolitinib (Ruxo.). Frequencies were determined relative to the values in stimulated cell cultures without any inhibitors (set at 100%). In **B–F**, symbols represent individual values; bars show the mean \pm SD. * = $P < 0.05$; ** $P < 0.01$; *** = $P < 0.001$; **** = $P < 0.0001$, by unpaired Student's t -test for comparisons between 2 groups (**B–D**) and one-way analysis of variance with Tukey's multiple comparisons test for comparisons between >2 groups (**E** and **F**). Non-PB = non-plasmablast; n.s. = not significant (see Figure 1 for other definitions). Color figure can be viewed in the online issue, which is available at <http://onlinelibrary.wiley.com/doi/10.1002/art.41913/abstract>.

available on the *Arthritis & Rheumatology* website at <http://onlinelibrary.wiley.com/doi/10.1002/art.41913/abstract>.

The frequency of PD-1^{high} T cells was highest in the SF from patients with oligoarticular JIA and those with polyarticular JIA and was lowest in the SF from patients with enthesitis-related arthritis (Figures 5A and B). Since ANA-positive patients within the oligoarticular JIA, polyarticular JIA, and psoriatic arthritis–JIA group seem to constitute a clinically homogeneous group of patients characterized by an early age at disease onset (27,28), we further compared the ANA-positive patients to the ANA-negative patients. Indeed, the frequency of PD-1^{high} T cells was significantly higher within the SF of ANA-positive patients compared to ANA-negative JIA patients (Figure 5B). However, the frequencies of PD-1^{high} T cells did not correlate with age at onset ($r = 0.09$, $P = 0.57$) (data not shown), and no differences were observed between patients with early or later disease onset (Figure 5B).

Next, we used an existing flow cytometry B cell data set derived from the patients analyzed above to address the distribution of different SF B cell populations in order to explore the association between the expansion of SF PD-1^{high} T cells and distinct effector B cell subsets (5). Whereas the frequency of CD21^{low/-}CD11c+ DN B cells significantly correlated with that of SF PD-1^{high} T cells, the frequency of CD27++CD38++ plasmablasts/plasma cells did not show a significant correlation with PD-1^{high} T cells (Figure 5C). Therefore, we conclude that the accumulation of PD-1^{high}CXCR5–HLA–DR+CD4+ T cells together with CD21^{low/-}CD11c+ DN B cells represents a characteristic cellular pattern within the inflamed joints of JIA patients who are ANA positive.

B cell differentiation skewed toward CD21^{low/-}CD11c+ cells in vitro in the presence of SF PD-1^{high}CD4+ T cells. The correlation between SF PD-1^{high}CXCR5–HLA–DR+CD4+ T cells and CD21^{low/-}CD11c+ DN B cells in situ, as well as the distinct cytokine patterns of these T cells with coexpression of IL-21 and IFN γ , suggests a different functional impact on B cell differentiation than that expected from classic Tfh cells. Therefore, we utilized activation assays in vitro to compare the functional impact on B cell differentiation between this PD-1^{high}CD4+ T helper cell subset derived from SF of JIA patients and Tfh cells derived from the tonsils of control individuals. While SF PD-1^{high}CD4+ T cells induced plasmablast differentiation and Ig secretion that was as potent as classic tonsil Tfh cells, the SF PD-1^{high} T cells, but not tonsil Tfh cells, skewed B cell differentiation toward a CD21^{low/-}CD11c+ phenotype (Figures 6A–D and Supplementary Figure 10, available on the *Arthritis & Rheumatology* website at <http://onlinelibrary.wiley.com/doi/10.1002/art.41913/abstract>).

Blocking IFN γ , and particularly IL-21, impaired plasmablast differentiation induced by SF PD-1^{high} T cells (Figure 6E), whereas blocking each cytokine alone did not significantly impair

CD21^{low/-}CD11c+ B cell differentiation (Figure 6F). However, a strategy of co-cytokine blockade, with blocking of IFN γ together with IL-21, partially impaired the induction of CD21^{low/-}CD11c+ B cells by SF PD-1^{high} T cells (Figure 6F). Additionally, inhibiting JAK/STAT signaling with ruxolitinib completely blocked plasmablast differentiation and effectively impaired, but did not totally abrogate, the SF PD-1^{high} T cell-induced differentiation of CD21^{low/-}CD11c+B cells in vitro (Figure 6F).

Since T-bet has been characterized as one of the defining transcription factors of CD21^{low/-}CD11c+ B cells, we additionally analyzed whether SF PD-1^{high}CD4+ T cells would also induce T-bet expression in B cells in vitro. Indeed, SF PD-1^{high}CD4+ T cells induced T-bet expression in control B cells with levels that tended to be higher than those obtained using coculture with tonsil Tfh cells (Supplementary Figure 11, available on the *Arthritis & Rheumatology* website at <http://onlinelibrary.wiley.com/doi/10.1002/art.41913/abstract>).

Paralleling this observation and in accordance with the different cytokine profiles observed in the SF and tonsil PD-1^{high}CD4+ T cells, the addition of IFN γ , but not IL-21 alone, significantly induced in vitro T-bet expression in CD40L-stimulated control B cells (Supplementary Figure 12, available on the *Arthritis & Rheumatology* website at <http://onlinelibrary.wiley.com/doi/10.1002/art.41913/abstract>). However, adding IL-21 had a synergistic effect on T-bet expression in IFN γ /CD40L-stimulated B cells (Supplementary Figure 12). Hence, the SF PD-1^{high}CD4+ T cell subset exerts a potent B helper function, not only inducing plasma cell differentiation, but also particularly skewing B cell differentiation toward a T-bet-expressing CD21^{low/-}CD11c+ phenotype, partly through the influence of IL-21 and IFN γ .

DISCUSSION

Synovial inflammation in ANA-positive JIA is characterized by B cell hyperactivity; however, the mechanisms driving aberrant B cell activation at the site of inflammation are not yet understood (3,4,6,7). We have previously demonstrated that the SF CD4+ T helper cell pool in ANA-positive JIA patients is particularly enriched in IL-21-secreting cells (21). We have also shown that CD21^{low/-}CD11c+ DN B cells accumulate in the joints of these patients (5). In the present study, we demonstrate that the expansion of IL-21-secreting cells is attributable to a distinct subset of PD-1^{high}CXCR5–HLA–DR+ CD4+ T cells. This CD4+ T helper cell subset exerts a potent B helper function and particularly skews B cell differentiation toward a CD21^{low/-}CD11c+ phenotype in vitro, suggesting a functional relationship between both cell subsets.

High expression of activation and proliferation markers, as well as contraction of the *TCRVB* repertoire within SF PD-1^{high}CXCR5–HLA–DR+CD4+ T cells, indicates clonal expansion of this T cell subset within the joints of JIA patients.

Furthermore, the increased clonal overlap of PD-1^{high}CXCR5–HLA–DR+CD4+ T cells between different joint sites in individual patients and between different JIA patients, as well as the preferential accumulation in the joints of ANA-positive JIA patients, may also suggest that clonal expansion has been elicited after encountering currently unknown autoantigens/antigens that are present at the site of inflammation. Therefore, PD-1^{high}CXCR5–HLA–DR+CD4+ T cells appear to represent a pathogenic T cell subset that is expanded in a subgroup of JIA patients, particularly in ANA-positive patients. Dysregulation of T helper cells has been observed in the PB of JIA patients (29,30). A circulating subset of “pathogenic-like” CD4+ T helper cells has been detected in the PB of JIA patients that partially resembles the PD-1^{high}CXCR5–HLA–DR+CD4+ T cell subset described in the present report (29). However, whereas these circulating CD4+ T helper cells displayed an inflammatory cytokine pattern, including increased expression of IFN γ , TNF, and IL-17, the PD-1^{high}CXCR5–HLA–DR+CD4+ T cell subset in the SF of JIA patients in the present study also showed increased expression of IFN γ and TNF, but did not show an increase in IL-17 levels. Furthermore, high PD-1 expression on CD4+ T cells in the SF of JIA patients was particularly correlated with increased expression of IL-21.

Hence, high PD-1 expression on SF CD4+ T helper cells seems to represent a surrogate marker of a clonally expanded T helper cell subset that is characterized by IL-21 expression, thereby suggesting a B helper function. This T helper cell subset appears to be functionally distinct from other proinflammatory T helper cell subsets that have previously been characterized in the joints of JIA patients, e.g., Th1, Th17, and Th1/Th17 cells (24,26). However, CD161 expression on a majority of these IL-21+IFN γ +IL-17–PD-1^{high} CD4+ T cells suggests that these cells may have originated from the Th17 subset of T helper cells, as has been described previously as the potential origin of non-classic Th1 cells (24–26,31–33). IL-12, which, in an environment of inflammation, has been shown to induce a shift from Th17 to Th1/Th17 or nonclassic Th1 cells and has been shown to induce IL-21 and IFN γ –coexpressing T helper cells in vitro, might be one of the factors involved in the conversion of Th17 cells to IL-21+IFN γ +IL-17–PD-1^{high} CD4+ T cells (7,24–26).

The PD-1^{high}CXCR5–HLA–DR+CD4+ T cells in the joints of JIA patients shared a distinct phenotype with other IL-21–secreting CD4+ T helper cell subsets detected within the inflamed tissue in patients with different autoimmune diseases (20,34). In particular, expression of activation markers (PD-1, OX40, HLA–DR) and a high BLIMP-1:Bcl-6 ratio in conjunction with c-MAF expression, as well as an extrafollicular/inflammatory chemokine receptor pattern (CCR2+CXCR5–), also characterize the transcriptional program of synovial Tph cells first described in patients with seropositive RA (20). Since then, using PD-1^{high}CXCR5– as the common denominator in the phenotype of Tph cells, a potential circulating counterpart of this subset has been detected in the PB of patients with systemic lupus erythematosus and type

1 diabetes and is thought to contribute to disease pathogenesis by inducing autoantibody/antibody-secreting plasma cells (35,36). Indeed, synovial Tph cells in seropositive RA displayed a potent B helper function, as assessed by the capacity to induce plasma cell differentiation and Ig secretion in vitro (20).

Consistent with those studies, we also provide the first evidence of a potent B helper cell function of PD-1^{high}CXCR5–HLA–DR+ T helper cells derived from the SF of ANA-positive JIA patients. Extending the previous work on Tph cells, our current analysis establishes a more differentiated functional impact of Tph cells on B cell differentiation. Indeed, the results we have presented from in vitro experiments and ex vivo studies highly suggest that SF PD-1^{high}CXCR5–HLA–DR+ CD4+ T cells not only induce plasma cell differentiation and Ig secretion but also particularly skew B cell differentiation toward CD21^{low}–CD11c+DN B cells. We assume that the cellular pattern observed in the SF of JIA patients mirrors that in the synovia. However, we were not able to extend our analysis to include synovial tissue from JIA patients, since synovectomy is rarely performed in JIA and ethical considerations prevented collecting synovial biopsy specimens from the children included in the analysis.

CD4+ T helper cells coexpressing IL-21 and IFN γ have been detected in several infections and autoimmune diseases, according to the corresponding setting and cellular phenotype: “Th1-Tfh cells,” Tfh-like cells or, as discussed above, Tph cells (18,19,37–44). Concomitantly, differentiation of CD21^{low}–CD11c+ DN B cells appeared to depend on IFN γ and IL-21, and expansion of Th1-Tfh cells correlates with the presence of CD21^{low}–CD11c+ DN B cells (10,41,45).

Consistent with the results from these studies, several findings from our experiments also suggest that Tph cells secreting IL-21 in conjunction with IFN γ support the differentiation of CD21^{low}–CD11c+ DN B cells in the joints of JIA patients. These findings include 1) the correlation between numbers of CD21^{low}–CD11c+ DN B cells and numbers of IL-21 and IFN γ –coexpressing PD-1^{high}CD4+ T cells in the SF of JIA patients, 2) the need for co-cytokine blockade with blocking of IFN γ together with IL-21 to impair SF PD-1^{high}CD4+ T cell–induced B cell differentiation toward CD21^{low}–CD11c+ B cells in vitro, 3) the lack of in vitro induction of CD21^{low}–CD11c+ B cells by tonsil Tfh cells that predominantly express IL-21 and IL-4 but do not show increased expression of IFN γ , and 4) the synergistic effect of IFN γ and IL-21 on T-bet induction in CD40L-stimulated control B cells in vitro. However, whereas plasmablast/plasma cell differentiation in vitro was essentially dependent on JAK/STAT signaling, and in particular was dependent on the expression of IL-21, the mechanisms underlying the induction of CD21^{low}–CD11c+ B cells by SF Tph cells seem to be more complex, since blocking JAK/STAT signaling (thereby blocking the effects of IFN γ and IL-21) only partially impaired differentiation in vitro.

Of note, another essential prerequisite for the formation of CD21^{low}–CD11c+DN B cells is the engagement of B cell–intrinsic

Toll-like receptors (TLRs), including TLR-7 and TLR-9, which sense components of nuclear antigens that are delivered via antinuclear B cell receptors (BCRs) (10,12,13,46). Although this process could not be addressed in the present study, it is tempting to speculate that expansion of CD21^{low/-}CD11c+ DN B cells in the joints of ANA-positive JIA patients might have been induced after concomitant signaling through antinuclear BCRs and TLR-7/TLR-9 in the presence of IL-21 and IFN γ secreted by Tph cells (10,47).

In summary, we have characterized a distinct subset of PD-1^{high}CXCR5-HLA-DR+ CD4+ T cells that is clonally expanded in the joints of ANA-positive JIA patients and that displays a phenotype similar to that of Tph cells. These Tph cells functionally differ from classic Tfh cells and particularly promote differentiation of CD21^{low/-}CD11c+ DN B cells that are concomitantly expanded in the joints of ANA-positive JIA patients. These cells are potentially triggered by autoantigens/antigens present at the site of inflammation. Hence, the characteristic expansion of Tph cells and CD21^{low/-}CD11c+ DN B cells in the joints of ANA-positive JIA patients might reflect the autoimmune response at the site of inflammation.

ACKNOWLEDGMENT

We would like to thank the FACS Core Unit of the IZKF Würzburg for supporting this study.

AUTHOR CONTRIBUTIONS

All authors were involved in drafting the article or revising it critically for important intellectual content, and all authors approved the final version to be published. Dr. Morbach had full access to all of the data in the study and takes responsibility for the integrity of the data and the accuracy of the data analysis.

Study conception and design. Fischer, Dirks, Girschick, Morbach.

Acquisition of data. Fischer, Dirks, Klaussner, Haase, Holl-Wieden, Hofmann, Hackenberg, Girschick, Morbach.

Analysis and interpretation of data. Fischer, Dirks, Klaussner, Haase, Hofmann, Hackenberg, Girschick, Morbach.

REFERENCES

- Prakken B, Albani S, Martini A. Juvenile idiopathic arthritis [review]. *Lancet* 2011;377:2138–49.
- Mijnheer G, van Wijk F. T-cell compartmentalization and functional adaptation in autoimmune inflammation: lessons from pediatric rheumatic diseases. *Front Immunol* 2019;10:940.
- Gregorio A, Gambini C, Gerloni V, Parafioriti A, Sormani MP, Gregorio S, et al. Lymphoid neogenesis in juvenile idiopathic arthritis correlates with ANA positivity and plasma cells infiltration. *Rheumatology (Oxford)* 2007;46:308–13.
- Corcione A, Ferlito F, Gattorno M, Gregorio A, Pistorio A, Gastaldi R, et al. Phenotypic and functional characterization of switch memory B cells from patients with oligoarticular juvenile idiopathic arthritis. *Arthritis Res Ther* 2009;11:R150.
- Dirks J, Fischer J, Haase G, Holl-Wieden A, Hofmann C, Girschick H, et al. CD21^(lo/-)CD27⁽⁻⁾IgM⁽⁻⁾ double-negative B cells accumulate in the joints of patients with antinuclear antibody-positive juvenile idiopathic arthritis. *Front Pediatr* 2021;9:635815.
- Marasco E, Aquilani A, Cascioli S, Moneta GM, Caiello I, Farroni C, et al. Switched memory B cells are increased in oligoarticular and polyarticular juvenile idiopathic arthritis and their change over time is related to response to tumor necrosis factor inhibitors. *Arthritis Rheumatol* 2018;70:606–15.
- Morbach H, Wiegering V, Richl P, Schwarz T, Suffa N, Eichhorn EM, et al. Activated memory B cells may function as antigen-presenting cells in the joints of children with juvenile idiopathic arthritis. *Arthritis Rheum* 2011;63:3458–66.
- Isnardi I, Ng YS, Menard L, Meyers G, Saadoun D, Srdanovic I, et al. Complement receptor 2/CD21- human naive B cells contain mostly autoreactive unresponsive clones. *Blood* 2010;115:5026–36.
- Rakhmanov M, Keller B, Gutenberger S, Foerster C, Hoenig M, Driessen G, et al. Circulating CD21low B cells in common variable immunodeficiency resemble tissue homing, innate-like B cells. *Proc Natl Acad Sci U S A* 2009;106:13451–6.
- Cancro MP. Age-associated B cells [review]. *Annu Rev Immunol* 2020;38:315–40.
- Floudas A, Neto N, Marzaioli V, Murray K, Moran B, Monaghan MG, et al. Pathogenic, glycolytic PD-1+ B cells accumulate in the hypoxic RA joint. *JCI Insight* 2020;5:e139032.
- Jenks SA, Cashman KS, Zumaquero E, Marigorta UM, Patel AV, Wang X, et al. Distinct effector B cells induced by unregulated Toll-like receptor 7 contribute to pathogenic responses in systemic lupus erythematosus. *Immunity* 2018;49:725–39.
- Rubtsova K, Rubtsov AV, Cancro MP, Marrack P. Age-associated B cells: a T-bet-dependent effector with roles in protective and pathogenic immunity [review]. *J Immunol* 2015;195:1933–7.
- Crotty S. T follicular helper cell biology: a decade of discovery and diseases [review]. *Immunity* 2019;50:1132–48.
- Ueno H, Banchereau J, Vinuesa CG. Pathophysiology of T follicular helper cells in humans and mice [review]. *Nat Immunol* 2015;16:142–52.
- Crotty S. T follicular helper cell differentiation, function, and roles in disease [review]. *Immunity* 2014;41:529–42.
- Schmitt N, Ueno H. Human T follicular helper cells: development and subsets [review]. *Adv Exp Med Biol* 2013;785:87–94.
- Hutloff A. T follicular helper-like cells in inflamed non-lymphoid tissues [review]. *Front Immunol* 2018;9:1707.
- Rao DA. T cells that help B cells in chronically inflamed tissues [review]. *Front Immunol* 2018;9:1924.
- Rao DA, Gurish MF, Marshall JL, Slowikowski K, Fonseka CY, Liu Y, et al. Pathologically expanded peripheral T helper cell subset drives B cells in rheumatoid arthritis. *Nature* 2017;542:110–4.
- Fischer J, Dirks J, Haase G, Holl-Wieden A, Hofmann C, Girschick H, et al. IL-21+ CD4+ T helper cells co-expressing IFN- γ and TNF- α accumulate in the joints of antinuclear antibody positive patients with juvenile idiopathic arthritis. *Clin Immunol* 2020;217:108484.
- Janssen E, Morbach H, Ullas S, Bannock JM, Massad C, Menard L, et al. Deducator of cytokinesis 8-deficient patients have a breakdown in peripheral B-cell tolerance and defective regulatory T cells. *J Allergy Clin Immunol* 2014;134:1365–74.
- Canavan M, Floudas A, Veale DJ, Fearon U. The PD-1:PD-L1 axis in inflammatory arthritis [review]. *BMC Rheumatol* 2021;5:1.
- Cosmi L, Cimaz R, Maggi L, Santarlasci V, Capone M, Borriello F, et al. Evidence of the transient nature of the Th17 phenotype of CD4+CD161+ T cells in the synovial fluid of patients with juvenile idiopathic arthritis. *Arthritis Rheum* 2011;63:2504–15.
- Maggi L, Cimaz R, Capone M, Santarlasci V, Querci V, Simonini G, et al. Etanercept inhibits the tumor necrosis factor α -driven shift of Th17 lymphocytes toward a nonclassical Th1 phenotype in juvenile idiopathic arthritis. *Arthritis Rheumatol* 2014;66:1372–7.

26. Nistala K, Adams S, Cambrook H, Ursu S, Olivito B, de Jager W, et al. Th17 plasticity in human autoimmune arthritis is driven by the inflammatory environment. *Proc Natl Acad Sci U S A* 2010;107:14751–6.
27. Ravelli A, Varnier GC, Oliveira S, Castell E, Arguedas O, Magnani A, et al. Antinuclear antibody-positive patients should be grouped as a separate category in the classification of juvenile idiopathic arthritis. *Arthritis Rheum* 2011;63:267–75.
28. Ravelli A, Felici E, Magni-Manzoni S, Pistorio A, Novarini C, Bozzola E, et al. Patients with antinuclear antibody-positive juvenile idiopathic arthritis constitute a homogeneous subgroup irrespective of the course of joint disease. *Arthritis Rheum* 2005;52:826–32.
29. Spreafico R, Rossetti M, van Loosdregt J, Wallace CA, Massa M, Magni-Manzoni S, et al. A circulating reservoir of pathogenic-like CD4+ T cells shares a genetic and phenotypic signature with the inflamed synovial micro-environment. *Ann Rheum Dis* 2016;75:459–65.
30. Foley C, Floudas A, Canavan M, Biniecka M, MacDermott EJ, Veale DJ, et al. Increased T cell plasticity with dysregulation of follicular helper T, peripheral helper T, and Treg cell responses in children with juvenile idiopathic arthritis and Down syndrome-associated arthritis. *Arthritis Rheumatol* 2020;72:677–86.
31. Basdeo SA, Cluxton D, Sulaimani J, Moran B, Canavan M, Orr C, et al. Ex-Th17 (nonclassical Th1) cells are functionally distinct from classical Th1 and Th17 cells and are not constrained by regulatory T cells. *J Immunol* 2017;198:2249–59.
32. Basdeo SA, Moran B, Cluxton D, Canavan M, McCormick J, Connolly M, et al. Polyfunctional, pathogenic CD161+ Th17 lineage cells are resistant to regulatory T cell-mediated suppression in the context of autoimmunity. *J Immunol* 2015;195:528–40.
33. Cosmi L, De Palma R, Santarlasci V, Maggi L, Capone M, Frosali F, et al. Human interleukin 17-producing cells originate from a CD161+ CD4+ T cell precursor. *J Exp Med* 2008;205:1903–16.
34. Christophersen A, Lund EG, Snir O, Sola E, Kanduri C, Dahal-Koirala S, et al. Distinct phenotype of CD4+ T cells driving celiac disease identified in multiple autoimmune conditions. *Nat Med* 2019;25:734–7.
35. Bocharnikov AV, Keegan J, Wacleche VS, Cao Y, Fonseka CY, Wang G, et al. PD-1hiCXCR5- T peripheral helper cells promote B cell responses in lupus via MAF and IL-21. *JCI Insight* 2019;4:e130062.
36. Ekman I, Ihantola EL, Viisanen T, Rao DA, Nanto-Salonen K, Knip M, et al. Circulating CXCR5^{hi}PD-1^{hi} peripheral T helper cells are associated with progression to type 1 diabetes. *Diabetologia* 2019;62:1681–8.
37. Carpio VH, Opata MM, Montanez ME, Banerjee PP, Dent AL, Stephens R. IFN- γ and IL-21 double producing T cells are Bcl6-independent and survive into the memory phase in plasmodium chabaudi infection. *PLoS One* 2015;10:e0144654.
38. Ma X, Nakayamada S, Kubo S, Sakata K, Yamagata K, Miyazaki Y, et al. Expansion of T follicular helper-T helper 1 like cells through epigenetic regulation by signal transducer and activator of transcription factors. *Ann Rheum Dis* 2018;77:1354–61.
39. Morita R, Schmitt N, Bentebibel SE, Ranganathan R, Bourdery L, Zurawski G, et al. Human blood CXCR5⁺CD4⁺ T cells are counterparts of T follicular cells and contain specific subsets that differentially support antibody secretion. *Immunity* 2011;34:108–21.
40. Obeng-Adjei N, Portugal S, Tran TM, Yazew TB, Skinner J, Li S, et al. Circulating Th1-cell-type Tfh cells that exhibit impaired B cell help are preferentially activated during acute malaria in children. *Cell Rep* 2015;13:425–39.
41. Unger S, Seidl M, van Schouwenburg P, Rakhmanov M, Bulashevskaya A, Frede N, et al. The T_H1 phenotype of follicular helper T cells indicates an IFN- γ -associated immune dysregulation in patients with CD21^{low} common variable immunodeficiency. *J Allergy Clin Immunol* 2018;141:730–40.
42. Velu V, Mylvaganam GH, Gangadhara S, Hong JJ, Iyer SS, Gumber S, et al. Induction of Th1-biased T follicular helper (Tfh) cells in lymphoid tissues during chronic simian immunodeficiency virus infection defines functionally distinct germinal center Tfh cells. *J Immunol* 2016;197:1832–42.
43. Vu Van D, Beier KC, Pietzke LJ, Al Baz MS, Feist RK, Gurka S, et al. Local T/B cooperation in inflamed tissues is supported by T follicular helper-like cells. *Nat Commun* 2016;7:10875.
44. Xiao L, Jia L, Zhang Y, Yu S, Wu X, Yang B, et al. Human IL-21+ IFN- γ +CD4+ T cells in nasal polyps are regulated by IL-12. *Sci Rep* 2015;5:12781.
45. Naradikian MS, Myles A, Beiting DP, Roberts KJ, Dawson L, Herati RS, et al. Cutting edge: IL-4, IL-21, and IFN- γ interact to govern T-bet and CD11c expression in TLR-activated B cells. *J Immunol* 2016;197:1023–8.
46. Zumaquero E, Stone SL, Scharer CD, Jenks SA, Nellore A, Mousseau B, et al. IFN γ induces epigenetic programming of human T-bet^{hi} B cells and promotes TLR7/8 and IL-21 induced differentiation. *Elife* 2019;8:e41641.
47. Marshak-Rothstein A. Toll-like receptors in systemic autoimmune disease [review]. *Nat Rev Immunol* 2006;6:823–35.

Variants on the *UBE2L3/YDJC* Autoimmune Disease Risk Haplotype Increase *UBE2L3* Expression by Modulating CCCTC-Binding Factor and YY1 Binding

Jaanam Gopalakrishnan,¹ Kandice L. Tessneer,² Yao Fu,² Satish Pasula,² Richard C. Pelikan,² Jennifer A. Kelly,² Graham B. Wiley,² and Patrick M. Gaffney¹ 

Objective. Genetic variants spanning *UBE2L3* are associated with increased expression of the *UBE2L3*-encoded E2 ubiquitin-conjugating enzyme H7 (UbcH7), which facilitates activation of proinflammatory NF- κ B signaling and susceptibility to autoimmune diseases. We undertook this study to delineate how genetic variants carried on the *UBE2L3/YDJC* autoimmune risk haplotype function to drive hypermorphic *UBE2L3* expression.

Methods. We used bioinformatic analyses, electrophoretic mobility shift assays, and luciferase reporter assays to identify and functionally characterize allele-specific effects of risk variants positioned in chromatin accessible regions of immune cells. Chromatin conformation capture with quantitative polymerase chain reaction (3C-qPCR), chromatin immunoprecipitation (ChIP)-qPCR, and small interfering RNA (siRNA) knockdown assays were performed on patient-derived Epstein-Barr virus-transformed B cells homozygous for the *UBE2L3/YDJC* nonrisk or risk haplotype to determine if the risk haplotype increases *UBE2L3* expression by altering the regulatory chromatin architecture in the region.

Results. Of the 7 prioritized variants, 5 demonstrated allele-specific increases in nuclear protein binding affinity and regulatory activity. High-throughput sequencing of chromosome conformation capture coupled with ChIP (HiChIP) and 3C-qPCR uncovered a long-range interaction between the *UBE2L3* promoter (rs140490, rs140491, rs11089620) and the downstream *YDJC* promoter (rs3747093) that was strengthened in the presence of the *UBE2L3/YDJC* risk haplotype, and correlated with the loss of CCCTC-binding factor (CTCF) and gain of YY1 binding at the risk alleles. Depleting YY1 by siRNA disrupted the long-range interaction between the 2 promoters and reduced *UBE2L3* expression.

Conclusion. The *UBE2L3/YDJC* autoimmune risk haplotype increases *UBE2L3* expression through strengthening a YY1-mediated interaction between the *UBE2L3* and *YDJC* promoters.

INTRODUCTION

The ubiquitin-conjugating enzyme E2 L3 gene (*UBE2L3*), located on 22q11.21, encodes E2 ubiquitin-conjugating enzyme H7 (UbcH7). UbcH7 is a functional subunit of the linear ubiquitin chain assembly complex (LUBAC), a crucial regulator of the canonical NF- κ B signaling pathway (1–4). In the LUBAC, UbcH7 facilitates formation of linear polyubiquitin chains that are conjugated to the NF- κ B essential modulator (NEMO). Ubiquitinated NEMO dissociates from the IKK, allowing activated IKK to

degrade the inhibitory subunit, I κ B. Activated NF- κ B then translocates to the nucleus to initiate transcription of proinflammatory mediators (2–4). In human primary B cells and monocytes, increased UbcH7 expression enhanced LUBAC-mediated NF- κ B activation, as well as the proliferation of plasmablasts and plasma cells (5,6), thus implicating *UBE2L3/UbcH7* as a critical regulator of proinflammatory responses in immune cells.

UBE2L3 is a prominent genetic susceptibility locus for several autoimmune diseases, including systemic lupus erythematosus (SLE) (5–13), rheumatoid arthritis (5,13–15), celiac disease (5,16),

The content of this publication is solely the responsibility of the authors and does not represent the official views of the NIH or the Presbyterian Health Foundation.

Supported by the National Institute of General Medical Sciences, the National Institute of Arthritis and Musculoskeletal and Skin Diseases, and the National Institute of Allergy and Infectious Diseases of the NIH (grants R01-AR-063124, R01-AR-073606, R01-AR-056360, P30-GM-110766, and U19-AI-082714) and by the Presbyterian Health Foundation. The Oklahoma Rheumatic Disease Research Cores Center supplied the Epstein-Barr virus-transformed B cell lines and is supported by the NIH (grants U54-GM-104938, P30-AR-073750, and UM1-AI-144292).

¹Jaanam Gopalakrishnan, PhD, Patrick M. Gaffney, MD: Oklahoma Medical Research Foundation and University of Oklahoma Health Sciences Center, Oklahoma City; ²Kandice L. Tessneer, PhD, Yao Fu, PhD, Satish Pasula, PhD, Richard C. Pelikan, PhD, Jennifer A. Kelly, MPH, Graham B. Wiley, PhD: Oklahoma Medical Research Foundation, Oklahoma City.

Address correspondence to Patrick M. Gaffney, MD, Oklahoma Medical Research Foundation, 825 NE 13th Street, MS 57, Oklahoma City, OK 73104. Email: patrick-gaffney@omrf.org.

Submitted for publication March 12, 2021; accepted in revised form July 8, 2021.

Crohn's disease (5,17,18), inflammatory bowel disease (5,19), juvenile idiopathic arthritis (5,20), and psoriasis (5,21). Transracial mapping of European, Asian, and African American SLE populations identified a single 67-kb autoimmune disease-associated risk haplotype that spans the *UBE2L3* gene body and extends to the nearby *YDJC* gene (10). Although it has been established that this risk haplotype is correlated with increased *UBE2L3* messenger RNA and UbcH7 protein expression (5,6,10), the genetic regulatory mechanisms driving increased expression in the context of the *UBE2L3/YDJC* autoimmune risk haplotype remain poorly understood.

In this study, we prioritized 7 risk variants spanning the *UBE2L3/YDJC* autoimmune risk haplotype positioned in regions of high chromatin accessibility. We discovered that 4 of the 7 risk variants co-bound the transcription factors YY1 and CCCTC-binding factor (CTCF). The risk alleles at each variant demonstrated increased binding affinity for YY1 at the expense of CTCF and strengthened the long-range interactions between the promoters of *UBE2L3* and *YDJC*. Our findings delineate a novel mechanism that explains how the risk haplotype likely drives elevated *UBE2L3* expression in autoimmune disease.

MATERIALS AND METHODS

Cell lines and reagents. Jurkat and THP-1 cells were procured from ATCC. Epstein-Barr virus (EBV)-transformed B cell lines were obtained from the Lupus Family Registry and Repository housed by the Oklahoma Rheumatic Disease Research Cores Center at the Oklahoma Medical Research Foundation with institutional review board approval (22). Sanger sequencing was used to verify the genotype of EBV B cell lines carrying the risk allele (A) or nonrisk allele (C) of the index single-nucleotide polymorphism (SNP), rs140490. Jurkat, THP-1, and EBV B cells were maintained in RPMI 1640 medium supplemented with 10% fetal bovine serum, 1× penicillin/streptomycin antibiotic mixture (Atlanta Biologicals) and 2 mM L-glutamine (Lonza). THP-1 cell medium was also supplemented with 50 μM β-mercaptoethanol. Where indicated, cells were stimulated with phorbol 12-myristate 13-acetate and ionomycin (P/I; 50 ng/ml, 500 ng/ml, respectively) for 2 hours prior to harvest. For the small interfering RNA (siRNA) knockdown of CTCF or YY1, EBV B cells homozygous for the *UBE2L3/YDJC* nonrisk or risk haplotype were transiently transfected with 10 nM siRNA using 4D Amaxa Nucleofactor Unit for EBV B cells (Nucleofactor SF kit no. V4XC-2032; Lonza). On-Target plus human CTCF siRNA SmartPool (no. L-020165-00-0005), human YY1 siRNA SmartPool (no. L-011796-00-0005), and nontargeting scrambled siRNA pool (no. D-001810-10-05) were purchased from Dharmacon. All stock laboratory chemicals were from Sigma-Aldrich or ThermoFisher.

Electrophoretic mobility shift assays (EMSAs).

Complementary pairs of 41-bp nonrisk and risk probes of individual variants were chemically synthesized by Integrated DNA Technologies (Supplementary Table 1, available on the *Arthritis &*

Rheumatology website at <http://onlinelibrary.wiley.com/doi/10.1002/art.41925/abstract>), annealed, and end-labeled with $\gamma^{32}\text{P}$ -adenosine triphosphate (PerkinElmer) using T4 polynucleotide kinase (no. M0201S; New England Biolabs). Nuclear proteins were extracted from Jurkat cells, EBV B cells, and THP-1 cells that were unstimulated or were stimulated with P/I for 2 hours. Ten micrograms of nuclear protein were incubated with labeled 50,000 counts per minute of nonrisk or risk probes in binding buffer (1 μg poly dl-dC, 20 mM HEPES, 1 mM MgCl_2 , 100 mM Tris HCl, pH 7.4, and 0.5 mM EDTA) for 30 minutes at room temperature. DNA-protein complexes were resolved on a non-denaturing 5% acrylamide gel in 0.5× Tris-borate/EDTA. Gels were dried and exposed overnight on a phosphor screen. DNA-protein complexes were visualized on a Phosphorimager (GS-360; Bio-Rad) and quantified using Bio-Rad Quantity 1D Analysis software. For competition assays, 10-, 50-, and 100-fold excess of unlabeled nonrisk or risk probes were added to the EMSA binding reactions.

Dual-luciferase reporter assay. We cloned ~350 bp of the DNA sequences surrounding the nonrisk or risk alleles of selected *UBE2L3* or *YDJC* variants (Supplementary Table 2, <http://onlinelibrary.wiley.com/doi/10.1002/art.41925/abstract>) into the promoterless firefly luciferase plasmid, pGL4.14, or the minimal promoter firefly luciferase plasmid, pGL4.23 (Promega). Site-directed mutagenesis was used to separate the physically close risk variants, rs140491 and rs11089620 or rs12484550, rs5998599, and rs9621715 (Supplementary Table 2). The empty vector, nonrisk clone, or risk clone was transiently cotransfected with the transfection control *Renilla* luciferase plasmid, pRL-TK, into homozygous nonrisk EBV B cells using a 4D Amaxa Nucleofactor Unit for EBV B cells (Nucleofactor SF kit no. V4XC-2032; Lonza). Twenty-four hours posttransfection, cells were left unstimulated or were stimulated with P/I for 2 hours. Promoter or enhancer activity was determined using a Promega dual-luciferase reporter assay according to the instructions of the manufacturer. Relative luciferase units (RLUs) for each sample were determined by normalizing the firefly luciferase activity to the *Renilla* luciferase activity. RLU was further normalized to the vector only control and reported as normalized RLU.

High-throughput sequencing of chromosome conformation capture coupled with chromatin immunoprecipitation (HiChIP). H3K27ac- and CTCF-mediated chromatin interactions were measured for the whole genome of EBV B cells as part of a previously published study (GEO accession no. GSE116193) (23). HiChIP raw reads (fastq files) were aligned to the hg19 human reference genome using HiC-Pro (24). Aligned data were processed and analyzed through the hicchipper pipeline (25). MACS2 was used for anchor calling based on ChIP-enriched regions (26). Loops were derived from the linked paired-end reads that overlapped with anchors. DNALandscapeR was used to visualize the long-range interactions in 2 dimensions.

Chromatin conformation capture with quantitative PCR (3C-qPCR). As previously described (27), 3C-qPCR was performed with minor modifications. Ten million cells from EBV B cell lines homozygous for the *UBE2L3/YDJC* nonrisk or risk haplotype were used per 3C library preparation. For 3C analysis of YY1 knockdown, EBV B cells transfected with YY1-targeted or scrambled siRNA were harvested after 24 hours, and 3 million cells were used per 3C library preparation. Cells were crosslinked with 2% formaldehyde at room temperature for 10 minutes, then quenched with 125 mM glycine for 5 minutes at room temperature. Cells were lysed, then the nuclei were pelleted and resuspended in 1.25× CutSmart Buffer (no. B7204S; New England Biolabs). Nuclei were treated with 0.3% sodium dodecyl sulfate (SDS) at 37°C for 1 hour, then 2% Triton X-100 for 1 hour. Chromatin was digested overnight at 37°C using 200 units of BssSI-v2 (no. R0680L; New England Biolabs). Ligation was performed overnight at 16°C or on ice using T4 DNA ligase (no. M0202M; New England Biolabs), with similar results. Chromatin was then de-crosslinked by adding proteinase K and incubating overnight at 65°C. RNase A treatment was used to remove RNA contamination from the chromatin. Next, 3C DNA template was purified by phenol–chloroform–isoamyl alcohol extractions, repeated twice.

The 3C-qPCR primers were designed to anneal in close proximity to BssSI-v2 cutting sites and amplify 9 fragments spanning the *UBE2L3/YDJC* 3C locus (Supplementary Table 3, <http://onlinelibrary.wiley.com/doi/10.1002/art.41925/abstract>). Primer efficiency was validated and normalized using template DNA from bacterial artificial chromosome (BAC) clone CTD3095B9 (no. 96012; ThermoFisher Scientific), digested with BssSI-v2. All qPCR assays were performed using LightCycler480 SYBR Green probe according to instructions of the manufacturer (Roche Diagnostics). The relative interaction frequency (RIF) was calculated by normalizing the interaction frequencies to the interaction frequency of the random ligation control (fragment 2). Interactions were considered positive if the RIF was greater than the interactions between the anchor and the negative control of the locus (fragments 3, 4, 5, 6, 9) (28,29).

ChIP-qPCR. ChIP assays were performed using a TruChIP chromatin shearing reagent kit (no. 520154; Covaris) to test CTCF and YY1 binding at the *UBE2L3* and *YDJC* promoter regions. Briefly, 1.5×10^7 EBV B cells that were homozygous for the *UBE2L3/YDJC* nonrisk or risk haplotype were crosslinked with 1% formaldehyde. Nuclei were isolated and sonicated in 1 ml of shearing buffer with a Covaris S1 sonicator (no. E220). Sheared chromatin was precleared using Magna ChIP Protein A + G magnetic beads (no. 16-663; Millipore) blocked in phosphate buffered saline (PBS) with bovine serum albumin, protease inhibitor cocktail (no. 539132; EMD Millipore), and Halt phosphatase inhibitors (no. 1862495; ThermoFisher Scientific). Chromatin–protein complexes were then immunoprecipitated overnight at 4°C by mild agitation with blocked and precleared Magna Protein A + G magnetic beads and

antibodies specific for CTCF (no. D31H2; Cell Signaling Technology), YY1 (no. sc-7341X; Santa Cruz Biotechnology), or respective normal IgG isotype controls (normal rabbit IgG [no. 2729S] or normal mouse IgG [no. 5415S]; Cell Signaling Technology). DNA was eluted from the immunoprecipitated chromatin complexes, reverse-cross-linked, purified by Agencourt AMPure XP beads (Beckman Coulter), and subjected to real-time qPCR analysis using LightCycler480 SYBR Green and primers flanking the *UBE2L3* or *YDJC* risk variants (Supplementary Table 4, <http://onlinelibrary.wiley.com/doi/10.1002/art.41925/abstract>). All primer pairs were validated using input DNA prior to performing ChIP-qPCR.

Western blotting. EBV B cells were harvested 24 hours, 48 hours, or 72 hours posttransfection with targeted or scrambled siRNA, pelleted, washed in cold PBS, and lysed with RIPA lysis buffer (no. 9806S; Cell Signaling Technology) containing protease inhibitor cocktail (no. 539132; EMD Millipore). Cell lysates were collected and protein concentrations were determined by Qubit Protein Assay Kit (no. Q33212; ThermoFisher Scientific). Proteins were denatured in 4× SDS loading buffer at 95°C for 5 minutes, separated by SDS–polyacrylamide gel electrophoresis, transferred to PVDF membrane (no. 1620177; Bio-Rad), blocked with 5% nonfat dairy milk, and analyzed by Western blotting, as indicated, using antibodies against *UBE2L3/UbcH7* (no. 3848S; Cell Signaling Technology), YY1 (no. sc-7341; Santa Cruz Biotechnology); CTCF (no. D31H2; Cell Signaling Technology), and β -actin (no. 4967S, loading control; Cell Signaling Technology). Blots were developed using Clarity Western ECL Substrate (no. 1705060) and visualized using a ChemiDocMP Imaging System (both Bio-Rad).

RNA extraction and real-time quantitative reverse transcription-PCR (qRT-PCR). Total RNA was isolated from EBV B cells carrying the *UBE2L3/YDJC* nonrisk or risk haplotype using a Direct-zol RNA MiniPrep Plus kit, according to the instructions of the manufacturer (Zymo Research). Complementary DNA synthesis was performed using a QuantiTect reverse transcriptase kit, according to the instructions of the manufacturer (Qiagen). Gene expression was measured by real-time PCR analysis using Light Cycle480 SYBR Green. Gene expression primers for human *UBE2L3*, human *YDJC*, human *SDF2L1*, and human *PPIL2* were purchased from Integrated DNA Technologies (Supplementary Table 5, <http://onlinelibrary.wiley.com/doi/10.1002/art.41925/abstract>); human *GAPDH* (no. PPH00150F) was from Qiagen.

RESULTS

Prioritization of candidate variants spanning the *UBE2L3/YDJC* autoimmune risk haplotype. We hypothesized that candidate variants positioned in regions of open chromatin would have an increased potential to modulate transcription factor binding and *UBE2L3* expression (30,31). We

identified 7 variants that colocalized with assay for transposase accessible chromatin sequencing (ATAC-seq) peaks from publicly available data from primary B cells, T cells, and monocytes using the UCSC Genome Browser (GEO accession nos. GSE74912, GSE74310) (32) (Supplementary Figures 1 and 2A–C, <http://onlinelibrary.wiley.com/doi/10.1002/art.41925/abstract>). One variant, rs140490, located in the *UBE2L3* promoter, has been the most frequently reported index SNP marking the *UBE2L3/YDJC* risk haplotype (5, 10) (Supplementary Figure 1). Of the remaining 6 variants, 2 are located in the *UBE2L3* promoter region (rs140491, rs11089620), 3 in the *UBE2L3* first intron (rs12484550, rs5998599, rs9621715), and 1 in the *YDJC* promoter region (rs3747093). These variants also colocalized with areas enriched for ENCODE-reported chromatin marks of functional regulatory elements, including the following: 1) the epigenetic marker of active enhancers, acetylation at lysine 27 on histone H3 (H3K27ac; Supplementary Figure 2D, [http://](http://onlinelibrary.wiley.com/doi/10.1002/art.41925/abstract)

onlinelibrary.wiley.com/doi/10.1002/art.41925/abstract); 2) the epigenetic marker of promoters, trimethylation at lysine 4 on histone H3 (H3K4Me3; Supplementary Figure 2E); 3) genomic regions enriched with guanine-cytosine dinucleotide repeats (CpG islands) that are DNA methylation regions in promoters (Supplementary Figure 2F); and 4) ChIP sequencing (ChIP-seq) clusters of transcription factor binding sites (Supplementary Figure 2G).

Risk alleles on the *UBE2L3/YDJC* autoimmune risk haplotype increase nuclear protein complex binding.

To assess the functional potential of the prioritized variants, we performed EMSAs using radiolabeled oligonucleotides carrying the risk or nonrisk alleles of each variant and nuclear proteins extracted from 3 immune-relevant human immortalized cell lines left unstimulated or stimulated with P/I for 2 hours: EBV B cell lines, Jurkat cell lines, and THP-1 cell lines representing B cell, T

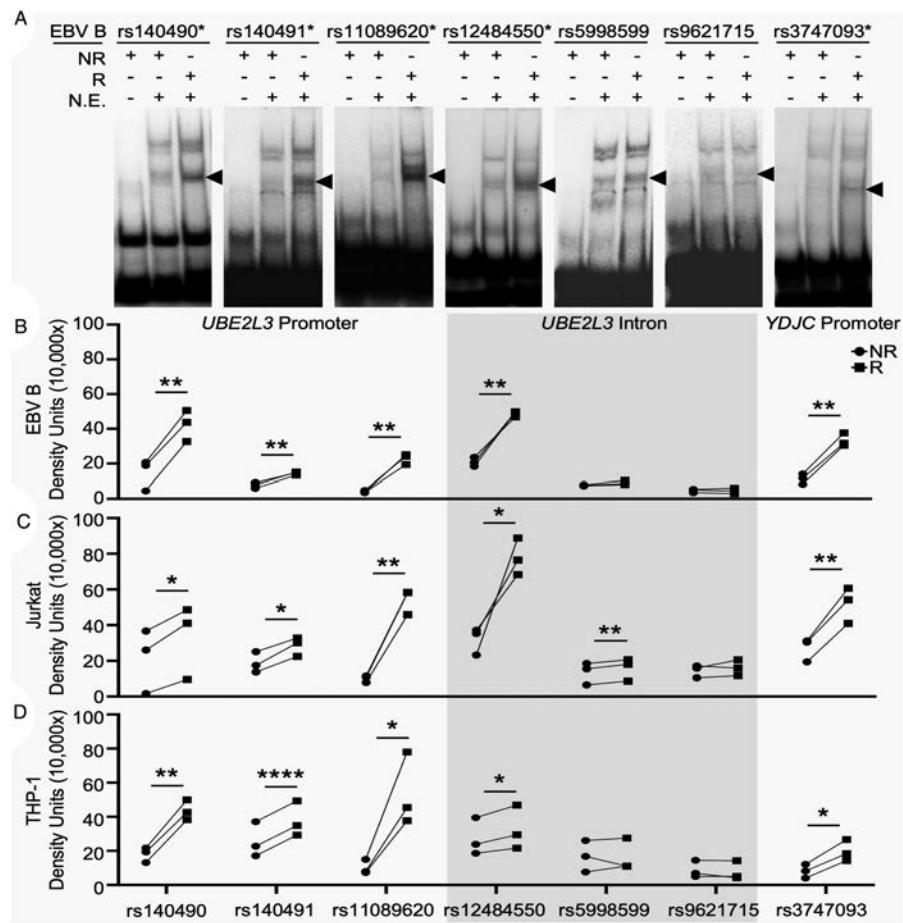


Figure 1. Risk alleles on the *UBE2L3/YDJC* autoimmune risk haplotype increase the binding affinities of nuclear protein complexes. Electrophoretic mobility shift assays were performed using radiolabeled oligonucleotides containing the nonrisk (NR) or risk (R) alleles of the indicated risk variants carried on the *UBE2L3/YDJC* autoimmune haplotype. Nuclear extracts (NE) were isolated from Epstein-Barr virus (EBV)-transformed B cells (A and B), Jurkat cells (C), or THP-1 cells (D) at rest (Supplementary Figure 3, <http://onlinelibrary.wiley.com/doi/10.1002/art.41925/abstract>). In A, images are representative of 3 experiments, * represents variants that exhibit allele-specific mobility shift, and arrowheads indicate the allele-specific mobility shift that was quantified in B for each indicated nuclear protein-bound probe. B–D, Quantitative densitometry of the nuclear protein-bound oligonucleotides shown in A and Supplementary Figures 3B and C. * = $P < 0.05$; ** = $P < 0.01$; **** = $P < 0.0001$, by paired t -test ($n = 3$ experiments).

cell, and monocytoid lineages, respectively. For the 3 *UBE2L3* promoter variants (rs140490, rs140491, rs11089620), 1 *UBE2L3* intronic variant (rs12484550), and the *YDJC* promoter variant (rs3747093), we observed significant increases in the nuclear protein binding to the risk alleles compared to the nonrisk alleles, in all 3 cell lines at rest and after P/I stimulation (Figure 1 and Supplementary Figures 3 and 4, <http://onlinelibrary.wiley.com/doi/10.1002/art.41925/abstract>). In unstimulated Jurkat cells only, the *UBE2L3* intronic variant, rs5998599, showed a modest increase in binding to the risk allele, compared to nonrisk allele (Figure 1C and Supplementary Figure 3B), which was lost after P/I stimulation (Supplementary Figures 3B and 4B, <http://onlinelibrary.wiley.com/doi/10.1002/art.41925/abstract>). The *UBE2L3* intronic variant, rs9621715, was the only tested variant that did not exhibit allele-specific binding in any of the 3 cell lines (Figure 1 and Supplementary Figures 3 and 4). The specificity of

our EMSA probes were confirmed by competition binding with unlabeled probes using EBV B cell nuclear extracts (Supplementary Figure 5, <http://onlinelibrary.wiley.com/doi/10.1002/art.41925/abstract>).

Risk variants on the *UBE2L3*/*YDJC* autoimmune risk haplotype exhibit allele-specific increases in reporter gene expression.

Using a promoterless luciferase reporter construct, we observed that the risk alleles of the *UBE2L3* and *YDJC* promoter region variants, rs140490 and rs3747093, exhibited significant increases in reporter gene expression, which was further increased following P/I stimulation (Figures 2A and B). In contrast, the risk alleles of the *UBE2L3* promoter region variants, rs140491 and rs11089620, cloned in combination (due to close positional proximity) or separately, demonstrated significant allele-specific promoter activity only after P/I stimulation (Figure 2C).

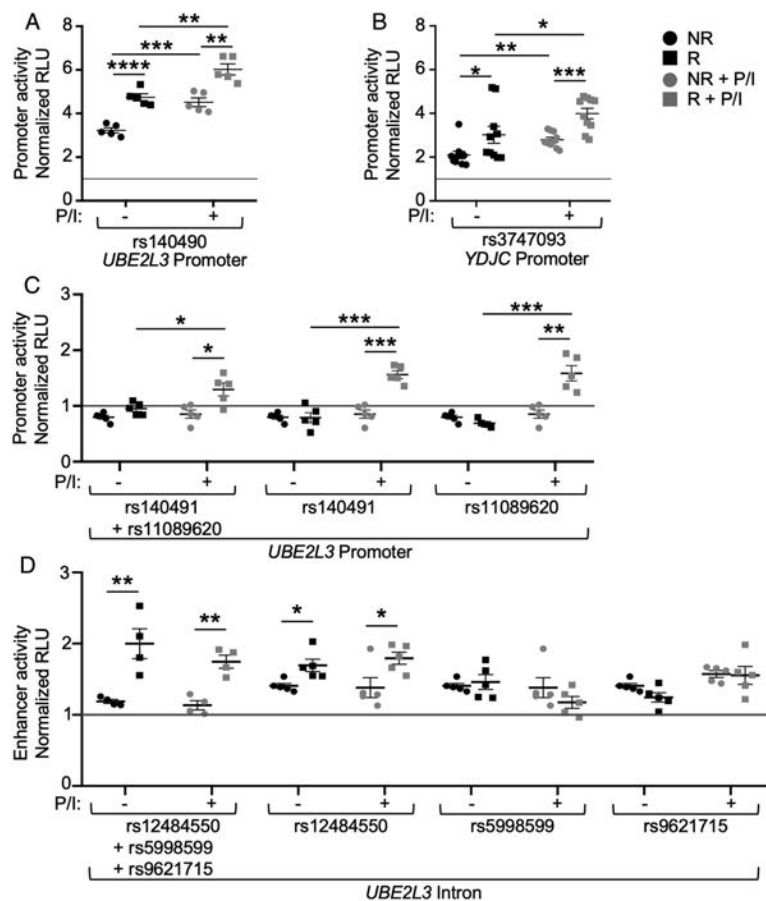


Figure 2. Risk variants on the *UBE2L3*/*YDJC* autoimmune risk haplotype exhibit allele-specific increases in reporter gene expression. Sequences carrying the nonrisk or risk alleles of the indicated variants were cloned into a promoterless vector (pGL4.14) (A–C) or minimal promoter vector (pGL4.23) (D). See Supplementary Tables 1 and 2 for nonrisk (NR) and risk (R) sequences (<http://onlinelibrary.wiley.com/doi/10.1002/art.41925/abstract>). Site-directed mutagenesis was used to dissect physically close variants that were originally cloned together (C and D). Luciferase activity was measured after transient transfection of Epstein-Barr virus B cells homozygous for the *UBE2L3*/*YDJC* nonrisk haplotype at rest or after 2 hours of stimulation with phorbol 12-myristate 13-acetate and ionomycin (P/I). Luciferase activity was normalized to *Renilla* transfection control, then the vector-only control (gray line), and reported as the mean \pm SEM of normalized relative fluorescence units (RLUs). * = $P < 0.05$; ** = $P < 0.01$; *** = $P < 0.001$; **** = $P < 0.0001$, by Student’s *t*-test ($n \geq 4$ experiments).

We then tested the *UBE2L3* intronic region variants, rs12484550, rs5998599, and rs9621715, using a minimal-promoter luciferase construct that measures enhancer-like function. We found that the risk alleles of these variants demonstrated enhancer activity when tested in combination (due to positional proximity) independent of stimulation (Figure 2D). When tested individually, each variant demonstrated enhancer-like function; however, the allele-specific effect was only observed for the rs12484550 risk allele (Figure 2D). Taken together, the increases in nuclear protein binding in the EMSA and the increased expression of the luciferase reporter gene in the context of the risk alleles are concordant with the elevated expression of *UBE2L3* observed in previously published studies (5,6,10).

***UBE2L3/YDJC* autoimmune risk haplotype strengthens long-range looping between the *UBE2L3* and *YDJC* promoter regions.** Since changes in transcription activity are often accompanied by changes in chromatin conformation, we leveraged a H3K27ac and CTCF HiChIP data set from EBV B cell lines

(GEO accession no. GSE116193) to assess chromatin organization in the region of *UBE2L3/YDJC* (23). A robust H3K27ac loop was observed between the *UBE2L3* and *YDJC* promoter elements, while a weaker interaction was seen with both promoters and the *UBE2L3* intronic enhancer (Supplementary Figure 6, <http://onlinelibrary.wiley.com/doi/10.1002/art.41925/abstract>). In addition, the *YDJC* promoter element was positioned in a CTCF loop anchor that interacts with the 3'UTR of *UBE2L3*. Thus, the *UBE2L3/YDJC* haplotype risk alleles may alter the regulatory function of the *UBE2L3* and *YDJC* promoters, as well as the *UBE2L3* intronic enhancer, by modulating long-distance DNA interactions.

To confirm the HiChIP results and determine the effect of the risk haplotype on chromatin organization, we performed 3C-qPCR in EBV B cell lines homozygous for the *UBE2L3/YDJC* non-risk or risk haplotype. Long-range interactions between the *UBE2L3* promoter region (anchor fragment 1, upstream of rs140490) and other potential contact points across the *UBE2L3/YDJC* locus (fragments 2–9) were measured (Figure 3A).

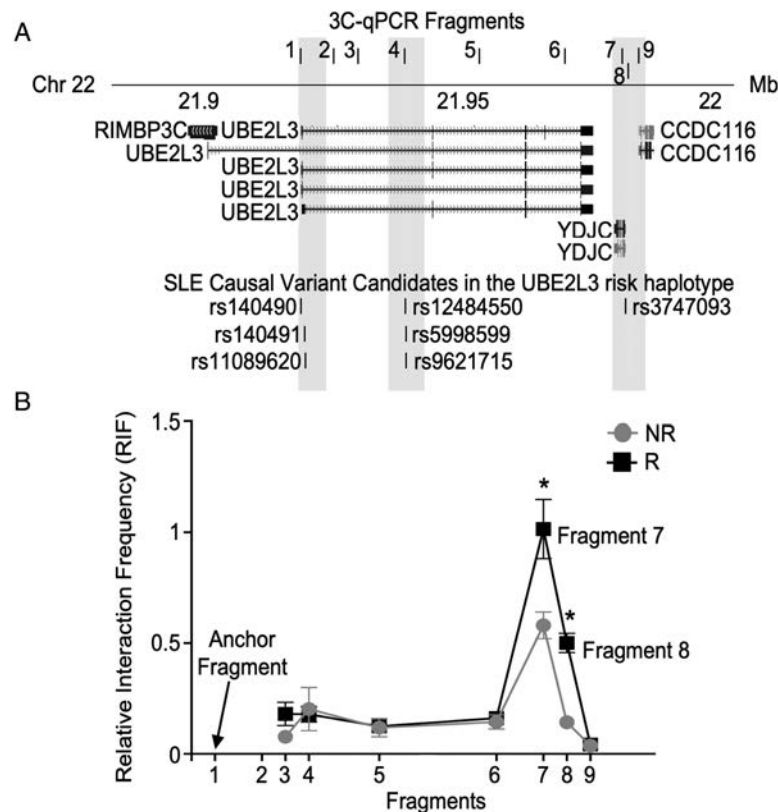


Figure 3. Risk variants carried on the *UBE2L3/YDJC* autoimmune risk haplotype strengthen long-range interactions between the *UBE2L3* and *YDJC* promoters. **A**, Schematic depiction of chromatin conformation capture with quantitative polymerase chain reaction (3C-qPCR) primers relative to the *UBE2L3/YDJC* locus and indicated systemic lupus erythematosus (SLE) risk variants in the UCSC Genome Browser is shown. **B**, Chromatin conformation capture with qPCR was performed in quiescent Epstein-Barr virus-transformed B cells homozygous for the *UBE2L3/YDJC* nonrisk (NR) or risk (R) haplotype using the anchor fragment (fragment 1) and test fragments shown in **A** (see Supplementary Table 3, <http://onlinelibrary.wiley.com/doi/10.1002/art.41925/abstract>). Relative interaction frequency between the anchor fragment and each test fragment was normalized to the *UBE2L3* bacterial artificial chromosome clone, then to the random ligation control, and plotted according to the interaction fragment number from the anchor as the mean \pm SEM. * = $P < 0.05$ by Student's t -test ($n = 3$ experiments).

Consistent with the HiChIP data, we observed a long-range interaction between the *UBE2L3* promoter (anchor fragment 1) and the *YDJC* promoter (fragments 7 and 8) in EBV B cells homozygous for the *UBE2L3/YDJC* nonrisk haplotype (Figure 3B). Moreover, we observed evidence of significantly increased long-range interactions between the same fragments in EBV B cells homozygous for the *UBE2L3/YDJC* risk haplotype. In contrast to the HiChIP data, we did not detect an interaction between either promoter element and the *UBE2L3* intronic enhancer (fragment 4) using 3C-qPCR (Figure 3B). Overall, these results suggest that the risk alleles of the selected variants in the promoter regions of *UBE2L3* and *YDJC* strengthen long-range physical interactions between the 2 promoters.

Alteration of CTCF and YY1 transcription factor binding due to risk variants on the *UBE2L3/YDJC* autoimmune risk haplotype.

CTCF and YY1 are ubiquitously expressed proteins that function to regulate mammalian gene expression through their influence on 3-dimensional (3-D) chromatin organization (33–38). In addition, co-binding of CTCF and YY1 has been shown to regulate gene transcription for a large number of mammalian promoters, with YY1 playing a dominant role in promoting transcription (35). Analysis of transcription factor ChIP-seq clusters from ENCODE revealed CTCF and YY1 binding

motifs in the *UBE2L3* and *YDJC* promoter regions (Supplementary Figures 7A and C, <http://onlinelibrary.wiley.com/doi/10.1002/art.41925/abstract>), but not in the *UBE2L3* intronic region (Supplementary Figure 7B).

Furthermore, *UBE2L3* promoter variants, rs140491 and rs11089620, are positioned in the ENCODE reported YY1 binding site (Supplementary Figure 7A), and the *YDJC* promoter variant, rs3747093, is positioned in an overlapping CTCF and YY1 binding site (Supplementary Figure 7C). Therefore, we hypothesized that the binding of CTCF and/or YY1 might be altered in the presence of the risk alleles. To test this hypothesis, we performed ChIP-qPCR for each variant and observed significantly lower CTCF binding to the risk alleles of rs140491, rs11089620, rs12484550, and rs3747093, relative to the respective nonrisk alleles (Figure 4A). CTCF binding to rs140490 was near baseline and exhibited no allele-specific differences. In contrast, we observed significant increases in YY1 binding in the presence of the *UBE2L3* (rs140490, rs140491, rs11089620) and *YDJC* (rs3747093) promoter variant risk alleles compared to the nonrisk alleles (Figure 4B). YY1 enrichment was not observed with the *UBE2L3* intronic variant, rs12484550. These results suggest that the autoimmune risk alleles exert their effect on *UBE2L3* transcription by preferentially binding YY1, at the expense of CTCF, at the promoters of both *UBE2L3* and *YDJC*.

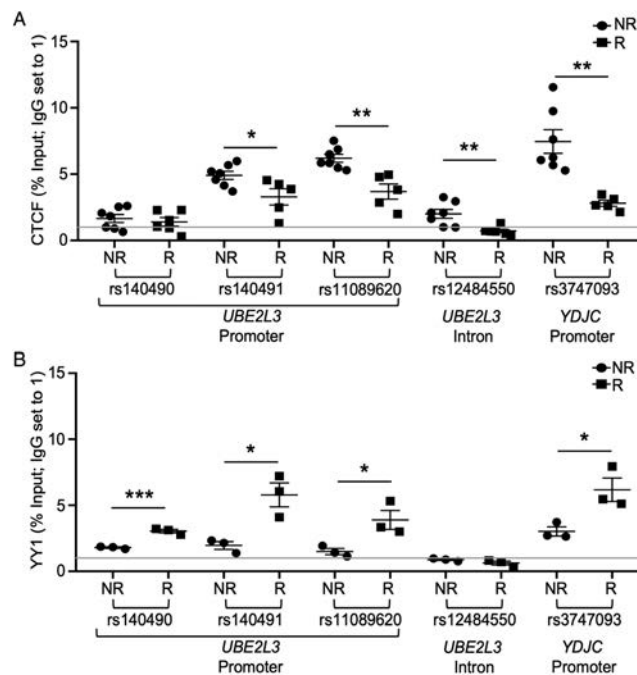


Figure 4. Risk variants carried on the *UBE2L3/YDJC* autoimmune risk haplotype exhibit allele-specific binding to CCCTC-binding factor (CTCF) and YY1 transcription factors. Chromatin immunoprecipitation with quantitative polymerase chain reaction was performed in Epstein-Barr virus-transformed B cells homozygous for the *UBE2L3/YDJC* nonrisk (NR) or risk (R) haplotype using antibodies against CTCF (A) or YY1 (B). Primers were designed to flank indicated variants (see Supplementary Table 4, <http://onlinelibrary.wiley.com/doi/10.1002/art.41925/abstract>). Rabbit or mouse IgG was used as an isotype control. Data show the mean \pm SEM. * = $P < 0.05$; ** = $P < 0.01$; *** = $P < 0.001$, by Student's *t*-test ($n \geq 5$ experiments for CTCF, and $n = 3$ experiments for YY1).

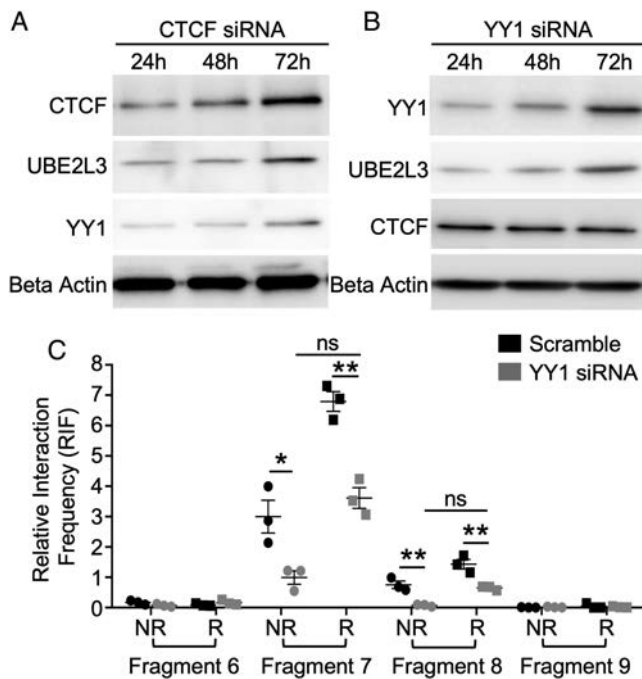


Figure 5. YY1 knockdown reduces *UBE2L3* expression and impairs the long-range DNA looping between the *UBE2L3* and *YDJC* promoters. **A** and **B**, Western blotting was performed to analyze expression levels of YY1, ubiquitin-conjugating enzyme E2 L3 (*UBE2L3*), CCCTC-binding factor (CTCF), and β -actin at 24 hours, 48 hours, and 72 hours post-transient transfection of CTCF small interfering RNA (siRNA) (**A**) or YY1 siRNA (**B**) in Epstein-Barr virus (EBV)-transformed B cells homozygous for the nonrisk *UBE2L3/YDJC* haplotype. In **A**, images are representative of 3 experiments. Expression in scrambled siRNA-transfected EBV B cells is shown in Supplementary Figures 8A and C (<http://onlinelibrary.wiley.com/doi/10.1002/art.41925/abstract>). Quantitative densitometry normalized to β -actin is shown in Supplementary Figures 8B and D. **C**, Chromatin conformation capture with quantitative polymerase chain reaction was performed with scrambled or YY1 siRNA-transfected EBV B cells carrying the *UBE2L3/YDJC* nonrisk (NR; circle) or risk (R; square) haplotype. Relative interaction frequency was normalized to the *UBE2L3* bacterial artificial chromosome clone, then to the random ligation control, and plotted as the mean \pm SEM. * = $P < 0.05$; ** = $P < 0.01$, by Student's *t*-test ($n = 3$ experiments). NS = not significant.

Knockdown of YY1 disrupts the *UBE2L3/YDJC* regulatory network and subsequent *UBE2L3* expression. We hypothesized that, if a gain in YY1 binding was responsible for increased interactions between the *UBE2L3* and *YDJC* promoter regions and increased *UBE2L3* transcription, then loss of YY1 expression would attenuate these interactions. To test this, we transfected EBV B cells homozygous for the *UBE2L3/YDJC* nonrisk haplotype with YY1 or CTCF siRNA, then measured CTCF, YY1, and *UBE2L3/UbcH7* protein levels at 24 hours, 48 hours, and 72 hours posttransfection. CTCF knockdown (Figure 5A and Supplementary Figures 8A and B, <http://onlinelibrary.wiley.com/doi/10.1002/art.41925/abstract>) and YY1 knockdown (Figure 5B and Supplementary Figures 8C and D) reached $\sim 80\%$ at 24 hours, relative to the scrambled control. Interestingly, the transient

knockdown of YY1 reduced *UBE2L3/UbcH7* expression (Figure 5B and Supplementary Figures 8C and D), while CTCF knockdown resulted in the loss of both *UBE2L3/UbcH7* and YY1 protein expression (Figure 5A and Supplementary Figures 8A and B), suggesting that CTCF might be an upstream regulator of YY1 expression. Furthermore, *UBE2L3/UbcH7* protein levels paralleled the recovery of both CTCF and YY1 protein expression 72 hours posttransfection.

The reduction in *UBE2L3/UbcH7* protein expression after YY1 knockdown, despite sustained CTCF protein levels (Figures 5A and B), suggests that YY1 binding at the *UBE2L3* and *YDJC* promoters likely modulates *UBE2L3* expression by promoting long-range interactions. To further assess the effect of YY1 knockdown in mediating the long-range interaction between the *UBE2L3* and *YDJC* promoters, we performed 3C-qPCR after siRNA-mediated knockdown of YY1 in EBV B cells homozygous for the *UBE2L3/YDJC* nonrisk or risk haplotype. YY1 knockdown significantly decreased the interaction frequency between the *UBE2L3* promoter and *YDJC* promoter (fragments 7 and 8) proportionally in both risk and nonrisk EBV B cell lines relative to scrambled siRNA transfection (Figure 5C). Although our YY1 knockdown was not allele-specific, the experiments do support a mechanism whereby increased binding of YY1 at the *UBE2L3* and *YDJC* promoters in the presence of the risk alleles strengthens the interaction between the 2 promoters and increases expression of *UBE2L3*.

Genes that share long-range DNA contacts with the *UBE2L3* and *YDJC* promoters also demonstrate increased expression in the context of the risk haplotype. We noticed that our HiChIP analysis also revealed several additional H3K27ac-mediated long-range interactions between anchors in the *UBE2L3* locus and genes downstream: *YDJC*, *CCDC116*, *SDF2L1*, and *PPIL2* (Supplementary Figure 6, <http://onlinelibrary.wiley.com/doi/10.1002/art.41925/abstract>). Of these, only *YDJC*, *SDF2L1*, and *PPIL2* demonstrated expression in EBV B cell lines (Supplementary Figure 9, <http://onlinelibrary.wiley.com/doi/10.1002/art.41925/abstract>); thus, we limited our qRT-PCR studies to these 3 genes and *UBE2L3* in EBV B cells homozygous for the risk or nonrisk haplotype. We observed the expected increase in *UBE2L3* transcript expression, but also found significantly increased expression of *YDJC*, *SDF2L1*, and *PPIL2* in cells homozygous for the risk haplotype compared with the nonrisk haplotype (Figure 6A). These results suggest that the mechanisms defined herein, which result in increased *UBE2L3* expression from the autoimmune risk haplotype, extend to a larger chromatin network that includes *YDJC*, *SDF2L1*, and *PPIL2*.

DISCUSSION

The primary objective of this study was to develop a mechanistic understanding of how functional risk variants carried on the

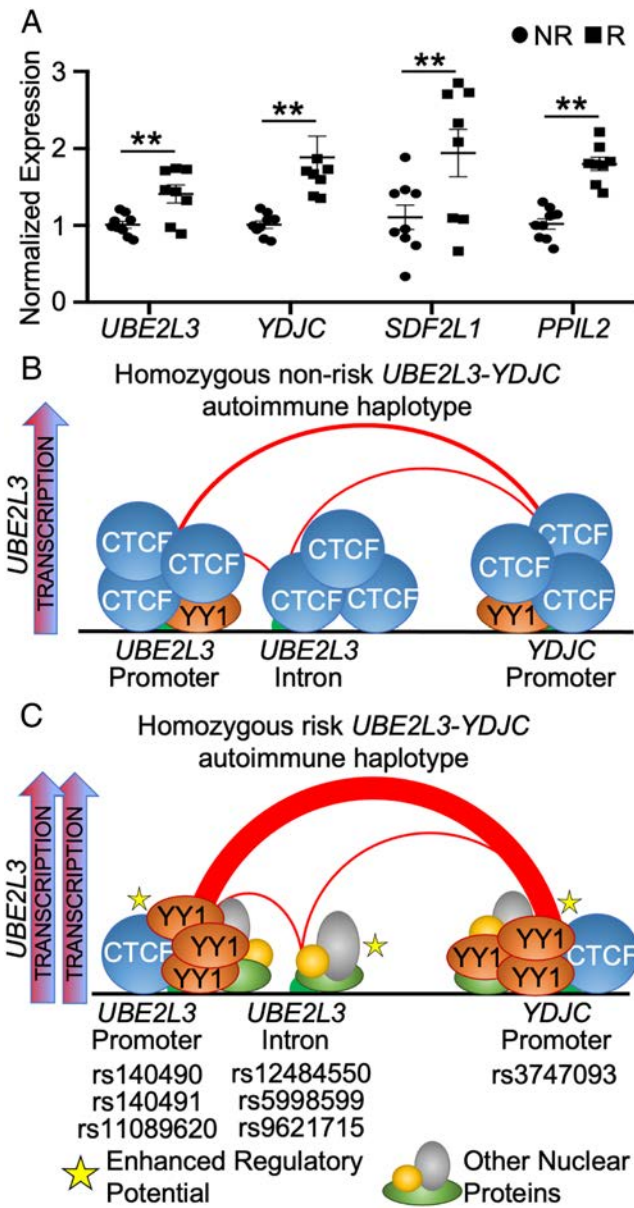


Figure 6. The *UBE2L3*/*YDJC* haplotype functions by differentially binding CCCTC-binding factor (CTCF) and YY1 to strengthen interactions between *UBE2L3* and *YDJC* promoters to increase *UBE2L3* expression. **A**, Real-time quantitative reverse transcription–polymerase chain reaction was used to measure the expression of the indicated genes in quiescent Epstein-Barr virus B cells homozygous for the nonrisk (NR) (circle) or risk (R) (square) *UBE2L3*/*YDJC* haplotype. Expression was normalized to *GAPDH* in nonrisk EBV B cells. Data are the mean ± SEM ($n \geq 8$ experiments). ** = $P < 0.01$, by Student’s *t*-test. **B** and **C**, Schematic depiction of how risk alleles carried on the *UBE2L3*/*YDJC* autoimmune risk haplotype increase YY1 binding affinity, at the expense of CTCF binding, is shown. Increased YY1 binding strengthens a long-distance interaction between the *UBE2L3* and *YDJC* promoters that facilitates both *UBE2L3* and *YDJC* expression, relative to the nonrisk haplotype.

UBE2L3/*YDJC* autoimmune disease risk haplotype drive hypermorphic *UBE2L3* expression implicated in autoimmune disease pathogenesis. We used a combination of in vitro assays designed

to measure the allele-specific regulatory effects of 7 risk variants, positioned in regions of high chromatin accessibility in several immune cell types. We discovered that 3 variants in the *UBE2L3* promoter (rs140490, rs140491, rs11089620) and 1 in the *YDJC* promoter (rs3747093) likely facilitate the hypermorphic expression effect of the *UBE2L3*/*YDJC* risk haplotype by increasing the binding of YY1 over CTCF, strengthening a long-range DNA interaction between the 2 promoters, and increasing the transcriptional activity of the regulatory network (Figures 6B and C).

YY1 and CTCF are both implicated in transcriptional regulation and stabilization of long-range DNA interactions and chromatin regulatory networks. In primate lymphoblastoid cells, co-bound YY1 and CTCF were shown to be enriched in transcriptionally active regions across the genome and function to stabilize and modulate transcription within chromatin regulatory networks (35). Furthermore, YY1 was shown to mediate interactions between enhancer and promoter elements to promote global transcription in murine embryonic stem cells (33). In this model, loss of YY1 significantly reduced global gene expression, supporting a role of YY1 as a global regulator of transcription and stability of long-range interactions. Consistently, we observed a loss of *UBE2L3* expression in EBV B cells after YY1 siRNA knock-down. Loss of *UBE2L3* expression coalesced with reduced long-range interaction frequencies between the *UBE2L3* and *YDJC* promoters in YY1-depleted EBV B cells.

Interestingly, we discovered that risk alleles of variants carried on the *UBE2L3*/*YDJC* risk haplotype increased YY1 binding and strengthened the long-range interaction between the 2 promoters. Similar allele-specific changes in the binding affinity of YY1 and subsequent disruptions in enhancer–promoter interactions were reported for several risk variants associated with type 1 diabetes mellitus (37). To our knowledge, this is the first report implicating co-bound YY1 and CTCF in the regulation of *UBE2L3*. Additionally, given that YY1 is ubiquitously expressed and exhibits global regulation in other cell models, it is tempting to speculate that altered affinity for YY1 may affect gene expression in the context of other autoimmune disease risk haplotypes.

Our study should be interpreted in the context of the following caveats. First, we utilized immortalized cell lines from 3 different immune cell subtypes to perform in vitro assays to independently assess the allele-specific binding affinity and regulatory function of each selected risk variant, and immortalized cell lines do not precisely replicate the transcriptional regulation of primary immune cells. Second, the in vitro assays precluded our ability to determine how allele-specific effects of each variant function within the context of the native chromatin architecture. However, the increase we observed in nuclear protein binding and enhanced regulatory activity for 5 of the 7 risk alleles across all cell types are consistent with the established hypermorphic effect of the *UBE2L3*/*YDJC* risk haplotype. Moreover, these results were internally consistent with 3C-qPCR analyses performed in EBV B cells that demonstrated strengthened DNA looping in the context of

the *UBE2L3/YDJC* risk haplotype. While EBV B cells do not precisely replicate the genomic architecture of primary B cells, they represent an important resource for evaluating allele-specific effects of genetic variants in the context of native chromatin architecture (23,39–41). Finally, we acknowledge that the bioinformatic approach we used to prioritize candidate variants based on positioning in chromatin accessible regions potentially omitted other functional variants.

Despite these caveats, we successfully characterized 5 functional variants carried on the largely uncharacterized *UBE2L3/YDJC* risk haplotype and delineated a novel mechanism that explains how the risk haplotype likely drives hypermorphic *UBE2L3* expression in autoimmune disease pathogenesis. Furthermore, analysis of available HiChIP data and our qRT-PCR studies suggest the presence of additional, higher-order chromatin interactions that may extend the effect of the *UBE2L3/YDJC* risk haplotype to other genes within the shared 3-D chromatin network, including *SDF2L1* and *PPIL2*. Future targeted gene-editing strategies in an isogenic cell line will be important to further elucidate the effects of differential CTCF/YY1 binding on *UBE2L3* expression and downstream cellular signaling.

ACKNOWLEDGMENT

We thank Kiely Grundahl from the Oklahoma Medical Research Foundation Genes and Human Disease Research Program for her technical assistance and helpful discussions.

AUTHOR CONTRIBUTIONS

All authors were involved in drafting the article or revising it critically for important intellectual content, and all authors approved the final version to be published. Dr. Gaffney had full access to all of the data in the study and takes responsibility for the integrity of the data and the accuracy of the data analysis.

Study conception and design. Gopalakrishnan, Fu, Gaffney.

Acquisition of data. Gopalakrishnan, Fu, Pasula, Pelikan, Wiley, Gaffney.

Analysis and interpretation of data. Gopalakrishnan, Tessneer, Fu, Pelikan, Kelly, Gaffney.

REFERENCES

- Rittinger K, Ikeda F. Linear ubiquitin chains: enzymes, mechanisms and biology [review]. *Open Biol* 2017;7:170026.
- Iwai K. Linear polyubiquitin chains: a new modifier involved in NF κ B activation and chronic inflammation including dermatitis. *Cell Cycle* 2011;10:3095–104.
- Tokunaga F, Sakata SI, Saeki Y, Satomi Y, Kirisako T, Kamei K, et al. Involvement of linear polyubiquitylation of NEMO in NF- κ B activation. *Nat Cell Biol* 2009;11:123–32.
- Fujita H, Rahighi S, Akita M, Kato R, Sasaki Y, Wakatsuki S, et al. Mechanism underlying I κ B kinase activation mediated by the linear ubiquitin chain assembly complex. *Mol Cell Biol* 2014;34:1322–35.
- Lewis MJ, Vyse S, Shields AM, Boeltz S, Gordon PA, Spector TD, et al. *UBE2L3* polymorphism amplifies NF- κ B activation and promotes plasma cell development, linking linear ubiquitination to multiple autoimmune diseases. *Am J Hum Genet* 2015;96:221–34.
- Lewis M, Vyse S, Shields A, Boeltz S, Gordon P, Spector T, et al. Effect of *UBE2L3* genotype on regulation of the linear ubiquitin chain assembly complex in systemic lupus erythematosus. *Lancet* 2015;385 Suppl 1:9.
- International Consortium for Systemic Lupus Erythematosus Genetics (SLEGEN), Harley JB, Alarcón-Riquelme ME, Criswell LA, Jacob CO, Kimberly RP, et al. Genome-wide association scan in women with systemic lupus erythematosus identifies susceptibility variants in *ITGAM*, *PXK*, *KIAA1542* and other loci. *Nat Genet* 2008;40:204–10.
- Taylor KE, Chung SA, Graham RR, Ortmann WA, Lee AT, Langefeld CD, et al. Risk alleles for systemic lupus erythematosus in a large case-control collection and associations with clinical subphenotypes. *PLoS Genet* 2011;7:e1001311.
- Bentham J, Morris DL, Graham DS, Pinder CL, Tomblinson P, Behrens TW, et al. Genetic association analyses implicate aberrant regulation of innate and adaptive immunity genes in the pathogenesis of systemic lupus erythematosus. *Nat Genet* 2015;47:1457–64.
- Wang S, Adrianto I, Wiley GB, Lessard CJ, Kelly JA, Adler AJ, et al. A functional haplotype of *UBE2L3* confers risk for systemic lupus erythematosus. *Genes Immun* 2012;13:380–7.
- Agik S, Franek BS, Kumar AA, Kumabe M, Utset TO, Mikolaitis RA, et al. The autoimmune disease risk allele of *UBE2L3* in African American patients with systemic lupus erythematosus: a recessive effect upon subphenotypes. *J Rheumatol* 2012;39:73–8.
- Sun C, Molineros JE, Looger LL, Zhou XJ, Kim K, Okada Y, et al. High-density genotyping of immune-related loci identifies new SLE risk variants in individuals with Asian ancestry. *Nat Genet* 2016;48:323–30.
- Orozco G, Eyre S, Hinks A, Bowes J, Morgan AW, Wilson AG, et al. Study of the common genetic background for rheumatoid arthritis and systemic lupus erythematosus. *Ann Rheum Dis* 2011;70:463–8.
- Stahl EA, Raychaudhuri S, Remmers EF, Xie G, Eyre S, Thomson BP, et al. Genome-wide association study meta-analysis identifies seven new rheumatoid arthritis risk loci. *Nat Genet* 2010;42:508–14.
- Okada Y, Wu D, Trynka G, Raj T, Terao C, Ikari K, et al. Genetics of rheumatoid arthritis contributes to biology and drug discovery. *Nature* 2014;506:376–81.
- Dubois PC, Trynka G, Franke L, Hunt KA, Romanos J, Curtotti A, et al. Multiple common variants for celiac disease influencing immune gene expression. *Nat Genet* 2010;42:295–302.
- Fransen K, Visschedijk MC, van Sommeren S, Fu JY, Franke L, Festen EA, et al. Analysis of SNPs with an effect on gene expression identifies *UBE2L3* and *BCL3* as potential new risk genes for Crohn's disease. *Hum Mol Genet* 2010;19:3482–8.
- Franke A, McGovern DP, Barrett JC, Wang K, Radford-Smith GL, Ahmad T, et al. Genome-wide meta-analysis increases to 71 the number of confirmed Crohn's disease susceptibility loci. *Nat Genet* 2010;42:1118–25.
- Jostins L, Ripke S, Weersma RK, Duerr RH, McGovern DP, Hui KY, et al. Host-microbe interactions have shaped the genetic architecture of inflammatory bowel disease. *Nature* 2012;491:119–24.
- Hinks A, Cobb J, Marion MC, Prahallad S, Sudman M, Bowes J, et al. Dense genotyping of immune-related disease regions identifies 14 new susceptibility loci for juvenile idiopathic arthritis. *Nat Genet* 2013;45:664–9.
- Tsoi LC, Spain SL, Knight J, Ellinghaus E, Stuart PE, Capon F, et al. Identification of 15 new psoriasis susceptibility loci highlights the role of innate immunity. *Nat Genet* 2012;44:1341–8.
- Rasmussen A, Sevier S, Kelly JA, Glenn SB, Aberle T, Cooney CM, et al. The lupus family registry and repository. *Rheumatology (Oxford)* 2011;50:47–59.
- Pelikan RC, Kelly JA, Fu Y, Lareau CA, Tessneer KL, Wiley GB, et al. Enhancer histone-QTLs are enriched on autoimmune risk haplotypes

- and influence gene expression within chromatin networks. *Nat Commun* 2018;9:2905.
24. Servant N, Varoquaux N, Lajoie BR, Viara E, Chen CJ, Vert JP, et al. HiC-Pro: An optimized and flexible pipeline for Hi-C data processing. *Genome Biol* 2015;16:259.
 25. Lareau CA, Aryee MJ. hicppper: a preprocessing pipeline for calling DNA loops from HiChIP data. *Nat Methods* 2018;15:155–6.
 26. Zhang Y, Liu T, Meyer CA, Eeckhoutte J, Johnson DS, Bernstein BE, et al. Model-based analysis of ChIP-Seq (MACS). *Genome Biol* 2008;9:R137.
 27. Hagège H, Klous P, Braem C, Splinter E, Dekker J, Cathala G, et al. Quantitative analysis of chromosome conformation capture assays (3c-qpcr). *Nat Protoc* 2007;2:1722–33.
 28. Dekker J, Rippe K, Dekker M, Kleckner N. Capturing chromosome conformation. *Science* 2002;295:1306–11.
 29. Naumova N, Smith EM, Zhan Y, Dekker J. Analysis of long-range chromatin interactions using Chromosome Conformation Capture. *Methods* 2012;58:192–203.
 30. Buenrostro JD, Wu B, Chang HY, Greenleaf WJ. ATAC-seq: a method for assaying chromatin accessibility genome-wide. *Curr Protoc Mol Biol* 2015;109:21.29.1–9.
 31. Klemm SL, Shipony Z, Greenleaf WJ. Chromatin accessibility and the regulatory epigenome [review]. *Nat Rev Genet* 2019;20:207–20.
 32. Corces MR, Buenrostro JD, Wu B, Greenside PG, Chan SM, Koenig JL, et al. Lineage-specific and single-cell chromatin accessibility charts human hematopoiesis and leukemia evolution. *Nat Genet* 2016;48:1193–203.
 33. Weintraub AS, Li CH, Zamudio AV, Sigova AA, Hannett NM, Day DS, et al. YY1 is a structural regulator of enhancer-promoter loops. *Cell* 2017;171:1573–88.
 34. Beagan JA, Duong MT, Titus KR, Zhou L, Cao Z, Ma J, et al. YY1 and CTCF orchestrate a 3D chromatin looping switch during early neural lineage commitment. *Genome Res* 2017;27:1139–52.
 35. Schwalie PC, Ward MC, Cain CE, Faure AJ, Gilad Y, Odom DT, et al. Co-binding by YY1 identifies the transcriptionally active, highly conserved set of CTCF-bound regions in primate genomes. *Genome Biol* 2013;14:R148.
 36. Pentland I, Campos-León K, Cotic M, Davies KJ, Wood CD, Groves IJ, et al. Disruption of CTCF-YY1-dependent looping of the human papillomavirus genome activates differentiation-induced viral oncogene transcription. *PLoS Biol* 2018;16:e2005752.
 37. Gao P, Uzun Y, He B, Salamati SE, Coffey JK, Tsalikian E, et al. Risk variants disrupting enhancers of T_H1 and T_{REG} cells in type 1 diabetes. *Proc Natl Acad Sci U S A* 2019;116:7581–90.
 38. Stik G, Vidal E, Barrero M, Cuartero S, Vila-Casadesús M, Mendieta-Esteban J, et al. CTCF is dispensable for immune cell transdifferentiation but facilitates an acute inflammatory response. *Nat Genet* 2020;52:655–61.
 39. Hernando H, Shannon-Lowe C, Islam AB, Al-Shahrour F, Rodríguez-Ubreva J, Rodríguez-Cortez VC, et al. The B cell transcription program mediates hypomethylation and overexpression of key genes in Epstein-Barr virus-associated proliferative conversion. *Genome Biol* 2013;14:R3.
 40. Hernando H, Islam AB, Rodríguez-Ubreva J, Forné I, Ciudad L, Imhof A, et al. Epstein-Barr virus-mediated transformation of B cells induces global chromatin changes independent to the acquisition of proliferation. *Nucleic Acids Res* 2014;42:249–63.
 41. Çalişkan M, Cusanovich DA, Ober C, Gilad Y. The effects of EBV transformation on gene expression levels and methylation profiles. *Hum Mol Genet* 2011;20:1643–52.

LETTERS

DOI 10.1002/art.41938

Hypogammaglobulinemia in rheumatoid arthritis patients treated with rituximab: should we switch biologics? Comment on the article by Fraenkel et al

To the Editor:

We read with great interest the 2021 guideline for the treatment of rheumatoid arthritis (RA) from the American College of Rheumatology (1) as reported by Dr. Fraenkel and colleagues. Among the various issues covered by the guideline was hypogammaglobulinemia in RA patients receiving treatment with rituximab. Hypogammaglobulinemia has been reported in ~17–43% of rituximab-treated patients with RA (2). Risk factors for hypogammaglobulinemia are not well defined, but the number of treatment cycles with rituximab and patients' baseline levels of immunoglobulins are the factors that have received the most study (2–7).

In the guideline it is conditionally recommended that in the setting of persistent hypogammaglobulinemia without infection, rituximab should be continued rather than having the patient switch to another biologic disease-modifying antirheumatic drug (bDMARD) (1). Although there are no data to support arguments for or against this recommendation, we believe the reasons behind it could be further clarified by referring to a handful of studies of hypogammaglobulinemia in patients with RA (2–10). These studies could help the reader in forming a more comprehensive opinion.

First, results from studies on the risk of infection in rituximab-treated RA patients who develop hypogammaglobulinemia have been conflicting, as at least 50% of the larger studies failed to show such risk (2,5–7,10). It should be highlighted that all studies refer to serious infections, which are defined as those requiring intravenous antibiotics (2), and there are no available data about the frequency of infections that could lead to the interruption/switching of treatment.

Second, the definition of hypogammaglobulinemia differed across studies (8,9). Therefore, providing a cutoff value for defining the range of low and high serum immunoglobulin levels would be helpful. As was also stated in the recommendations, the degree of hypogammaglobulinemia might play some role in a clinician's decision to switch treatment from rituximab to another bDMARD. In a recently published study from our group, the reduction in IgG levels was mild (500–700 mg/dl) in the majority of patients (2).

It should be stressed that the definition of “hypogammaglobulinemia” usually encompasses low IgG, IgM, and/or IgA levels, with the latter being very rarely affected in patients treated with anti-CD20 therapy (2). In fact, in RA patients treated with rituximab, low IgM levels are encountered more frequently than low

IgG levels (2,7,9). This is being increasingly appraised by the rheumatology community. However, its clinical significance is still vague. Of note, in a recently published study, including 83 RA patients with a mean \pm SD follow-up of 4.4 ± 2.2 years, low IgM levels were associated with better outcomes in patients with RA (assessed with the Disease Activity Score in 28 joints using the C-reactive protein level [11]) and the achievement of low disease activity state at the end of follow-up (2). Moreover, the term “persistent hypogammaglobulinemia” might be confusing. Although a study from our group showed that none of the patients developed transient hypogammaglobulinemia, other authors have described transient hypogammaglobulinemia in this setting, with older age being a risk factor (7).

In conclusion, given the lack of data in support of switching treatment to another bDMARD in cases of hypogammaglobulinemia in patients with RA, we do not disagree with the conditional recommendation to continue rituximab therapy. However, we wanted to shed light on the issues mentioned above (type and frequency of infections, degree and persistence of hypogammaglobulinemia, and type of immunoglobulins affected), which may help clinicians in their decision.

Gerasimos Evangelatos, MD, MSc 
Melina Moschopoulou, BSc
National and Kapodistrian University of Athens
Alexios Iliopoulos, MD
417 Army Share Fund Hospital (NIMTS)
George E. Fragoulis, MD, PhD 
National and Kapodistrian University of Athens
Athens, Greece

1. Fraenkel L, Bathon JM, England BR, St.Clair EW, Arayssi T, Carandang K, et al. 2021 American College of Rheumatology guideline for the treatment of rheumatoid arthritis. *Arthritis Rheumatol* 2021;73:1108–23.
2. Evangelatos G, Fragoulis GE, Klavdianou K, Moschopoulou M, Vassilopoulos D, Iliopoulos A. Hypogammaglobulinemia after rituximab for rheumatoid arthritis is not rare and is related with good response: 13 years real-life experience. *Rheumatology (Oxford)* 2021;60:2375–82.
3. Boleto G, Avouac J, Wipff J, Forien M, Dougados M, Roux C, et al. Predictors of hypogammaglobulinemia during rituximab maintenance therapy in rheumatoid arthritis: a 12-year longitudinal multi-center study. *Semin Arthritis Rheum* 2018;48:149–54.
4. De La Torre I, Leandro MJ, Valor L, Becerra E, Edwards JC, Cambridge G. Total serum immunoglobulin levels in patients with RA after multiple B-cell depletion cycles based on rituximab: relationship with B-cell kinetics. *Rheumatology (Oxford)* 2012;51:833–40.
5. Einarsson JT, Evert M, Geborek P, Saxne T, Lundgren M, Kapetanovic MC. Rituximab in clinical practice: dosage, drug adherence, Ig levels, infections, and drug antibodies. *Clin Rheumatol* 2017;36:2743–50.

6. Keystone E, Fleischmann R, Emery P, Furst DE, van Vollenhoven R, Bathon J, et al. Safety and efficacy of additional courses of rituximab in patients with active rheumatoid arthritis: an open-label extension analysis. *Arthritis Rheum* 2007;56:3896–908.
7. Van Vollenhoven RF, Emery P, Bingham CO III, Keystone EC, Fleischmann R, Furst DE, et al. Longterm safety of patients receiving rituximab in rheumatoid arthritis clinical trials. *J Rheumatol* 2010;37: 558–67.
8. Md Yusof MY, Vital EM, McElvenny DM, Hensor EM, Das S, Dass S, et al. Predicting severe infection and effects of hypogammaglobulinemia during therapy with rituximab in rheumatic and musculoskeletal diseases. *Arthritis Rheumatol* 2019;71:1812–23.
9. Van Vollenhoven RF, Fleischmann RM, Furst DE, Lacey S, Lehane PB. Longterm safety of rituximab: final report of the rheumatoid arthritis global clinical trial program over 11 years. *J Rheumatol* 2015;42: 1761–6.
10. Vassilopoulos D, Delicha EM, Settas L, Andrianakos A, Aslanidis S, Boura P, et al. Safety profile of repeated rituximab cycles in unselected rheumatoid arthritis patients: a long-term, prospective real-life study. *Clin Exp Rheumatol* 2016;34:893–900.
11. Prevoo ML, van 't Hof MA, Kuper HH, van Leeuwen MA, van de Putte LB, van Riel PL. Modified disease activity scores that include twenty-eight-joint counts: development and validation in a prospective longitudinal study of patients with rheumatoid arthritis. *Arthritis Rheum* 1995;38:44–8.

DOI 10.1002/art.41942

Reply

To the Editor:

We thank Dr. Evangelatos and colleagues for their interest in the 2021 guideline for the treatment of rheumatoid arthritis from the American College of Rheumatology and for their efforts to further clarify the recommendations for rituximab therapy in patients with RA and persistent hypogammaglobulinemia. During the process of developing the guideline, the voting panel thoroughly discussed many of the aspects of hypogammaglobulinemia during rituximab treatment that Evangelatos et al have adeptly described. The conditional recommendation to continue treatment with rituximab over switching to another biologic or targeted synthetic disease-modifying antirheumatic drug among patients at target with persistent hypogammaglobulinemia without infection was informed by the paucity of evidence and consideration by the voting panel.

Liana Fraenkel, MD, MPH 
Berkshire Medical Center
Pittsfield, MA
and Yale University School of Medicine
New Haven, CT

Joan M. Bathon, MD 
Columbia University Irving Medical Center
and Presbyterian Hospital
New York NY

Bryant R. England, MD, PhD 
University of Nebraska Medical Center
and VA Nebraska–Western Iowa Health Care System
Omaha NE
 E. William St.Clair, MD
Duke University Medical Center
Durham NC
 Elie A. Akl, MD, MPH, PhD
American University of Beirut
Beirut Lebanon
On behalf of the ACR RA guideline author group

DOI 10.1002/art.41919

Importance of internal and external validity in clinical research: comment on the article by Fatima et al

To the Editor:

In a cohort study recently published in *Arthritis & Rheumatology*, Dr. Fatima and colleagues showed that a higher Health Assessment Questionnaire (HAQ) disability index score (1) was associated with higher mortality among patients with early rheumatoid arthritis (RA) (2). This study is important because the authors focused on functional disability as measured by HAQ disability index in patients with early RA, which they found to be more strongly associated with mortality than a measure of disease activity and damage, the Disease Activity Score in 28 joints (DAS28) (3), in patients with established RA (4). The study by Fatima et al will contribute to further clinical research regarding physical functioning by predicting mortality in patients with early RA. However, we have some concerns with regard to this study's internal and external validity.

Our first concern is the fact that separate statistical models were used in the study by Fatima et al. In one model, the authors evaluated the association of baseline HAQ disability index scores with mortality, and in the other model, they assessed the association of HAQ disability index scores at 1 year with mortality. However, the baseline HAQ disability index score correlated with the HAQ disability index score at 1 year, and therefore these HAQ scores from both time points should have been included in the same statistical model in the evaluation of an association with mortality. One way to solve this problem would be to change the definition of exposure; for example, defining progression of the HAQ disability index score between designated time points as a difference of 2 points may be a suitable alternative for describing the progression of disability in patients with early RA (5). Another alternative would be to adjust the 1-year HAQ disability index scores for the baseline HAQ disability index scores in a single model. A higher HAQ disability index score at baseline is frequently found to be associated with a higher HAQ disability index score at 1 year, leading to increased mortality rates (6); therefore, if the baseline HAQ disability index score is not taken into account, confounding

bias may occur. To estimate the association between disability measured by HAQ and mortality without the influence of bias, it is necessary to either use the suggested definition of HAQ progression or adjust for baseline HAQ score in the HAQ at 1-year models.

Our second concern is with regard to the study's external validity. Fatima and colleagues emphasized that their study had good external validity because the cohort used in their study, the Canadian Early Arthritis Cohort (CATCH), was designed with a sample size that they seem to have considered to be sufficient for reliable estimation of an association with mortality (2); however, of the 3,195 participants with early RA in their cohort, only 1,724 participants (54.0%) were eligible in the final analysis, which suggests a reduction in external validity. Furthermore, there were no details regarding missing data, which may cause a reduction in sample size.

In addition, Fatima et al presented the DAS28 using C-reactive protein level (DAS28-CRP) and the DAS28 using erythrocyte sedimentation rate (DAS28-ESR) as comparable disease activity measures, but each of these (DAS-CRP and DAS-ESR) are calculated using different formulas and thus may not be interchangeable among patients with high disease activity, such as the participants in the study by Fatima et al (7). Such an incomplete presentation of the data implies that data are missing. To avoid further reduction of sample size due to missing data, the authors should have described the missing data and dealt with them in an appropriate manner (e.g., multiple imputations) (8).

In summary, the results of the study by Fatima et al and the interpretations of those results may be biased due to insufficient internal validity (i.e., inaccurate statistical models) and reduced external validity (i.e., reduced sample size regarding eligible participants and missing data). Both internal and external validity are essential in clinical research; therefore, further studies that compensate for the limitations mentioned above are still warranted.

Yusuke Matsuo, MD, PhD
Tokyo Kyosai Hospital
and Tokyo Medical and Dental University
Tokyo Japan
 Yoshie Yamada, MD
Kyoto University School of Public Health
and Graduate School of Medicine
Kyoto Japan
 Jun Miyata, MD
Osaka University Graduate School of Medicine
Osaka Japan
 Tetsuro Aita, MD
Fukushima Medical University
 Takashi Yoshioka, MD, MPH, PhD 
Center for Innovative Research for Communities
and Clinical Excellence
and Fukushima Medical University
Fukushima Japan

2. Fatima S, Schieir O, Valois MF, Bartlett SJ, Bessette L, Boire G, et al. Health assessment questionnaire at one year predicts all-cause mortality in patients with early rheumatoid arthritis. *Arthritis Rheumatol* 2021;73:197–202.
3. Prevoo ML, van't Hof MA, Kuper HH, van Leeuwen MA, van de Putte LB, van Riel PL. Modified disease activity scores that include twenty-eight-joint counts: development and validation in a prospective longitudinal study of patients with rheumatoid arthritis. *Arthritis Rheum* 1995;38:44–8.
4. Sokka T, Abelson B, Pincus T. Mortality in rheumatoid arthritis: 2008 update. *Clin Exp Rheumatol* 2008;26 Suppl 51:S35–61.
5. Norton S, Fu B, Scott DL, Deighton C, Symmons DP, Wailoo AJ, et al. Health Assessment Questionnaire disability progression in early rheumatoid arthritis: systematic review and analysis of two inception cohorts [review]. *Semin Arthritis Rheum* 2014;44:131–44.
6. Hernán MA, Hernández-Díaz S, Robins JM. A structural approach to selection bias. *Epidemiology* 2004;15:615–25.
7. Fleischmann RM, van Der Heijde D, Gardiner PV, Szumski A, Marshall L, Bananis E. DAS28-CRP and DAS28-ESR cut-offs for high disease activity in rheumatoid arthritis are not interchangeable. *RMD Open* 2017;3:2–6.
8. Enders CK. Multiple imputation as a flexible tool for missing data handling in clinical research. *Behav Res Ther* 2017;98:4–18.

DOI 10.1002/art.41916

Considerations for a study using the Health Assessment Questionnaire to predict all-cause mortality in early rheumatoid arthritis: comment on the article by Fatima et al

To the Editor:

We read with great interest the article by Dr. Fatima and colleagues (1), in which the authors concluded that higher Health Assessment Questionnaire (HAQ) disability index scores (2) and higher Disease Activity Scores in 28 joints (3) at 1 year were significantly associated with all-cause mortality in patients with early rheumatoid arthritis (RA). We agree with the use of discrete multivariate analysis to analyze these data in the Canadian Early Arthritis Cohort (CATCH) in the study by Fatima et al. However, we would like to point out some issues with the methodology used in their study.

First, the inclusion criteria should have been described in greater detail. Though solid administrative data were obtained from the CATCH cohort (4), precise information with regard to how the duration of joint swelling was documented was not provided. Furthermore, the enrollment criteria used (presence of swollen joints for <1 year and treatment with 1 or more disease-modifying antirheumatic drugs [DMARDs]) might not be perfectly representative of the entire population of patients with early RA. More comprehensive criteria, including presence of morning stiffness and presence of joint pain (as determined by the metatarsophalangeal joint squeeze test) should have been included, as was done in a previously published study that used data from the CATCH cohort (5). In addition, determination of the serum levels of anti-cyclic citrullinated peptide (anti-CCP) is a well-known method that has excellent

1. Fries JF, Spitz P, Kraines RG, Holman HR. Measurement of patient outcome in arthritis. *Arthritis Rheum* 1980;23:137–45.

specificity and sensitivity for the identification of early RA, and can be useful as a diagnostic criterion for RA (6). Therefore, if the anti-CCP level had been considered as part of the inclusion criteria in the study by Fatima et al, the study cohort may have been more representative of an early RA population.

Second, in the study by Fatima et al, patients who had not completed a HAQ disability index at either baseline or 12 months and patients who had not received treatment with a DMARD or biologic agent in their first year of follow-up were excluded, and therefore selection bias may have had some influence on the results. It is possible that patients with incomplete HAQ information had poorer adherence to treatment and subsequently worse outcomes. As for patients who did not receive DMARDs/biologic agents in the first year of follow-up, this group of patients may have already been experiencing severe symptoms at baseline, and therefore they may have been reluctant to allow the addition of DMARDs to their existing treatment regimen. In summary, the exclusion criteria used in the study by Fatima et al could have overlooked early RA patients who were either poorly adherent to treatment or were experiencing severe underlying disease, making the study sample less representative.

Finally, we have some sincere concerns with regard to the potential influence of several residual confounders. Although the authors utilized the Rheumatic Disease Comorbidity Index (7) to minimize the effect of comorbidities on all-cause mortality, there are still a few factors to consider in terms of those that might potentially convey a risk of confounding of the study results, including frequency of alcohol consumption, presence of cirrhosis or chronic kidney disease, and each patient's nutrition status and body mass index at baseline and over follow-up.

Drs. Ko and Yeh contributed equally to this work. Author disclosures are available at <https://onlinelibrary.wiley.com/action/downloadSupplement?doi=10.1002%2Fart.41916%file=art41916-sup-0001-Disclosureform.pdf>.

Po-Yun Ko, MD 
 Chung Shan Medical University School of Medicine
 Taichung, Taiwan
 and MacKay Memorial Hospital
 Taipei, Taiwan
 Da-Ming Yeh, MD
 Chung Shan Medical University Hospital
 and Chung Shan Medical University
 School of Medical Imaging and Radiological Science
 James Cheng-Chung Wei MD, PhD
 Chung Shan Medical University Institute of Medicine
 Chung Shan Medical University Hospital
 and China Medical University Graduate
 Institute of Integrated Medicine
 Taichung Taiwan

1. Fatima S, Schieir O, Valois MF, Bartlett SJ, Bessette L, Boire G, et al, on behalf of the CATCH Investigators. Health Assessment Questionnaire at one year predicts all-cause mortality in patients with early rheumatoid arthritis. *Arthritis Rheumatol* 2021;73:197–202.

2. Fries JF, Spitz P, Kraines RG, Holman HR. Measurement of patient outcome in arthritis. *Arthritis Rheum* 1980;23:137–45.
3. Baker JF, Conaghan PG, Smolen JS, Aletaha JS, Shults J, Emery P, et al. Development and validation of modified disease activity scores in rheumatoid arthritis: superior correlation with magnetic resonance imaging-detected synovitis and radiographic progression. *Arthritis Rheumatol* 2014;66:794–802.
4. Kudaeva F, Speechley M, Klar N, Schieir O, Bartlett SJ, Bessette L, et al. Association of arthritis onset with influenza: analysis of the Canadian Early Inflammatory Arthritis Cohort. *ACR Open Rheumatol* 2019; 1:63–9.
5. Holdren M, Schieir O, Bartlett SJ, Bessette L, Boire G, Hazlewood G, et al. Improvements in fatigue lag behind disease remission in early rheumatoid arthritis: results from the Canadian Early Arthritis Cohort. *Arthritis Rheumatol* 2021;73:53–60.
6. Aletaha D, Neogi T, Silman AJ, Funovits J, Felson DT, Bingham CO III, et al. 2010 rheumatoid arthritis classification criteria: an American College of Rheumatology/European League Against Rheumatism collaborative initiative. *Arthritis Rheum* 2010;62:2569–81.
7. Michaud K, Wolfe F. Comorbidities in rheumatoid arthritis. *Best Pract Res Clin Rheumatol* 2007;21:885–906.

DOI 10.1002/art.41915

Functional capacity at 1 year predicts all-cause mortality in patients with rheumatoid arthritis: comment on the article by Fatima et al

To the Editor:

We read with interest the article by Dr. Fatima and colleagues on the use of the Health Assessment Questionnaire (HAQ) to predict all-cause mortality in patients with early rheumatoid arthritis (RA) (1). The conclusion of their study demonstrated that higher HAQ disability index scores (2) and Disease Activity Scores in 28 joints (DAS28) (3) at 1 year are significantly associated with all-cause mortality in a large cohort of patients with early RA.

We would like to point out our earlier findings from a prospective follow-up survey of a cohort of 100 RA patients, in which patients were followed up at 11 years (4), 15 years (5,6), 25 years (7), and 40 years (8) after study inception, and data on clinical features and incidence of death were collected at each time point. The unique aspect of this series was the fact that we were able to obtain follow-up data from all 100 patients in the cohort, in contrast to the survey from the Canadian Early Arthritis Cohort (CATCH) used by Fatima et al, which captured follow-up data on 1,724 patients from a cohort that initially included 3,195 participants. Our original cohort of 100 sequential patients with RA seen within the first year of disease was referred to The Royal National Hospital for Rheumatic Diseases in Bath, England between 1957 and 1963. The patients were referred to one of the consultants (John A. Cosh), who documented all of the data available at that time. This series of studies predated the introduction of the HAQ and DAS28 as measures of physical function and disease activity. At that time, the diagnosis of RA was categorized as classical, definite, or possible RA according

to the original American College of Rheumatology diagnostic criteria (9), and functional capacity was assessed using the Steinbrocker criteria (10). Other details were collected and sequentially reported at the designated follow-up time points. At study inception, all patients had a diagnosis of definite or classical RA.

In our cohort of 100 RA patients, the functional capacity of the patients, as measured with the Steinbrocker criteria after 1 year, had been significantly worse among those who died by the 15-year follow-up ($P < 0.001$) (5). This finding was confirmed in the subsequent studies of patients in the Bath series (6–8).

Features at 1 year after the start of the disease that were associated with mortality up to 40 years after onset of RA symptoms by regression analysis included older age ($P < 0.0001$), lower hemoglobin level ($P = 0.0461$), and reduced functional capacity ($P < 0.0001$) (8). The standardized mortality ratio of the cohort at 40 years was 2.13 (95% confidence interval 1.26–3.60). The median survival was reduced by 10 years for men and 11 years for women, compared with the general population in Bath and the surrounding area. It is worth noting that all of the patients recruited lived within a 10-mile radius of the hospital and over the 40 years of reporting they all lived within 30 miles of Bath.

One other aspect to consider is that our cohort was inadequately treated by today's standards. Several received gold injections and subsequently penicillamine. Thus, the natural course of RA was observed in that earlier cohort, which would not be seen today in the majority of RA patients undergoing treatment in modern health care systems, since most are receiving the current optimal treatments for the disease.

The study of the Bath cohort in 1981 demonstrated that functional capacity at 1 year predicts all-cause mortality in patients with early RA, even when measured with the crude Steinbrocker method. It is interesting to see that the HAQ score showed similar prognostic significance in the CATCH survey ~40 years later.

Author disclosures are available at <https://onlinelibrary.wiley.com/action/downloadSupplement?doi=10.1002%2Fart.41915&file=art41915-sup-0001-Disclosureform.pdf>.

Richard K. Jacoby, MD, FRCP
Royal Devon and Exeter Hospital
Exeter UK

Johannes J. Rasker, MD, PhD 
University of Twente
Enschede The Netherlands

1. Fatima S, Schieir O, Valois MF, Bartlett SJ, Bessette L, Boire G, et al, on behalf of the CATCH Investigators. Health Assessment Questionnaire at one year predicts all-cause mortality in patients with early rheumatoid arthritis. *Arthritis Rheumatol* 2021;73:197–202.
2. Fries JF, Spitz P, Kraines RG, Holman HR. Measurement of patient outcome in arthritis. *Arthritis Rheum* 1980;23:137–45.
3. Baker JF, Conaghan PG, Smolen JS, Aletaha JS, Shults J, Emery P, et al. Development and validation of modified disease activity scores

in rheumatoid arthritis: superior correlation with magnetic resonance imaging–detected synovitis and radiographic progression. *Arthritis Rheumatol* 2014;66:794–802.

4. Jacoby RK, Jayson MIV, Cosh JA. Onset, early stages, and prognosis of rheumatoid arthritis: a clinical study of 100 patients with 11-year follow up. *Br Med J* 1973;2:96–100.
5. Rasker JJ, Cosh JA. Cause and age at death in a prospective study of 100 patients with rheumatoid arthritis. *Ann Rheum Dis* 1981;40:115–20.
6. Rasker JJ, Cosh JA. The natural history of rheumatoid arthritis: a fifteen-year follow-up study; the prognostic significance of features noted in the first year. *Clin Rheumatol* 1984;3:11–20.
7. Reilly PA, Cosh JA, Maddison PJ, Rasker JJ, Silman AJ. Mortality and survival in rheumatoid arthritis: a 25-year prospective study of 100 patients. *Ann Rheum Dis* 1990;49:363–9.
8. Minaur NJ, Jacoby RK, Cosh JA, Taylor G, Rasker JJ. Outcome after 40 years with rheumatoid arthritis: a prospective study of function, disease activity, and mortality. *J Rheumatol* 2004;31 Suppl 69:3–8.
9. Ropes MV, Bennett GA, Cobb S, Jacox R, Jessar R. Diagnostic criteria for rheumatoid arthritis; 1958 revision. *Ann Rheum Dis* 1959;18:49–51.
10. Steinbrocker O, Traeger CH, Batterman RC. Therapeutic criteria in rheumatoid arthritis. *JAMA* 1949;140:659–62.

DOI 10.1002/art.41918

Reply

To the Editor:

We appreciate the interest in our article concerning the HAQ disability index (1) in an early RA incident cohort (the CATCH), which we assessed at baseline and at several follow-up time points for its predictive capacity in estimating the risk of all-cause mortality among patients with RA. We will now address the concerns outlined by each set of authors.

Dr. Matsuo and colleagues suggested that the HAQ disability index score at 1 year of follow-up depends on the HAQ disability index score at baseline. This is a true but different study question. We aimed to understand if residual disability at 1 year of treatment in early RA is associated with all-cause mortality, rather than whether change in disability over 1 year predicts mortality. We therefore performed additional analyses, as suggested, in which we adjusted for the baseline HAQ disability index score, with the results showing similar levels of association with mortality but without improvement in the fit of the model (Table 1).

A second point that was raised by Matsuo and colleagues was regarding the potential impact of missing data on the validity and generalizability of the findings of our study. Our colleagues point out that at the time that our report was published, CATCH had enrolled 3,195 participants, yet only 1,724 participants (54%) were included in the analysis. Our study, however, had additional inclusion and exclusion criteria, such as including patients enrolled between January 2007 and March 2016, as we wanted to allow time for the event of interest (death) to occur. Treatment for RA was required during the first year, and only

Table 1. Association of HAQ disability index scores at baseline and 1 year with risk of mortality in patients with early rheumatoid arthritis, as determined in the original model versus models with different adjustments*

	HAQ–mortality risk model	
	Baseline HAQ, HR (95% CI)	1-year HAQ, HR (95% CI)
Original model (no adjustments)	1.30 (0.84–2.00)	1.73 (1.09–2.74)
Model substituting DAS28-ESR	1.33 (0.84–2.00)	1.72 (1.20–3.09)
Model substituting DAS28-CRP	1.35 (0.86–2.13)	1.72 (1.02–2.88)
Model adjusted for baseline HAQ score	–	1.79 (1.05–3.04)

* Values are the hazard ratio (HR) with 95% confidence interval (95% CI) for associations of baseline or 1-year Health Assessment Questionnaire (HAQ) disability index scores with risk of mortality, based on the model originally published in Fatima et al (6) and in models adjusted for the Disease Activity Score in 28 joints using the erythrocyte sedimentation rate (DAS28-ESR), DAS28 using the C-reactive protein level (DAS28-CRP), and baseline HAQ disability index score.

patients with active disease were eligible for this study. After applying the aforementioned criteria, there were 2,407 eligible participants and for 1,724 of the patients, we had complete data on the HAQ disability score at baseline and 1 year, DAS28 scores (2) from baseline and 1 year, data on an inflammation marker (either the ESR or the CRP level) available at baseline and 1 year, and data on the known vital status of each patient. This represented 72% of all eligible participants. It is up to clinicians to presume whether these patients with early RA could be generalizable to their clinic patients. The reasons for the missing data in our study are likely to be similar to those in other cohorts of patients with early RA, in which patients may have missed a visit or did not complete all forms at key time points, or laboratory tests may have been performed outside of the visit time window.

To address other concerns raised by Dr. Ko and colleagues, the inclusion criteria of the CATCH cohort were well described, including establishing the date of disease onset as the date at which the initial symptoms of RA (i.e., presence of joint swelling) were recorded, and determining eligibility on the basis of application of the RA criteria at the time of enrollment (3). Nearly all of the patients in the CATCH cohort met the American College of Rheumatology/European League Against Rheumatism 2010 criteria for RA (4), but patients with a suspected diagnosis of RA were included in this study if the patient began treatment with a DMARD. However, in many studies of patients with early RA, only ~50–60% of patients are positive for anti-CCP antibodies, so we would have removed many patients with RA if that criterion had been applied to the cohort (3).

We agree with Ko and colleagues that inclusion of patients without follow-up or missing baseline HAQ disability index data could bias the study, but likely this bias would skew the results toward a more conservative estimate of mortality risk, as patients

who do not attend follow-up visits may be less adherent to treatment and often have lower socioeconomic status. Nearly 100% of the CATCH cohort was prescribed DMARDs, and in the majority of these patients the prescription was provided at the first rheumatology visit, and therefore a lack of treatment with DMARDs would be very rare. Ko et al are correct in assuming that some serious comorbidities, such as cirrhosis and renal failure, are not necessarily part of the Rheumatic Disease Comorbidity Index (5) and could increase the rate of all-cause mortality and also may be a confounder in the patient's function scores, potentially resulting in a higher HAQ disability index score. However, some of these patients would not have been prescribed a DMARD due to severe comorbidity and contraindications to methotrexate; therefore they would have been excluded from the analyses. However, as mentioned, the frequency of use of DMARDs in the first year of follow-up in the CATCH cohort was nearly 100%. Therefore, any patients who had no history of DMARD use would have been very rare in this cohort.

There was a concern that DAS28-ESR and DAS28-CRP scores are not interchangeable. In our study, continuous scores of DAS28-ESR and DAS28-CRP were used. Thus, in our cohort, the DAS28-ESR and DAS28-CRP disease state scores were not interchangeable, because the DAS28-CRP scores were lower; nevertheless, the continuous scores for the DAS28-ESR and DAS28-CRP were highly correlated (>0.9) (7). In some jurisdictions in Canada, reimbursement for ESR testing was discontinued over the study period. Therefore, given that data on ESR or CRP were missing due to a system change, and that continuous DAS28 scores were used for covariate adjustment, we were able to use both the DAS28-ESR score (in 93% of patients) and the DAS28-CRP score (in 7% of patients); the latter was only imputed when the ESR result was missing. We repeated the analyses using only DAS28-ESR data and this did not substantially change the results.

Finally, Dr. Jacoby and colleagues described the results from their study of 100 patients with incident RA who were followed up for 4 decades, in which it was observed that poor functional capacity was predictive of mortality. A diagnosis of RA ascertained decades ago would likely be very different due to lack of early RA clinics, lack of classification criteria, and fewer available DMARDs. Worse functional class in their study and impaired patient self-reported function as measured by the HAQ disability index in our study were both predictive of mortality. We appreciate the comparison of the unique observations made by following up patients closely for decades.

We thank these colleagues for raising interesting points with respect to the methods and generalizability of our findings and comparing our results to those in a historical cohort of patients with incident RA who were followed up for 40 years.

The CATCH study was independently designed and implemented by the investigators. It has been financially supported through unrestricted research grants from Amgen, Pfizer Canada, AbbVie, Medexus, Inc., Eli Lilly Canada, Merck Canada, Sandoz, Canada Biopharmaceuticals, Hoffmann-LaRoche,

Janssen Biotech, UCB Canada, Bristol Myers Squibb Canada, and Sanofi Genzyme.

Safoora Fatima, MD
*University of Western Ontario
 London Ontario, Canada*
 O. Schieir, PhD
 E. C. Keystone, MD 
*University of Toronto
 Toronto Ontario, Canada*
 M. F. Valois, PhD
 S. J. Bartlett, PhD 
*McGill University
 Montreal Quebec, Canada*
 L. Bessette, MD
*CHU de Québec-Université Laval
 Laval Quebec, Canada*
 G. Boire, MD
*Centre Intégré Universitaire de Santé
 et de Services Sociaux de l'Estrie
 CHU de Sherbrooke
 and Université de Sherbrooke
 Sherbrooke Quebec, Canada*
 G. Hazlewood, MD, PhD 
*University of Calgary
 Calgary Alberta, Canada*
 C. Hitchon, MD 
*University of Manitoba
 Winnipeg Manitoba, Canada*
 D. Tin, BScPhm
 C. Thorne, MD
*Southlake Regional Health Centre
 Newmarket Ontario, Canada*
 V. P. Bykerk, MD
*University of Toronto
 Toronto, Ontario, Canada
 Hospital for Special Surgery
 and Weill Cornell Medical College
 New York, NY*

J. E. Pope, MD 
*University of Western Ontario
 Schulich School of Medicine and Dentistry
 and St. Joseph's Health Care London
 London Ontario, Canada
 on behalf of the CATCH Investigators*

1. Maska L, Anderson J, Michaud K. Measures of functional status and quality of life in rheumatoid arthritis: Health Assessment Questionnaire Disability Index (HAQ), Modified Health Assessment Questionnaire (MHAQ), Multidimensional Health Assessment Questionnaire (MDHAQ), Health Assessment Questionnaire II (HAQ-II), Improved Health Assessment Questionnaire (Improved HAQ), and Rheumatoid Arthritis Quality of Life (RAQoL). *Arthritis Care Res (Hoboken)* 2011; 63:Suppl 11:S4–13.
2. Prevoost ML, van't Hof MA, Kuper HH, van Leeuwen MA, van de Putte LB, van Riel PL. Modified disease activity scores that include twenty-eight-joint counts: development and validation in a prospective longitudinal study of patients with rheumatoid arthritis. *Arthritis Rheum* 1995;38:44–8.
3. Kuriya B, Schieir O, Lin D, Xiong J, Pope J, Boire G, et al. Thresholds for the 28-joint disease activity score (DAS28) using C-reactive protein are lower compared to DAS28 using erythrocyte sedimentation rate in early rheumatoid arthritis. *Clin Exp Rheumatol* 2017;35:799–803.
4. Aletaha D, Neogi T, Silman AJ, Funovits J, Felson DT, Bingham CO III, et al. 2010 rheumatoid arthritis classification criteria: an American College of Rheumatology/European League Against Rheumatism collaborative initiative. *Arthritis Rheum* 2010;62:2569–81.
5. England BR, Sayles H, Mikuls TR, Johnson DS, Michaud K. Validation of the rheumatic disease comorbidity index. *Arthritis Care Res (Hoboken)* 2015;67:865–72.
6. Fatima S, Schieir O, Valois MF, Bartlett SJ, Bessette L, Boire G, et al. Health assessment questionnaire at one year predicts all-cause mortality in patients with early rheumatoid arthritis. *Arthritis Rheumatol* 2021; 73:197–202.
7. Minaur NJ, Jacoby RK, Cosh JA, Taylor G, Rasker JJ. Outcome after 40 years with rheumatoid arthritis: a prospective study of function, disease activity, and mortality. *J Rheumatol Suppl* 2004;69:3–8.

Arthritis & Rheumatology

An Official Journal of the American College of Rheumatology
www.arthritisrheum.org and wileyonlinelibrary.com

Editor

Daniel H. Solomon, MD, MPH, *Boston*

Deputy Editors

Richard J. Bucala, MD, PhD, *New Haven*

Mariana J. Kaplan, MD, *Bethesda*

Peter A. Nigrovic, MD, *Boston*

Co-Editors

Karen H. Costenbader, MD, MPH, *Boston*

David T. Felson, MD, MPH, *Boston*

Richard F. Loeser Jr., MD, *Chapel Hill*

Social Media Editor

Paul H. Sufka, MD, *St. Paul*

Journal Publications Committee

Amr Sawalha, MD, *Chair, Pittsburgh*

Susan Boackle, MD, *Denver*

Aileen Davis, PhD, *Toronto*

Deborah Feldman, PhD, *Montreal*

Donnamarie Krause, PhD, OTR/L, *Las Vegas*

Wilson Kuswanto, MD, PhD, *Stanford*

Michelle Ormseth, MD, *Nashville*

R. Hal Scofield, MD, *Oklahoma City*

Editorial Staff

Jane S. Diamond, MPH, *Managing Editor, Atlanta*

Lesley W. Allen, *Assistant Managing Editor, Atlanta*

Ilani S. Lorber, MA, *Assistant Managing Editor, Atlanta*

Stefanie L. McKain, *Manuscript Editor, Atlanta*

Sara Omer, *Manuscript Editor, Atlanta*

Emily W. Wehby, MA, *Manuscript Editor, Atlanta*

Christopher Reynolds, MA, *Editorial Coordinator, Atlanta*

Brittany Swett, MPH, *Assistant Editor, Boston*

Associate Editors

Marta Alarcón-Riquelme, MD, PhD, *Granada*

Heather G. Allore, PhD, *New Haven*

Neal Basu, MD, PhD, *Glasgow*

Edward M. Behrens, MD, *Philadelphia*

Bryce Binstadt, MD, PhD, *Minneapolis*

Nunzio Bottini, MD, PhD, *San Diego*

John Carrino, MD, MPH, *New York*

Lisa Christopher-Stine, MD, MPH,
Baltimore

Andrew Cope, MD, PhD, *London*

Nicola Dalbeth, MD, FRACP, *Auckland*

Brian M. Feldman, MD, FRCPC, MSc, *Toronto*

Richard A. Furie, MD, *Great Neck*

J. Michelle Kahlenberg, MD, PhD,
Ann Arbor

Benjamin Leder, MD, *Boston*

Yvonne Lee, MD, MMSc, *Chicago*

Katherine Liao, MD, MPH, *Boston*

Bing Lu, MD, DrPH, *Boston*

Anne-Marie Malfait, MD, PhD, *Chicago*

Stephen P. Messier, PhD,
Winston-Salem

Janet E. Pope, MD, MPH, FRCPC,
London, Ontario

Christopher T. Ritchlin, MD, MPH,
Rochester

William Robinson, MD, PhD, *Stanford*

Georg Schett, MD, *Erlangen*

Sakae Tanaka, MD, PhD, *Tokyo*

Maria Trojanowska, PhD, *Boston*

Betty P. Tsao, PhD, *Charleston*

Fredrick M. Wigley, MD, *Baltimore*

Edith M. Williams, PhD, MS, *Charleston*

Advisory Editors

Ayaz Aghayev, MD, *Boston*

Joshua F. Baker, MD, MSCE,
Philadelphia

Bonnie Bermas, MD, *Dallas*

Jamie Collins, PhD, *Boston*

Kristen Demoruelle, MD, PhD, *Denver*

Christopher Denton, PhD, FRCP, *London*

Anisha Dua, MD, MPH, *Chicago*

John FitzGerald, MD, *Los Angeles*

Lauren Henderson, MD, MMSc, *Boston*

Monique Hinchcliff, MD, MS, *New Haven*

Hui-Chen Hsu, PhD, *Birmingham*

Mohit Kapoor, PhD, *Toronto*

Seoyoung Kim, MD, ScD, MSCE, *Boston*

Vasileios Kytтарыs, MD, *Boston*

Carl D. Langefeld, PhD,
Winston-Salem

Dennis McGonagle, FRCPI, PhD, *Leeds*

Julie Paik, MD, MHS, *Baltimore*

Amr Sawalha, MD, *Pittsburgh*

Julie Zikherman, MD, *San Francisco*

AMERICAN COLLEGE OF RHEUMATOLOGY

Kenneth G. Saag, MD, MSc, *Birmingham*, **President**

Douglas White, MD, PhD, *La Crosse*, **President-Elect**

Carol Langford, MD, MHS, *Cleveland*, **Treasurer**

Deborah Desir, MD, *New Haven*, **Secretary**

Steven Echard, IOM, CAE, *Atlanta*, **Executive Vice-President**

© 2022 American College of Rheumatology. All rights reserved. No part of this publication may be reproduced, stored or transmitted in any form or by any means without the prior permission in writing from the copyright holder. Authorization to copy items for internal and personal use is granted by the copyright holder for libraries and other users registered with their local Reproduction Rights Organization (RRO), e.g. Copyright Clearance Center (CCC), 222 Rosewood Drive, Danvers, MA 01923, USA (www.copyright.com), provided the appropriate fee is paid directly to the RRO. This consent does not extend to other kinds of copying such as copying for general distribution, for advertising or promotional purposes, for creating new collective works or for resale. Special requests should be addressed to: permissions@wiley.com.

Access Policy: Subject to restrictions on certain backfiles, access to the online version of this issue is available to all registered Wiley Online Library users 12 months after publication. Subscribers and eligible users at subscribing institutions have immediate access in accordance with the relevant subscription type. Please go to onlinelibrary.wiley.com for details.

The views and recommendations expressed in articles, letters, and other communications published in *Arthritis & Rheumatology* are those of the authors and do not necessarily reflect the opinions of the editors, publisher, or American College of Rheumatology. The publisher and the American College of Rheumatology do not investigate the information contained in the classified advertisements in this journal and assume no responsibility concerning them. Further, the publisher and the American College of Rheumatology do not guarantee, warrant, or endorse any product or service advertised in this journal.

Cover design: Todd Machen

©This journal is printed on acid-free paper.